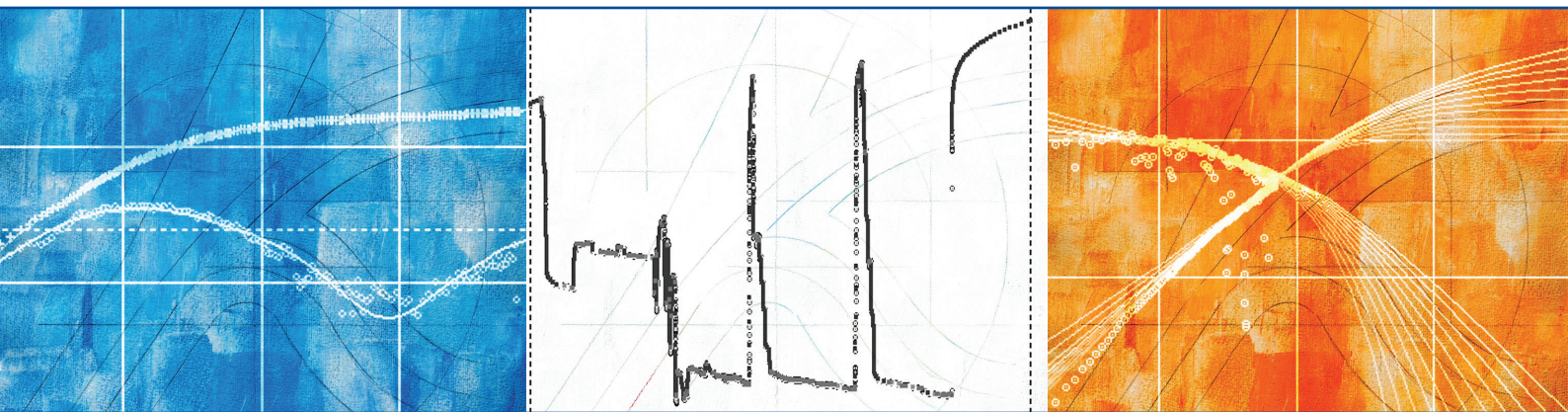




Dynamic Data Analysis



The theory and practice of Pressure Transient, Production Analysis, Well Performance Analysis, Production Logging and the use of Permanent Downhole Gauge data.

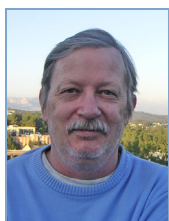
Olivier Houzé - Didier Viturat - Ole S. Fjaere
(et al)

**Olivier Houzé (OH) - Author**

Engineering Degree from Ecole Polytechnique (France, 1982) and MSc in Petroleum Engineering from Stanford University (USA, 1983). After four years as a Field Engineer with Flopetrol Schlumberger, co-founded KAPPA in 1987 and has been its Managing Director since 1991. Author of several papers on Pressure Transient Analysis and co-author of the 2009 SPE monograph on Pressure Transient Testing.

**Didier Viturat (DV) - Author**

Engineering Degree from Ecole Centrale de Lyon (France, 1975) and from the IFP school (France, 1976). Thirteen years as a Field Engineer, Reservoir engineer and Instructor with Flopetrol and Schlumberger Testing. Eight years as Reservoir Engineer with Geoservices and Geopetrol. Head of technical support, principal trainer and consultant in KAPPA Engineering since 1999. Author of several papers on Well Test Analysis methods.

**Ole S. Fjaere (OSF) - Author**

BSc in Petroleum Engineering from Rogaland Regional College (Norway, 1975). Ten years with Flopetrol Schlumberger as a well test and wireline operator, well test interpretation engineer and line management. Joined KAPPA in 1989 as an instructor and consultant in Pressure Transient Analysis.

**Simon Trin (ST) - Project Coordinator (the one who lost sleep)**

Engineering Degree from Ecole Supérieure de l'Electricité (France, 2006), Msc and Engineer's degree in Petroleum Engineering from Imperial College (United Kingdom, 2006). After two years as a Field Reservoir Engineer with Shell International, joined KAPPA in 2008 as a R&D Reservoir Engineer.

**Olivier Allain (OA) - Technical author on some chapters**

Engineering Degree from Ecole Nationale des Ponts et Chaussées (France, 1987), MSc and Engineer's degree in Petroleum Engineering from Stanford University (USA, 1987-88). After two years as a Field Engineer with Schlumberger Testing and Production Services, joined KAPPA in 1990 and has been its Technical Director since 1998.

**Eric Tauzin (ET) - Technical author on some chapters**

Engineering Degree in fluid mechanics from ENSEEIHT (France, 1992). MSc in Petroleum Engineering from Stanford University (USA, 1995). Joined KAPPA in 1998 as a Reservoir Engineer.

Other contributors

Véronique Chassignol: Technical author, final formatting

Benoît Berthoud: Artworks

Kevin Siggery: Reviewer

Joop de Wit: Reviewer

David Wynne: Reviewer



1.A What is the purpose of this book?

This book is a living document delivered in electronic (PDF) format. The advantage of this is that it can be updated regularly with new content. The downside is that you may have to reprint from time to time.

This publication has three objectives:

- To be a stand-alone technical book that registered users can freely download.
- It constitutes the reference notes for many of the KAPPA training courses:
 - Foundation Pressure Transient Analysis
 - Advanced Pressure Transient Analysis
 - Production Analysis and PDG data
 - Dynamic Data Analysis (Parts I & II)
 - Specific in-house courses

Based on the particular course, only relevant chapters are compiled. To make the course easy to follow, all slides used during the course are replicated in this document.

- Finally, although a generic document, it is part of the technical reference manual for the KAPPA software suite:
 - KAPPA Server, a client-server application for PDG reservoir surveillance
 - Ecrin, an engineering workstation integrating several dedicated modules:
 - Saphir NL for Pressure Transient Analysis
 - Topaze NL for Production Analysis
 - Rubis for History Matching
 - Amethyste for Well Performance Analysis (though we acknowledge that in this first version on the subject the dedicated chapter is somewhat sparse)
 - In this latest version of the DDA book we have added a chapter on Emeraude, the Production Logging software, that is currently a stand-alone product.

This book is not designed to teach software functionality. Guided sessions, online videos and online help exist for that purpose. Here we focus on the methodology involved in the analysis of dynamic data. However we shamelessly refer to our software and exclusively use KAPPA screen dumps. This version is synchronized with Ecrin v4.12.

Actually, let us put things in the right order. At KAPPA we do not promote methods because they are integrated in our software products, it is the other way around. We implement in our products what we think is right at a given time, and this is what we then show here.

The challenge of this book then was similar to that of Ecrin: to write something that covers a wide range of disciplines, whilst avoiding duplication and confusion for those who are only interested in one subject.

We hope you will enjoy reading it as much as it was a painful process to put it together...

The authors

A boring note on Copyrights

Sorry to talk about this dull detail but this is a sign of the times. This book is the intellectual and commercial property of KAPPA. It is available on our WEB site at no cost to registrants. You are welcome to download it and print it for your own use. If you are in the academic world, or even if you are a professional instructor, you are welcome to have it printed for your students. You are also permitted to take any part of it and integrate it into other media on the condition that the copyright of KAPPA is added and visible. This applies to the copies of the copies, etc, etc.

You are NOT allowed (and KAPPA reserves the right to take legal action and would):

- To commercialize this book in whole or in part;
- To use any part of this book in any media format without a clear reference and acknowledgement to KAPPA.

We have seen in the past that some of our diagrams and figures, available from our software, on-line help or the support material we deliver with our courses, have been used in other publications. KAPPA has no objection to this however we do ask, and expect, to be acknowledged. Since the foundation of the Company KAPPA has regularly and systematically officially registered its software and supporting diagrams and figures. In addition the figures we insert in our published documents are bitmap exports of vector (Illustrator™) original documents that we also keep and register. So we can prove both the chronological and technical history of our supporting material.

1.B What is Dynamic Data Analysis?

Not so long ago the only source of dynamic data was the welltest. When KAPPA started in 1987 with was still the case, and all this was called welltest interpretation (WTI).

Things started to drift when the same tools were applied to other operations: particularly nice formation test data, unplanned shut-ins recorded by the first permanent measurements, etc. Welltest interpretation was then rebranded **Pressure Transient Analysis (PTA)**.

Things drifted even more when people started to look at rates and pressures at the much larger time scale of the well production life. People started entering data in PTA software, but this was wrong, as models and hypotheses to apply at these time scales were different.

The basic, empirical tools of rate decline analysis were given more substance with ad-hoc superposition, various loglog plots and models already developed for PTA. We ended up in the early 2000's with what is called today Rate Transient Analysis (RTA) or **Production Analysis (PA)**. Though both terms are valid, in this book we will use the latter.

The development of **Permanent Downhole Gauges (PDG)** brought an unexpected mine of PTA and PA data. However data sets were massive, and data usable only with the development of smart filters and dedicated client-server applications. The amount of processing required dedicated software tools, and a first workflow was defined, mainly by KAPPA.

Then came the 'Intelligent Fields'. They are not so intelligent yet, but they should become so by a smart combination of permanent measurements, a federating data model and an enhanced workflow that would let automatic processes do most of the ground work while engineers would work by exception on data / cases / wells that require remedial decisions.

Even simulation ended up in the area of dynamic data. Dedicated numerical model could **History Match (HM)** the production information and permanent gauge data. In order to be reasonably fast this would not be done by large simulators, but by numerical models intermediate between a single tank material balance and full field simulators.

In KAPPA the four elements above were integrated in Ecrin (French word for jewel box), including Saphir NL (PTA), Topaze NL (PA) and Rubis (HM). PDG data processing was handled by Diamant Master, a client-server application.

In the meantime other methods were integrated in the workflow:

Production Logging (PL) used to be run when something was wrong with the well production, and Emeraude was developed separately by KAPPA in the mid-1990s. In the past twenty years this perception has evolved, and PL is now a full scale reservoir tool, especially in multilayered formations and for complex well geometries.

If we consider that all the above deal with transient data (even very long transients) **Well Performance Analysis (WPA)** is somewhat at the junction between the transient and the steady state (or pseudo-steady state) worlds. Though it generally uses steady-state models it is applied in transient analysis to correct responses to datum. It shares the IPR's with the PTA, and used the same well models and flow correlations as the PL.

After this long introduction we may get to our basic definitions:

Dynamic Flow describes any intended or unintended flow process, during exploration or production operations, where diffusion of fluid takes place within a reservoir. In most cases the dynamic flow will be human made, by putting one or several wells in production, and/or by injecting fluids into one or several wells. This however is not strictly required. Drilling and completing a well crossing several commingled zones may create a crossflow without the well producing, and this will also qualify as a dynamic flow.

Dynamic Data are the set of measurements of physical properties that are somewhat impacted by the dynamic flow. This data may be versus depth (e.g. production and temperature logs), versus time (e.g. usual pressure, temperature and rate data) or both (e.g. fiber optics data).

Dynamic Data Analysis is simply the process of interpreting and modeling the dynamic data. As introduced before, this includes Pressure Transient Analysis (PTA), Production Analysis (PA), History Matching (HM), Well Performance Analysis (WPA), Production Logging (PL). In the figure below we have even added a specific item for Formation Testers, even though it is not yet the focus of a specific KAPPA product.

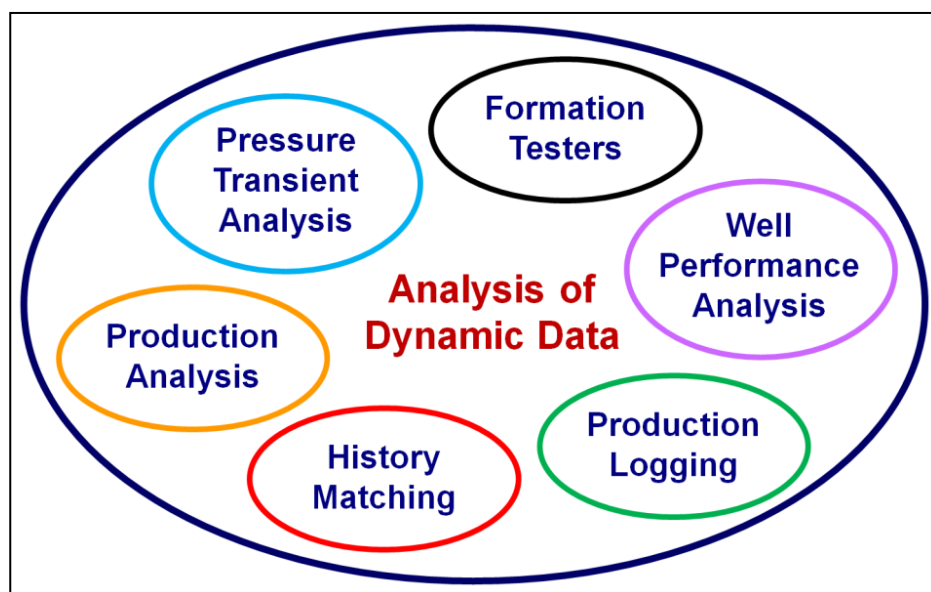


Fig. 1.B.1 – Dynamic Data Analyses

The previous version of the KAPPA book was called Dynamic Flow Analysis. When we released it we believed this term would become the industry standard. It was the name of a specific SPE ATW in Kota Kinabalu in 2004: "From Well Testing to Dynamic Flow Analysis".

However the term Dynamic Flow Analysis was not embraced in the industry and had somewhat become a KAPPA brand (thanks to the good success of this book), which is absolutely not what we had in mind. Also DFA was an acronym already used in the industry for Formation Tests.

As the industry accepted term now seems to be 'Dynamic Data' we have decided to eat our hat and rename the technique as per the industry standards.

The schematics below show the space scales of the different components of Dynamic Data Analysis. Areas are naturally not exclusive, and there are overlaps:

- Formation Testers (FT, yellow) share some diagnostic and modeling tools with PTA. It brings a vertical understanding beyond what standard PTA can do. The diffusion allows FT to see beyond the direct surrounding of the well. However the connection between the duration of the test and the investigation area does not match, despite some opposite claims, what a standard welltest will laterally see.
- PTA (blue disk) brings information in an intermediate area around the well (the infamous radius of investigation). Deconvolution on several shut-ins provides information beyond the investigation zone of individual build-ups (blue circle).
- Though it can use multi-well models and diagnostics, PA (orange) typically gives long term information on individual wells in their respective drainage areas.
- HM (red) will do the same in multiple-well mode, exclusively using a numerical model
- PL (green) provides detailed information inside the well in front of the producing intervals
- WPA (purple) models the well productivity, its evolution in time and sensitivity to completion options. It also provides a means to correct pressure and rates to datum.

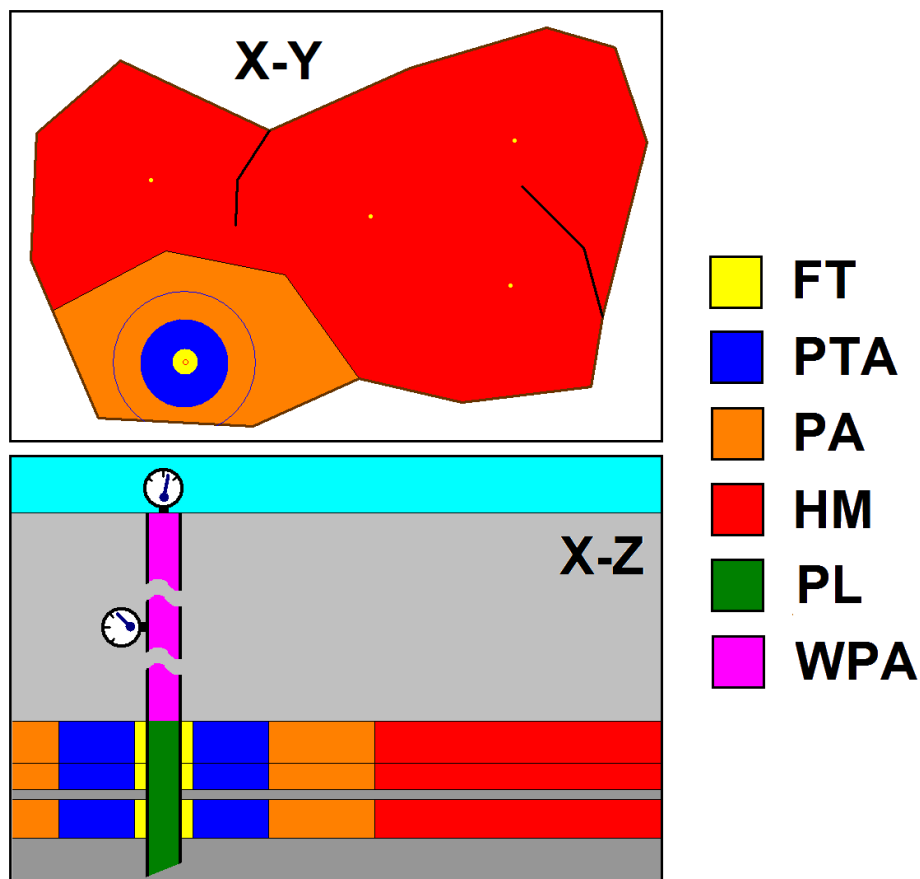


Fig. 1.B.2 – Schematics in the X-Y and X-Z planes

1.C Pressure Transient Analysis (PTA)

When PTA was still called Well Test Interpretation, analyses were performed on data acquired during dedicated operations called well tests.

A typical well test set-up is shown in the figure below. Temporary equipment is installed downhole and at surface, the well is put on production under a predefined program and the diagnostic is performed, generally on a shut-in period after a clean-up phase, an initial shut-in and a stable production phase during which producing rates are measured at the separator.

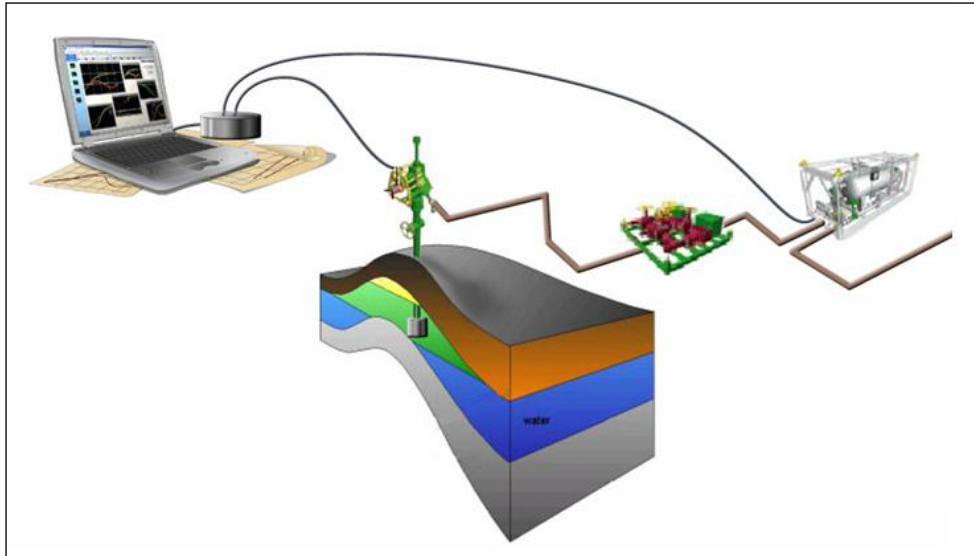


Fig. 1.C.1 – Typical well test setup

The data absolutely required to perform a PTA are the rates, the pressures (preferably downhole), the fluid PVT and a few additional parameters (well radius, pay zone, etc) required to switch from a qualitative to a quantitative analysis.

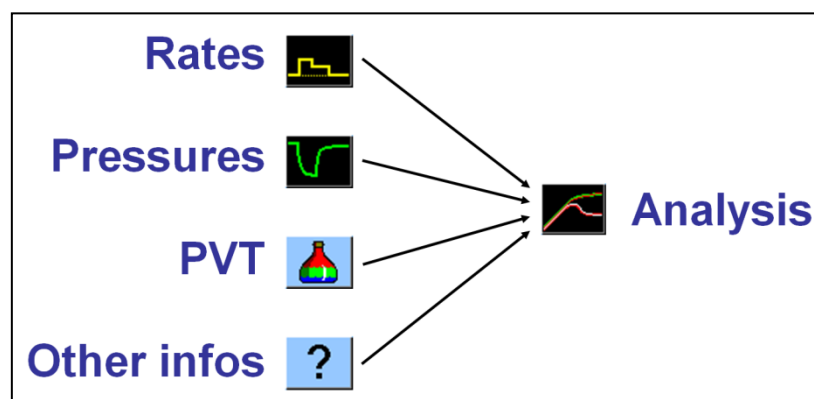


Fig. 1.C.2 – Required data for Analysis

The main flow regime of interest is the Infinite Acting Radial Flow, or IARF, which occurs after well effects have faded and before boundaries are detected. IARF may not always be seen. IARF provides an average reservoir permeability around the well, the well productivity (skin). When the well is shut in we also get an estimate of the reservoir static pressure (p^* or p_i). The first PTA methods were specialized plots (MDH, Horner) introduced in the 1950's to identify and quantify IARF. Other specialized plots dedicated to other flow regimes followed through.

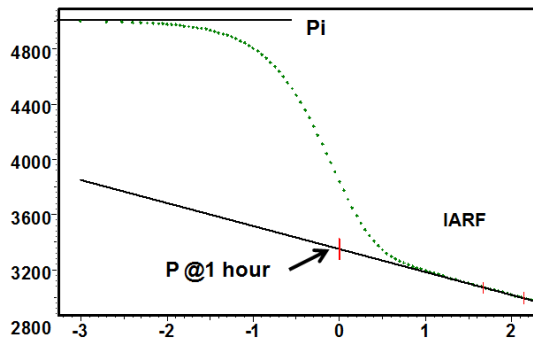


Fig. 1.C.3 – MDH plot

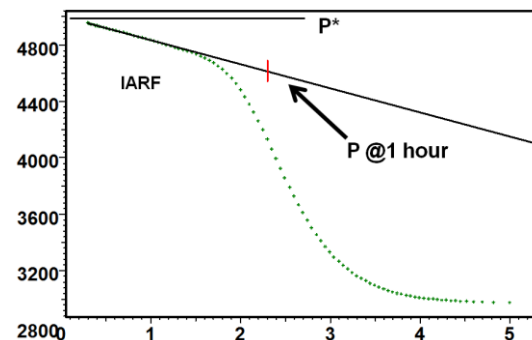


Fig. 1.C.4 – Horner plot

In the 1970's loglog type-curve matching techniques were developed to complement straight lines. One would plot the pressure response on a loglog scale on tracing paper and slide it over pre-printed type-curves until a match is obtained. The choice of the type-curve and the relative position of the data (the match point) provided physical results. These methods were of poor resolution until the Bourdet derivative was introduced.

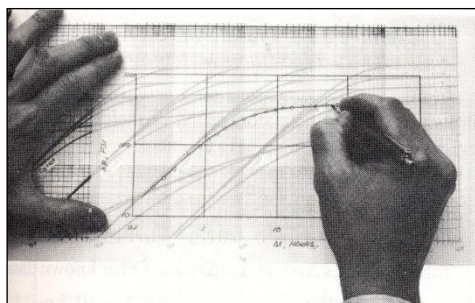


Fig. 1.C.5 – Manual Drawdown type curve matching

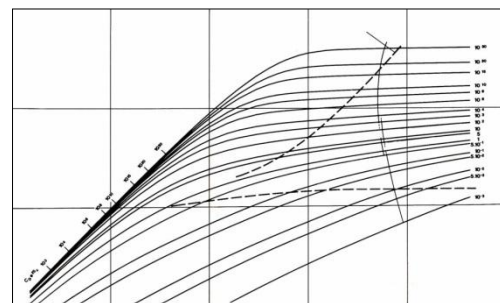


Fig. 1.C.6 – Drawdown Type Curve

In 1983, the Bourdet derivative, i.e. the slope of the semilog plot displayed on the loglog plot, increased the resolution and reliability of a new generation of type-curves.

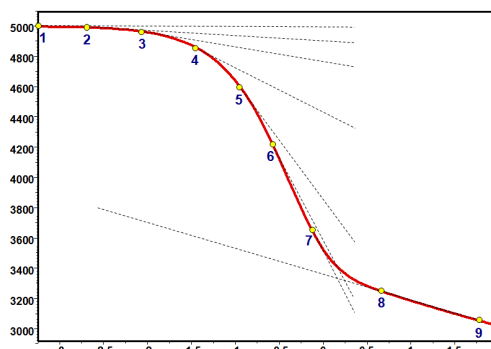


Fig. 1.C.7 – Superposition plot

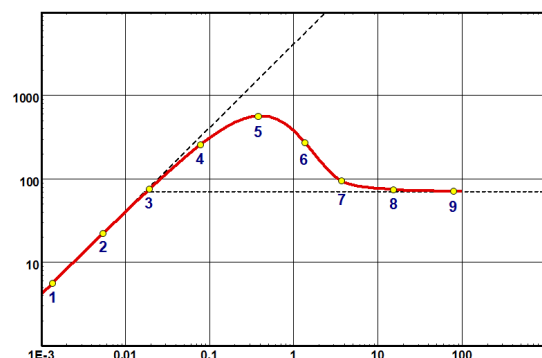


Fig. 1.C.8 – Derivative plot

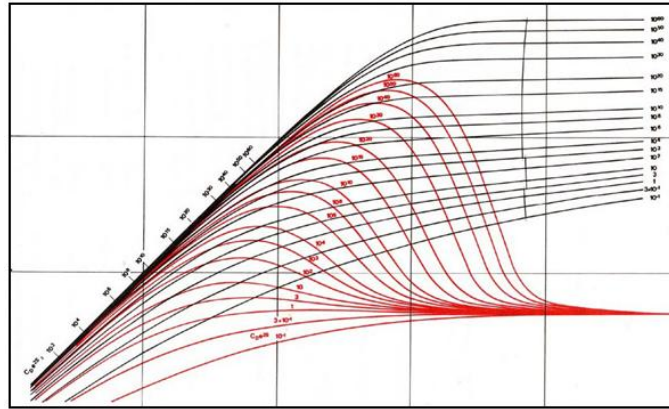


Fig. 1.C.9 – Bourdet derivative type curve

Type-curve techniques turned obsolete in the mid-1980s with the development of PC based software and the direct generation of more and more sophisticated analytical models, taking into account the complete pressure and flow rate history.

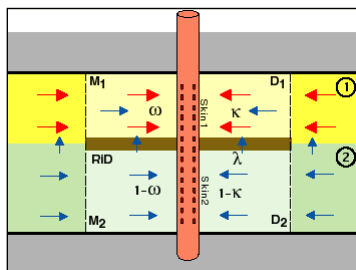


Fig. 1.C.10
2K Composite reservoir

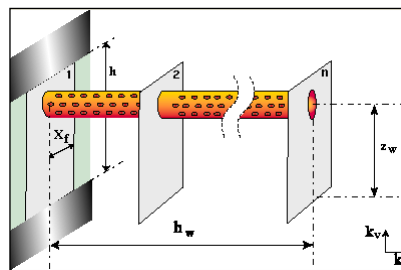


Fig. 1.C.11
Fractured horizontal well

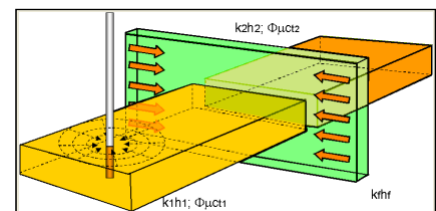


Fig. 1.C.12
Conductive fault

The core diagnostic tool remained the Bourdet derivative. Solutions were no longer unique, and the engineer was challenged to search for the most consistent answer by considering information available from all sources. The match of the model on the real data governed the validity of these analysis, while straight-line methods were made redundant.

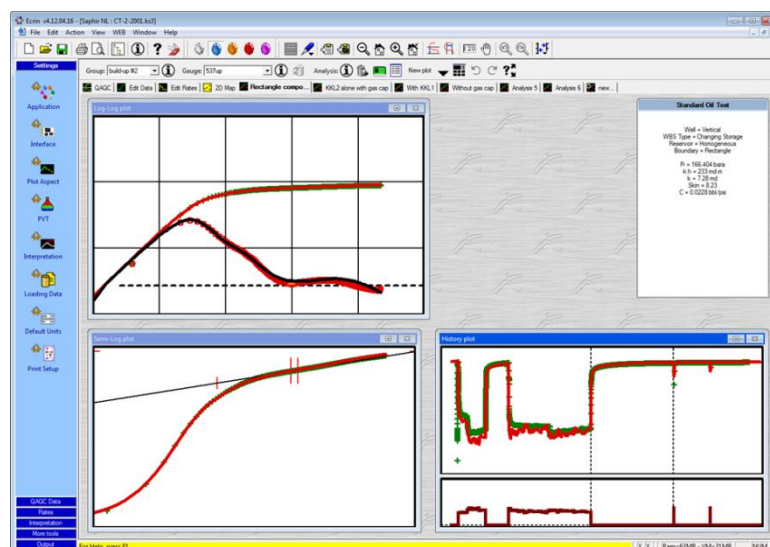


Fig. 1.C.13 – 1990-2000's – PC based PTA

Beyond superposition and the use of more sophisticated models, PC based software allowed nonlinear regression to improve results by history matching the data with the models.

Despite the spread of more and more complex analytical models and various pseudopressures developed to turn nonlinear problems into pseudolinear problems accessible to these analytical models, there was a point where analytical models would not be able to handle the complexity of some geometries and the high nonlinearity of some diffusion processes. The 1990's saw the development of the first numerical models dedicated to well testing, though the spread of usage of such models only took place in the early 2000's.

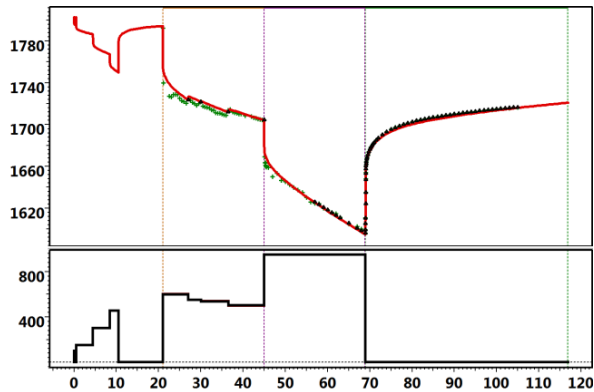


Fig. 1.C.14 – History match

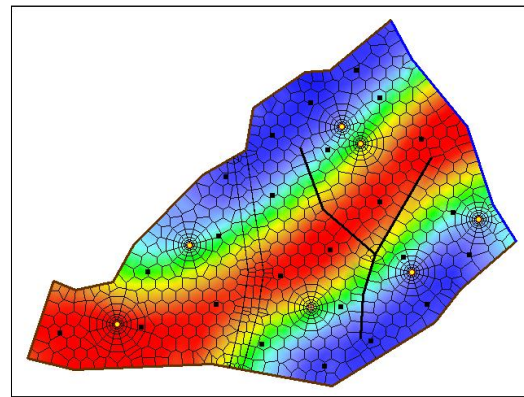


Fig. 1.C.15 – Numerical models

One would expect that most developments to come will be technology related, with more powerful processing, higher graphics and higher amount of data available. For sure we are also going to see in the years to come expert systems that will be able to approach the capacity of human engineers, in a more convincing way than the work done on the subject in the 1990's.

However the surprise is that we may also see fundamental methodology improvements. The 'surprise' of the past decade has been the successful publication of a deconvolution method which, at last (but we caveats) can be useful to combine several build-ups in a virtual, long and clean production response. Other surprises may be coming...

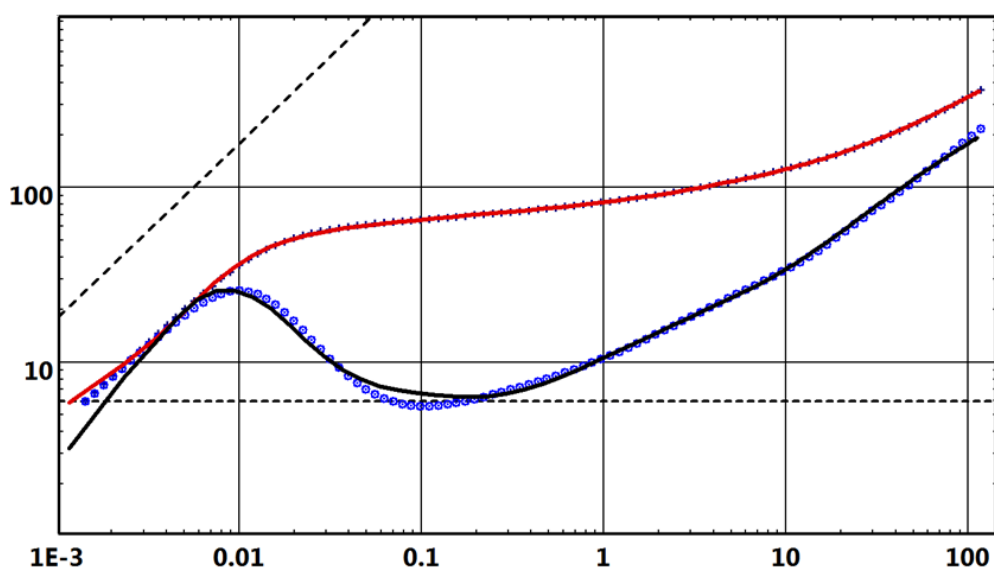


Fig. 1.C.16 – Deconvolution

1.D Production Analysis (PA)

PA started in the 1920's, when Arnold and Cutler established the first empirical relations for economic purpose but with no physical relation to actual reservoir engineering. The objective was more or less to find the right scale, draw a straight line and extrapolate.

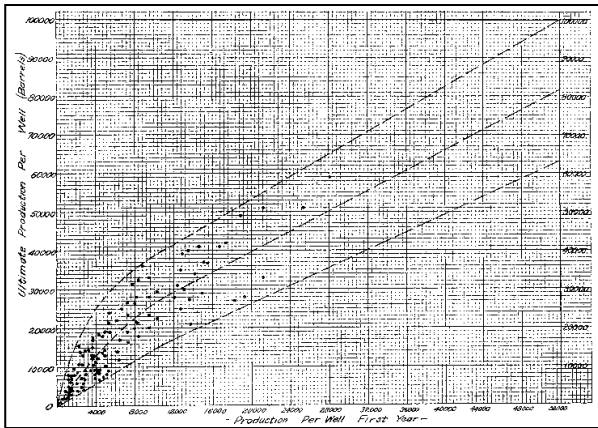


Fig. 1.D.1 – Arnold plot (1919)

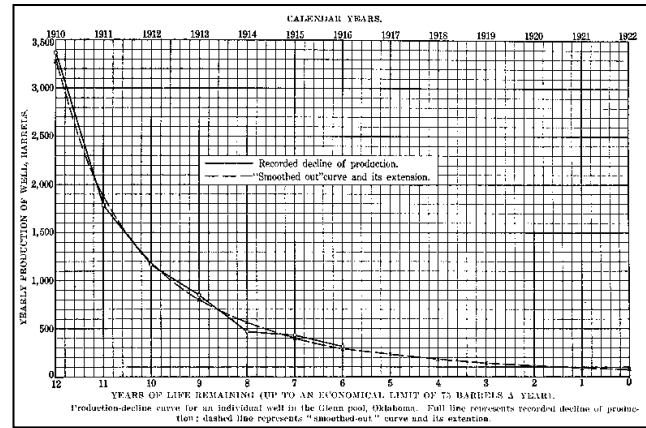


Fig. 1.D.2 – Cutler plot (1924)

Things improved marginally with Arps in the 1940's, with the formulation of constant pressure exponential, hyperbolic and harmonic decline responses:

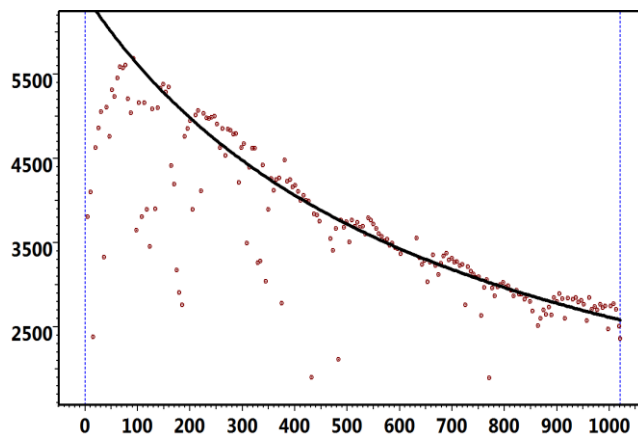


Fig. 1.D.3 – Arps plot

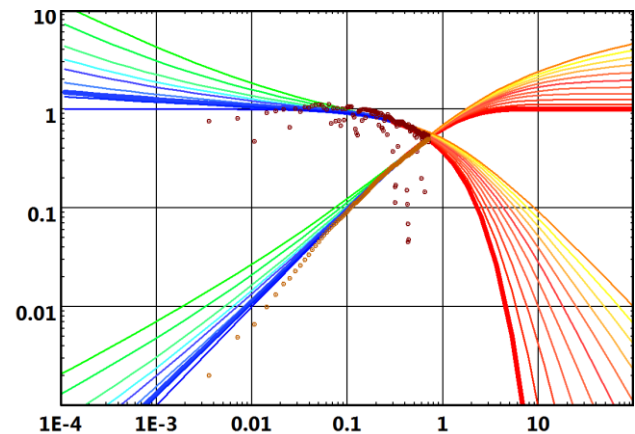


Fig. 1.D.4 – Fetkovich type curve

The first loglog, well test style type-curves came with Fetkovich in the 1970's, still assuming constant flowing pressure at a time where the well test community was moving towards superposition / convolution of the flow rates.

Superposition and derivative came ten years later, with the work of Blasingame et al., and a new presentation was proposed, with normalized rate pressure instead of normalized pressure rate values, and an adjusted time scale (material balance time):

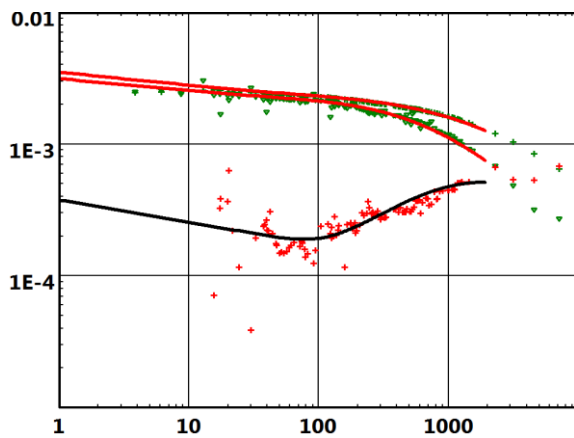


Fig. 1.D.5 – Blasingame plot:
Normalized rate Pressure

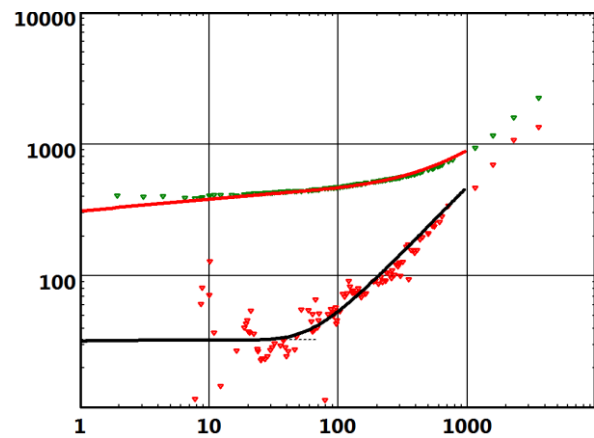


Fig. 1.D.6 – The loglog plot:
Normalized pressure rate

At this stage, PA's theory had caught up with PTA, but with no effect on day-to-day PA which remained, until very recently, constrained to 'old' tools implemented at the periphery of production databases. Producing pressures would be overlooked, hence missing the opportunity to account for superposition. When forward-thinking people wanted to use both pressure and rates, they would do this in a PTA software. However this was wrong, as assumptions made in PTA are not necessarily valid over the time scale of the well production.

The move to modern PA commercial software is recent. One key factor was the spread of permanent surface and downhole pressure gauges, making real analysis using both production and pressure data. Commercial PA packages such as KAPPA's Topaze, were then released.

The complementarity with PTA was also the key to the recent success of modern PA.

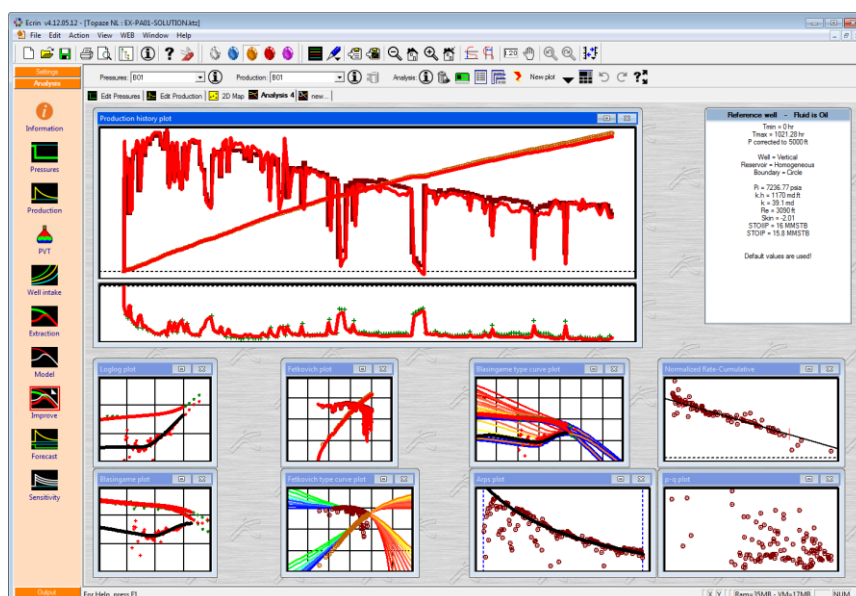


Fig. 1.D.7 – The 21st Century – PC based PA

1.E Permanent Downhole Gauges

With the increasingly frequent installation and use of permanent downhole gauges (PDG) and other measuring instruments we are receiving data at a high acquisition rate and over a long time interval. Put crudely, if we multiply high frequency by long duration we get a huge number of data points; typically 30 million, but sometimes up to 300 to 500 million.

Conversely, the number of data points needed for an analysis remains small:

- Low frequency data for production analysis and history matching. If rates are acquired daily, a pressure point per hour will do. This means less than 100,000 points for ten years.
- High frequency data or Pressure Transient Analysis. Assuming 100 build-ups with 1,000 points extracted on a logarithmic time scale for analysis, coincidentally this is another, albeit different, 100,000 points.

Even for huge data sets, 200,000 points are plenty to cope with the required processing, i.e. two orders of magnitude less than the median size of the actual raw data set. Unlike the size of the raw data, 200,000 points is well within the processing capability of today's PC.

However we need some smart filtering algorithms to obtain these points.

In addition we generally have high frequently, high quality pressure data. We cannot say the same for rates, which are generally of poor quality. In most cases individual well productions are not measure but allocated using simplistic methods. A successful automatic processing of the pressures also requires a successful automatic identification of events of interests and a correction of the allocated rates.

Though such processing cannot qualify as 'analysis', it is an essential element to define our ability to process permanent data. This will be presented in a dedicated chapter of this book.

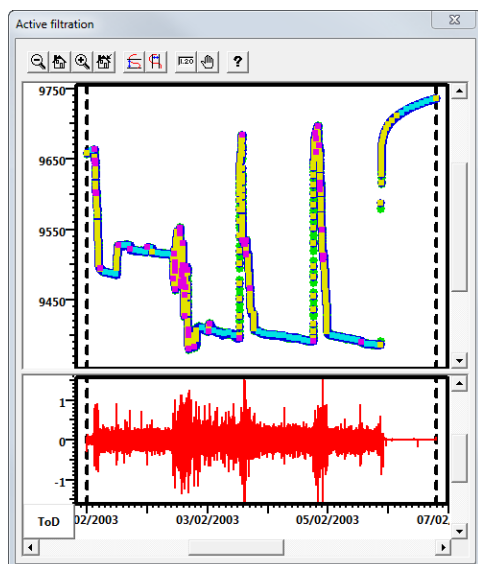


Fig. 1.E.1 – Filter window for 200,000 PDG data points

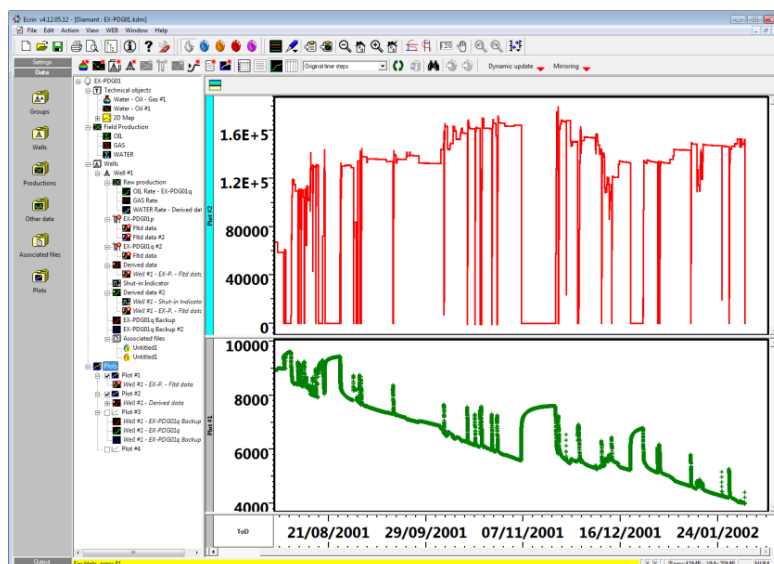


Fig. 1.E.2 – Pressures from PDG and rate data ready for PA and PTA analyses

1.F Other candidates for Dynamic Data Analysis (DDA)

1.F.1 Formation testers

These are tools run on electric line and that can push a probe into the formation or set two packers over a short interval of the reservoir. This allows production of formation fluid into a small closed chamber. The tool is primarily used to obtain formation pressures versus depth to determine the formation fluid gradients and pick fluid contacts. With accurate pressure gauges, permeability and skin estimates can be obtained. Fluid samples can also be obtained using this tool.

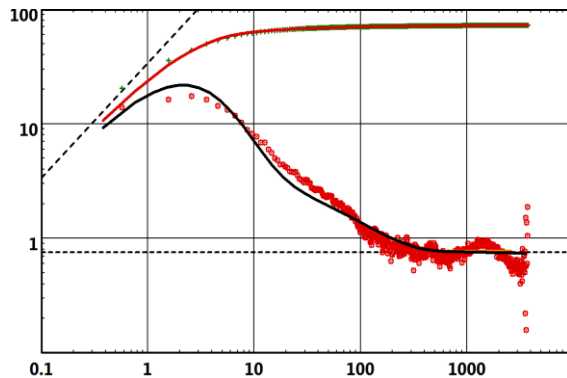


Fig. 1.F.1 – Formation tester loglog plot

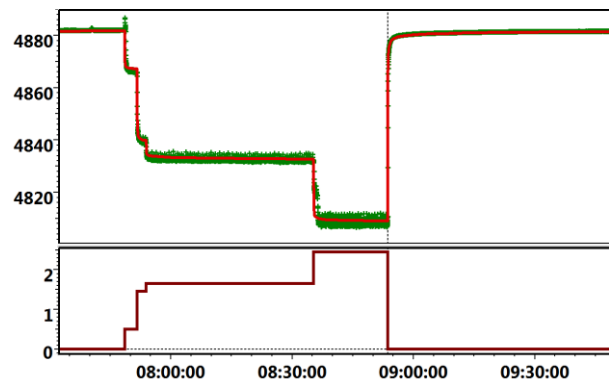


Fig. 1.F.2 – Formation tester history plot

1.F.2 Temperature diffusion

DTS Distributed Temperature Sensor

This technology allows us to measure temperature, and other parameters, at any time and depth along a fiber optic cable placed in the well.

Once installed in the well, the cable may be interrogated at any time using nanosecond bursts of laser light. As it travels down the optical fiber the light interacts with the structure of the fiber causing the emission of short pulses of light that bounce back along the cable to the source. This is then analyzed by the surface instrumentation to determine the temperature, or other parameters, at the point of origin of the 'bounce back'. The continuous monitoring of the returning light allows the construction of a continuous temperature profile along the producing zones. This can then be used to assess the layer contributions, water and/or gas breakthrough, monitor the effectiveness of gas lift systems and help in detecting problems with the optimum productivity potential of the well.

ATS Array Temperature Sensing

The main difference between ATS and DTS is that in an ATS installation the measuring of the returning light bursts are not continuous along the fiber; instead dedicated measuring nodes along the fiber are used. The advantage is that shorter parameter sampling rate can be used.

1.G Book content

Version 4.12 of this book is synchronized with the release of Ecrin v4.12, and with Emeraude v2.60. However the process is not complete, and we have deliberately by-passed some specific issues to focus on what we consider to be the fundamentals that are needed before performing analyses.

Chapter 1 – (this) Introduction

Chapter 2 – Theory

Includes the hypotheses, equations and solutions at the root of the models and methods implemented in PTA and PA.

Chapter 3 – PTA – General Methodology (PTA)

Includes the classical tools and modern methods that were developed in well test interpretation, then pressure transient analysis, for both gas and oil. We also cover some operational issues in well testing such as test design, data acquisition and quality control.

Chapter 4 – Production Analysis (PA)

As for PTA, this covers the classical tools and modern methods that were developed to perform production analysis and history match production data.

Chapter 5 to 8 – wellbore (5), well (6), reservoir (7) and boundary (8) models

These chapters are an itemized review of models used in both PTA and PA. We follow the logic implemented in the definition of the analytical models used in the Ecrin modules, PTA (Saphir) and PA (Topaze). We split models by category, progressing away from the wellhead, moving from wellbore, to well, reservoir and finally boundaries.

Chapter 9 – PVT

Describes the PVT models and flow correlations used by both PTA and PA.

Chapter 10 – Numerical models

Includes the additional capabilities offered by numerical models in handling complex geometries and nonlinear problems such as gas diffusion, multiphase flow and non-Darcy flow.

Chapter 11 – PTA Special test operations

Includes techniques that are not usually considered as standard well tests, such as formation testing, slug, multilayer and interference tests.

Chapter 12 – Well modeling and Performance Analysis

Includes the tools (VLP, IPR, etc) developed in well modeling and performance analysis.

Chapter 13 – Permanent Downhole Gauges

Includes the new information available from PDG data, the issues linked to the massive amount of data acquired and stored, and the solutions the industry has developed.

Chapter 14 – Production Logging

This introduction to production logging covers the governing principles, typical tools and operations and interpretation methods. It is a fairly high level yet complete overview.

What is NOT yet in this book:

We wanted to get this book released and therefore faced a dilemma; wait for everything to be ready or wait for later versions to include some additional content. We took the latter option and so the following subjects are not in this current version: Temperature diffusion, Unconventional reservoirs

1.H How many equations do you want?

As we know people love or hate equations. Of course people want to have 'practical' training; because the silly alternative is 'impractical' training. But it would be a mistake to completely turn our back on the equations, and 'dumb down' the learning.

Although we know that people with a solely academic background may miss the point if they do not understand the practical world, likewise it makes little sense for wholly practical people to have no understanding of the theoretical background.

Engineers with an excellent practical experience but no theory may be making mistakes of which they are blissfully and completely unaware.

So, as with anything else, this is just a matter of common sense.

Knowing the theory means knowing the assumptions, and knowing the assumptions means knowing the limitations of the theory.

There is one thing for sure: PTA and PA are not just about knowing how to operate the software. That's the easy bit. The software is just a tool. It is the Engineer who makes the interpretation.

So we have decided to provide two levels of reading in this book, and we leave you to choose:

- The main, white sections will only show the practical side of things, the qualitative explanations, and the behavior equations, i.e. those you would have to apply for, say, a specialized analysis using your own spreadsheet. It will also show basic equations, but not the details of derivation of these equations. You will be spared disappearing into dimensionless and Laplace space (Captain).
- If you would like, at least once in your life, to follow the process of the derivation of the diffusion equation, line source solution, finite radius well, closed systems, gas pseudopressures, the yellow sections are just for you.

1.I Other books for reference

If you want to learn how to perform DDA the KAPPA book you have in your hands right now is certainly the most practical you will find ☺. If you do not believe it, or if you wish to expand your reading, we invite you to plough through some, or for the real masochist, all of the following learned tomes:

For normal people:

1. 'Advances in Well Test Analysis': SPE Monograph Vol. 5 by Robert C. Earlougher, Jr. in 1977: This is a monument. Get one even if the content is a bit outdated (no Bourdet Derivative). It will remain for a long time a mine of references.
2. 'Transient Well Testing': SPE Monograph Vol. 23, published in 2009 though it was supposed to get out in 1990. Ten different authors (including OH), 850 pages that are sometimes pretty heterogeneous, but still a must-have.
3. 'Modern Well Test Analysis, a computer-aided approach' by Roland Horne, Petroway Inc. 1995: The first book which really integrated the current methodology based on the Bourdet derivative. Still today a very good complement.
4. 'Well Test Analysis: The use of advanced interpretation models', by Dominique Bourdet, Elsevier 2002: Three good reasons to get it: (1) with the Bourdet derivative, Dominique certainly made the single most important contribution to modern Pressure Transient Analysis and, indeed, to Production Analysis; (2) Dominique started KAPPA with Olivier Houzé in 1987, and he left in 1991; (3) his book is very close to our philosophy. It now lacks Production Analysis, deconvolution and numerical models, but it is still a must-have.

For those from the dark side who love equations and wish to understand everything:

1. 'Conduction of Heat in Solids', Carslaw & Jaeger: A mother lode from where the petroleum industry has been mining many ideas. Equations need adaptation, but they are all there.
2. 'Handbook of Mathematical Functions', Abramowitz & Stegun: All you need to navigate your starship through Laplace Space and Bessel Functions. A must-have if you write code.
3. Raj Raghavan: 'Well Test Analysis', Prentice Hall 1993: Raj just loves equations. Do not try to count. He must have been paid by the Integral and this is, actually, the strength of this book. An excellent set of theoretical references.

There are other very good books, apology for not referencing them all...



2 – Theory

OH – OSF – DV



2.A Diffusion equation

2.A.1 Darcy's law

Darcy's original experiment (Henry Darcy, France, 1856) is shown below. It was initially set to study the pressure loss due to the flow of water in sand filters.

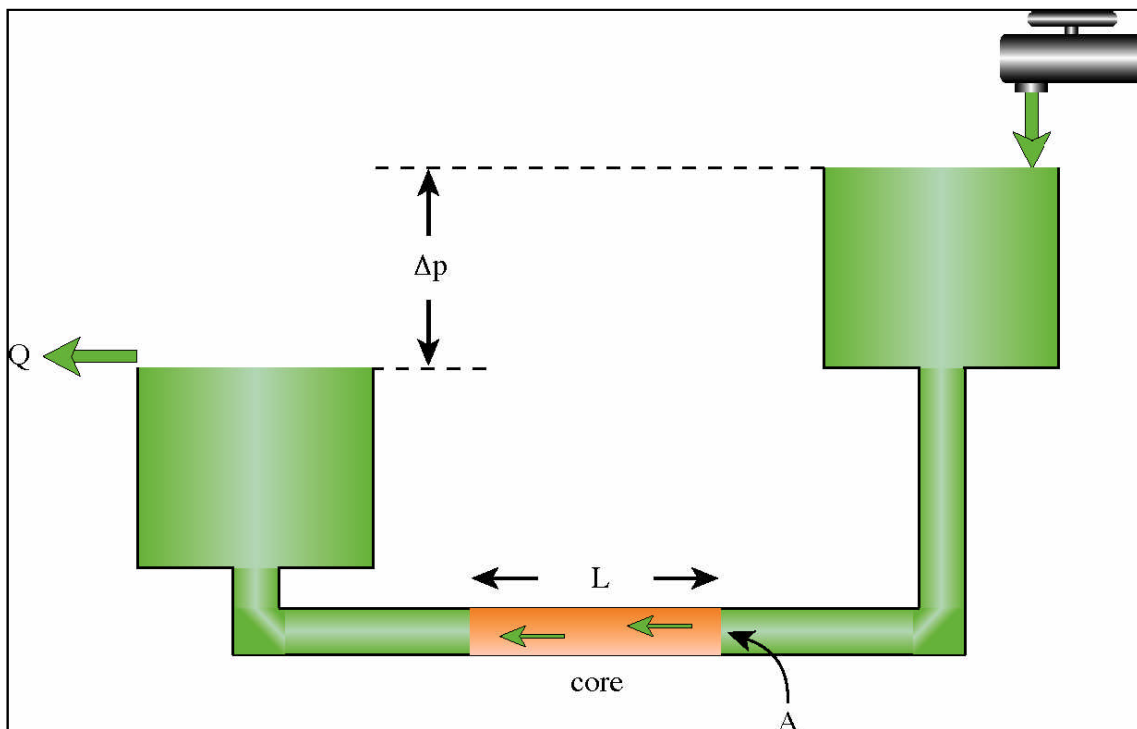


Fig. 2.A.1 – Darcy's experiment

In this experiment, Henry Darcy established a linear relation between the horizontal flow rate across a section of porous medium and the pressure gradient across the same section.

Using today's conventions, in Field Units, the relation discovered by the Darcy's experiment can be written:

$$\frac{\Delta p}{L} = -887.2 \frac{Q\mu}{kA}$$

Its differential form can be given in linear coordinates for linear flow and in cylindrical coordinates for radial flow. For radial coordinates the flow rate is assumed to be positive for a producing well, i.e. flow towards the well:

Darcy's law in linear coordinates, in the x direction:

$$\frac{\partial p}{\partial x} = -887.2 \frac{q_x \mu}{k_x A}$$

Darcy's law in radial coordinates:

$$r \frac{\partial p}{\partial r} = 141.2 \frac{q \mu}{kh}$$

Darcy's Law states that the pressure drop between two points, close enough to consider all parameters to be constant, will be:

- proportional to the flowrate density (q/A)
- proportional to the fluid viscosity (μ)
- inversely proportional to the reservoir permeability (k)

Darcy's Law is a fundamental law in dynamic data analysis. It is used to model the flow in several compartments in the reservoir:

- At any point of the reservoir, it is one of the three equations that will be used to define the diffusion equation (see next section).
- When the well is flowing, it determines the pressure gradients at the sandface.
- Close to reservoir boundaries it determines that the pressure gradient towards a no-flow boundary is flat, or it allows the determination of the inflow from the pressure gradient.

Darcy's law assumes a linear relation between the flow of fluid in one direction and the pressure gradient, corrected for gravity, in the same direction. This assumes that the density of flow is small enough to avoid turbulent behaviour.

When there is turbulence, a quadratic term is added and Darcy's law is replaced by the Forchheimer's equation. We then speak about non-Darcy flow. In most cases, non-Darcy problems will be solved with a numerical model.

2.A.2 The diffusivity equation

The diffusivity equation describes how, in an elementary piece of rock, the pressure will react in time as a function of the local pressure gradient around this piece of rock.

There may be as many diffusivity equations as there are assumptions on what is happening downhole. The basic theory in Dynamic Data Analysis uses the simplest possible diffusivity equation, assuming the following:

- The reservoir is homogeneous and isotropic.
- The fluid is single-phase and only slightly compressible.
- Gravity effects are ignored. If they were not the diffusivity equation would be written in terms of potential and not pressure.
- Darcy's law applies.
- Reservoir and fluid properties are independent of the pressure.

Under these conditions, the diffusivity equation is derived from the combination of:

- (1) The principle of conservation of mass
- (2) Darcy's law
- (3) Slightly compressible fluid equation

Some more complex versions of the diffusivity equation will have different components: Darcy's law may be replaced by the Forchheimer's equation, and more complex PVT models may be used: real gas diffusion, multiphase black oil correlations or an Equation of state.

Derivation of the diffusivity equation:

The diffusion equation is derived from the combination of three elementary equations:

The law of **conservation of mass**: this is a 'common sense' law that states that nothing is ever created or lost; things just move or transform themselves (Antoine Lavoisier, France, 1785). The formulation for an elementary piece of rock is that 'mass in' minus 'mass out' = 'accumulation'.

We consider the flow in the x direction of a fluid through a (small) area A, between x and x+δx and between time t and t+δt. Considering that 1 bbl/day = 0.23394 ft³/hr, we get the following equation

$$\text{Conservation of mass: } Mass_{in} - Mass_{out} = Accumulation = Mass_{after} - Mass_{before}$$

$$\text{Conservation of mass: } [0.23394 \rho q_x \delta t]_x - [0.23394 \rho q_x \delta t]_{x+\delta x} = [\rho \phi A \delta x]_{t+\delta t} - [\rho \phi A \delta x]_t$$

$$\text{Differential form: } -0.23394 \frac{\partial \rho q_x}{\partial x} = A \frac{\partial (\rho \phi)}{\partial t}$$

The second equation we will use relates the rate in a direction to the pressure gradient in this direction. The simplest among these equations is **Darcy's law** (Henry Darcy, France, 1856), which establishes a linear relation between the speed and the pressure gradient, the linear factor being a function of one reservoir property (the permeability) and one fluid property (the viscosity).

$$\text{Darcy's law in the x direction: } q_x = -\frac{k_x A}{887.2 \mu} \frac{\partial p}{\partial x}$$

$$\text{So we get: } -0.23394 \frac{\partial}{\partial x} \left[-\frac{k_x A \rho}{887.2 \mu} \frac{\partial p}{\partial x} \right] = A \frac{\partial (\rho \phi)}{\partial t}$$

$$\text{This simplifies to: } \frac{\partial (\rho \phi)}{\partial t} = 0.0002637 k_x \frac{\partial}{\partial x} \left[\frac{\rho}{\mu} \frac{\partial p}{\partial x} \right]$$

It is from the equation above that we will start when dealing with real gas. Now we are going to focus on slightly compressible fluids. The first term can be developed as:

$$\text{First term: } \frac{\partial (\rho \phi)}{\partial t} = \frac{\partial (\rho \phi)}{\partial p} \frac{\partial p}{\partial t} = \left[\rho \frac{\partial \phi}{\partial p} + \phi \frac{\partial \rho}{\partial p} \right] \frac{\partial p}{\partial t} = \rho \phi \left[\frac{1}{\phi} \frac{\partial \phi}{\partial p} + \frac{1}{\rho} \frac{\partial \rho}{\partial p} \right] \frac{\partial p}{\partial t}$$

$$\text{New differential form: } 0.0002637 \frac{k_x}{\rho \phi} \frac{\partial}{\partial x} \left[\frac{\rho}{\mu} \frac{\partial p}{\partial x} \right] = \left[\frac{1}{\phi} \frac{\partial \phi}{\partial p} + \frac{1}{\rho} \frac{\partial \rho}{\partial p} \right] \frac{\partial p}{\partial t}$$

The two terms between brackets in the second member of the equation are the formation compressibility and the fluid compressibility:

$$\text{Formation compressibility: } c_f = \frac{1}{\phi} \frac{\partial \phi}{\partial p}$$

$$\text{Fluid compressibility: } c_{fluid} = \frac{1}{\rho} \frac{\partial \rho}{\partial p}$$

New differential form:

$$\frac{\partial p}{\partial t} = 0.0002637 \frac{k_x}{\rho \phi [c_f + c_{fluid}]} \frac{\partial}{\partial x} \left[\frac{\rho}{\mu} \frac{\partial p}{\partial x} \right]$$

The last equation required is PVT related, in order to assess the relation between the fluid compressibility and the pressure. The simplest equation that can be used is the **slightly compressible fluid**, assuming that the fluid compressibility is constant, i.e. independent of the pressure. So we get a total constant compressibility:

Slightly compressible fluid: $c_t = c_f + c_{fluid} = \text{Constant}$

Also we can consider that:

$$\frac{\partial}{\partial x} \left[\frac{\rho}{\mu} \frac{\partial p}{\partial x} \right] \approx \frac{\rho}{\mu} \frac{\partial^2 p}{\partial x^2}$$

We finally get the diffusion equation in the x direction:

Diffusion equation; direction x: $\frac{\partial p}{\partial t} = 0.0002637 \frac{k_x}{\phi \mu c_t} \frac{\partial^2 p}{\partial x^2}$

The process above was dealing with the flux in only one direction. If we consider now the flux through an arbitrarily small cube in all three directions, we get:

Generic diffusion equation:
$$\frac{\partial p}{\partial t} = 0.0002637 \frac{\left[k_x \frac{\partial^2 p}{\partial x^2} + k_y \frac{\partial^2 p}{\partial y^2} + k_z \frac{\partial^2 p}{\partial z^2} \right]}{\phi \mu c_t}$$

If we consider an isotropic reservoir, all permeability components are equal to a unique permeability, k:

Isotropic diffusion equation:

$$\frac{\partial p}{\partial t} = 0.0002637 \frac{k}{\phi \mu c_t} \left[\frac{\partial^2 p}{\partial x^2} + \frac{\partial^2 p}{\partial y^2} + \frac{\partial^2 p}{\partial z^2} \right] = 0.0002637 \frac{k}{\phi \mu c_t} \nabla^2 p$$

The operator on the right end side is called the Laplace operator, or Laplacian. It is also written Δp , but we will avoid this form in order not to cause confusion with the pressure change in time, also noted Δp .

2.A.3 Diffusion in a homogeneous isotropic reservoir

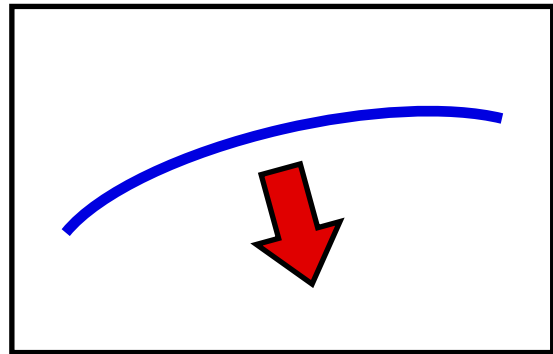
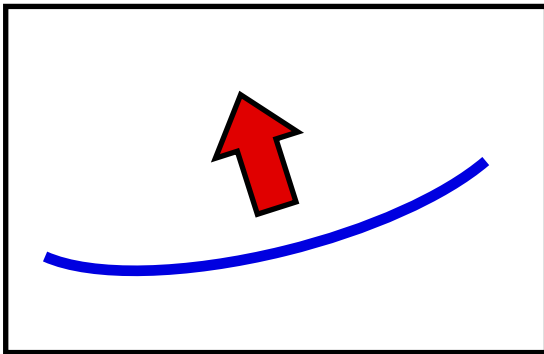
When combining the law of conservation of mass, the simplest pressure gradient equation (Darcy's law) and the simplest material balance relation (slightly compressible fluid assumption), we get the simplest version of the diffusion equation, given below in three different forms:

General form:
$$\frac{\partial p}{\partial t} = 0.0002637 \frac{k}{\Phi \mu c_t} \nabla^2 p$$

Radial flow:
$$\frac{\partial p}{\partial t} = 0.0002637 \frac{k}{\Phi \mu c_t} \frac{1}{r} \left[\frac{\partial}{\partial r} \left(r \frac{\partial p}{\partial r} \right) \right]$$

Linear flow:
$$\frac{\partial p}{\partial t} = 0.0002637 \frac{k}{\Phi \mu c_t} \frac{\partial^2 p}{\partial x^2}$$

Physical meaning: If we look at the last relation and consider the flow in only one direction:



- If the curvature of the pressure profile is positive, the pressure will locally increase. If the curvature is negative the pressure will decrease. The speed of the pressure change, in whatever direction, will be proportional to this curvature.
- If the permeability is large, the pressure change will be fast. Basically, the more permeable the formation, the quicker the formation fluid will react to a local pressure disturbance.
- If the viscosity is large, the pressure change will be slow. Basically, the more viscous the fluid, the slower the formation fluid will react to a local pressure disturbance.
- The ratio k/μ , to which the speed of reaction is proportional, is also called the mobility.
- If the porosity is large, the pressure change will be small, and therefore, at a given time, relatively slow. Basically, the more porous the formation, the lower the pressure change that will be required to produce / receive the same mass of fluid.
- If the total compressibility is large, the pressure change will be small, and therefore, at a given time, slow. Basically, the more compressible the formation is, the lower the pressure change required to produce / receive the same mass of fluid.
- The term $1/\phi c_t$, to which the amplitude of the reaction is proportional, is also called the storativity.
- Mobility and productivity seems to play the same role in the diffusion equation. However the mobility will also be found in the inner boundary conditions and this is where the role of the different parameters will diverge.

Generally, the diffusion equation used in most analytical models is the radial formulation. The reference point of such a radial solution is the producing or injecting well. This system of coordinates is well suited to model radial flow to and from the well. In the following we will stay in radial coordinates.

The diffusion equation shown above describes the flow of what we call a homogeneous reservoir where this same, unique equation will be applied everywhere in the reservoir. More complex reservoirs can be modelled, and this diffusion equation will be replaced by formulations involving different pressures at the same point (double-porosity, double-permeability reservoirs) or changing diffusivity and mobility in different locations (composite reservoirs). The different reservoir models are detailed in the chapter on the subject.

2.B Initial, well and outer boundary conditions

The diffusion equation describes how the fluid pressure in a local piece of rock will locally react to a pressure disturbance. This equation defines how the system will react far from the boundaries and the wells.

In order to define a problem completely we need to know a starting point, i.e. the initial state of the system, and how the fluid flow will be constrained at the well and at the natural limits of the reservoir.

2.B.1 Initial conditions

The most common condition, and the only easy state to model analytically, is to assume that at a reference time 0, corresponding to the time when the sequence of production starts, the reservoir was at initial uniform pressure p_i . This simple equation can be written:

In Cartesian coordinates: $\forall x, y, z \quad p(t=0, x, y, z) = p_i$

Assuming a radial symmetry: $\forall r \quad p(t=0, r) = p_i$

In the case of a multilayer analysis, if the reservoir layers are commingled there could be one such equation for each independent layer. If the pressure difference between the different layers is not the static gradient in the wellbore, it means that cross-flow will occur between the different layers as soon as the well is perforated, even if it is not flowing.

It is also possible to start a problem with a dynamic pressure situation. This will be, typically, the 'restart' of a simulator run from which one wants to run a test on a new, additional well. This kind of situation is however only possible when using a numerical model.

2.B.2 Well conditions

All equations above (diffusion, initial and outer boundary conditions) lead to a nicely uniform reservoir at initial pressure, forever. What changes this million-year-old equilibrium is the disturbance created by man-made producing or injecting wells. We generally take 0 as the time of the initial disturbance.

The simplest realistic model is a vertical well, of radius r_w , fully penetrating the formation. The inner condition is nothing more than Darcy's law calculated at the sandface. In the case of a

homogeneous reservoir this will write: Finite radius well: $\left[r \frac{\partial p}{\partial r} \right]_{r_w, t} = 141.2 \frac{q B \mu}{k h}$

As the flow rate q is generally given at standard conditions, the volumetric downhole rate q_{sf} is calculated by multiplying the standard rate by the reservoir volume factor B . In the simplest cases this volume factor is considered constant. Otherwise a PVT equation must be used to dynamically calculate the volume factor.

An unrealistic but very convenient model of well condition is the line source, corresponding to the same Darcy's law but for the limit case of a well of radius zero.

Line source well:
$$\lim_{r \rightarrow 0, t} \left[r \frac{\partial p}{\partial r} \right] = 141.2 \frac{qB\mu}{kh}$$

The line source problem is interesting because it is easier to solve, faster to run and the calculation of this solution at $r=r_w$ is a good approximation of the finite radius solution and for any practical purpose it is exactly the same solution within the formation, when $r > r_w$. It is the solution of choice to simulate interference tests and image wells for boundary effects (see the chapter on boundary models).

Other inner boundary conditions correspond to Darcy's law applied to more complex well geometries (fractures, limited entry, horizontal, slanted, multilateral, etc), and are detailed in the chapter on well models.

In most cases, the production of the well will be affected by wellbore effects, generally modelled using what we call the wellbore storage. This notion is developed in the Wellbore chapter.

In these cases there is a time delay in the production / shut-in, and the well condition also includes a wellbore component. The simplest model is a constant wellbore storage applied to a well opened and shut in at surface. The modified equation, for a finite radius well, with wellbore storage:

$$\left[r \frac{\partial p}{\partial r} \right]_{r_w, t} = \frac{141.2 \left[qB + 24C \frac{\partial p}{\partial t} \right] \mu}{kh}$$

2.B.3 Outer boundary conditions

Another set of equations is needed to define how the fluid reacts close to a natural boundary. This could be the outer boundary of the system, or even intermediate faults.

The simplest condition to model analytically is that there is no boundary at all, i.e. that the reservoir is of infinite extent in all directions. The equation for such system is:

Assuming radial symmetry:
$$\lim_{r \rightarrow \infty} [p(r, t)] = p_i$$

Naturally and unfortunately, no reservoir is infinite. However, in pressure transient analysis this model is easier to generate and will match the data over the duration of the well test, as long as the test is short enough for no lateral boundary to be seen.

Infinite reservoir models are unlikely to be used in production analysis, where such a hypothesis is unlikely to be met over the extended time range of such analysis.

2.C Line Source Solution in a homogeneous infinite reservoir

We now consider the simplest problem we can find: the diffusion in a homogeneous infinite reservoir, starting at initial uniform pressure p_i , produced by a vertical line source well. The derivations in the following section can be skipped.

2.C.1 Derivation

The complete real problem is described with the four following equations:

Homogeneous radial diffusion:
$$\frac{\partial p}{\partial t} = 0.0002637 \frac{k}{\Phi \mu c_i} \frac{1}{r} \left[\frac{\partial}{\partial r} \left(r \frac{\partial p}{\partial r} \right) \right]$$

Uniform initial pressure:
$$p(t = 0, r) = p_i$$

Infinite reservoir:
$$\lim [p(r, t)]_{r \rightarrow \infty} = p_i$$

Line source well:
$$\lim \left[r \frac{\partial p}{\partial r} \right]_{r \rightarrow 0, t} = 141.2 \frac{qB\mu}{kh}$$

The problem is simplified by introducing dimensionless variables that will integrate all other parameters and end up with a unique set of equations that we will solve analytically once and for all. These dimensionless parameters are not only useful to solve the problem. They have a historic importance, as they were at the origin of the method of type-curve matching (see the 'old stuff' in the PTA Chapter). Though it does not look like it, there are not so many ways to simplify the complete set of equations. The dimensionless parameters are defined as:

Dimensionless radius:
$$r_D = \frac{r}{r_w}$$

Dimensionless time:
$$t_D = 0.0002637 \frac{kt}{\Phi \mu c_i r_w^2}$$

Dimensionless pressure:
$$p_D = \frac{kh}{141.2qB\mu} (p_i - p)$$

Please note that it is not strictly necessary to introduce the dimensionless radius to solve the problem. However we will approximate the solution at the well by taking the line source solution at $r=r_w$. In addition, these dimensionless terms with this definition of r_D will be used to exactly solve the finite radius problem, later in this chapter. Injecting the dimensionless terms in the physical problem brings us to the dimensionless problem:

Homogeneous radial diffusion:
$$\frac{\partial p_D}{\partial t_D} = \frac{1}{r_D} \left[\frac{\partial}{\partial r_D} \left(r_D \frac{\partial p_D}{\partial r_D} \right) \right]$$

Uniform initial pressure:
$$p_D(t_D = 0, r_D) = 0$$

Infinite reservoir:
$$\lim [p_D(r_D, t_D)] = 0$$

Line source well:

$$\lim_{r_D \rightarrow 0, t_D} \left[r_D \frac{\partial p_D}{\partial r_D} \right] = -1$$

We will now focus on the dimensionless diffusion equation. As for any diffusion problem, the equation can be further simplified by moving the problem into Fourier space (Joseph Fourier, France, 1822) or Laplace space (Pierre-Simon de Laplace, France, 1820). We will use here the Laplace transform, under which the diffusion equation, combined with the initial condition becomes:

Laplace Transform:
$$\bar{p}_D(u, r_D) = \int_{t_D=0}^{\infty} p_D(t_D, r_D) \exp(-ut_D) dt_D$$

Diffusion Equation in Laplace space:
$$u \bar{p}_D = \frac{1}{r_D} \left[\frac{\partial}{\partial r_D} \left(r_D \frac{\partial \bar{p}_D}{\partial r_D} \right) \right]$$

This equation is known to be a modified Bessel equation (Wilhem Bessel, Germany, 1824), the generic form of the solution uses modified Bessel functions:

Generic Modified Bessel solution:
$$\bar{p}_D(u, r_D) = A(u)K_0(r_D \sqrt{u}) + B(u)I_0(r_D \sqrt{u})$$

K_0 and I_0 are the modified Bessel functions of order zero. The unknown functions A and B are taken from the inner and outer boundary conditions. This gives:

From the outer boundary condition:
$$B(u) = 0$$

From the inner boundary condition:
$$A(u) = \frac{1}{u}$$

Line source solution in Laplace space:
$$\bar{p}_D(u, r_D) = \frac{1}{u} K_0(r_D \sqrt{u})$$

The real dimensionless solution is the inverse Laplace transform of this function. Generally, the inverse Laplace transform is numerically obtained using the Stehfest algorithm (Harald Stehfest, Germany, 1970). In this particular case, and this is the interest of the Line Source Solution, we know the inverse transform. It is called the Exponential Integral function and it can be written:

Exponential Integral solution:
$$p_D(r_D, t_D) = -E_i \left(-\frac{r_D^2}{4t_D} \right)$$

Before we return to the physical world, let us notice an interesting property of the Exponential Integral: for small negative arguments, it has a logarithmic approximation that will be the basis of 'Infinite Acting Radial Flow'. It can be written:

for $t_D \geq 100r_D^2$
$$p_D(r_D, t_D) \approx \frac{1}{2} \left[\ln \frac{t_D}{r_D^2} + 0.80907 \right]$$

We now just have to replace dimensionless parameters by their real values to get the physical solution.

2.C.2 The Line Source Solution

The solution, at any point and time, for a Line Source well producing a homogeneous infinite reservoir, is given by the following:

Line Source Solution:

$$p(r,t) = p_i - \frac{70.6qB\mu}{kh} \left[-E_i \left(-\frac{948.1\Phi\mu c_i r^2}{kt} \right) \right]$$

A typical line source response is displayed in the figures below, on a loglog scale (with the Bourdet derivative) and a semilog scale. For first readers, the notions of loglog and semilog plots are described in the PTA methodology chapter.

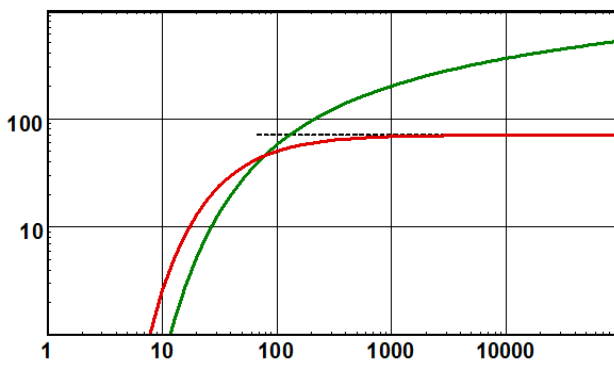


Fig. 2.C.1 – Line source loglog plot

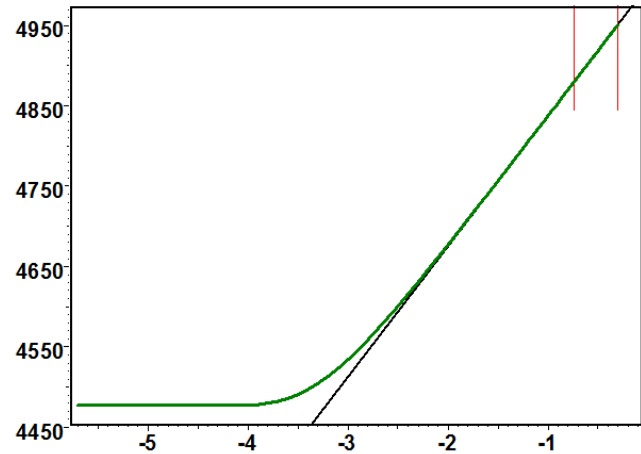


Fig. 2.C.2 – Line source semilog plot

The line source equation shows that the pressure change is a unique function of the parameter group r^2/t , or more conveniently r/\sqrt{t} . This has an important implication on the physical understanding of the diffusion process. If one considers, for example, the time it requires for the pressure change to reach a certain value (for example 1 psi), it will amount to a certain value of r/\sqrt{t} that we will calculate from the Line Source Solution, and therefore the relation:

Radius of investigation:

$$r_{inv} = a\sqrt{t}$$

In the chapter on boundary models we recommend at one does not use the notion of radius of investigation, as it may be misleading when one considers how such result is used afterwards. However, it is an interesting means of understanding the diffusion process. To extend this notion to cases where the flow geometry may not be strictly radial, we may consider that the area of investigation is proportional to r^2 , and we therefore have:

Area of investigation:

$$A_{inv} = bt$$

If the flow is not strictly horizontal and/or the thickness h is not constant, we will use:

Volume of investigation:

$$V_{inv} = ct$$

Although the following is valid at any point in the reservoir, we will now focus on the well response, that will be taken at $r=r_w$. As demonstrated in the previous section, there is a value of time above which the Line Source Solution reaches a 'regime' where one can use an approximation of the highest interest to the well test interpretation engineer. It is the semilog approximation and this regime is called **Infinite Acting Radial Flow**, or **IARF**.

$$\text{IARF: For } t \geq \frac{379200\Phi\mu c_t r_w^2}{k} \quad p(t) \approx p_i - \frac{162.6q\mu}{kh} \left[\log(t) + \log\left(\frac{k}{\Phi\mu c_t r_w^2}\right) - 3.228 \right]$$

Convention: $\ln(x)$ is the natural logarithm; $\log(x)$ is the decimal logarithm

IARF is characterized by linearity between the pressure change and the logarithm of time. This is why we also call this the semilog approximation. The slope of the response allows the calculation of the permeability-thickness, kh .

But before we develop further the IARF, we are going to introduce two other effects commonly accounted for in Pressure Transient Analysis: Wellbore storage and Skin effect.

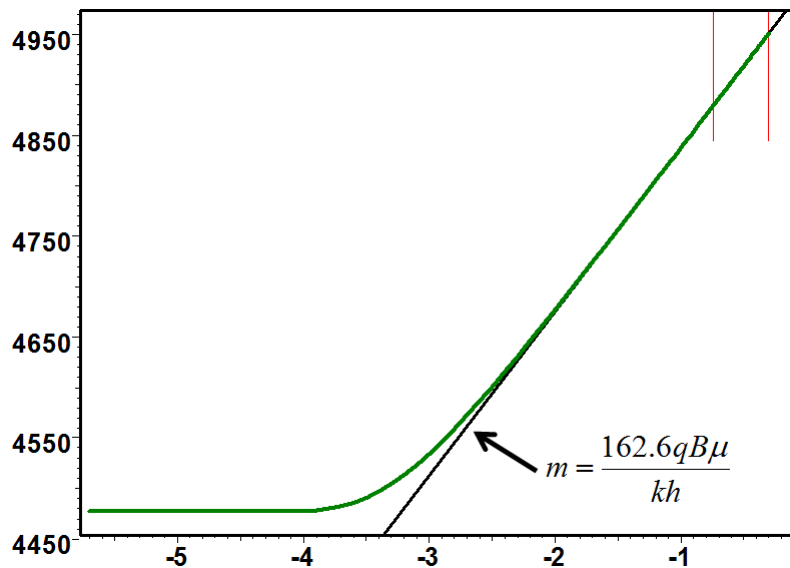


Fig. 2.C.3 – Semilog plot

2.D Wellbore storage and skin

2.D.1 Wellbore storage

In most cases the valve used to open the well and shut it in is not exactly at sandface level. In most cases it will be at surface. Even in the case of downhole shut in there is always a volume that will act as a cushion between the sandface and the valve. As a result, wellbore dynamics create a time lag between the sandface and the surface, or the valve, or the choke. This is what we generally call wellbore storage.

Let us take the case of a well opened and shut in at surface. When you open the well the initial surface production will be coming from the decompression of the fluid trapped in the wellbore. In the initial seconds or minutes of the flow the sandface will not even 'know' that the well is opened and the sandface rate will remain virtually zero. Naturally, at some stage we get to a mass equilibrium, i.e. the sandface mass rate reaches the surface mass rate. This is the time of the end of the wellbore storage. Conversely, if the well is shut in at surface, the surface rate will go immediately to zero while the sandface does not know about it. The time of wellbore storage is this transition time between the effective shut-in time and the time at which the reservoir stops flowing into the well.

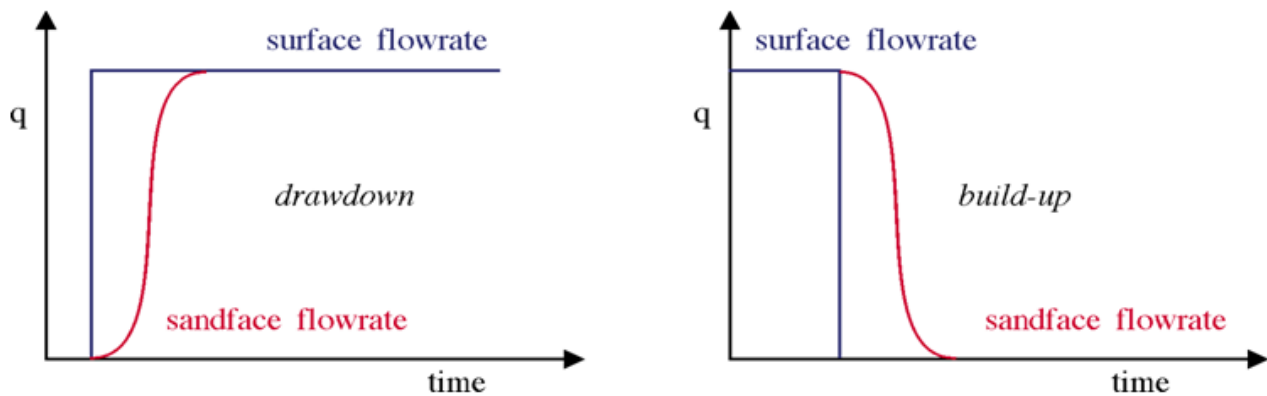


Fig. 2.D.1 – Wellbore storage

There are two main types of wellbore storage. The first one is modelled by the compression or decompression of the wellbore fluid in the wellbore volume. This is expressed as:

Wellbore storage by fluid compression: $C = V_w c_w$

Where V_w is the wellbore volume and c_w the fluid compressibility.

The second type of wellbore storage is linked to the rise of the liquid level present in the wellbore. A simplified version is expressed as:

Wellbore storage from liquid level: $C = 144 \frac{A}{\rho}$

Where A is the flow area at the liquid interface, ρ is the fluid density.

The relation between the surface and the sandface rate is then given by:

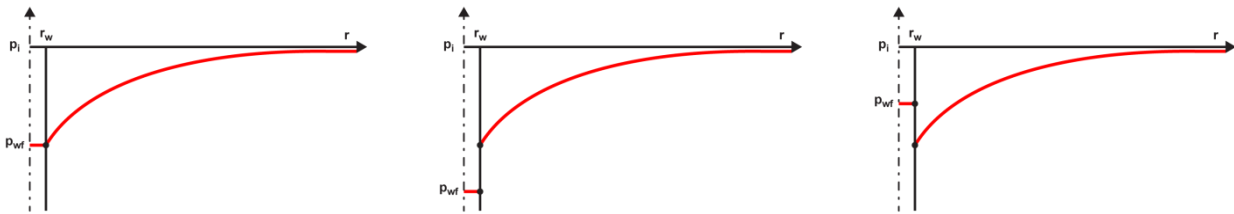
Wellbore storage equation:
$$q_{sf} = qB + 24C \frac{\partial p}{\partial t}$$

The simplest wellbore storage model implies that C is constant. However this is not always the case, and the various models of storage are described in the Wellbore chapter.

2.D.2 Skin

The skin effect quantifies the difference between the productivity of a well in an ideal case and its effective productivity in reality:

- If, after drilling, completion, cementing and perforating, the pressure drop for a given production into the wellbore is identical to the one you would forecast in the ideal case for the same geometry, the skin is zero.
- Very often, the reservoir near the wellbore had been invaded and the effective permeability around the well is lowered, thus a higher pressure drop results for a given production. The skin is then positive.
- Conversely, a stimulated well will have better productivity, hence a lower pressure drop for a given production. The skin is then considered negative.
- Skin may not be constant in time. During the initial 'clean-up' period in a well test, skin has a tendency to reduce. Conversely, over long period of times, completed wells may get damaged reducing productivity, hence an increasing skin.



Non damaged skin = 0

Damaged Skin > 0

Stimulated Skin < 0

Fig. 2.D.2 – Skin sign convention

We will consider that a well has a constant skin when the additional pressure drop, or Δp_{skin} , is proportional to the sandface rate. The skin S is a dimensionless factor representative of a pressure change, and integrates the same coefficients as the one in Darcy's law:

Constant skin S:
$$\Delta p_{skin} = p(r_w, t) - p_{wf}(t) = 141.2 \frac{q_{sf} \mu}{kh} S$$

Where p is the pressure in the formation, at a given time, at distance r_w , i.e. just beyond the sandface, while p_{wf} , at a given time, is the well flowing pressure.

A way to model a positive skin effect is to consider an equivalent composite system, with an invaded zone, or skin damage zone of radius r_{ws} larger than r_w and permeability k_s lower than k .

Darcy's law gives the relation between the equivalent skin factor, s and k_s :

Skin from a radial composite equivalent:
$$S = \left(\frac{k}{k_s} - 1 \right) \ln \left(\frac{r_{ws}}{r_w} \right)$$

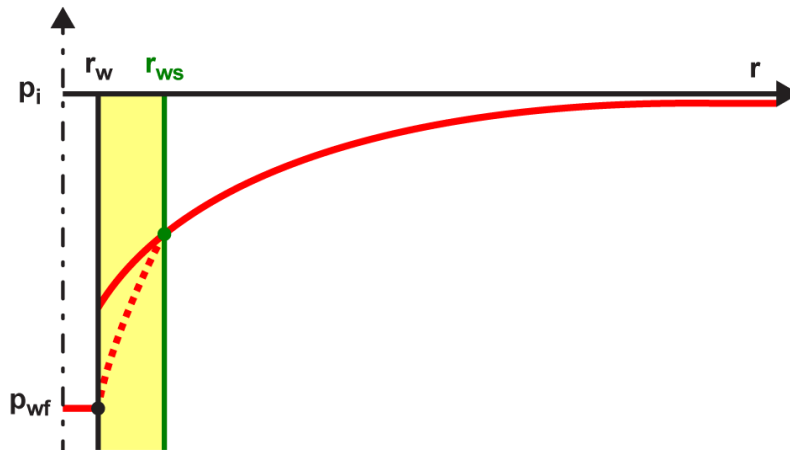


Fig. 2.D.3 – Equivalent composite system

Another way to model skin is the notion of equivalent radius, applicable to both positive and negative skins. The idea is to consider that the well with skin has the same productivity as a larger or smaller well with no skin. If the skin is positive, the equivalent wellbore radius will be smaller than r_w . If the skin is negative, the equivalent wellbore radius will be larger than r_w . The equation, again, straight from Darcy's law, can also be found at the limits when the permeability k_s above tends to infinity (open hole), and will be given by:

Equivalent wellbore radius:
$$S = -\ln \left(\frac{r_{we}}{r_w} \right) \quad \text{or} \quad r_{we} = r_w e^{-S}$$

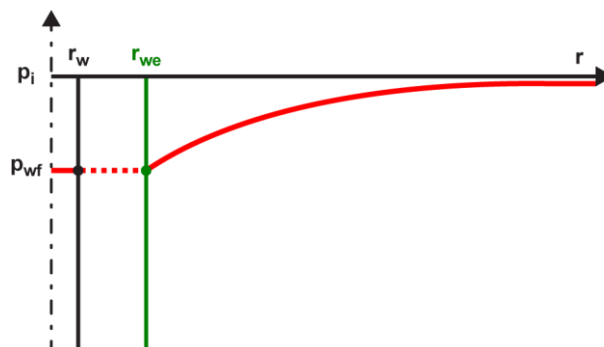


Fig. 2.D.4 – Skin: equivalent wellbore radius

We now consider the case of a homogeneous, infinite reservoir produced by a vertical well with constant wellbore storage and constant skin.

2.D.3 Derivation

We now have a slightly more complex problem to solve:

Homogeneous radial diffusion:
$$\frac{\partial p}{\partial t} = 0.0002637 \frac{k}{\Phi \mu c_t} \frac{1}{r} \left[\frac{\partial}{\partial r} \left(r \frac{\partial p}{\partial r} \right) \right]$$

Finite radius well:
$$\left[r \frac{\partial p}{\partial r} \right]_{r_w, t} = 141.2 \frac{q_{sf} \mu}{kh}$$

Initial pressure & infinite reservoir:
$$p(t=0, r) = p_i \quad \lim_{r \rightarrow \infty} [p(r, t)] = p_i$$

Wellbore storage & skin:
$$q_{sf} = qB + 24C \frac{\partial p_{wf}}{\partial t} \quad p - p_{wf} = 141.2 \frac{q_{sf} \mu}{kh} S$$

We will now repeat the definition of the dimensionless terms and add dimensionless sandface rate and dimensionless wellbore storage. The Skin, being dimensionless, does not need any conversion:

Dimensionless radius, time & pressure:

$$r_D = \frac{r}{r_w} \quad t_D = 0.0002637 \frac{kt}{\Phi \mu c_t r_w^2} \quad p_D = \frac{kh}{141.2 qB \mu} (p_i - p)$$

Dimensionless sandface rate & storage:
$$q_D = \frac{q_{sf}}{qB} \quad C_D = \frac{0.8936C}{h \phi c_t r_w^2}$$

We now get the equivalent dimensionless problem:

Homogeneous radial diffusion:
$$\frac{\partial p_D}{\partial t_D} = \frac{1}{r_D} \left[\frac{\partial}{\partial r_D} \left(r_D \frac{\partial p_D}{\partial r_D} \right) \right]$$

Initial pressure & infinite reservoir:
$$p_D(t_D=0, r_D) = 0 \quad \lim_{r_D \rightarrow \infty} [p_D(r_D, t_D)] = 0$$

Finite radius well:
$$\left[r_D \frac{\partial p_D}{\partial r_D} \right]_{r_D=1, t_D} = -1$$

Wellbore storage & skin:
$$\left[r_D \frac{\partial p_D}{\partial r_D} \right]_{r_D=1, t_D} = -q_D \quad p_{wfD} = p_D + q_D S \quad q_D = 1 - C_D \frac{dp_{wfD}}{dt_D}$$

The solution process will be the same as the line source problem and will not be detailed here.

For the finite radius problem (without storage, without skin), the general form is like the line source:

Generic Modified Bessel solution:
$$\bar{p}_D(u, r_D) = A(u)K_0(r_D \sqrt{u}) + B(u)I_0(r_D \sqrt{u})$$

As the line source, the infinite reservoir conditions arrives at $B(u)=0$. The only difference is that we now calculate the well equation at $r_D=1$ and not $r_D=0$. This gets us to a different value for $A(u)$:

From the inner boundary condition:
$$A(u) = \frac{1}{u\sqrt{u}K_1(\sqrt{u})}$$

If we define the function:
$$K_0^1(x) = \frac{K_0(x)}{xK_1(x)}$$

The finite radius solution at the well is
$$\bar{p}_D(u) = \frac{1}{u} K_0^1(\sqrt{u})$$

In the wellbore storage and skin solution we eliminate q_D and p_{wFD} in the top equations, we take the Laplace transform, etc, etc. In fact, we can make the generic demonstration that, if we know the Finite Radius solution of a given problem in Laplace space, wellbore storage and skin can be added by the following transform:

We obtain a modified Bessel equation and solve for inner and outer boundaries; a term K_1 appears corresponding to the finite radius well condition, and we finally get the following results:

Adding wellbore storage & skin:
$$\bar{p}_{wFD}(u) = \frac{1}{u} \left[\frac{S + u\bar{p}_{FRD}(1, u)}{1 + uC_D[S + u\bar{p}_{FRD}(1, u)]} \right]$$

In the homogeneous infinite case:
$$\bar{p}_{wFD}(u) = \frac{1}{u} \left[\frac{S + K_0^1(\sqrt{u})}{1 + uC_D[S + K_0^1(\sqrt{u})]} \right]$$

The problem is then solved in real space by taking the inverse Laplace transform using Stehfest numerical algorithm. Though the solution is more complex, the difference between this solution and the Exponential Integral solution will stabilize when wellbore storage effects vanish, the residual difference remaining is the skin factor. This links to the IARF by:

After wellbore storage:
$$p_{wFD}(t_D) \approx -E_i\left(-\frac{1}{4t_D}\right) + S$$

Dimensionless IARF: for $t_D \geq 100$
$$p_{wFD}(t_D) = \frac{1}{2} [\ln t_D + 0.80907 + 2S]$$

2.D.4 Behavior

The two figures below show the drawdown response of a vertical well with wellbore storage and skin in a homogeneous infinite reservoir. The plot on the left shows the response on semilog scale, with the pressure as a function of $\log(t)$. The plot on the right shows the loglog plot of $\log(\Delta p)$ and derivative vs $\log(\Delta t)$.

The derivative is developed in the chapter on 'PTA – General methodology'. The derivative shown on the right is the absolute value of the slope of the semilog plot on the left. When the model on the left becomes a straight line, the derivative stabilizes horizontally. The level of this stabilization is the slope of the model on the left. As all responses end up parallel on the left plot, then all derivatives merge to the same level on the right plot.

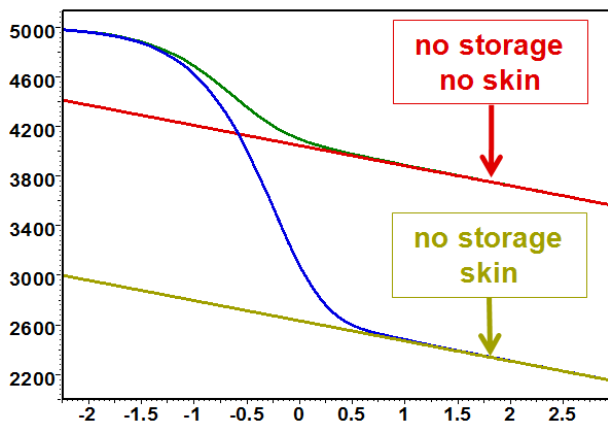


Fig. 2.D.5 – Finite radius solution, semilog scale

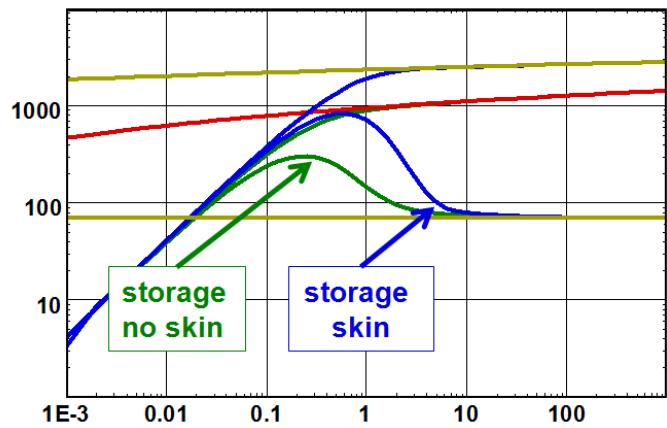


Fig. 2.D.6 – Finite radius solution, loglog scale

At early time, the flow is governed by wellbore storage and there is a linear relation between pressure change and elapsed time:

Early time pure wellbore storage:
$$p(\Delta t) = p_i - \frac{qB}{24C} \Delta t$$

At late time, Infinite Acting Radial Flow (IARF) is reached, and there is a linear relation between the pressure change and the logarithm of the elapsed time:

IARF Equation:
$$p(\Delta t) = p_i - \frac{162.6qB\mu}{kh} \left[\log(\Delta t) + \log\left(\frac{k}{\Phi\mu c_t r_w^2}\right) - 3.228 + 0.8686S \right]$$

2.E Outer boundary conditions

The previous sections only considered reservoir of infinite extent. An outer boundary will be made up of one or several sections of various type and shape combinations. In this section we will introduce the most usual types of boundaries, solve the case of a simple closed system and introduce the notion of pseudo-steady state (PSS).

2.E.1 Major types of boundaries

The most common type of boundary or boundary section is sealing, or no flow. It is given by applying Darcy's law orthogonally to the boundary surface, with a rate equal to zero:

No-flow boundary section:
$$\left[\frac{\partial p}{\partial \vec{n}} \right]_{\Sigma} = 0$$

The second most common type of boundary or boundary section is an approximation of pressure support (gas drive or water drive) considering that the pressure remains constant:

Constant pressure boundary section:
$$[p]_{\Sigma} = p_i$$

There are many other types of boundaries: leaky boundaries, conductive boundaries, water drives and gas caps. They will be described in detail in the chapter on boundary models.

In this section we focus on closed systems constituted by only no-flow sections, as we want to introduce the notion of pseudo-steady state (PSS), the main regime of interest in Production Analysis (PA).

The simplest case of a closed system (because it is the simplest to model analytically) is a reservoir of circular shape centered at the well and of radius r_e . Such model may be used to simulate the behavior of a really closed system or the production of a well in its drainage area:

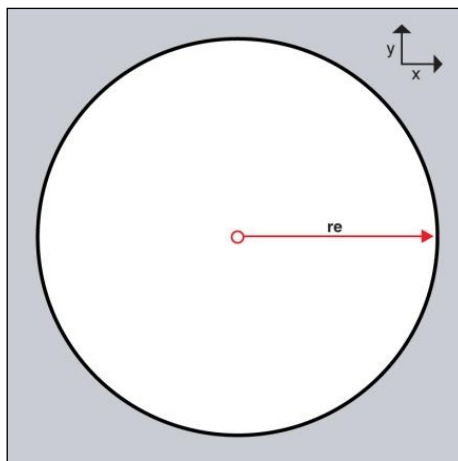


Fig. 2.E.1 – Closed circular boundary

2.E.2 Derivation for a circular reservoir

We consider a finite radius well to which we will add later wellbore storage and skin. Because it is an easy extension we are going to solve both cases of no-flow and constant pressure.

The problem is defined by the following set of equations:

Homogeneous radial diffusion:
$$\frac{\partial p}{\partial t} = 0.0002637 \frac{k}{\Phi \mu c_t} \frac{1}{r} \left[\frac{\partial}{\partial r} \left(r \frac{\partial p}{\partial r} \right) \right]$$

Finite radius well:
$$\left[r \frac{\partial p}{\partial r} \right]_{r_w, t} = 141.2 \frac{q_{sf} \mu}{kh}$$

Uniform initial pressure:
$$p(t=0, r) = p_i$$

Boundary equation, closed circle:
$$\left[\frac{\partial p}{\partial r} \right]_{r_e, t} = 0$$

Boundary equation, ct pressure circle:
$$p(t, r_e) = p_i$$

Dimensionless parameters are exactly the same as for the infinite finite radius solution and will not be repeated here. We end up with the following dimensionless problem:

Homogeneous radial diffusion:
$$\frac{\partial p_D}{\partial t_D} = \frac{1}{r_D} \left[\frac{\partial}{\partial r_D} \left(r_D \frac{\partial p_D}{\partial r_D} \right) \right]$$

Initial pressure & finite radius well:
$$p_D(t_D=0, r_D) = 0 \quad \left[r_D \frac{\partial p_D}{\partial r_D} \right]_{r_D=1, t_D} = -1$$

Closed circle OR Ct pressure circle:
$$\left[\frac{\partial p_D}{\partial r_D} \right]_{r_{eD}, t} = 0 \quad \text{OR} \quad p_D(t_D, r_{eD}) = 0$$

As for the line source problem we move the diffusion equation into Laplace space and get the following generic solution using modified Bessel functions:

Solution of the diffusion equation:
$$\bar{p}_D(u, r_D) = A(u)K_0(r_D \sqrt{u}) + B(u)I_0(r_D \sqrt{u})$$

The terms A(u) and B(u) will be defined by the initial, inner boundary (well) and outer boundary equations. Long story short we end up with the following solutions:

For a closed circle:
$$\bar{p}_{FRD}(u) = \frac{\frac{K_0(\sqrt{u})}{u\sqrt{u}K_1(\sqrt{u})}}{1 - \frac{K_1(r_{eD}\sqrt{u})}{I_1(r_{eD}\sqrt{u})} \frac{I_1(\sqrt{u})}{K_1(\sqrt{u})}} - \frac{\frac{I_0(\sqrt{u})}{u\sqrt{u}I_1(\sqrt{u})}}{1 - \frac{I_1(r_{eD}\sqrt{u})}{K_1(r_{eD}\sqrt{u})} \frac{K_1(\sqrt{u})}{I_1(\sqrt{u})}}$$

For a ct pressure circle:
$$\bar{p}_{FRD}(u) = \frac{\frac{K_0(\sqrt{u})}{u\sqrt{u}K_1(\sqrt{u})}}{1 + \frac{K_1(r_{eD}\sqrt{u})}{I_1(r_{eD}\sqrt{u})} \frac{I_1(\sqrt{u})}{K_1(\sqrt{u})}} - \frac{\frac{I_0(\sqrt{u})}{u\sqrt{u}I_1(\sqrt{u})}}{1 + \frac{I_1(r_{eD}\sqrt{u})}{K_1(r_{eD}\sqrt{u})} \frac{K_1(\sqrt{u})}{I_1(\sqrt{u})}}$$

To the finite radius solution we can add wellbore storage and skin in Laplace space:

Adding wellbore storage & skin:
$$\bar{p}_{wFD}(u) = \frac{1}{u} \left[\frac{S + u\bar{p}_{FRD}(u)}{1 + uC_D[S + u\bar{p}_{FRD}(u)]} \right]$$

The problem is once again transferred to real space using the Stehfest algorithm. The behavior is studied in the next section. As for IARF we will use an interesting late time approximation:

Late time approximation:
$$p_{wFD}(t_D) = \frac{2t_D}{r_{eD}^2} + \ln r_{eD} - \frac{3}{4} + S$$

This will be the origin of the pseudo-steady state behavior. Converting the dimensionless radius back dimensionless variables to physical variables we get the PSS equation:

PSS equation:
$$p_{wFD}(t_D) = \frac{2\pi r_w^2}{A} t_D + \frac{1}{2} \ln \left(\frac{A}{C_A r_w^2} \right) + 0.4045 + S$$

C_A is the Dietz shape factor, characteristic of the shape of the reservoir and the position of the well in the reservoir. In the case of a well at the center of a closed circle we get $C_A=31.62$.

2.E.3 Pseudo-Steady State flow

At late time the pressure response of a well flowing at the center of a homogeneous reservoir of circular shape will be approximated by:

Circular PSS equation:
$$p(t) = p_i - 0.03723 \frac{qB}{\phi c_i h r_e^2} t - 141.2 \frac{qB\mu}{kh} \left[S + \ln \frac{r_e}{r_w} - \frac{3}{4} \right]$$

We see that the slope of this linear approximation is inversely proportional to the square of the circle radius. More generally the slope will be inversely proportional to the reservoir area.

In the case where the reservoir thickness is not the constant h the slope will be inversely proportional to the volume of the reservoir (or the drainage area). In other words quantifying the PSS slope will provide an estimate of the reservoir volume and therefore the reserves.

The figures below show the drawdown response of a vertical well with wellbore storage and skin in a homogeneous reservoir and under three boundary configurations: an infinite reservoir (green), a circular reservoir of 6,000 ft of radius (blue) and an even smaller reservoir with a radius of 3,000 ft (red). Responses are shown on a linear scale (left) and a loglog scale (right) together with the Bourdet derivative defined in the PTA chapter.

During production, when the boundary is detected, the behavior deviates from Infinite Acting Radial Flow to reach Pseudo-Steady State according to the equation above. PSS is characterized by linearity between the pressure change and the elapsed time on the linear scale.

On the loglog plot PSS is characterized by a unit slope of the Bourdet derivative. Though it is slower, the pressure change also tends towards merging with the pressure derivative on the same unit slope.

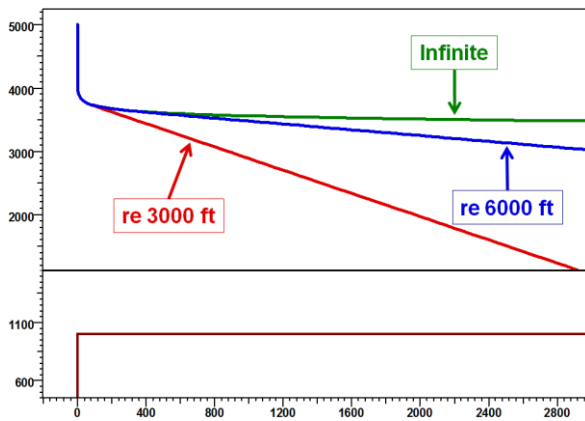


Fig. 2.E.2 – Finite radius PSS solution, linear scale

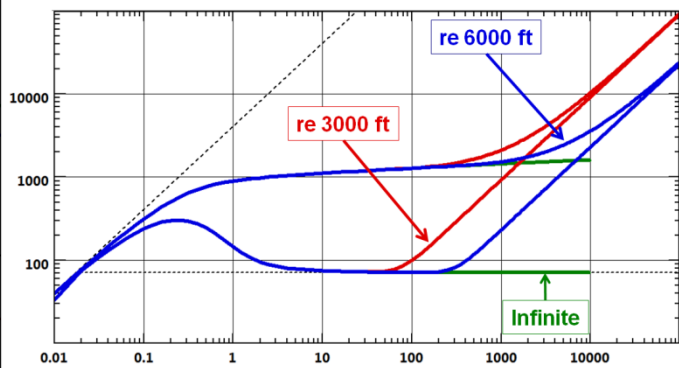


Fig. 2.E.3 – Finite radius PSS solution, loglog scale

Comparing the two circular responses:

- Drawing a straight line on the linear plot will show that the slope of the 're 3,000 ft' line is twice larger than the slope of the 're 6,000 ft' line.
- Looking at the time of deviation from IARF on the loglog plot, we see that this occurs 4 times earlier for the 3,000 ft case than for the 6,000 ft case.

In both cases we see the inverse proportionality of the slope and the time of divergence to the square of the reservoir radius or, more generally to the reservoir area.

The circular model is only one example of closed systems, and Pseudo-Steady State exists for all closed systems. It is a regime encountered after a certain time of constant rate production.

Although it is a flow regime of interest for Pressure Transient Analysis, it is THE flow regime of interest in Production Analysis. Pseudo-Steady State may sometimes not only be seen as a result of reaching the outer boundary of the reservoir; in a producing field, for example, there is a time when equilibrium between the production of all the wells may be reached, and, for each well, Pseudo-Steady State will occur within the well drainage area.

For a slightly compressible fluid, Pseudo-Steady State is characterized by a linear relation between the pressure change and the time. When PSS is reached, the pressure profile in the reservoir will 'freeze' and the pressure will deplete linearly and uniformly throughout the connected reservoir. Things are somewhat different when the PVT becomes complex.

2.F Complex production histories – Superposition in time

2.F.1 The principle of superposition

Derivations as shown before assumed a constant rate production. In practice we need to model more complex flow histories. This is done using the principle of superposition. We generate the solution of a complex problem as the linear combination and superposition, in time and/or space, of simpler components. The most popular superpositions are:

- Simulation of complex production histories by linear combinations of simple drawdown solutions with different weights and starting times. This is called superposition in time.
- Simulation of simple linear boundaries by linear combinations of infinite well and interference solutions coming from virtual wells (also called image wells).

For any problem involving a linear diffusion equation, the main superposition principles are:

- Linear combinations of solutions honoring the diffusion equation also honor this equation.
- At any flux point (well, boundary), the flux resulting from the linear combination of solutions will be the same linear combination of the corresponding fluxes.
- If a linear combination of solutions honors the diffusion equation and the different flux and boundary conditions at any time, then it is THE solution of the problem.

From these principles it is easy to build the following series of rules for superposition in time:

- The pressure change due to the production q of a given system is q times the unit rate solution of the same system. This extends to injections using a negative rate.
- To simulate the sequence of a constant rate q_1 from time zero to time t_1 , followed by the production q_2 from time t_1 to infinity, you can superpose the production at rate q_1 from time zero to infinity and a production of rate $(q_2 - q_1)$ from time t_1 to infinity.
- As a particular case, to simulate a constant production q of duration t_p , followed by a shut-in, you can superpose the production of q from time zero and an injection of q from time t_p .
- This is then easily extends to more complex production sequences.

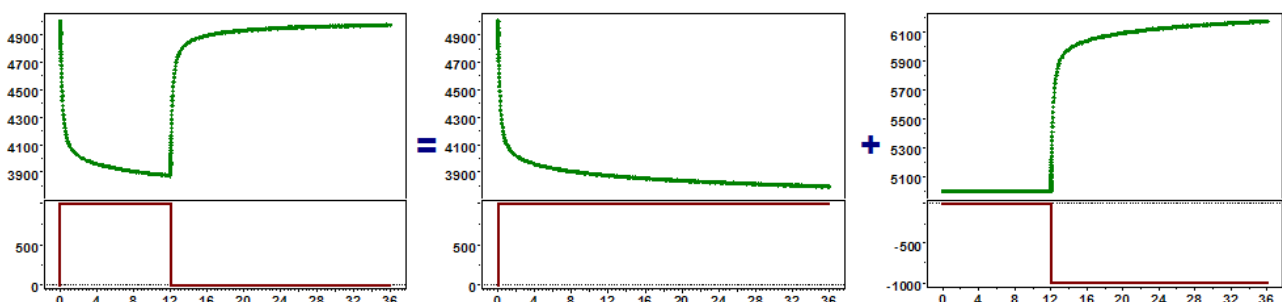


Fig. 2.F.1 – Graphical illustration of simple superposition

2.F.2 Build-up superposition

$\Delta p_{unit}(\Delta t)$ is the solution of a problem for a constant production of unit rate. We also consider $\Delta p_{DD}(\Delta t)$, solution of a given problem in the case of a constant production at rate q . We have:

Drawdown solution:
$$\Delta p_{DD}(\Delta t) = q \Delta p_{unit}(\Delta t)$$

We now consider a production at rate q of duration t_p , followed by a shut-in:

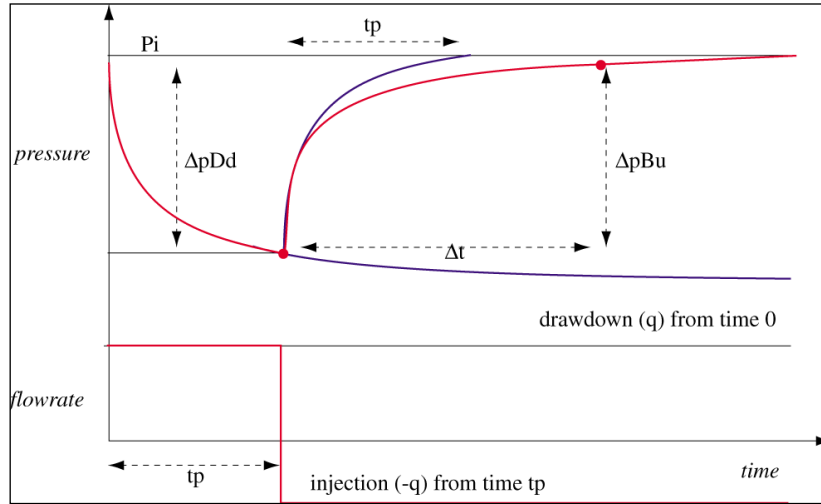


Fig. 2.F.2 – Buildup superposition

During the initial production phase, the pressure will be given by:

Production phase:
$$p_{DD}(t) = p_i - \Delta p_{DD}(t) = p_i - q \Delta p_{unit}(t)$$

The pressure change during the build-up is the superposition of the pressure change due to the production of q from time 0 and an injection of q starting at time t_p . This will be written:

Build-up pressure:
$$p_{BU}(t) = p_{BU}(t_p + \Delta t) = p_i - q \Delta p_{unit}(t_p + \Delta t) + q \Delta p_{unit}(\Delta t)$$

or:
$$p_{BU}(t_p + \Delta t) = p_i - \Delta p_{DD}(t_p + \Delta t) + \Delta p_{DD}(\Delta t)$$

The initial pressure may not be known at this stage. We generally start from the pressure change observed during the shut-in, i.e. starting from the last flowing pressure before shut-in:

Build-up pressure change:
$$\Delta p_{BU}(\Delta t) = p_{BU}(t_p + \Delta t) - p_{BU}(\Delta t = 0) = p_{BU}(t_p + \Delta t) - p_{DD}(t_p)$$

Replacing, we get:
$$\Delta p_{BU}(\Delta t) = [p_i - \Delta p_{DD}(t_p + \Delta t) + \Delta p_{DD}(\Delta t)] - [p_i - \Delta p_{DD}(t_p)]$$

And we get the build-up superposition relationship: The pressure change during a build-up, i.e. the difference between the current pressure and the last flowing pressure, can be calculated as the simple superposition of elementary drawdown solutions:

Build-up superposition:
$$\Delta p_{BU}(\Delta t) = \Delta p_{DD}(t_p) + \Delta p_{DD}(\Delta t) - \Delta p_{DD}(t_p + \Delta t)$$

As the drawdown solution is an increasing function of time, we get the inequalities:

Inequalities:
$$\Delta p_{BU}(\Delta t) < \Delta p_{DD}(t_p) \text{ and } \Delta p_{BU}(\Delta t) < \Delta p_{DD}(\Delta t)$$

In other words the build-up response will be 'flatter' than the drawdown response, and the pressure will never get back above initial pressure...

2.F.3 Multirate superposition

Multi-rate superposition is the natural extension of the build-up superposition to any type of production history. A sequence of rates q_1, q_2, \dots, q_n , of respective durations T_1, T_2, \dots, T_n , with respective starting times $t_1=0, t_2, \dots, t_n$.

We calculate the pressure at any time t during the period of flow q_n . In the diagram below, we have $q_n=0$. For Pressure Transient Analysis we often deal with shut-in pressures after more or less complex production histories. However the following equations are valid for any rates.

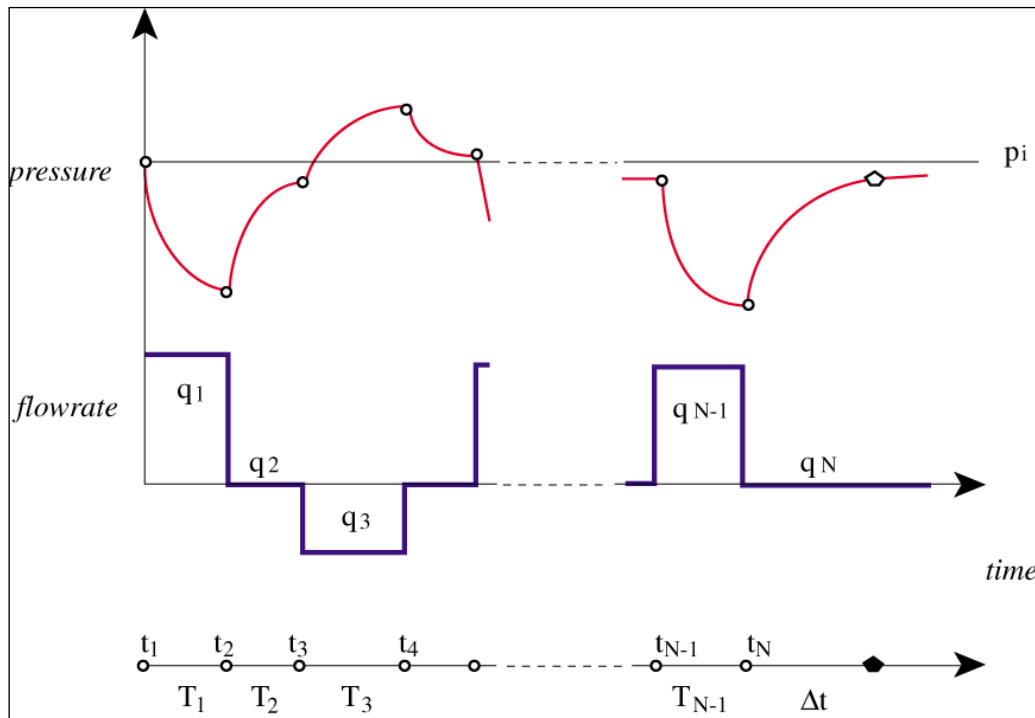


Fig. 2.F.3 – Multirate superposition

Using the principle of superposition we calculate the pressure change by superposing drawdown responses, starting from the beginning of each flow period to the current time, and of respective rates $q_1-q_0, q_2-q_1, \dots, q_n-q_{n-1}$ (with $q_0=0$).

$$\text{Multirate superposition: } p(t) = p_i - \sum_{i=1}^n (q_i - q_{i-1}) \Delta p_{unit}(t - t_i)$$

If the period of interest is a producing period, or multi-rate drawdown, the pressure change of interest will correspond to the above formula. In case of a shut-in after a multi-rate production, the interpretation engineer will, as for a simple build-up, consider the pressure change since the well was shut-in.

$$\text{Multirate shut-in: } \Delta p_{BU}(\Delta t) = p(t_n + \Delta t) - p(t_n)$$

$$\text{From superposition: } \Delta p_{BU}(\Delta t) = \sum_{i=1}^{n-1} (q_i - q_{i-1}) \Delta p_{unit}(t_n - t_i) - \sum_{i=1}^n (q_i - q_{i-1}) \Delta p_{unit}(t_n + \Delta t - t_i)$$

We have shown how multirate solutions can be derived from elementary drawdown solutions. Horner time, superposition time, etc, will be introduced in the PTA methodology chapter.

2.G Other means to solve and model a diffusion problem

The three models presented so far were solved analytically. Analytical models are fast and accurate. Unfortunately a lot of problems are too complicated to be directly solved analytically. This section presents the main tools used in the industry to provide such solutions.

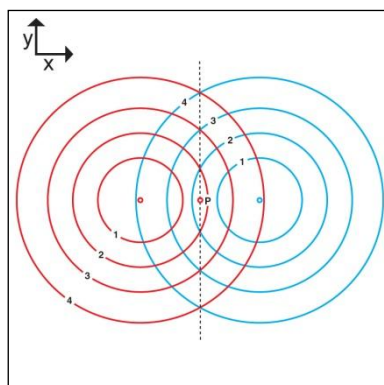
2.G.1 Superposition in space of analytical models (image wells)

It is possible but relatively complex and CPU intensive to model linear boundaries and radial diffusion at the same time. However, for some geometries, linear boundaries can be replaced by a superposition of interferences from virtual wells. This is called the method of image wells, which in turn requires the notion of superposition in space.

In a way similar to the superposition in time introduced in the previous section, superposition in space tells us that if two or more solutions honor the diffusion equation, for example two line sources coming from different wells, any linear combination of these solutions will honor the diffusion equation. The resulting inner and outer boundary conditions will be the same linear combination of the conditions generated by the individual solutions.

Using this principle, the method of image wells consists of superposing individual mirrored infinite solutions to create a pseudo-boundary. In the case of a single sealing fault of infinite extent, we will add two pressure changes: (1) the pressure change due to the well response in an infinite reservoir, and (2) the interference solution of an image well, symmetric to the well with respect to the fault.

The sum of these two pressure changes, at any point of our half plane reservoir, will honor the diffusion equation (superposition in space). Because the response will be symmetric with respect to the fault, the continuous pressure gradient orthogonal to the fault will have to be zero, and the no flow boundary condition will be honored. All other conditions, initial and well, being honored, we have built the exact solution to our problem.



*Fig. 2.G.1 – X-Y representation of an image well.
The pressure drop of a fixed value is shown at different times.
Effective pressure drop is the sum of these two signals*

Strictly speaking, the interference solution added to the infinite solution is not always a line source. It has to be the exact interference solution from the image well. The time delay due to wellbore storage may need to be taken into account. In the case of a fracture with a sealing fault this will involve an image fracture properly positioned. In most cases the difference between the proper interference solution and a line source will be negligible, but not always.

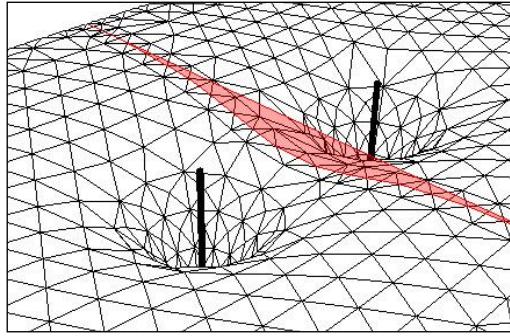


Fig. 2.G.2 – 3D representation of the pressure profile in a 2D plane, with an image well

Note: one could argue that, when the number of image wells is limited (sealing faults, intersecting faults for some angles) the sum of the image solutions constitute the exact analytical model. Conversely, when the sum is infinite the resulting solution could be classified as a semi-analytical solution. This is correct, but still solutions using image wells are an important category of models that we wanted to single out.

2.G.2 Semi-analytical solutions

When a complex problem cannot be solved rigorously i.e. with a simple closed form solution, it has to be approximated by cutting the solution into steps, either time steps or bits and pieces of boundary / well segment / fracture segment. Then the solution will show an integral function or a time-by-time matrix inversion. Such a solution is called semi-analytical, because some components are calculated analytically but put together numerically.

Integral solutions are generally computationally slower than closed form solutions, and the difficulty is to re-formulate the integrals, optimize the components and use extrapolation whenever feasible, in order to reduce the calculation time to a level acceptable to the end user. This is especially so in the case of nonlinear regression. As an example, the equation below is the solution in Laplace space for a horizontal well in a closed circle.

$$\overline{p_D}(u) = \frac{\tilde{q}\mu}{2\pi k h_D u} \left\{ \int_{-\tilde{L}_h}^{\tilde{L}_h} \left[K_0(\tilde{r}_D \sqrt{u}) + \frac{(-1)^{n+1} I_0(\tilde{r}_D \sqrt{u}) K_s(r_{eD} \sqrt{u})}{I_s(r_{eD} \sqrt{u})} \right] d\alpha \right. \\ \left. + 2 \sum_{n=1}^{\infty} \cos \frac{n\pi z_w}{h} \cos \frac{n\pi z_w}{h} \int_{-\tilde{L}_h}^{\tilde{L}_h} F_n(\alpha) d\alpha \right\}$$

$$\text{where } F_n(\alpha) = K_0(\tilde{r}_D \varepsilon_n) + \frac{(-1)^{n+1} I_0(\tilde{r}_D \varepsilon_n) K_s(r_{eD} \varepsilon_n)}{I_s(r_{eD} \varepsilon_n)}$$

Application: linear composite, leaky faults, combinations of linear and radial geometries.

2.G.3 Boundary elements

A particular case of approximate analytical solutions are boundary elements. The principle is to honor the boundary condition by adding to the infinite solution an integral function on the boundary that will 'compensate' for the infinite solution to honor this boundary condition.

This solution has the advantage of focusing on the boundary only, and solves a 3-D problem with a 2-D solution, or a 2-D problem with a 1-D solution.

However there are two major shortcomings: (1) each block delimited by a boundary must be homogeneous, and (2) it involves the inversion of a densely populated matrix, and this can be very computer intensive.

Because of these two shortcomings, numerical models are currently preferred and more developed in the industry.

2.G.4 Numerical models

The application to PTA and PA of specifically designed numerical models is one of the major technical developments of recent years, especially for KAPPA.

Numerical models address the two major limitations of the modelling methods presented above: they can model complex geometries, and they can model nonlinear diffusion problems for which the superposition in time and space of analytical models will not work.

Numerical models are the subject of a dedicated chapter in this book.

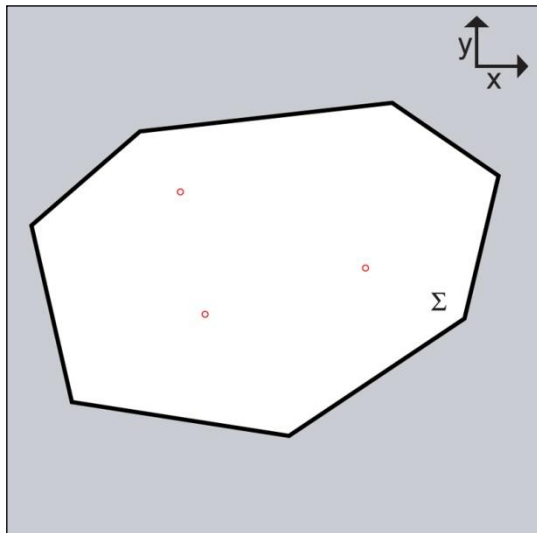


Fig. 2.G.3 – Boundary elements

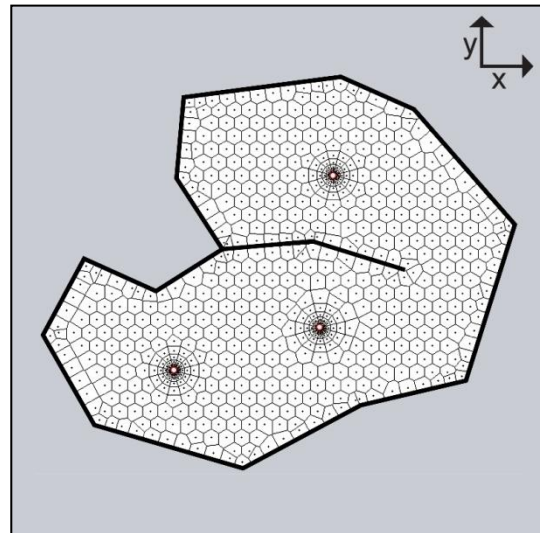


Fig. 2.G.4 – Numerical model

2.H Physical meaning of Diffusion

In Pressure Transient Analysis and Production Analysis, we use the diffusion assumptions described in the previous section to process measured data, analyze them using models and finally forecast the well and reservoir response. To do this we have two groups of parameters; the 'known' parameters that we will input and the 'unknown' parameters that we calculate.

In the process, we may be tempted to ignore the impact of the known parameters and focus on unknown parameters. Worse, engineers with improper training may use software defaults for 'known' parameters without considering the impact on the results.

This section is a summarized guide to the influence of all parameters involved in the diffusion process, whether we input or calculate them.

2.H.1 Reference case

To do this we select a reference case, with arbitrarily long production and shut-in periods.

You may wish to reproduce the whole process in the chapter below by running successive test designs in Saphir and compare the results using the multi-gauge or multi model option.

We simulate the simplest model that can reproduce the three following flow regimes: Wellbore Storage and Skin, Infinite Acting Radial Flow and Pseudo-Steady State. We model a vertical well in a circular homogeneous reservoir centered at the well:

Input parameters: $r_w=0.3$ ft; $h=100$ ft; $\phi=10\%$; $c_t=1.e-5$ psi-1; $\mu=1$ cp

Flow rate history: $q=1,000$ stb/day with $B=1$; 1,000 hours of flow; 1,000 hours of shut-in

Interpretation 'results': $p_i=5,000$ psi; $C=0.01$ bbl/psi; $Skin=0$; $k=10$ mD; $r_e=1,500$ ft

The result of such design, on both production and buildup, is shown below. The loglog plot shows both drawdown and buildup periods.

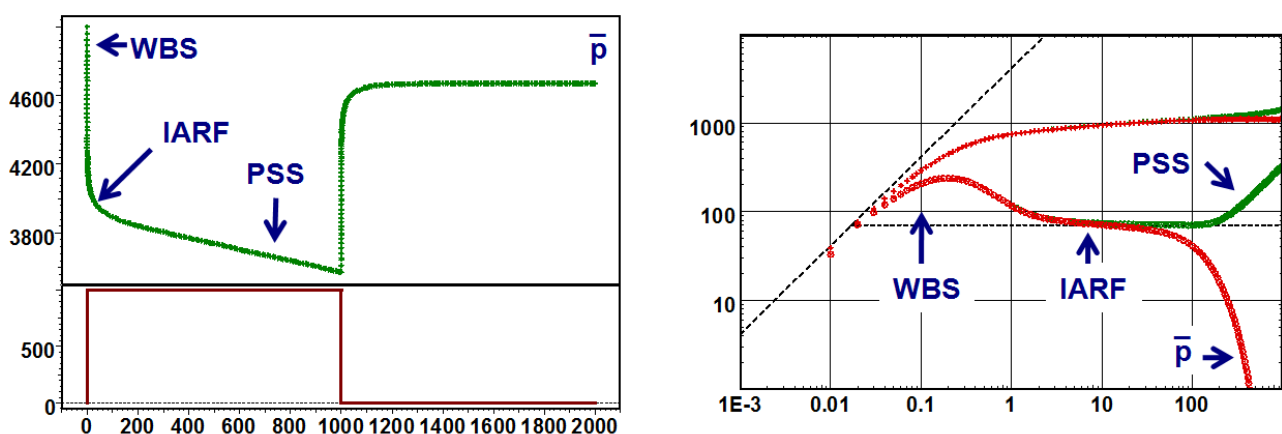


Fig. 2.H.1 – Test Design of the reference case: history and loglog plots

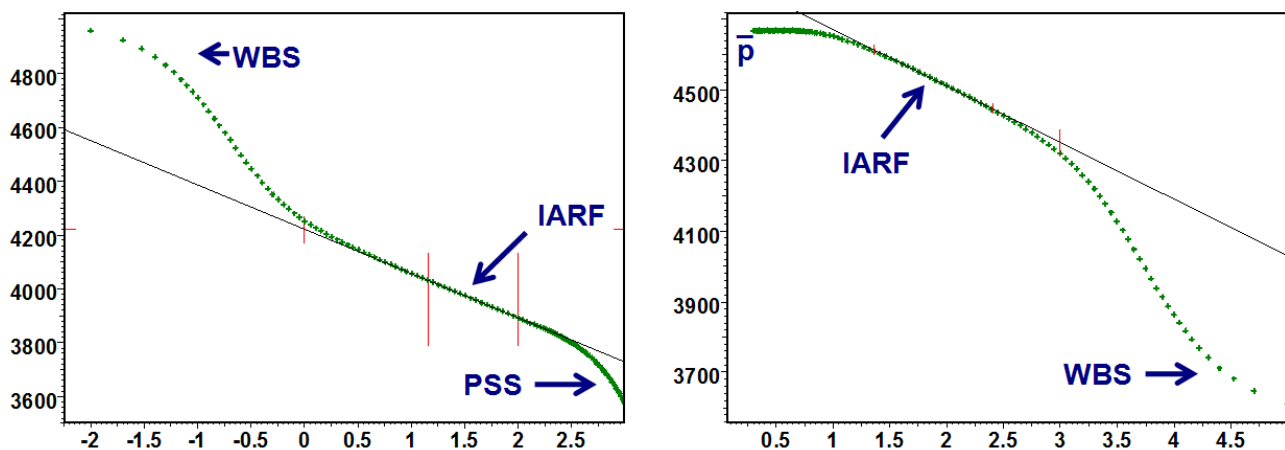


Fig. 2.H.2 – Semilog plot (drawdown) and Horner plot (buildup)

As developed in the PTA chapter we can observe the following:

- The early time hump of the derivative is the transition between pure wellbore storage (early time unit slope; the magnitude of the hump is the skin).
- Infinite Acting Radial Flow (IARF) corresponds to the stabilization of the Bourdet derivative.
- At late time, the production (drawdown) period shows a unit slope corresponding to Pseudo-Steady State, whilst during the shut-in the pressure stabilizes at the average pressure and the derivative takes a dive (also see the chapter on 'Boundary models').

In the following we are focusing on the production (drawdown) and study the effect caused by changes in both 'known' and 'unknown' parameters.

In this design we know ALL parameters. In the following, however, we will make a split between 'unknown' and 'known' parameters. 'Unknown' parameters are those for which we generally look for in a Pressure Transient or Production Analysis.

In the case of the simulated example, they are the wellbore storage coefficient, the skin factor, the reservoir permeability and the radius of the circular boundary.

'Known' parameters are those we generally assume to be given as an input in order to calculate the 'unknown' parameters from the analysis. Usually, they are r_w , h , ϕ , c_t and μ . We will show how sensitive the response is to the 'known' and 'unknown' parameters, and how an error in the estimation of such parameters will impact our analysis.

2.H.2 Effect of 'unknown' parameters

2.H.2.a Wellbore storage

The figure below presents the response with all default parameters except for the wellbore storage. Values for C are 0.001, 0.003, 0.01, 0.03 and 0.1 (stb/psi).

The value of C has a major effect, which is actually exaggerated by the logarithmic time scale. You can see on the linear history plot that all responses seem to be the same, however.

Infinite Acting Radial Flow: When the influence of wellbore storage is over all responses merge together, both in terms of pressure and derivative. Wellbore storage does not play any role except that it masks infinite acting radial flow on a time that is proportional to the value of C .

PSS: Wellbore storage does not affect the late time response.

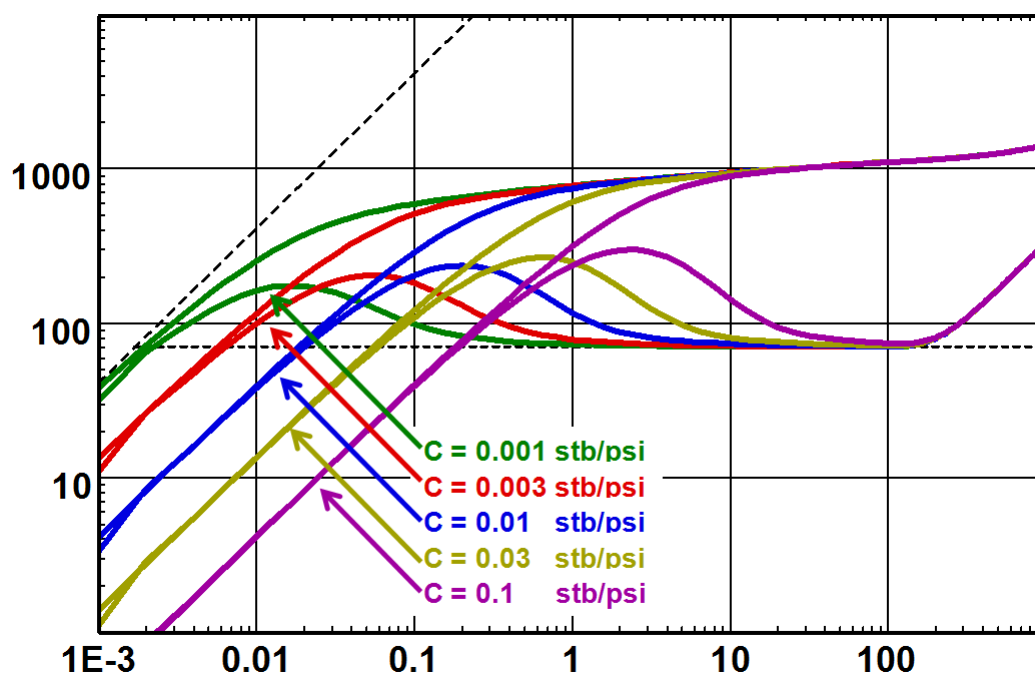


Fig. 2.H.3 – Effect of wellbore storage, loglog plot

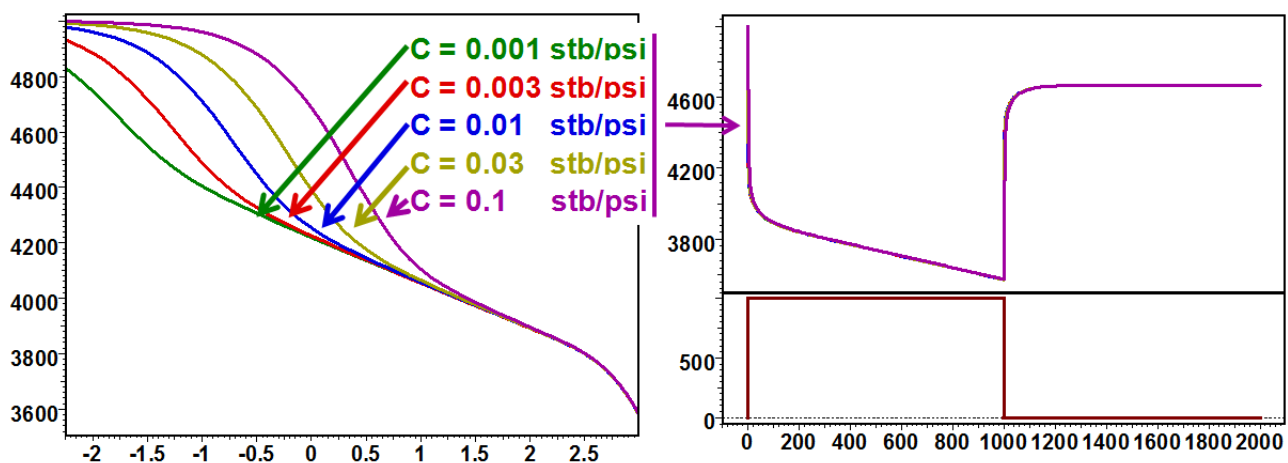


Fig. 2.H.4 – Effect of wellbore storage, semilog and history plot plot

2.H.2.b Skin

Below is shown the response with all default parameters and a variable skin. Values for skin are -3, 0, 2, 5 and 10.

Storage: Skin does not change the position of the early time unit slope (pure wellbore storage) but affects the amplitude of the hump. A larger skin will produce a larger hump, hence delaying the time at which Infinite Acting Radial Flow is reached.

IARF: Once IARF is reached, the skin has no effect on the vertical position of the derivative, but has a cumulative effect on the amplitude of the pressure.

PSS: Skin does not have an effect on the time at which PSS is reached or on the derivative response at the end. However the cumulative effect on the pressure remains and all responses 'bend' and remain parallel when PSS is reached (see history plot below).

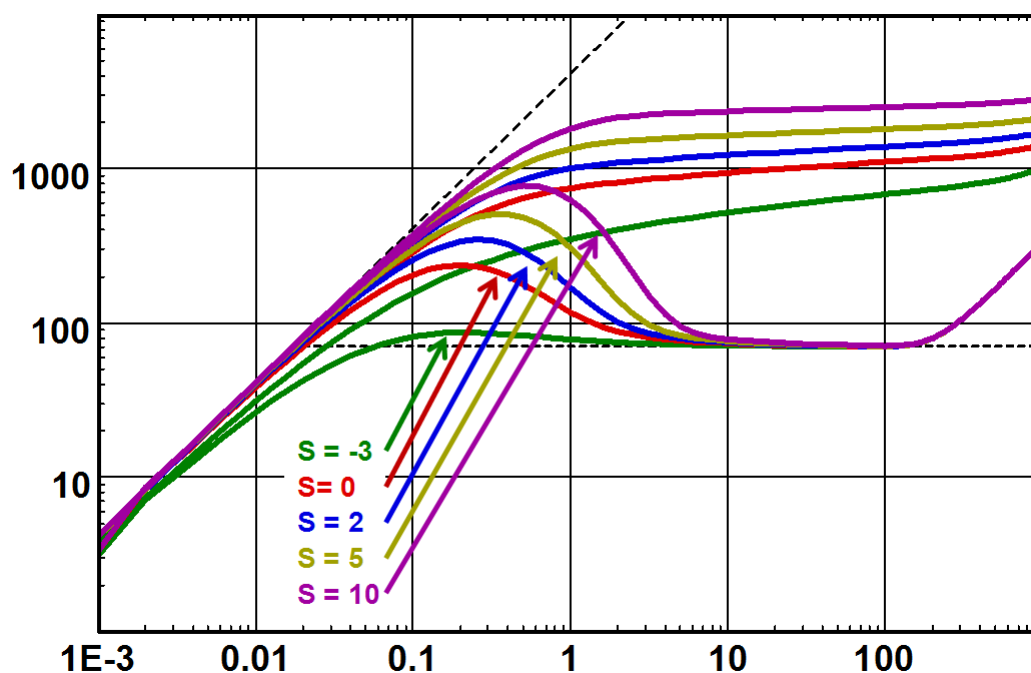


Fig. 2.H.5 – Effect of skin, loglog plot

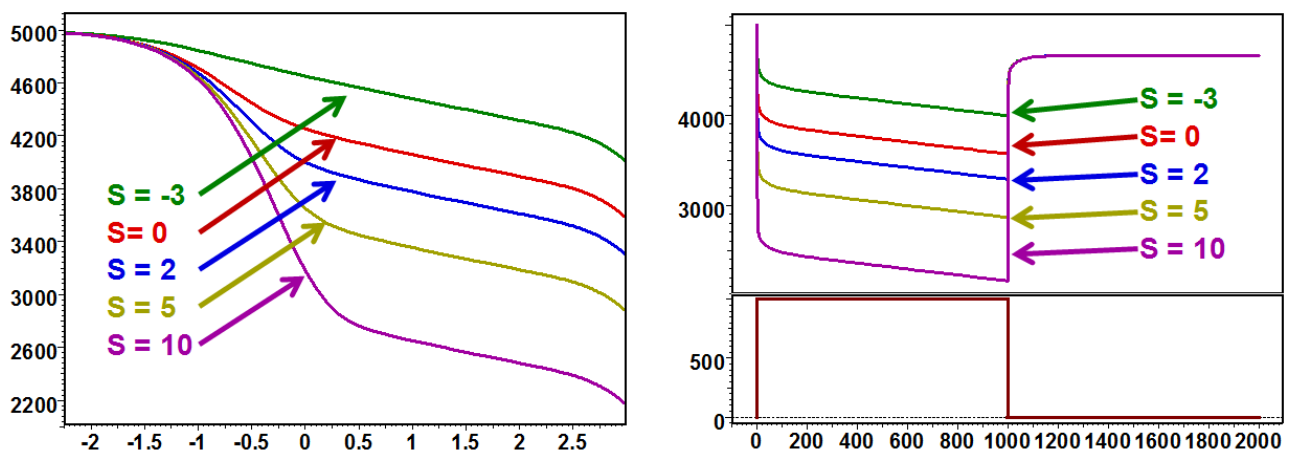


Fig. 2.H.6 – Effect of skin, semilog and history plot

2.H.2.c Permeability

The figure below presents the response with all default parameters except the permeability. Values for k are 2, 5, 10, 20 and 50 mD.

Storage and IARF: The derivative responses have the same shape but they are translated along the wellbore storage line of unit slope. When the permeability is higher, the reservoir reacts faster and deviates earlier from pure wellbore storage. The level of stabilization of the derivative, i.e. the slope of the semilog plot, is inversely proportional to k . For this reason the responses diverge on the semilog plot, the different slopes being inversely proportional to k .

PSS: At late time all derivative signals merge to a single unit slope. This is linked to the fact that permeability has no effect on the material balance equation.

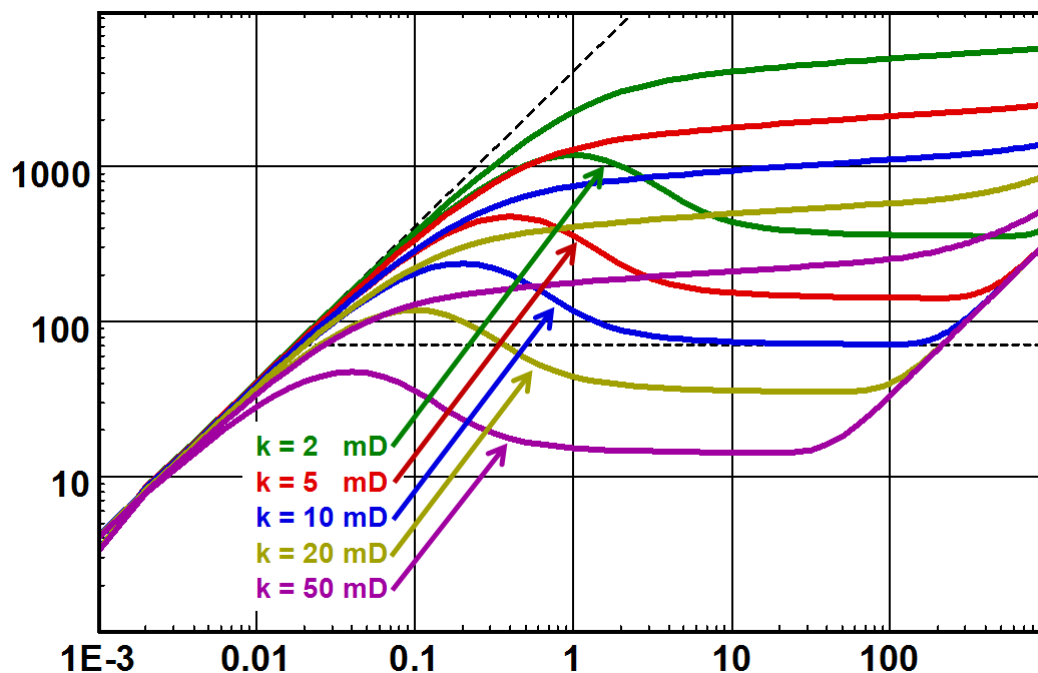


Fig. 2.H.7 – Influence of the reservoir permeability, loglog plot

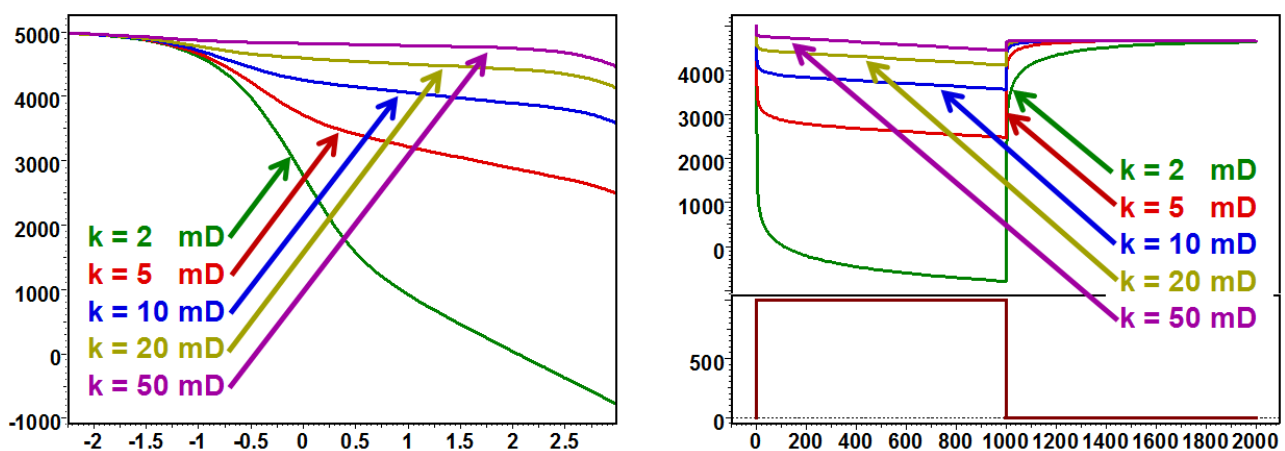


Fig. 2.H.8 – Influence of the reservoir permeability, semilog and history plot

2.H.2.d Reservoir size

Below is presented the response with all default parameters except the reservoir size, the radius r_e . From the reference case we have successively divided / multiplied by 1.5, and the values of r_e are 667, 1000, 1500, 2250 and 3375 ft.

The time at which PSS occurs depends on r_e . As the governing group in the diffusion equation is t/r^2 , when r_e is multiplied by 2 the time at which PSS occurs is multiplied by 4. When PSS occurs the slope of the pressure response, on the history plot, is inversely proportional to the volume of the reservoir, and therefore inversely proportional to r_e^2 .

In the shut-in the pressure stabilizes to the average pressure obtained by simple material balance. Unlike the cases above, the pressures, for a given production, do not stabilize at the same value. Again the depletion $(p_i - p_{av})$ is inversely proportional to the reservoir pore volume, i.e. inversely proportional to r_e^2 .

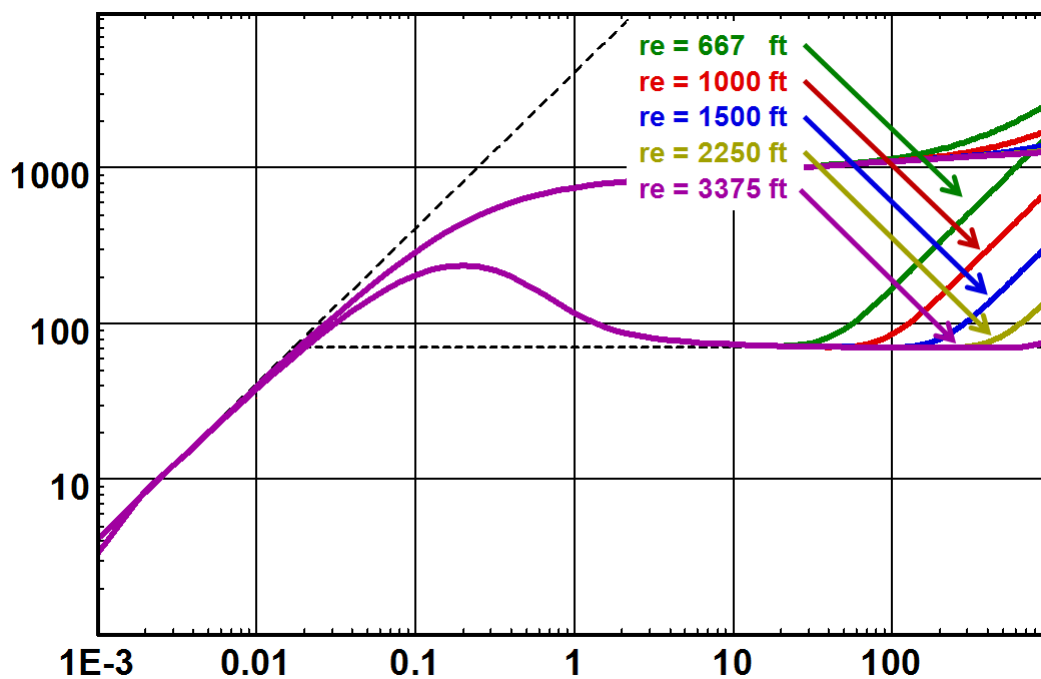


Fig. 2.H.9 – Effect of the reservoir size, loglog plot

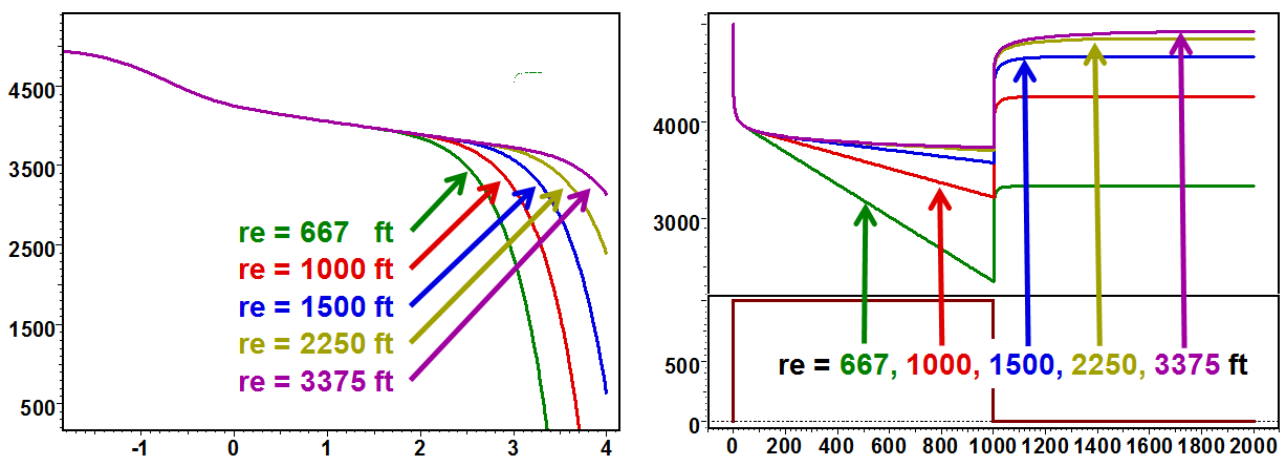


Fig. 2.H.10 – Effect of the reservoir size, semilog and history plot

2.H.3 Effect of 'known' parameters

2.H.3.a Wellbore radius

The response with all default parameters but varying the wellbore radius is illustrated below. Values of r_w are 0.1, 0.3, 1 and 3 ft.

The effect of a change in the wellbore radius is strictly the same as the consequence of a skin change: Early time amplitude of the derivative hump, no middle time and late time effect on the derivative, but a shift in the pressure that stays constant once wellbore storage effects are over. The equivalence between wellbore radius and skin is hardly a surprise, as skin can also be defined with respect to an equivalent wellbore radius. The well response is in fact a function of the equivalent wellbore radius $r_{we} = r_w \cdot e^{-S_{kin}}$.

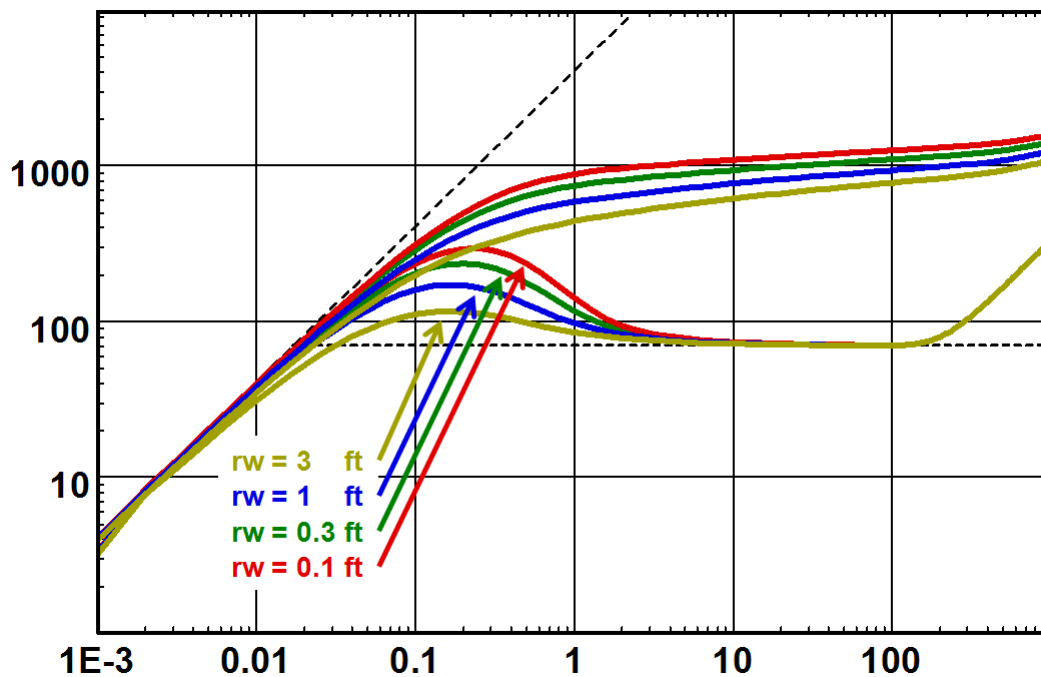


Fig. 2.H.11 – Effect of wellbore radius r_w , loglog plot

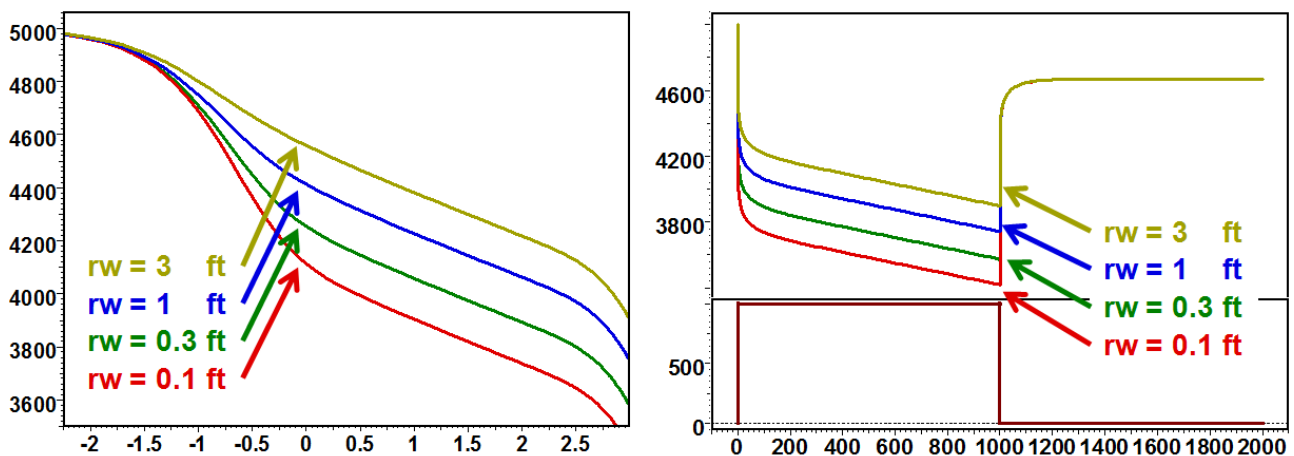


Fig. 2.H.12 – Effect of wellbore radius r_w , semilog and history plot

2.H.3.b Porosity

The figure below presents the response with all default parameters but varying the porosity. Values for ϕ are 3%, 10% and 30%.

Storage and IARF: Porosity behaves like the skin or the well radius. A smaller porosity produces a higher hump on the derivative but does not change the derivative IARF level. The equivalence between porosity and skin is used in two different areas. In interference tests the skin has a marginal influence, and the pressure amplitude is used to assess the porosity.

Hydrogeology: Hydrogeology will assess a value of skin (generally zero) and use the absolute value of the pressure change to assess the Storativity S , i.e. the porosity.

For a given reservoir size, the time for PSS is proportional to ϕ . Underestimating the porosity by 10% will provide an overestimation of the reservoir bulk volume of 10%, and therefore an overestimation of the boundary distance. The total pore volume will remain correct.

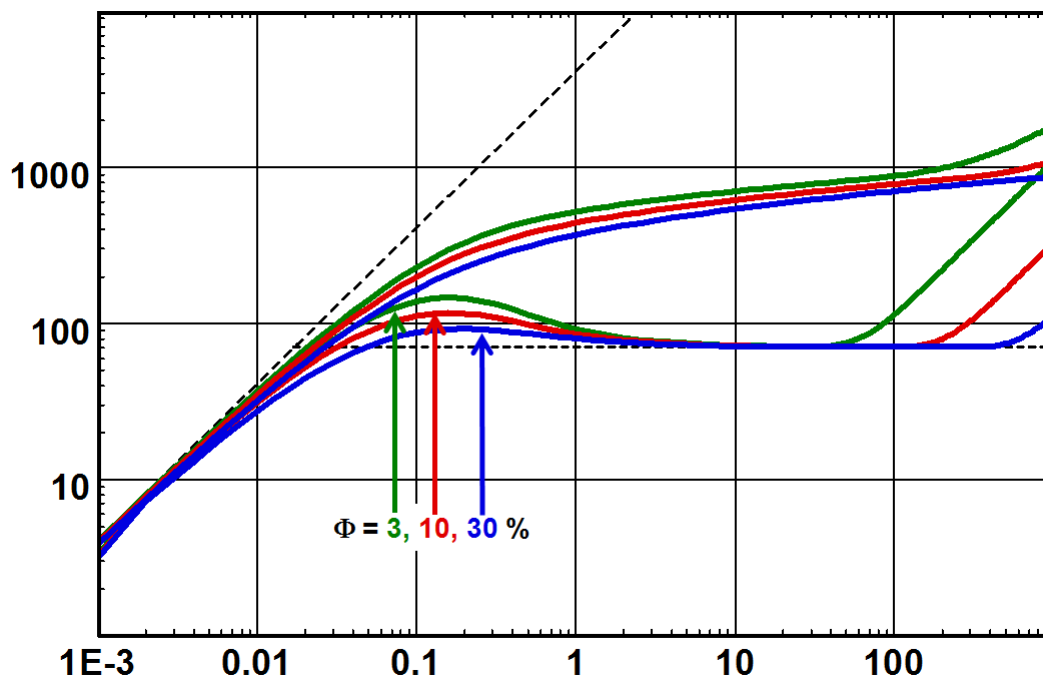


Fig. 2.H.13 – Effect of the reservoir porosity, loglog plot

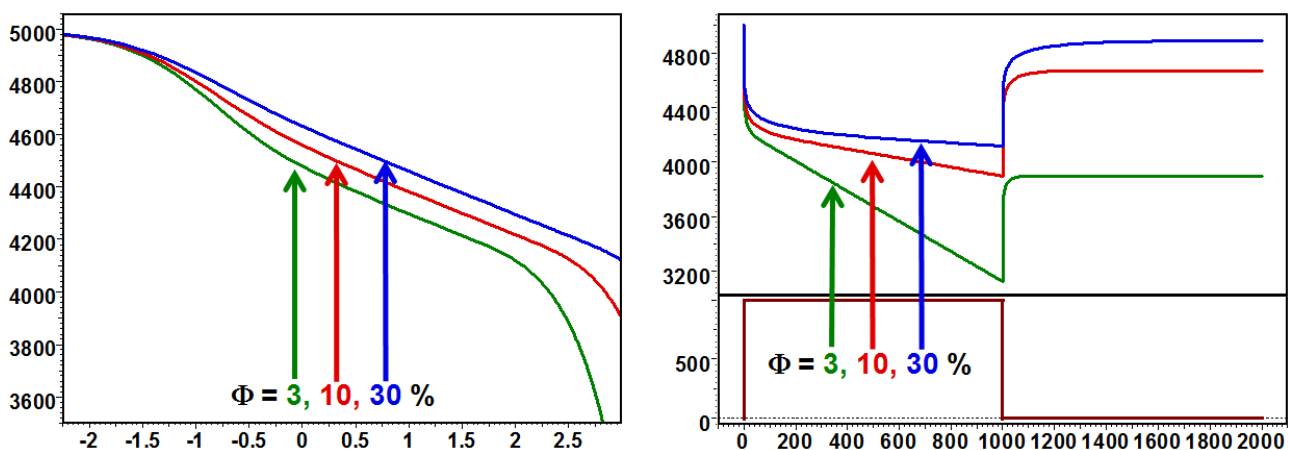


Fig. 2.H.14 – Effect of the reservoir porosity, semilog and history plot

2.H.3.c Total compressibility

Illustrated below is the response simulated with default parameters varying the total compressibility. Values for c_t are $3 \cdot 10^{-6}$, $1 \cdot 10^{-5}$ and $3 \cdot 10^{-5}$ psi⁻¹. The sensitivities at Early Time (Storage), Middle time (IARF) and late time (PSS) are strictly the same as for the porosity: A smaller compressibility produces a higher hump of the early time derivative. Compressibility does not affect the derivative level when IARF is reached but has a cumulative effect on the pressure. At late time, compressibility affects the time at which the boundary is detected and the material balance equation. As for porosity, under-estimating c_t by 10% will provide an over-estimation of the reservoir size by 10%, and therefore an over-estimation of the boundary distance. In fact, on all parts of the response, the influence of porosity and compressibility will be a function of their product $\phi \cdot c_t$.

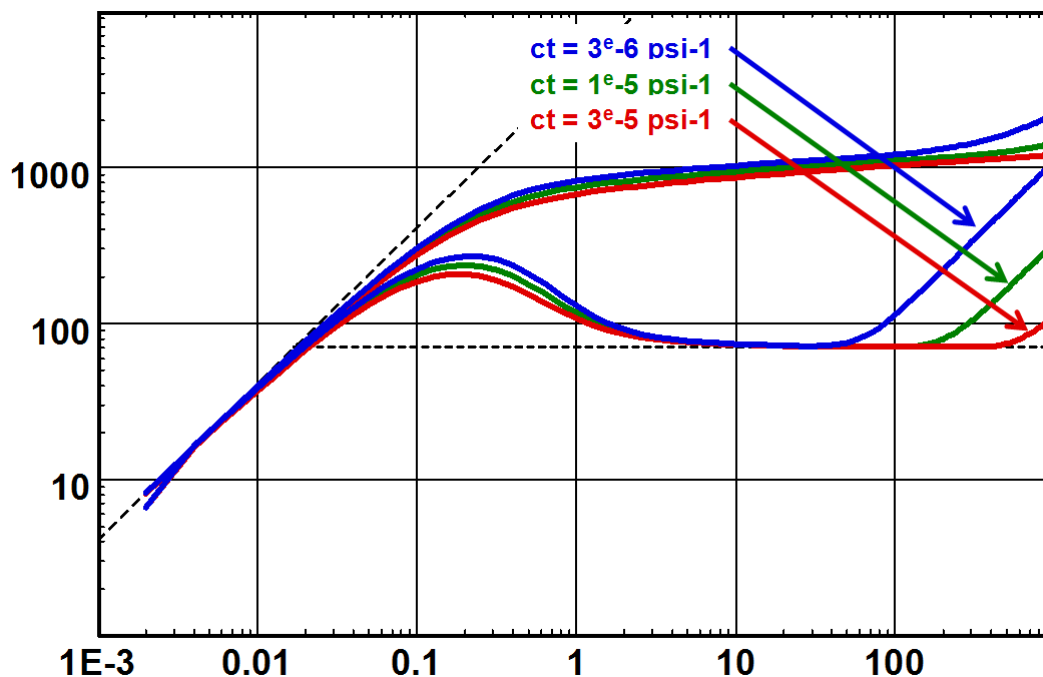


Fig. 2.H.15 – Effect of total compressibility, loglog plot

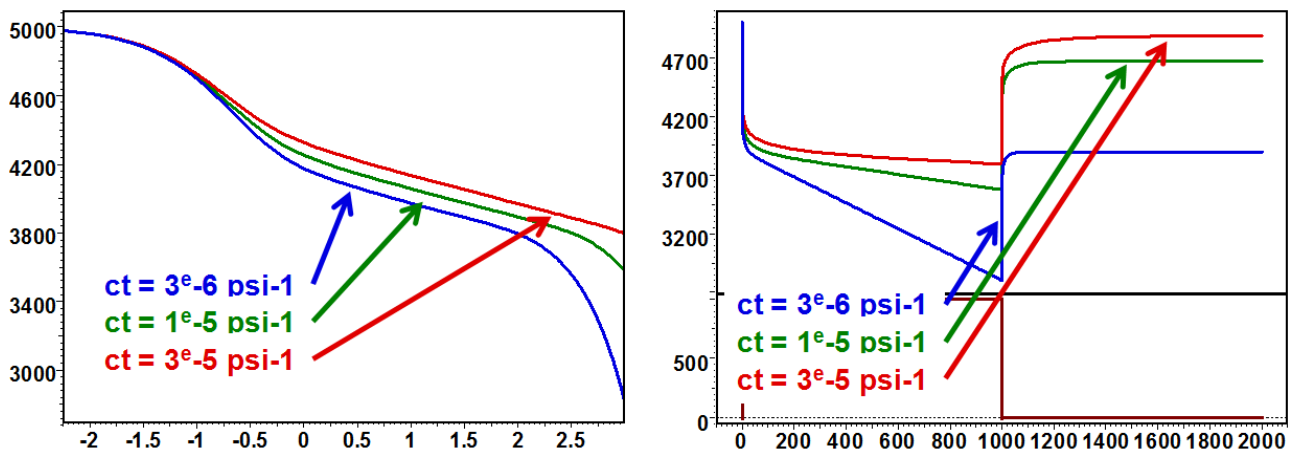


Fig. 2.H.16 – Effect of the total compressibility, semilog and history plot

2.H.3.d Viscosity

The next figure illustrates the response with default parameters but varying the fluid viscosity. Values for μ are 0.2, 0.5, 1, 2 and 5 cp. If we compare the response with the Fig. 2.H.8 illustrating the effect of a permeability change (above), we see that the sensitivity to viscosity is exactly opposite to the sensitivity to permeability. At early time (Storage) and middle time (IARF), the derivative responses have the same shape but translated along the wellbore storage line of unit slope. When the viscosity is lower, the reservoir reacts faster and deviates earlier from pure wellbore storage. The levels of stabilization of the derivative and the semilog slopes are proportional to μ . At late time all derivative signals merge to a single unit slope. In other words, the sensitivity on $1/\mu$ is the same as the sensitivity to k on all parts of the response. This means that we have another governing group with k/μ , also called the mobility.

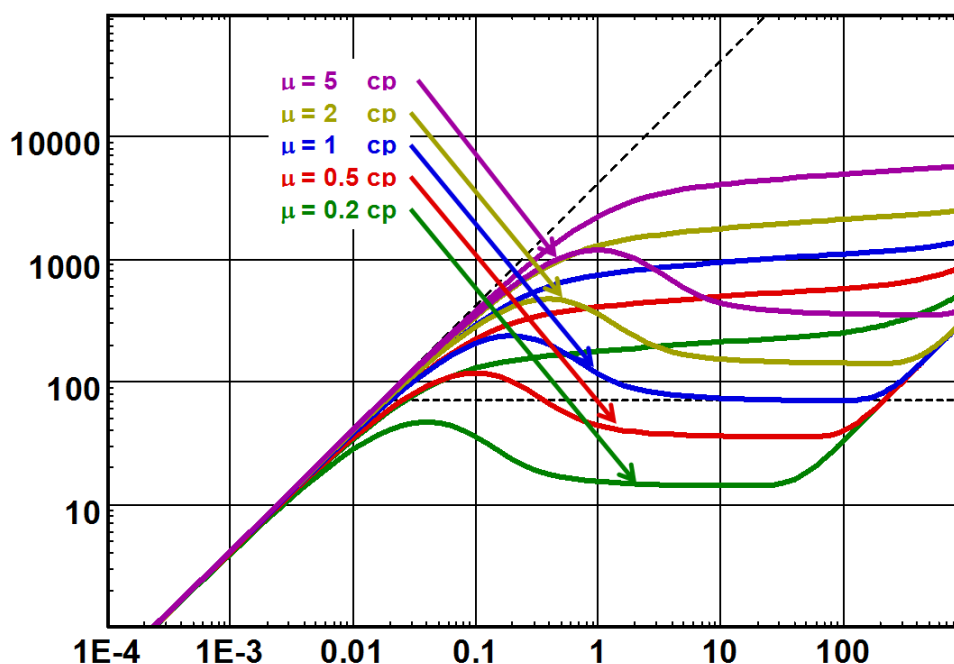


Fig. 2.H.17 – Effect of the fluid viscosity, loglog plot

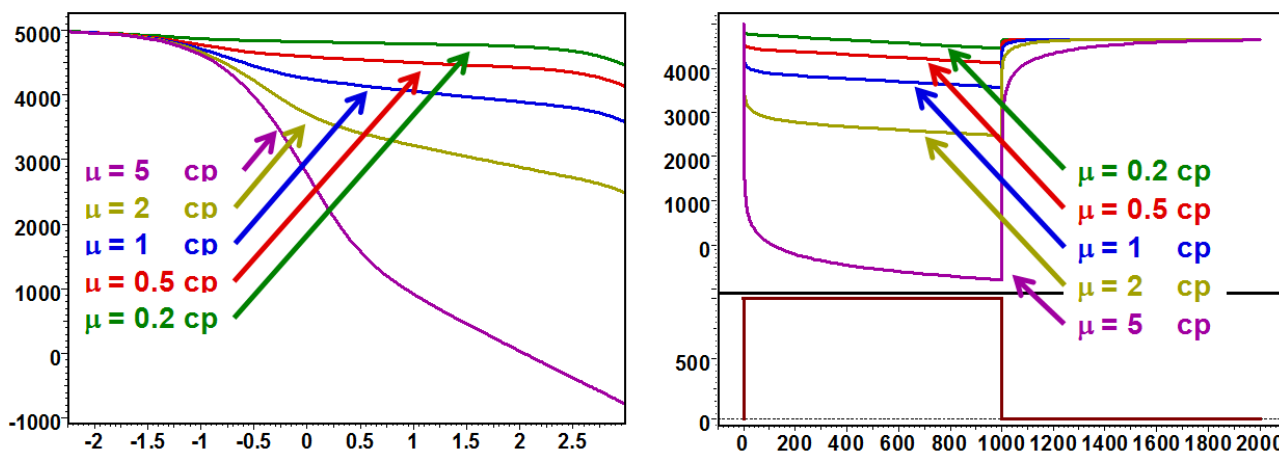


Fig. 2.H.18 – Effect of the fluid viscosity, semilog and history plot

2.H.3.e Thickness

Illustrated below is the response with all default parameters constant and a varying net drained thickness. Values for h are 20, 50, 100, 200 and 500 ft.

Storage and IARF: Changing the thickness has a similar effect to changing the permeability and an effect opposite to changing the viscosity. In other words, the governing group that defines the early time response, apart from wellbore storage and skin, is kh/μ .

PSS: Unlike permeability and viscosity, the reservoir thickness also has an effect on the late time material balance calculation. Also, the time at which the derivative deviates from IARF towards PSS does not change, and therefore the influence of the thickness on the position of the PSS straight line is similar to the sensitivity to the reservoir porosity or the compressibility.

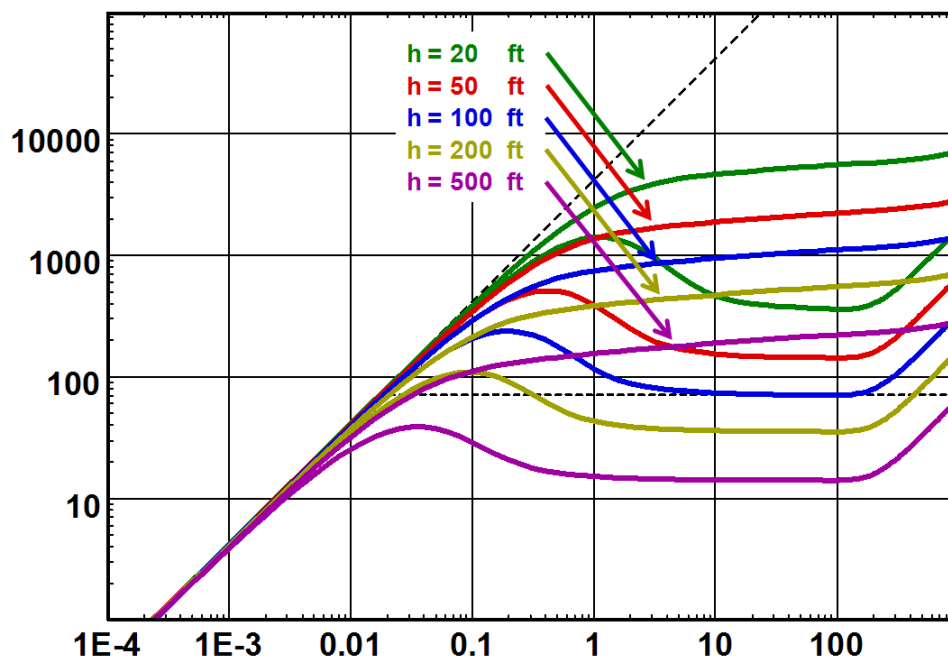


Fig. 2.H.19 – Effect of the reservoir thickness, loglog plot

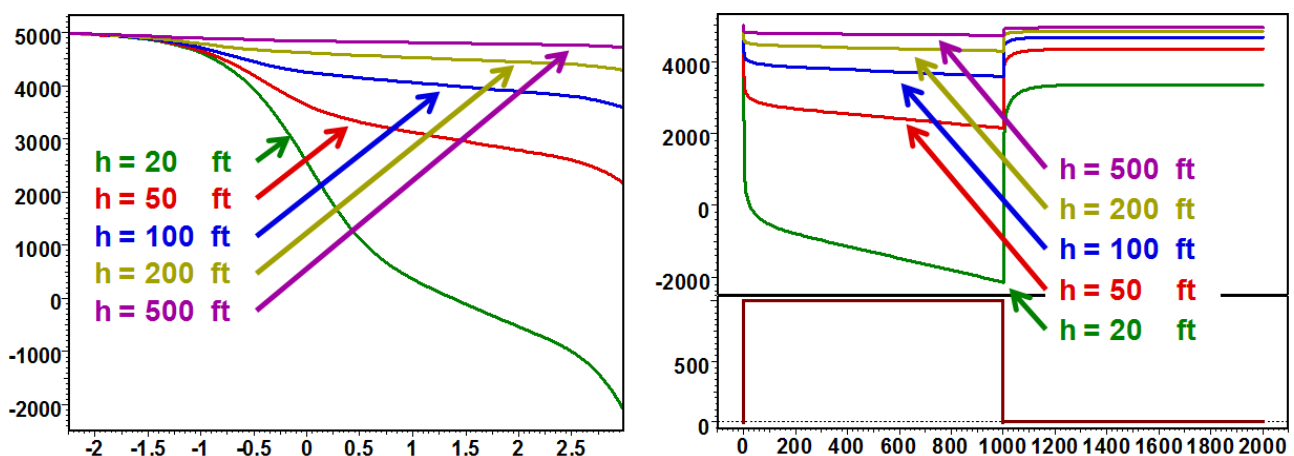


Fig. 2.H.20 – Effect of the reservoir thickness, semilog and history plot

2.H.3.f How about rates?

We are not referring to superposition effects, but to the plain value of the rate, i.e. the effect of a systematic error on the rate values and/or the formation volume factor B.

Fig. 2.H.22 below illustrates the response with all default parameters constant, but with a variable rate for each simulation. Values for q_B are 600, 800, 1000, 1200 and 1400 rb/d.

The result of varying q_B corresponds to a straight multiplication of the pressure change from p_i . The loglog response is shifted vertically, and the semilog and history plots are vertically compressed or expanded, the fixed point being the initial pressure.

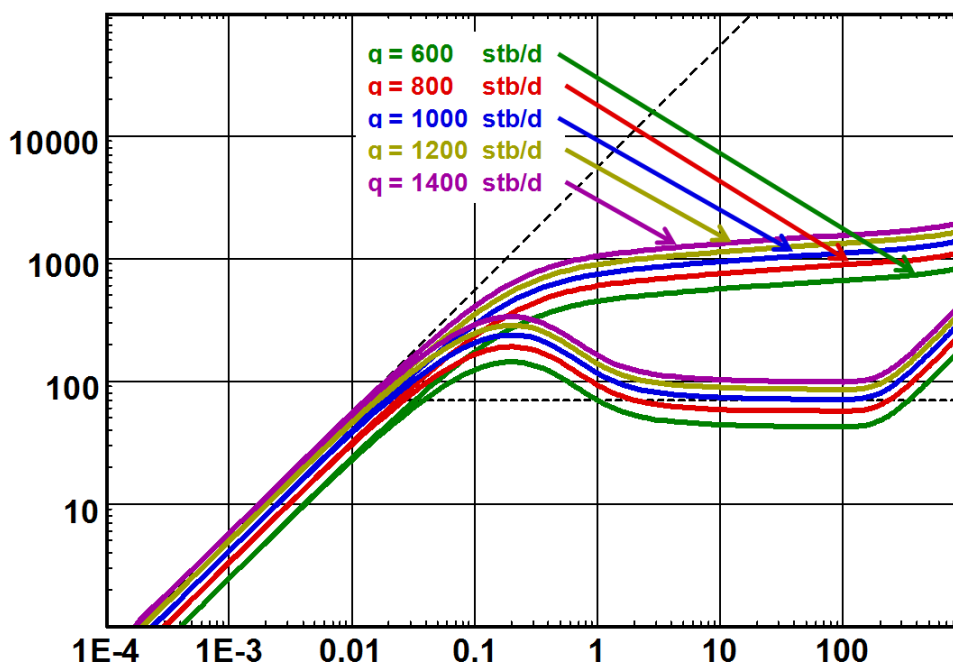


Fig. 2.H.21 – Effect of the rate– q_B , loglog plot

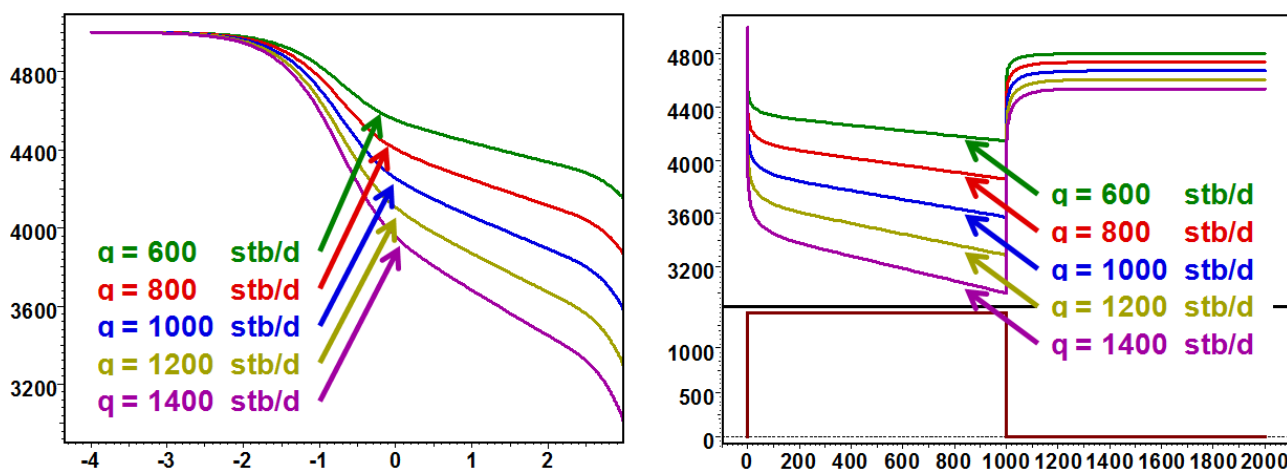


Fig. 2.H.22 – Effect of the rate– q_B , semilog and history plot

2.H.4 Conclusions

2.H.4.a on this series of designs

Beyond the arbitrary split between input and output parameters set in the methodology of Pressure Transient Analysis, we see that several groups of parameters govern the response of the well / reservoir system.

- Pure wellbore storage: The absolute position of the early time unit slope is only a function of the wellbore storage C.
- Transition from pure wellbore storage to IARF: The shape of the hump, which originally was set to $C_D e^{2.Skin}$ when dealing with type curves, is actually a function of C and $r_w e^{-Skin}$, and is also slightly affected by ϕ and c_t . The whole curve is translated along the unit slope as a function of k , μ and h , the governing group being kh/μ .
- IARF: The governing group is kh/μ defining the semilog slope, hence the level of the derivative stabilization when IARF is reached.
- There is a residual effect of r_w , $skin$, ϕ and c_t that defines the constant term of the IARF straight line. Generally the Skin factor is calculated from this constant term.
- At late time the parameters that govern the position of the PSS unit slope are r_e , ϕ , c_t and h . The governing group is $\phi.c_t.h.r_e^2$. You may actually prefer the group $2\pi.r_e^2.h.\phi.c_t$, and you get $V_{pore}.C_t$, where V_{pore} is the reservoir pore volume. What we arrived at here is nothing more than material balance.
- There is a residual effect of all factors that affected the transient diffusion before PSS was reached, and which constitute the constant term of the PSS straight line.

2.H.4.b on the equations

If we consider the IARF equation given in previous section:

$$p(t) = p_i - \frac{162.6qB\mu}{kh} \left[\log(t) + \log\left(\frac{k}{\Phi\mu c_t r_w^2}\right) - 3.228 + 0.8686.Skin \right]$$

...and if we re-shuffle it a bit, we get:

$$\Delta p(t) = \frac{162.6qB}{\frac{kh}{\mu}} \left[\log(t) + \log\left(\frac{kh}{\mu}\right) - \log(h\Phi c_t) - 3.228 - 2\log(r_w e^{-Skin}) \right]$$

One can see that the slope is a function of kh/μ , and that there is a constant term that shows, among other things, the residual effect of $r_w e^{-Skin}$, ϕ and c_t .

If we consider the PSS equation given previously:

$$p(t) = p_i - 0.234 \frac{qB}{\phi c_t h A} t - 141.2 \frac{qB\mu}{kh} \left[\frac{1}{2} \ln\left(\frac{A}{C_A r_w^2}\right) + 0.4045 + Skin \right]$$

...and if we re-shuffle it a bit again, without worrying about calculating a few constants, including the value of the shape factor for a circle, we get:

$$\Delta p(t) = a_1 qB \frac{t}{2\pi r_e^2 h \phi c_i} + a_2 qB \frac{a_3 + \ln(r_e^2) - \ln(r_w e^{-Skin})}{\frac{kh}{\mu}}$$

Or...

$$\Delta p(t) = a_1 qB \left[\frac{1}{V_{pore} c_i} t + f \left(r_w e^{-Skin}, \frac{kh}{\mu}, r_e \right) \right]$$

One can see that the slope is a function of the porous volume times the compressibility, while the constant term is a function of all the transients that happened before PSS occurred.

2.H.5 Effect of errors on the different input parameters

What we have seen so far is the sensitivity of a test / production design on the different parameters. In the case of a real analysis we will input the 'known' parameters, calculate the model response and vary the 'unknown' parameters until the model matches the measured response. This will 'calculate' the 'unknown' parameters.

What we will do now is consider that the truth is our reference case. From this reference case we will change one of the 'known' parameters to a wrong value, off by, say, 10%. Then optimize the model by varying the 'unknown' parameters to match the reference case and see how this affects these parameters (the results from Pressure Transient or Production Analyses).

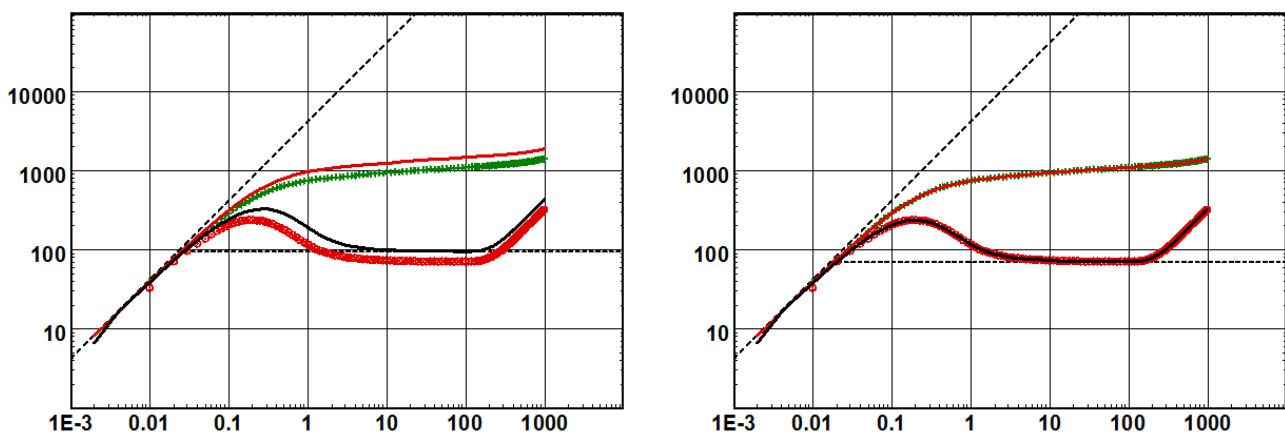


Fig. 2.H.23 – h at 25% below 'true' – Left plot is the model using all other 'exact' unknown
 Right plot is the match after optimization of the unknown parameters
 kh is OK – k is 33% above 'true' – r_e is 15% above 'true' – Skin at -0.14 instead of 0

The action here is fairly straightforward, so we will spare you the figures and only show you the results:

- **Well radius:** If we over-estimate r_w by 10%, the calculated skin will be over-estimated with a shift of 0.1. The general rule is that the false skin induced by this incorrect r_w will be in the ratio (r_{w_wrong}/r_{w_right}). All other parameters will be OK.
- **Porosity:** If we over-estimate ϕ by 10%, k and kh will be OK, there will be a marginal error on the skin, the reservoir size will be underestimated by 10%, and hence the boundary distances will be underestimated by 5%.
- **Compressibility:** Same as above. If we over-estimate c_t by 10%, k and kh will be correct, there will be a marginal error on the skin, however the reservoir size will be underestimated by 10%, hence the boundary distances will be underestimated by 5%.
- **Viscosity:** If we over-estimate μ by 10%, k and kh will be overestimated by 10%, there will be no error on skin and the reservoir size will be evaluated correctly.
- **Thickness:** If we over-estimate h by 10%, kh will be correct and k will be underestimated by 10%. There will be a marginal error in the skin, the reservoir size will be underestimated by 10%, and hence the boundary distances will be underestimated by 5%.
- **Rate:** If we over-estimate $q.B$ by 10%, C , $k.h$ and k will be overestimated by 10%. The reservoir size will also be overestimated by 10%, and hence the boundary distances will be overestimated by 5%. There will also be a minor skin difference.

This is summarized in the table below:

	Storage & Skin		Permeability		Boundary	
	C	Skin	k.h	k	Area	Distance
$r_w \uparrow 10\%$	-	$\uparrow 0.1$	-	-	-	-
$\phi \uparrow 10\%$	-	ε	-	-	$\downarrow 10\%$	$\downarrow 5\%$
$c_t \uparrow 10\%$	-	ε	-	-	$\downarrow 10\%$	$\downarrow 5\%$
$\mu \uparrow 10\%$	-	-	$\uparrow 10\%$	$\uparrow 10\%$	-	-
$h \uparrow 10\%$	-	ε	-	$\downarrow 10\%$	$\downarrow 10\%$	$\downarrow 5\%$
$q.B \uparrow 10\%$	$\uparrow 10\%$	ε	$\uparrow 10\%$	$\uparrow 10\%$	$\uparrow 10\%$	$\uparrow 5\%$

2.I The case of dry gas

2.I.1 The PVT of real dry gas

When the problem is no longer linear, the superposition of drawdown solutions is replaced by more complex semi-analytical models or numerical models. Superposition time functions may no longer be strictly valid, but they will be kept as diagnostic tools. Ultimately, only nonlinear numerical models will be strictly valid.

In some cases we can try to keep using the principle of superposition by substituting the pressure, and in some cases the time, with a function of the pressure that makes the equation a bit more linear. This is the case for the nonlinear diffusion of dry gas, where we will use what is called pseudopressure and pseudotime.

We have considered so far that the reservoir fluid was slightly compressible and that viscosity and compressibility were constant. This assumption is not valid for gases.

Regarding compressibility, the PVT relation is given by:

Ideal gas: $PV = nRT$

Real gas law: $PV = ZnRT$

The gas viscosity is also a function of pressure and temperature. The Z factor and viscosity may be input from tables at a given temperature or we may use correlations. The correlations for Z factor (Beggs & Brill, Dranchuk et al, Hall and Yarborough) and for viscosity (Lee et al, Carr et al) can also be matched using flash reference data. From the Z factor table / correlation, one can then calculate the volume factor and compressibility correlations.

The two figures below give a typical relation between Z and μ as a function of p at a given T:

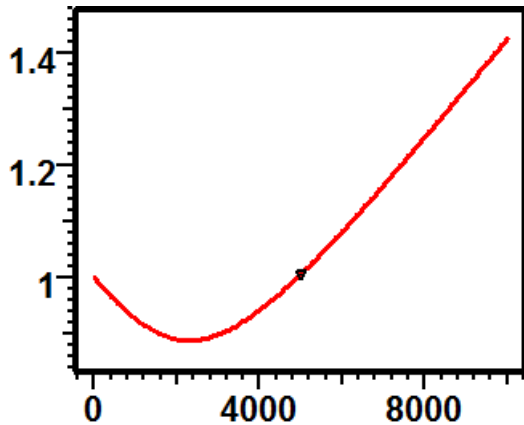


Fig. 2.I.1 – Z factor vs p [psia]

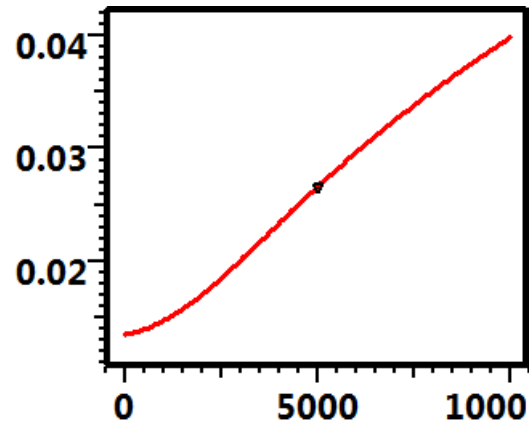
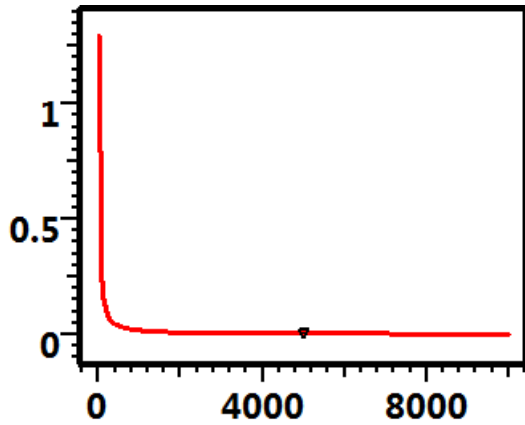
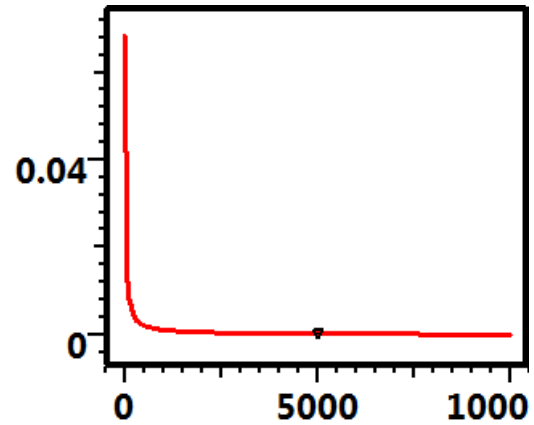


Fig. 2.I.2 – μ_g [cp] vs p [psia]

Volume factor and compressibility are then calculated from the Z factor:

Volume factor and compressibility: $B_g = \frac{Zp_{sc}T}{pT_{sc}}$ $c_g = -\frac{1}{B_g} \frac{dB_g}{dp} = \frac{1}{p} - \frac{1}{Z} \frac{dZ}{dp}$

Fig. 2.I.3 – B_g [SCF/RCF] vs p [psia]Fig. 2.I.4 – c_g [psi⁻¹] vs p [psia]

We could just use these PVT elements straight into a numerical simulator. However we would be short of diagnostic plots if we were just blindly simulating and matching.

The idea is to rearrange the equations by changing variables in a gas diffusion equation that looks like the slightly compressible fluid equation. If we do so we could extend the methodology and diagnostic plots developed for the linear process to the nonlinear process of gas diffusion. This is done by introducing pseudopressures.

2.1.2 Derivation of the real dry gas diffusion

We deviate from our initial derivation just before the slightly compressible fluid assumption:

Raw diffusion equation:
$$0.0002637k_x \frac{\partial}{\partial x} \left[\frac{\rho}{\mu} \frac{\partial p}{\partial x} \right] = \frac{\partial(\rho\phi)}{\partial t}$$

The real gas law gives:
$$PV = ZnRT \quad \text{where} \quad n = \frac{m}{M}$$

This gives the gas density:
$$\rho = \frac{m}{V} = \frac{M}{RT} \frac{p}{Z}$$

Diffusion equation becomes:
$$0.0002637k_x \frac{\partial}{\partial x} \left[\frac{M}{RT} \frac{p}{\mu Z} \frac{\partial p}{\partial x} \right] = \frac{\partial}{\partial t} \left[\frac{M}{RT} \frac{p}{Z} \phi \right]$$

Which simplifies to:
$$\frac{\partial}{\partial t} \left[\frac{p}{Z} \phi \right] = 0.0002637k_x \frac{\partial}{\partial x} \left[\frac{p}{\mu Z} \frac{\partial p}{\partial x} \right]$$

The first term develops as:
$$\frac{\partial}{\partial t} \left[\frac{p}{Z} \phi \right] = \phi \frac{p}{Z} \left[\frac{1}{\phi} \frac{\partial \phi}{\partial p} + \frac{Z}{p} \frac{\partial}{\partial p} \left(\frac{p}{Z} \right)_T \right] \frac{\partial p}{\partial t}$$

The gas compressibility is written:
$$c_g = \frac{1}{\rho} \left(\frac{\partial \rho}{\partial p} \right)_T = \frac{RTZ}{Mp} \frac{\partial}{\partial p} \left(\frac{Mp}{RTZ} \right)_T = \frac{Z}{p} \frac{\partial}{\partial p} \left(\frac{p}{Z} \right)_T$$

So:
$$\frac{\partial}{\partial t} \left[\frac{p}{Z} \phi \right] = \phi \frac{p}{Z} (c_f + c_g) \frac{\partial p}{\partial t} = \phi c_t \frac{p}{Z} \frac{\partial p}{\partial t}$$

And the diffusion equation becomes:

$$\phi c_t \frac{p}{Z} \frac{\partial p}{\partial t} = 0.0002637 k_x \frac{\partial}{\partial x} \left[\frac{p}{\mu Z} \frac{\partial p}{\partial x} \right]$$

Or:

$$\frac{p}{Z} \frac{\partial p}{\partial t} = 0.0002637 \frac{k_x}{\phi c_t} \frac{\partial}{\partial x} \left[\frac{p}{\mu Z} \frac{\partial p}{\partial x} \right]$$

We add the viscosity μ on both sides of the equation:

Gas diffusion equation:

$$\frac{p}{\mu Z} \frac{\partial p}{\partial t} = 0.0002637 \frac{k_x}{\phi \mu c_t} \frac{\partial}{\partial x} \left[\frac{p}{\mu Z} \frac{\partial p}{\partial x} \right]$$

We introduce the pseudopressure in order to eliminate the additional terms in the gas diffusion equation (there is an historic factor 2 in this equation):

Gas pseudopressure:

$$m(p) = 2 \int_0^p \frac{p}{\mu Z} dp$$

Taking the partial differential:

$$\frac{\partial m(p)}{\partial t} = \frac{\partial m(p)}{\partial p} \frac{\partial p}{\partial t} = \frac{2p}{\mu Z} \frac{\partial p}{\partial t}$$

And, the same way:

$$\frac{\partial m(p)}{\partial x} = \frac{\partial m(p)}{\partial p} \frac{\partial p}{\partial x} = \frac{2p}{\mu Z} \frac{\partial p}{\partial x}$$

The gas diffusion equation becomes:

$$\frac{\partial m(p)}{\partial t} = 0.0002637 \frac{k_x}{\phi \mu c_t} \frac{\partial^2 m(p)}{\partial x^2}$$

Extending to x, y, z directions:

$$\frac{\partial m(p)}{\partial t} = 0.0002637 \frac{k}{\Phi \mu c_t} \nabla^2 m(p)$$

We now arrive at the same formulation as the case of a slightly compressible fluid.

2.I.3 Diffusion of real dry gas

2.I.3.a Standard pseudopressures

In order to extend the methodology of Dynamic Data Analysis to gas cases, one introduces a function of the pressure called the pseudopressure. It is given by:

Gas pseudopressure:

$$m(p) = 2 \int_0^p \frac{p}{\mu Z} dp$$

The Field unit for pseudopressures is psi²/cp. A typical pseudopressure response as a function of pressure, and for a given temperature, is shown below. There is a rule of thumb regarding the behavior of this function:

- Below 2000 psia, μZ is fairly constant, and $m(p)$ behaves like p^2
- Above 3000 psia, μZ is fairly linear, and $m(p)$ behaves like p

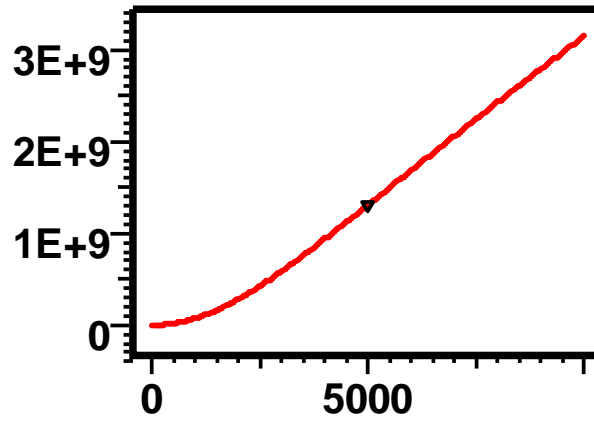


Fig. 2.I.5 – Pseudopressure vs. pressure

Gas diffusion equation:

$$\frac{\partial m(p)}{\partial t} = 0.0002637 \frac{k}{\Phi \mu c_t} \nabla^2 m(p)$$

The principle of traditional real gas analysis is to replace the pressure by the pseudopressure and interpret the data as if the fluid was slightly compressible.

However, there is an important shortcoming in this method. Although the equation looks the same, it will only be linear as long as we can consider the diffusion term $k/\phi\mu c_t$ constant. This is valid as long as the average reservoir pressure does not substantially decrease which is a reasonable assumption for a standard, relatively short, well test. In the case of extended tests such as limit tests and production well tests, this may not be the case.

2.I.3.b Normalized pseudopressures

The gas diffusion equation remains valid if we multiply the pseudopressures by a fixed number. Because the unit and orders of value of the standard pseudopressures are not intuitive, one possibility is to use normalized pseudopressures by selecting a reference pressure p_{ref} , with the condition:

Normalized pseudopressures:
$$m_{Norm}(p) = p_{ref} \frac{m(p)}{m(p_{ref})}$$

Normalized pseudopressure at:
$$p_{ref}: \quad m_{Norm}(p_{ref}) = p_{ref}$$

The normalized pseudopressures have the dimension and unit of the pressure, it follows the same diffusion equation and it coincides with the pressure at p_{ref} :

Normalized pseudopressures:
$$\frac{\partial m_{Norm}(p)}{\partial t} = 0.0002637 \frac{k}{\Phi \mu c_t} \nabla^2 m_{Norm}(p)$$

2.I.4 Non-Darcy flow

The diffusion equation used as the basis of the methodology in Dynamic Data Analysis is based on three components: the conservation of mass, a PVT equation and Darcy's law. We have seen above that the gas PVT required some adjustments in the equations and the method: pseudopressures, changing storage, material balance. In complement there are some cases, and especially for gas, where the assumption of Darcy flow is invalid. Sections of the reservoir, generally close to the well, will flow at such speed that turbulence will occur and have a strong impact on the well response. We now need to add a turbulence component to the flow equation, replacing Darcy's law by a second degree equation, such as Forchheimer's.

Darcy's law expressed in terms of speed, in SI units:

$$\frac{\partial P}{\partial x} = \frac{\mu}{k} \cdot u$$

Forchheimer's equation, same references and units:

$$\frac{\partial P}{\partial x} = \frac{\mu}{k} \cdot u + \beta \cdot \rho \cdot u^2$$

β is called the turbulence factor. There are two main options to address non-Darcy flow:

- The first is to focus on the impact of non-Darcy flow on the well productivity. This is what was done historically using rate dependent skin. Normal diffusion is used, but an additional, rate related skin component is added.
- The other way is to model non-Darcy flow by numerically integrating the Forchheimer equation in the model.

A diagram of the two options is shown in the figure below:

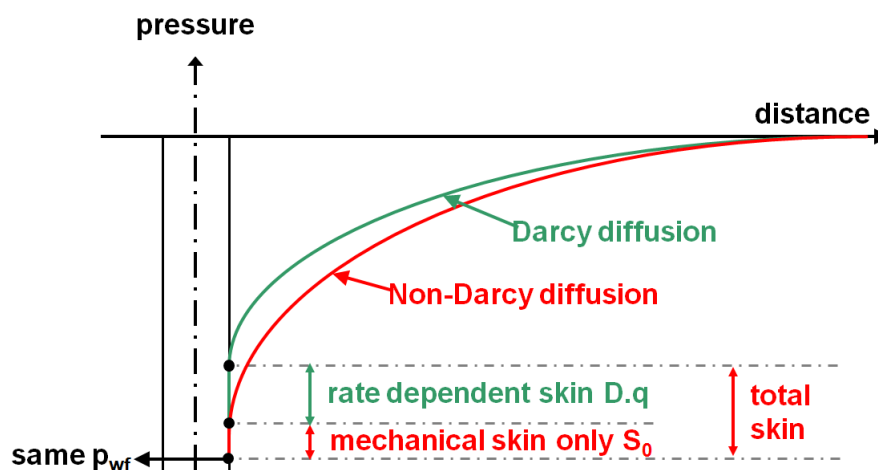


Fig. 2.I.6 – Two ways to model non-Darcy flow

The application of these two approaches is detailed in the chapter 'PTA General methodology' and in 'Production Analysis – The case of dry gas'.



3 – Pressure Transient Analysis

OH – OSF – DV



3.A Introduction

The following sections present the classical and modern methodology and tools developed for Pressure Transient Analysis (PTA). We will present the typical path recommended to perform an analysis and to design a test. The final sections are dedicated to operational considerations on well testing i.e. what data to gather and its validation

Twenty years ago PTA was still named 'Well Test Interpretation', as only well test operations could provide such data. In the last years well tests have been complemented and partially replaced by formation tests and any shut-in monitored by permanent downhole gauges, hence the new, more generic name.

Today's definition of PTA is less about the operation that produces the data than the processing applied to them. In PTA we gather pressures and rates, preferably downhole, and we focus on one or several periods of interest, generally shutins (buildup or falloff) to perform a diagnostic. The diagnostic leads to the choice of a model and this model is then used to simulate pressure values to be matched on the data. The model is then tried against a larger portion of the recorded data, if available. Part of the process involves matching the model parameters on the data by trying to achieve the best possible match, either by trial and error or using nonlinear regression.

The two major analysis methods described in this book are Pressure Transient Analysis (PTA) and Production Analysis (PA). Several key items differentiate the processing of PTA from PA:

- PTA is preferably on clean, shutin data, while PA uses the production data.
- As a consequence PTA data are cleaner, with a high capacity for diagnostics compared to PA, where one will typically match clouds of simulated and data points.
- PTA is performed over a relatively short period, hours / days / weeks rather than the months and years analysed in PA.
- In PTA we analyse pressure data using the rates as the corrective function. In PA it tends to be the opposite, where the input is the flowing pressure and the output is the rates and the cumulative production.

In the next two sections we will make a clear distinction between the traditional tools (the 'old stuff') and modern tools (the 'right stuff'). Traditional tools had their use in the past, and they are still in use today, but have become largely redundant in performing analysis with today's software. Modern tools are at the core of today's (2010) modern methodology, and they are of course on the default path of the processing.

3.B The old stuff

Twenty years ago, the core of well test interpretation was the dual use of specialized plots and type-curve matching:

- Specialized plots correspond to a selected scale where some flow regime of interest such as infinite acting radial flow, linear flow, bilinear flow, spherical flow or pseudo-steady state are characterized by a straight line. The slope and the intercept of this straight line will generally give two parameters of the system.
- Type-curve matching consists in sliding a plot of the data, generally on a loglog scale, on pre-printed type-curves. The relative position between the data and the type-curve, also called the time match and pressure match, provides two quantitative parameters. The choice of type-curve will give additional information.

We will start with the semilog plots, the main specialized plots used to quantify the main flow regime in PTA: Infinite Acting Radial Flow, or IARF.

3.B.1 IARF and Semilog plots

We have seen in Chapter 'Theory' that IARF is the main regime of interest in Pressure Transient Analysis. In the case of a production at a constant rate, IARF is characterized by linearity between the pressure change and the logarithm of time. We will see that such linearity is also found for more complex production history, provided that the right time function is used.

3.B.2 Drawdown response and MDH plot

In the case of a constant production from time 0 to infinity, the IARF is characterized, for a finite radius well in a homogeneous reservoir, by the equation:

$$\Delta p = \frac{162.6q\mu}{kh} \left[\log(\Delta t) + \log\left(\frac{k}{\Phi\mu c_t r_w^2}\right) - 3.228 + 0.8686S \right]$$

In the case of more complex well geometries and reservoir heterogeneities, the constant term may be more complicated, as it will integrate the cumulative effect of these geometries and heterogeneities. Still the response will have the same shape. The value of skin S calculated from the equation above may not be the right value in terms of well damage according to Darcy's law, but it will have some meaning. It is called the 'equivalent skin'.

The Miller-Dyes-Hutchinson (MDH) plot is a graph of the pressure or the pressure change as a function of the logarithm of time. IARF is characterized by a linearity of the response.

Drawing a straight line through these points gives a slope and an intercept:

IARF straight line:
$$Y = \frac{162.6qB\mu}{kh} \log(\Delta t) + b = m \log(\Delta t) + b$$

Where:
$$b = \Delta p_{LINE}(\log(\Delta t) = 0) = \Delta p_{LINE}(\Delta t = 1hr)$$

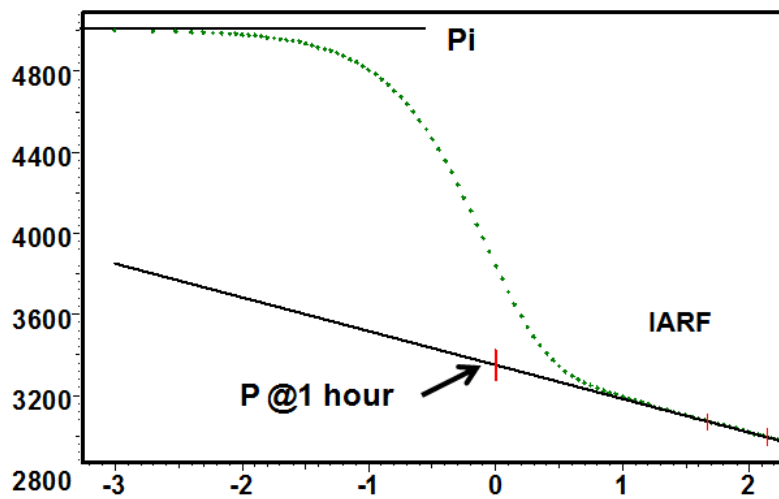


Fig. 3.B.1 – Drawdown MDH plot

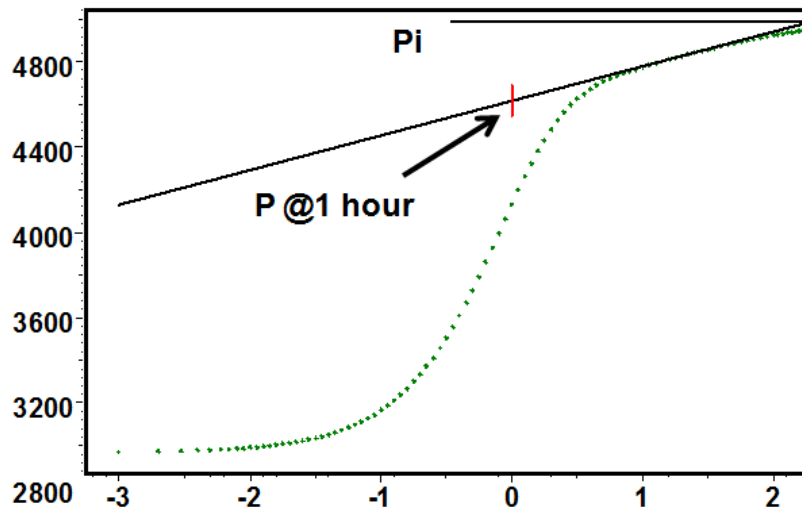


Fig. 3.B.2 – Buildup MDH plot

Important: The value of b corresponds to the value of Δp on the straight line, not on the data.

Permeability and the skin are then given by:

Permeability:
$$k = \frac{162.6qB\mu}{mh}$$

Skin factor:
$$S = 1.151 \left[\frac{\Delta p_{LINE}(\Delta t = 1hr)}{m} - \log \left(\frac{k}{\Phi \mu c_i r_w^2} \right) + 3.228 \right]$$

3.B.3 Build-up response and Horner plot

The MDH plot, with the simple $\log(\Delta t)$ time function, results directly from the log approximation to the drawdown solution for infinite-acting radial flow. In order to use semilog analysis for any flow period other than the first drawdown, it is necessary to take into account superposition effects.

How to get the Horner plot:

Build-up superposition: $\Delta p_{BU}(\Delta t) = \Delta p_{DD}(t_p) + \Delta p_{DD}(\Delta t) - \Delta p_{DD}(t_p + \Delta t)$

IARF approximation: $\Delta p_{DD}(X) = \frac{162.6qB\mu}{kh} \left[\log(X) + \log\left(\frac{k}{\Phi\mu c_t r_w^2}\right) - 3.228 + 0.8686S \right]$

If Δt is large enough to reach IARF, so will $t_p + \Delta t$. A lot of terms cancel out and we get:

Build-up superposition: $\Delta p_{BU}(\Delta t) = \frac{162.6qB\mu}{kh} \log\left(\frac{\Delta t}{t_p + \Delta t}\right) + \Delta p_{DD}(t_p)$

Rearranging: $\Delta p_{BU}(\Delta t) = \frac{162.6qB\mu}{kh} \log\left(\frac{t_p \Delta t}{t_p + \Delta t}\right) + \left[\Delta p_{DD}(t_p) - \frac{162.6q\mu}{kh} \log(t_p) \right]$

If the production time was too short, IARF was not reached during the flow period and $\Delta p_{DD}(t_p)$ cannot be turned into a log approximation. The constant term on the right of the equation becomes unknown. In this case, the analysis described below will give the permeability, but not the skin factor. If the production time was long enough, then the term t_p can also be turned into a logarithmic approximation and we get:

IARF at t_p : $\Delta p_{DD}(t_p) - \frac{162.6qB\mu}{kh} \log(t_p) = \frac{162.6qB\mu}{kh} \left[\log\left(\frac{k}{\Phi\mu c_t r_w^2}\right) - 3.228 + 0.8686S \right]$

So: $\Delta p_{BU}(\Delta t) = \frac{162.6qB\mu}{kh} \left[\log\left(\frac{t_p \Delta t}{t_p + \Delta t}\right) + \log\left(\frac{k}{\Phi\mu c_t r_w^2}\right) - 3.228 + 0.8686S \right]$

We introduce the Horner Time as: $\frac{t_p \Delta t}{t_p + \Delta t}$

Infinite-acting radial flow for a build-up is characterized by linearity between the pressure response and the logarithm of Horner time. Drawing a straight line through this point gives a slope and an intercept:

IARF straight line: $Y = \frac{162.6qB\mu}{kh} \log\left(\frac{t_p \Delta t}{t_p + \Delta t}\right) + b = m \log\left(\frac{t_p \Delta t}{t_p + \Delta t}\right) + b$

If the producing time t_p was long enough to reach IARF, the IARF approximation for a build-up will be similar to the drawdown relation, replacing time by Horner time, and will be given by:

IARF for a build-up: $\Delta p_{BU}(\Delta t) = \frac{162.6qB\mu}{kh} \left[\log\left(\frac{t_p \Delta t}{t_p + \Delta t}\right) + \log\left(\frac{k}{\Phi\mu c_t r_w^2}\right) - 3.228 + 0.8686S \right]$

After transformation, we get the equation of the Horner plot straight line in terms of pressure:

$$p_{BU} = p_i - \frac{162.6qB\mu}{kh} \log\left(\frac{t_p + \Delta t}{\Delta t}\right)$$

Permeability-thickness product and the skin are then calculated.

Permeability-thickness product: $k = \frac{162.6qB\mu}{mh}$

Skin factor if t_p is large enough: $S = 1.151 \left[\frac{p_{1hr} - p_{wf}}{m} + \log\left(\frac{t_p + 1}{t_p}\right) - \log\left(\frac{k}{\Phi\mu c_t r_w^2}\right) + 3.23 \right]$

Note that the time function is such that the data plots 'backwards', as when Δt is small, at the start of the build-up, the Horner function ($\log(t_p + \Delta t)/\Delta t$) will be large, and when Δt tends to infinite shut-in time the Horner time tends to 1, the log of which is 0.

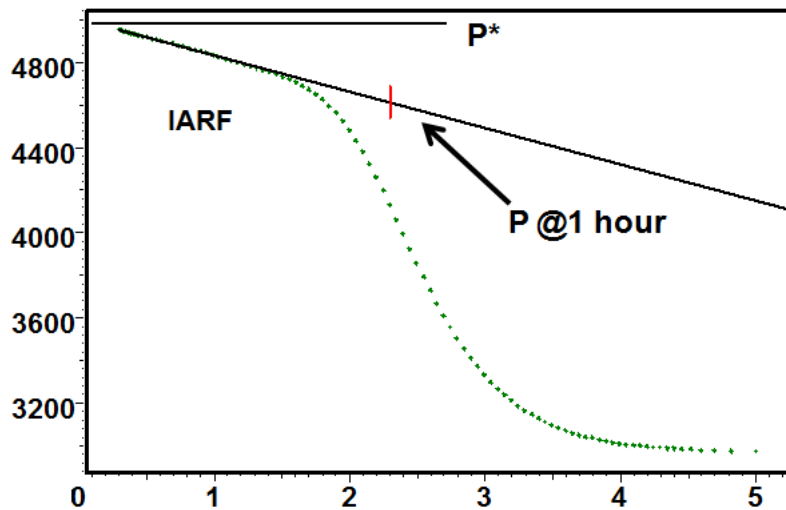


Fig. 3.B.3 – Horner plot

If the reservoir were truly infinite, the pressure would continue to build-up in infinite-acting radial flow and eventually intercept the y-axis at p_i , the initial pressure. However, as no reservoir is infinite, the extrapolation of the radial flow line at infinite shut-in time is called p^* , which is simply an extrapolated pressure.

If the reservoir is infinite: $p_i = p^*$

It is important to notice that the calculation of the permeability is valid even in the case of a short production before the shut-in, while the validity of the calculation of skin is conditioned to a producing time long enough, so IARF was reached before t_p .

3.B.4 Shut-in after a complex production and superposition plot

When a shut-in follows a complex production / injection history, the process is equivalent to that for a simple build-up, but the Horner time must be replaced by the superposition time function defined by:

$$S_n(\Delta t) = \sum_{i=1}^{n-1} \frac{q_i - q_{i-1}}{q_n - q_{n-1}} \log(t_n - t_i + \Delta t) + \log \Delta t$$

A plot of pressure versus superposition time is the 'general semi-log' plot:

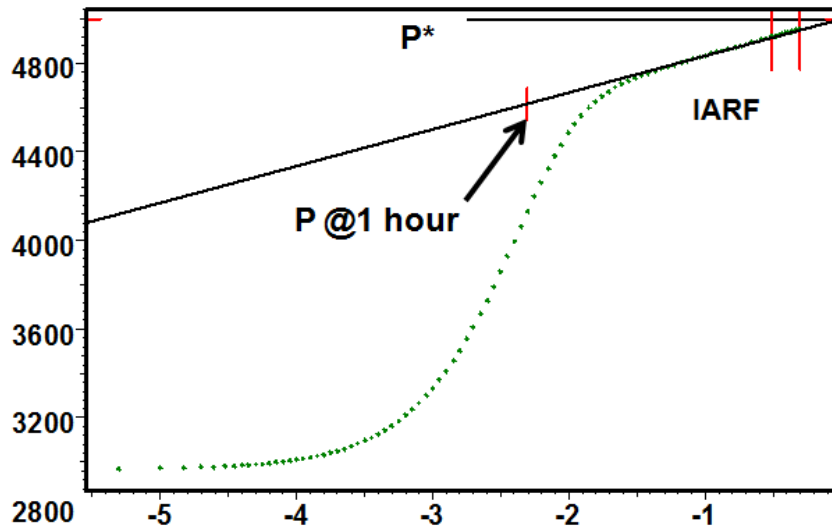


Fig. 3.B.4 – General semilog: superposition plot

Calculations of permeability is the same as for the Horner plot, and the skin factor is calculated by taking one point on the straight line, say (X,Y), and is given by:

$$S = 1.151 \left\{ \frac{Y - p_{wf}}{m} - X - \log \left(\frac{k}{\Phi \mu c_t r_w^2} \right) - \sum_{i=1}^n \left[\frac{q_i - q_{i-1}}{q_n - q_{n-i}} \log(t_{n+1} - t_i) \right] + 3.23 \right\}$$

3.B.5 Complex productions and rate normalized superposition plot

In some cases the engineer will want to interpret producing periods when the rate is not stabilized, or the rates data will be sandface rate, and therefore the value of the rate will not instantaneously go down to zero during the shut-in period. These cases are a little more complex than the cases above. However the principle of the semi-log analyses will be kept with the following modifications:

For a multi-rate production or injection (whether rates are measured at surface or downhole), the adequate semi-log plot will still have the same superposition time as the X axis, but the pressure will be replaced by:

$$\frac{Q}{q(t)}[p_i - p(t)]$$

Where Q is a reference value for normalization, that will be generally chosen to be the last stabilized rate of the interpreted period so that the function tends to Δp at late time.

For a multi-rate build-up or fall-off using sandface rates, the Y axis will still be

$$p(t) - p_{wf}$$

but the calculation of the superposition time will allow rates to be changed during the period. Furthermore the reference rate will not be the difference of rates before N and N-1 (this has no meaning when dealing with continuous downhole rate measurements), but the last stabilized rate before shut-in.

Loglog type-curves Type-curve matching originally consisted in plotting a loglog plot of the pressure response versus time on tracing paper that could then be slid over a set of pre-printed type-curves, the log cycles being square and of the same size in both plots. The selection of the type-curve matching the data can provide one or several parameters, and the relative positions of the two plots in the X and Y direction, also called the match point, will give two other interpretation results.

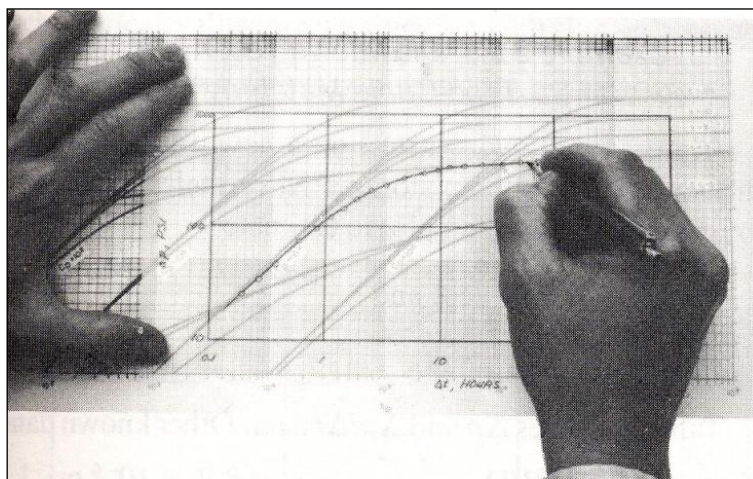


Fig. 3.B.5 – Type-curve matching

The type-curve used for wellbore storage and skin in an infinite homogeneous reservoir (in the following Figure), the pressure match (relative positions in the Y direction) will give the permeability. The time match (relative positions in the X direction) will give the wellbore storage, and the selection of the curve will give the skin factor.

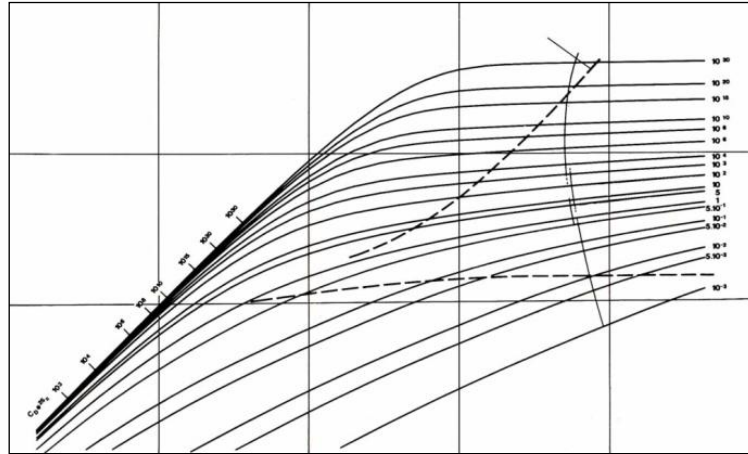


Fig. 3.B.6 – Wellbore storage and skin type-curve

The origin of type-curves

We have seen in Chapter 'Theory' that diffusion problems were solved by replacing the real variables by dimensionless variables that eliminate other parameters influence in order to arrive at a set of equations that are solved, hopefully quite simply and once and for all, in dimensionless space. Two critical variables are the dimensionless time and dimensionless pressure.

Dimensionless time:
$$t_D = 0.0002637 \frac{k}{\Phi \mu c_i r_w^2} \Delta t = A \Delta t \text{ where } A = f(k, \mu, r_w, \dots)$$

Dimensionless pressure:
$$p_D = \frac{kh}{141.2qB\mu} \Delta p = B \Delta p \text{ where } B = g(k, h, \mu, \dots)$$

This is still used today in modern software to generate analytical models. The solution is solved in dimensionless space, then the variables are converted to real variables and superposition is applied to the solution, and then matched with the real data.

However, this was not possible, or at least not easy, before personal computers and related software were available. So the 'trick' was to use a simple and remarkable property of the logarithmic scales, historically used to create slide rules. Taking the logarithm of the equations above we would get:

Logarithmic relations:
$$\log(t_D) = \log(\Delta t) + \log(A)$$

and
$$\log(p_D) = \log(\Delta p) + \log(B)$$

In other words, the dimensionless response, also called a type-curve, and the real response, taken on a loglog scale, have the same shape. By translation, it is possible to match the data on the dimensionless response and this is called a type-curve match. The value of the translation, also called match point, in the X direction (the time match) and in the Y direction (the pressure match) will give A and B, which in turn provides two quantitative pieces of information. The time match will give different, model dependent, information. The pressure match will typically give the permeability-thickness product.

3.B.6 Other specialized plots

Infinite Acting Radial flow is the most important but not the only flow regime characterized by linearity of the pressure response when plotted versus the right time scale. Different flow regimes require a specific plot of pressure versus the appropriate time scale to quantify parameters specific to the flow regime.

The main flow regimes are:

Regime	Model	Linearity vs
Infinite Acting Radial Flow	Homogeneous Infinite	logarithm of time
Pseudo-Steady State	Closed systems	time
Pure wellbore storage	Wells with storage	time
Spherical flow	Limited Entry wells	inverse of square root of time
Bilinear flow	Fractures with Finite Conductivity	fourth root of time
Linear flow	Fractures	square root of time
Linear flow	Channel shaped reservoirs	square root of time
Semi-linear flow	U-shaped reservoirs	square root of time
Semi-radial flow	Sealing fault	logarithm of time
Partial radial flow	Intersecting fault	logarithm of time
Early time IARF	Horizontal well	logarithm of time
Linear flow	Horizontal well	square root of time

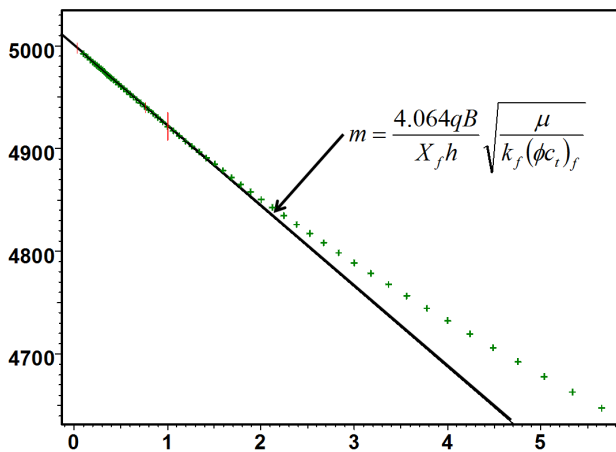


Fig. 3.B.7 – Square root plot

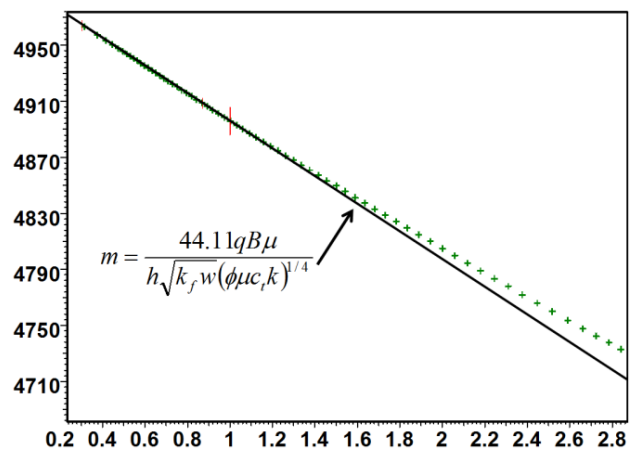


Fig. 3.B.8 – Fourth root plot

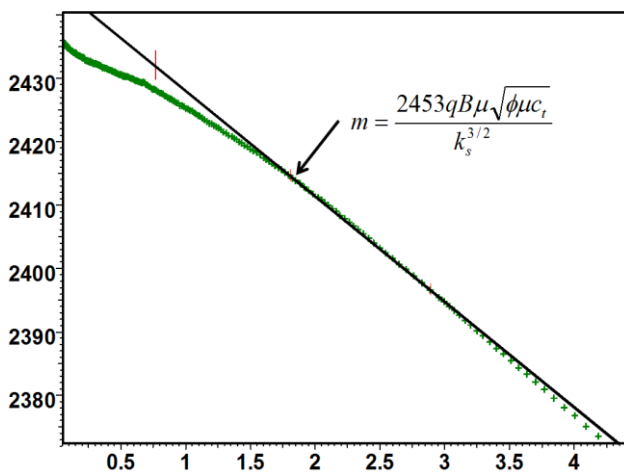


Fig. 3.B.9 – One over square root of time plot

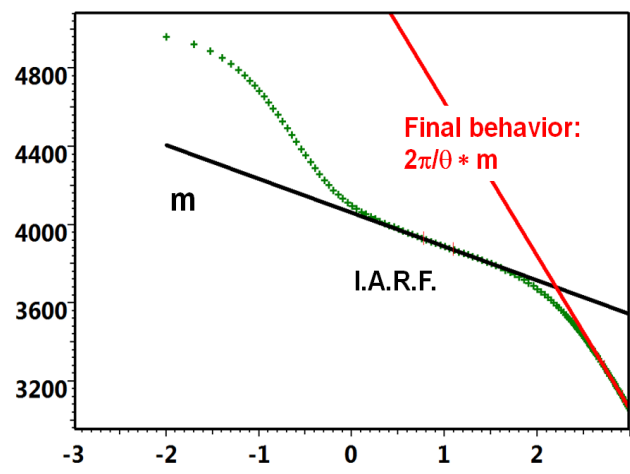


Fig. 3.B.10 – MDH plot for intersecting faults

3.B.7 IPR & AOF

A common measure of the performance of any gas, or oil, well is its ability to deliver against atmospheric pressure. It is certainly unrealistic if we consider the bottom hole pressure; however this measurement provides an input value for IPR calculations, and it is an accepted 'universal indicator' for gas wells. It is called the 'Absolute Open Flow' potential of the well. The concept of AOF is more useful if one uses wellhead instead of bottomhole pressures, as this indicates now the maximum achievable flowrate.

In order to evaluate the AOF, the well is tested at multiple rates. The bottom hole pressure is measured during each drawdown and buildup. These data are plotted on the adequate plot in order to deduce the leading parameters values for the equations governing the rate and the stabilized flowing pressure relationship. The most classical plot is $\Delta m(p)$.vs q , on a log-log scale, leading to the C and n parameters values of the Rawlings and Schellhardt equation:

$$Q = C(m(\bar{p}) - m(p_{wf}))^n$$

The same equation is used to describe the Inflow Performance Relationship and to create the very useful IPR plot $m(p_{wf})$ versus q .

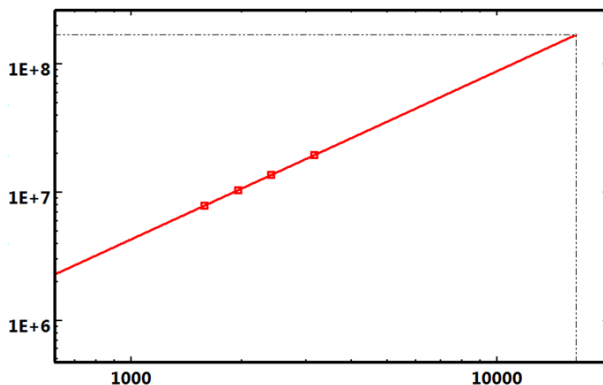


Fig. 3.B.11 – AOFP plot

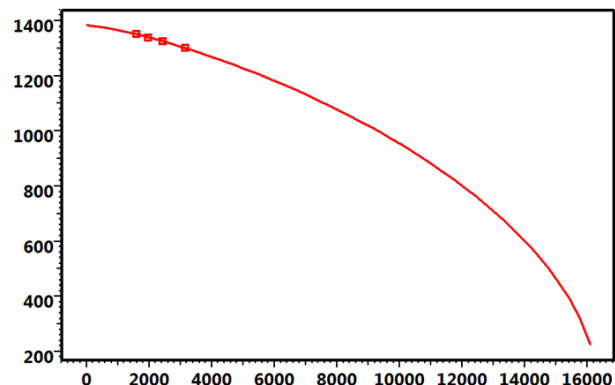


Fig. 3.B.12 – IPR plot

The AOF is obtained by extrapolating the deliverability curve to a $\Delta m(p)$ value corresponding to a flowing bottom hole pressure of 14.7 psi.

Cullender and Katz improved later the method in order to reduce the well test duration by using short and non stabilized flow period data. The various well test types and IPR and AOF methods are detailed in the chapter on Well Performance Analysis.

3.C The 'right' stuff

To speak about 'right stuff' vs. 'old stuff' is deliberately provocative. Old stuff is not always wrong. Old stuff was smartly developed to adapt to what we had before modern PC's: slide rules, graph paper, basic calculators, programmable calculators, etc. Old stuff has been of great benefit to the industry and was on the critical path to get the modern tools we have today.

What is sometimes wrong is to continue using old techniques that are less accurate than more recent developments. What is definitely wrong is to continue using such tools today, simply out of inertia, while everybody knows that their limitations are successfully addressed by more modern techniques. What is near criminal is using the good old stuff to address completely new problems that were never encountered when this good old stuff was developed.

Simpler is better when simple is right.

3.C.1 Before the Bourdet Derivative

Until 1983, PTA methodology was a manual process alternating type-curve matching and specialized analyses. Type-curves without derivative had poor diagnostic capabilities. The results from specialized plots would help position the data on the type-curve.

For example, drawing the IARF straight line on the Horner plot would give a permeability that could be used to set the pressure match on the type-curve. Selecting a type-curve would give the approximate time of start of IARF, which in turn would help define the Horner plot line. For gas we would complement this with AOF / IPR analyses.

The shortcomings of this methodology were numerous:

- Type-curves with pressure only had very poor resolution on a loglog scale.
- Type-curves were generally printed for drawdown responses, and ruined by superposition.
- Type-curves were set for a discrete number of parameter values.
- Specialized plots required a pure flow regime that may never have been established.
- Skin calculation on the Horner plot required that IARF was reached during the drawdown.
- Drawing a straight line through the two last pressure points was a common practice.
- The process required moving back and forth between at least two or more different plots.

To most engineers the replacement of manual techniques by computer based analysis in their day-to-day work occurred in the 1980s, and came from three major breakthroughs:

- Electronic downhole pressure gauges, either run with memory or on electric line, became cheap and reliable, detecting repeatable behaviors far beyond what the previous generation of mechanical gauges could offer.
- The spread of Personal Computers allowed the development of PC-based pressure transient analysis software. The first PC based programs appeared in the 1980's, initially reproducing the manual methods on a computer. Since then, new generations of tools have been developed, with modern methodology at its core.
- The Bourdet derivative is certainly the single most important breakthrough in the history of Pressure Transient Analysis. It is still today (2010) the cornerstone of modern technology.

Let us start with the Bourdet derivative...

3.C.2 Definition of the Bourdet Derivative

As any breakthrough idea, the principle of the Bourdet derivative is very simple:

The Bourdet Derivative is the slope of the semilog plot displayed on the loglog plot...

... to be more accurate, it is the slope of this semilog plot when the time scale is the natural log. It has to be multiplied by $\ln(10)=2.31$ when the decimal logarithm is used in the semilog plot. The semilog plot is not 'any' semilog plot (MDH, Horner, etc). To be correct the reference logarithmic time scale must be the superposition time.

$$\text{For the first drawdown: } \Delta p' = \frac{d\Delta p}{d \ln(\Delta t)} = \Delta t \frac{d\Delta p}{d\Delta t}$$

$$\text{In the more general multirate case, and in particular for shut-ins: } \Delta p' = \frac{d\Delta p}{d \sup(\Delta t)}$$

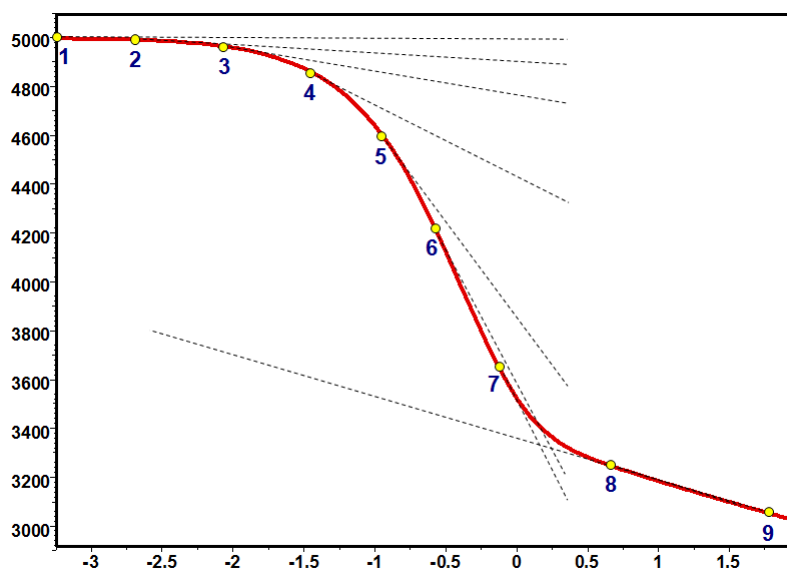


Fig. 3.C.1 – Bourdet derivative, semilog plot

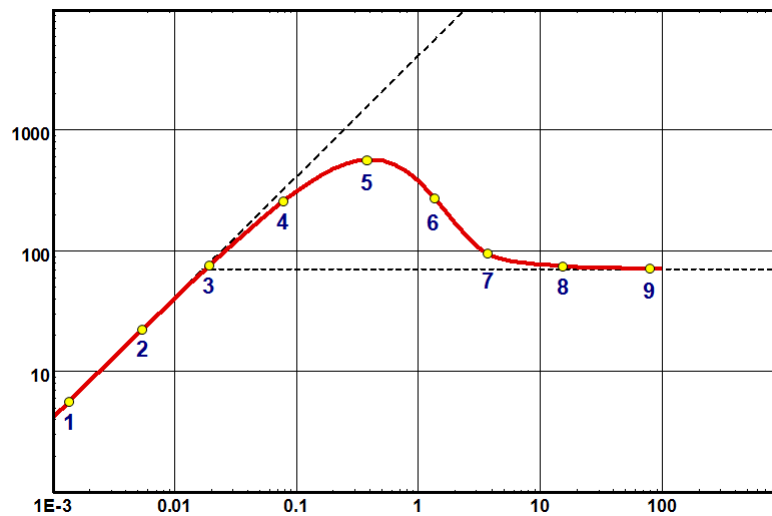


Fig. 3.C.2 – Bourdet derivative, loglog plot

3.C.3 Bourdet Derivative & Infinite Acting Radial Flow (IARF)

When IARF occurs we have the approximation: $\Delta p = m' \text{sup}(\Delta t)$

Where m' is the slope of the semilog straight line. In the following the drawdown response is a specific case of the multirate response, and the logarithm of time is the specific superposition time for a drawdown. The derivative is therefore:

Derivative when IARF has been reached:
$$\Delta p' = \frac{d\Delta p}{d \text{sup}(\Delta t)} = m'$$

When IARF is reached, the derivative stabilized to a level equal to the slope of the semilog straight line. This property was the main reason for the development of the derivative, as it is easy and straight forward to identify IARF on the loglog plot, something which is virtually impossible on the semilog plot. One can say that the derivative is a 'magnifying glass' of the semilog behavior, conveniently placed on the same plot, used historically for type-curve matching.

Combined with the early time unit slope during wellbore storage, the derivative provides an immediate way to define the pressure and the time match on the loglog plot, just by positioning a unit slope line on the wellbore storage regime and positioning the horizontal line on the IARF response.

This alone would have made the Bourdet derivative a key diagnostic tool. The delightful surprise was that the derivative could do much more, and that most well, reservoir and boundary models carry a specific signature on the derivative response. It is this remarkable combination that allowed the derivative to become **THE** diagnostic and matching tool in Pressure Transient Analysis.

3.C.4 Bourdet Derivative & Wellbore Storage

Pure wellbore storage effects are only observed at very early time when the well pressure behavior is dominated by the well fluid decompression or compression.

In case of pure wellbore storage: $\Delta p = C\Delta t$

Even for multirate solutions at early time: $\sup(\Delta t) \approx \ln(\Delta t)$

The derivative is therefore: $\Delta p' = \Delta t \frac{dC\Delta t}{d\Delta t} = C\Delta t = \Delta p$

At early time, when pure wellbore storage is present, pressure and the Bourdet derivative curves will merge on a unit slope straight line on the loglog plot.

Other early time flow regimes, such as linear and bilinear flow, covered in more detail later, will exhibit a different and specific behavior for both pressure and the Bourdet derivative.

3.C.5 The original idea behind the Bourdet Derivative

The simplest and most frequently used analytical model in Pressure Transient Analysis is the case of a vertical well, with wellbore storage and skin, producing a homogeneous reservoir of infinite extent. This 'new' formulation of the derivative by Bourdet et al. was solving at once this case, on a single loglog plot, and in a very accurate way:

When plotting the pressure and the Bourdet derivative on a loglog scale, at 'late time' the derivative would stabilize, and the stabilization level would define the type-curve pressure match (hence the permeability) in a unique way. The only possible movement then would be left and right to define the time match.

At early time the Pressure and the Bourdet derivative would merge on a single unit slope, that was also found on the type-curves, hence providing a unique value of this time match, and an instant calculation of the wellbore storage.

Luckily enough, the shape of the derivative (drawdown) type-curve and the Bourdet derivative of the data (multirate) was seldom affected by the superposition, unlike the pressure data, so it was reasonably valid to match the data derivative with the type-curve derivative, hence getting a unique identifier of the type-curve (generally $C_D e^{2S}$), which in turn would give the value of Skin.

So, on a single action, a type-curve using the Bourdet derivative would provide the definitive answer on a single, accurate diagnostic plot.

This was already brilliant, but it turned out that the Bourdet derivative could bring much more for all type of models, whether by identification of other flow regimes or by the signature that the Bourdet derivative would carry for such or such model...

3.C.6 Bourdet Derivative & other flow regimes

We are not going to describe exhaustively the list of flow regimes that can be successfully identified using the Bourdet derivative. The short answer is: 'a lot'. The table below shows a list of the most frequently used flow regimes in PTA, together with the chapter of the DDA book where this will be covered in more details:

Model	Regime	Δp slope	$\Delta p'$ slope	DDA chapter
Storage	Storage	1	1	Wellbore
Fracture	Linear	0.5	0.5	Well
Fracture	Bilinear	0.25	0.25	Well
Limited Entry	Spherical	-	-0.5	Well
Homogeneous	IARF	-	0	Reservoir
Channels	Linear	0.5 (late)	0.5	Boundary
Closed	PSS	1 (late)	1	Boundary

As an appetizer, below is a loglog plot of some of these flow regimes:

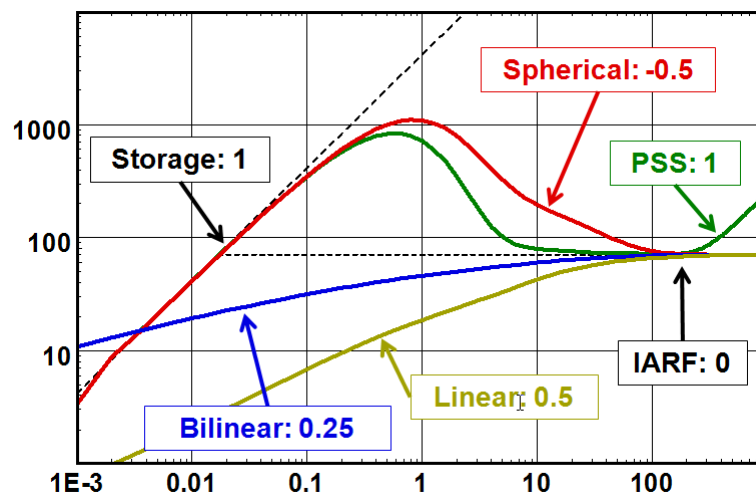


Fig. 3.C.3 – Bourdet Derivative and various flow regimes

3.C.7 Bourdet Derivative & Other models

The use of the Bourdet derivative does not stop with flow regimes. The Bourdet derivative can display the signature of numerous well, reservoir and boundary behaviors. Again the loglog plot below shows some typical behaviors detected from the observation of the Bourdet derivative.

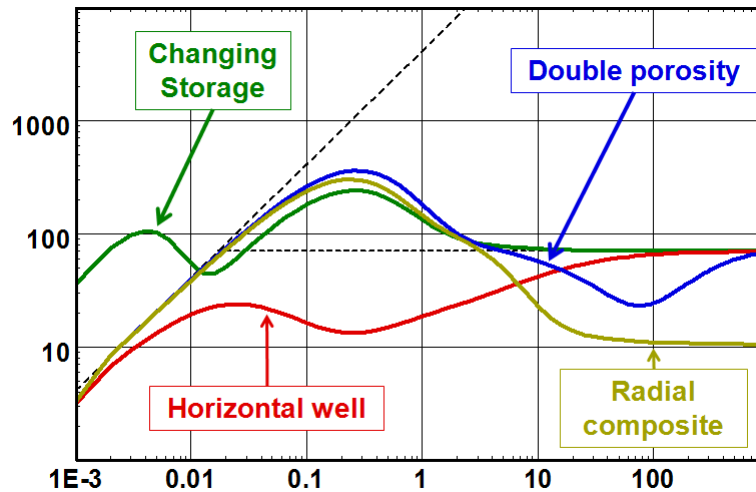


Fig. 3.C.4 – Bourdet derivate and other models

3.C.8 Modeling

The actual measured data is matched to a full model response selected by the interpreter from the identified flow regimes, including the appropriate well and boundary models and the actual production history.

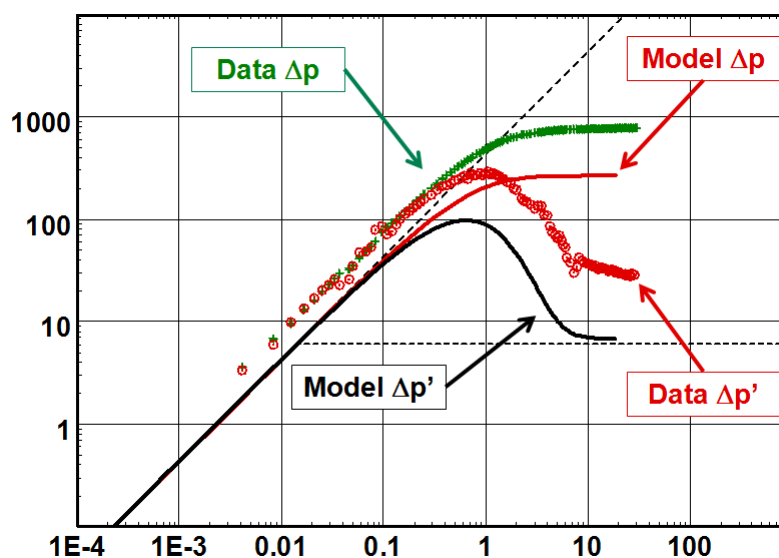


Fig. 3.C.5 – Modeling

3.D The use of modern deconvolution

Deconvolution in Pressure Transient Analysis has been the subject of numerous publications. Deconvolution could tentatively be used (1) to remove wellbore storage effects in order to get to IARF earlier, (2) to turn a complex noisy production history into an ideal drawdown ready for interpretation, (3) to explore boundaries not detected by individual build-ups.

Despite the good hard work done on the subject, true deconvolution is fundamentally unstable. To add stability into the deconvolution process one has to make assumptions that bias the response. Until recently, when a new paper was published on the subject, the natural question would not be “does it work?” but rather “where’s the trick?”.

This is no longer the case. A set of publications, initiated by Imperial College and complemented by bp (e.g. SPE #77688 and SPE #84290), offer a method that actually works, especially, although not exclusively, to identify boundaries from a series of consecutive build-ups. There is a trick, and there are caveats, but the trick is acceptable and the method can be a useful complement to PTA methodology.

Saphir offered on October 2006 the first commercially available version of this method. It was since improved by adding additional methods and it is now a totally recognized and helpful method, able to provide additional information, unseen through other techniques.

3.D.1 What is deconvolution? Why do we need it?

3.D.1.a The need

Analytical models are developed assuming a perfectly constant production as drawdown type-curves. In reality a well test, or a well production, is anything but constant. Rates vary in time, and the producing responses are generally so noisy that we usually focus on shut-in periods only.

In the simulated example shown on the plot below, the total production history is 3,200 hours, and the build-up is only 100 hours long. What we see on the loglog plot corresponds to only 100 hours of diffusion. We use the superposition of the rate history in the derivative calculation, but this is only to correct superposition effects; we really only see 100 hours of diffusion.

But there is more than 100 hours of information in the total response. Pressure has been diffusing for 3,200 hours, some locations far beyond the radius of 100 hours of investigation have felt the effect of the production and this information has bounced back to the well. So there is more information somewhere in the data, but not in the build-up alone.

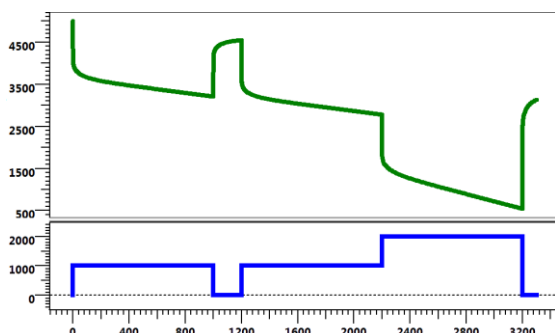


Fig. 3.D.1 – History: $p_w(t)$ & rates

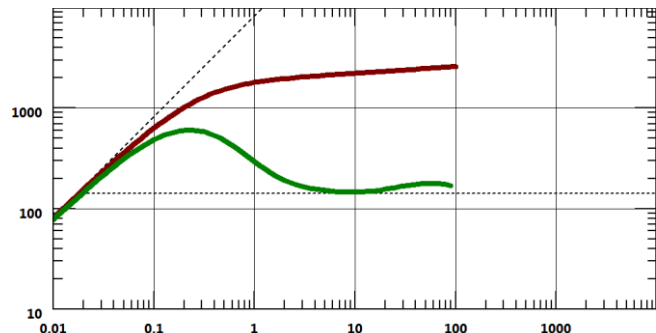


Fig. 3.D.2 – Build-up: $\Delta p_w(t)$ & $\Delta p'_w(t)$

The idea behind deconvolution is, in this example, to recreate from the real data, the ideal pressure response to a constant production over the same period (see below). If such a response was created, we could extract a loglog response of 3,200 hours duration, and the virtual data extracted this way would show much more of the reservoir than the 100 hour build-up could possibly reveal alone.

In other words, if we extract the deconvolved data from the real pressure response without assumptions, we will be able to get a much longer response, or the same response for a much shorter test.

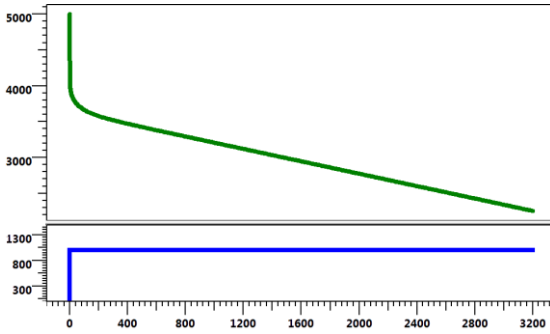


Fig. 3.D.3 – Deconvolution: $p_u(t)$

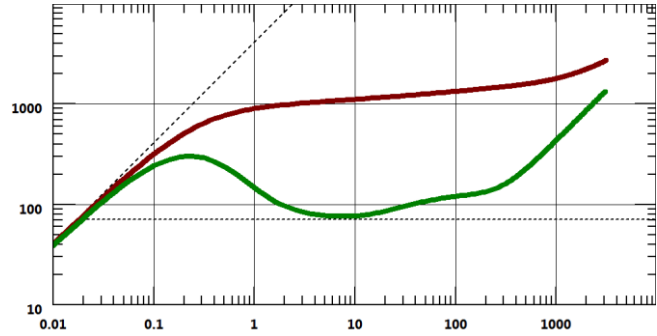


Fig. 3.D.4 – Deconvolution: $\Delta p_u(\Delta t)$ & $\Delta p'_u(\Delta t)$

In theory we may not even need to shut the well in. With deconvolution we would make a stepwise construction of an ideal constant pressure response and be able to perform a Pressure Transient Analysis whenever we have some rates and pressures recorded at the same time. One of the Holy Grails of transient analysis has been found?

3.D.1.b Mathematical formulation

Before looking at deconvolution, we need to know a little about what constitutes convolution. The mathematical definition of the convolution of two real functions is:

$$[f \otimes g](t) = \int_0^t f(\tau)g(t-\tau)d\tau$$

Convolution is what we do when we apply the principle of superposition (see Chapter 2) in order to get the pressure response $\Delta p(t)$ for a complex rate history $q(t)$ knowing the ideal pressure drop $\Delta p_u(t)$ for a constant, unit production. We have:

$$\Delta p_w(t) = \int_0^t q(\tau) \frac{\partial \Delta p_u(t-\tau)}{\partial (t-\tau)} d\tau = \int_0^t q(\tau) \Delta p'_u(t-\tau) d\tau$$

Where

$$\Delta p'_u(t) = \frac{\partial \Delta p_u}{\partial t}$$

In other words:

$$\Delta p = q \otimes \Delta p'_u = q' \otimes \Delta p_u$$

Note that, when the rate history is a step function, the calculation of this integral will bring the 'usual' superposition equation, seen in Chapter 2:

$$p(t) = p_i - \sum_{i=1}^n (q_i - q_{i-1}) \Delta p_u(t-t_i)$$

What we know from the test data is the pressure response $\Delta p(t)$ and the rate history $q(t)$. What we are interested in is $\Delta p_u(\Delta t)$, the ideal response for a constant production. The process of getting a convolution component (Δp_u) from one convolution component (q) and the convolution product (Δp) is called deconvolution.

We will not get into the details of the past work on deconvolution. There was what we call 'blind' deconvolution, i.e. a stepwise 'de-superposition' of the pressure data assuming nothing. This is an unstable and divergent process. There was also 'constrained deconvolution', such as moving to Laplace space and dividing the Laplace pressure response by the Laplace rate history. The weak point was generally in the assumptions made. Other deconvolution targets were more limited, such as getting an early IARF response by deconvolving the early time build-up with the 'assumed' downhole rates corrected by wellbore storage. However all these attempts had limited success. Deconvolution was considered a nice but unrealistic idea.

However, a new approach has recently been developed by Imperial College and bp. This approach has generated much enthusiasm, and although it is valid and useful, it is most important to bear in mind the assumptions and the limitations, as there are, indeed, some. It is based on a change of variable corresponding to what we really look for, ie the derivative on a loglog scale.

We define $\sigma = \ln(\Delta t)$ and $z(\sigma) = \ln \left[\frac{dp_u(\Delta t)}{d \ln(\Delta t)} \right] = \ln \left[\frac{dp_u(\sigma)}{d\sigma} \right]$

With this change of variable, the convolution equation becomes:

$$p(t) = p_i - \int_{-\infty}^{\ln t} q(t - e^\sigma) e^{z(\sigma)} d\sigma$$

3.D.2 Deconvolution Method 1 (von Schroeter et al., 2004)

This method was initially presented by von Schroeter et al. (Imperial College) in 2004. The suggested reference SPE Paper is #77688.

3.D.2.a Problem unknowns

Instead of looking numerically for the pressure response for a unit rate $\Delta p_u(\Delta t)$, we change the unknown and consider the response upon which we will base our diagnostic. i.e. the logarithm of the pressure derivative response as a function of the logarithm of time:

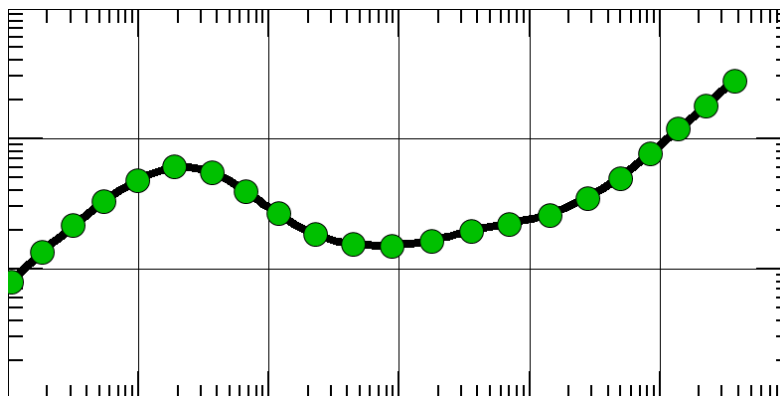


Fig. 3.D.5 – 1st (and main) unknown: $z(\sigma)$

$$\sigma = \ln(\Delta t) \quad \text{and} \quad z(\sigma) = \ln \left[\frac{dp_u(\Delta t)}{d \ln(\Delta t)} \right] = \ln \left[\frac{dp_u(\sigma)}{d\sigma} \right]$$

The principle of the new deconvolution method is to find the derivative curve $z(\sigma)$ which, using a modified convolution expression, will match the data. The curve $z(\sigma)$ is defined as a polyline or a spline. It has an initial point, as (0,0) makes no sense on a loglog scale. Its time range is the elapsed time between the beginning of the production history and the last data point we will try to match (3,200 hr in the previous example).

The curve $z(\sigma)$ is the main unknown. There are two additional sets of optional unknowns: the first is the initial pressure p_i , which may or may not be known. The last unknown is a tolerance to errors in the rate history, which we need to introduce for the optimization process to converge.

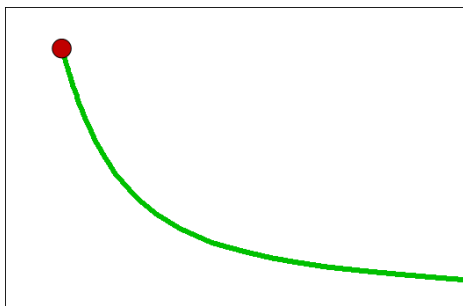


Fig. 3.D.6 – 2nd unknown: p_i

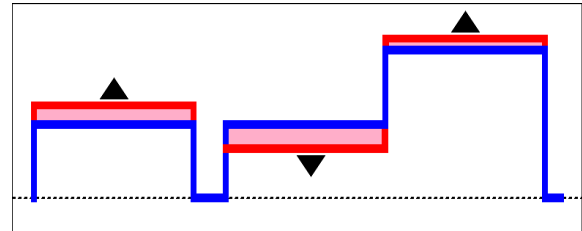


Fig. 3.D.7 – 3rd unknown: Δq 's

3.D.2.b Problem objective function

The three unknowns above are adjusted, in a nonlinear regression process, to minimize an objective function. This objective function has three components.

Naturally, the first and main component of the objective function we want to minimize is the standard deviation between the convolved model and the pressure data (Fig. 3.D.8 below). This may be all pressure data or, more likely, a series of time intervals where the pressure data is considered reliable. Typically, successive build-ups are a good candidate, unless the producing pressures are exceptionally smooth as in the case of clean gas tests for example.

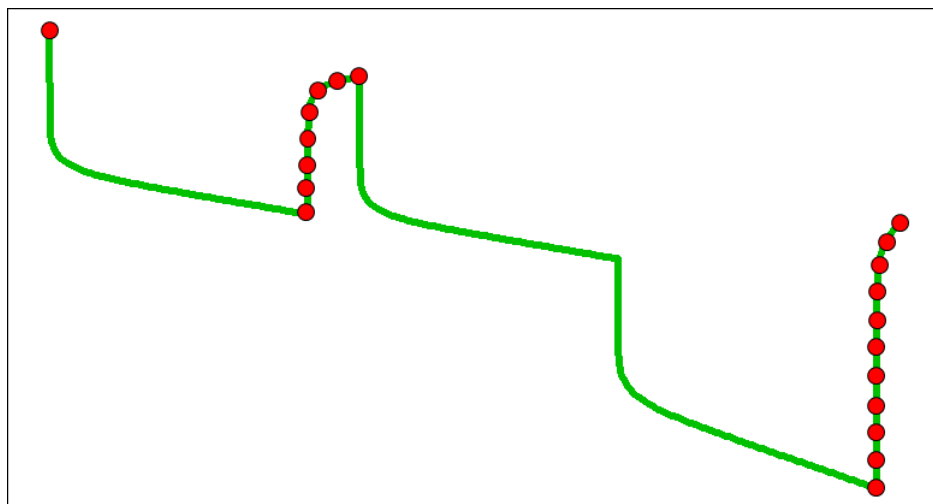


Fig. 3.D.8 – 1st objective function
minimize distance between simulated and real data

The second component of the objective function is the total curvature of the derivative response. When several derivative responses provide an equivalent match, the idea is 'the simpler the better'. Among the candidate responses, the one with the smallest total curvature is selected. In other words, if several variations give a good fit, the one that transits smoothly between the points is preferred to those that oscillate.

The third and last component of objective function is the modification in the rate values required to obtain a match. Again, for the same quality of match, the solution that requires the smallest changes in the rates is selected.

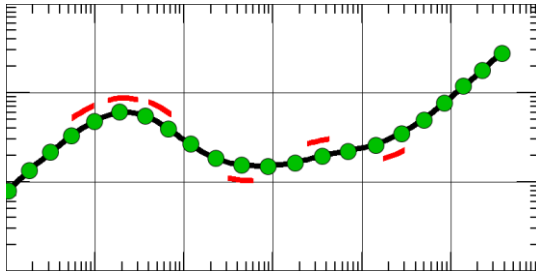


Fig. 3.D.9 – 2nd objective function
minimize total curvature

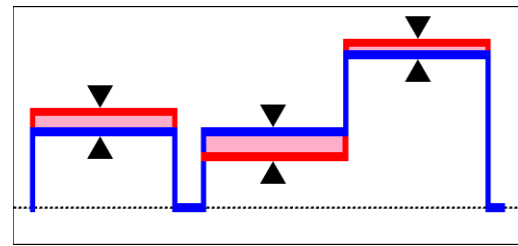


Fig. 3.D.10 – 3rd objective function
minimize rate correction

3.D.2.c Deconvolution in plain English

This essence of this new deconvolution method is optimization. Instead of optimizing model parameters at the end of the interpretation, we take a discrete representation of the derivative we are looking for, and we shift it and bend it until it honors the selected data after integration, to give us a unit pressure change response from the derivative, and convolution, to take the rates into account.

Because we need to account for some uncertainties on the rates and for better behavior of the optimization algorithm, we allow the rates to change a bit, but we try to make this change as small as possible.

We want the resulting derivative curve to have the same kind of signature as the various analytical and numerical models we use. To achieve this we make sure that the total curvature of the response is reasonable, i.e. the resulting curve is not too twisted.

Once we get our deconvolved derivative, we integrate to get the pressure response and show both pressure and derivative on a loglog plot. As this is the theoretical response for a constant rate, we match the deconvolved data with drawdown models, not superposed models.

Because this deconvolved response is not data, but 'only' the result of an optimization that may be imperfect, we keep an eye on the real data by superposing the model and looking at the history match on the real, not the deconvolved signal.

3.D.2.d Field data application

The history plot below shows 3,000 hours of permanent pressure and rate recordings. The three longest build-ups are extracted and shown on a loglog scale below.

The green and red build-ups are strictly telling exactly 'the same story', while the blue build-up is consistent at late time but diverges at early time, with apparently a different wellbore storage and skin.

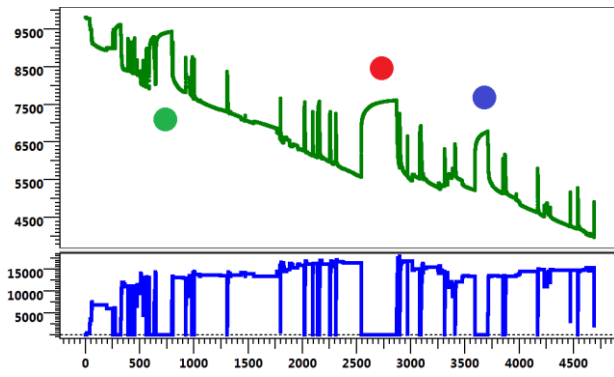


Fig. 3.D.11 – Production and pressure history

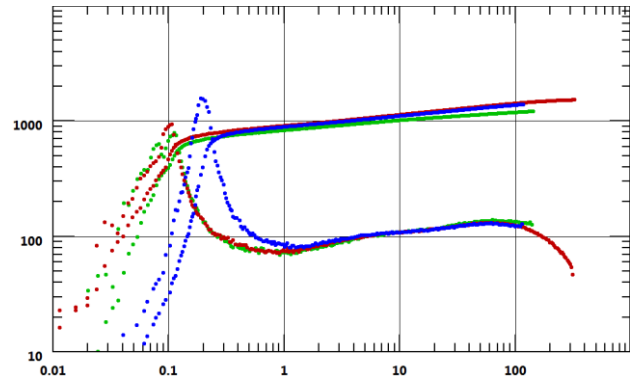


Fig. 3.D.12 – Normalized loglog plot

If we apply the von Schroeter et al. method on the two coherent build-ups (green and red) the process is successful and the resulting deconvolution is shown in the figure below. The late derivative dip in both build-ups does not correspond to a pressure support but the beginning of a closed system. The late time unit slope in the deconvolution derivative will provide a fair estimate of the well drainage area. Because we had two build-ups the deconvolution process could also back calculate a consistent value for the initial pressure.

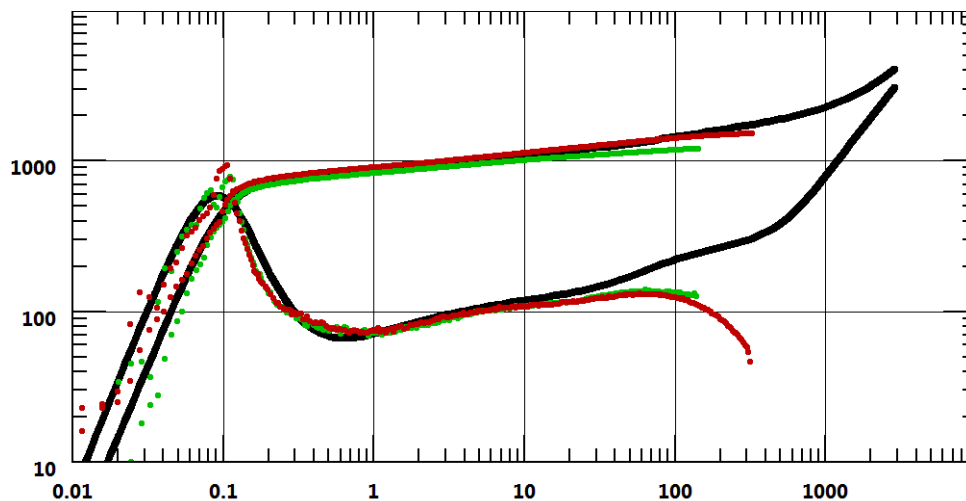


Fig. 3.D.13 – Deconvolution with the two consistent BU's

3.D.2.e Main limitation of von Schroeter et al. method

We take the same real example as in the previous section, but we consider the third build-up later in the same well production history. If we extract and compare the derivative response of the three build-ups, they tell more or less the same story at late time but the early time response is inconsistent with the two initial build-ups.

If we calculate the convolution with no constraint from the three build-ups, or even using any of the two first build-ups and the last, we get an erratic deconvolved signal (see figure below). Coming back to Earth, we should remember that deconvolution is, after all, only a nonlinear regression process.

Any engineer that has been using nonlinear regression on analytical models knows how this process is impressive when it succeeds and pathetic when it fails. It is the same here. The inconsistencies at early time have forced the spline to oscillate to the best, actually least bad, fit for the early time of the three build-ups. This had a residual effect at late time and the spline had to oscillate again to get back on track. It is frustrating, because we do not really care about the early time, and the late time of the three build-ups were telling more or less the same thing. But the process has failed, because it is just a brainless numerical process that is not able to incorporate this early / late time distinction. Hence, the process is doomed, looking for a global solution that does not exist.

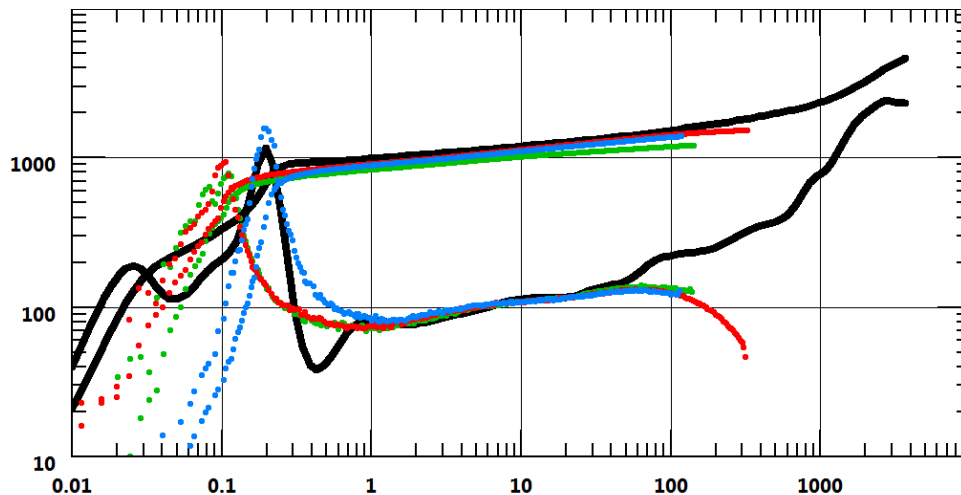


Fig. 3.D.14 – Deconvolution from the three BU's

If we want to use deconvolution for, say, volumetrics from PDG data, we are likely to see the wellbore storage and skin change over time. We face here a major potential limitation of the deconvolution. It also kills any hope to have the deconvolution become a single button option that would give the engineer a reliable late time response at no risk.

To be fair to the von Schroeter et al. method, it could give a more stable answer if we increased the smoothing of the algorithm. This amounts to give more weight to the 'minimum curvature' part of the error function at the expense of the 'match data' part. The algorithm then sacrifices the accuracy of the match in order to get a simpler, smoother derivative curve.

The danger of using smoothing is to hide a failure of the optimization and get a good looking but absolutely irrelevant deconvolution response. Such irrelevance could be detected when comparing the reconvolved pressure response to the recorded data on a history plot. However this problem is one of the main, frustrating shortcomings of the original von Schroeter et al. method.

3.D.3 Deconvolution Method 2 (Levitan, 2005)

It is possible to perform a deconvolution for a single build-up if we combine the shut-in data with a known value of initial pressure (see the consequences below in the paragraph 'Pi influence on the deconvolution').

The workaround suggested by Levitan is to replace a single deconvolution for all build-ups by one deconvolution for each build-ups.

As deconvolution can be done using p_i and any build-up, the idea of the Levitan method is to perform one deconvolution for each build-up with a common value of initial pressure. The first guess of p_i may produce divergent deconvolution responses. The value of p_i is reiteratively changed until one gets a consistent late time response for all deconvolutions. Because each deconvolution only honors one build-up data at a time, there will not be any instability at early time.

This process is easily accessed in Saphir: this Levitan et al. deconvolution method is proposed when multiple periods are extracted: 'Separate deconvolutions with a common p_i ' (Levitan et al). The checkbox 'force P_i to:' is automatically tagged 'on' and p_i must be entered manually. This option calculates automatically one deconvolution per extracted period. The results working on the 3 build ups is shown below:

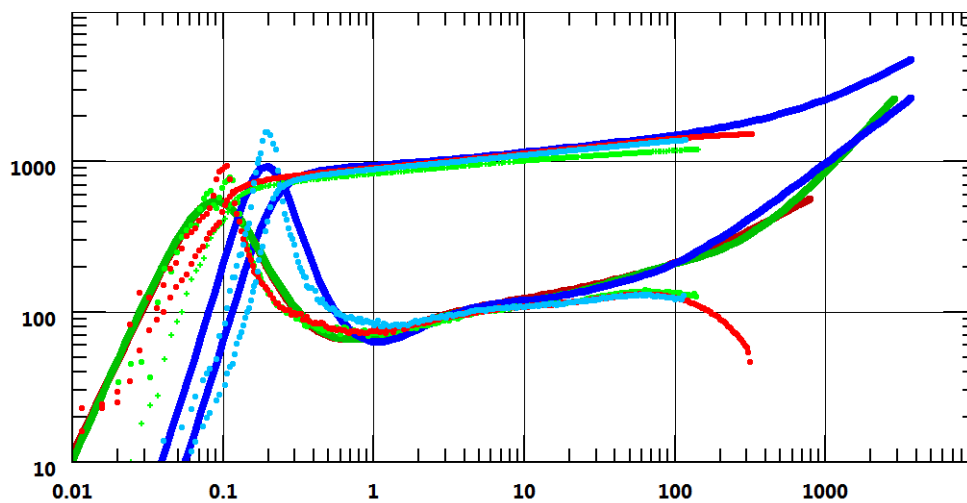


Fig. 3.D.15 – Automatic 'separate deconvolution with a common p_i '

When ignoring the P_i :

The process would be a bit more complicated if we did not have a couple of coherent build-ups to start with. If we had, say, only Build-up #1 and Build-up #3, we would have to 'play' with the initial pressure until the late time behaviors are coherent and give the same reservoir size. Attempts at deconvolution with values that are both too low too high for p_i are shown in the plots below.

This becomes a trial-and-error process, until the late time behavior is coherent for the two build-ups although this just may not be possible. We see on the plots below that the late time behavior are reasonably coherent but crossing each other.

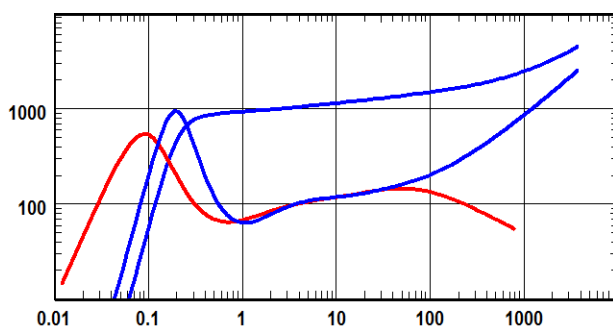


Fig. 3.D.16 – Separate deconvolutions
initial pressure too low
early build-up 'below' late build-up

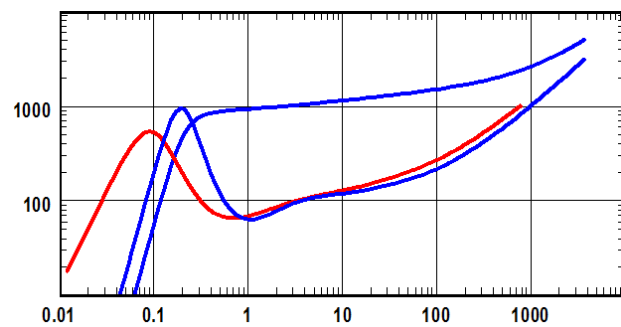


Fig. 3.D.17 – Separate deconvolutions
initial pressure too high
early build-up 'above' late build-up

The Levitan method addresses the main limitation of the von Schroeter et al. method. However two problems remain:

- a) It requires a re-iterative process where the initial pressure is assessed and corrected until the coherence of all convolutions is reached. Attempts to add an optimization loop on p_i have failed so far.
- b) A deconvolution using a given build-up and a single additional point (the initial pressure) will not provide additional, intermediate behaviors that we may detect if we were running a single optimization on all build-ups. Some information is therefore potentially lost in the separation process.

3.D.4 Deconvolution Method 3 (Houzé et al., 2006-2010)

When we extract several shut-ins from PDG data and compare them together on a rate normalized loglog plot, they often, remarkably exhibit the same behavior at late time but vastly differ at early time, with different wellbore behaviors and apparent skin factors.

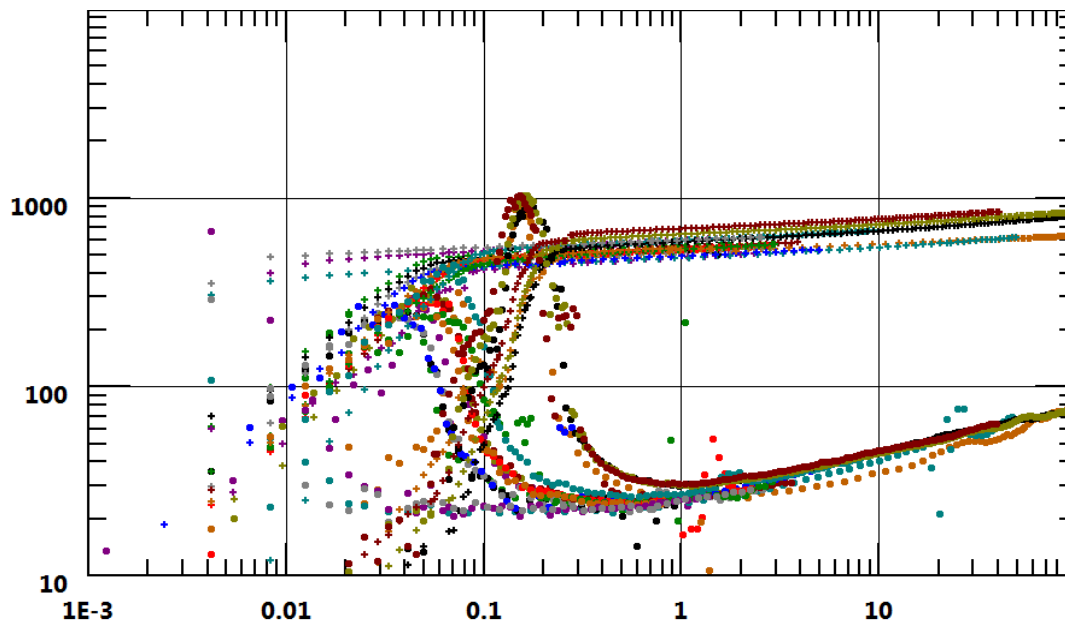


Fig. 3.D.18 – Multiple build-ups from PDG data

This inconsistency ruins the stability of the von Schroeter et al. method and forces the engineer to go into the tedious process of trial and error of the Levitan method.

When the inconsistency comes from different behavior at early time, a solution is proposed.

To illustrate this we can run a very simple simulation, or test design, of two systems with different wellbore storages and skins but the same reservoir / boundary model. In this example we use the simplest homogeneous infinite behavior but it applies to more complex systems. The loglog plot of both responses is shown below left. Simulation 1 has a constant wellbore storage. Simulation 2 has a larger, changing wellbore storage and a higher skin value.

The plot below right compares both simulations on a linear scale and displays the difference between them. During the production phase, the simulations differ with an early time transient corresponding to the different wellbore effects and the skin. When wellbore effects fade the difference stabilizes at a level corresponding to $\Delta P_{Skin}(\Delta Skin)$. When the well is shut-in there is again a transient behavior, but when the wellbore effect fades the difference stabilizes to zero. We will call this limit time the convergence time.

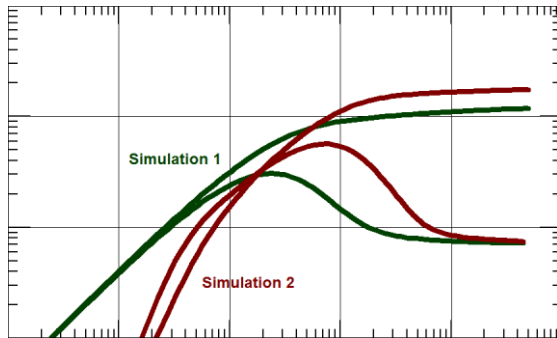


Fig. 3.D.19 – Two simulations: log log plot

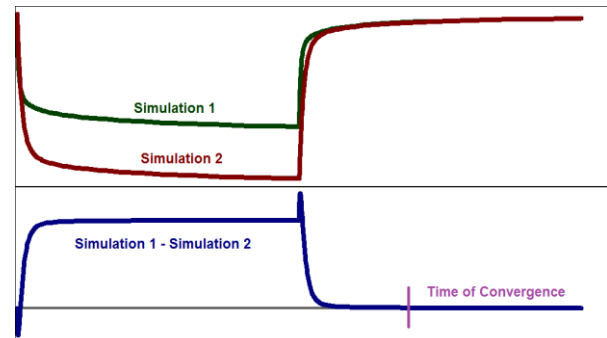


Fig. 3.D.20 – Two simulations: linear plot

On the loglog plot, pressures do not merge at late time because we are plotting $\Delta P(\Delta t) = P_{Shut-in}(\Delta t) - P_{wf}(\Delta t=0)$. The $P_{Shut-in}$ values converge, and ΔP stabilizes at $P_{wf1} - P_{wf2}$.

The deconvolution is an optimization on P , not ΔP . We will get a stable process, not affected by early time discrepancies, if we run an optimization on one build-up and the last part of the other build-ups after convergence.

The Houze et al. method (called 'Deconvolution on one reference period and the end on the other periods' in Saphir), allows specifying which period (blue in our case) will be taken as a reference and all its data taken into account and the other periods (green and red) will be taken into account at late time after the convergence time specified by the user.

It gives a single deconvolution matching with the reference period early time and corresponding to all the periods at late time as shown below:

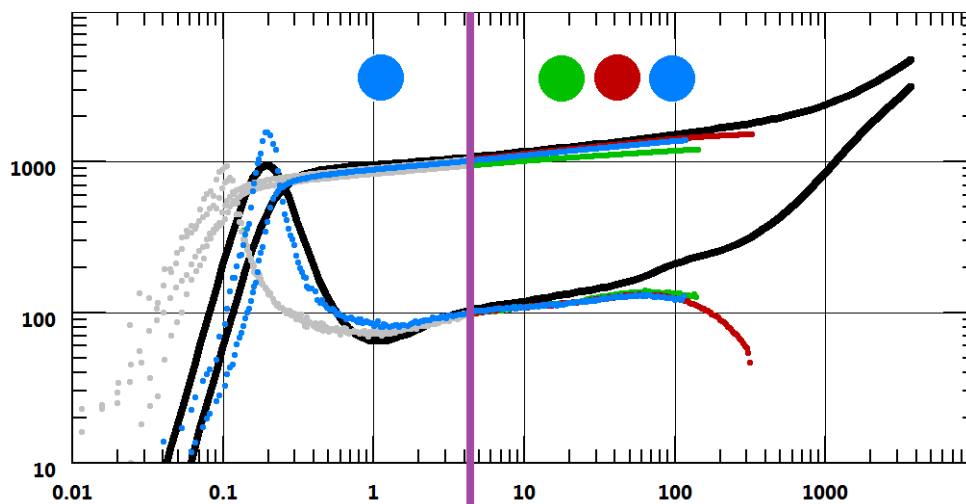


Fig. 3.D.21 – Deconvolution with a period reference early time and all periods late time

3.D.4.a Variant 1: Using Levitan method after Method 3

The main variable in the Levitan method is the initial pressure. Method 3 brings a value for p_i which is meant to be compatible with all selected build-ups and is a good candidate for the Levitan method. Without any engineer interaction, the initial pressure resulting from Method 3 is used to execute the Levitan method immediately after Method 3, with no more trial-and-error.

From experience, this combination does not bring much. The problem with the Levitan method is that each deconvolution will be the simple combination of a given build-up and a single value of initial pressure. Even if we add one or two log-cycles between the build-up and the deconvolution, all this addition will be coming from a single pressure value, and therefore deconvolution will have no chance to pick-up intermediate behaviors.

3.D.4.b Variant 2: Using Method 3 on all build-ups

Method 3 consists in picking the convergence time, selecting a build-up and running the optimization. This can be successively applied to all build-ups.

Compared to the Levitan method, we get the same number of deconvolution responses and the post-processing is the same. However it has the advantage of using a 'proven' convergence time instead of a wildly guessed initial pressure, and there is no reiteration. In complement, each deconvolution uses positive information from all build-ups, and it is possible to pick intermediate behaviors that are beyond the reach of the Levitan method.

There is no guaranty that the late behavior of all deconvolution curves will be the same. This will be the case only if the material balance information is consistent. If not, it will point out that the deconvolution process may not be valid, either because of poor data or because the hypotheses behind this deconvolution are not valid

3.D.4.c Remaining limitations

The deconvolution method presented in this paper clears some of the limitations of the von Schroeter et al. method without some of the inconvenience of the Levitan method. However limitations remain and should not be overlooked:

- Deconvolution works if convolution, i.e. the principle of superposition is valid. This in turn implies that the equations governing our system are linear. This rules out any nonlinearity such as nonDarcy flow, multiphase flow, etc. In such case the optimization will give 'something' but this something may be plain wrong and misleading.
- For any practical purpose, the new deconvolution only works on shut-in periods. This observation is the basis of this Method 3, which otherwise would not be valid.
- Attempts to integrate interference wells in the deconvolution process have failed so far.
- Deconvolution apparently adds one or two log cycles but there is no magic. We had this information before. When interpreting a build-up, a properly trained engineer checks the coherence of the model on the pressure history plot. If the simulation was inconsistent it was the sign that 'something' had affected the long term response that was not detected during this build-up. Adding this 'something' would often amount to adding some late time boundary behaviors, in order for the model to follow the data throughout the well history. The new deconvolution just does that, but in a very elegant way.
- Deconvolution is not a video game that turns bad data into good ones... When successive build-ups are inconsistent, the deconvolution optimization will fail. At best it will be speculatively, but in the worst case it will look OK and will be misleading.
- With Method 3 different wellbore storage and skin factors may be handled. However the rest of the model must remain constant. The idea of getting all shut-ins from ten years of a permanent gauge, then run a deconvolution is perfectly ludicrous. In real life the system changes and the convolution of a single model over several years just does not make sense.

3.D.5 Pi influence on the deconvolution

In the case illustrated in the figures below, we have run a test design with a homogeneous infinite model. So we know that the right response is homogeneous infinite. It starts from an initial pressure of 5,000 psia. There was a 400 hours constant rate production period followed by a 100-hours shut-in.

When the deconvolution is run with too high a value of p_i (red dot), there is an additional depletion compared to the infinite case. In order for the deconvolution to honor both the build-up and the initial pressure, it will have to exhibit at late time an increase of the derivative level, typical of a sealing boundary. Conversely, if we entered too low a value of p_i (blue dot), there needs to be some kind of support to produce depletion smaller than the infinite case. The deconvolution will exhibit a dip in the late time derivative.

In other words, deconvolution honors the data of the first 100 hours of the build-up, and then uses the flexibility of the 400 last hours to 'bend' in order to be compatible with the entered value of p_i . Why is the shape so smooth? Because, on top of this, the optimization process minimizes the total curvature of the derivative curve.

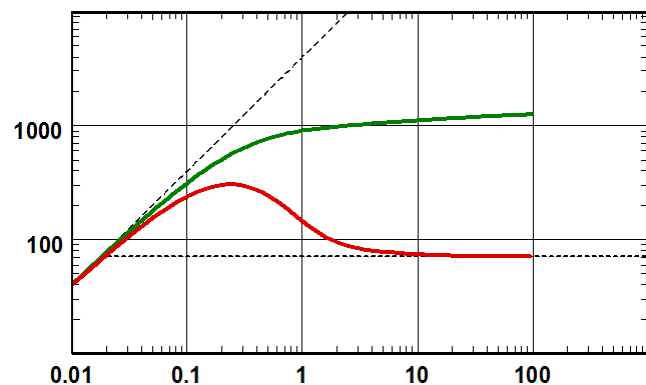
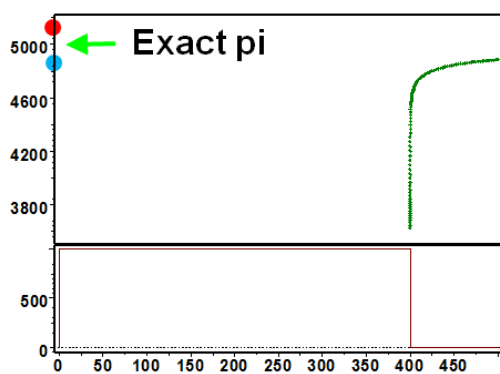


Fig. 3.D.22 – Deconvolution of a single build-up with different values of p_i
For an infinite reservoir - Left: Simulation; Right: extracted build-up

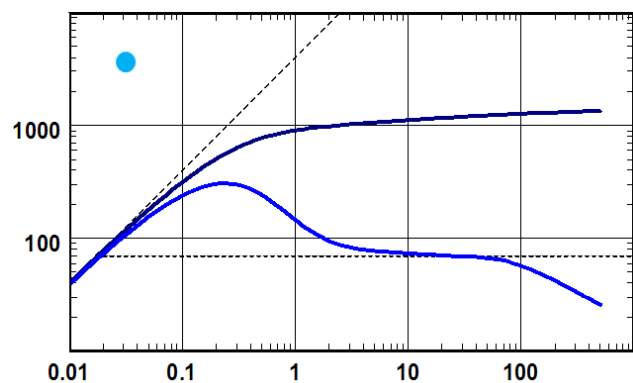
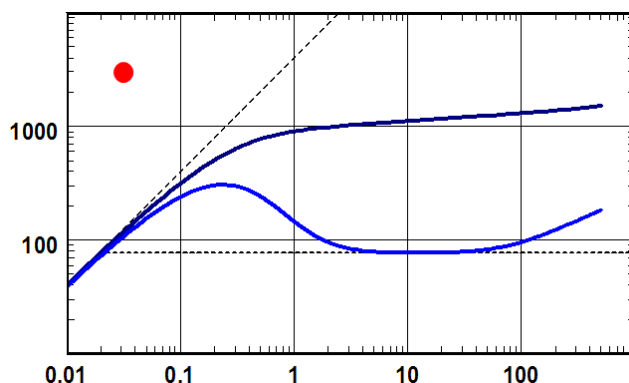


Fig. 3.D.23 – Deconvolution with p_i too high (red) or too low (blue)

How does this work?

We had 400 hours of production and 100 hours of shut-in. Deconvolution is attempting to provide 500 (theoretical) hours of constant production. The first 100 hours of the spline representation are rigid, because they have to match the build-up. We have a loose tail between 100 and 500 hours. The regression moves the tail up or down in order to match the initial pressure p_i after superposition, i.e. to match the depletion during the producing phase.

If the initial pressure is higher than the infinite case, the depletion is greater, and the reservoir has to be bounded. If the initial pressure is lower, the depletion is less and the derivative of the deconvolution will tail down and exhibit pressure support.

Now, there are hundreds of tail responses that could produce a specific depletion. Which one is picked? The simplest one, because the regression selects the solution with the lowest curvature, i.e. the one that will go smoothly from the part of the response that is fixed to whatever PSS level. The first part of the data is rigid, the last part is more or less set by the depletion and the transition is as smooth as possible.

Naturally, if we had more intermediate data, like some reliable flowing pressures, this would 'firm up' the deconvolution algorithm. The optimization first focuses on matching the data before trying to get a smooth response.

3.D.5.a Implementation in Saphir

The implementation in Saphir gives access to any of the above mentioned methods, through a very logical workflow.

The periods to analyze must be first selected for extraction, they may be picked interactively:

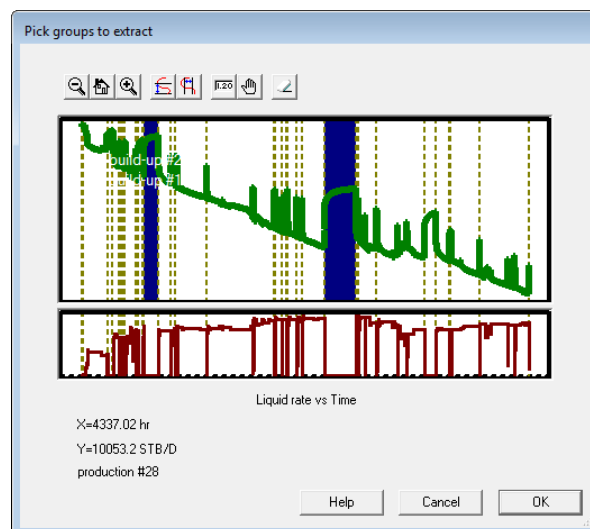


Fig. 3.D.24 – Selecting the periods

Having selected more than one build-up, when the deconvolution process is called its dialog offers the various available methods:

- Looking for a common solution to all the extracted periods (Von Shroeter et al.)
- Separate solutions with a common P_i (Levitan et al.)
- Deconvolution on one period as reference, and the end of the other periods (Houze et al.)
- Variant 1 : Levitan et al. after Houzé et al.

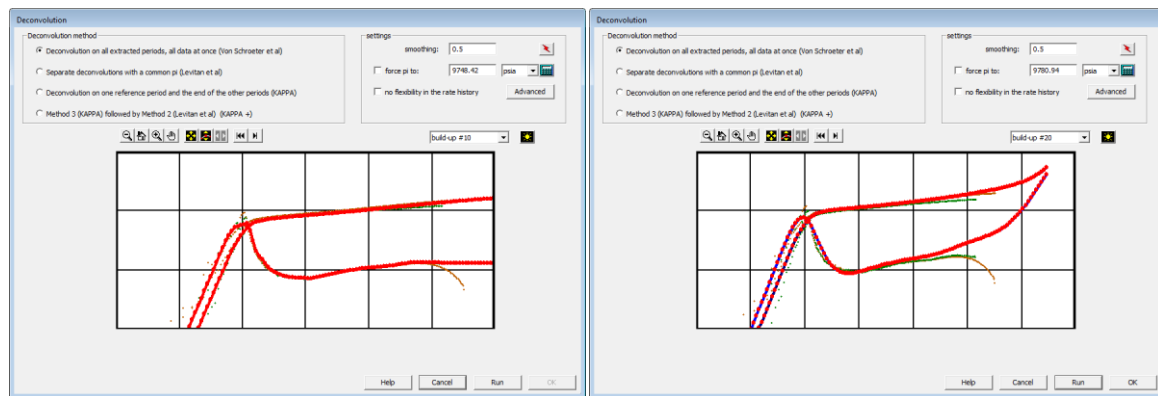


Fig. 3.D.25 – Deconvolution dialog before and after run

The Pi can be forced to a fixed value to improve the process efficiency.

The rate history correction can be deactivated.

It is possible to superimpose the deconvolved signal and the individual build-up data in a rate normalized way. The reconvolved responses corresponding to the build-ups can also be plotted.

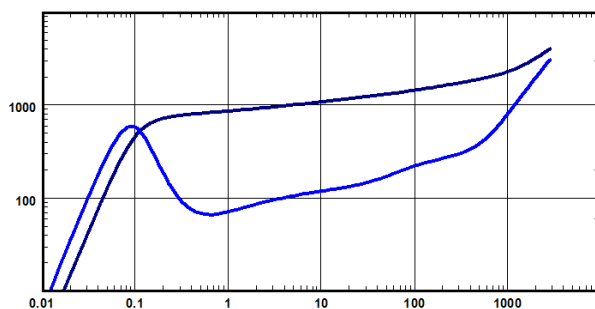


Fig. 3.D.26 – Deconvolved response

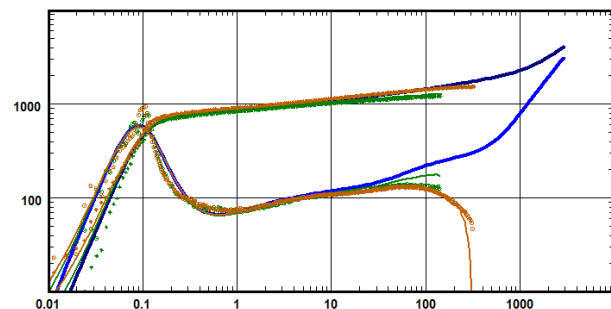


Fig. 3.D.27 – Compared to BU data and reconvolved response

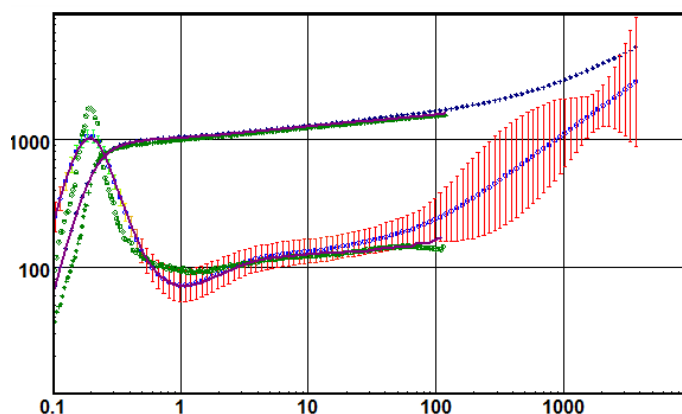
3.D.6 Using sensitivity to assess the validity of a deconvolution

The early time part of the deconvolution response is constrained by the build-up data, and the tail end is adjusted to honor other constraints, such as the pressure drop between the successive build-ups. When no constraint is applicable to a part of the data, the deconvolution picks the smoothest possible path to minimize the curvature. There may be intermediate boundary effects in the 'real' reservoir, but we have no way to know. An issue is to assess which part of the deconvolved data is positive information, and which part is just a smooth transition between positive information.

This is a very serious issue, and may be one of the main dangers of the deconvolution process. When we interpret data and choose the simplest model that honors whatever we have, we know the assumptions we make. When we add a closed system to a model matching individual build-ups in order to reproduce the depletion, we know that we are taking the simplest model, but that there may be additional and intermediate boundaries that we may not see. In its apparent magic, deconvolution presents a long term response that is NOT positive information but just a best match. So how can we discriminate positive information and information by default?

One element of answer is to calculate a sensitivity. The deconvolution parameters include the points of the $z(\sigma)$ response, the curvature of this response and the rate changes. Looking in the Jacobian of the deconvolution matrix we can see the sensitivity of the match to the individual points of the $z(\sigma)$ response. In Saphir we normalize this and show it as a vertical sensitivity band for each point of $z(\sigma)$.

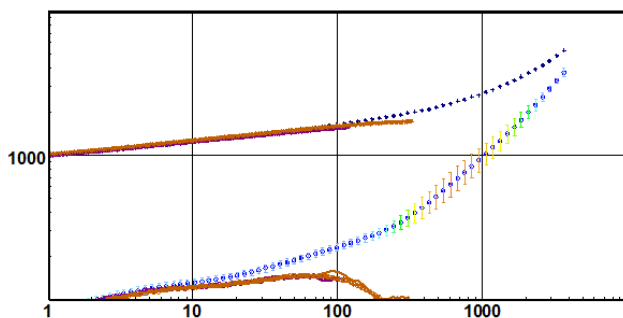
This band does not quantify the real, physical, uncertainty. It only provides a blunt statistical description of the problem around the solution point and answers the question, "By how much can I move this node until the match is affected?" If the sensitivity is high, we are close to positive information and the uncertainty band is narrow. If, on the contrary, moving a point up and down has no or little effect on the global response, then we know that this section of the response may not be very relevant. In order to illustrate this we have taken two extreme examples.



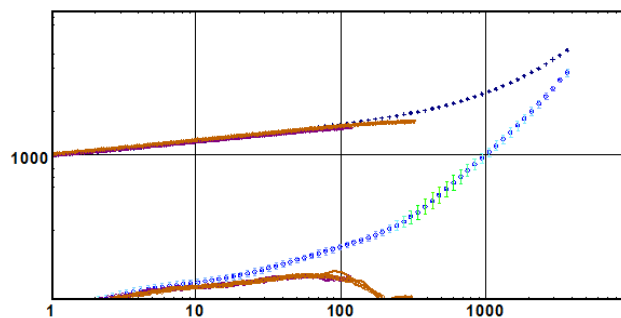
*Fig. 3.D.28 – Sensitivity representation
single build-up and no π (1/2)*

In the above figure we have done what we should never do: calculate a deconvolution with a single build-up WITHOUT imposing a value of π . The problem is completely under-defined, because we can move the tail end of the deconvolution and get a perfect match of the data by compensating π . So the tail end is completely irrelevant and it shows on the sensitivity plot.

In the below left figure, we have run the deconvolution with the two build-ups of the original example. We let π be calculated by the deconvolution process. As one can see, the sensitivity is much better, but intermediate behavior could have been different. What made the deconvolution pick the selective curve was its smoothness. Now, in the right side figure the same deconvolution was run but the value of π was fixed. This makes the sensitivity graph even better.



*Fig. 3.D.29 – Sensitivity representation
two build-ups and no π*



*Fig. 3.D.30 – Sensitivity representation
two build-ups and π*

3.D.7 Conclusion (in 2010)

The recent deconvolution is a nonlinear regression on a model derivative, without knowing the model. The main unknown are these derivative points on a loglog scale. We curve is bent, integrated and superposed in order to best fit the data of interest, generally consecutive and reasonably consistent build-ups. Additional unknown may be the initial pressure and some slack on the rate history. Additional constraints include a minimization of the curvature and of the amplitude of the rate changes.

This new deconvolution provides, in one run, a synthesis of information present in different parts of the pressure / rate history. When you combine two build-ups that are far apart in time, you do not only check their coherence but you integrate, in the deconvolved response, the information of depletion that took place between these two build-ups.

There is nothing really that a conscientious and trained engineer could not do before having this tool, but all this information is calculated in a single run, early in the interpretation process, instead of being a trial-and-error, last minute analysis following the interpretation of the individual build-ups.

So the tool is useful and interesting, but we must emphasize its uses and limitations:

- For any practical purpose, today it only works on shut-ins.
- It should not be used as a black box. It is only an optimization process, and optimization processes are typically impressive when they work and pathetic when they do not. Any error in the deconvolution process will be carried over during the rest of the interpretation.
- Deconvolution should be considered a complement to, not an alternative to, standard build-up analysis. It can be useful, early in the interpretation process, to run a deconvolution and see if it carries any information that could be integrated in the engineer thinking process, but the reference and ultimate decision should come from a match on the real data (typically the history match and the individual build-ups), not only the match on the product of an optimization process that carries some assumptions.
- To work at once it requires us to bundle together coherent, typically build-up, responses. When build-ups are incoherent, it is still possible to run individual deconvolutions based on the same value of p_i , and modify p_i until the different deconvolutions are coherent.
- Deconvolution only works if superposition works and if the system does not change in time. Superposition works if the running equations are linear. If the flow is nonlinear (e.g., material balance depletion, nonDarcy, multiphase, etc) deconvolution will fail and may be misleading. Same will apply, even if the diffusion is perfectly linear, if other wells are interfering with the analyzed pressure response (multi-well case).

So, as with any new tool there is the 'buzzword' syndrome. It should not be oversold nor overbought. Deconvolution is NOT the silver bullet that will provide your reserves that we could not see before.

Still, it is great to have something new in an area where the last really innovative theoretical tool was the 1983 Bourdet derivative.

3.E Modern PTA methodology

Modern Pressure Transient Analysis is based on the use of PC based PTA software products. The key for any modern software is to combine user friendliness and a powerful technical kernel, with both analytical and numerical capabilities. In terms of methodology, the central diagnostic tool is the loglog plot, showing both pressure and the Bourdet derivative used for the diagnostics and the match with the selected model(s). The sections below describe the typical path of today's Pressure Transient Analysis. It was our understanding of what this typical path should be that led us to implement this in Saphir.

Once the interpretation is initialized the first task is to get a coherent and representative set of rate and pressure data. This includes loading the data, quality check and validation and editing to prepare for analysis. One or several periods of interests, typically buildups, will then be extracted and the diagnostic plot created and the data diagnosed. The interpretation engineer can select one or several candidate analytical and/or numerical models, set their parameters and generate these models. For candidate models that are retained, the engineer can refine the parameters, either manually or using nonlinear regression. Once the model parameters are finalized, the user may assess the sensitivity and/or cross-correlations of the parameters using confidence intervals from the nonlinear regression and run sensitivity analysis. Finally, a report is issued.

The path above is the default path when all goes well. In reality, for complex problems, it may be a trial-and-error process where the interpretation engineer may decide to go backwards before continuing forward again when a segment of the process is not satisfactory.

3.E.1 Initialization

The interpretation engineer must first input information required to identify the test and select the main options that will set up the interpretation process: the type of fluid (that will determine the function of the pressure to be used) and the type of test (standard, interference). The engineer may start with a standard analysis, nonlinear numerical, shale gas or coalbed methane (CBM), multilayer analytical or linear numerical, or a formation tester type of analysis. The final input will be the parameters that are assumed to be known which are required to calculate the interpretation results: porosity, net drained vertical thickness, well radius, etc.

Fig. 3.E.1 – General conditions

For a slightly compressible fluid, only a few PVT properties, assumed to be constant, are needed: formation volume factor, viscosity, and total system compressibility.

Fig. 3.E.2 – Slightly compressible fluid

For other phase combinations, a choice of correlations or input of PVT tables is required to calculate the pseudo pressure and pseudo time functions.

Fig. 3.E.3 – Defining the PVT

3.E.2 Loading Data

Import from flat ASCII files, manual input and copy-paste from a spreadsheet are the main methods used to load data. However, data is increasingly read from databases sometimes with a direct real time link to the running acquisition systems of service companies during the test.

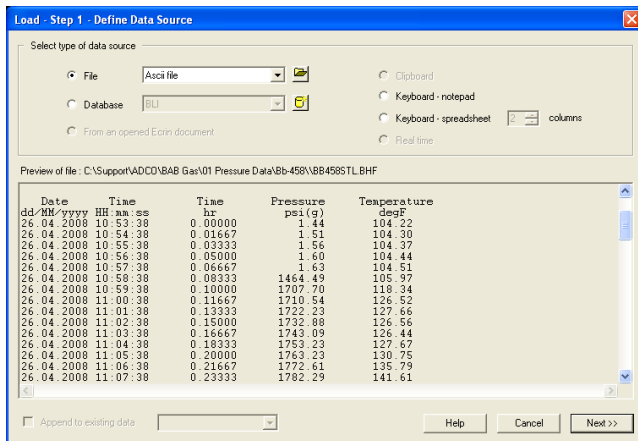


Fig. 3.E.4 – Loading Data: Define data source

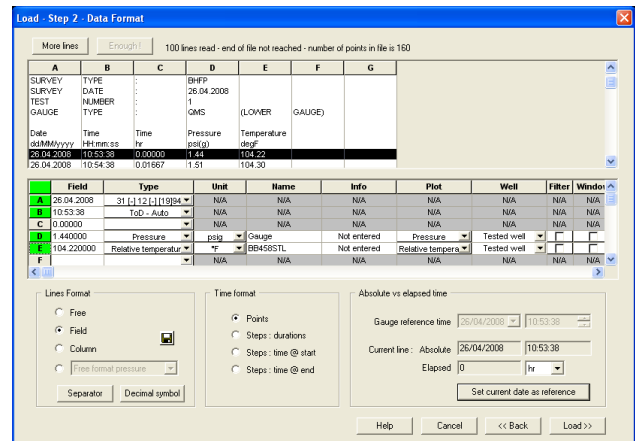


Fig. 3.E.5 – Loading Data: Define data format

Unlike for open-hole logs and despite several attempts in the past, as of today (2010) no industry-standard ASCII format has emerged to execute the load with a click. In Canada the EUB has published a format (PAS) for compulsory electronic submission of test data and results, but this remains very oriented towards local legal procedures. So software packages have to provide the engineer with the flexibility to interactively define the file format, in order to cover the wide variety of existing files.

Originally, the amount of data was a real issue because of limited available memory running under DOS, the cost of computer memory, and the fact that the size of the data arrays had to be declared and set by the software programmers at compilation time. All these limitations have gone. Today's software can easily handle multiple gauges and volume of gauge data acquired during a well test which is sometimes more than a million data points.

The recommended procedure is to load all data acquired from all gauges during the well test, and not just a filtered subset. Filtering can always been applied later, on duplicate data sets. However, things are changing with the spread of permanent downhole gauges and the increased usage of production data in Pressure Transient and Production Analysis. The amount of production data is one order of magnitude higher, and is much less smooth than a typical buildup. Smart filters, such as wavelets, are increasingly required to reduce the volume of the data, retaining any trends and significant changes and at the same time eliminate noise. The processing of Permanent Downhole Gauge (PDG) data is covered in another chapter.

3.E.3 Quality Control

Quality Control is an essential part of the interpretation, too often overlooked in the past, it includes:

- Validation of the gauges: identification of failures, drift, clock failure, resolution, etc.
- Identification of operational problems.
- When applicable, identification and correction of tidal effects.
- Discrimination of wellbore effects from reservoir effects.

Quality Control has fortunately become a growing concern. Previously, an interpretation engineer would often consider the buildup data only and match it with, for example, a radial composite model; whilst all too readily ignoring the possibility that the test behavior could indeed be related to wellbore phase redistribution. An efficient tool to diagnose wellbore effects is the dynamic calculation of the difference between the gauges measuring the same data. The value of the difference itself is of little interest as long as it stays within the gauges accuracy. However, variations of the difference may be a valuable source of information.

When two pressure sensors are set at the same depth, as with a dual gauge carrier, their difference can be used to check their synchronization (time shift) and their coherence. Gauge failure and gauge drift may be identified.

When the gauges are set at different levels, as in a tandem configuration, any change of the pressure gradient occurring between the gauges may be detected. In the presence of phase segregation problems, the proper placement of dual gauges may help qualifying and even quantifying these problems. The engineer will avoid pointlessly interpreting and using a complex reservoir model behavior that has absolutely nothing to do with the reservoir.

In the absence of dual gauges, one can calculate the derivative of the gauge versus time, and plot it on a linear or log-log scale. This will act as a 'magnifying glass' of the pressure behavior.

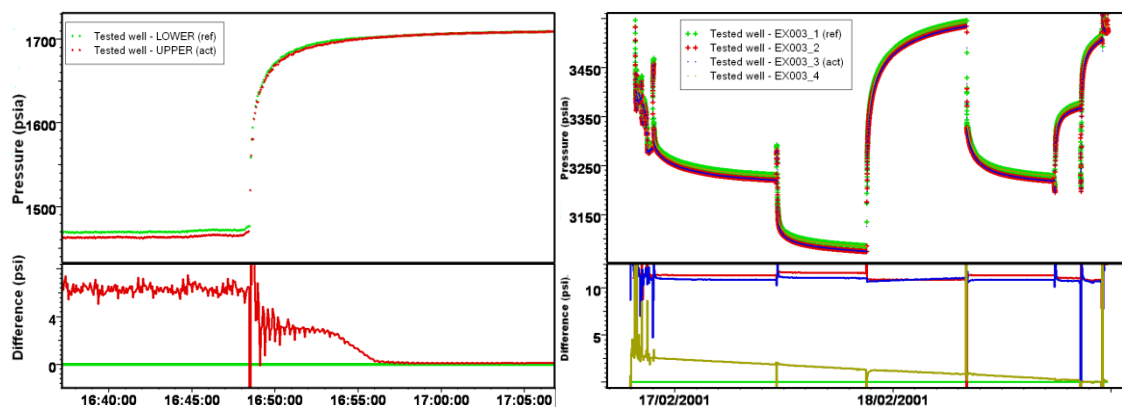


Fig. 3.E.6 – Data Quality control using dual gauges and Drifting gauge

Even though people associate the difficulty of well test interpretation to the modelling part, a lot of thinking takes place at this stage of the interpretation, as it defines the starting point from which the diagnostic will take place. Failing to identify any operational problems can potentially jeopardize the whole interpretation process.

There is a side advantage in performing a comprehensive Quality Control: after going back and forth between the data and the well test report, the interpretation engineer will know what happened during the test, even if he/she was not on-site.

3.E.4 Editing data

Loaded data may be the result of careful post-processing by the data acquisition company, in which case no or little editing may be needed. But very often the interpretation engineer will have to gather data of unequal quality and from different sources. Pressures will often be acquired downhole in real time or with a memory gauge, while rates will still be measured at surface and come from the well test report with a different time sampling.

Beyond the usual cleaning of irrelevant data and the correction of load errors, the main challenge will be to end up with at least one coherent, synchronized set of rate and pressure data. To get there the engineer may have to perform the following tasks:

- Get all data acquired electronically to the same reference time.
- If not already loaded, create the rate history graphically by identifying the pressure breaks and get the rate values from the well test report. Use a facility to automatically identify the shutin periods and automatically correct the production history from volumes to rates.
- Refine the production history, when the time sampling of rate measurements is too crude.
- Conversely, if the production history goes into useless details, simplify the rate history to reduce the CPU time required to run the models.

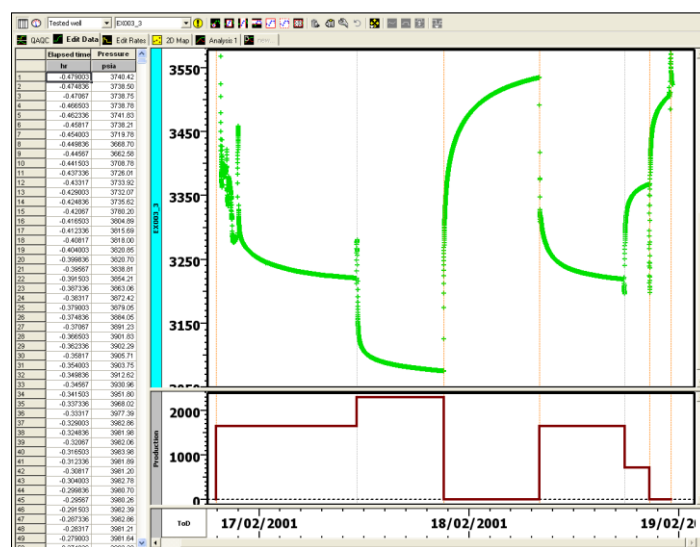


Fig. 3.E.7 – Editing data:
Pressure and production history adjustment

3.E.5 Extraction and diagnostic

Once the data have been synchronized and validated, the analysis itself will start. The engineer will focus on one or several gauges, one or several flow periods, and will create the appropriate diagnostic tools, starting with the loglog and the semilog plots. When several gauges are used, they will be overlaid. When several production and/or shutin periods are extracted, they will be rate-normalized, then overlaid. In the case of Saphir, this extraction is followed by an automatic positioning of a horizontal line for IARF on the Bourdet derivative and a unit slope line for pure wellbore storage on both pressure and the Bourdet derivative. This positioning is set by a relatively simple filtration, the main goal being to put these lines in the same 'range' as the data. Surprisingly, this sort of processing works quite well in the case of simple responses, giving an instantaneous estimate of the wellbore storage and permeability-thickness product. In case of complex behavior, the software may have selected the wrong level of the derivative for IARF and or the wrong unit slope for wellbore storage. The interpretation engineer will then interactively move the two straight lines in order to properly position these flow regimes.

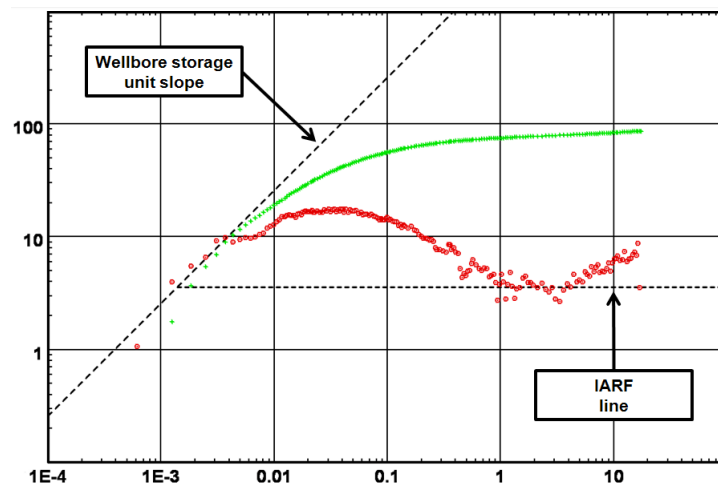


Fig. 3.E.8 – Match lines

During the extraction process, and possibly later, the engineer may decide to control the derivative smoothing, apply a logarithmic filter, and in the case of a shut-in, control the last flowing pressure.

3.E.6 Deconvolution

The new deconvolution method developed in the last few years was presented in a previous section. Extraction of the deconvolution may occur right after the extraction of the individual shut-ins, or much later after the interpretation of the individual shut-ins.

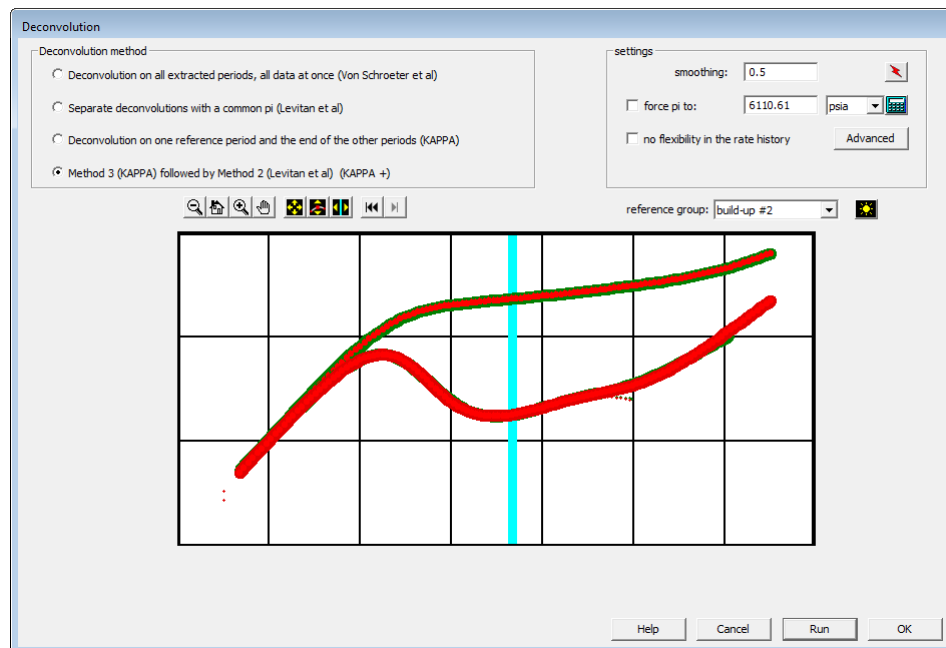


Fig. 3.E.9 – Deconvolution dialog

3.E.7 Diagnostic

After extraction, data problems overlooked in the initial quality control may become apparent, requiring further data editing, and a new extraction.

Looking at the derivative response will generally be the starting point of this process. Individual features in the derivative signature will be considered, validated or rejected, and potentially associated to a well, reservoir or boundary model. These possible assumptions must then be compared to what is already known from other sources.

Depending on the diagnostic, the loglog and semilog plots can be complemented by other specialized plots to identify specific flow regimes by straight line analysis. However this approach has been made largely redundant by the introduction of the modern approach. The engineer will have the choice of the pressure function, the time function and the type of superposition that will be applied to the time function; raw function, tandem superposition for simple buildups, or multirate superposition.

Depending on the prior knowledge and the complexity of the response, the problem may be very quickly restricted to one or two alternatives, or the range of possibilities may remain large. For exploration wells, the uncertainty in the explanation may stand, and alternative explanations may be presented in the 'final' report. Further tests and increased knowledge of the reservoir could allow, later, narrowing down the range of possibilities, months or years after the initial interpretation.

3.E.8 Model generation

The engineer, after diagnosing the behavior, will then select one or several candidate models. The process below will be duplicated for each considered model.

The objective is to use the modelling capability of the software to match in part or in totality the pressure response. This will consist of selecting one or several models, which may be analytical or numerical. Then, entering a first estimate of the model parameters, running the model and comparing the simulated results with the real data, on all relevant plots.

AI based Model advisers may be used to speed up the process by detecting if a derivative response can be explained by a certain combination of well, reservoir and boundary models, and produce a first estimate of the model parameters with no user interaction.

Today's software products offer a wide choice of analytical models. Typically the user will select a wellbore, a well, a reservoir and a boundary model. Unfortunately, our ability to solve problems mathematically is limited, and all combinations of well, reservoir and boundary models may not be available. This is sometimes frustrating to the engineer, as in this case only portions of the response can be matched at any one time.

There are many ways to estimate parameters: (1) from the results of specialized plots that may have been created in the analysis; (2) from straight lines drawn on the loglog plot (wellbore storage, IARF, fractures, closed systems, etc.); (3) from interactive features picking the corresponding part of the derivative signature; (4) by manual input.

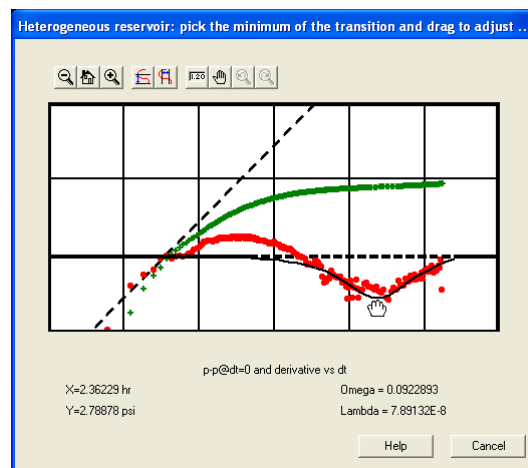


Fig. 3.E.10 – Interactive pick

For complex analytical models, only a few parameters, or relationships between parameters, will be determined in a unique way from the well test response. The other parameters or missing relations will be input from other sources of information. If this missing information is not available, the problem will remain under-specified.

The previous remark on parameter estimation is even more critical when using numerical models, where the geometry will essentially be built from prior knowledge of the reservoir, and only a few 'global' unknowns will be deduced from the test.

It is no longer a technical problem to transfer information and data directly and dynamically between applications, and there are dozens of public or proprietary protocols to do so (OLE, COM, DCOM, Corba, etc.). As a consequence models generated from third party applications may be transferred and run in pressure transient analysis software. The most common example is a 'standard' reservoir simulator run.

The model is generated and compared to the data, in terms of both pressure and Bourdet derivative on the history plot, the loglog and semilog plots. In case other specialized plots are used, the model will also be compared on these different scales. At this point, the engineer may decide to reject the candidate model, or keep it and refine the parameter calculations.

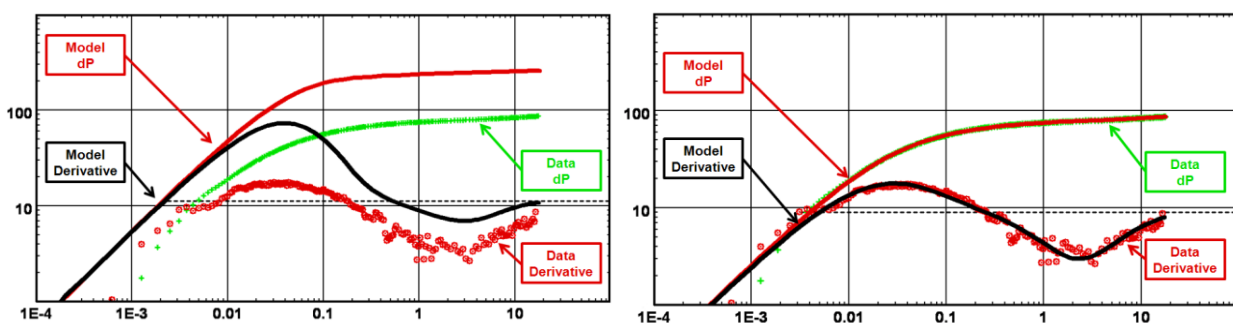


Fig. 3.E.11 – Initial and Final model match

3.E.9 Model refinement

Modification of the parameters: Before leaving the parameter refinement to an optimization routine, the engineer should deal with the gross parameter errors if there are any. This will increase the chance for the regression to succeed and converge faster, and it will secure the choice of the model. Software will generally provide facilities to ease this process. For example, parameters may be corrected if the engineer shifts the match on the loglog plot. However, an experienced interpretation engineer with a good understanding of the sensitivity to the model parameters will often do it faster by changing the values by hand.

Nonlinear regression: The principle is to use numerical optimization to refine the parameter estimates by minimizing an error function, generally the standard deviation between the simulated pressures and the real pressures at carefully selected times. The derivative may also be integrated in the error function. The most commonly used optimization algorithm is Levenberg-Marquardt, but there are many variants.

Among the model parameters, some may be fixed by the engineer. For the others, the engineer may control their upper and lower limits. The data points on which the error function will be calculated may also be user controlled. One major choice will be whether the optimization is restricted to the analyzed period, or if it is extended to data outside the analysis. In the first case, the match at the end of the optimization process will be as good as or better than the starting point. If the optimization is performed on points beyond the analyzed period, the overall history match will be improved, but potentially at the expense of the quality of the match on the period used for the diagnostic.

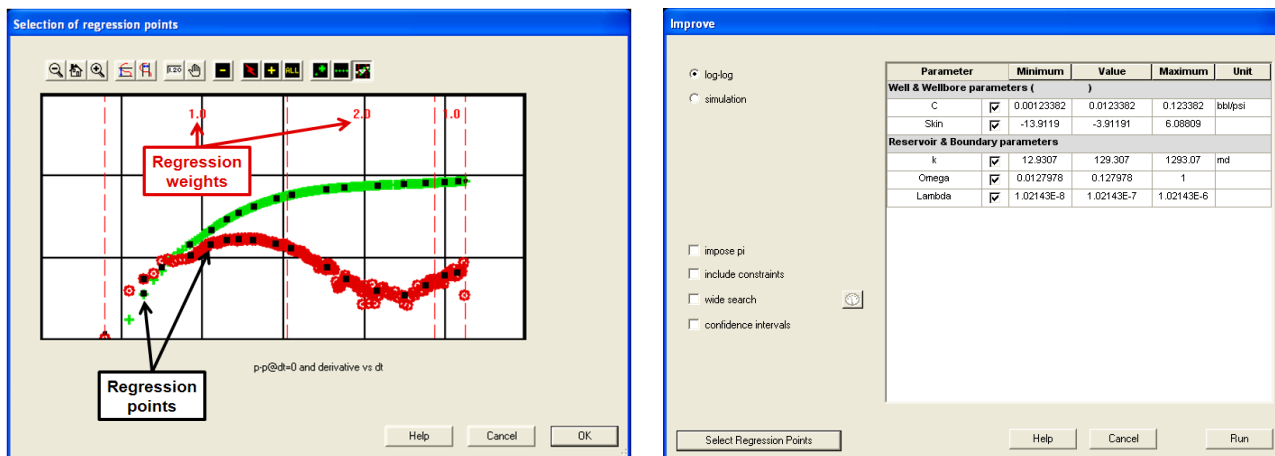


Fig. 3.E.12 – Setting regression points and controlling the optimization bounds

3.E.10 Sensitivity study

At the end of the nonlinear regression it is also possible to recover the confidence intervals. They can be used to assess the sensitivity to individual parameters and eventual parameters cross-correlations.

One can also run and display series of model generations corresponding to different values of a given parameter in order to compare them on a single loglog plot. This is, to a certain extent, the modern version of the type-curves, where dimensionless drawdown solutions are replaced by the generation and extraction of detailed models with user preset ranges of parameters. The figure below shows the sensitivity to the distance between a well and one single sealing fault.

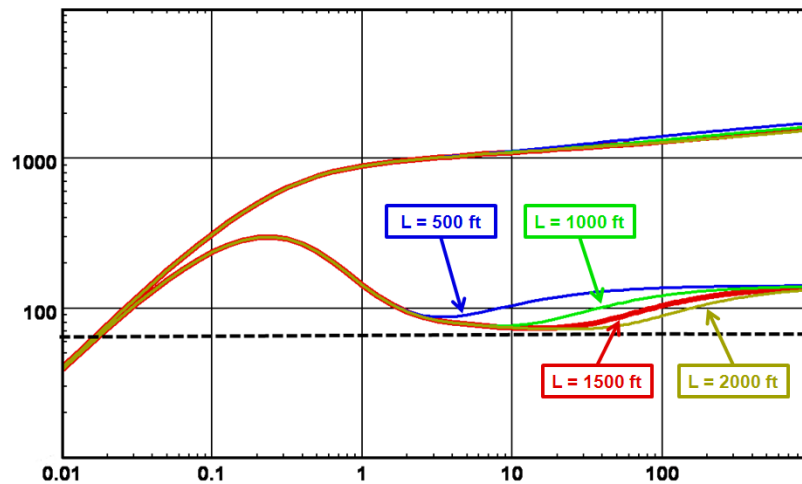


Fig. 3.E.13 – Sensitivity to distance

3.E.11 Reporting Guidelines

A typical interpretation report will be split into two components: the 'mechanical' part, basically the result tables and plots generated, directly or indirectly, by the Pressure Transient Analysis package, and the 'verbose' part, where the engineer will report the objectives, the operations, the interpretation, the confidence one could have on his interpretation, and possible recommendations for well treatments and/or future tests.

There has never been an industry standard for reporting, except the Canadian EUB format that is restricted to very basic results. Typically, professional interpretation reports will be generated with two possible set-ups:

- A header document, from a word processor, with some 'copy-paste' of plots and results from the PTA software, but with most of the 'mechanical' report delivered as an annex.
- An integrated document, typically from a word processor, where some plots and tables are dynamically connected to the PTA software using some OLE or COM automations. The advantage of this solution is that it is much more flexible. Once a model template has been set up the reporting process will get shorter and shorter from one interpretation to the next.

In any case the engineer must keep in mind that an interpretation is, at best, a best guess at a given time, and 'truth' can evolve with time. The key word here is 'interpretation'.

'The reservoir is a circle of radius 4123.93 ft'.

This is probably the worst possible statement we can imagine in PTA. The reservoir is very unlikely to be an exact circle. What we have in PTA is a range of models that we KNOW to be over-simplified. We simplify to turn the qualitative into quantitative, and one must always be factual. Also, the number of significant figures of a result must be reasonable, or at least not ridiculous. It is not because the nonlinear regression finished at a given number that we must keep all the significant figures of this number. So a much more reasonable statement would be: 'If we consider that the late time behavior is linked to a close system, a reasonable match was obtained with a circular reservoir with a radius of 4,100 ft.'

'The more I know about well testing, the more I worry'. H.J. Ramey Jr, 1989

3.F Test design

Pressure Transient Analysis is performed on data that were acquired during dedicated operations (well tests) or from permanent gauges. In order to optimize a coming well test, one can use the modelling capabilities of the PTA software to run a test design, i.e. simulate the response of a well test from the parameters or range of parameters we expect. It is then possible to play with the different scenarios and adapt them to the various constraints and the test objectives.

In order to run the scenarios the engineer must rely on known information and data or make reasonable assumptions. To explore 'what-if' scenarios, sensitivity studies are carried out and based upon these the engineer can choose both downhole and surface equipment including, amongst others, pressure gauges with adequate accuracy and resolution. Surface equipment must be selected which includes facilities to measure the flowrate of gas, oil and water. This done, the engineer can make the safest and most economical plan to reach the test objectives.

3.F.1 Safety

Safety is the primary concern in all well testing operations and is the mandatory objective that must be met before any other. With the safety constraints applied the objectives of the test must be defined, operational limitations identified and scenarios considered that clearly show if the objectives will be met and if not, why not. The safety aspects of well testing are covered in a variety of documents and books available on the internet and elsewhere. All companies have their own procedures and standards and they should all be fairly common as they have to conform to rules and regulations set down by the various regulatory bodies overseeing different parts of the world. This section is just to remind the reader that Hazard and Operational studies (HAZOPS) for well test operations exist and they must always be applied to ensure safe practice and operation.

3.F.2 Objectives

It sounds obvious but you must know what you want to achieve. What are the ultimate results you would like to obtain from the considerable investment involved in running such a test, and what are the results going to be used for. An assessment of the value of the results is also necessary to avoid 'overkill' and unnecessary expenditures. Below is a non-exhaustive list of parameters one may want to determine in a well test:

- Well model (fractures, partial penetration, slanted and horizontal well parameters)
- Reservoir model (double porosity, layer and composite parameters)
- Boundary model (distance and type of boundaries)
- Permeability
- Skin
- Heterogeneities (double-porosity, layer and composite parameters)
- Static pressure
- Layer parameters (properties and pressure)
- Layer contributions

3.F.3 What data, what quality at what cost?

In order to gather the data necessary to meet the test objectives it is required to define the type of tools that will achieve this. How critical is the accuracy of the downhole measurements and what are the requirements with respect to surface flow rates? What is the requirement with respect to frequency of sampling?

As a general rule the higher the sampling rate of a tool, the better it is for pressure transient analysis. This is certainly the case with respect to downhole pressure and temperature measurements, but is less critical with the surface flow rate measurements.

The tools must be carefully selected. The downhole gauges must have accuracy adequate for the expected pressure response. If the differential pressure during a test is expected to be small (e. g. high permeability and low formation damage) then the accuracy and resolution becomes an important issue. It is also important to consider if high sampling rate of a tool will have an adverse effect on its accuracy. How to program a memory gauge or decide to use real time surface read-out gauge is an issue that needs to be resolved.

If multiphase production is expected in the wellbore or even in the formation then certain considerations must be addressed. To decrease the wellbore volume, downhole shutin may be considered to minimize the chances of phase segregation during a buildup and careful placement of the gauge in the test string is important.

The below figure illustrates the programmed change in pressure acquisition rate just prior to a buildup. The increase in sampling rate increases the noise.

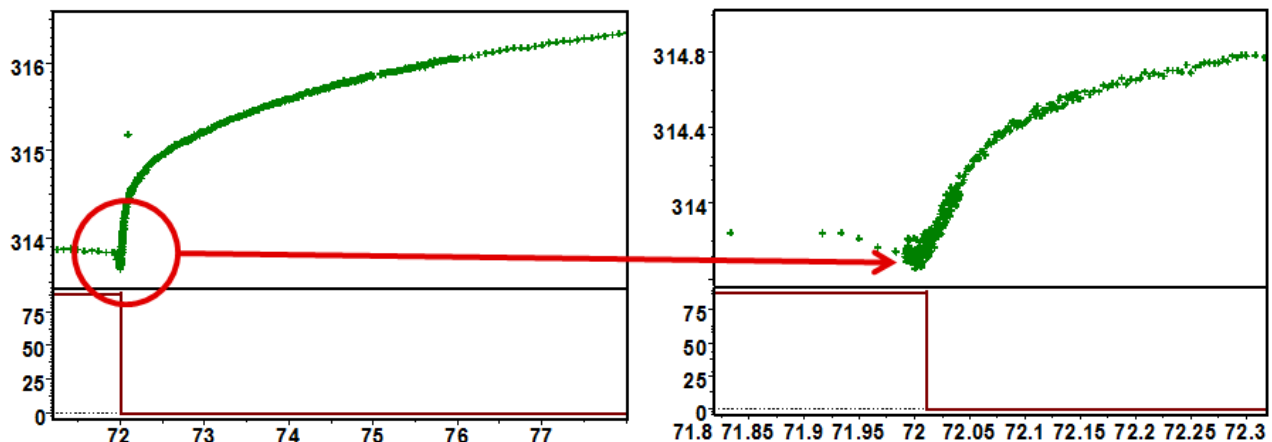


Fig. 3.F.1 – Increase in acquisition rate

When the diagnostic plot is affected by noise the recognition of the flow regimes becomes more difficult and the choice of the correct interpretation model becomes ambiguous. See following illustration.

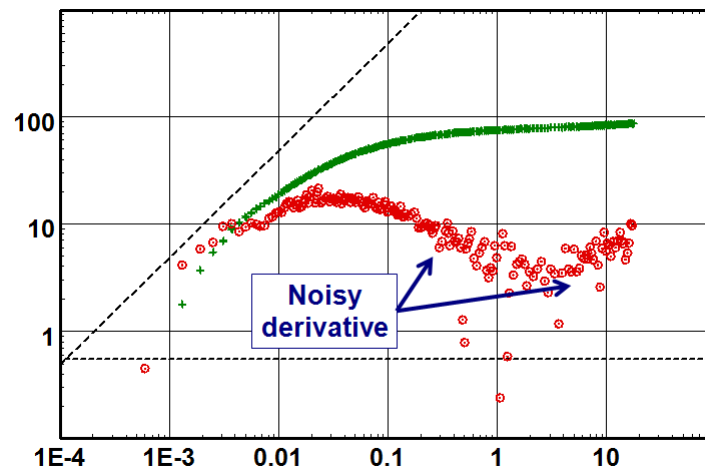


Fig. 3.F.2 – Ambiguous model identification

The behaviour of the period that will be analysed is very dependent upon the previous history and in particular any disturbances immediately before the period in question. If flow rate changes or small shutin periods immediately prior to the subject period cannot be avoided, at least the value of the flow rates should be captured. This is a detail that should be stressed in any test program.

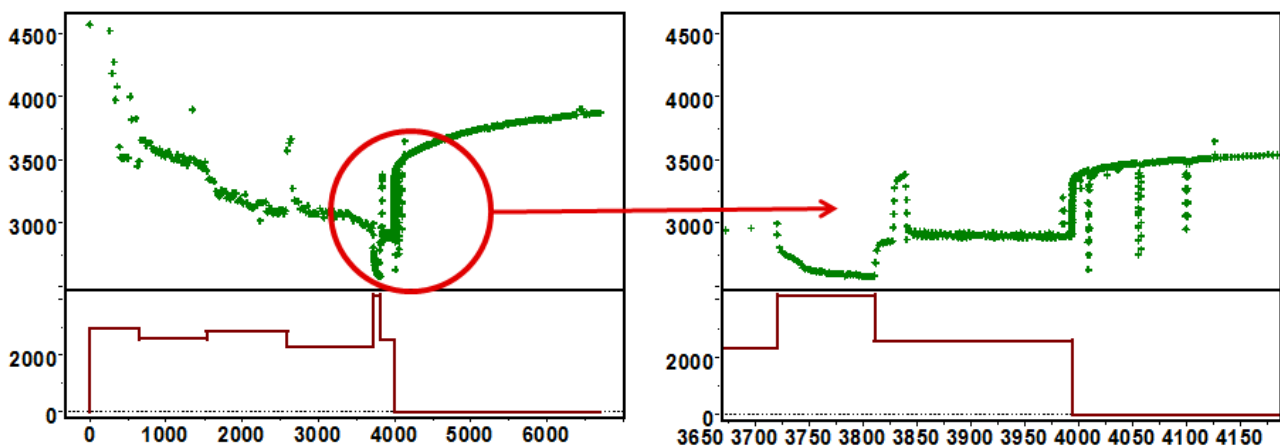


Fig. 3.F.3 – Disturbing the period for analysis

During a buildup that was designed for analysis purposes avoid as far a safety permits any surface operations that may jeopardize the usefulness of the period. The example below illustrates a real case where some surface operations affected the buildup period and rendered it for all practical purposes useless for any analysis with confidence.

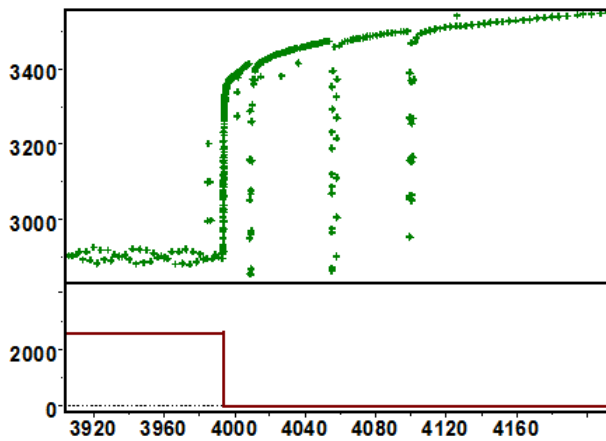


Fig. 3.F.4 – History plot

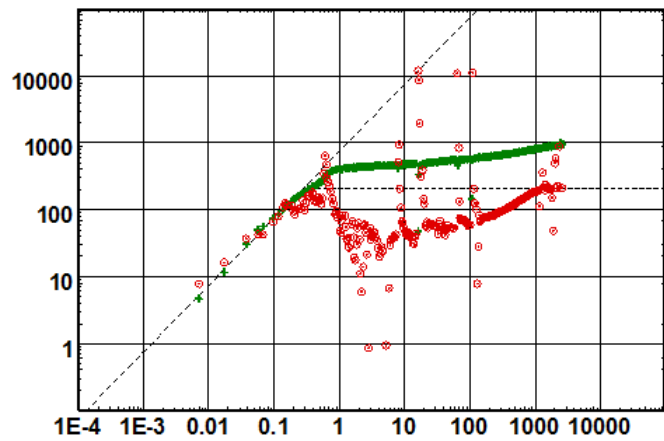


Fig. 3.F.5 – Loglog plot

3.F.4 Type of test

There are several different tests mainly depending upon the type of well.

- Exploration
- DST
- Formation testing
- Appraisal
- Production
- Dynamic gradient
- Static gradient

The planning of any of these types of tests involves setting a scenario to theoretically evaluate if the objectives of the tests will be met.

3.F.5 Scenario

In order to set a scenario some of the information is usually known and some are assumed. The quality and quantity of the known parameters are dependent upon the amount of work already carried out on a prospect, if the planned test is to be carried out in a known field, if the well has already been tested at some earlier stage, etc. The below table summarises some of the data necessary to set the scenario which will be used to theoretically simulate the test which will be used for the final program.

Well completion	PVT parameters	Rock properties	Reservoir description
rw	Specific gravity	Net pay h	Distance to limit
Perforated interval	Volume factor B	porosity f	Limit types
hw	Viscosity m	formation	Estimated Pi (initial pressure)
Estimated damage	Compressibility co, cg, cw	compressibility cf or cr	pressure)
Depth	Estimated Pi (initial pressure)	Estimated permeability k	
Deviation			

In order to illustrate the concept we will devise a scenario where the main objective of the test is to determine skin, permeability and the distance to a seismic defined fault at some distance away from the well (1500 ft).

The analysis of nearby wells has indicated the nature of the reservoir to be homogenous with a permeability-thickness of some 1000 mDft. The skin is of course unknown but believed to become positive after drilling in this relatively high permeability rock. PVT parameters are known in this saturated reservoir, and porosity and net drained thickness have easily been determined from open hole logs in advance of the planned test.

The well has been on production in excess of a year. The well will be shut in to run two memory gauges in tandem and set in a nipple 100 ft above top of perforations. The sampling rate of the gauges is set at a minimum sampling of one second. The below plot illustrates how a five second sampling rate with a quartz gauge of 0.01 psi resolution and 1 psi noise should look on a diagnostic loglog plot.

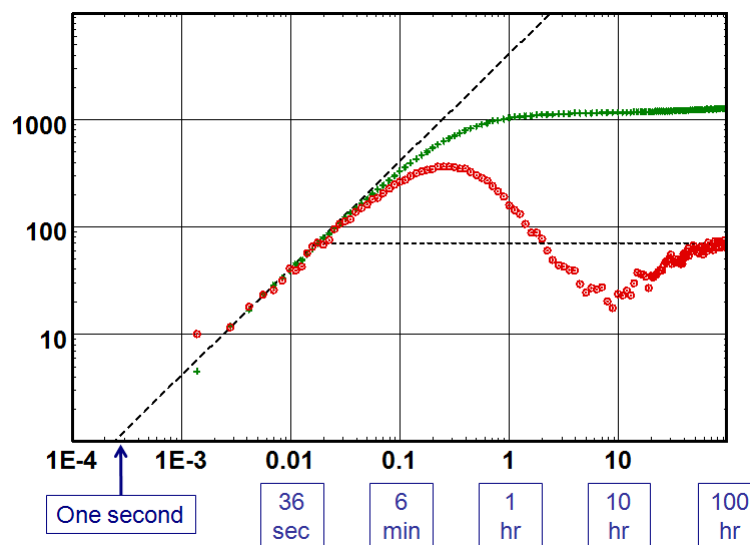


Fig. 3.F.6 – Logarithmic scale

The duration of the shutin that permits for the running and setting of the gauges is set to 24 hours to allow the pressure to stabilize. Then a one single constant production step of 1000 stb/d for 24 hours. This will be followed by a build up of 100 hours. The 100 hours was chosen as the limit of buildup time. The reason is not necessarily to build up for the actual 100 hours, but it is a duration that, from most practical viewpoints is the limit of most buildups in production wells due to the production loss. This allows determining the optimum buildup time in order to find the permeability, skin and distance to fault. The test design option of the software was then used to calculate different scenarios and 'what if' sensitivities. The simulated pressure history is shown in the figure below.

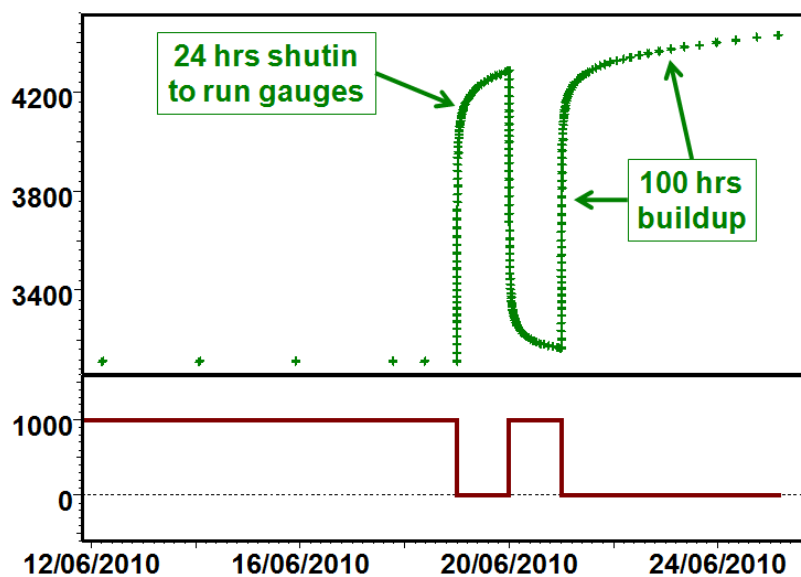


Fig. 3.F.7 – Simulated pressure history

The defined production history and the model were used to study the sensitivity to the skin by running various models and make a comparison. From the figure below it can be seen that infinite acting radial flow will be reached for skin equal -2 at 7 hours shutin time, and skin of 5 at 14 hours shutin time. The combination of skin above 5 and the fault will mask the radial flow thus permeability cannot be determined with any confidence. The sealing fault is detected after about 25 hours shutin time, however the doubling of the slope will only happen after the end of the 100 hours shutin.

The next figure illustrates that when the storage increases above 0.01 bbl/psi and the skin is maintained at +10, then radial flow will not be reached and the identification of the fault becomes ambiguous.

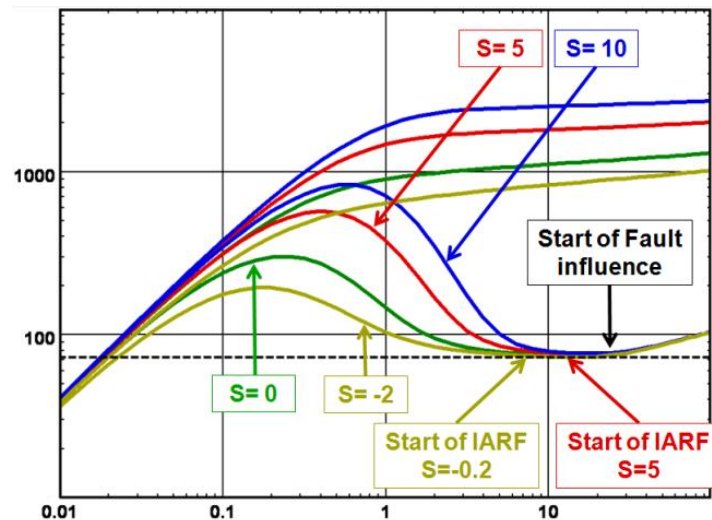


Fig. 3.F.8 – Skin sensitivity

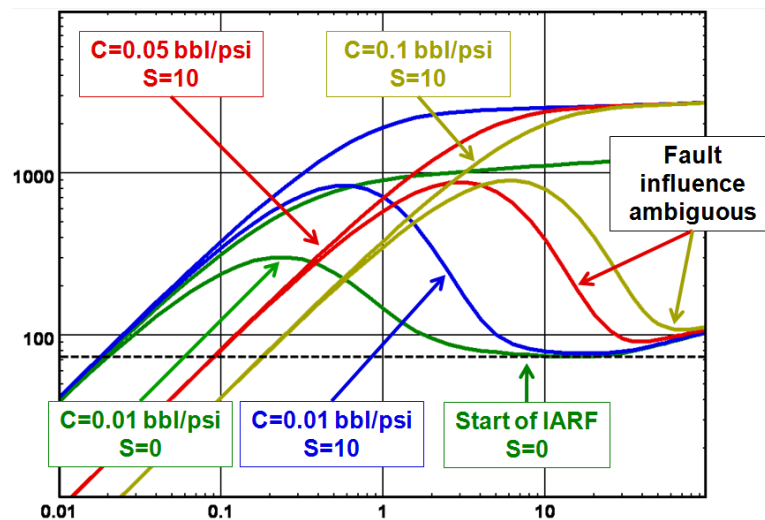


Fig. 3.F.9 – Wellbore storage sensitivity

3.F.6 The final program

A final program is issued and contains all the necessary information to allow the field personnel to safely carry out the well test and assure that all necessary equipment is available.


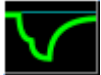



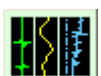
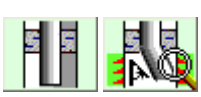


Specific responsibility levels and who is accountable for what part of the operation is defined in the document.

Each phase of the operation is identified and durations of flow and shutin periods are clearly defined. Usually a flow sequence is defined with one single and constant flowrate, this is sometime confusing and the field personnel may try to achieve such a constant flowrate by continuously adjusting the choke. To increase the chances of obtaining a solid analysis from the data it is however recommended to avoid any choke changes during a single defined flowing period as long as the flow rates are measured.

Finally the program is just that, a program; proper field supervision is of course indispensable and adjustments to the plan must be continuous as conditions change.

3.G Operational considerations: Gathering data

It is absolutely necessary, before running a test, to really identify what the test objectives are and which data should be acquired. Part of this work will be achieved with the test design. However, in complement the engineers and operators on site will need to clearly know what information is needed. The following table can be used as a guide, but the list is by no means exhaustive.

	Type of data	PTA
	Production history	Yes
	Pressure history	Yes
	PVT, correlations, tables or constraints	Yes
r_w	Wellbore radius	Yes
Φ	Porosity	Yes except interference
h	Net vertical drained thickness	Yes
	Field map with surrounding wells based on seismic interpretation	Preferably
	Production history of surrounding wells	Preferably
	Complete completion log preferably with a permeability log. Core and core analysis	Preferably
	Completion diagram and geometry, deviation, perfos, gauge depths.	Preferably
	All gauges, well test and operations reports	Yes
	Choice of flow correlations or availability of lift curves from third party software	If pressure far from sandface

3.H Quality Assurance and Quality Control

3.H.1 Introduction

During the early 1980's the oil industry, especially in Northern Europe, went through a totally justifiable drive to increase the quality and efficiency of work carried out in most of the commonly related services involved in the production of oil and gas.

Quality control manuals and procedures had to be presented to prove that every effort was fulfilled by the involved parties to assure that work, equipment and preparation procedures were documented and followed. These documents had to be approved by a 'controlling body' before the company was qualified as an approved contractor. The QA/QC manuals described and identified the procedures to follow, backed up by checklists, tests, inspections and certification by approved inspectorates.

This drive was mainly directed towards offshore construction and sub-sea technology to optimize equipment performance and the quality of engineering works, including the safety of oil and gas installations and oil field operations.

Service companies were no exception, but QA/QC was limited to planned and regular calibration of mechanical and electronic measuring devices. As service companies claim no responsibility for any loss or damage due to faulty measurements and interpretations, there was no procedure to validate measured data before analysis.

However methods were developed in the early 1990's. They allow quality control of downhole pressure and temperature measurements, and they ensure that the data is valid and usable by the engineer for further analysis. Such validation increases the confidence in the results of the analysis and eliminates, to a large degree, errors that could lead to major mistakes in the decision process of optimum development and production of petroleum reserves.

3.H.2 Background

The introduction of the Bourdet derivative revolutionized the approach to PTA. It gave us deeper sensitivity and multiplied our analysis ability. It also complicated the diagnostics by revealing phenomena unseen and not understood until this time.

This sensitivity had a price: as both reservoir response and operational problems affect the same pressure response, too often the Bourdet derivative response to fluid movements in the wellbore, phase segregation and temperature anomalies would wrongly be associated to a reservoir feature and interpreted as such.

It was necessary to enable the engineer to differentiate between the representative data of the reservoir response and the part caused as a result of a signal from other phenomena.

The techniques described in this chapter were developed as a result of severe interpretation problems encountered in many fields and led to the introduction of the concept of Differential Pressure Analysis.

It will be shown how the use of pressure differentials measured between pressure gauges placed at different levels in the test string can help the interpreter to identify the pressure data that is valid for interpretation, and enable him to save time by eliminating useless data caused by anomalies and wellbore phenomena. The method brings 'Quality Control' one step further, and should be an integral part in the overall QA/QC programs of any company dealing with downhole measurements of pressure and temperature.

3.H.3 The concept of Differential Pressure Analysis

The analysis is based upon the difference in pressure measured between tandem pressure gauges, the simplest case, or a combination of pressure differences if multiple gauges are used during a pressure survey.

The study of these differences can reveal the following problems and has a direct impact on the choice of the data measurements for a valid PTA:

- Detect phase segregation in the wellbore;
- Establish phases for pressure correction;
- Identify the movement of the fluid interface movements (water / oil / gas);
- Identify temperature anomalies or other gauge technical problems;
- Check the gauge accuracy and resolution;
- Identify gauge drift;
- Other technical or electronic malfunctions;
- Selection of the most representative data channel, if any.

By convention the pressure difference between gauges is calculated so that that an increase in the 'difference channel' represents an increase in the fluid density between the gauges sensing points, and a decrease a reduction of the fluid density, i.e.:

$$\Delta p = p_{lower} - p_{upper}$$

The 'difference channel' behaviour is the same whatever the gauge offset. The upper gauge may well read a higher pressure than the lower gauge, possibly due to a gauge problem or just because of accuracy, but the 'difference channel' would have the same identifiable shape.

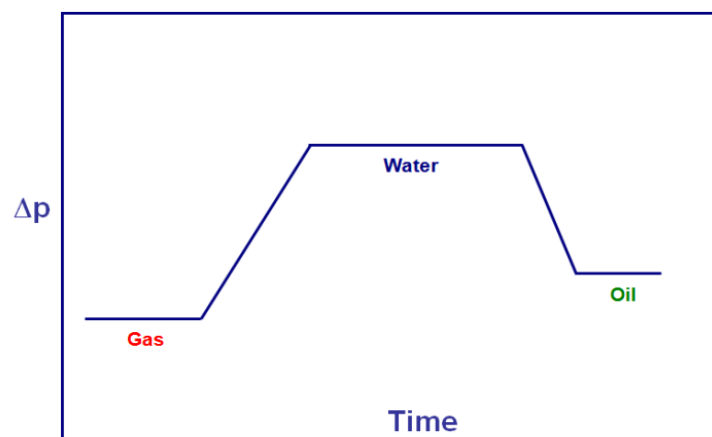


Fig. 3.H.1 – Difference channel

3.H.4 Basics

The simple analysis is based upon the study of the pressure and temperature differences between two or more gauges placed in the test string at different depths. The figure below shows schematically what happens to the pressure at the different sensors, if a 'gas-oil' interface is moving downwards and passes the sensors.

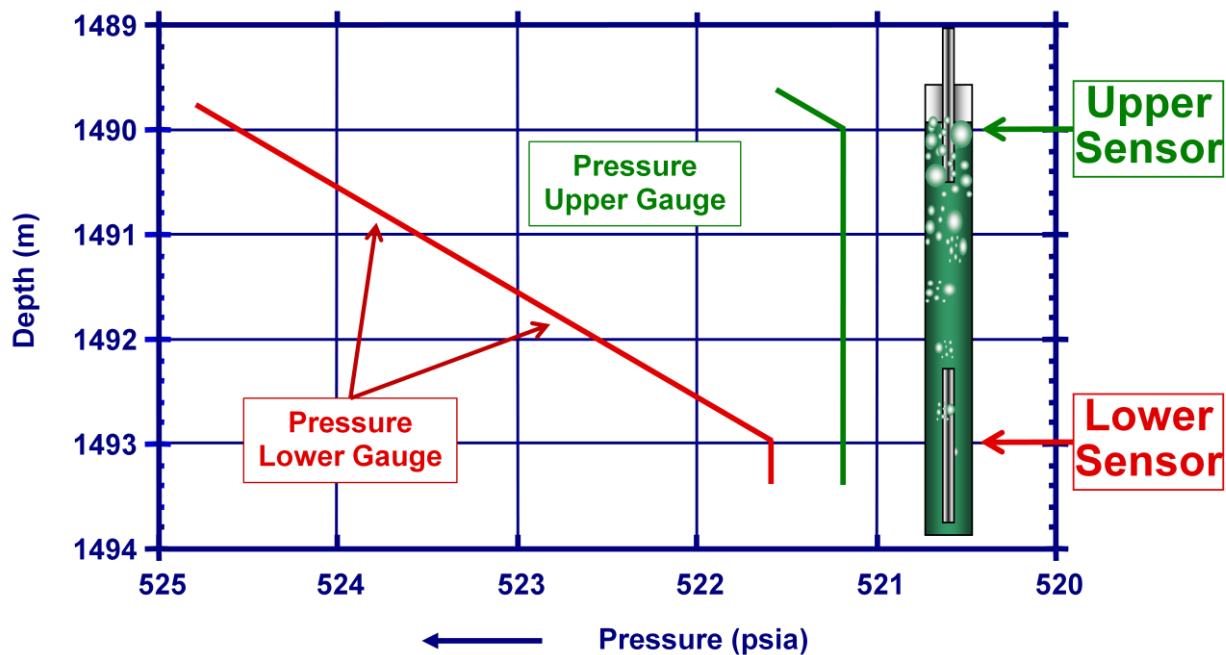


Fig. 3.H.2 – Fluid movement downwards

The example assumes that any background behavior is following a constant transient (trend) or is in Pseudo-Steady state (PSS).

Once the gas-oil interface hits the upper sensor, the pressure at this sensing point remains 'constant' while the interface moves towards the lower pressure point.

The pressure at the lower sensor declines linearly if the fluid interface movement is constant. It becomes constant again after the interface has moved below the lower pressure sensor. The difference in pressure between the two sensing points is represented by the difference in fluid gradient between oil and gas.

The following illustration represents the 'difference channel' between the two sensing points, and by simple analysis it can be determined what fluid phase changes have caused the observed phenomenon (see QA/QC).

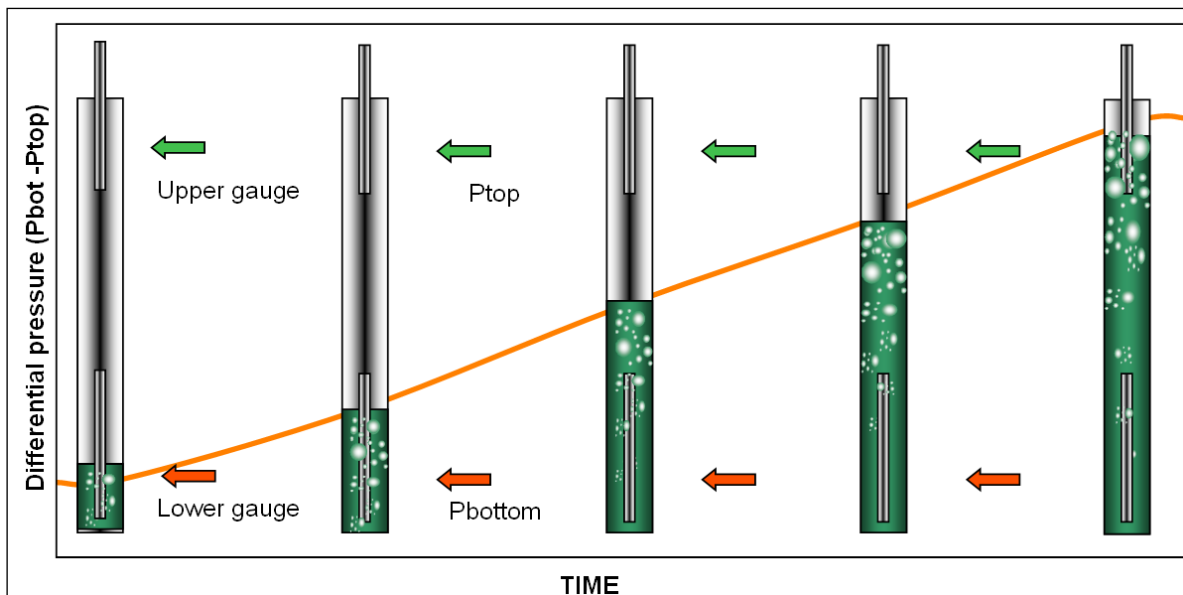


Fig. 3.H.3 – Pressure difference

3.H.5 Pressure correction

Clearly it would be desirable to be able to correct for any perturbation in the pressure caused by the 'phase segregation', which also in the majority of cases has an adverse effect on the Bourdet derivative used for the diagnostics in pressure transient analysis.

In practice this has proved to be near on impossible although using models that takes into account changing wellbore storage can sometimes reproduce the observed effects, but with little added quantitative value. The important task is to identify the problem and discount the period of perturbation when the data is being analysed by simply ignoring this part of the data and being able to explain why the data was ignored.

The simple identification that a problem exists will also help the engineer in making static pressure corrections. The fact that the pressure gauges sensing points are seldom at the level of the sandface is often overlooked by the interpretation engineer.

Classically, the static pressure (p_i , p^* , p bar, final build-up pressure) is corrected:

- From the gauge depth to the sandface using a static well static gradient.
- From the sandface to a common reservoir datum using the reservoir gradient taking into account any gradient changes.

This correction is usually done manually and is essential to establish reservoir pressure trends, declines and depletion rates.

In the past the dynamic pressure was not corrected as this involved advanced modeling with multiphase flow. Today many such flow models are available. The advanced correction of dynamic pressure data is covered in the chapter on wellbore models.

3.I More on QA/QC

3.I.1 Diagnosing phase segregation from differential pressure

Differential Pressure Analysis is an intelligent evaluation observed anomalies, and an attempt to identify the fluid phases in the wellbore near the gauge sensing points. It gives a reasonable idea of wellbore occurrences and the fluid distribution.

This only gives approximate results and it cannot be used for all types of wellbore phenomena. Nevertheless it enhances the operational understanding and allows for an intelligent correction to reservoir datum with more confidence. Such analysis will also enhance the confidence in the material balance calculation and the identification of drainage patterns.

Practically it involves a choice of several recognizable events on the difference channel (blue circles in the figure below) and transfers the different delta pressure values to a simple spreadsheet. Estimation of fluid gradients is based on the known fluid densities and resulting changes in the pressure gradient, that makes the total picture logical by applying a global gauge offset.

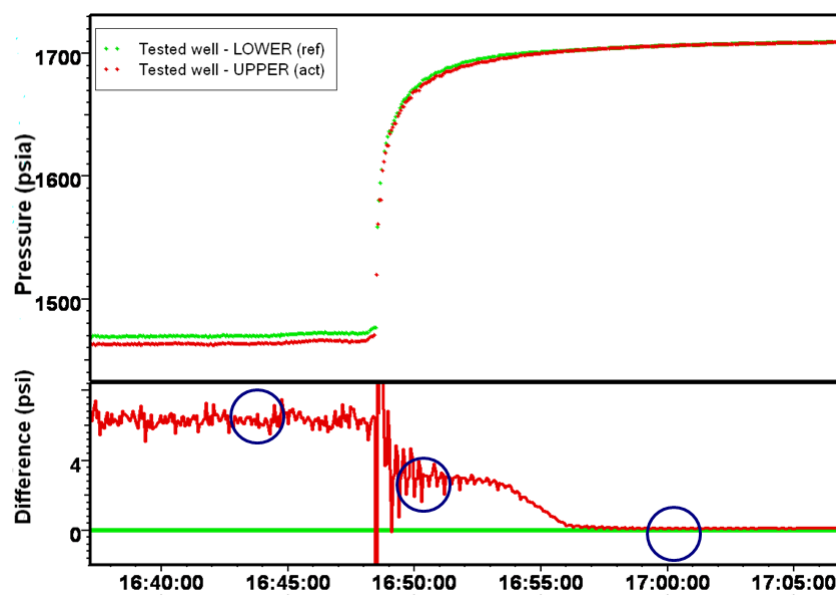


Fig. 3.I.1 – QAQC plot with events marked on difference channel

This method does not only reveal wellbore anomalies. It also determines the pressure gauge offset, which will have to be within the range of the gauge manufacturer's claimed accuracy and resolution.

DIFFERENTIAL PRESSURE ANALYSIS

Events	From Difference Channel		dp Gradient	Assumed Fluid	Assumed Gradient	Calculated dp	Implied Offset	Observed dp	Residual difference
	Time	dp							
[1]	(hrs) [2]	(psi) [3]	(psi/ft) [4]	[5]	(psi/ft) [6]	(psi) [7]	calculated [8]	corrected [9]	(psi) [10]
Event 1	17.10	6.30	0.69	Friction	0.714	6.510	-0.210	6.510	0.000
Event 2	17.18	2.90	0.317	Oil	0.341	3.110	-0.210	3.110	0.000
Event 3	17.33	0.20	0.02	Gas	0.045	0.410	-0.210	0.410	0.000
Distance between sensors:			9.12 ft	Assumed Accuracy Offset:			-0.21 psi		

Column (2) and (3) are read directly from the difference channel from the quality control plot. Column (4) is the differential gradient calculated from column (3). Column (5) and (6) are intelligent guesses or assumptions by the user that will normalize column (8), i.e. the same implied gauge offset applies whatever the assumed fluid phase is present.

The implied offset is then entered by the user in its appropriate box below the table, and the residual differences will become close to zero or zero, if the correct assumption as to the fluids present in the wellbore have been made.

The implied offset becomes the gauge offset which has to be within the gauge specifications to be acceptable to the operator.

This analysis gives a much better idea as to which of the fluid gradients to use to correct the gauge pressure to top of sandface.

Another product of this approach is being able to decide which part of the data is really valid for pressure transient analysis as all data affected by the segregation or fluid movements must be discounted in the interpretation process. The impact of not knowing and understanding the wellbore environment is now described.

3.1.2 Impact on the diagnostic

The impact on the Pressure Transient Analysis can be substantial, as illustrated below. The upper gauge is affected by phase segregation and the shape of the derivative is clearly distorted, resulting in the wrong choice of interpretation model.

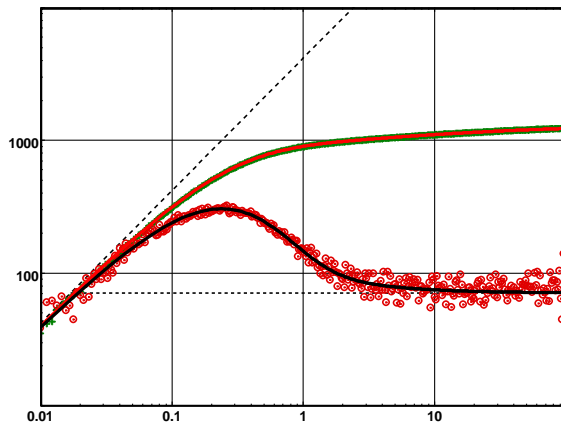


Fig. 3.1.2 – Lower gauge; homogeneous

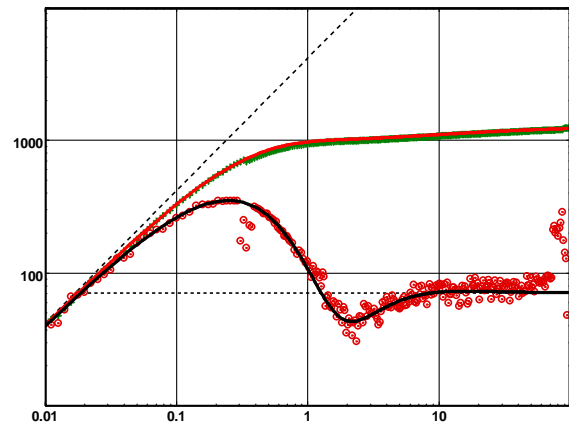


Fig. 3.1.3 – Upper gauge; double porosity

3.1.3 Gauge drift

Gauge drift is caused by unstable electronic components and fatigue of the sensing material used in the instruments. Strain gauges are particular susceptible to this problem.

Drift during a relatively short well test is uncommon, especially today as the quality of electronic gauges has increased immensely. However, it still does happen, and a severe drift will lead to a wrong PTA diagnostic.

The drift problem is more common during long term measurements and can therefore be a real problem in permanent downhole gauges (PDG).

In any case it is important to check the data for validity through the QA/QC procedures described in this document before attempting any serious analysis. To identify a drifting gauge it is necessary to have two or more measurements and study the difference channel constructed between a reference gauge and all the other gauges.

The following figures illustrate the difference channel and the impact on the analysis of the drifting gauge if we did not know that such drift exists.

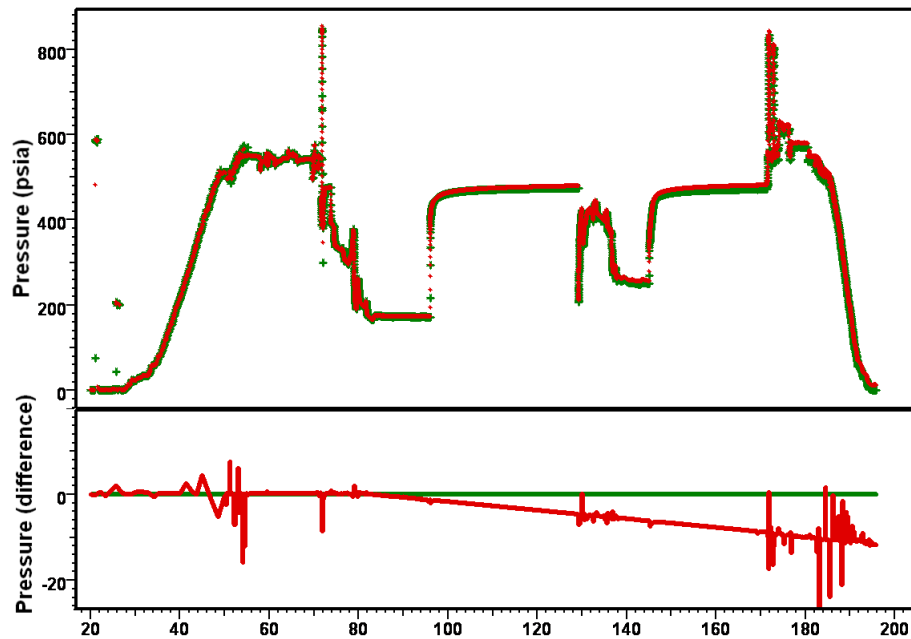


Fig. 3.I.4 – QA/QC plot with difference

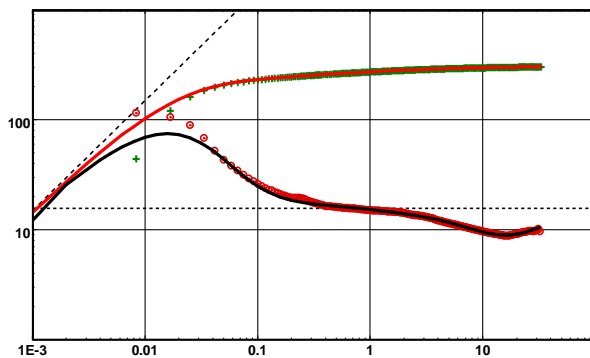


Fig. 3.I.5 – Match non drifting gauge, no fault

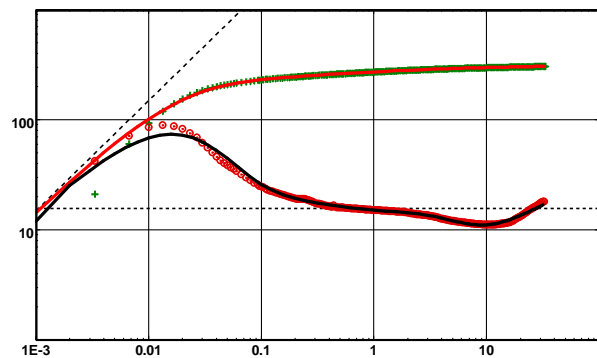


Fig. 3.I.6 – Match drifting gauge, with fault

3.I.4 Phase redistribution

When different phases are produced the redistribution of fluids in the wellbore at shut-in may be almost instantaneous and produce what is called 'gas humping'. This may (seldom) be seen in a water / oil case also. At shut-in the fluid mixture separates and a total reversal of fluids occurs in the wellbore. The heavier fluid moves to the bottom of the well and the lighter fluid, usually gas, accumulates at the top. This can produce a hump in the pressure at shut-in sometimes above the reservoir pressure.

Only when the two phases are stabilized will the buildup return to a normal pressure difference and the response may be analyzed.

The below figure illustrates how the pressure at the sandface at early time can actually rise above reservoir pressure. Imagine a well with a well head pressure A . The upper part of the well is filled with a liquid/gas mixture of a certain weight and in the lower part of the well gas is predominant (admittedly, a rather theoretical assumption). The gas phase at the bottom is considered weightless. In between the two phases is a frictionless piston. The gauge pressure at the bottom of the well is therefore the wellhead pressure plus the weight of the oil mixture, $A+P$. Let's now assume that we turn this cylinder upside down, the wellhead pressure stays at $A+P$ and the bottom hole pressure increases to $A+2P$. This induces an abnormal rise in the bottom hole gauge pressure that can be above reservoir pressure.

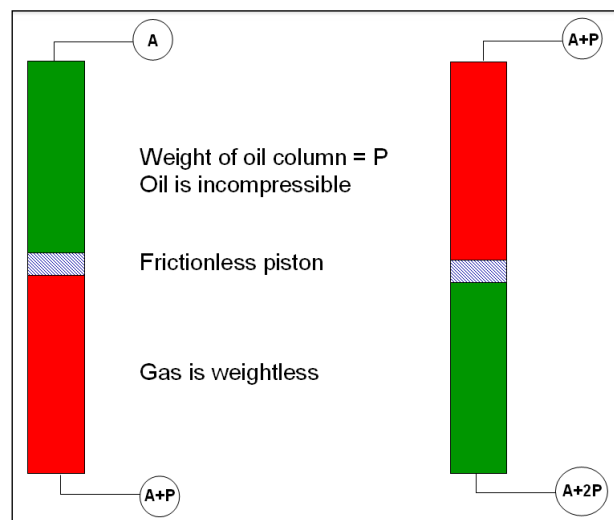


Fig. 3.I.7 – Gas humping

See the following figure that illustrates the hump caused by this phenomenon. This is a classical feature in Pressure Transient Analysis.

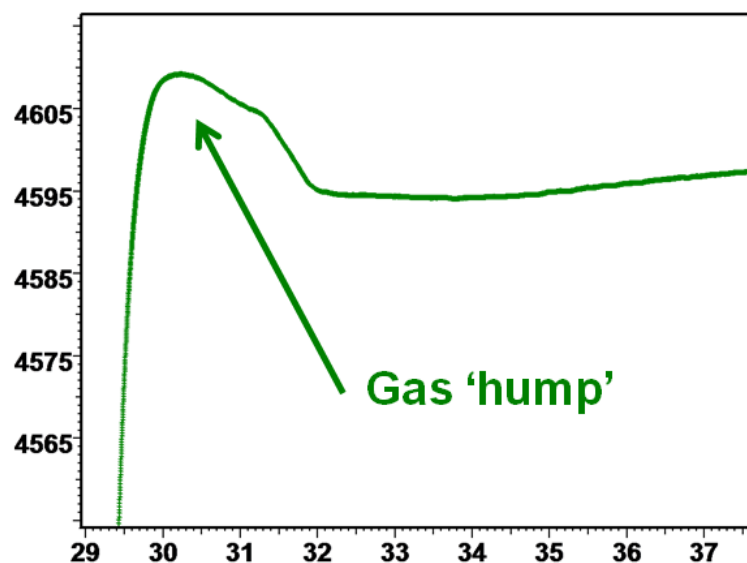


Fig. 3.I.8 – Gas humping

3.J The case of dry gas

3.J.1 Diffusion of real dry gas

As mentioned in the 'Theory' chapter, in order to extend the methodology of Dynamic Data Analysis to gas cases, we introduce a function of the pressure called the pseudopressure. It is given by:

Gas pseudopressure:

$$m(p) = 2 \int_0^p \frac{p}{\mu Z} dp$$

Using the gas pseudo pressure instead of the pressure, the diffusion equation remains valid the same methodology presented above can apply.

In addition to these methods, the gas case presents few particularities presented here.

3.J.2 Correcting the pressure to sandface

Usually the pressure gauge is not set at the sandface due to mechanical constraints in the completion. Because of this, the results obtained from the pressure transient analysis are at the level of the gauge and not the sandface which, in terms of pressure (P_i) and skin (S), will not reflect the true sandface conditions.

It is necessary first to define the vertical pressure profile in the well. The Saphir/Topaze internal flow correlations or an actual lift curve generated by some specialized program (i.e. Amethyste) can be used for this.

The available correlation for gas is an external lift curve or the internal Cullender & Smith method, but with two modifications for handling water and condensate.

The correlation is based on the gas properties as defined in the PVT setup, and a general friction factor is calculated using the Colebrook and White equation. Note that when you deal with a condensate case with equivalent gas gravity and total rates, the proper gradient and rates are used in the correlation to account for the condensate presence. The presence of water can be accounted for, based on a constant water to gas production ratio.

The solution selected in Saphir is to include both the hydrostatic and friction pressure loss in the model and correct the generated model response to the actual gauge depth, and then to return all the results at the sandface.

In fact, the gauge pressure is not transformed, nor corrected hence it is the model that is brought to the level of the gauge.

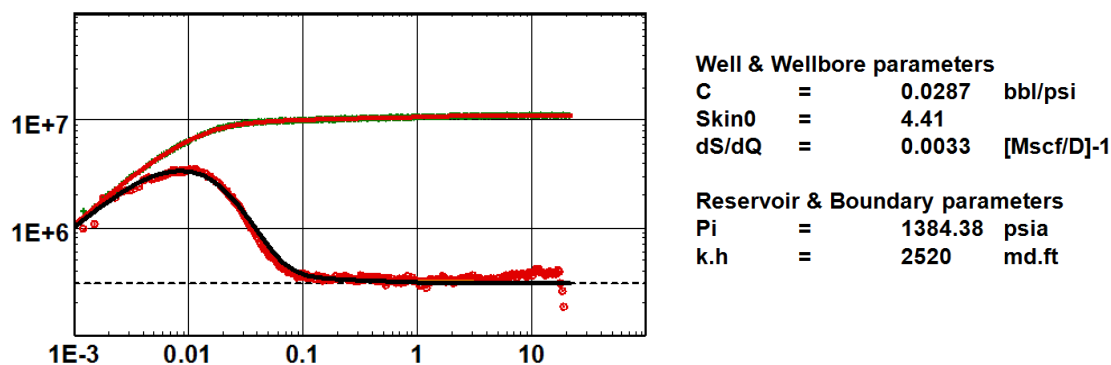


Fig. 3.J.1 – Analysis at gauge level

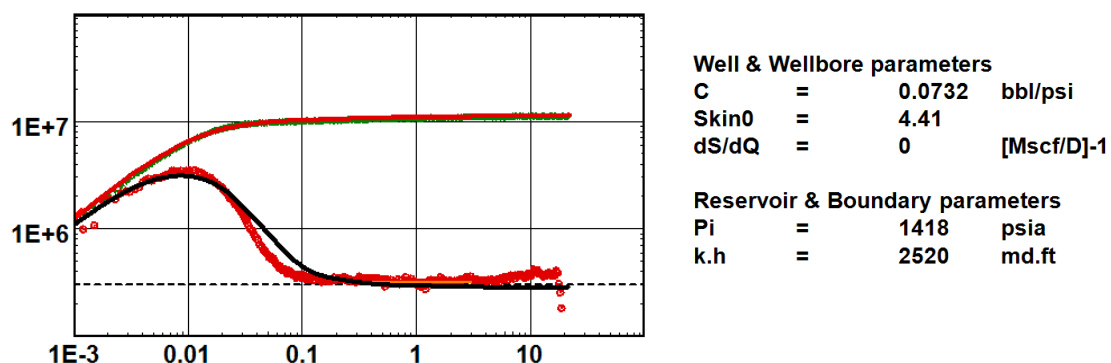


Fig. 3.J.2 – Analysis after model correction to gauge level

You can observe that results (P_i and skin) are now returned at the sandface and that the rate dependent skin attributed to the formation is now a lot smaller and should be attributed to the pressure loss through, in this example, the 1000 ft of 1.5"ID tubing.

Once the sandface parameters have been returned by the model match, the sandface pressure can be properly corrected to a common reservoir datum though the, hopefully appropriate, knowledge of the fluid gradients in the reservoir.

3.J.3 Gas material balance

The issue of material balance in gas diffusion has become increasingly critical in recent years with the spread of permanent gauges. The origin is the same as for changing wellbore storage. Even with the use of pseudopressures, the diffusion equation can be considered linear for as long as the diffusion terms left outside the time and pressure variables remain constant. This time, we are not facing problems of changing wellbore storage, a process only linked to the pressure in the wellbore, but to the whole diffusion process throughout the reservoir.

Diffusion equation:

$$\frac{\partial m(p)}{\partial t} = 0.0002637 \frac{k}{\Phi \mu c_i} \nabla^2 m(p)$$

As soon as we have a pressure gradient in the reservoir, the diffusion term, and especially the product μc_t , will become different from one reservoir block to the next.

Although one could consider that it also happens during any well test, this becomes critical when the reservoir average pressure declines in the reservoir and/or in the well drainage area. It is therefore necessary to adjust the models or the data.

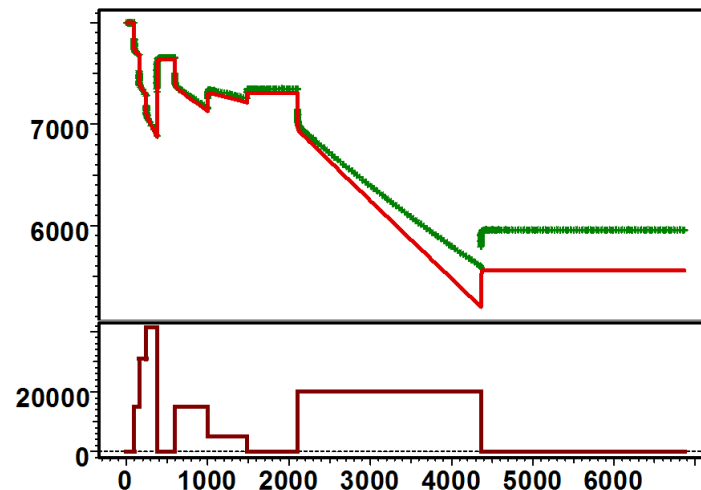


Fig. 3.J.3 – Match without a material balance correction

If we look at a real gas simulation for a long term limit test, or a production survey using permanent gauges, and use it to match with an analytical model where the diffusion was taken at initial pressure, we can see a divergence between the simulated pressure and the measured data, even though the reservoir geometries and the PVT used are strictly the same.

There are again three ways to handle this problem:

3.J.3.a Using pseudotime functions

It is the same principle as for the changing wellbore storage, but this time the pressure from which the pseudotime function is calculated will be the reservoir, or drainage area, average pressure:

- The process starts from an initial estimate of the reservoir initial pressure and volume. These two parameters are required to calculate the initial gas in place G_i .
- At each time step, the cumulative production is calculated and subtracted from the initial gas in place. A standard p/Z calculation is used to estimate the reservoir average pressure at this time, to be used to calculate the pseudotime integral, and then the pseudo time. This pseudotime is used on the loglog plot, and the data is therefore expanded to the right, allowing the match with a classic closed system type-curve.

This method was useful at the time when one only had type-curves as models. Today computers can do much better and faster. The main shortcoming was that the initial estimate of the volume and the initial pressure was made before the model was matched. The model would give a value of initial pressure and volume, which might not be the same as the initial guess, hence requiring another modification of the data, another match, and so on. The process would however, converge quickly.

3.J.3.b Integrating the material balance correction in the analytical model

The theory behind this solution is the same, but the use of a model makes the process simpler and more coherent. The model includes a reservoir size and an initial pressure. So the initial gas in place can be calculated as an integral part of the model. At any time step the algorithm calculates the average pressure from the cumulative production using p/Z , and replaces the viscosity and total compressibility in the superposition by the one coming from the average pressure. So at any time step the simulated pressure is coherent with the material balance of the model. The optional derivation is shown below:

We consider the total gas in place at initial pressure. V_{res} is the pore volume occupied by the gas. T_{res} is the fluid temperature at reservoir conditions. G_i is the initial gas in place at standard conditions.

Real gas equation at initial pressure:
$$p_i V_{res} = Z_i n R T_{res}$$

Same amount of fluid at standard conditions:
$$p_{sc} G_i = n R T_{sc}$$

So we get immediately G_i :

$$G_i = \frac{p_i}{Z_i} \cdot \frac{V_{res} T_{sc}}{p_{sc} T_{res}}$$

We now consider, at time t , the same situation after a total cumulative production of $Q(t)$. We now want to calculate the average reservoir pressure:

Real gas equation at initial pressure:
$$\bar{p} V_{res} = \bar{Z} n(t) R T_{res}$$

Same amount of fluid at standard conditions:
$$p_{sc} (G_i - Q(t)) = n(t) R T_{sc}$$

So we get immediately G_i :

$$G_i - Q(t) = \frac{\bar{p}}{\bar{Z}} \cdot \frac{V_{res} T_{sc}}{p_{sc} T_{res}}$$

We calculate the average pressure from:

$$\frac{\bar{p}}{\bar{Z}} = \frac{p_{sc} T_{res}}{V_{res} T_{sc}} (G_i - Q(t))$$

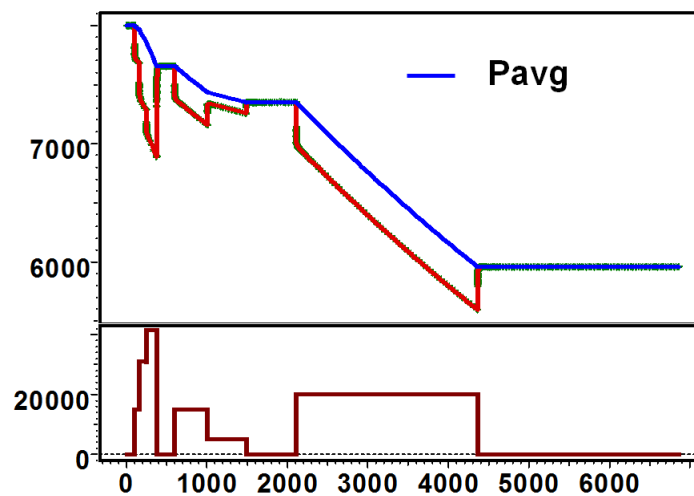


Fig. 3.J.4 – Match with a material balance correction

3.J.3.c Using a numerical model

The use of a numerical model is, conceptually, even simpler. As the gas equation is entered at the level of each cell, the material balance is automatically honoured, not only globally, as above, but at the level of each cell. Solving the problem numerically is by far the most rigorous approach.

As the problem is nonlinear, this requires Saphir NL and the use of a nonlinear solver, but in the case of single gas this will rarely require more than one iteration. So this sort of model, for reasonably simple geometries, will be both fast and accurate.

For information, the case presented above is an actual simulation using Saphir NL.

3.J.4 Non-Darcy flow

As mentioned previously, there are two main options to address non-Darcy flow: using a rate dependent skin model or integrating the Forchheimer equation in a numerical model.

3.J.4.a Simulating non-Darcy flow with a rate dependent skin model

There are two complimentary approaches to determine the rate dependency caused by high flow velocities and turbulence using the simplified assumption that the relationship is linear. In an analytical model the non-Darcy flow effect is simulated by an additional skin using the linear function of the rate.

$$S_{total} = S_0 + (ds/dq)q \quad ds/dq = D$$

This is illustrated in the figure above. D is called the (linear) non-Darcy flow coefficient.

In order to access the rate dependency it is necessary to conduct a multi flowrate test, these tests are described in the chapter Well Performance Analysis.

The classical way of determining the skin versus rate relationship is to use semilog analysis of each flow period if this analysis is valid. Then plot the resulting skin versus the corresponding rate as illustrated in the figure below. This will return the skin without turbulence ie: the mechanical skin, the intercept of the assumed straight-line, S_0 and the rate dependency D derived from the slope. Here it is important to remember that a flow/after flow test with only one single shut-in may not produce the required results as a semilog analysis of a producing period may be impossible due to the inherent fluctuation of the rates masking the pressure response where semilog analysis is valid.

It is therefore recommended to use the type of tests that have intermediate shut-ins, isochronal or modified isochronal, where we stand a better chance of obtaining the skin from the analysis of these shut-ins. The plot of skin versus rate is done automatically in Saphir. The results can then automatically be transferred and the model generated with regression to improve the model match as necessary.

If the skin versus rate plot fails because semilog analysis is not valid, the rate dependency parameters can still be set in the model dialog using an initial guess. Then the model match can be refined by regression.

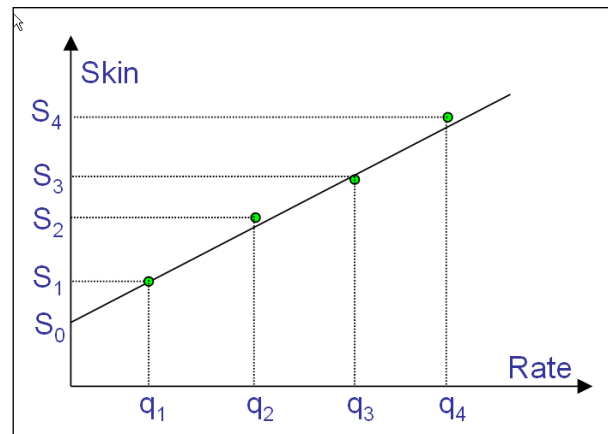


Fig. 3.J.5 – Skin versus rate plot

The figures below show the comparison between a simulation run with a constant skin and a rate dependant skin:

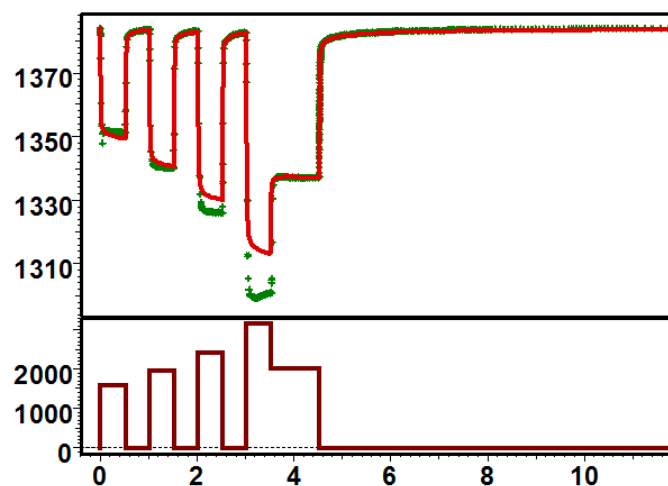
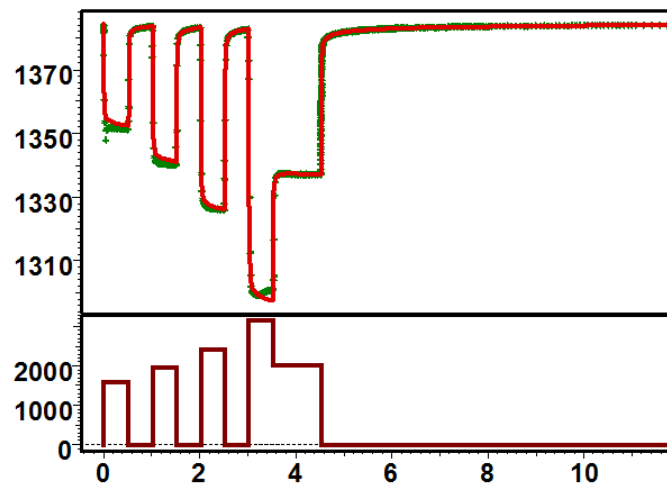


Fig. 3.J.6 – Isochronal test matched with a constant skin



*Fig. 3.J.7 – Test data matched
with a rate dependant skin*

3.J.4.b Simulating non-Darcy flow with a numerical model

In a numerical model the (non linear) non-Darcy flow effect is included in the flow equation through the value of the (non linear) non-Darcy flow coefficient, β which appears in the Forchheimer equation:

$$\frac{\partial P}{\partial x} = \frac{\mu}{k} \cdot u + \beta \cdot \rho \cdot u^2$$

It can be evaluated from the linear assumption described above using ds/dq with:

$$\beta \approx ds/dq \cdot \frac{2\pi r_w \cdot h \cdot \mu}{k}$$

or from an empirical equation:

$$\beta = \frac{0.005}{[\Phi \cdot (1 - S_w)]^{5.5} \cdot k^{0.5}}$$



4 – Production Analysis (PA)

OH – OSF – DV



4.A Introduction and a brief history

Production Analysis (PA) is seen as a natural complement of Pressure Transient Analysis when one has pressure and rate data and wants to make some kind of analysis. This is the case with the spread of Permanent Downhole Gauge (PDG) data, which contain candidate data for both analysis techniques.

PA and PTA share a large technical kernel, and are often performed by the same engineers. This was not always the case, and we will start with a short history of PA.

PA started in the 1920s on a purely empirical basis, and as a financial tool. There was no technical background to these relations, the objective was to find the right decline function that fit the past history and would be able to assess the US\$ revenue in the future.

In the 1940s, the formulation of constant pressure exponential, hyperbolic and harmonic rate decline was published (Arps, 1945). This was still partly empirical, but some parameters could be quantified using specific analyses.

In the 1960s came the first series of type-curves, still assuming constant flowing pressure. The Fetkovich type-curve combined two families of curves: one for the transient flowing period and one for the late time boundary dominated response. Ten years later Carter extended it to the gas case. Other type-curves were later published to address further complex configurations including layered and fractured reservoirs. This was done in parallel to the theoretical work done in PTA.

At this stage the methodology was somewhat equivalent to the standard procedure in PTA in the late 1970s. The Arps plot was the counterpart of the Horner plot, and the constant pressure type-curves were the counterpart of the well test drawdown type-curves.

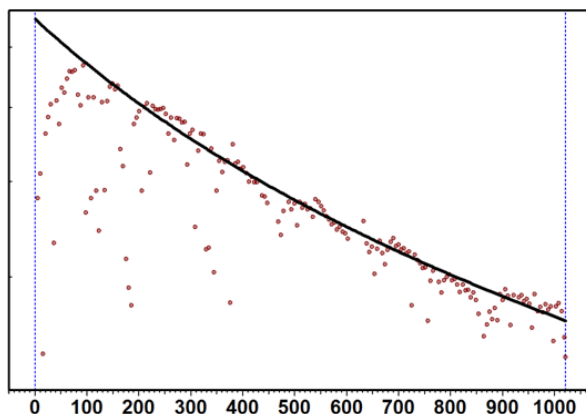


Fig. 4.A.1 – Arps plot

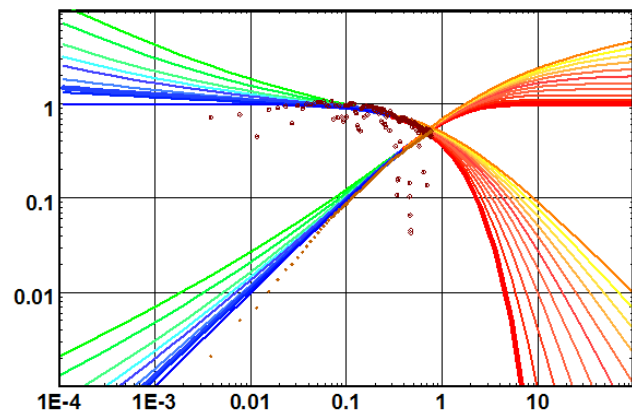


Fig. 4.A.2 – Fetkovich type-curve

As we have seen the introduction of the Bourdet derivative and PCs dramatically changed PTA in the 1980s and 1990s. This did not happen as fast in PA, where most work continued to be done using Arps and Fetkovich methods, generally as side applications linked to the production databases. Unlike PTA, classical methodology in PA was not phased out. In many mature reservoirs, permanent gauges cannot be justified economically, and PA methods will stay as they are, because there are generally no data to justify a more sophisticated approach.

However the theory had evolved in ways akin to those in PTA. Blasingame et al. introduced a variable rates/variable pressure type-curve as a loglog plot of productivity index vs. material balance time, complemented by the equivalent of the Bourdet derivative. An adapted version of the loglog plot, where rate-normalized pressure replaces the productivity index, was also published. Additional solutions accounted for various well and reservoir configurations. So the modern tools were available in theory before the end of the 1980s, but they were only recently implemented in commercial PA applications, such as Topaze.

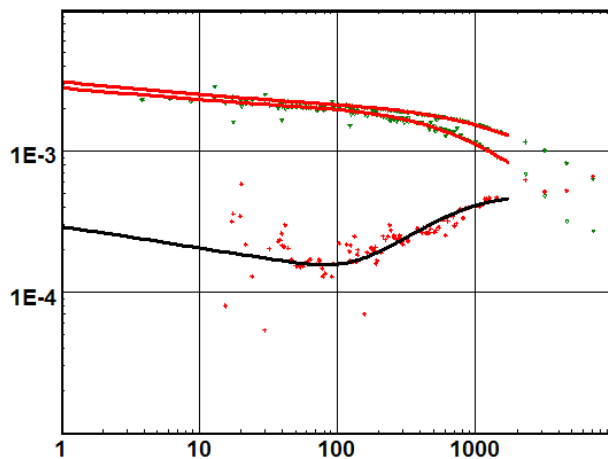


Fig. 4.A.3 – Blasingame plot

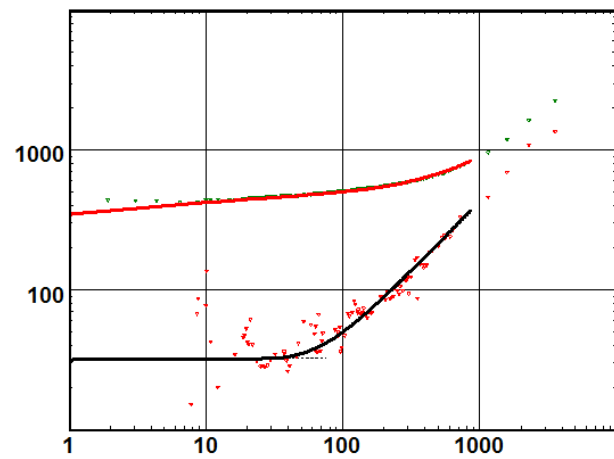


Fig. 4.A.4 – Loglog plot

Advancements in PA started to progress in the late 1990s and early 2000s, partly due to the development of permanent pressure gauges. When engineers started receiving long term continuous pressure data, the first reaction was to load this into a PTA program: "I have rates; I have pressures, so I treat this as a well test". However PTA methodology was not designed for this type of data, and engineers would sometimes perform incorrect interpretation by overlooking specific assumptions that are no longer valid on the time scale of a permanent gauge survey. Material balance errors and over-simplifications using Perrine's approach for multiphase flow property evaluation were, and are, among the most frequently encountered errors.

4.B The old stuff

4.B.1 Arps

Decline Curve Analysis methods, as formalized by Arps in 1945, have been for many years the conventional technique for analysis and forecasting of well production data. Decline type-curves are based on an empirical rate-time and associated cumulative-time equation, which can be expressed in the general form:

$$q(t) = \frac{q_i}{[1 + bD_i t]^{\frac{1}{b}}} \quad Q(t) = \frac{q_i^b}{D_i(1-b)} (q_i^{1-b} - q(t)^{1-b})$$

where: q_i is the initial rate, D_i is the decline factor, and b a parameter varying between 0 and 1, defining the decline type. Three types are usually considered: hyperbolic, exponential and harmonic.

Exponential decline, $b = 0$

It can be shown that the general decline equation tends to an exponential decline when b tends to 0:

$$q(t) = q_i e^{-D_i t} \quad Q(t) = \frac{q_i - q(t)}{D_i}$$

Harmonic decline, $b = 1$

$$q(t) = \frac{q_i}{[1 + D_i t]} \quad Q(t) = \frac{q_i}{D_i} \ln \left(\frac{q_i}{q(t)} \right)$$

Hyperbolic decline, $b \in]0,1[$

The expressions are those above.

Decline curve equations are applicable only after the transient part of the response has ceased, i.e. during boundary dominated flow. A general approach consists in the determination of the three parameters directly, by non-linear regression. The traditional usage however, is centered on the use of some specific presentations where linearity is sought after the value of b has been fixed. Practically, the following scales / linearity can be used:

$\log(q)$ vs t : Linear plot if the decline is exponential, concave upward otherwise.

q vs Q : Linear plot if the decline is exponential, concave upward otherwise.

$\log(q)$ vs Q : Linear plot if the decline is harmonic, concave downward otherwise.

Most PA software allows the scale to be set to the above and more. The regression of the decline is non linear, i.e. it is possible to have the value of b determined from the regression rather than assuming a value of b linked to the particular scale.

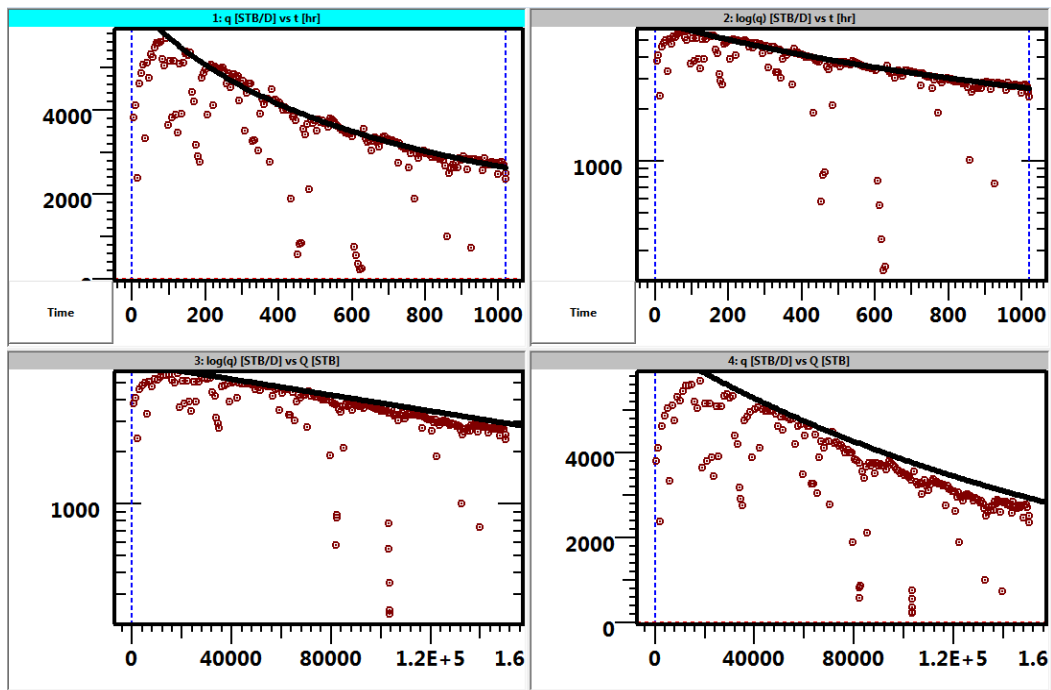


Fig. 4.B.1 – Arps

Once the decline parameters have been obtained, and since the analytical expression of the rate and cumulative are known, it is possible, from a given abandonment rate, to calculate the corresponding abandonment time, and hence the recovery at abandonment.

The abandonment rate is usually defined as either q_a or the ratio $\frac{q_a}{q_i}$.

The abandonment time is noted t_a and the recovery at abandonment $N_p(t_a)$. The figure below illustrates this extrapolation of the Arps plot.

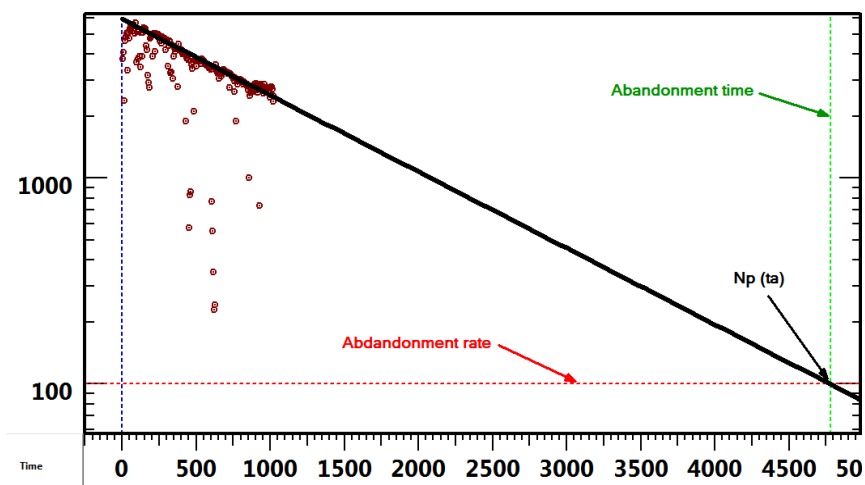


Fig. 4.B.2 – Abandonment

Exponential decline is widely used because of the simplicity of the associated graphical methods. It leads to conservative reserves estimates. Besides, it can be demonstrated that exponential decline is the late time behavior of a constant pressure production in a closed reservoir, with a slightly compressible fluid assumption.

The equation governing the PSS behaviour is:

$$\Delta p = mQ + bq$$

With

$$\Delta p = p_i - p_w$$

Q = cumulative production

q : instantaneous production rate

and

$$m = \frac{1}{Nc_i}$$

Differentiating the two terms of the equation with respect to the time:

$$\frac{d\Delta p}{dt} = m \frac{dQ}{dt} + b \frac{dq}{dt}$$

Under constant production well pressure conditions

$$\frac{d\Delta p}{dt} = 0 = m \frac{dQ}{dt} + b \frac{dq}{dt}$$

We have

$$\frac{dQ}{dt} = q$$

Therefore

$$\frac{dq}{dt} = -\frac{m}{b}q \quad \text{or} \quad \frac{dq}{q} = -\frac{m}{b}dt$$

$$\int \frac{dq}{q} = -\frac{m}{b} \int dt \quad \text{or} \quad \ln q = -\frac{m}{b}t + cst$$

$$q = \exp\left(-\frac{m}{b}t + cst\right)$$

that can be written

$$q = q_i \exp\left(-\frac{m}{b}t\right)$$

There are many situations however, where the general hyperbolic decline is more adequate. This is the case in solution gas drive reservoirs.

In our opinion, and given the power of the non-linear regression, it is better to try and determine all three parameters, including b , systematically.

Above all, it is important to stress that decline curves have many limitations:

- The bottom-hole pressure must be fairly constant.
- The well behavior is assumed constant, e.g. no change in skin with time.
- The drainage area of the considered well is constant, i.e. the producing behavior of surrounding wells must also be stabilized.

A refinement can be made for the case where the decline in the oil rate is caused by an increase in the water cut, mostly in water drive reservoirs with unfavourable mobility ratio. If one replaces the oil rate by the oil cut, f_o the Arps equation can be used for wells with variable gross production. The same plots can be made and extrapolated: $\log(f_o)$ vs t , f_o vs Q and $\log(f_o)$ vs Q .

4.B.2 Fetkovich

In 1980, Fetkovich introduced a type-curve combining the theoretical response of a well in a closed reservoir, and the standard Arps decline curves. The motivation behind this work was to come up with a loglog matching technique applicable to both the transient part of the data and the boundary dominated flow period. By presenting both periods, the Type-Curve would avoid incorrectly matching transient data on decline curves.

A determining preliminary step was that the exponential decline can be shown to be the long-term solution of the constant pressure case. The Fetkovich type-curve is derived assuming a slightly compressible fluid and constant flowing pressure. Extension to gas can be made with the appropriate dimensionless rate expression, as described below. The original type-curve presented by Fetkovich displayed rate only. A composite presentation including the cumulative was later introduced to bring more confidence in the matching process and to reduce the effect of the noise.

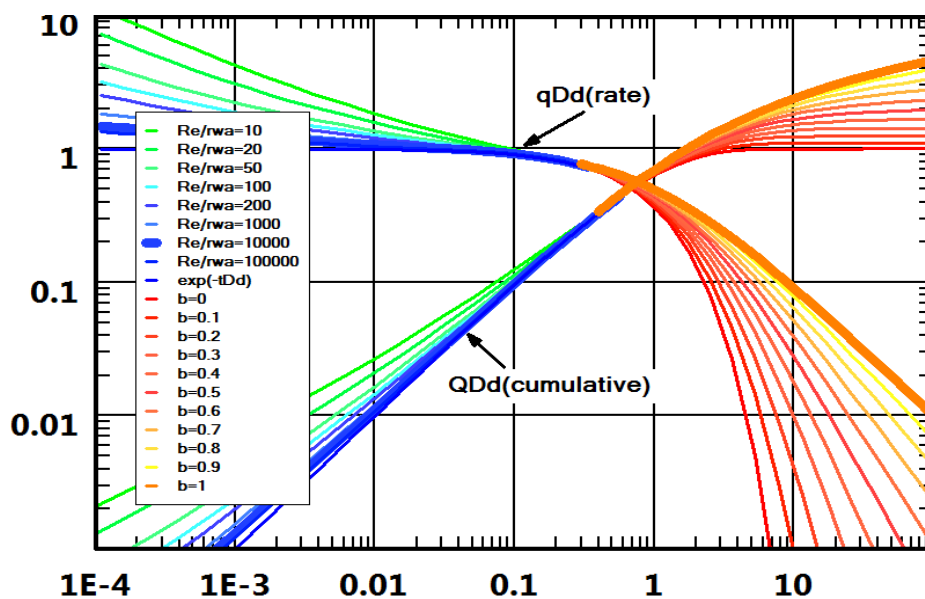


Fig. 4.B.3 – Fetkovich type curve

In the above figure the left region of the curves (green to blue) corresponds to the transient part of the response. On the right hand side, are the Arps decline curves (red to yellow). Note the legend on the left: the red Arps curve is for an exponential decline ($b=0$), the last yellow curve is for a harmonic decline ($b=1$).

The Fetkovich type-curve displays dimensionless values q_{Dd} , Q_{Dd} versus t_{Dd} as defined below. The dimensionless variables can be expressed in terms of the Arps decline curve parameters, or in terms of the transient response parameters. The duality is due to the composite nature of the type-curve showing once again a merge of a theoretical closed reservoir response, and the empirical Arps stems.

All the following equations are in Oil Field Units.

Time

Decline curve dimensionless time: $t_{Dd} = D_i t$

Dimensionless time: $t_D = \frac{0.00634kt}{\phi\mu c_i r_w^2}$

Related by:
$$t_{Dd} = \frac{t_D}{\frac{1}{2} \left[\left(\frac{r_e}{r_w} \right)^2 - 1 \right] \left[\ln \left(\frac{r_e}{r_w} \right) - \frac{1}{2} \right]}$$

Rate

Decline curve dimensionless rate: $q_{Dd} = \frac{q(t)}{q_i}$

Dimensionless flow rate, oil: $q_{D \text{ oil}} = \frac{141.2q(t)\mu B}{kh(p_i - p_w)}$

And the equivalent expression for gas is:

$$q_{D \text{ gas}} = \frac{50300Tq(t)p_{sc}}{T_{sc}kh(m(p_i) - m(p_w))}; \text{ with } m(p) = \int_0^p \frac{2pdp}{\mu Z}$$

q_{Dd} and q_D are related by:
$$q_{Dd} = q_D \left[\ln \left(\frac{r_e}{r_w} \right) - \frac{1}{2} \right]$$

Cumulative production

Decline curve dimensionless cumulative: $Q_{Dd} = \frac{Q(t)}{N_{pi}}$

Where N_{pi} defines the ultimate recovery.

A match will bring values of r_e and kh , D_i and q_i . The type of decline, b is not linked to any of the match ratios, obtained by selecting the correct type-curve. From the external boundary distance, the reservoir pore volume can be calculated. From the Arps parameters, the future performance can be forecast; N_{pi} can be calculated as well as N_p for any specified abandonment rate.

4.B.3 Gas material balance \bar{P}/Z vs Q plot

In case of dry gas reservoir a classical method can also be applied, using the \bar{P}/Z vs Q plot. The method assumes to get several reliable static average pressure values in the well history.

The method is based on the simple material balance equation:

$$Gi = \frac{QB_g}{B_g - B_{gi}}$$

Where Gi is the gas initially in place and Q the cumulative gas production.

Estimating the B_g by:

$$B_g = \frac{0.00504TZ}{\bar{P}}$$

The equation becomes:

$$\frac{\bar{P}}{Z} = \left(-\frac{P_i}{GZ_i} \right) Q + \frac{P_i}{Z_i}$$

This equation indicates that a plot of $\frac{\bar{P}}{Z}$ versus Q extrapolates to the gas initially in place Gi .

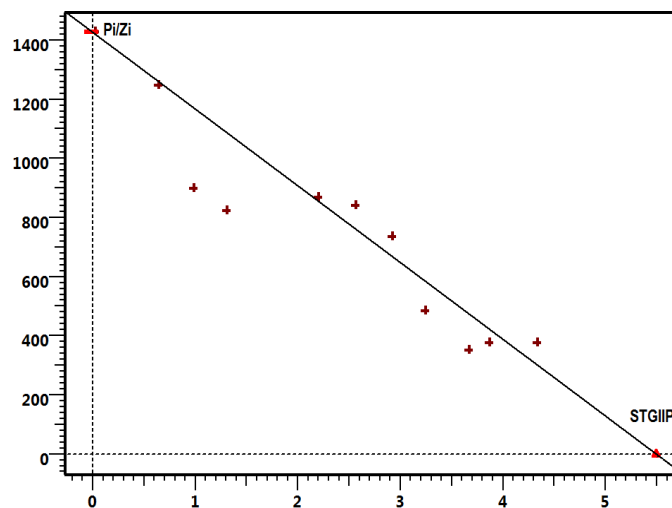


Fig. 4.B.4 – \bar{P}/Z vs Q plot

The validity and the accuracy of this method depend directly on the validity of the static pressure and of the PVT parameters.

4.C The right stuff

4.C.1 Blasingame plot

Previous sections have described the conventional Decline Curve Analysis methods, and their extension using Fetkovich type-curves. We recall that the latter were obtained by combining a theoretical model response and the empirical decline stems of Arps.

Broadly speaking, one could say that the introduction of type-curve matching techniques in production analysis has opened the way to applying methods developed for well test interpretation to the analysis of production data. The main limitation in the Fetkovich type-curve is the assumption of constant flowing pressure. Blasingame and McCray noted that using a pressure normalized flow rate when the bottom-hole pressure varies significantly did not remedy the problem. They sought functions that would transform the variable pressures/variable rates solution into an equivalent constant pressure or constant rate solution. They introduced two specific time functions, t_{cr} the constant rate time analogy, and t_{cp} for constant pressure. For the liquid case, the constant rate analogy time function is defined as the ratio of the cumulative and the flow rate:

$$t_{cr} = \frac{Q(t)}{q(t)}$$

When the normalized rate $\frac{q(t)}{p_i - p_w(t)}$ is plotted versus this function on a loglog scale, the boundary dominated flow period follows a negative unit slope line:

The Black Oil Pseudo Steady State flow rate equation is:

$$\frac{q_o}{\Delta p} = \frac{1}{b_{o,ps} + m_{o,ps} \bar{t}}$$

With:

$$m_{o,ps} = \frac{1}{N C_t} \frac{B_o}{B_{oi}} ;$$

$$b_{o,ps} = 141.2 \frac{\mu_o B_o}{kh} \left[\frac{1}{2} \ln \left[\frac{4}{e^\gamma} \frac{1}{C_A} \frac{A}{r_w^2} \right] + s \right] ;$$

and

$$\bar{t} = \frac{N_p}{q_o}$$

When the Pseudo Steady States dominates $\frac{q_o}{\Delta p}$ is function of \bar{t} at exponent (-1).

Therefore a loglog plot of $\frac{q_o}{\Delta p}$ vs \bar{t} will show a negative unit slope straight line.

Note: Periods of very low rates give artificially high values of $\bar{t} = \frac{N_p}{q_o}$ then the equation

$\frac{q_o}{\Delta p} = \frac{1}{b_{o,pss} + m_{o,pss}\bar{t}}$ tends to $\frac{q_o}{\Delta p} = \frac{1}{m_{o,pss}\bar{t}}$ the points are found on the same -1 unit slope straight line.

Based on this result, Palacio and Blasingame introduced type-curves that could be used for variable flowing pressure conditions. In order to improve the type-curve analysis the Bourdet derivative was also considered. However, due to the noise inherent to the production data, the derivative was not applied to the normalized flow itself but to its integral. More precisely, the Palacio-Blasingame type-curve plot shows the following:

Normalized rate:

$$PI(t) = \frac{q(t)}{p_i - p_w(t)}$$

Normalized rate integral:

$$PI\ Int. = \frac{1}{t_e} \int_0^{t_e} PI(\tau) d\tau = \frac{1}{t_e} \int_0^{t_e} \frac{q(\tau)}{p_i - p_w(\tau)} d\tau$$

Normalized rate integral derivative:

$$PI\ Int.\ Derivative = \frac{\partial(PI_{Int})}{\partial \ln(t_e)}$$

All three curves are plotted against t_e on a loglog scale:

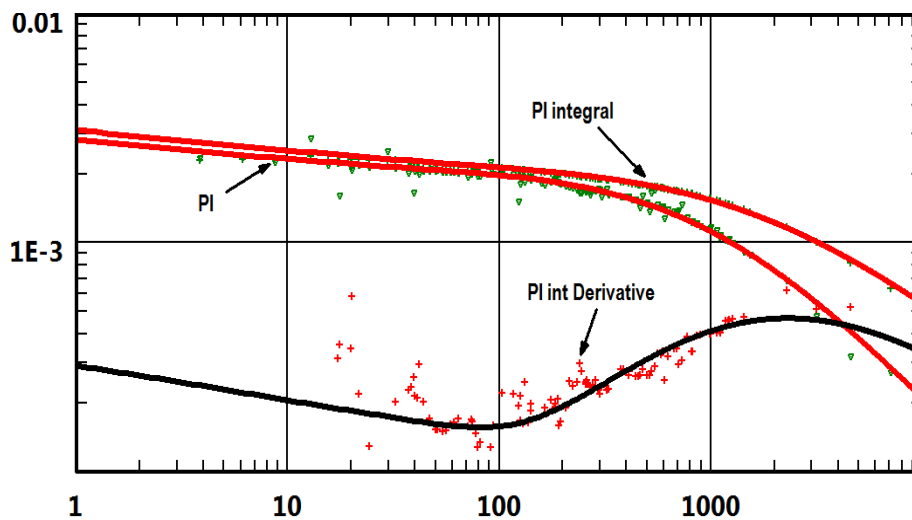


Fig. 4.C.1 – Blasingame plot

The traditional method of using this presentation is in conjunction with type-curves for a particular well model (see figure below).

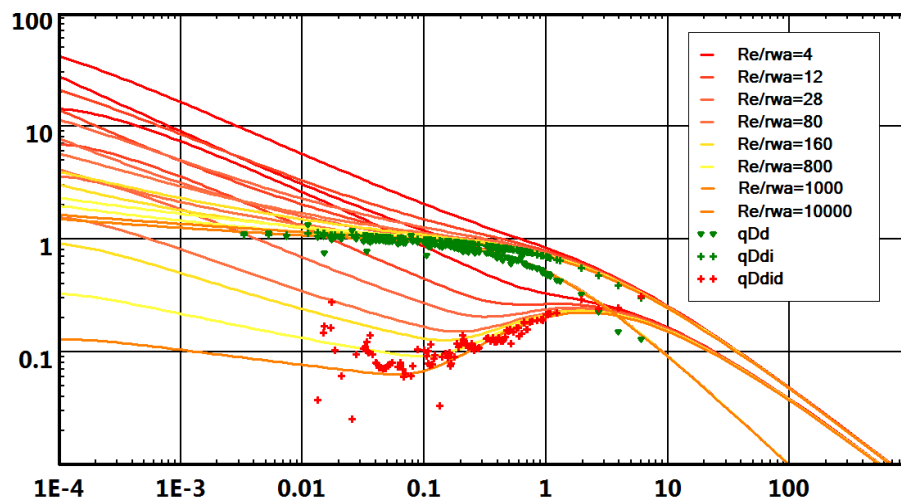


Fig. 4.C.2 – Blasingame type curve

This plot is used as a diagnostic tool, where the data and a model response are compared. The model can be any model, analytical or numerical, single or multi-well, etc. One can either display the 'true' model response, i.e. the response to the full pressure history, or the response to a single pressure step. The single step response shows the signature of the model in a clear, and usable form, whereas the response to the real history is usually very erratic, because the equivalent time is jumping back and forth in time.

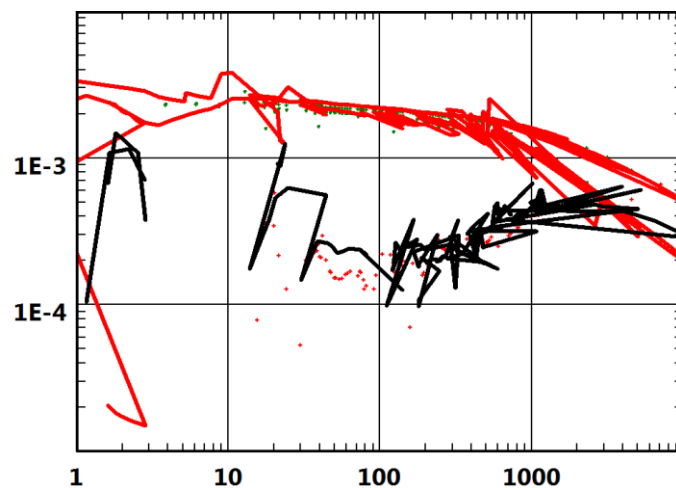


Fig. 4.C.3 – Blasingame plot with 'true' model response

4.C.2 Loglog plot

By replacing the time with an equivalent time, defined as the ratio of the cumulative to the flow rate, one can transform a variable flowing pressure test into a constant rate equivalent, at least for a liquid case. The parallel with constant rate solution can be taken one step further if, rather than working with a pressure-normalized rate, we work with rate-normalized pressure.

In other words for the liquid case, if we plot $\frac{p_i - p_w(t)}{q(t)}$ versus $t_e = \frac{Q(t)}{q(t)}$ on a loglog scale the boundary dominated flow will exhibit a unit slope line, similar to pseudo-steady state in Pressure Transient Analysis. Furthermore, if we take the derivative of the normalized pressure with respect to the logarithm of t_e , the transient part will exhibit a stabilization at a level linked to the mobility.

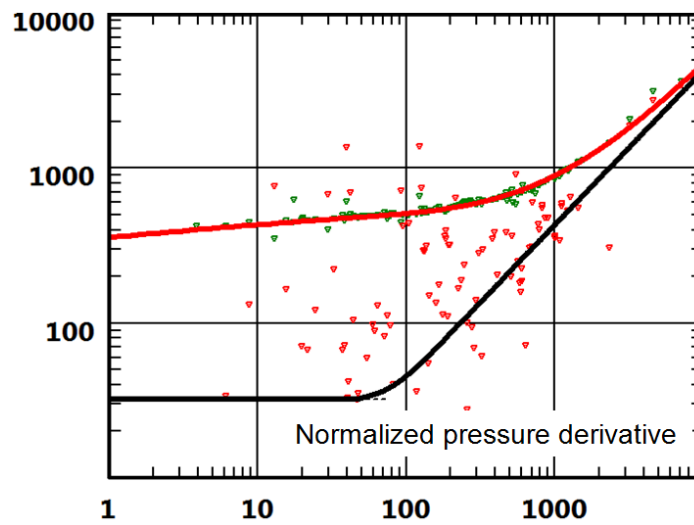


Fig. 4.C.4 – Loglog plot with normalized pressure derivative

The similarity with PTA is thus complete. Yet, the noise level on the derivative is usually too high, see the figure above. One workaround is to work with a normalized pressure integral, in a manner analogous to what was done on the Palacio-Blasingame type-curves.

Integral of normalized pressure:

$$I(t_e) = \frac{1}{t_e} \int_0^{t_e} \frac{p_i - p_w(\tau)}{q(\tau)} d\tau$$

Bourdet derivative of the Integral of normalized pressure: $I'(t_e) = \frac{\partial I(t_e)}{\partial \ln(t_e)}$

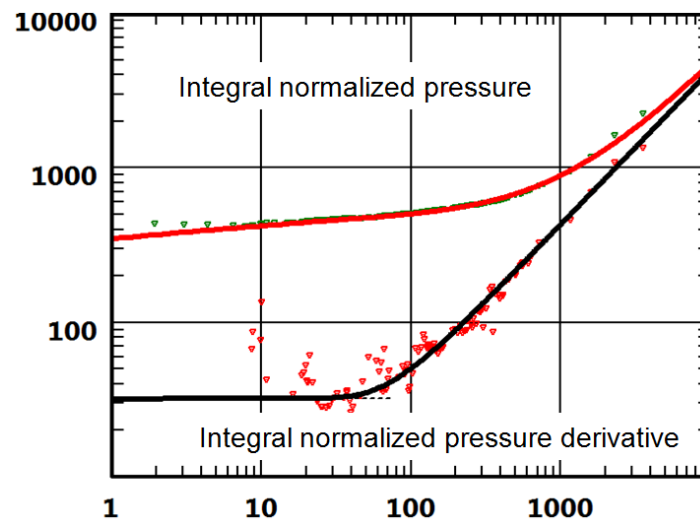


Fig. 4.C.5 – Loglog plot, integral of normalized pressure and derivative

Using the integral preserves the signature of the flow regimes while significantly reducing the noise. Hence such definitions provide a diagnostic tool where most of the usual well test methods can be used. In particular, it is clearly possible to get an estimate of the reservoir kh from the derivative stabilization level. The kh being known, one can then get a first estimate of the reservoir size from the unit slope late time trend. These calculations are an integral part of the loglog plot. It is possible to either display the 'true' model response, i.e. the response to the full pressure history, or the response to a single pressure step. The single step response, used in all the figures above, shows the signature of the model in a clear and usable whereas the response to the real history is usually very erratic, because the equivalent time is jumping back and forth in time as illustrated in the figure below.

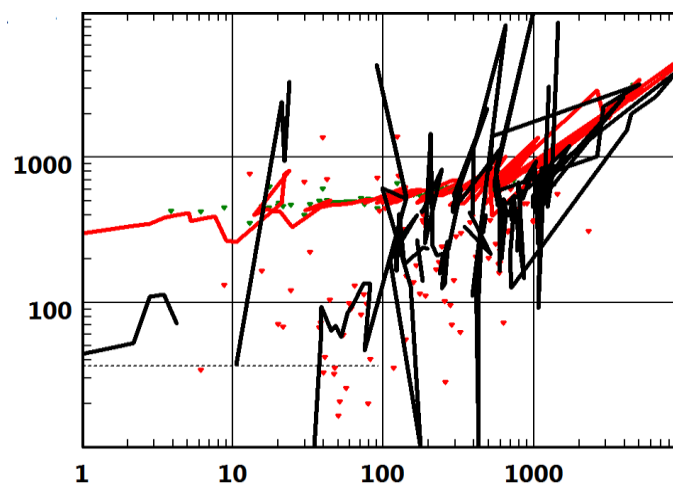


Fig. 4.C.6 – Loglog plot with 'true' model response

4.C.3 Material balance (Normalized rate-cumulative) plot

Agarwal et al. presented a Cartesian plot of dimensionless rate q_D versus dimensionless cumulative Q_{DA} .

They show that the responses corresponding to distinct reservoir sizes all exhibit a straight line with a negative slope during boundary dominated flow, and all curves converge to the same value on the X axis, equal to $1/2\pi$. In other words, the following relation is established in all cases during boundary dominated flow:

$$q_D = \frac{1}{2\pi} - Q_{DA}$$

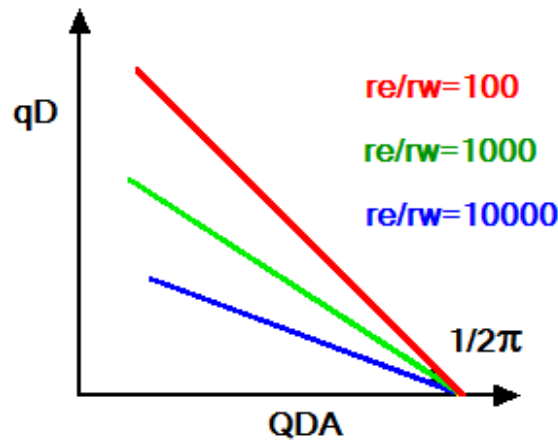


Fig. 4.C.7 – Agarwal et al plot

The expression of the dimensionless variables varies depending of the fluid type and a specific treatment must be applied in each case.

Oil

For an oil case, the expression of the dimensionless parameters is defined below:

$$q_D = \frac{141.2qB\mu}{kh(p_i - p_w)} \quad \text{and} \quad Q_{DA} = \frac{0.8936QB}{\phi hAc_t(p_i - p_w)}$$

All equations are in Oil Field units.

The dimensionless cumulative production can be expressed in terms of the fluid in place, in STB/D:

$$N = \frac{\phi hA}{5.615B}$$

$$Q_{DA} = \frac{0.8936Q}{5.615Nc_t(p_i - p_w)} = \frac{Q}{2\pi Nc_t(p_i - p_w)}$$

So the linear relationship between dimensionless rate and cumulative becomes:

$$\frac{141.2qB\mu}{kh(p_i - p_w)} = \frac{1}{2\pi} - \frac{0.8936QB}{5.615Nc_t(p_i - p_w)}$$

Using the full definition of the dimensionless variables requires an a priori estimate of PV, basically what we are after. Therefore the method presented by Agarwal-Gardner is iterative.

However we see from the above equation that if we plot $\frac{q}{p_i - p_w}$ versus $\frac{Q}{c_t(p_i - p_w)}$ boundary dominated flow will exhibit a straight line which intercept with the X axis gives directly N.

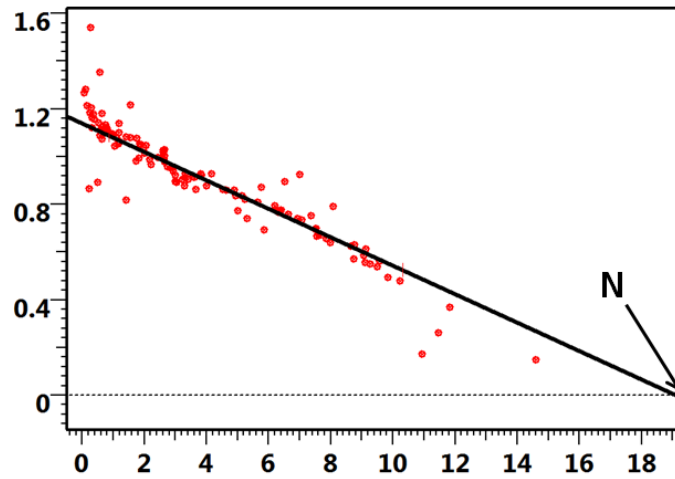


Fig. 4.C.8 – Material balance plot

Note: In the case of constant flowing pressure, it is interesting to draw a parallel between this rate cumulative plot and the rate cumulative plot used in traditional decline curve analysis. The traditional decline methods yield a maximum recovery rather than fluid in place. The relation between the two methods is established by considering a recovery factor of $RF = c_t(p_i - p_w)$.

4.C.4 Flowing gas material balance plot

The principle is to get from flowing data a plot that resembles a normal P/Z plot made in terms of reservoir average pressure. As always the problem with this kind of analysis is that one needs the results sought to build the plot, leading to an iterative procedure.

The Material Balance equation in gas is written:

$$\frac{m_n(p_i) - m_n(\bar{p})}{q_{(t)}} = \frac{1}{(c_t^i G_i)} \times t_a + b \quad (1)$$

Where the normalized pseudo pressure and equivalent time functions are defined as:

$$m_n(p_i) = \frac{\mu_i z_i}{2p_i} \int_{p_{base}}^p \frac{2p}{\mu z} dp$$

$$\bar{t}_{egas} = \frac{\mu_{gi} c_{ti}}{q_g(t)} \int_0^t \frac{q_g(t)}{\mu_g(\bar{p}) c_t(\bar{p})} dt$$

Using the equality derived from the P.S.S. equation:

$$t_a = \frac{\mu_i c_i^i Z_i G_i}{q(t) 2 p_i} [m(p_i) - m(\bar{p})]$$

equation (1) can be changed to give:

$$m_n(\bar{p}) = m_n(p_w) + b \times q_{(t)} \quad (2)$$

The principle of the flowing material balance method is:

Create a plot of $\frac{m_n(p_i) - m_n(\bar{p})}{q_{(t)}}$ versus t_a

As the system goes into pseudo steady state flow, the points will converge towards a straight line: the intercept at $t_a = 0$ hrs is b.

Having b:

1. The equation (2) is used to calculate \bar{p} from p_w , b, and $q(t)$.
2. \bar{p}/Z is plotted versus Q :

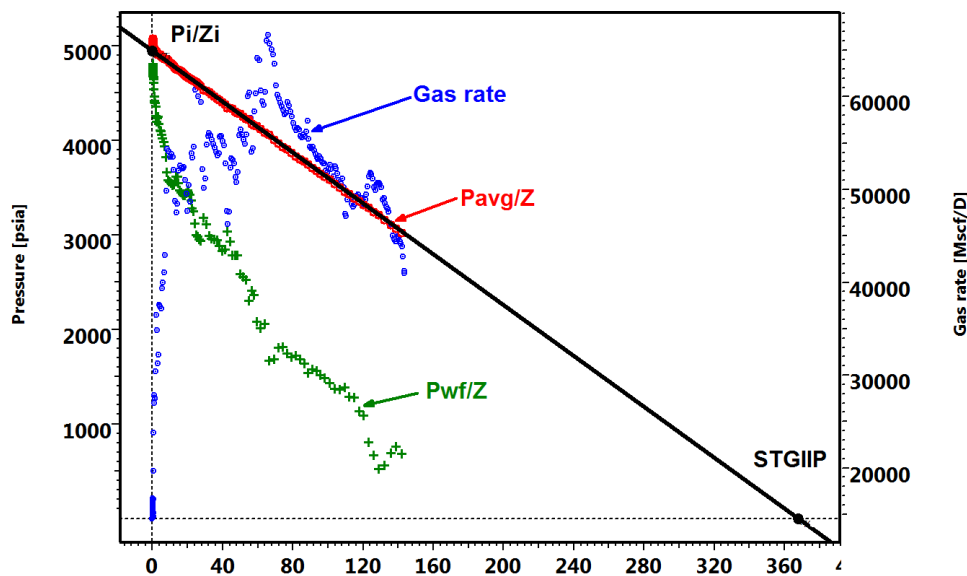


Fig. 4.C.9 – \bar{p}/Z versus Q plot

3. A straight line is drawn through the P_{avg}/Z and extrapolated to get G_i .

Only problem is that the time function used by the first plot, t_a involves the reservoir average pressure hence it requires an estimate of the reserves.

In this Topaze example, the complete procedure follows:

- (1) Estimate G_i beforehand.
- (2) By selecting a time range where the system is believed to be in pseudo steady state, the software performs an automatic regression to determine b using equation (1) and the method defined above.

(3) Then the straight line method will be applied in the plot \bar{p}/Z versus Q , P_i/Z_i can be input to find G_i (STGIIP).

Like most of the methods extrapolating a behavior the constraint is that the well status and production conditions must be constant in the interval used for the analysis.

4.C.5 P-Q diagnostic plot

The two methods presented above require selecting data set during the P.S.S. flow period.

Kabir et al. presented a cartesian plot of P vs q which provides a simple way to perform a diagnosis.

The life of a production well can be divided in three type of behavior:

1. The infinite acting radial flow
2. A period during which the production is maintained and imposed by the completion.
3. The Pseudo Steady State, when the well behavior is boundary dominated.

During the P.S.S. it is demonstrated that the slope dp/dq is governed by the equation:

$$\frac{dp_{wf}}{dq} = \frac{0.2339Bq}{\Phi h c_t A} \left/ \frac{dq}{dt} \right.$$

In a closed system, the rate has an exponential decline, therefore, the slope dp/dq will be constant and function of the drained volume.

A typical P vs Q plot behaviour would be:

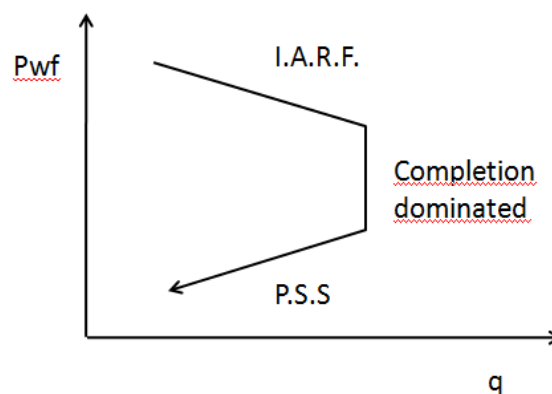


Fig. 4.C.10 – Typical P vs Q plot

That allows diagnosing the various behaviour types on a p vs q plot of any well field data:

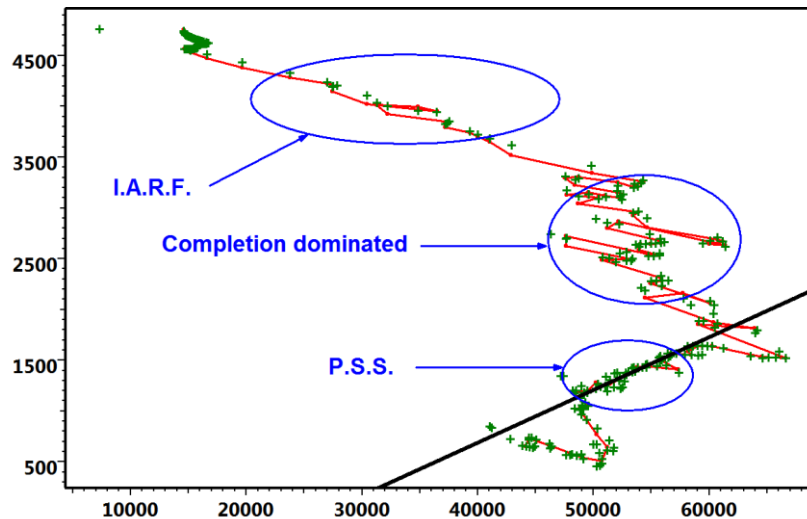


Fig. 4.C.11 – Field example P vs Q plot

Then, the adequate subset of points can be selected to be used in the corresponding methods. It also allows comparing the behaviours from wells to wells in order to detect a possible compartmentalization: if the plot exhibits two different slopes in the P.S.S., that tends to demonstrate that they are depleting two different compartments.

4.C.6 History plot

For complex cases and noisy data where no specific behavior is seen on these diagnostic plots, the linear plot of pressure and rates vs. time becomes the main tool. There is no real diagnostic, just an optimization process. Under these conditions, it is not realistic to expect to estimate more than a productivity index, mobility and a drainage area. In the absence of any other information, the simplest analytical solution, homogeneous circular reservoir, will usually be suitable to model the well drainage area. The use of more complex models can be acceptable if complementary information is available from other sources, and the number of parameters allowed to change in the optimization process is reduced to a minimum.

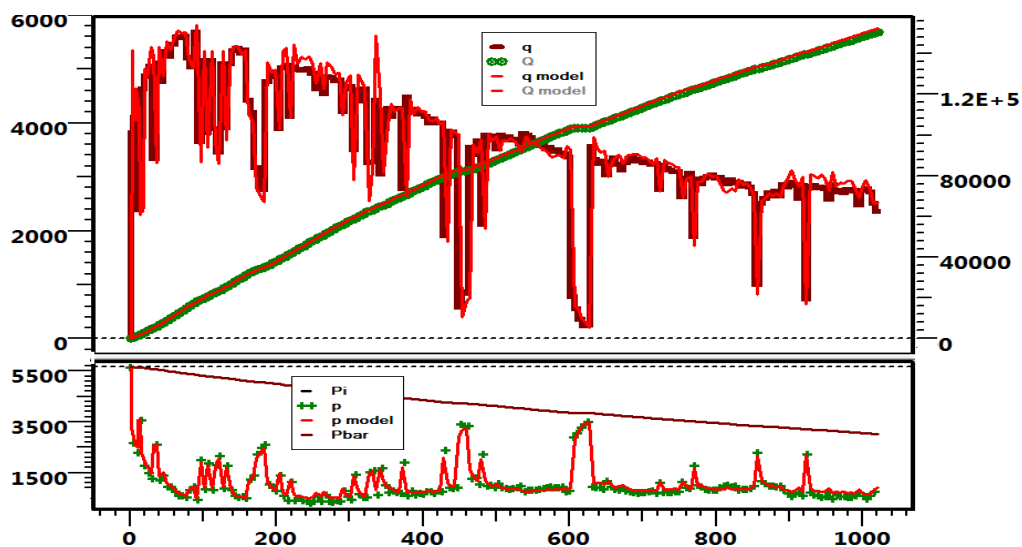


Fig. 4.C.12 – Production history match

4.D The case of dry gas

In this paragraph we present the way the methods created for oil production analysis are modified and adapted to take into account the gas properties specificity.

The original methods specific to gas (and only to gas) production analysis are directly presented in the chapters 'Old Stuff' and 'Right Stuff'.

4.D.1 Diffusion of real dry gas

As mentioned in the 'Theory' chapter, in order to extend the methodology of Dynamic Data Analysis to gas cases, we introduce a function of the pressure called the pseudopressure. It is given by:

Gas pseudopressure:

$$m(p) = 2 \int_0^p \frac{p}{\mu Z} dp$$

Using the gas pseudo pressure instead of the pressure, the diffusion equation remains valid the same methodology presented above can apply.

In addition to these methods, the gas case presents few particularities presented here.

4.D.2 The old Stuff

4.D.2.a Fetkovich

It is worth noting that specific methods or extensions have been studied for gas production, such as the Carter type-curve. When using the Fetkovich type curve with gas, the expression of the rate match is modified to use the pseudo pressure $m(p)$, in a similar manner to what is done in Pressure Transient Analysis. In addition, Fraim and Wattenbarger suggested the use of a normalized time rather than time itself, with the following definition:

$$t_n = \int_0^t \frac{(\mu c_t)_i}{\mu(\bar{p}) c_t(\bar{p})} dt$$

The gas diffusion equation can then be re-written in terms of pseudo pressure $m(p)$:

$$\frac{\partial m(p)}{\partial t} = 0.0002637 \frac{k}{\Phi \mu c_t} \nabla^2 m(p)$$

When the pressure varies significantly, the term μc_t and therefore the diffusion term varies. If we introduce the pseudotime:

$$t_n(t) = \int_0^t I(p_{wf}(\tau)) d\tau \quad \text{where} \quad I(p) = \frac{(\mu c_t)_i}{\mu(\bar{p}) c_t(\bar{p})}$$

The diffusion equation becomes:

$$\frac{\partial m(p)}{\partial t_n} = 0.0002637 \frac{k}{\Phi (\mu c_t)_i} \nabla^2 m(p)$$

Note: the use of the normalised pseudo time requires the knowledge of the average pressure at each step, that makes its use difficult.

They demonstrated that the real gas constant pressure solution, when plotted using normalized time, exhibits a boundary-dominated period that matches the exponential decline. The major drawback however, is that the normalized time expression requires an a priori knowledge of the average pressure, hence of the reserves. The method is thus iterative in nature.

Note: if the normalized time is not used a gas response in depletion mode will not necessarily follow the exponential decline.

Using Fetkovich type-curves

It is important to remember that the Fetkovich type-curve is based, for the depletion part, on the Arps decline curves. Like the decline curves it suffers some limitations:

- It is assumed that the bottom-hole pressure is fairly constant. Fetkovich suggests that if the pressure is smooth, and uniformly decreasing, one could use a Δp normalized rate.
- The well behavior is assumed constant, e.g. no change in skin with time.

The drainage area of the considered well is constant, i.e. the producing behavior of surrounding wells must also be stabilized.

4.D.2.b Gas material balance \bar{P}/Z vs Q plot

This method is specific to gas. It is not an 'adapted' oil method to gas, it is presented in the chapter 'The old stuff'.

4.D.3 The right stuff

4.D.3.a Blasingame plot

The cornerstone of the Blasingame plot is the linearity between the normalized rate

$\frac{q(t)}{p_i - p_w(t)}$ and $\frac{1}{t_e}$ during boundary dominated flow. This relation, valid for a slightly

compressible fluid, does not apply to gas unless the rate is normalized with respect to $\Delta m(p)$ and the time is modified as follows:

$$\bar{t}_{egas} = \frac{\mu_{gi} c_{ti}}{q_g(0)} \int_0^t \frac{q_g(t)}{\mu_g(\bar{p}) c_t(\bar{p})} dt$$

In the PSS oil flow rate equation $\frac{q_o}{\Delta p} = \frac{1}{b_{o,pss} + m_{o,pss} \bar{t}}$, the slope $m_{o,pss}$ is a function of the fluid compressibility, which is highly pressure dependent in gas cases.

The objective is to keep the linearity and the PSS flow rate equation for gas in the same shape as for oil:

$$\frac{q_g}{\Delta p} = \frac{1}{b_{g,pss} + m_{g,pss} \bar{t}_{gas}} \text{ with a constant slope } m_{g,pss}$$

We take the varying viscosity and compressibility into account by introducing the 'pseudo' pressure and 'pseudo' normalized time:

$$p_p = \frac{\mu_{gi} z_i}{p_i} \int_{p_{base}}^p \frac{p}{\mu_g z} dp$$

$$\bar{t}_{gas} = \frac{\mu_{gi} c_{ti}}{q_g(t)} \int_0^t \frac{q_g(t)}{\mu_g(\bar{p}) c_t(\bar{p})} dt$$

The slope is then:

$$m_{g,pss} = \frac{1}{G c_t}$$

The intersect becomes:

$$b_{g,pss} = 141.2 \frac{\mu_{gi} B_{gi}}{kh} \left[\frac{1}{2} \ln \left[\frac{4}{e^{\gamma}} \frac{1}{C_A} \frac{A}{r_w^2} \right] + s \right]$$

The consequence of not using this time function is that the linearities expected during the various flow regimes may be distorted.

It is not necessary in the Blasingame plot since this plot only provides a basis for comparing the data and a model response calculated for the particular case. Handling the non linearities is the model responsibility, not that of the plot. If the model is representative, the model and the data will be consistent. So it does not matter whether such or such period exhibits a linearity or not.

This is different when using a type curve as the type curve embeds modelling assumptions. That is why this time function is used in Topaze in the match with the Blasingame type curve.

4.D.3.b Loglog plot

The linearities expected during the various flow regimes may be distorted when the diffusion does not follow a linear equation, with gas or in multiphase cases, it is important to realize that the loglog plot, like the Blasingame plot, only provides a basis for comparing the data and a model response. Handling the non-linearities is the model responsibility, not that of the plot. If the model is representative, the model and the data will be consistent. It does not really matter whether such or such period exhibits linearity or not. When using a type-curve this is different as the type-curve embeds modelling assumptions.

4.D.3.c Material balance (Normalized rate-cumulative) plot

The boundary dominated flow obeys the same equation:

$$q_D = \frac{1}{2\pi} - Q_{DA}$$

Provided that the dimensionless rate and cumulative production be defined as:

$$q_D = \frac{1422.T.q}{kh(m(p_i) - m(p_w))} \quad \text{and} \quad Q_{DA} = \frac{4.50.T.z_i.G_i.[m(p_i) - m(\bar{p})]}{\phi h A . p_i . [m(p_i) - m(p_w)]}$$

All equations are in Oil Field units.

Unlike the oil case, we cannot find a simple expression of a normalized cumulative that is independent of the fluid in place. This is because the gas in place is involved in a non-linear fashion in the expression of the dimensionless cumulative. However by extension with the previous method for oil we can choose to plot:

$$\frac{q}{m(p_i) - m(p_w)} \quad \text{versus} \quad Q_{DA} = \frac{G_i.[m(p_i) - m(\bar{p})]}{[m(p_i) - m(p_w)]}$$

The value of 'X' at the intercept is:

$$\frac{G_i.[m(p_i) - m(\bar{p})]}{[m(p_i) - m(p_w)]} @ \text{Intercept} = \frac{\phi . h . A . p_i}{4.50.2.\pi.T.z_i} = \frac{PV.p_i}{4.50.2\pi.T.z_i} = \frac{PV.p_i.p_{sc}.T}{4.50.2\pi.T.B_{gi}.T_{sc}.p_i} = \frac{PV}{B_{gi}} = G_i$$

Note: the X-axis value $Q_{DA} = \frac{G_i.[m(p_i) - m(\bar{p})]}{[m(p_i) - m(p_w)]}$ depends on the gas in place G_i value, therefore

a change in the straight line coefficients changes the intersect therefore the abscissa of the data, in other word moving the straight line will move the data points through which we draw it, it becomes an iterative process that converges easily.

4.D.3.d Flowing gas material balance plot and P-Q diagnostic plot

Like the P/Z vs q plot, these methods, specific to gas, and not 'adapted' oil analyses methods, are presented in the chapter 'The right stuff'.

4.D.4 General major gas issues

4.D.4.a Correcting the pressure to sandface

Usually the pressure gauge is not set at the sandface due to mechanical constraints in the completion. Because of this, the results obtained from the pressure transient analysis are at the level of the gauge and not the sandface which, in terms of pressure (P_i) and skin (S), will not reflect the true sandface conditions.

It is necessary first to define the vertical pressure profile in the well. The Saphir/Topaze internal flow correlations or an actual lift curve generated by a specialized program (Amethyste) can be used for this.

The available correlation for gas, in Topaze, is an external lift curve or the internal Cullender & Smith method, but with two modifications for handling water and condensate.

The correlation is based on the gas properties as defined in the PVT setup, and a general friction factor is calculated using the Colebrook and White equation. Note that when you deal with a condensate case with equivalent gas gravity and total rates, the proper gradient and rates are used in the correlation to account for the condensate presence. The presence of water can be accounted for, based on a constant water to gas production ratio.

The solution selected in Topaze is to include both the hydrostatic and friction pressure loss in the model and correct the measured pressure to the sandface depth.

An important consequence is that the dependent skin attributed to the formation can be a lot smaller because a large part is now attributed to the pressure loss through.

4.D.4.b Gas material balance correction

The Production Analysis is performed on large duration data set and the material balance in gas diffusion is a critical issue.

The diffusion equation can be considered linear for as long as the diffusion terms left outside the time and pressure variables remain constant. Diffusion equation:

$$\frac{\partial m(p)}{\partial t} = 0.0002637 \frac{k}{\Phi \mu c_t} \nabla^2 m(p)$$

As soon as we have a pressure gradient in the reservoir, the diffusion term, and especially the product μc_t , will become different from one reservoir block to the next.

If we look at a real gas simulation for a long term production survey and use it to match with an analytical model where the diffusion was taken at initial pressure, we can see a divergence between the simulated pressure and the measured data, even though the reservoir geometries and the PVT used are strictly the same.

There are two ways to handle this problem in Production Analysis.

Integrating the material balance correction in an analytical model

The model includes a reservoir size and an initial pressure. So the initial gas in place can be calculated as an integral part of the model. At any time step the algorithm calculates the average pressure from the cumulative production using p/Z , and replaces the viscosity and total compressibility in the superposition by the one coming from the average pressure. So at any time step the simulated pressure is coherent with the material balance of the model. The optional derivation is shown as follows:

We consider the total gas in place at initial pressure. V_{res} is the pore volume occupied by the gas. T_{res} is the fluid temperature at reservoir conditions. G_i is the initial gas in place at standard conditions.

Real gas equation at initial pressure:
$$p_i V_{res} = Z_i n R T_{res}$$

Same amount of fluid at standard conditions:
$$p_{sc} G_i = n R T_{sc}$$

So we get immediately G_i :
$$G_i = \frac{p_i}{Z_i} \cdot \frac{V_{res} T_{sc}}{p_{sc} T_{res}}$$

We now consider, at time t , the same situation after a total cumulative production of $Q(t)$. We now want to calculate the average reservoir pressure:

Real gas equation at initial pressure:
$$\bar{p} V_{res} = \bar{Z} n(t) R T_{res}$$

Same amount of fluid at standard conditions:
$$p_{sc} (G_i - Q(t)) = n(t) R T_{sc}$$

So we get immediately G_i :
$$G_i - Q(t) = \frac{\bar{p}}{\bar{Z}} \cdot \frac{V_{res} T_{sc}}{p_{sc} T_{res}}$$

We calculate the average pressure from:
$$\frac{\bar{p}}{\bar{Z}} = \frac{p_{sc} T_{res}}{V_{res} T_{sc}} (G_i - Q(t))$$

Using a numerical model

The use of a numerical model is, conceptually, even simpler. As the gas equation is entered at the level of each cell, the material balance is automatically honoured, not only globally, as above, but at the level of each cell. Solving the problem numerically is by far the most rigorous approach.

As the problem is nonlinear, this requires Topaze NL and the use of a nonlinear solver.

4.D.4.c Non-Darcy flow

As mentioned in the 'Theory' chapter, there are two main options to address non-Darcy flow: using a rate dependent skin model or integrating the Forchheimer equation in a numerical model.

Simulating non-Darcy flow with a rate dependent skin model

A rate dependant skin model may be used in the pressure and rate history simulation:

$$S_{total} = S_0 + (ds/dq)q$$

The required parameters values are:

$$S_0 \text{ and } ds/dq$$

These values result from a necessary well test data analysis. The methods are developed in the Chapter 'PTA - General Methodology'.

Simulating non-Darcy flow with a numerical model

In a numerical model the (non linear) non-Darcy flow effect is included in the flow equation through the value of the (non linear) non-Darcy flow coefficient, β which appears in the Forchheimer equation:

$$\frac{\partial P}{\partial x} = \frac{\mu}{k} \cdot u + \beta \cdot \rho \cdot u^2$$

It can be evaluated from the 'Rate dependant skin' linear assumption described above using ds/dq with:

$$\beta \approx ds/dq \cdot \frac{2\pi r_w \cdot h \cdot \mu}{k}$$

or from an empirical equation:

$$\beta = \frac{0.005}{[\Phi \cdot (1 - S_w)]^{5.5} \cdot k^{0.5}}$$

4.E Modern PA methodology

Modern Production Analysis is based on the use of PC based PA software products. The key for any modern software is to combine user friendliness to a powerful technical kernel, requiring both analytical and numerical capabilities. In terms of methodology, the central diagnostic tools are the Blasingame and loglog plots, which are used whenever such a diagnostic is possible. However, because of the very scattered nature of production data, the ultimate diagnostic tool will often be the history plot, where the coherence of the model and the data, in terms of simulated pressures, rates and cumulative productions, will be the final decision tool for the interpretation engineer.


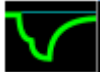



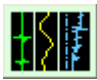
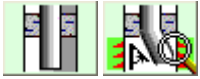


Once the interpretation is initialized and production data loaded, the first task will be to extract the interval of time on which the analysis will be performed. If the pressures are not available, only the 'old' tools can be used. If both rates and pressures are available, the interpretation will be performed with the four main diagnostic tools. The interpretation engineer can select one or several analytical and/or numerical models, set their parameters and generate these models for comparison with the actual data. For models that are believed applicable, the engineers can refine the model leading parameters, either manually or by using nonlinear regression.

Once this is finalized, the engineer may use the model(s) to forecast future production by defining a scenario of producing pressures. The user can then run a sensitivity analysis on a selection of the model parameters.

The path described is the default path when all is well. In reality, for complex problems, it becomes a trial-and-error process where the interpretation engineer may decide to go back and forth as needed when part of the process is unsatisfactory.

4.E.1 Preparing a project and loading data

The initialization procedure is largely the same as that used in PTA. The interpretation engineer inputs PVT data, geometric well and reservoir information, the following table can be used as a guide:

	Type of data	Required for PA
	Production history	Yes
	Pressure history	Old stuff: No Right stuff: Yes
	PVT, correlations, tables or constraints	Yes
r_w	Wellbore radius	Yes
Φ	Porosity	Yes
h	Net vertical drained thickness	Yes
	Field map with surrounding wells based on seismic interpretation	Preferably
	Production history of surrounding wells	Preferably
	Complete completion log preferably with a permeability log. Core and core analysis	Preferably
	Completion diagram and geometry, deviation, perfos, gauge depths.	Preferably
	All gauges, well test and operations reports	Yes
	Choice of flow correlations or availability of lift curves from third party software	If pressure far from sandface

The load option imports flat ASCII files, allows manual input, copy-paste from spreadsheets, and increasingly input through links to databases or intermediate repositories using advanced filtering tools.

After the load, the cumulative production is automatically calculated by integration of the production history, and is displayed on the history plot together with the rate. Pressures is loaded and displayed in the history plot.

Quality control is not as critical as in PTA, because wellbore effects are normally not dominant, except when the pressure is recorded at surface. In this case, the validity of the well intake curves used to correct the pressure to sandface during extraction can become a potential weak point.

4.E.2 Editing data

Loaded data may be the result of careful post-processing after the data has been acquired, in which case no or little editing may be needed. However, often the interpreter will gather data of unequal quality from different sources. Pressures will often be acquired downhole in real time or with a memory gauge or come from permanent gauges (PDG), while rates are mostly measured at surface but in some cases, can also come from permanent measuring devices downhole.

Beyond the usual cleaning of irrelevant data and the correction of load errors, the main challenge is to end up with at least one coherent, synchronized set of rate and pressure data. To get there the engineer may have to perform the following tasks:

- Synchronise all data acquired electronically to the same reference time.
- If rates are not loaded from a file, create the rate history by identifying the pressure breaks and get the rate values from hard copy reports.
- Refine the production history, when the time sampling of rate measurements is too crude.
- Conversely, if the production history goes into useless detail, simplify the rate history to reduce the CPU time required to run the models.

4.E.3 Extraction and diagnostics

Once the data have been synchronized and validated, the analysis itself will start. The time range over which the extraction of the data will take place is defined and the following plots are built by the software in addition to the history plot:

- ARPS plot
- Fetkovich type-curve plot
- Fetkovich plot
- Blasingame plot
- Loglog plot
- Normalized rate-cumulative plot

At extraction time the option to invoke a defined lift curve or flow correlation to correct the pressure profile from the measurement depth to sandface can be chosen.

The loglog plot (see below) is used for diagnostic purposes to identify the two main flow regimes hopefully present in production data, infinite acting radial flow (IARF) and pseudo steady state (PSS). The pressure match is fixed to coincide with a stabilization of the derivative of the normalized pressure integral and the time match is fixed to the unit slope line of PSS at late time. The pressure match and the time match are adjusted by click and drag of the mouse. The loglog plot is linked to the Blasingame and the Fetkovich plot so any change in the loglog match is mirrored in the others. In case the data is of high quality and the sampling frequency is high enough it is sometimes possible that more than the IARF transient develop thus extending the diagnostic possibilities to approach those of PTA and both well and reservoir models can be recognized in the test data. This is however rare in low frequency data typically used in production analysis.

If the loaded pressure history contains any decent build-ups with high frequency pressure data or a link to a database that allows the repopulation of this data without a filter then the interpreter is in luck. This data can be transferred to a PTA module to determine all of the classical parameters including the model and these can be transferred back to the PA package and finally the modelling can begin; adjusting for parameters that can typically change over the longer time intervals involved in production analysis (i.e. skin).

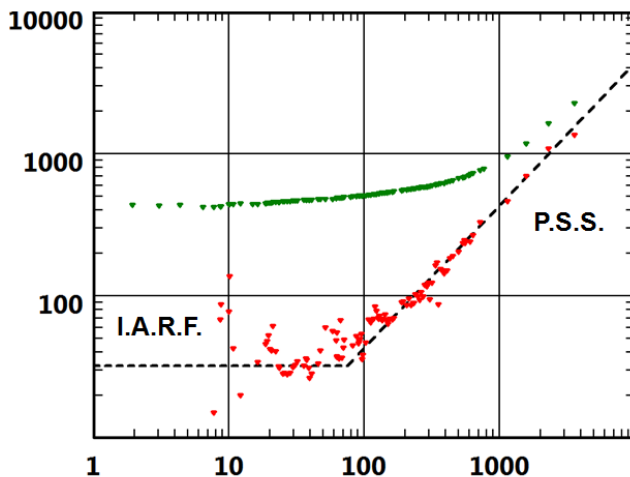


Fig. 4.E.1 – Match on the Loglog plot

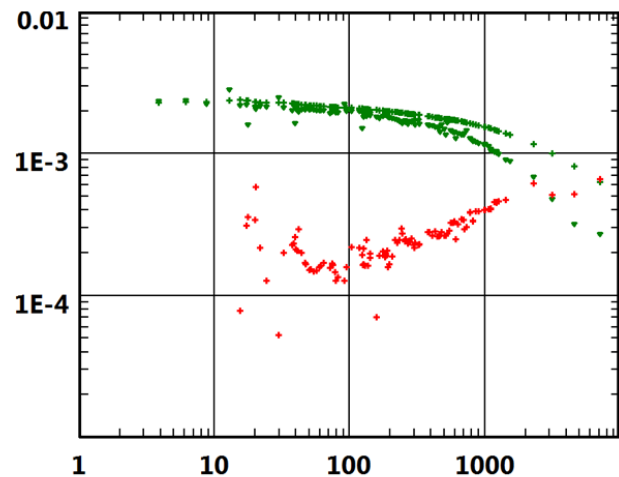


Fig. 4.E.2 – Blasingame plot

4.E.4 Model generation

After the diagnostics candidate models, analytical or numerical, are selected and an attempt is made to obtain a match between the models and the real data in all the relevant plots including the history plot. To obtain a match the interpreter will run with a first estimate of the model parameters generally obtained by generating the default, or automatic, model based on the initial match made in the loglog plot as described in the previous section. The default model is the homogenous model with constant skin in a closed circle. At generation time a first estimate of the constant skin is automatically made by the software.

After a comparison between the model and the data, changes can be made to the model parameters and any known well configuration can be imposed such as knowledge of the well being fractured, horizontal or partially penetrating. In the event that PTA was performed on part of the pressure data the model used can be transferred to the production analysis.

Finally the objective is to vary the model parameters until there is a reasonable match between the model and the data in all relevant plots, including the history plot.

4.E.5 Model refinement

Before using the software non linear regression routine to optimize the model parameters and the match, the engineer should manually deal with the gross parameter errors and change the values until the model and the data are closer. An experienced analyst with a good understanding of the sensitivity to the various model parameters should get a fit, by changing the parameters by hand, between the model and the data very quickly. This will increase the chance for the regression to succeed and converge faster.

The principle of non linear regression is to use numerical optimization to refine the parameter estimates by minimizing an error function, generally the standard deviation between the simulated and real values at selected times. The most commonly used optimization algorithm is Levenberg-Marquardt, but there are many variants. The engineer has the possibility to run with some or all the leading parameters of the model and he can also fix the upper and lower limits of the allowed parameter variation. The data points on which the error function will be calculated may also be controlled. See figure below:

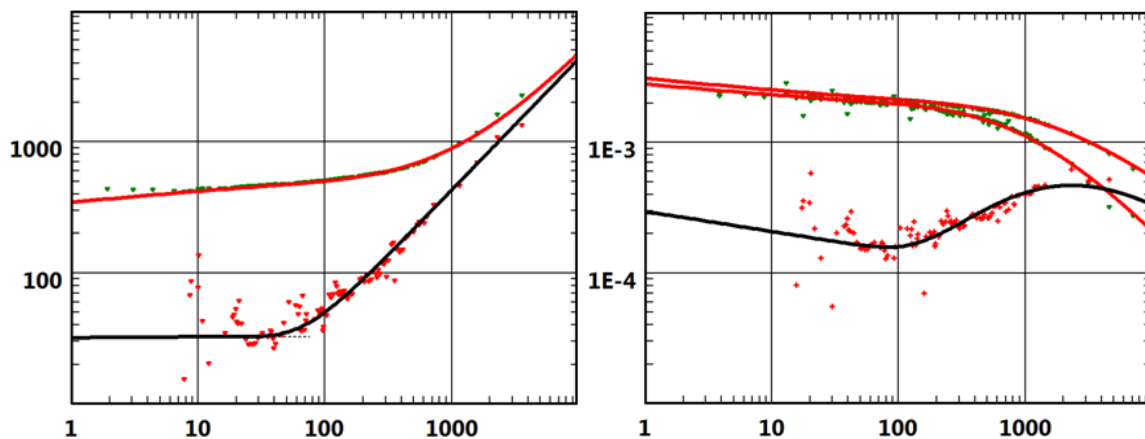


Fig. 4.E.3 – Final match after optimization

4.E.6 Forecast

Once the model has been selected a production forecast can be easily performed by defining a flowing (producing) pressure scenario. See the figure below illustrates this with a constant pressure production for 100 days.

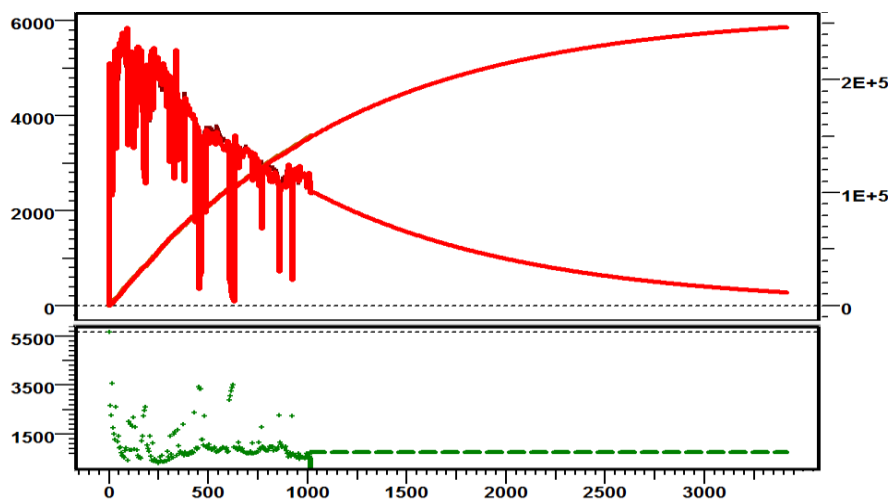


Fig. 4.E.4 – Forecast 100 days constant pressure production

4.E.7 Sensitivity study

At the end of the nonlinear regression it is also possible to recover some confidence intervals. They can be used to assess the sensitivity to individual parameters and any eventual parameters cross-correlations.

Another possibility is to run and display a series of model generations corresponding to different values of a given parameter, in order to compare theses on the history.

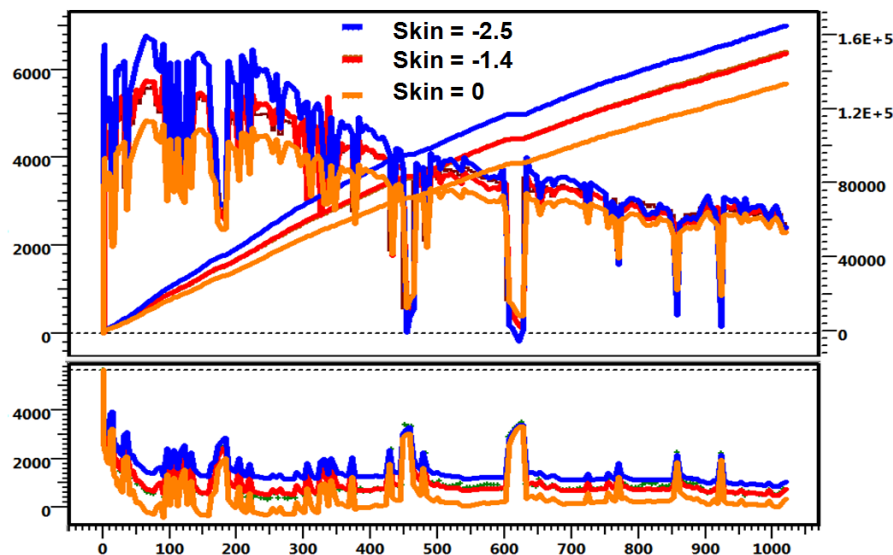


Fig. 4.E.5 – Sensitivity to skin

4.E.8 Reporting Guidelines

A typical analysis report will be split into two components: the 'mechanical' part, basically the result tables and plots generated, directly or indirectly, by the Production Analysis package, and the 'verbose' part, where the engineer will report the objectives, the operations, the analysis, his confidence in the results and forecast, and possible recommendations for stimulation, workover and continued or future measurements and equipment to use.

Typically, professional analysis reports are generated with two possible set-ups:

- A header document, from a word processor, with some 'copy-paste' of plots and results from the PA software, but with most of the 'mechanical' report delivered as an annex,
- An integrated document, typically from a word processor, where some plots and tables are dynamically connected to the PA software using some OLE or COM automations. The advantage of this solution is that it is much more flexible. Once a model template has been defined, the reporting process will get shorter and shorter from one analysis to the next.

4.F PA versus PTA

4.F.1 Introduction

The comparative table below shows a summary of the common and different aspects of the PTA and PA techniques.

The main aspects will be detailed later in this paragraph.

	Pressure Transient Analysis (PTA)	Production Analysis (PA)
Theoretical bases	Same equations, superposition, analytical and numerical model. Some assumptions are, however, specific.	
Time range	Hours, Days, sometimes Weeks	Weeks, Months, Years
Periods of interest	Mostly shut-ins Clean productions possible	Producing phases But build-ups may be included
Data sources	Well test measurements Formation tests Permanent gauges (PDG)	Measured/allocated production surface pressure readings Permanent gauges (PDG)
Reservoir areas of interest	Whatever volume of investigation during the test and/or the shut-in	Well or group drainage area
The good old plot(s)	MDH, Horner	Arps
The good old type-curve(s)	McKinley, Gringarten	Fetkovich
Modern diagnostic plots	Loglog with Bourdet derivative	Loglog & Blasingame with Bourdet derivative
Main flow regime of interest Main corresponding results	Infinite Acting Radial Flow kh & skin	Pseudo-Steady State (PSS) drainage area & shape factor
Diagnostic capability	High to very high	Average to low
Long term validity	Average to low	High to very high

4.F.2 Common tools

PA and PTA methods share the same assumptions in terms of the use of the diffusion equation and limiting conditions. Most of the analytical and numerical models developed in PTA may be used in PA with minor adjustments, such as the ability to use the pressures as the input to simulate the rates with superposition.

Modern PA and PTA share a similar path. After loading, synchronizing and extracting data, one first tries to run a diagnostic using specialized plots and straight lines. An analytical or numerical model is then run, and an optimization process adjusts the parameters to minimize the difference between the simulated model response and the observed data.

4.F.3 PSS vs. IARF

The main regime of interest in PTA is Infinite Acting Radial Flow (IARF). We look primarily for a stabilization of the Bourdet derivative. When IARF is detected, specialized analysis will give a value of mobility and a total equivalent skin factor. We can refine this and diagnose other well, reservoir and boundary behaviors from various parts of the response; however the starting point will always be IARF.

The main regime of interest in PA is Pseudo Steady State (PSS). We look primarily for a unit slope on the Loglog or the Blasingame plot. Specialized analysis will determine the size of the well drainage area from the slope, and the intercept will be a function of three main factors: the well productivity index, the mobility and a shape factor. More complex models could be used, but there may not be enough information to determine the additional parameters. However the pressure transient results may be used to determine these.

4.F.4 Diagnostic capabilities

One of the key steps in PTA is the diagnostics, where, based on the derivative behavior the engineer decides which model could most appropriately be used to perform the analysis. This is made possible by very clean data and constant production i.e. zero, during the build-up.

Production history may be so scattered that the responses will be dominated by transients. In this case there is no way to identify pseudo steady state behavior. This may happen even though the well is still producing and the pressure is declining globally.

Despite the lack of pure PSS behavior it will be possible with a model to history match the data and obtain a reliable drainage area estimate and even sometimes discriminate mobility, skin and shape factor. No specialized plot will show such a behavior. So the use of models and optimization is likely to change the way PA is performed completely, even more radically than happened with PTA.

4.F.5 Validity of the PTA hypothesis in Production Analysis

PTA can provide a clean snapshot of what the well and reservoir system is at a given time. PA covers a much wider time range, and some of the assumptions valid during a single well test will not be true over the well producing history. The three main differences are related to the well productivity, the drainage area and multiphase production.

PTA models account for rate-dependent skin. It is also known that the well may be cleaning up during the initial production phase. So the well productivity may not be constant during a well test. However this is a reasonable assumption for a single build-up, and optimization will be possible with a single mechanical skin model. In PA this is unlikely. Well productivity does change over time, and no optimization process is reasonably possible over a long period of time without considering a time-dependent skin.

In PTA, boundary effects are generally material boundaries, even though interfering wells can produce the same effects as boundaries. In PA we consider the well drainage area. Except when there is only one producing well, part or all of the drainage area boundaries are immaterial, depending on the flow equilibrium between the neighboring wells. The drainage area will change in time when new wells are produced, or even when the flow rates change asymmetrically. To account for these changes, a multi well model, either analytical or numerical, may be required.

In PTA we approximately handle multiphase cases using pseudo-pressures or considering that saturations are constant and the flow can be modelled with an equivalent single-phase fluid as in Perrine's method. In PA, solutions exist that consider that individual fluids develop PSS independently. However these solutions make a global correction for multiphase production but they are unable to forecast the breakthroughs. There is a point where only a history match with a numerical model can account for multiphase production.



5.A Introduction

Until we are able to beam the fluid directly from the pore space into the ship cargo bay we will need to use this route called the wellbore. Wellbore effects are seen very differently, depending where you stand:

- For the Pressure Transient Analysts anything related to the wellbore is a nuisance. Wellbore effects will spoil the early part of the pressure response, and may even persist throughout the whole test or shut-in survey.

So to the PT-Analyst Wellbore Effects = BAD.

- Production Analysts are a little luckier, because they work on a time scale where transient effects are not that important, and addressing wellbore effects amounts to connecting a lift curve. In fact, playing with the lift curves and implementing 'what if' scenarios is part of their jobs.

So to the Production Analyst Wellbore Effects = OK.

This Manichean split can be presented another way:

- The steady-state component of wellbore effects is a key element of the well productivity. It may be modeled using lift curves, or VLP curves, and this in turn requires flow correlations that are present in both Production Logging and Well Performance Analysis, a.k.a. Nodal Analysis™ (Trademark of Schlumberger).

Correction to datum may be either applied to the data in order to correct the real pressure to sandface, or integrated in the model in order to simulate the pressure at gauge level. Correction to datum and integration of VLP curves are detailed in the PTA (QA/QC) and the Well Performance Analysis chapters of this book.

- The transient component of wellbore effects often ruins the life of the PT-Analyst. The action at the origin of a sequence of flow (opening and shut-in of a valve, change of a choke) is occurring at a certain distance from the sandface, and any wellbore volume between the operating point and the sandface acts as a cushion. This induces a delay between what we want to see and what effectively occurs at the sandface.

In welltest operations, it is highly recommended to reduce this nuisance as much as possible by means of downhole shut-in tools.

In Production Analysis it is not much of an issue, as transient wellbore effects occur at a time scale of little interest for rate decline.

This chapter deals with the modeling of some of the simplest transient wellbore models, and is mainly applicable to Pressure Transient Analysis only.

5.B Constant Wellbore storage

The simplest wellbore model is the constant wellbore storage

As introduced in the 'Theory' chapter, the wellbore storage introduces a time delay between the rate we impose at the operating point (typically the choke manifold at surface) and the sandface rate. The wellbore storage equation was introduced in the 'Theory' chapter:

Wellbore storage equation:

$$q_{sf} = qB + 24C \frac{\partial p_{wf}}{\partial t}$$

Not surprisingly, the constant wellbore storage model assumes that the wellbore storage factor C is constant. The below figure illustrates the behavior of the sandface rate during the opening and shut-in of a well.

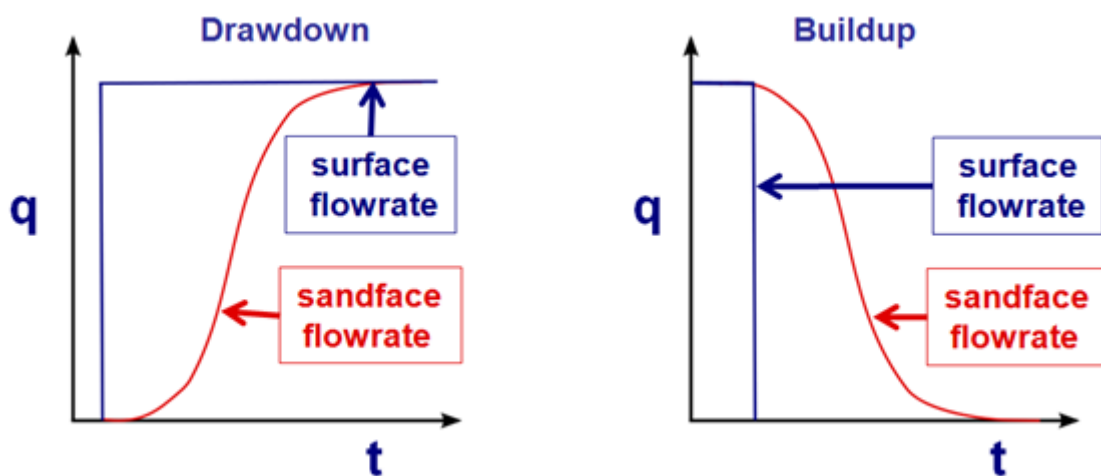


Fig. 5.B.1 – Wellbore storage

5.B.1 Loglog analysis

Fig. 5.B.2 with various constant wellbore storage constants is illustrated below. Pure wellbore storage is characterized by the merge of both Pressure and Bourdet Derivative curves on the same unit slope.

At a point in time, and in the absence of any other interfering behaviors, the Derivative will leave the unit slope and transit into a hump which will stabilize into the horizontal line corresponding to Infinite Acting Radial Flow. The form and the width of the hump is governed by the parameter group Ce^{2S} , where S is the Skin factor.

The horizontal position of the curve is only controlled by the wellbore storage coefficient C. Taking a larger C will move the unit slope to the right, hence increase the time at which wellbore storage will fade. More exactly, multiplying C by 10 will translate the curve to one log cycle to the right.

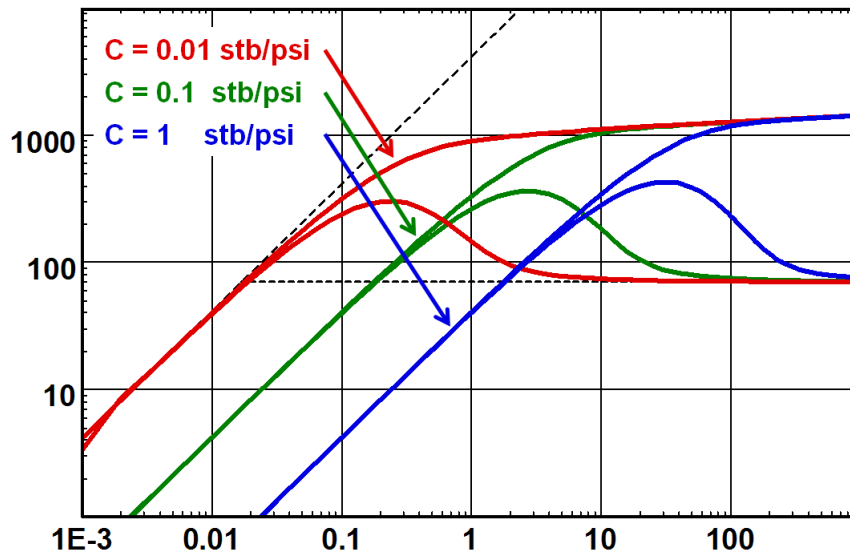


Fig. 5.B.2 – Wellbore storage loglog response

5.B.2 Specialized analysis (Cartesian plot)

A unique slope on the loglog plot corresponds to a linearity of the pressure response on a Cartesian plot. This Cartesian plot may show either P or ΔP vs. Δt .

Below is shown a Cartesian plot of pressure versus time.

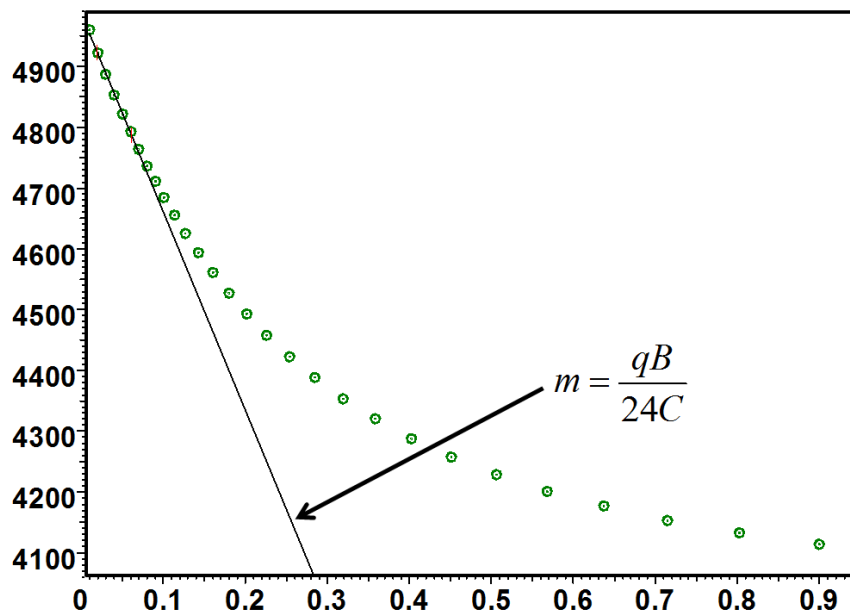


Fig. 5.B.3 – Cartesian plot of pressure vs. elapsed time

The early time straight line corresponding to the pure wellbore storage is given by:

$$\text{Wellbore Storage Straight line: } \Delta p = \frac{qB}{24C} \Delta t = m \Delta t$$

So one can get the wellbore storage constant with:

$$\text{Specialized plot result: } C = \frac{qB}{24m}$$

5.B.3 Sensitivity analysis on the wellbore storage coefficient

The figure below presents the response with wellbore storage values, C of 0.001, 0.003, 0.01, 0.03 and 0.1 (stb/psi).

The value of C has a major effect, which is actually exaggerated by the logarithmic time scale. You can see on the linear history plot that all responses seem to be the same, however.

When the influence of wellbore storage is over both the pressure change and the derivative merge together. Wellbore storage tends to mask infinite acting radial flow on a time that is proportional to the value of C . Wellbore storage will also tend to mask other flow regimes that can be present in a well test. Early time well responses such as linear, bi-linear, spherical and hemispherical flow will disappear if the storage effect is considerable. Effects of heterogeneous reservoirs can also be masked by wellbore storage. The wellbore storage effect on other well and reservoir models are covered in the individual chapters of these models.

Wellbore storage does not affect the late time pseudo steady state response.

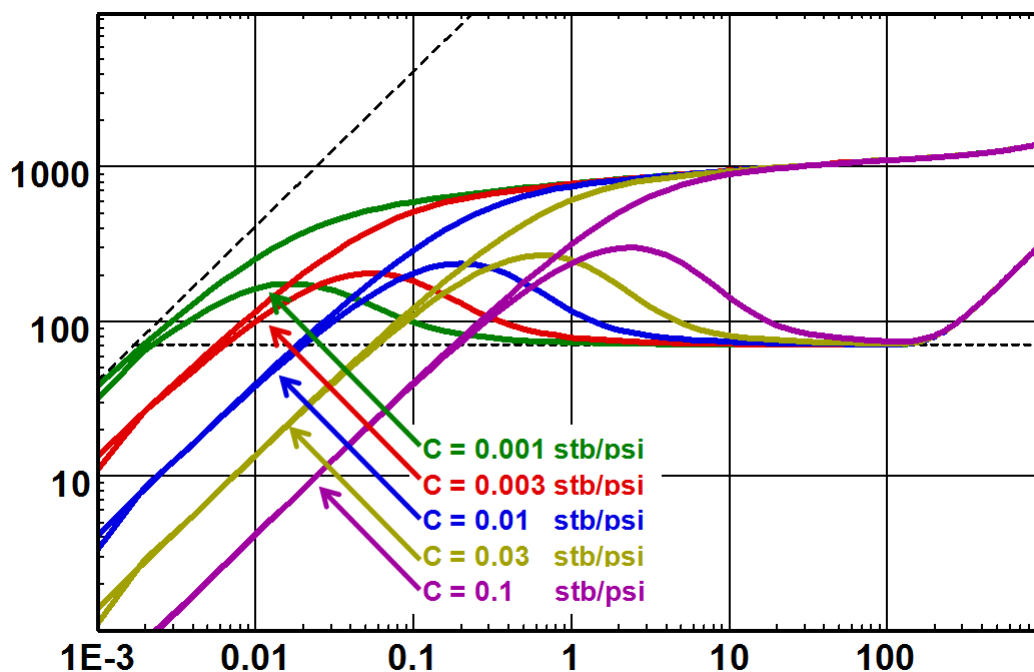


Fig. 5.B.4 – Effect of wellbore storage, loglog plot

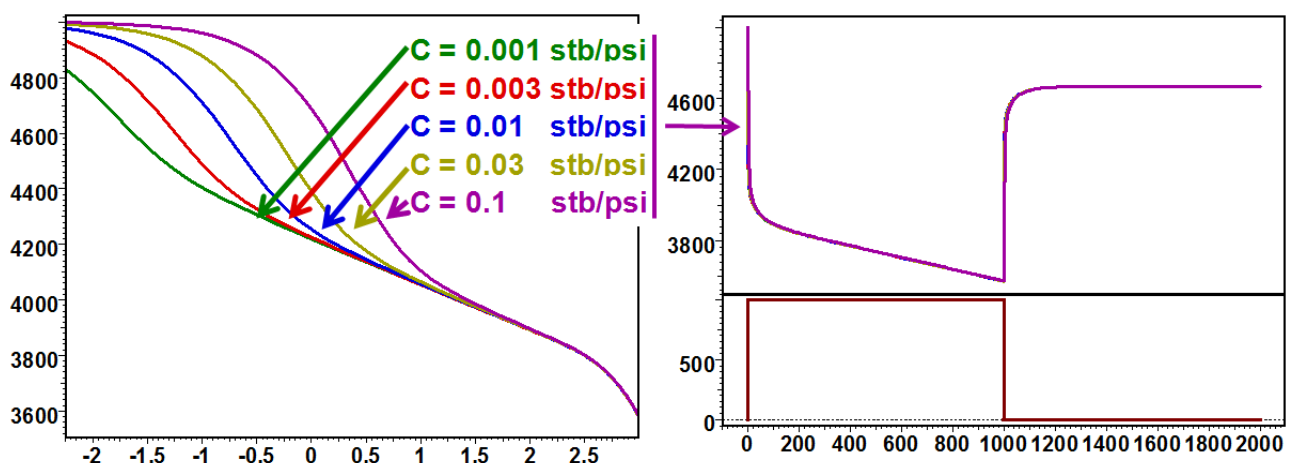


Fig. 5.B.5 – Effect of wellbore storage, semilog and history plot

5.C Changing wellbore storage

The most frequent case of changing wellbore storage is related to the compressibility change of the wellbore fluid.

A classic example is gas. When the well is flowing the pressure in the wellbore will decrease, and the gas compressibility will increase. In this fixed volume this will result in an increase of the wellbore storage parameter. The opposite will occur during the shut-in, where the increase of pressure will result in a decrease of the wellbore storage. Though it occurs in any gas test, this behavior will be visible, and become a nuisance, in the case of tight gas, where the high pressure gradient in the formation results in a high pressure drop in the wellbore.

Another typical example is an oil well flowing above bubble point pressure in the reservoir. At a stage (sometimes immediately) there will be a point in the wellbore above which the pressure gets below bubble point. In this place the oil compressibility will be progressively dominated by the compressibility of the produced gas, hence an increase of the wellbore storage which will evolve in time.

In both cases, the wellbore storage will be increasing during the production and decreasing during the shut-in.

Other sources of changing wellbore storage may be various PVT behaviors, change of completion diameter of a rising or falling liquid level, phase redistribution, falling liquid level during a fall-off, etc.

In some cases the wellbore effect will be so extreme that any modeling is hopeless. In this case the engineer will focus on matching the derivative response after the wellbore effect has faded, accepting that the early time response cannot be matched and may induce a (cumulative) incorrect value of the skin factor.

There are three main ways today to model changing wellbore storage:

- Analytical, time related wellbore storage
- PVT correction using the pseudotime function and a constant storage value
- Numerical, pressure dependent storage model

5.C.1 Analytical models

Most analytical formulations of changing wellbore storage involve an initial value of wellbore storage C_i , a final value C_f , some assumption for a transition function (Hegeman, Fair, etc) and a time at which this transition occurs. The main characteristic of these models is that the transition occurs at a given value of Δt , and is NOT related to the value of the pressure.

The figures below illustrate increasing and decreasing wellbore storage as modeled by the Hegeman model of changing wellbore storage.

The matching consists in setting the wellbore storage straight line on the FINAL value of wellbore storage, pick a second position corresponding to the INITIAL value of storage, and then pick the median time when the transition occurs. The initial model generation will seldom match the response perfectly, but this model, combined with a robust nonlinear regression, has the capacity to adjust to virtually any single trend early time response.

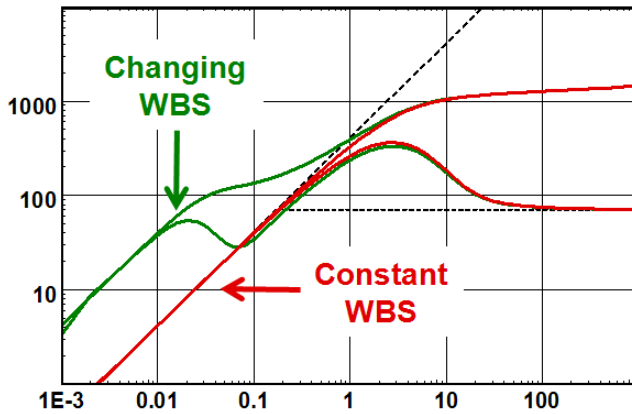


Fig. 5.C.1 – Increasing storage

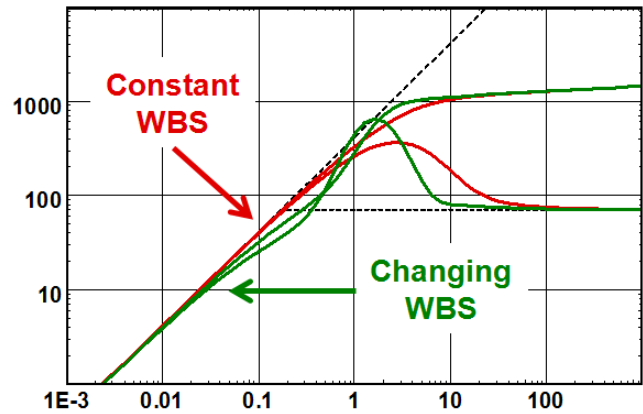


Fig. 5.C.2 – Decreasing storage

In practice, the Hegeman model is sharper and has more capabilities to match real data. This is related to the choice of transition function and does not mean that this model is physically better. Actually it does not mean that ANY of these models are correct, and they should be used with care for the following reasons:

- The models are just transfer functions that happen to be good at matching real data. There is no physics behind them. They may end up with an initial, final storage and transition time that makes no physical sense.
- These models are time related. There will be a wellbore storage at early time and a wellbore storage at late time. This is not correct when the model is pressure related. In the case of production, the real wellbore storage at early time will correspond to the storage at late time of the build-up, and the reverse. So, the superposition of a time related solution will be incorrect on all flow periods except the one on which the model was matched. This aspect is often ignored and/or overlooked.
- These models are 'dangerous' to the extent that they work beautifully to match 'anything that goes wrong' at early time, even when the use of such model is not justified. They are the early time version of the radial composite model at intermediate time. Actually, combining changing wellbore storage and radial composite will match any rubbish data.

5.C.2 Combining pseudo-time and a constant storage model

In a tight reservoir, the pressure changes can be large and the assumption that μc_t is constant leads to a distortion in the early time of the loglog plot. The response can in most cases be matched using the changing wellbore storage option described above. However the changes in μc_t can also be included in the diffusion equation and pseudo-time can be used during the extraction of the period to be analyzed. Pseudo-time is defined by

Pseudo-time:
$$t_{ps}(t) = \int_0^t I(p_{wf}(\tau)) d\tau \quad \text{where} \quad I(p) = \frac{1}{\mu(p)c_i(p)}$$

The following figures show a loglog response before and after pseudo time correction. The use of pseudo time is detailed in the chapter on 'Gas'.

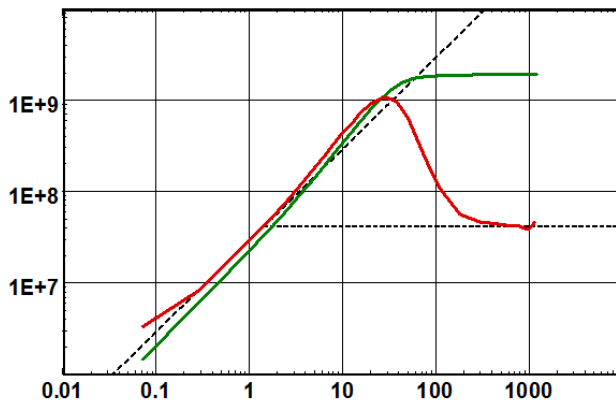


Fig. 5.C.3 – Without pseudo-time

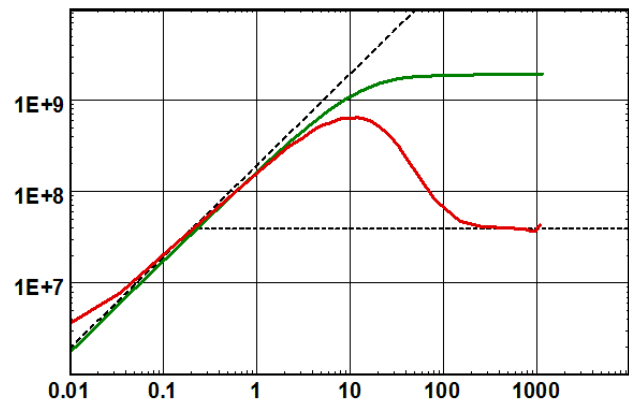


Fig. 5.C.4 – With pseudo-time

There are two drawbacks to this approach:

- This method modifies, once and for all, the data to match the model, and not the opposite. This excludes, for example, the possibility of comparing several PVT models on the same data. The method was the only one available at the time of type-curve matching, where models were limited to a set of fixed drawdown type-curves.
- In order to calculate the pseudotime function one needs the complete pressure history. When there are holes in the data, or if the pressure is only acquired during the shut-in, it will not be possible to calculate the pseudotime from the acquired pressure. There is a workaround to this: use the pressures simulated by the model, and not the real pressures. This amounts to the same thing once the model has matched the data, and there is no hole. However it is a bit more complicated for the calculation, as the pressure at a considered time requires the pseudotime function, and vice versa.

5.C.3 Numerical pressure dependent wellbore storage

The principle is to use a wellbore model which, at any time, uses the pressure to define the wellbore storage parameter. In order for the model to be stable, the wellbore storage has to be calculated implicitly at each time step. As the problem is not linear, this can only be done using a non linear model.

This is by far the most relevant way to simulate pressure related wellbore storage. The figure below illustrates a buildup matched with the changing wellbore storage model (Hegeman), the extracted buildup corrected for pseudo time and matched with this model, and the match with the non linear numerical model with pressure dependent wellbore storage.

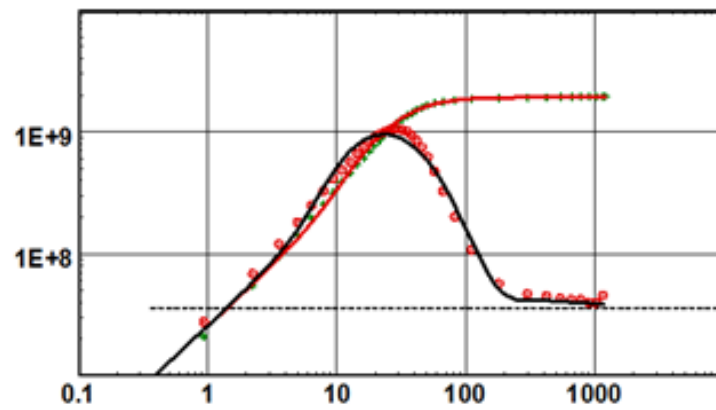


Fig. 5.C.5 – Changing wellbore storage match

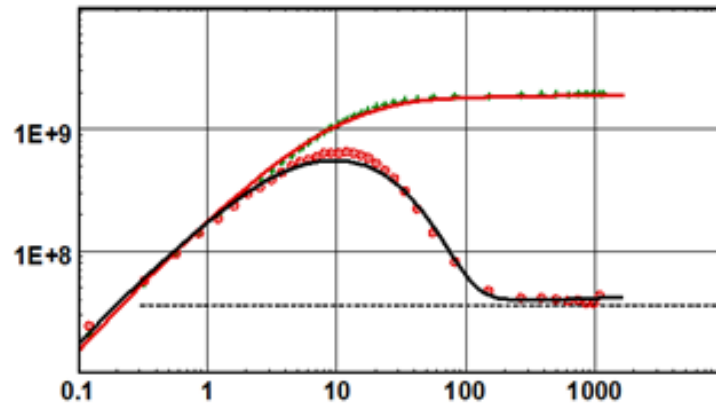


Fig. 5.C.6 – Pseudo time match

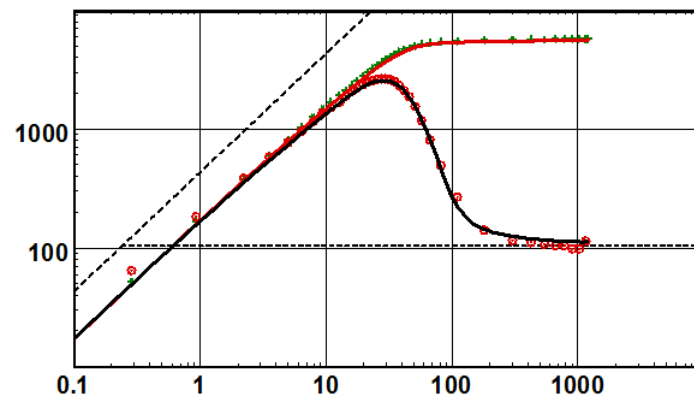


Fig. 5.C.7 – Match with non linear numerical model:
Pressure dependent wellbore storage



6.A Introduction

The geometry of the well, its trajectory in the formation, the way it is completed and/or stimulated, have a major impact on transient responses and the long term well productivity.

For the PT-Analyst, in most cases the well model will dominate the transient response after the wellbore storage has faded and before IARF is established.

The flow geometry around the well may create characteristic flow regimes, with a specific signature of the Bourdet derivative and linearity on a given specialized plot. Some long lasting flow geometries may also be identified by the Production Analyst.

After radial flow is reached the well model will produce a total equivalent skin, which can be calculated using the standard straight line method (MDH, Horner, Multirate semilog). This total skin is the sum of the 'real' skin, resulting from the well damage or stimulation, and a geometrical skin which will define the difference in productivity between the current well geometry and a fully penetrating vertical well.

However textbook responses are not that frequent. Wellbore effects may hide some specific well regime. Some well configurations, such as horizontal wells, will have a longer term impact, will be sensitive to heterogeneities and will seldom exhibit the expected behavior.

The problem of identifying and quantifying well behaviors is not trivial, and it is not expected to become any better in the years to come. Additional developments are very likely to blur the message even more:

- In extremely low permeability formations the geometry of the well may affect the pressure response for years, and IARF may never be reached for the practical duration of the well life. This is the case of fractured horizontal wells in shale gas formations, and it is developed in the unconventional gas chapter of this book.
- Increasingly complex and 'intelligent' completions, multi-drain wells, may be a dream for the production engineer but they are a nightmare for the analyst. The sensitivity of the solution to local heterogeneities, the lack of unique solutions, and the absence of any pure flow regime make the analysis almost impossible.

For these reasons, what is taught in this chapter may become less and less relevant when this sort of configuration becomes the norm. When no formal analysis technique is available we will end up using these complex models for test design and productivity design, and we will use history matching with a very limited number of diagnostic tools.

6.B Vertical well with Constant Skin

The simplest model is a vertical well fully penetrating the reservoir producing interval.

This is the model used to derive the basic equations in the chapter on 'Theory'. This model is sometimes called 'wellbore storage & skin', reference to the original type-curves of the 1970's. The reason is that the two only parameters affecting the loglog plot response will be the wellbore storage and the skin factor. However, wellbore storage is a wellbore effect and skin is used in complement of all other models.

So we will stick to the term 'vertical well', considering that 'fully penetrating' is the default status of a vertical well, otherwise the model will be called 'limited entry' or 'partial penetration' (see other sections in this chapter).

The behavior of a vertical well in a homogeneous infinite reservoir has already been presented in previous sections and is shown here as a reminder. The loglog and semilog plots below show the response for various values of the skin factor (S).

On the loglog plot, the shape of the derivative response, and with a much lower sensitivity the shape of the pressure response, will be a function of the group $C.e^{2S}$.

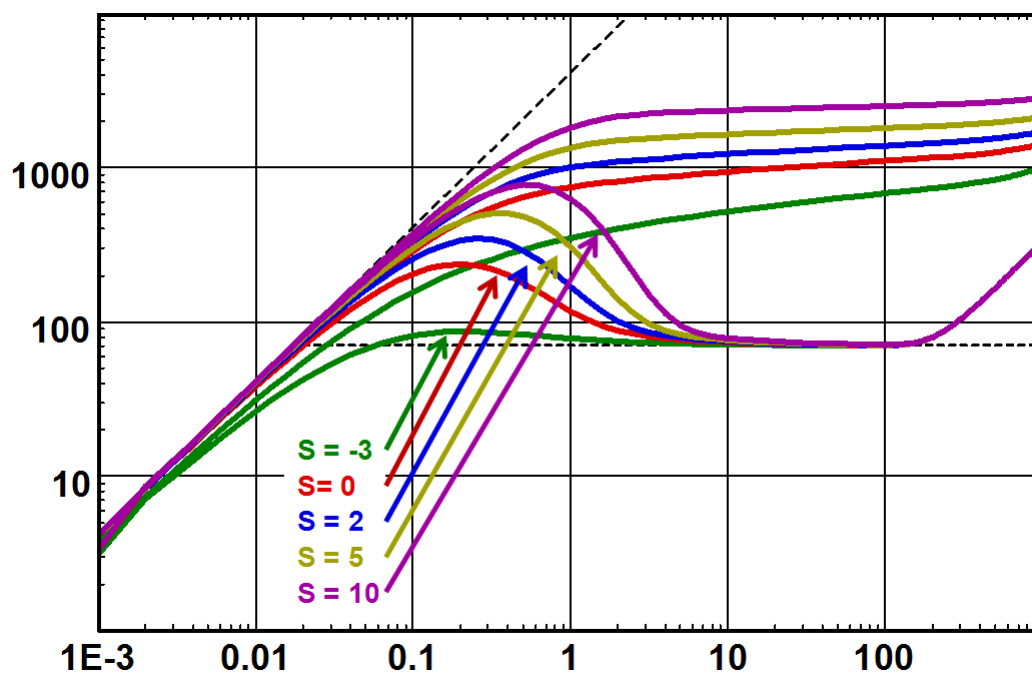


Fig. 6.B.1 – Effect of skin, loglog plot

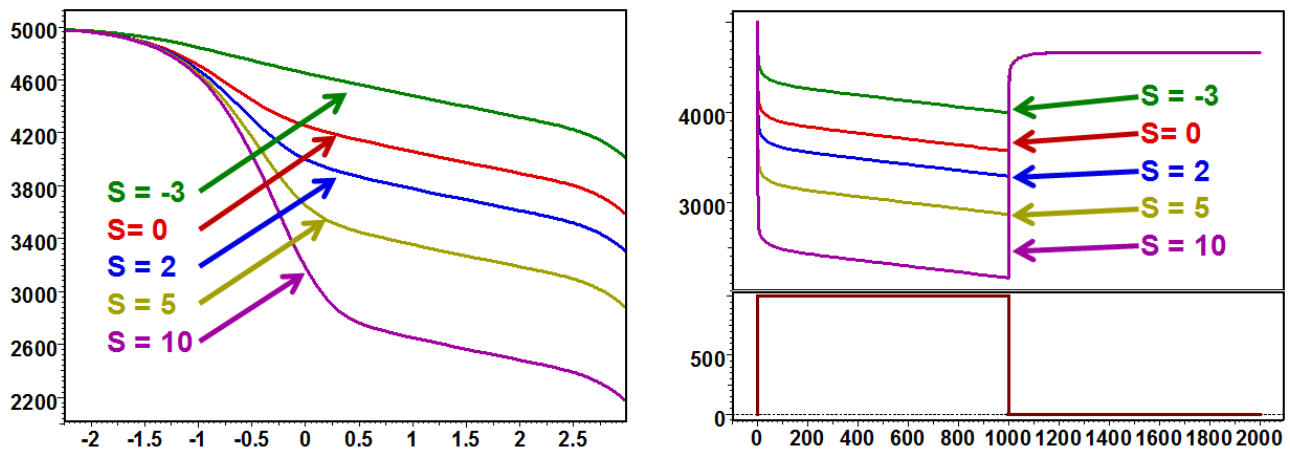


Fig. 6.B.2 – Effect of skin, semilog and history plot

The shape of the hump, which originally was set to $C_D e^{2.S_{skin}}$ when dealing with type curves, is actually a function of C and $r_w e^{-S_{skin}}$.

If we consider the IARF equation given in previous section:

$$p(t) = p_i - \frac{162.6qB\mu}{kh} \left[\log(t) + \log\left(\frac{k}{\Phi\mu c_t r_w^2}\right) - 3.228 + 0.8686.S_{skin} \right]$$

...and if we re-shuffle it a bit, we get:

$$\Delta p(t) = \frac{162.6qB}{\frac{kh}{\mu}} \left[\log(t) + \log\left(\frac{kh}{\mu}\right) - \log(h\Phi c_t) - 3.228 - 2\log(r_w e^{-S_{skin}}) \right]$$

One can see that the slope is a function of $k.h/\mu$, and that there is a constant term that shows, among other things, the residual effect of $r_w e^{-S_{skin}}$, ϕ and c_t .

6.C Vertical Well with Changing Skin

In this section, we keep the assumption of a vertical well fully penetrating the formation. However we now allow the skin factor to be changing over time and/or as a function of the producing rate.

6.C.1 Rate dependent skin

In high rate wells, especially but not only in gas wells, the flow velocity may become considerable and in some cases the flow becomes turbulent. When this happens, Darcy's law no longer applies and will be replaced by Forseheimer's equation:

$$\frac{dP}{dx} = \frac{\mu}{k} \cdot u + \beta \cdot \rho \cdot u^2, \quad \beta = \frac{0.005}{[\Phi \cdot (1 - S_w)]^{5.5} \cdot k^{0.5}}$$

The exact problem is nonlinear and can be solved numerically, as described in chapter on 'Numerical models'.

However, it can be simplified and analytical models can be used with a fair approximation by adding a rate dependent component to the skin factor. Under these conditions, the effective skin factor S' for a given rate q will be given by:

$$S' = S_0 + Dq \quad \text{or} \quad S' = S_0 + \frac{dS}{dq} q$$

D is called the non-Darcy flow coefficient. In order to assess the rate dependency the skin has to be solved for several rates.

In gas well testing the most common method is to plan for an isochronal or modified isochronal test, but this is done mainly to determine the deliverability of the well. Such a test procedure includes multiple buildups after different flowrates and the engineer can then profit for 'free' the fact that the buildups can be analyzed for skin and define the rate dependency. This can then be used in the model.

The following figures illustrate the loglog plot with four buildups with different skins and the corresponding history match using a constant skin in the model. It can be seen that the match is not consistent with the measured data.

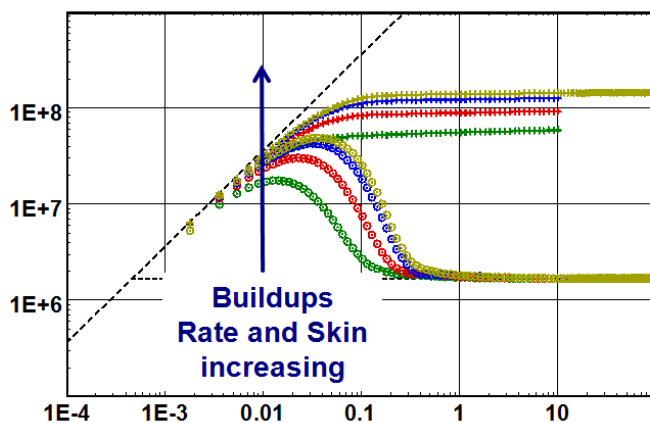


Fig. 6.C.1 – Loglog plot

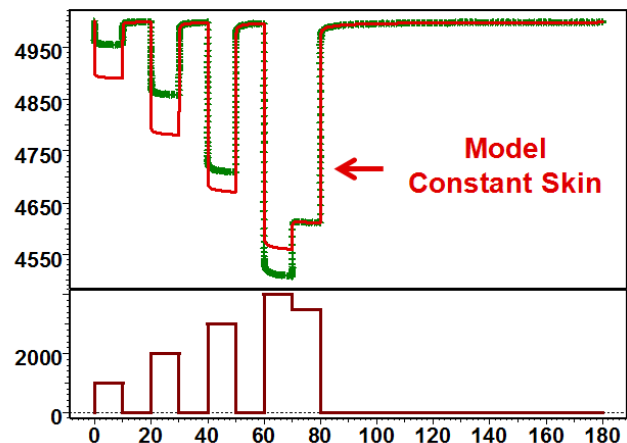


Fig. 6.C.2 – History match, constant skin

The next figures illustrate the 'skin versus rate' plot, which is used to evaluate the rate dependency and the skin if no turbulence was present. From this we can determine a rate dependent skin model. Finally we see in the history match plot that the model is consistent with the measured data.

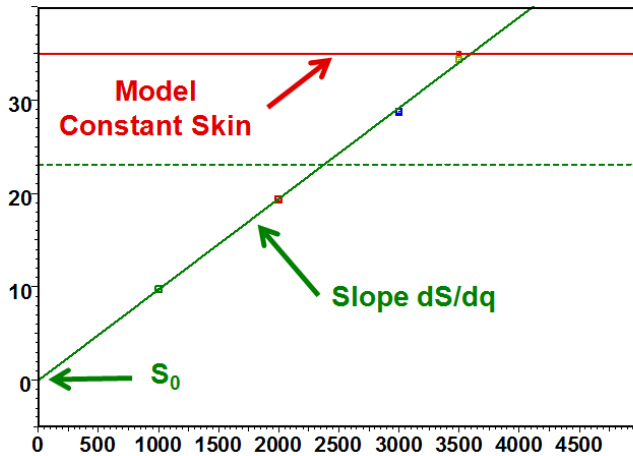


Fig. 6.C.3 – Skin vs. rate plot

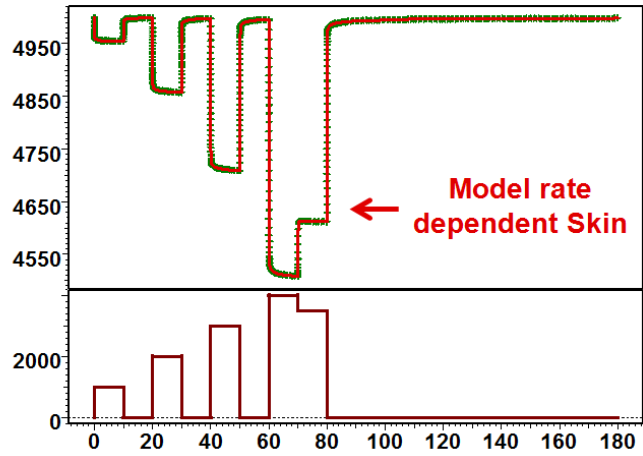


Fig. 6.C.4 – History match, rate dependant skin

6.C.2 Time dependent well model

After a stimulation job or a full workover, there is often a voluntary change from one well model to another. This can typically be the change of the well conditions from a wellbore storage and skin type to a fracture model after a 'frac' job. The skin can also change but the transformation of the model is more radical than just an improvement or deterioration of the skin. The other well models are discussed and developed later in this chapter but since the change of the full well model is similar to that of just a straight forward time dependent skin, we will briefly discuss it here.

The most common example of a well model transformation is when a well is subject to fracture stimulation. Typically the well is damaged and no fracture is intersecting the well during the first status or time period of a well test. Then the well is subject to the 'frac' job and the well model is changed to fracture model. It is possible to model this using a time dependent well model. The history is divided into time periods with a certain status, and each status can have the following definitions:

- Status with constant wellbore storage and skin
- Status with changing wellbore storage
- Rate dependent skin for each status
- Status with infinite, uniform flux or finite conductivity fractures
- Each status can have a different geometry limited entry
- Each status can have a different horizontal well geometry

The figure below illustrates the loglog match of the well behavior before and after a fracture stimulation job. The model matches the whole history of the test sequence including the fracture treatment.

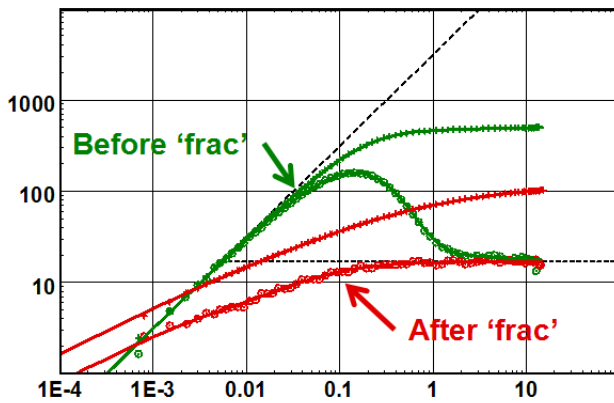


Fig. 6.C.5 – Changing well loglog match

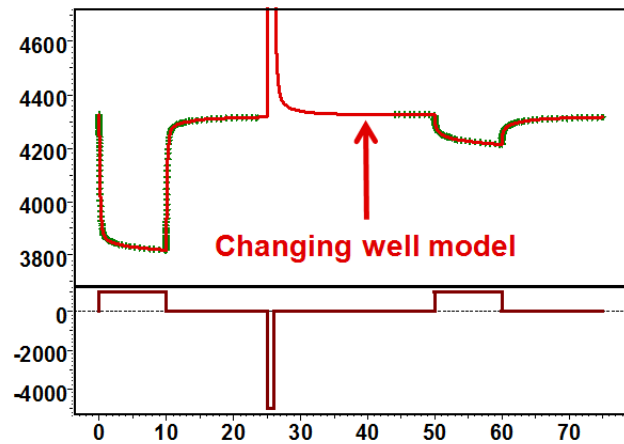


Fig. 6.C.6 – Changing well history match

6.C.3 Time dependent skin

When the well is cleaning up one will see a decrease of skin with time. Conversely a well may get progressively damaged during its producing life, hence an increase of the skin factor.

These effects may be modeled by allowing the mechanical skin to vary over the well life. This may actually be combined with a rate dependent component, though solving for both may often be an under-specified problem.

In Saphir, time dependent skin is just a subset of the changing well model where each status is assigned a skin. The figure below illustrates a well that is cleaning up matched with a constant and changing skin model.

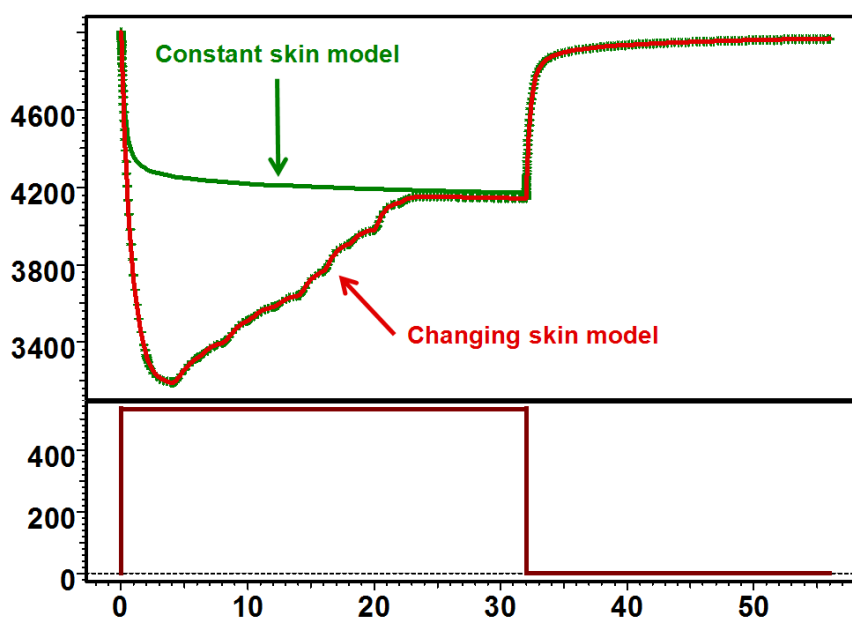


Fig. 6.C.7 – Well cleaning up

6.D High conductivity fracture

6.D.1 Hypotheses

Acidizing and fracturing are the basic choices when one wants to improve the productivity of a well. Acidizing requires an injectivity which will make it the typical treatment of choice for stimulating wells in high to medium permeability formations.

At the opposite, fracturing requires a mechanical stress induced by the resistance to the flow, and will be typically performed in low permeability formations. An extreme case today is the production of shale gas formations, which only occurs through series of fractures created along a horizontal drain. In a fracture job the bottom hole pressure rises above the fracture gradient of the formation, but within the pressure range allowed by the completion. Once the fracture is initiated, the bottom hole pressure is kept while a proppant such as sand or ceramic beads is included in the fracturing fluid. As the fracture 'screens out', the induced fracture faces remain open.

Rock mechanics suggests that in most cases the fracture has symmetrical 'bi-wing' geometry. The model we use in well testing assumes that the fracture wings are two perfect rectangles, each of length X_f , the half fracture length. For fully penetrating fractures the rectangles height is the formation thickness.

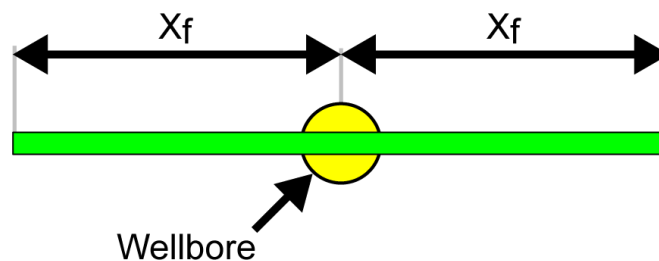


Fig. 6.D.1 – Schematic of a fracture model in the horizontal plane

There are two main types of fractured models: the high, or 'infinite conductivity' and the 'finite conductivity'. In the high conductivity we assume that the pressure drop along the inside of the fracture is negligible. In the low conductivity case we simulate diffusion within the fracture (see specific section).

There are two main high conductivity fracture models: the **Uniform Flux** model assumes a uniform production along the fracture. The **Infinite Conductivity** model assumes no pressure drop along the fracture. The latter is the one that makes sense physically. The former was initially developed because it is pretty straightforward to generate analytically. It is also used with a 'trick' (see below) to simulate the infinite conductivity response without the CPU cost of the true, semi-analytical solution.

6.D.2 Behavior

At early time only the part of the reservoir in front of the fracture will significantly contribute to the well production, orthogonal to the fracture plane. This is what we call the **linear flow**, and this is a characteristic feature (see figure below).

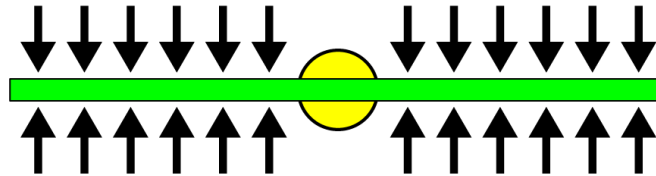


Fig. 6.D.2 – Early time linear flow

This linear flow is a particular case of a flow through a section of constant area A . Other examples of such flow are late time linear flow between two parallel faults. When such flow occurs there is a linear relation between the pressure change and the square root of the elapsed time, given by the following relation:

$$\Delta p = \frac{8.12 qB}{Area} \sqrt{\frac{\mu \Delta t}{k \phi c_t}}$$

Where 'Area' is the flowing section in ft². In the case of a fracture, the flowing section is the area of the fracture rectangle, so $Area = 2X_f h$. We then get:

$$\Delta p = \frac{4.06 qB}{hX_f} \sqrt{\frac{\mu \Delta t}{k \phi c_t}} = \sqrt{\frac{16.52 q^2 B^2 \mu}{h^2 \phi c_t}} \frac{\sqrt{\Delta t}}{\sqrt{kX_f^2}}$$

The flow will then progressively deviate from the early linear flow while the rest of the formation starts impacting the well production, and the area of investigation becomes elliptical. When the production continues the ellipse grows into a large circle and we reach Infinite Acting Radial Flow. At this stage the fracture behaves like a standard well with a **negative skin**.

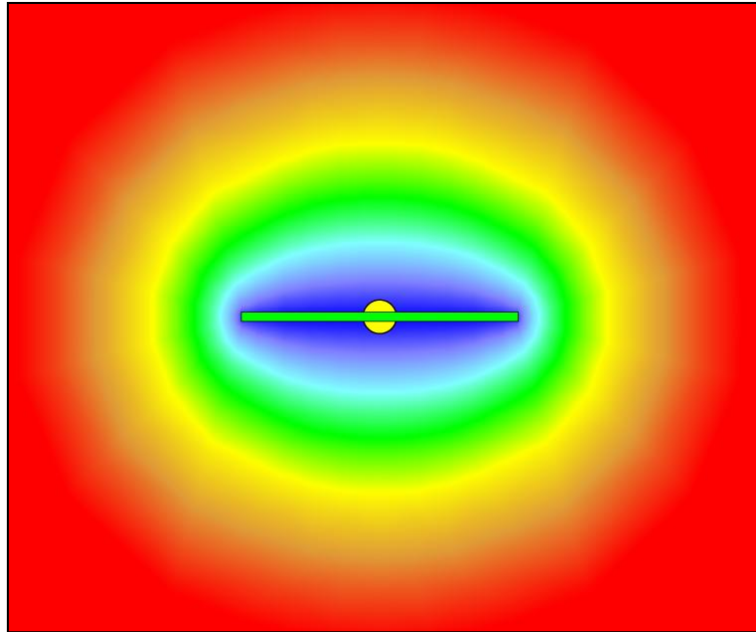


Fig. 6.D.3 – Evolution of the area of investigation

The figure below shows the normalized density of flow from the formation into the fracture. The red curve corresponds to the Uniform Flux fracture. At very early time the infinite conductivity solution will follow this profile. However this changes rapidly until it stabilizes at late time to the blue curve, showing that most of the flow at late time comes from the tips of the fracture, which are more exposed to the rest of the formation than the center part.

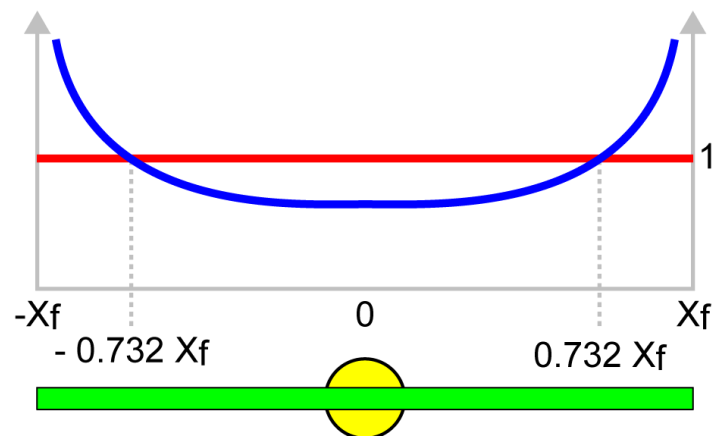


Fig. 6.D.4 – Flow profile along the fracture at early and late time

6.D.3 Loglog Analysis

From the previous section, the pressure change during the early time linear flow is:

$$\Delta p = m\sqrt{\Delta t} \quad \text{where} \quad m = \sqrt{\frac{16.52 q^2 B^2 \mu}{h^2 \phi c_t}} \frac{1}{\sqrt{kX_f^2}}$$

In the equations above, all parameters are inputs except the permeability and the fracture half length. During the linear flow, the result of any analysis will therefore provide a relation between permeability and fracture half length by determining the value of kX_f^2 .

The Bourdet derivative at early time is given by:

$$\Delta p' \approx \frac{d\Delta p}{d \ln(\Delta t)} = \Delta t \frac{d\Delta p}{d\Delta t} = \Delta t \frac{m}{2\sqrt{\Delta t}} = \frac{1}{2} m\sqrt{\Delta t} = \frac{1}{2} \Delta p$$

On a decimal logarithmic scale this writes:

$$\log(\Delta p) = \log(m) + \frac{1}{2} \log(\Delta t) \quad \text{and} \quad \log(\Delta p') = \log(\Delta p) - \log(2)$$

The early time flow regime of a high conductivity fracture is characterized on a loglog plot by a half unit slope on both the pressure and derivative curves. The level of the derivative is half that of the pressure. At later time there is a transition away from this linear flow towards Infinite Acting Radial Flow, where derivative stabilizes (see figure below).

The position of these two half slope straight lines will establish a link between the time match and the pressure match, providing a unique result for kX_f^2 . Fixing the stabilization level of the derivative will determine the value of k , and the half fracture length will be calculated from kX_f^2 . If there is no clear stabilization level the problem will become underspecified.

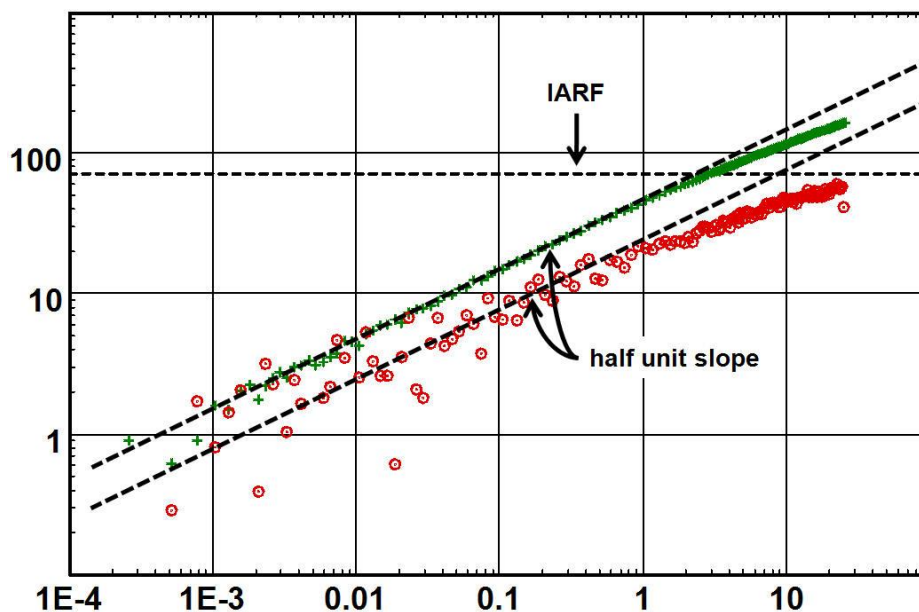


Fig. 6.D.5 – Infinite conductivity fracture behavior

6.D.4 Sensitivity to different parameters

6.D.4.a Choice of fracture model

The description above applies to both Infinite Conductivity and Uniform Flux models. It may be interesting at this stage to compare both solutions for the same parameters, see figure below.

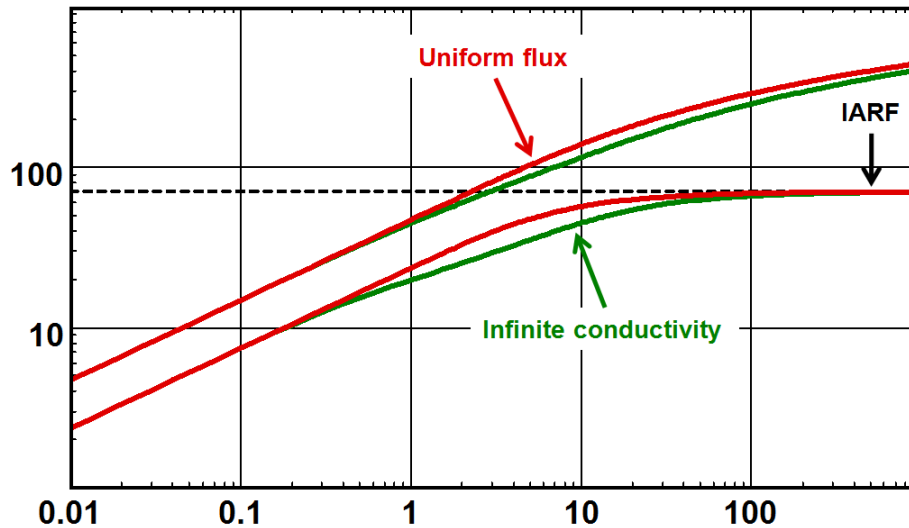


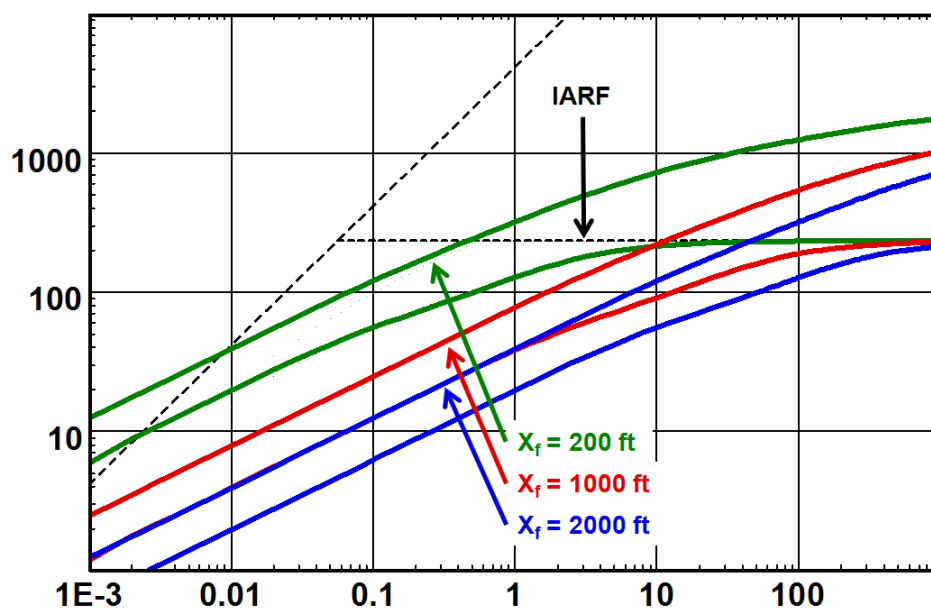
Fig. 6.D.6 – Uniform Flux vs. Infinite Conductivity

These solutions differ only slightly when plotted on a loglog scale. Purists consider that the uniform flux solution is physically incorrect and only the infinite conductivity solutions should be used. In real life the uniform flux transients generally offer a better match, and this can be explained by the fact that the productivity of the uniform flux fracture, for a given length, is slightly lower than the infinite conductivity, and that this, possibly, better simulates the slight pressure losses in the fracture.

The Uniform Flux model was published because it was fairly easy to calculate. The infinite conductivity fracture was solved semi-analytically (at high CPU cost) but it was shown that an equivalent response could be obtained by calculating the (fast) uniform flux solution at an off-centered point in the fracture ($x=0.732.X_f$). This position corresponds to the intercept of both flow profiles, as shown in the 'behavior' section.

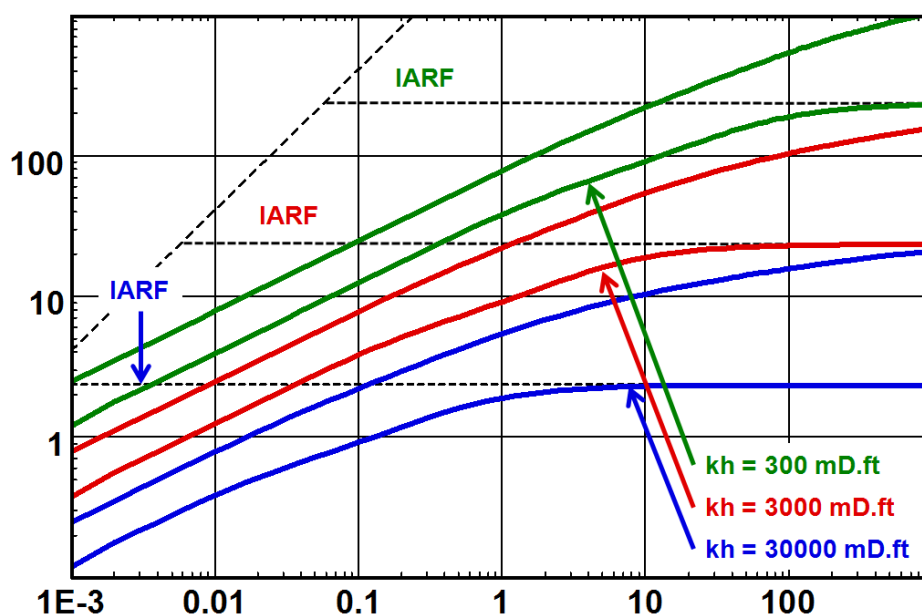
6.D.4.b Sensitivity to the half fracture length

The loglog plot below is the comparison of several infinite conductivity responses for different values of X_f , all other parameters, including the formation permeability, staying the same. Because the permeability does not change, the pressure match remains constant, and the loglog response is shifted left and right. Multiplying the fracture length by 10 will shift the responses two log cycles to the right. This will shift the early time half slope down one cycle.

Fig. 6.D.7 – Sensitivity to X_f

6.D.4.c Sensitivity to the reservoir permeability

The loglog plot below is the comparison of several infinite conductivity responses for different values of permeability, all other parameters, including the fracture half length, staying the same. Multiplying the permeability by 100 will shift the stabilization of the derivative down two log cycles, but the half slope of the linear flow will only be shifted down one log cycle.

Fig. 6.D.8 – Sensitivity to kh

6.D.5 Specialized Analysis

Let us repeat it. The loglog analysis with the Bourdet derivative (a.k.a. the 'right stuff') has all what is needed to perform the complete analysis of a fractured well. Positioning the half slopes of both pressure and Bourdet derivative exactly does what we will be showing below. The advantage of the loglog approach is that it will be valid even if a pure linear flow is not detected, and a successful nonlinear regression will not require pure behaviors to occur. Anyway, the specialized analyses have a historical value and do not hurt, anyway.

From the previous section, the relation between pressure and time during the linear flow is:

$$\Delta p = m\sqrt{\Delta t} \quad \text{where} \quad m = \sqrt{\frac{16.52 q^2 B^2 \mu}{h^2 \phi c_t}} \frac{1}{\sqrt{k X_f^2}}$$

A straight line can be drawn on a cartesian graph of pressure change versus $\sqrt{\Delta t}$:

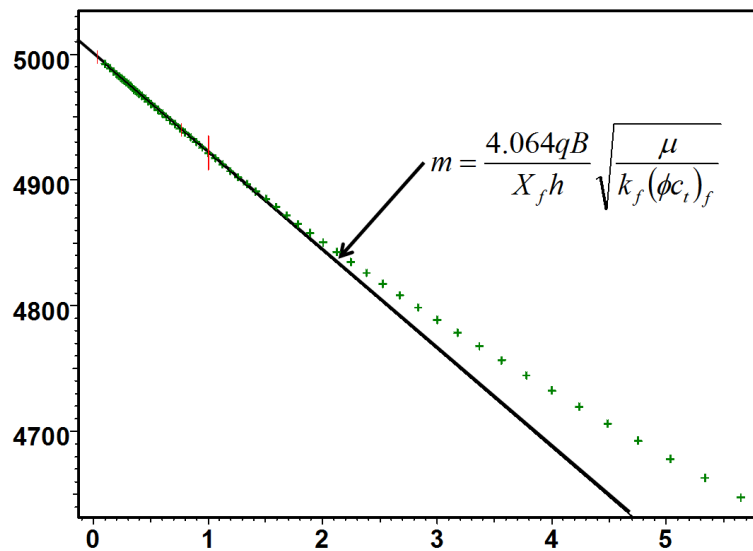


Fig. 6.D.9 – Square root plot

From this plot we get a value of $k X_f^2$, and therefore X_f if we do know k .

$$k X_f^2 = \frac{16.52 q^2 B^2 \mu}{m^2 h^2 \phi c_t} \quad \text{and / or} \quad X_f = \frac{4.06 q B}{m h} \sqrt{\frac{\mu}{k \phi c_t}}$$

Applying superposition? **NO!**

In a specialized plot (except the linear plot) it is possible to replace a time function by its rate superposition. For example we could use the tandem square root plot in the case of a build-up. This is the case when we assume that the flow regime we are studying is actually the superposition of these flow regimes. We do this for Infinite Acting Radial Flow or late time effects such as the linear flow between parallel faults. This does NOT apply here, or to any other early time behavior, and we should use the pure time function, not the superposed one. The only exception may be for shale gas, where the 'early time' behavior actually lasts years, and where superposition may be applicable.

6.D.6 Adding wellbore storage

The original publications on fracture solutions were without wellbore storage and skin. It is not that it was absent, but the solution with two additional parameters (C and S) was too complex to be turned into readable type-curves especially as the influence of skin is particularly messy.

Wellbore storage will affect the early time data by masking the linear flow. If the storage effect is high enough no fracture flow may be diagnosed from the loglog plot and the interpreter can no longer justify that a fracture may exist if the total skin is not highly negative. It will also become increasingly more difficult to make a choice between a low or high conductivity fracture, and the half fracture length X_f can no longer be determined from the square root plot.

If a fracture job had been done on the well this could be an indication that the job had not been very successful or that the fracture had propagated up or down rather than laterally.

The below figure illustrates the effect of wellbore storage on the linear flow in the loglog plot.

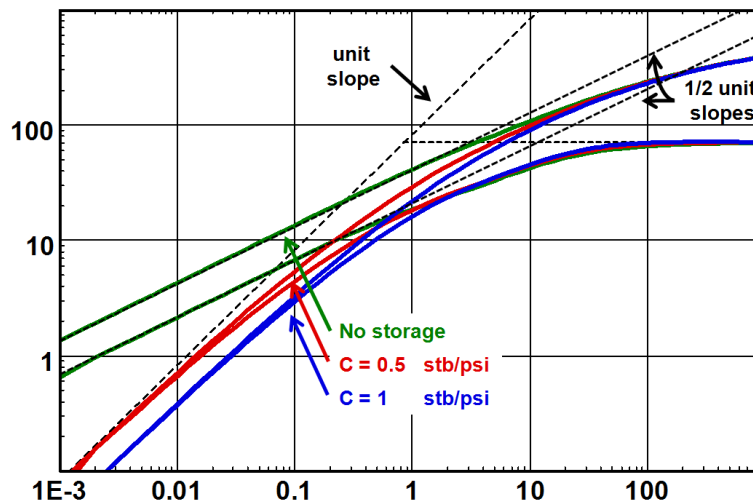


Fig. 6.D.10 – Loglog plot influence of wellbore storage

6.D.7 Skin effect

Total skin; geometrical skin; model skin: The concept of skin in configurations that are not based on a standard vertical well are sometimes confusing. This section describes the different skin components, and how they may be combined.

6.D.7.a Fracture Geometrical Skin

When we run a standard straight line analysis on a logarithmic scale (MDH, Horner, Superposition) we calculate a value of the skin factor. This is what we call the **Total Skin** S_T . This calculation may take place at any time after the extraction of the build-up, and is independent of the model chosen. The Total Skin is given by the equation:

$$\Delta p_{Skin} = 141.2 \frac{q_{sf} \mu}{kh} S_T$$

where Δp_{Skin} is the pressure difference between our data and the response of a standard, undamaged, fully penetrating vertical well.

When we generate a high conductivity fracture model with no specific damage or stimulation other than the fracture itself, and then perform a IARF straight line analysis, we will get a negative skin. This negative skin is not due to any pressure loss or gain at the sandface, it is just due to the geometry of the well. This is what we call the **Geometrical Skin** S_G . We can also link this geometrical skin to the equivalent wellbore radius. This is the radius of a theoretical vertical well that would have the same productivity as the fracture. The geometrical skin and equivalent radius depend on our choice of fracture model:

$$\text{Uniform Flux : } S_G = -\ln\left(\frac{X_f}{2.718r_w}\right) \quad r_{weq} = \frac{X_f}{e} \approx 37\% X_f$$

$$\text{Infinite Conductivity : } S_G = -\ln\left(\frac{X_f}{2.015r_w}\right) \quad r_{weq} = \frac{X_f}{2.015} \approx 50\% X_f$$

Another way to present this is that an infinite conductivity fracture with a half length of 200 ft will have the same productivity of a theoretical vertical well with a radius of 100 ft. If the well radius is 0.3 ft, the geometrical skin S_G will be $-\ln(333) = -5.8$.

The figure below shows the equivalent wellbore radius for an Infinite Conductivity Fracture (blue) and a Uniform Flux Fracture (orange).

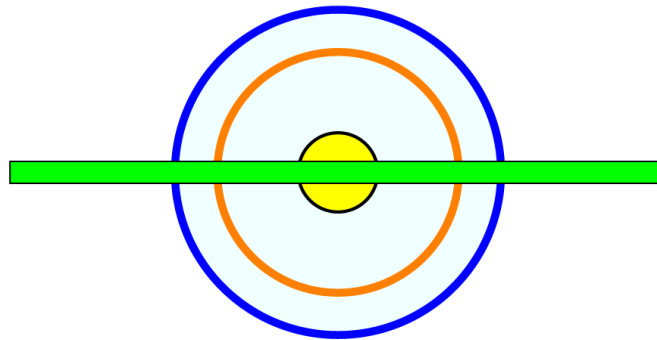


Fig. 6.D.11 – Equivalent wellbore radius

6.D.7.b Model Skin and Total Equivalent Skin

In complement there may be a pressure loss or gain at the sandface, which is quantified with the **Model Skin** S_M . At this stage one has to be careful about the convention of how the skin is defined. There are two ways to define the Skin factor in a fractured well model, and these are accessible in the Saphir settings page, Interpretation option, Skin tab:

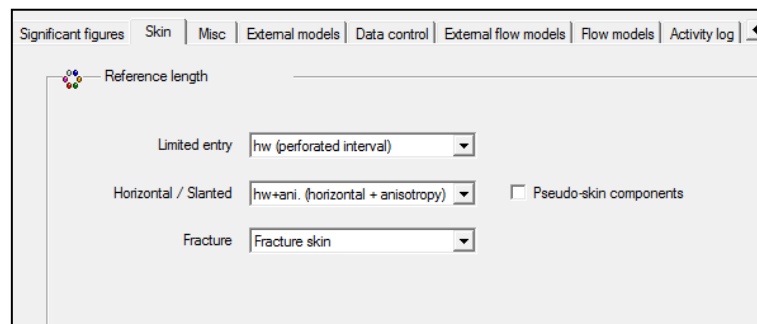


Fig. 6.D.12 – Skin convention dialog in Saphir v4.12

The **Standard Skin** considers that we keep the standard vertical well sandface as the flow area through which the skin factor is applied. This is as if the skin pressure drop was occurring at the well and not at the fracture sandface.

There are two ways to define the **Fracture Skin**:

$$A_{Flow} = 2\pi r_w h$$

Because the reference areas are the same, under this convention the component skins add up, and the total equivalent skin S_T will be:

$$S_T = S_G + S_M$$

$$\text{and } A_{Flow} = 4X_f h$$

Because the reference areas are different, under this convention the component skins will need a normalization to add up, and the total equivalent skin S_T will be:

$$S_T = S_G + \frac{\pi r_w}{2X_f} S_M$$

In Saphir v4.12 there was a third way, where h as a reference thickness was replaced by X_f , but it does not make any sense physically and will be removed in v4.20.

6.D.7.c Influence of skin

The figure below illustrates the influence of fracture skin on the behavior of the pressure change and the derivative. There is no effect on the derivative but the pressure change will no longer show the half slope behavior of linear flow as the pressure change become flatter as the fracture skin increases.

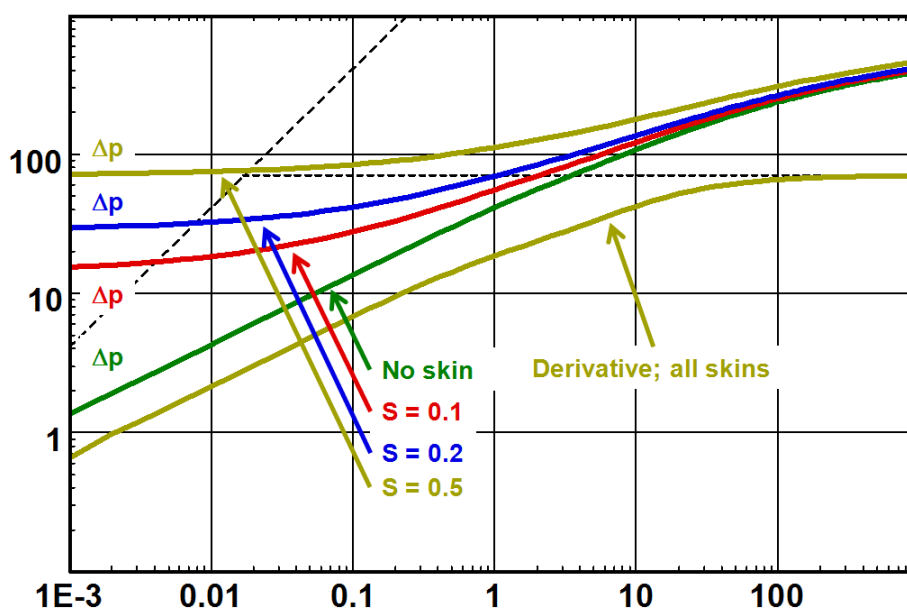


Fig. 6.D.13 – Fracture skin influence

6.E Low conductivity fracture

6.E.1 Hypothesis

The fracture geometry is the same as that of the high-conductivity models, but now it is assumed that there is a significant pressure gradient along the fracture.

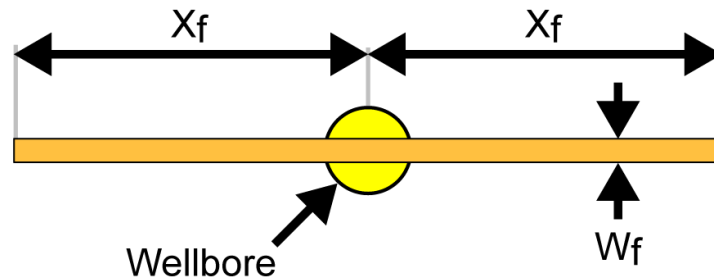


Fig. 6.E.1 – Schematic of a fracture model in the horizontal plane

6.E.2 Behavior

In the absence of storage, the first flow regime is linear flow along the fracture axis, this simultaneously induces a linear flow orthogonal to the fracture, the amplitude of which changes along the fracture length, i.e. there is a non-uniform flux into the fracture, in contrast to the high-conductivity models. This bi-linear flow regime, with linear flow along two axes, gives rise to a pressure response proportional to the fourth root of time. Both the loglog and the Bourdet derivative plots exhibit quarter slopes during bi-linear flow. Bi-linear flow is followed by the usual linear flow, characterized by a 1/2-unit slope on the loglog.

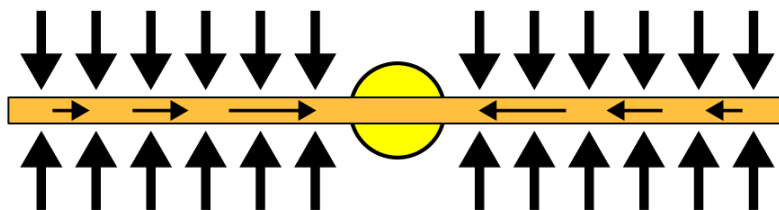


Fig. 6.E.2 – Early time bi-linear flow

The bi-linear flow regime is usually happening at very early time, and is not always seen. It represents the time at which the pressure drop along the fracture is significant, and in reality this time is very short. Even when there is no storage effect, the data sometimes does not exhibit a 1/4-slope and can be matched directly with a high-conductivity fracture model. However, the general model for an 'induced fracture' fractured well must be the finite-conductivity fracture model, as there will always be a pressure drop along the fracture, however small. This is however, not significant compared to the linear pressure drop in the reservoir into the fracture.

There are two additional parameters that needs to be specified in this model; the fracture width (w) and the fracture permeability (k_f), in fact it is the permeability thickness of the fracture that is specified (k_fw).

When the fracture conductivity is very high, the model approaches the infinite-conductivity response, with a $1/2$ -slope developing immediately. Conversely, with low k_fw the pressure drop along the fracture is significant almost to the onset of radial flow (IARF). When such flow occurs the relationship between the pressure change and the fourth root of elapsed time is given by the flowing relationship:

$$\Delta p = \frac{44.11qB\mu}{h\sqrt{k_fw}(\phi\mu c_k)^{1/4}} \Delta t^{1/4}$$

6.E.3 Loglog Analysis

From the previous section, the pressure change during bi-linear flow is:

$$\Delta p = m\sqrt[4]{\Delta t} \quad \text{where} \quad m = \frac{44.11qB\mu}{h\sqrt{k_fw}(\phi\mu c_k)^{1/4}}$$

$$\Delta p' \approx \frac{d\Delta p}{d \ln(\Delta t)} = \Delta t \frac{d\Delta p}{d\Delta t} = \Delta t \frac{m}{4\sqrt[4]{\Delta t}} = \frac{1}{4} m\sqrt[4]{\Delta t} = \frac{1}{4} \Delta p$$

On a decimal logarithmic scale this writes:

$$\log(\Delta p) = \log(m) + \frac{1}{4} \log(\Delta t) \quad \text{and} \quad \log(\Delta p') = \log(\Delta p) - \log(4)$$

During bi-linear flow the pressure change and the Bourdet derivative follows two parallel straight lines with a slope of one quarter ($1/4$). The level of the derivative is a quarter of that of the pressure change.

This is followed by the onset of linear flow and the pressure change and the Bourdet derivative follow then two parallel straight lines of half slope ($1/2$) with the level of the derivative half that of the pressure change.

When radial flow is reached we have the usual stabilization of the derivative curve.

The following figure illustrates this behavior on the loglog plot.

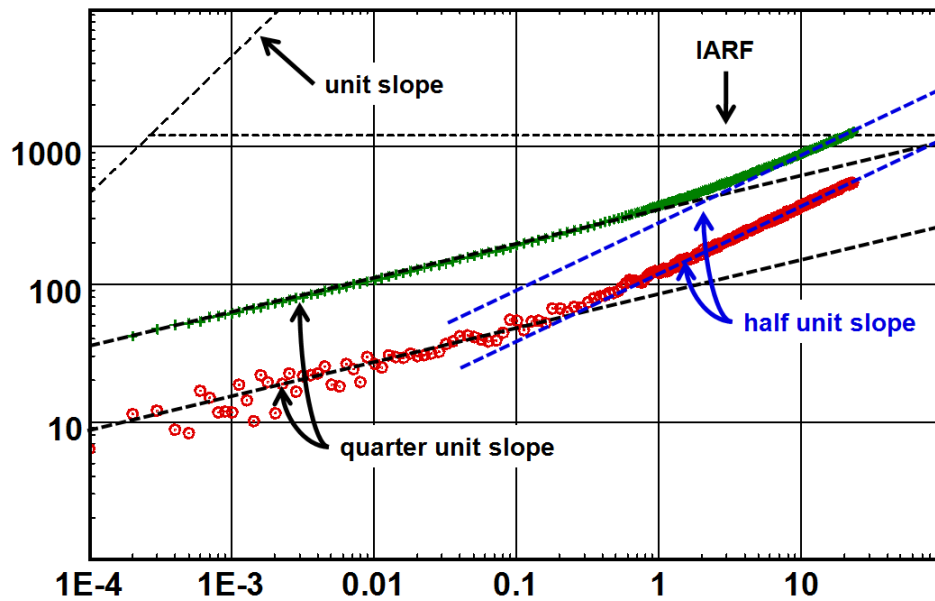


Fig. 6.E.3 – Finite conductivity fracture behavior

6.E.4 Sensitivity to different parameters

6.E.4.a Sensitivity to $k_f w_f$

For larger fracture conductivities the solution approaches that of an infinite conductivity fracture and the bi-linear flow will disappear completely as the derivative and the pressure change is shifted lower and lower, the $\frac{1}{4}$ slope will be completely replaced by the linear $\frac{1}{2}$ slope. See the illustration in the figure below.

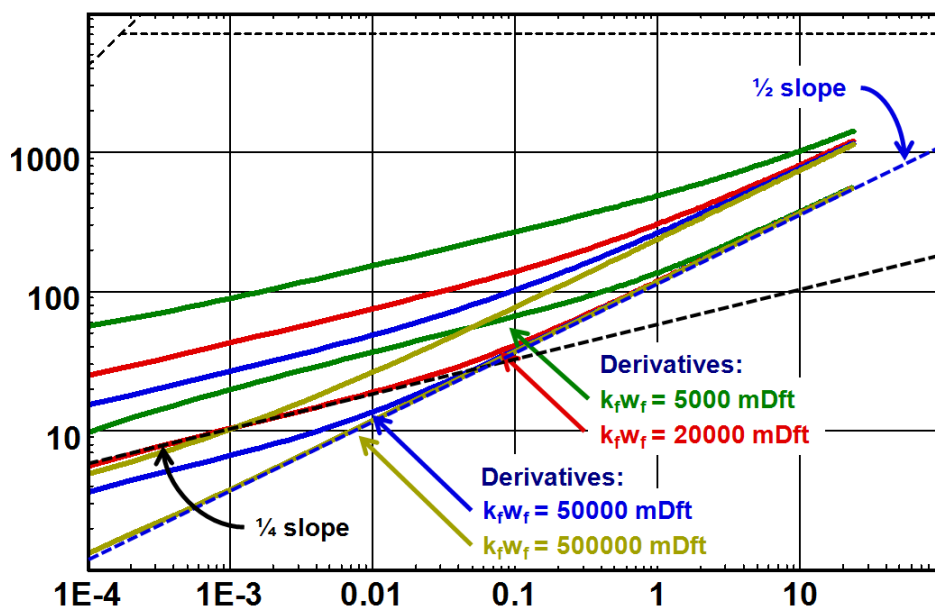


Fig. 6.E.4 – Finite conductivity fracture, sensitivity to $k_f w_f$

With very low fracture conductivity the linear flow will not develop and the bi-linear flow will be dominating until the onset of infinite acting radial flow.

6.E.4.b Sensitivity to the half fracture length

Keeping $F_{CD} = \frac{k_f w_f}{k X_f}$ constant the pressure change and the Bourdet derivative curves shift to the right as the fracture length increases. The longer the fracture, the longer it takes to reach IARF. The following figure illustrates this.

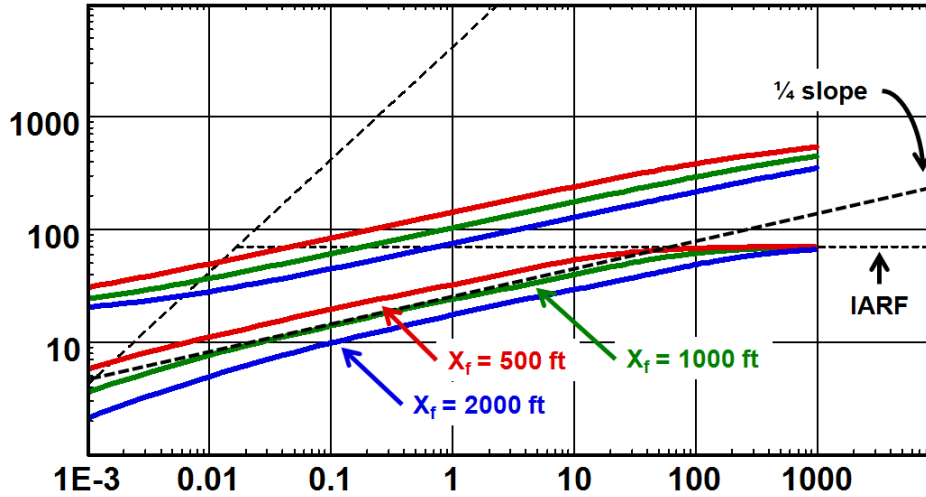


Fig. 6.E.5 – Constant F_{CD} ; sensitivity to half fracture length, X_f

In practice, massive hydraulic fracturing is only common in very low permeability formations. We typically encounter this sort of stimulation in Tight Gas, Shale Gas and Coal Bed Methane (CBM), type of reservoirs. This topic is covered in the chapter on 'Unconventional Reservoirs'. It suffices to say here that these types of wells would not be economically viable or would not produce at all without this sort of stimulation. It is now becoming popular not only to induce one single fracture in the well, but horizontal wells are selectively 'fraced', and multiple individual low conductivity fractures may exist. It goes without saying that the analyst's task can become more than just challenging.

It is easy to imagine that for a period subject to pressure transient analysis the time to reach infinite acting radial flow will be prohibitively long, and in some cases the transient will never reach this flow regime at all (well, maybe after thousands of years). Thus one can understand that lacking some of the flow regimes the interpretation of massive hydraulically fraced wells can be quite difficult.

It is therefore always recommended that a pre frac test be carried out to determine the permeability thickness product of the formation (kh).

6.E.5 Specialized analysis

The data that matches the quarter unit straight line in both the pressure change and the Bourdet derivative is in bi-linear flow. A plot of the pressure change versus the fourth root of elapsed time, $\sqrt[4]{\Delta t}$ will be on a straight line of slope:

$$m = \frac{44.11 q B \mu}{h \sqrt{k_f w_f (\phi \mu c_i k)^{1/4}}} \text{ and } k_f w_f = 1945 \sqrt{\frac{1}{\Phi \mu c_i k} \left(\frac{a B \mu}{h m} \right)^2}$$

The figure below illustrates the fourth root plot.

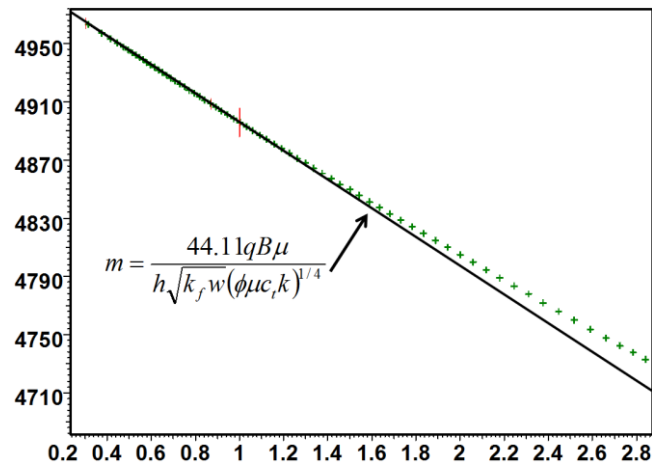


Fig. 6.E.6 – Fourth root plot

6.E.6 Adding wellbore storage

Wellbore storage will affect the early time data by masking both bi-linear and linear flow. The storage effect does not need to be very high in order to mask the fracture flow completely. The interpreter is faced with data that cannot prove that a fracture exists; only the very negative skin associated with the fracture and a marked increase in productivity will give him some arguments that the stimulation job was indeed successful or partly successful.

In fact, the analyst is often faced with this dilemma. From a design point of view the fracture job may be judged successful as we know what we pumped and the proppant disappeared, so the fracture must be in the ground. But often, the frac will propagate up or down, and parallel short fractures maybe induced thus masking the very long fracture that was designed for. It is just not manifesting itself in the bottom hole pressure data.

The figure below illustrates the effect of wellbore storage on the early time behavior.

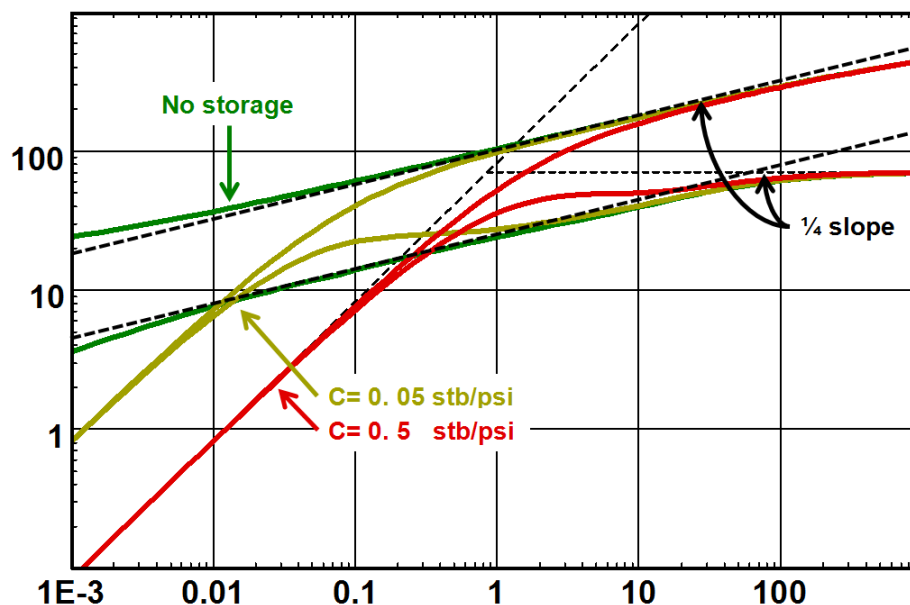


Fig. 6.E.7 – Wellbore storage influence

6.E.7 Skin effect

The total (semilog) skin of a fractured well is negative due to the fracture geometry. The mechanical skin of the fracture (damage) is the difference between the total skin and the geometrical skin. The total skin is given by the equation:

$$\Delta p_{Skin} = 141.2 \frac{q_{sf} \mu}{kh} S_T$$

where Δp_{Skin} is the pressure difference between our data and the response of a standard, undamaged, fully penetrating vertical well.

6.E.7.a Fracture Geometrical Skin

The skin of the finite conductivity fracture is defined by the geometrical skin defined for an infinite conductivity fracture and a correction factor to allow for the pressure drop caused by the low fracture conductivity.

The geometrical skin expresses the relation between the half fracture length and the skin for values of $\frac{k_f w}{k X_f} > 300$ and:

$$S_G = -\ln\left(\frac{X_f}{2.015 r_w}\right) \quad r_{weq} = \frac{X_f}{2.015} \approx 50\% X_f$$

6.E.7.b Model Skin and Total Equivalent Skin

In complement there may be a pressure loss or gain at the sandface, which is quantified with the **Model Skin** S_M . At this stage one has to be careful about the convention of how the skin is defined. There are two ways to define the Skin factor in a fractured well model, and these are accessible in the Saphir settings page, Interpretation option, Skin tab:

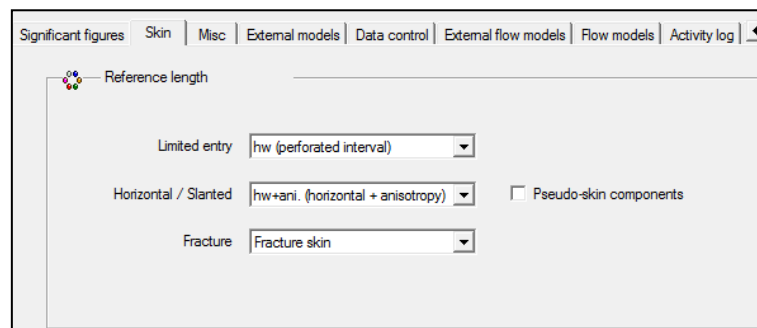


Fig. 6.E.8 – Skin convention dialog in Saphir v4.12

The **Standard Skin** considers that we keep the standard vertical well sandface as the flow area through which the skin factor is applied. This is as if the skin pressure drop was occurring at the well and not at the fracture sandface.

There are two ways to define the **Fracture Skin**:

$$A_{Flow} = 2\pi r_w h$$

Because the reference areas are the same, under this convention the component skins add up, and the total equivalent skin S_T will be:

$$S_T = S_G + S_M$$

If one consider

$$A_{Flow} = 4X_f h$$

The reference areas are different, under this convention the component skins will need a normalization to add up, and the total equivalent skin S_T will be:

$$S_T = S_G + \frac{\pi r_w}{2X_f} S_M \text{ Influence of skin}$$

The figure below illustrates the influence of fracture skin on the behavior of the pressure change and the Bourdet derivative. There is no effect on the derivative but the pressure change will no longer show the quarter slope behavior of bi-linear flow as the pressure change become flatter when the fracture skin increases.

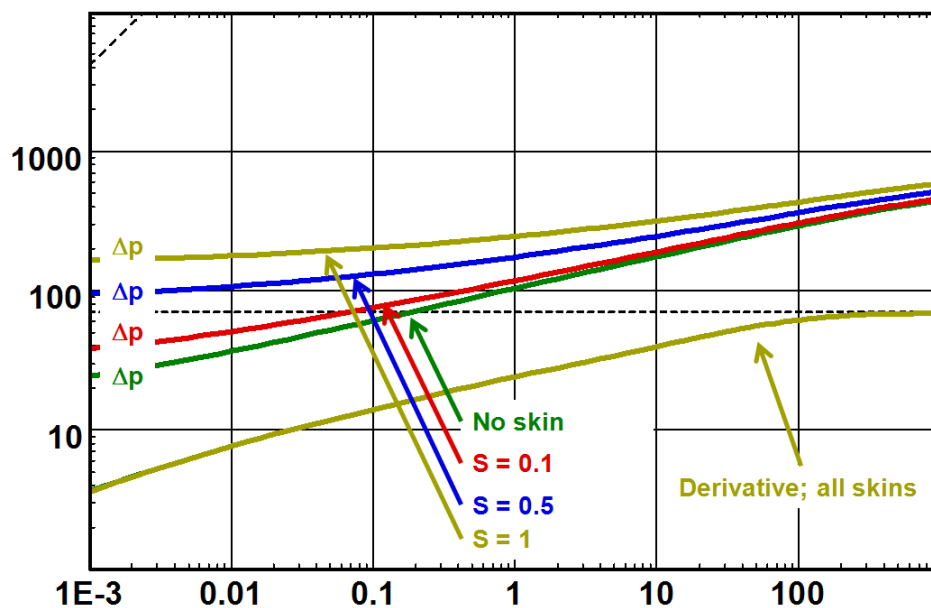


Fig. 6.E.9 – Fracture skin influence

6.F Limited entry well

6.F.1 Hypothesis

This model assumes that the well produces from an interval smaller than the net drained interval. The drained interval is not always fully perforated to avoid gas coning or cusping and/or water production from an underlying or lateral aquifer or bottom water. In this case the limited entry is voluntary. Partial penetration can also happen as a result of field operations gone awry; problems such as perforations off depth and plugging of perforations are amongst many reasons that a well has limited contribution to production.

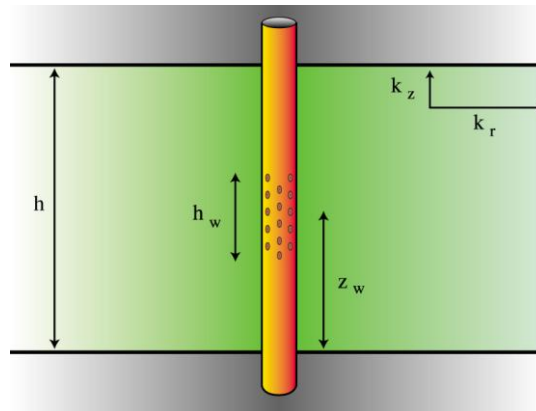


Fig. 6.F.1 – Limited entry schematic

The partial penetration effect also comes into play with all sorts of formation testing tools where the point of production can be just one single small ID probe, thus the pressure measurements maybe affected by the partial penetration spherical flow regime right through the measurement time. This particular test type is covered in the chapter on 'PTA - Special test operations'.

6.F.2 Behavior

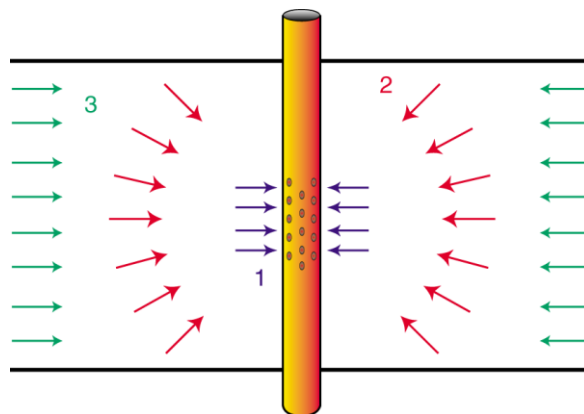


Fig. 6.F.2 – Limited entry flow regimes

In theory, after wellbore storage, the initial response is radial flow in the perforated interval h_w (see figure above), shown as '1'. This 'stabilization' gives the product $k_r h_w$ (the subscript r stands for radial) and it can be imagined that if there were no vertical permeability this would be the only flow regime present before the influence of any lateral boundaries. In practice this flow regime is more often than not masked by wellbore storage.

In flow regime '2' there is a vertical contribution to flow, and if the perforated interval is small enough a straight line of slope $-1/2$ (negative half slope) may develop in the Bourdet derivative, corresponding to spherical or hemi-spherical flow. The pressure is then proportional to $\frac{1}{\sqrt{\Delta t}}$.

The relation of the pressure change and the 'one over the square root' of the elapsed time is:

$$\Delta p = \frac{70.6qB\mu}{k_s r_s} - \frac{2453qB\mu\sqrt{\phi\mu c_i}}{k_s^{3/2}} \frac{1}{\sqrt{\Delta t}}$$

With: $k_s = (k_r^2 k_v)^{1/3}$

Finally, when the diffusion has reached the upper and lower boundaries, the flow regime becomes radial again, and the stabilization now corresponds to the classical product, $k_r h$.

In any model where there is a vertical contribution to flow, there must also be a pressure drop in the vertical direction, and vertical permeability has to be considered along with the radial permeability. The pressure drop due to the flow convergence (flow regime 2, spherical flow) is a 'near-wellbore' reservoir effect caused by the anisotropy. If the spherical flow is seen in the data it may be possible to separate the 'damage' and 'geometric' components of the total skin determined from the second IARF period.

6.F.3 Loglog Analysis

From the previous section, the pressure change during spherical flow is:

$$\Delta p = m \frac{1}{\sqrt{\Delta t}} \quad \text{where} \quad m = \frac{2453qB\mu\sqrt{\phi\mu c_i}}{k_s^{3/2}}$$

$$\Delta p' \approx \frac{d\Delta p}{d \ln(\Delta t)} = \Delta t \frac{d\Delta p}{d\Delta t} = \Delta t \frac{m}{-2\sqrt{\Delta t}} = -\frac{1}{2} m \sqrt{\Delta t} = -\frac{1}{2} \Delta p$$

The characteristic flow regime is spherical flow until upper and lower boundaries have been reached and then followed by radial flow in the reservoir.

The interesting flow regime here is spherical flow during which time the pressure change is proportional to $\frac{1}{\sqrt{\Delta t}}$, the Bourdet derivative will follow a negative half unit slope straight line.

From this flow regime it is possible to determine the anisotropy $\frac{k_v}{k_r}$. The below figure illustrates the behavior of a well with partial penetration.

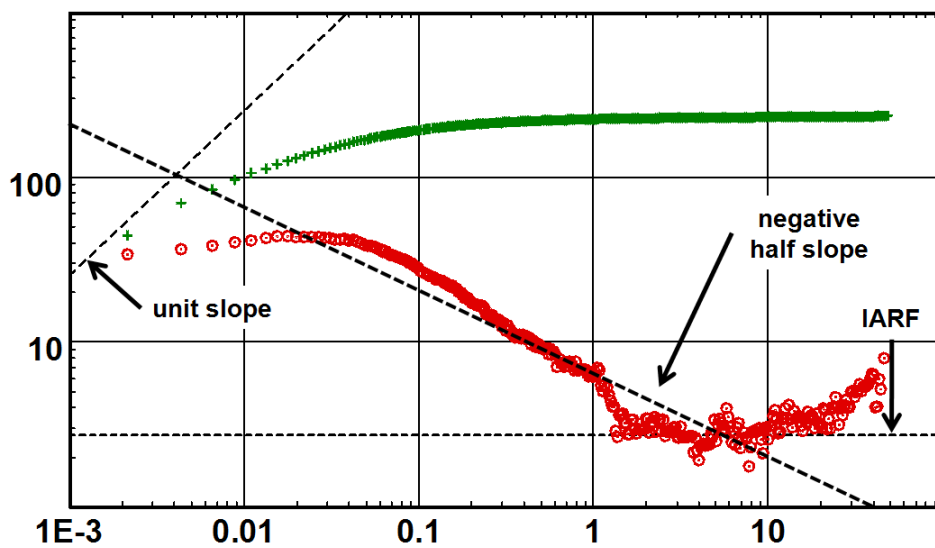


Fig. 6.F.3 – Limited entry well behavior

6.F.4 Sensitivity to different parameters

6.F.4.a Sensitivity to the anisotropy

As the anisotropy contrast becomes large the spherical flow regime becomes longer and the geometrical skin more severe. If the open interval is close to either the upper or lower boundary hemispherical flow will develop which is seen as a translation of the negative half slope in time, it develops later. If either of the boundaries is a constant pressure boundary (gas cap or active aquifer can act as a constant pressure boundary) then the Bourdet derivative will turn down. The below figures illustrates the sensitivity caused by the anisotropy on the Bourdet derivative in the loglog plot.

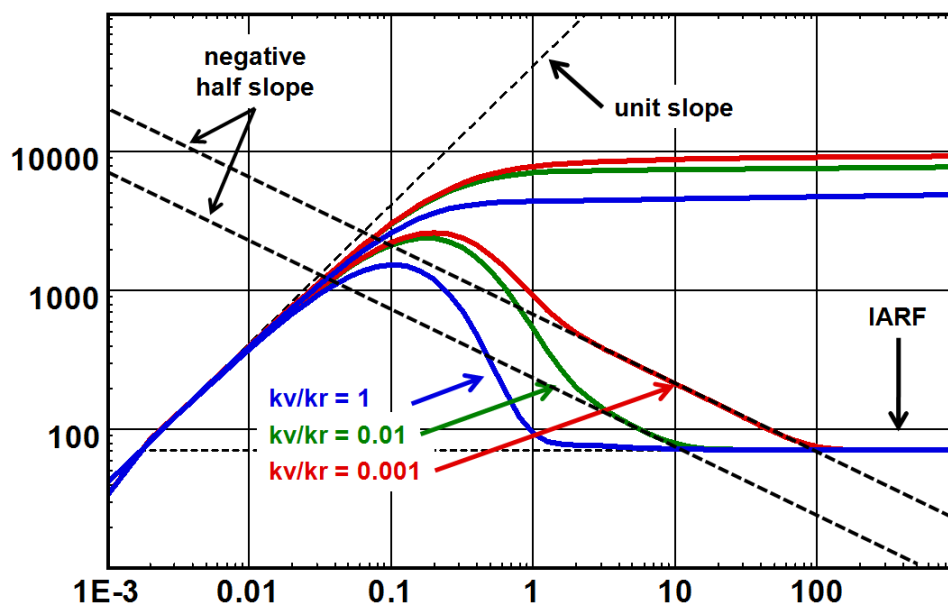


Fig. 6.F.4 – Sensitivity to anisotropy

The following figure shows the difference between spherical and hemi-spherical flow.

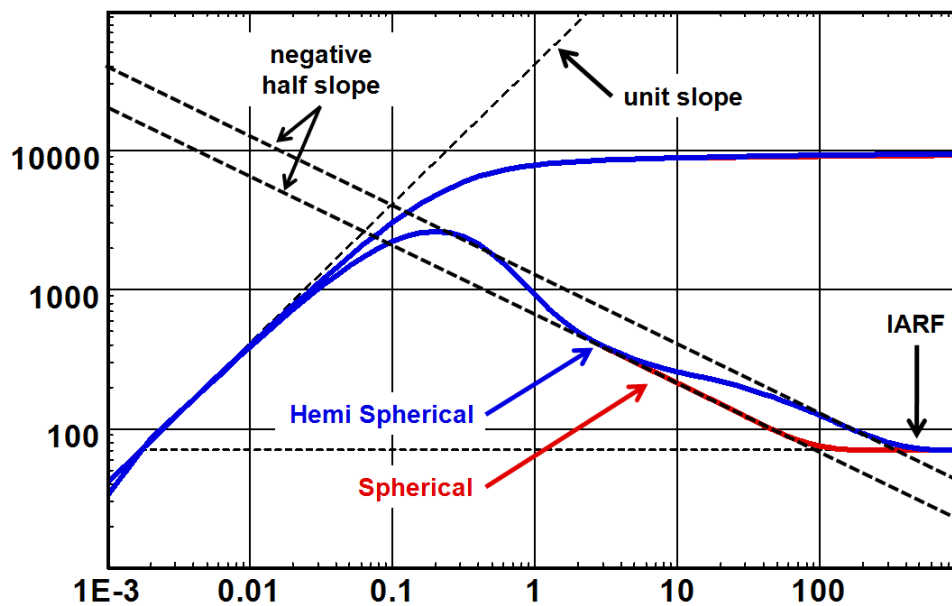


Fig. 6.F.5 – Spherical and hemi-spherical

6.F.4.b Sensitivity to the vertical distance to a constant pressure boundary

The next figure illustrates the influence of the proximity to a constant pressure boundary. The closer the perforated interval is to the boundary the stronger is the effect from it.

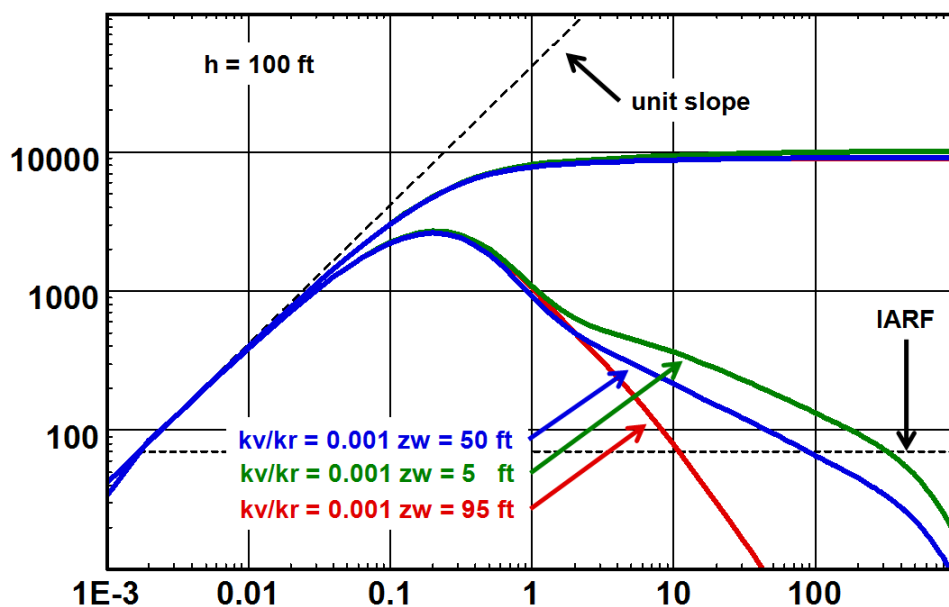


Fig. 6.F.6 – Limited entry with Gas Cap

With a high enough vertical permeability the spherical flow may not be seen at all; this is also dependent upon the ratio h_w/h , the fraction of the producing interval that is contributing and the level of wellbore storage. As k_v decreases the negative half slope spherical flow derivative becomes increasingly evident. The geometrical skin also increases.

6.F.5 Specialized analysis

The data that matches the negative half unit slope straight line on the Bourdet derivative in the loglog plot will also be on a straight line if the pressure change is plotted versus $\frac{1}{\sqrt{\Delta t}}$ in a cartesian plot. The straight line has a slope of:

$$m = \frac{2453qB\mu\sqrt{\phi\mu c_t}}{k_s^{3/2}}$$

The anisotropy can then be determined $\frac{k_v}{k_r} = \left(\frac{k_s}{k_r}\right)^3$

This is valid when the contribution interval is such that spherical flow develops. If the open interval is close to the upper or lower boundaries then hemispherical flow will develop and the slope of the specialized plot has to be divided by two.

The below figure illustrates the specialized plot of pressure change versus $\frac{1}{\sqrt{\Delta t}}$.

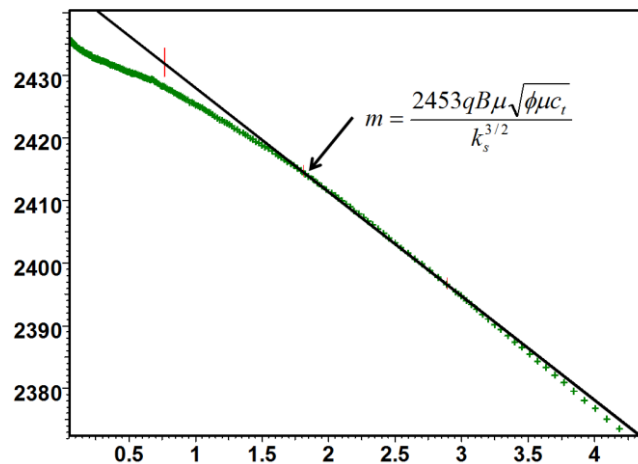


Fig. 6.F.7 – One over square root plot

6.F.6 Adding wellbore storage

Wellbore storage will quickly mask the spherical flow regime. In a well where there is no voluntary partial penetration the interpreter can easily miss the effect and as the limited entry can result in a high geometrical and thus a high total skin this can often be misdiagnosed as damage alone when coupled with the storage effect. Stimulation of a limited entry well will therefore often have no results.

The following figure illustrates the effect of increasing wellbore storage on a limited entry well.

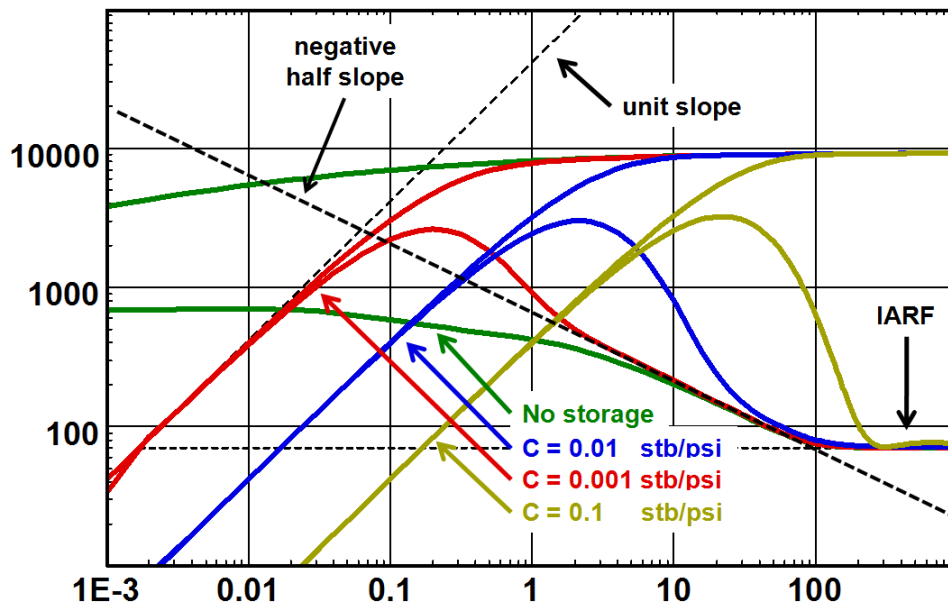


Fig. 6.F.8 – Sensitivity to wellbore storage

6.F.7 Skin effect

6.F.7.a Skin components

The total skin of a limited entry well is invariably positive due to the partial penetration. The mechanical skin of the open interval is the difference between the total skin and the geometrical skin.

A variety of correlations has been presented in the literature to estimate the geometrical skin. In Saphir the geometrical skin is determined by the difference between the model skin and the model skin for a fully penetrating vertical well with no skin damage, thus the various skin components adds up directly:

$$S_M = (S_T - S_G)$$

At this stage one has to be careful about the convention of how the skin is defined. There are two ways to define the Skin factor in limited entry well model, and these are accessible in the Saphir settings page, Interpretation option, Skin tab:

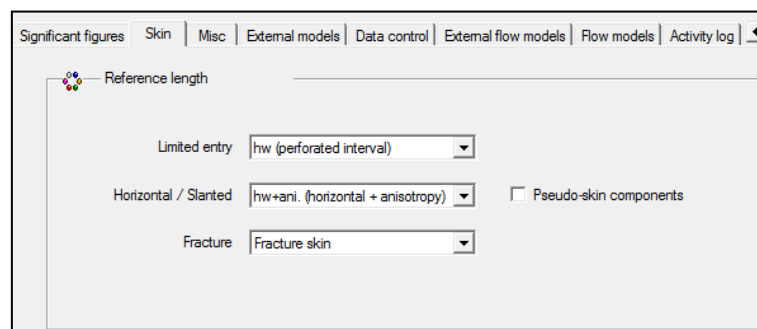


Fig. 6.F.9 – Skin convention dialog in Saphir v4.12

The skin can be referred to the perforated interval and the skin components needs to be normalized to add up, the total equivalent skin S_T will be:

$$S_T = \left(S_M \frac{h}{h_w} + S_G \right)$$

6.F.7.b Influence of skin

The figure below illustrates the influence of the mechanical skin on the pressure change and the Bourdet derivative. There is no effect on the derivative so a change in skin will not mask the spherical flow regime.

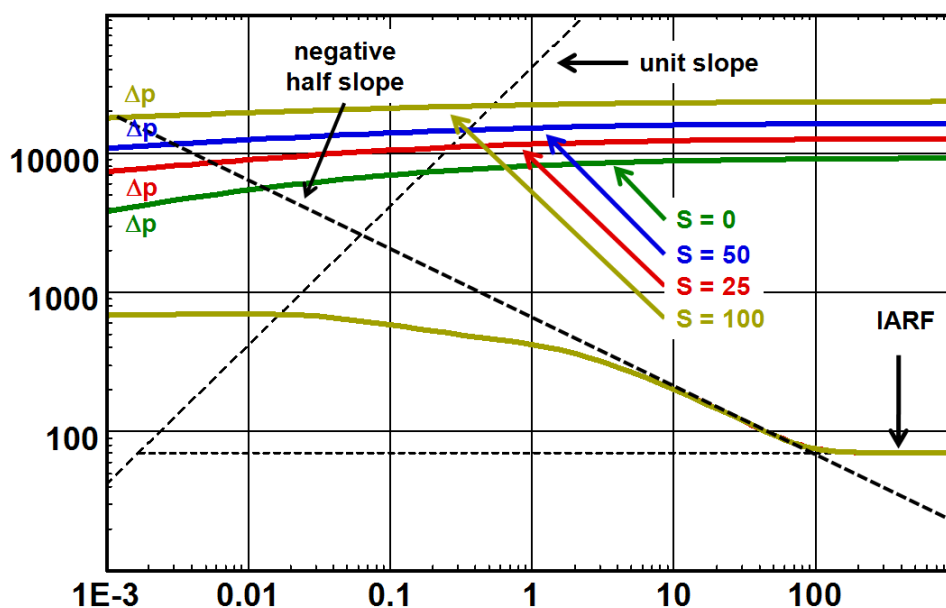


Fig. 6.F.10 – Limited entry skin sensitivity

There are often questions about how positive a skin can be in reality. The reality has to be seen in the proper light, that is with the appropriate reference. Imagine a test carried out with a 2 inch probe of a formation tester. The skin is determined to be 1 with reference to the probe dimension. If the test had reached radial flow a classical semilog analysis would reveal a skin (total skin) of 600 calculated with the appropriate net drained interval of 100 ft. So yes, very positive skin values may exist, the trick is to know what they mean.

6.G Horizontal wells

Horizontal wells are with no doubt a dream for the production engineer. However, they are a bit of a nightmare for the interpretation engineer trying to perform Pressure Transient Analysis. The nightmare started in the early 1990's, when the first horizontal well solutions were integrated into PTA software. It was quickly found out that the wells producing the textbook response given by the theory were in minority.

After the fact, the reason is pretty straightforward: the reality is far more complex than what we model. When dealing with vertical wells, we are making the same mistakes, but there is an enormous and fortuitous averaging effect taking place around the vertical well, and the response will be close to what theory predicts. In other words, we were lucky in the start when we used simplistic models for vertical wells and Infinite Acting Radial Flow and it worked (just). No such luck with horizontal wells, as the response is very sensitive to the assumptions that we make, whether it is the homogeneity of the formation, the part of the horizontal well that will produce effectively (the part of the horizontal section that is contributing to the production), the well geometry (the first rule of horizontal wells being that they are not horizontal) and multiphase flow behavior in the wellbore.

This warning is to say, yes fine, there are horizontal well models, and they give some theoretical behavior that will be described in this section. In the next section you will find 'textbook' data and some not so 'textbook' but overall you will realize that we can indeed make sense of the majority of data sets and achieve consistent analysis results. When we cannot, it is better to explain why and avoid at all costs inventing all sorts of schemes to try to explain the unexplainable.

6.G.1 Hypothesis

The well is assumed to be strictly horizontal, in a homogeneous formation which is also strictly horizontal and of uniform thickness h . As a start, we will consider that the reservoir is isotropic in the horizontal plane, but we will allow vertical anisotropy and other parameters to be defined as in the limited entry well.

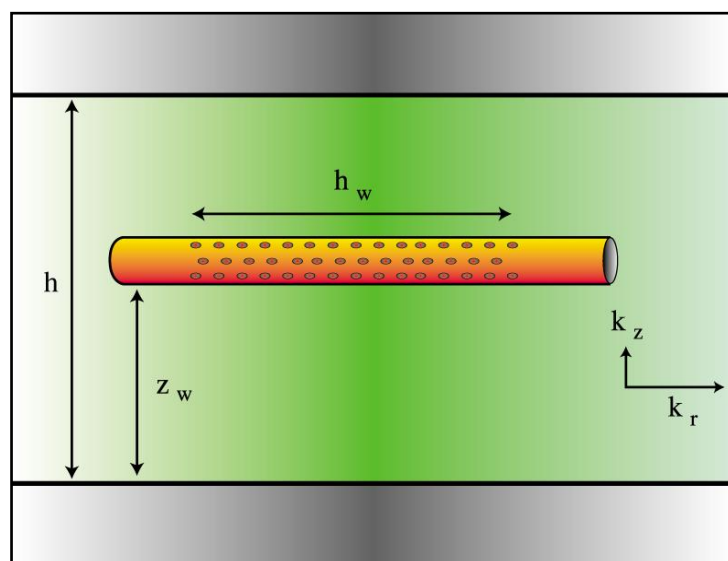


Fig. 6.G.1 – Horizontal well geometry

6.G.2 Behavior

The first flow regime, often obscured by wellbore storage, is pseudo-radial flow in the vertical plane, analogous to radial flow in a vertical well (see below figure). The average permeability combines the vertical and a radial (horizontal) component with horizontal anisotropy. In most cases the horizontal anisotropy is ignored and the permeability combination is just that of vertical and radial permeability. The thickness corresponds to the producing well contributing length. The level of the horizontal derivative, or the slope of the semilog straight-line, is therefore:

$$(kh)_{early} = h_w \sqrt{k_v k_r}$$

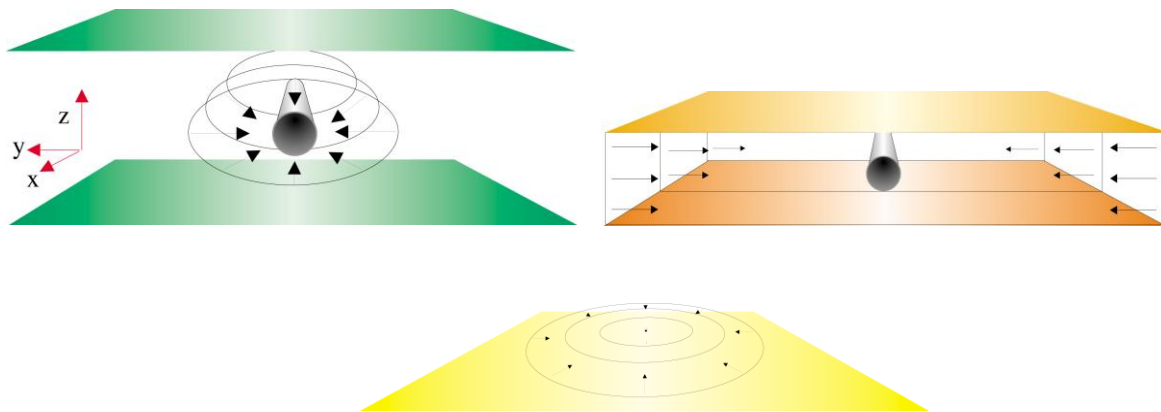


Fig. 6.G.2 – Main flow regimes: Pseudo-radial, linear flow and radial

If the vertical permeability is relatively large, the geometrical skin will be negative and the second flow regime is linear flow between the upper and lower boundaries. The Bourdet derivatives will follow a 1/2-unit slope.

$$(kh)_{linear} = k_r \left(\frac{h_w}{2} \right)^2$$

When the vertical permeability is small the geometrical skin becomes positive and the behavior of the second flow regime will be similar to that observed in limited entry wells.

The final flow regime is radial flow equivalent to that in a vertical well, with the second derivative stabilization representing the usual kh if the reservoir is considered isotropic.

$$(kh)_{late} = k_r h$$

6.G.3 Loglog analysis

The below figure illustrates a typical horizontal well behavior of a real horizontal well. Despite the changing wellbore storage at early time the 'early radial flow' is developed before linear flow sets in.

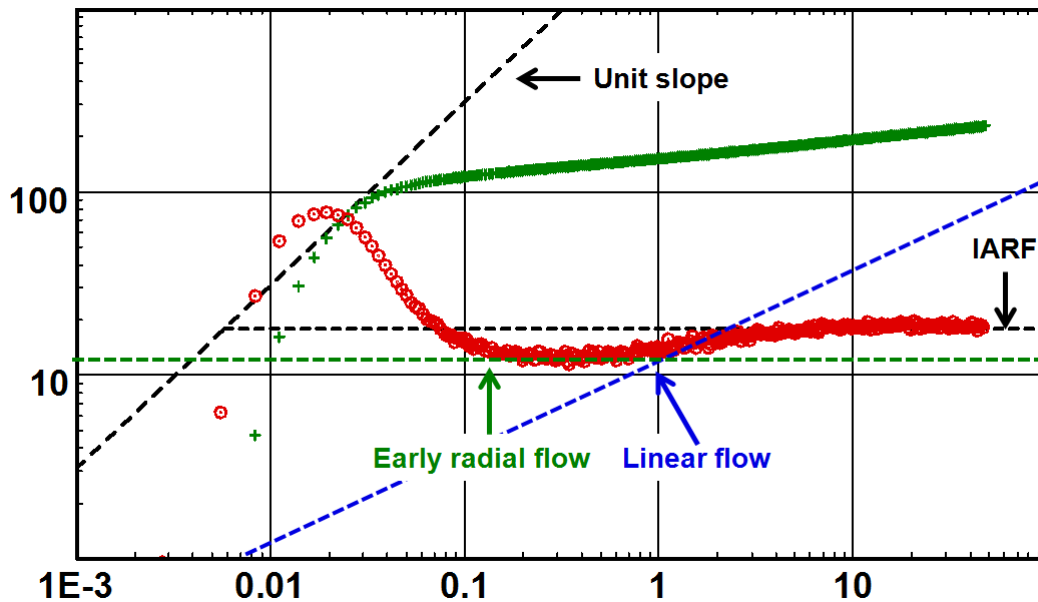


Fig. 6.G.3 – Horizontal well behavior

Looking end-on into a horizontal well is equivalent to looking down a vertical well. The first flow regime after storage in a vertical well is radial flow, and in a horizontal well the same applies. However due to the anisotropy the flow around the wellbore is not circular, but elliptical, as the diffusion will typically propagate more slowly in the vertical direction. Had the reservoir been totally isotropic in all directions then the diffusion around the horizontal well would be perfectly radial.

Once the diffusion has reached the upper and lower boundaries the flow becomes linear (if the geometrical skin is negative), equivalent to the parallel faults geometry in a vertical well but because of the finite length of the horizontal wellbore it cannot stay linear forever. Eventually the diffusion has reached sufficiently far from the wellbore that the dimensions of the horizontal section become irrelevant, and the flow again becomes radial, equivalent to radial flow in a vertical well.

6.G.4 Sensitivity to different parameters

6.G.4.a Contributing horizontal section, h_w and position

In a reservoir with no gas cap or aquifer, the well would typically be positioned as centrally as possible between the upper and lower boundaries, in which case the boundaries would be seen simultaneously and there would be a clean transition from radial to linear flow. The following figure illustrates the behavior with variable contributing horizontal sections (h_w), there is no wellbore storage.

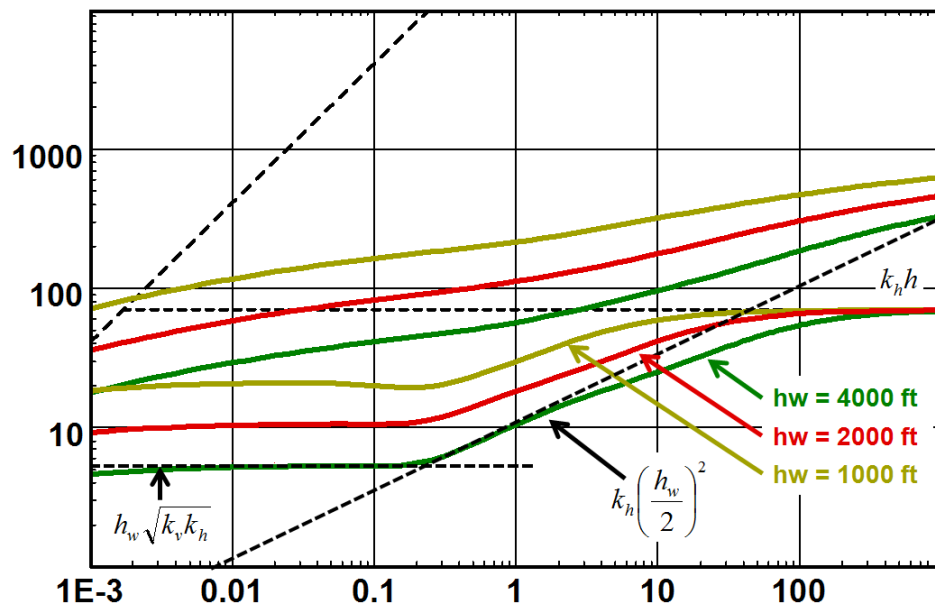


Fig. 6.G.4 – Horizontal well loglog response, variable horizontal drains

If the well is closer to one or the other boundary, there will first be a doubling of the derivative, as if seeing a fault in a vertical well, before the second boundary brings on the linear flow. The following figure illustrates this.

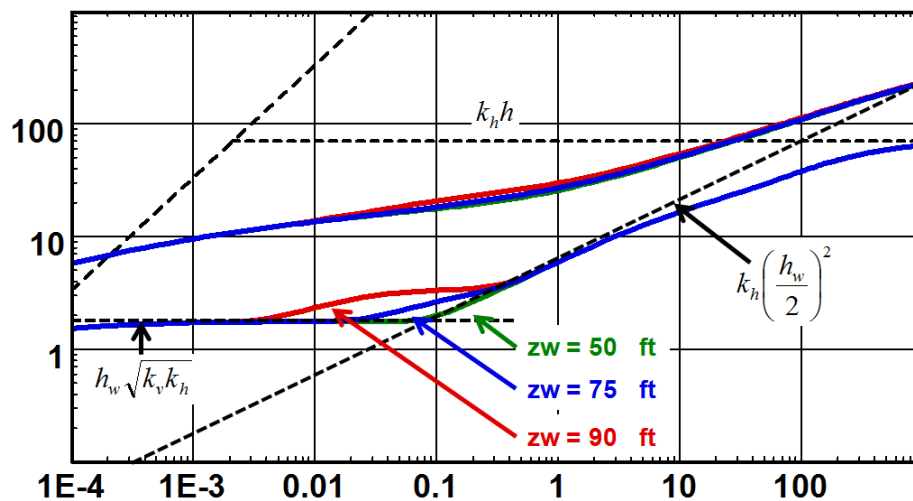


Fig. 6.G.5 – Horizontal well loglog response, variable well placements, z_w

If the upper or lower boundary is a gas cap or an aquifer, the well will probably be positioned close to the other sealing boundary. In that case there will again be a doubling of the derivative, similar to the 'fault' response in a vertical well, followed by a constant pressure response. In each case the doubling of the derivative will not always be fully developed before the arrival of the next flow regime, be it linear flow or a constant pressure boundary.

6.G.4.b Sensitivity to the anisotropy

Further, below, we are illustrating the behavior for a horizontal well with a variable k_v/k_h . When the permeability contrast increase, the shape of the Bourdet derivative loses the classic 'finger print' of the horizontal well. The shape of the derivative approaches that of a partial penetrating well.

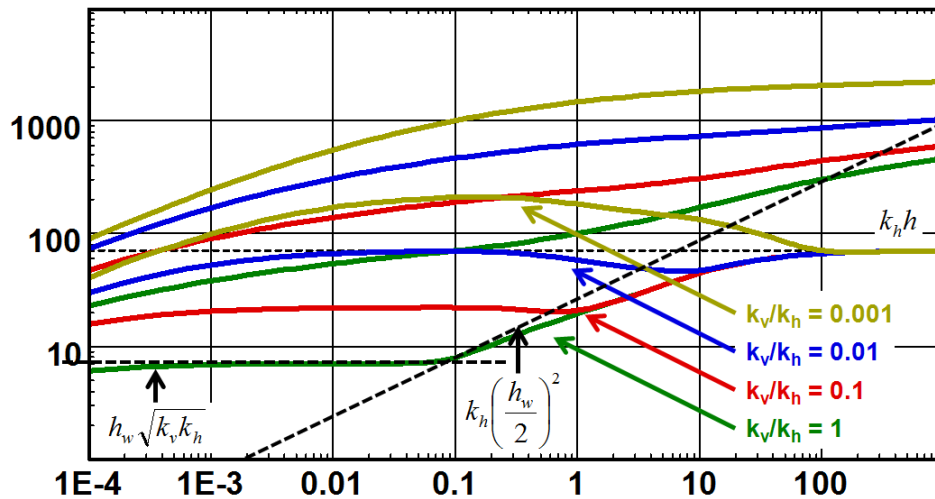


Fig. 6.G.6 – Horizontal well loglog response, variable vertical anisotropy

6.G.5 Adding wellbore storage

Wellbore storage will very quickly mask the 'early time radial flow'. Significant wellbore storage will also mask the half unit slope straight line of the linear flow. Both factors increase considerably the challenge facing the interpretation engineer since experience has shown that it is common not to develop infinite acting radial flow in the reservoir. Without any recognizable clear flow regimes to deal with, the task is certainly compounded and a consistent analysis can only be achieved if the reliability of the 'known' data is high. Refer to the following figure that shows the behavior with different wellbore storage constants.

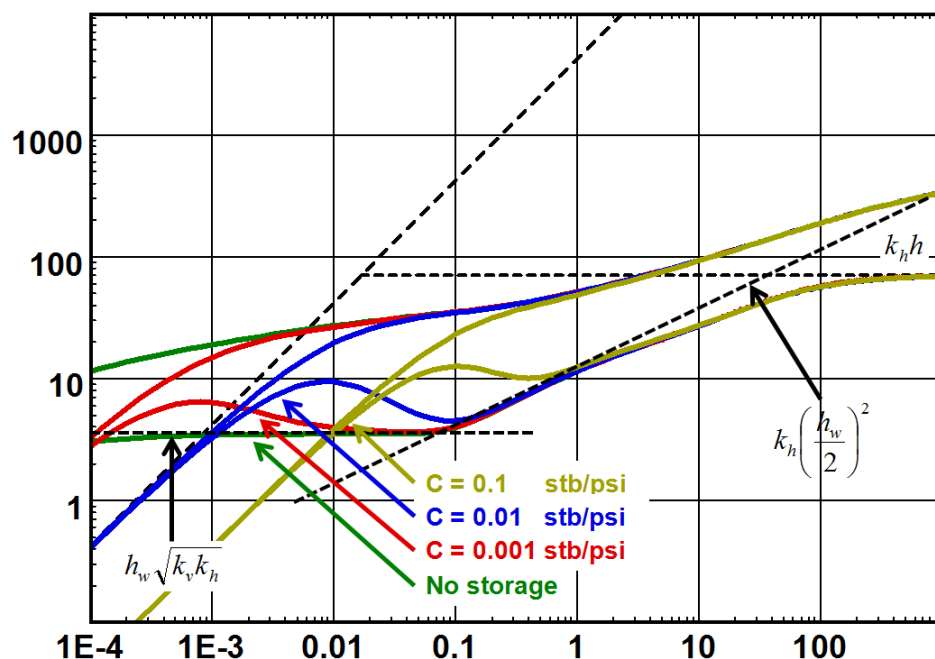


Fig. 6.G.7 – Sensitivity to wellbore storage

6.G.6 Skin effect

When the contrast between horizontal and vertical permeability (anisotropy) is small the geometry of a horizontal well will induce a negative skin components that reflects directly why we would want to drill horizontal wells in the first place. The mechanical skin S_M is the difference of the total skin S_T and the geometrical skin S_G .

A variety of correlations has been presented in the literature to estimate the geometrical skin. In Saphir the geometrical skin is determined by the difference between the model and the model for a fully penetrating vertical well with no skin damage.

$$S_T = (S_M + S_G)$$

The infinitesimal skin S_M is constant at the wellbore; however several references can be used to normalize the different skins.

If the skin is referred to the horizontal contributing length then:

$$S_T = \frac{h}{h_w} S_M + S_G$$

And including the anisotropy:

$$S_T = \frac{h}{h_w} \sqrt{\frac{k_r}{k_v}} S_M + S_G$$

The figure below illustrates the influence of the skin on the behavior of the pressure change and the Bourdet derivative. There is no effect on the derivative as long as the skin is 0 or positive. If the skin S_M becomes negative then both the pressure change and the derivative will mask the early time radial flow and the shape at will approach the behavior of the fractured well.

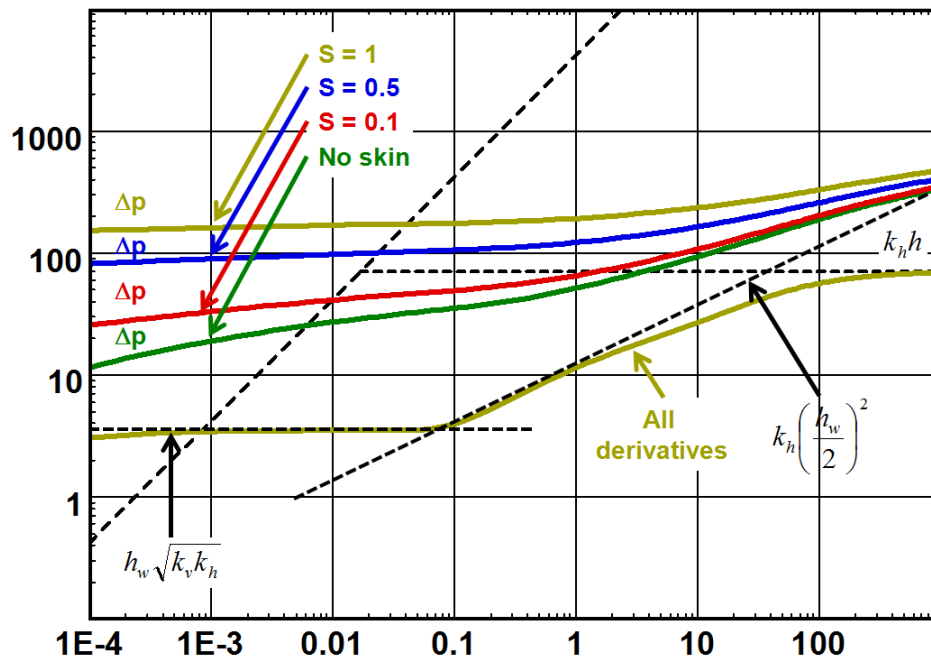


Fig. 6.G.8 – Horizontal well, sensitivity to skin

6.H More on horizontal wells

6.H.1 The flow regimes and incomplete data

During a test we should be able to easily identify the main flow regimes during the period that is being analyzed. Unfortunately this is the theory and 'real life' is not so accommodating. In fact it is rare to see a real test that exhibit the 'late time' or reservoir radial flow. The 'early' radial flow is often masked by wellbore storage and unfortunately too often by phase segregation in the wellbore. The well maybe close to an unidentified upper or lower boundary so what may look like 'early' radial flow is in fact just a boundary response. The reservoir is by most accounts not homogeneous so in addition, the analysis is complicated by having to use reservoir models with additional parameters to describe the heterogeneities.

In addition we know that most 'horizontal' wells are not horizontal at all and in almost all real cases they cut through various dipping layers.

The analysis of a horizontal well response is a challenge indeed.

Unfortunately there is not much we can do to produce miracles. The challenge is to recognize that a flow regime has been masked by another and if not, make the right diagnostics.

When a flow regime is missing in the response we have to rely on the 'known' parameters that were discussed in a previous chapter of this document. And, we are in luck, Saphir has some tools that are very useful and can help us produce a complete analysis with confidence even if the data recorded is incomplete.

6.H.1.a Early time radial flow

Let's say we have recorded a buildup in a horizontal well, but the test was stopped in the middle of the linear flow period, see the below figure.

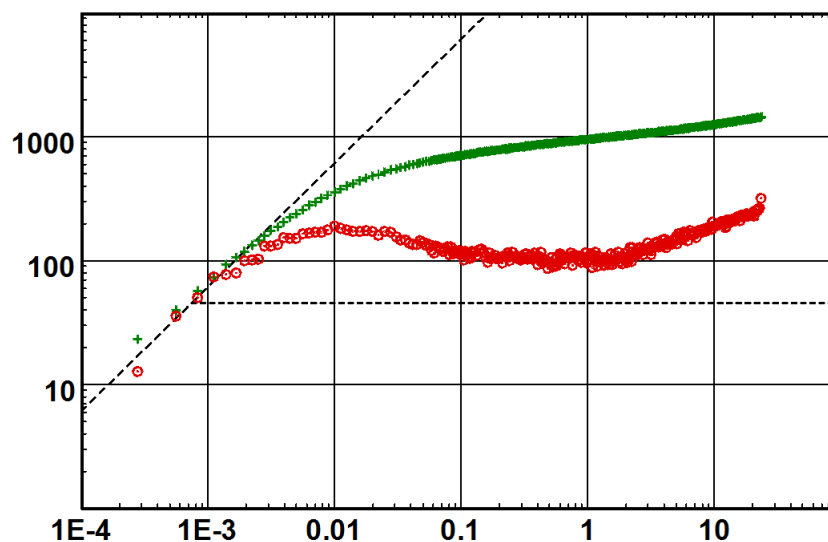


Fig. 6.H.1 – Loglog plot of incomplete data

Further, if we assume that seismic and log data is complete and that we have already good knowledge of expected horizontal contribution (h_w), vertical drainage (h) and the ratio of anisotropy, the below outlines a procedure that will help in the analysis of incomplete data.

The semilog plot will give:

$$(kh_w)_{early} = h_w \sqrt{k_v \cdot k_r} = 162.6 \frac{qB\mu}{m_{semi\log}}$$

and the skin:

$$S_{(k_v, k_r, h_w)} = S_M \frac{h}{h_w} \sqrt{\frac{k_r}{k_v}}$$

with:

$$h = h_w$$

We can also trace the 'early time radial flow' line on the loglog plot to determine $(kh_w)_{early} = h_w \sqrt{k_v \cdot k_r}$, and S_M directly.

'Knowing' h_w and k_v/k_r we estimate quickly what k_r should be if the 'known' parameters are right. We also 'know' the pressure match: $PM = 1.151k_r h / 162.6qB\mu$ and can quickly place the infinite acting radial flow line on the right level on the loglog plot.

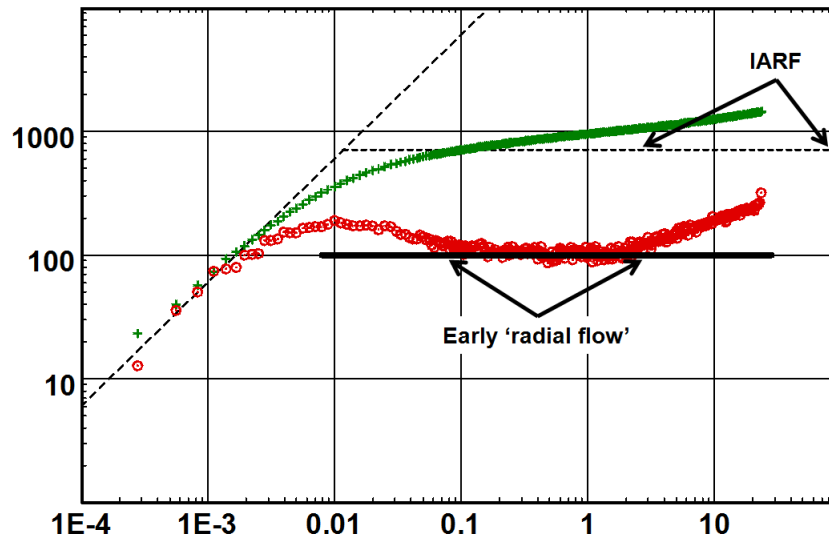


Fig. 6.H.2 – Loglog plot with 'early time' line and pressure match

6.H.1.b Linear flow

A plot of the pressure change versus $\sqrt{\Delta t}$ will return the length of the contributing drain (h_w) if $k = k_r$ and $h = h$. The special 'Channel' line in the loglog plot will also return this parameter.

$$k_h \left(\frac{h_w}{2} \right)^2 = 16.52 \left(\frac{qB}{mh} \right)^2 \frac{\mu}{\Phi c_i}, \quad m \text{ is the slope of the straight line in the pressure versus } \sqrt{\Delta t} \text{ plot.}$$

If we match the IARF line with the 'early time' radial flow and we replace the value of h with h_w the line in the square root plot and the specialized line, 'Channel' in the loglog plot, will return

$$\text{the vertical net drained, } h \text{ as follows: } h = (L_1 + L_2)_{Model} \sqrt{\frac{k_v}{k_r}}$$

This gives us a double check that our approach is consistent despite the missing data. The below plots illustrates the square root plot and the 'Channel' special line in the loglog plot.

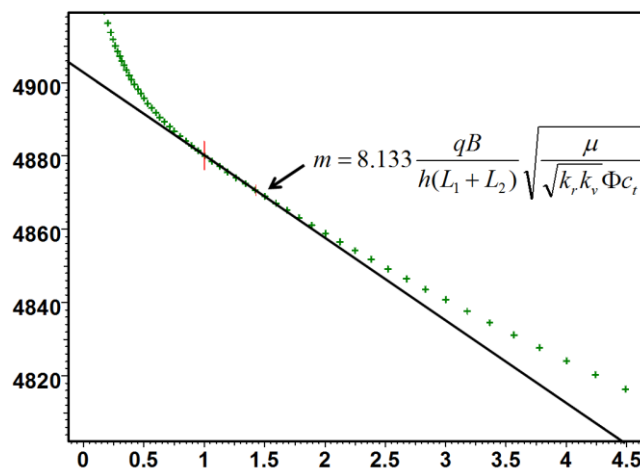


Fig. 6.H.3 – Square root plot

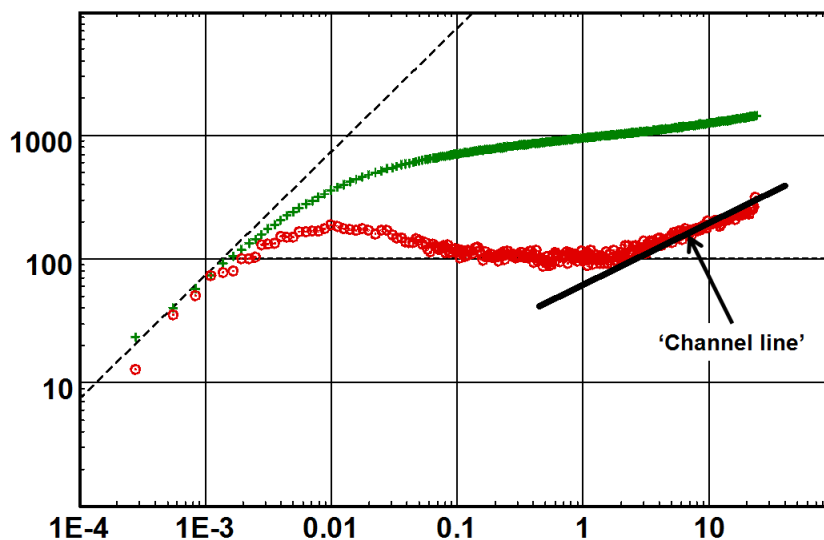


Fig. 6.H.4 – Loglog 'Channel' line

Finally we have enough information to be able to generate the model with the appropriate 'known' and 'unknown' parameters. The model match is illustrated below.

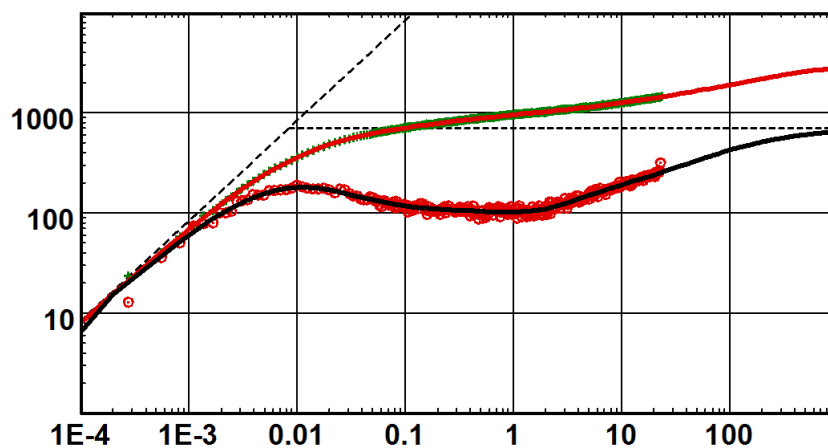


Fig. 6.H.5 – Final model match

In addition we can use a 'poly' line to set the level of 'early' radial flow, the linear and the 'late' radial flow. Just using the input of the 'known' parameter and transferring the 'poly' line results to the model we see that the results from the line gives a model very close to the data. A quick 'improve' of the leading parameters of the model will give us a perfect match with very reasonable results, see the figures below.

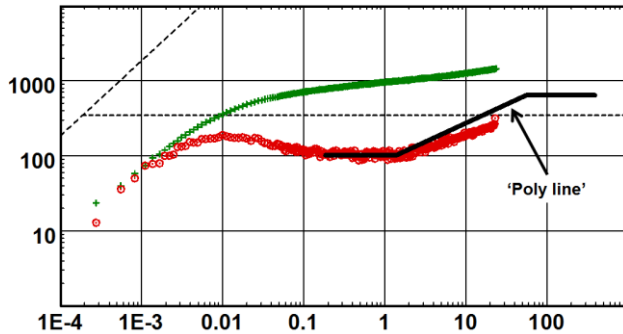


Fig. 6.H.6 – Loglog plot with 'poly' line

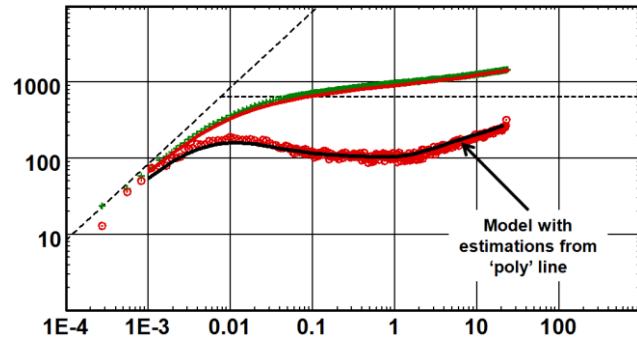


Fig. 6.H.7 – Loglog plot with model from 'poly' line

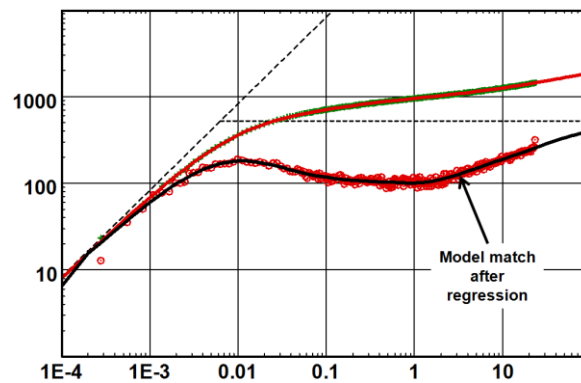


Fig. 6.H.8 – Loglog plot with model after regression

6.H.2 Horizontal anisotropy

The figure below illustrates the horizontal well behavior where the reservoir is anisotropic, vertically $k_z/k_r = 0.01$ (constant) and horizontally k_x/k_y , k_x is along the well and k_y is perpendicular to k_x . It shows clearly that the most efficient horizontal well crosses perpendicularly to the high permeability direction.

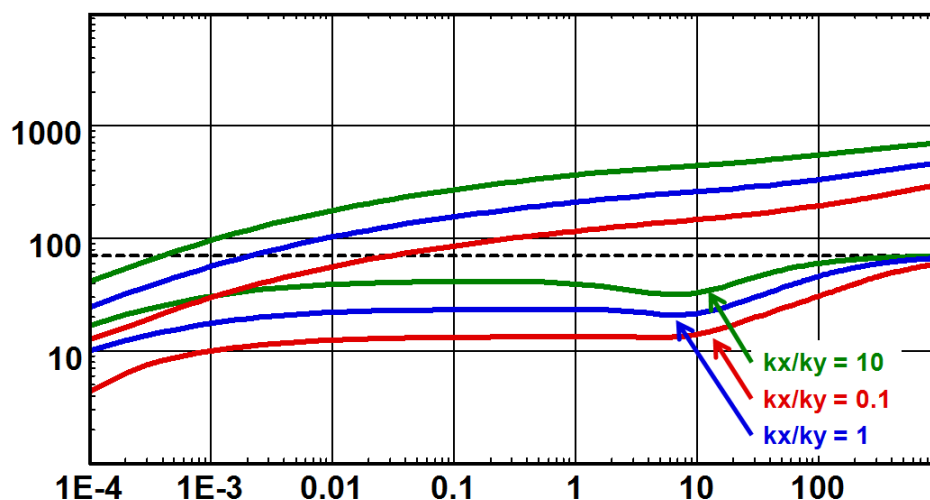


Fig. 6.H.9 – Horizontal well loglog response, variable horizontal anisotropy

6.H.3 Fractured horizontal well

When facing the challenge of producing very low permeability reservoirs (for example shale gas reservoirs), the completion type of choice is usually the fractured horizontal well in order to maximize productivity and increase the drainage area, as extremely low mobility is limiting significantly the extent of drainable volume further from the well. Consequently, this model is well adapted to unconventional gas analysis and production forecasting.

For those interested in the particular problem of production analysis in unconventional gas reservoir, it is further developed in the KAPPA shale gas papers: *The Analysis of Dynamic Data in Shale Gas Reservoirs – Part 1 and Part 2 (OH et al.)*.

In a tight matrix environment, the production from the interface drain - reservoir is negligible compared to the multiple fractures contribution. Consequently, the productivity index will be less sensitive to the drain damage than to the fracture quality. This will be illustrated below.

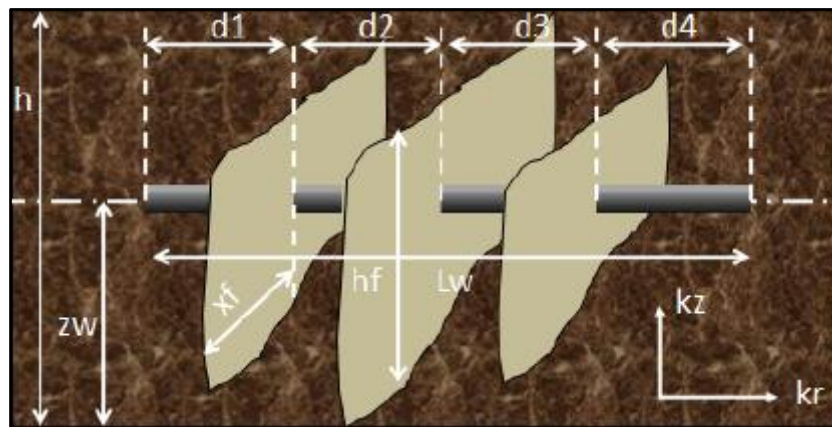


Fig. 6.H.10 – Fractured horizontal well

After the effects of wellbore storage, linear or bilinear flow behavior develops due to the fractures (1/2 or 1/4 unit slopes or both), then the response may correspond to radial flow in the vertical plane orthogonal to the horizontal borehole, with an anisotropic permeability $k = \sqrt{k_v k_r}$, this flow regime is usually always masked by the fracture influence.

As the top and bottom boundaries are sealing, the response shows the behavior of a vertical well between two parallel sealing faults and the derivative should follow a positive half unit slope during this linear flow, however there is no easy way to determine if the half slope is caused by the fractures or the horizontal wellbore between the upper and lower boundary.

At later time stabilization in the derivative is observed corresponding to infinite acting radial flow (IARF) in the horizontal plane relative to kh .

6.H.3.a Sensitivity

The below figure illustrates the behavior with various well configurations, flow through the fracture only, through the drain only and through both. It shows clearly that the contribution of the drain is negligible.

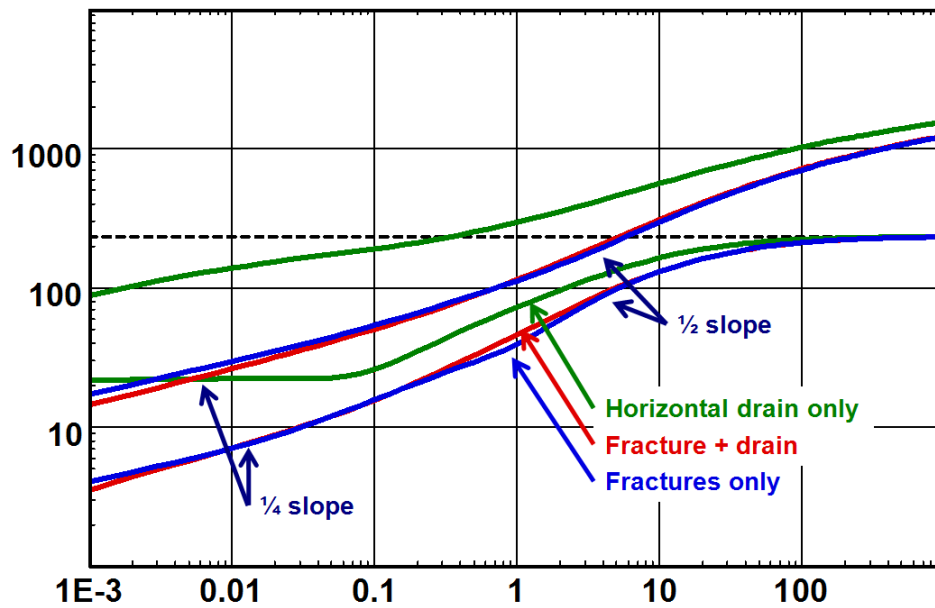


Fig. 6.H.11 – Flow through fractures, drain or both

The horizontal well behavior is totally dominated by the presence of the fractures, the typical shape of the horizontal well disappears and is replaced by the dominant behavior of the low conductivity fractures with the characteristic shape of bi-linear ($\frac{1}{4}$ slope) and linear ($\frac{1}{2}$ slope) flow. The rules discussed in the previous section will no longer apply.

The Horizontal fractured wells behavior is therefore dominated by the fracture quality, fracture half length, conductivity and number. The spacing also plays an important role in the behavior as seen in the following figure that show the influence of the length of the horizontal drain with equal number of identical fractures. The shorter the drain, with the equal number of fractures, the steeper the transition from bi-linear to infinite acting radial flow becomes and the less the overall shape resembles that of a horizontal well.

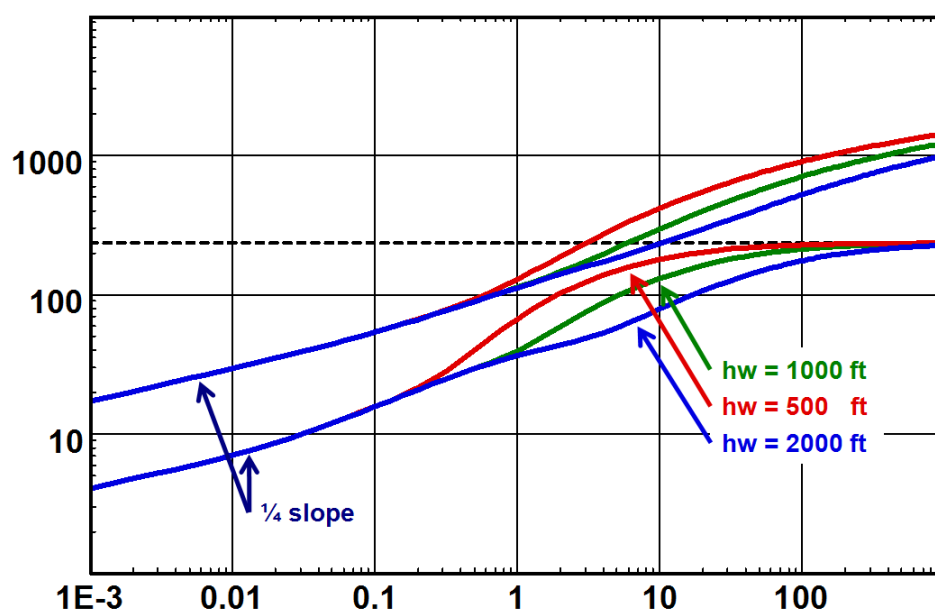


Fig. 6.H.12 – Equal number of identical fracture, sensitivity to horizontal drain length

The figure below illustrates the influence of the half length of the fractures. In this case there are four fractures at equal spacing. When the half fracture length is small it is possible to observe the classical 'early time' radial flow of the horizontal well behavior. This is however the rare occasion when we deal with multiple fractured horizontal wells.

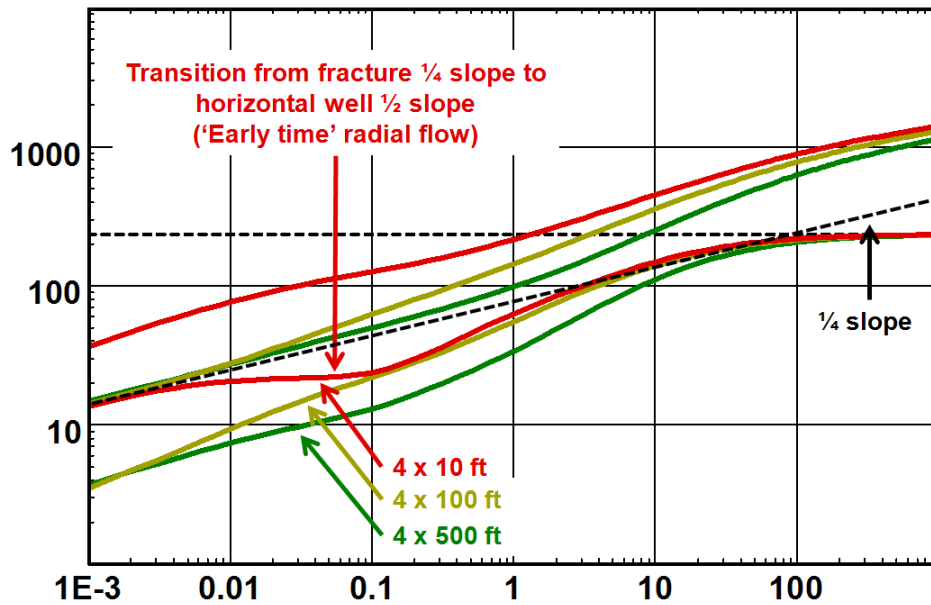


Fig. 6.H.13 – Influence of half fracture length

6.H.3.b Adding wellbore storage

The wellbore storage effect will mask the fracture flow regime, see the following figure.

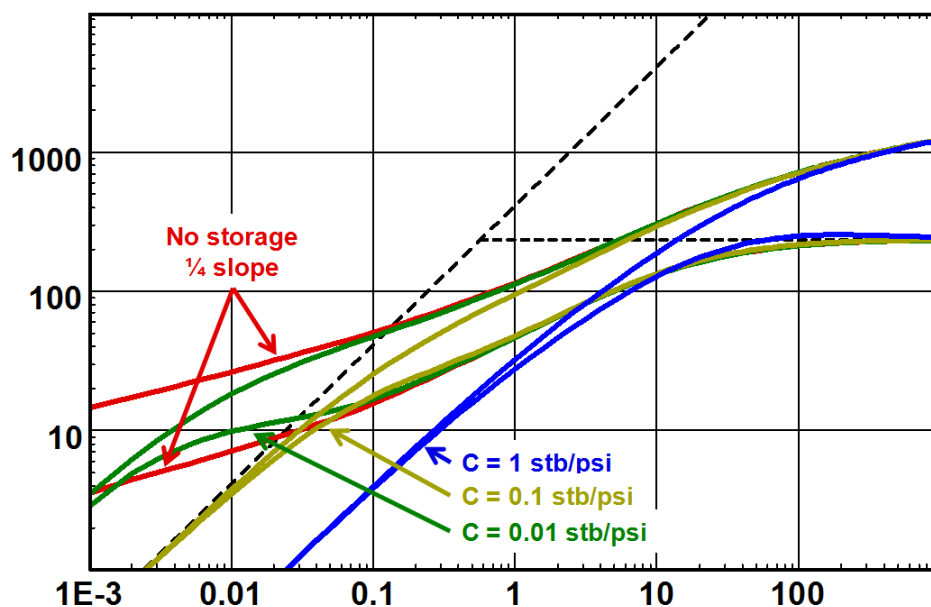


Fig. 6.H.14 – Influence of wellbore storage

6.H.3.c Skin

When a situation with multiple fractures in a horizontal well is facing us we are invariably up against low or 'no' permeable rock. In most cases we are dealing with 'unconventional gas'. Thus the damage of the actual well(bore) becomes a non issue.

The skin will not influence the derivative, thus we will retain the diagnostic tool, and be able to recognize the flow regimes present in the signal when no other influence is present, such as high or changing wellbore storage and phase segregation.

The figure below illustrates the multiple fracture model with the influence of skin.

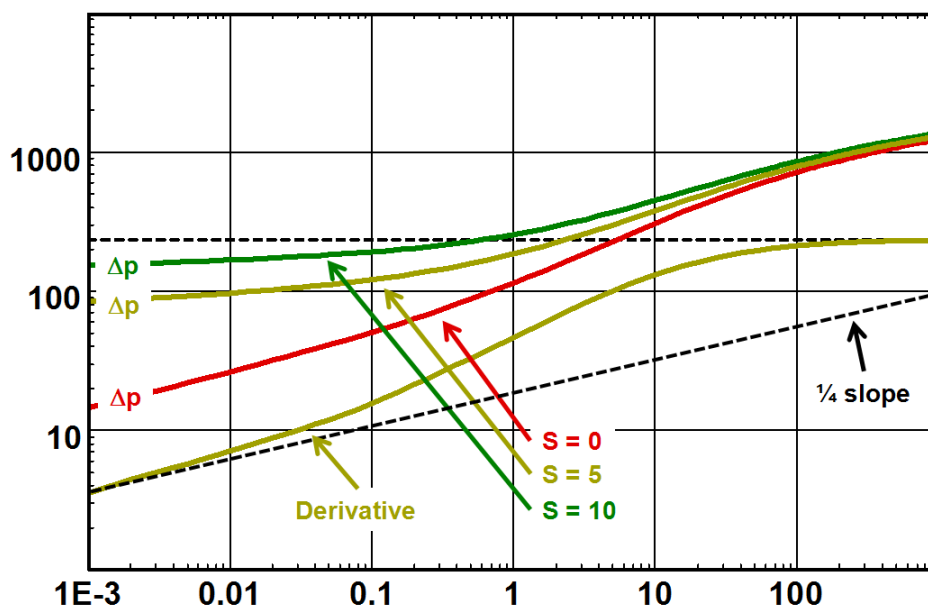


Fig. 6.H.15 – Skin influence

6.H.4 Field examples

Below we are illustrating two model matches with real data. The first well has a near textbook behavior of a horizontal well with changing wellbore storage at early time.

The second well is in an area where the vertical permeability is very low. This gives rise to the typical but unorthodox behavior of a horizontal well with positive geometrical skin.

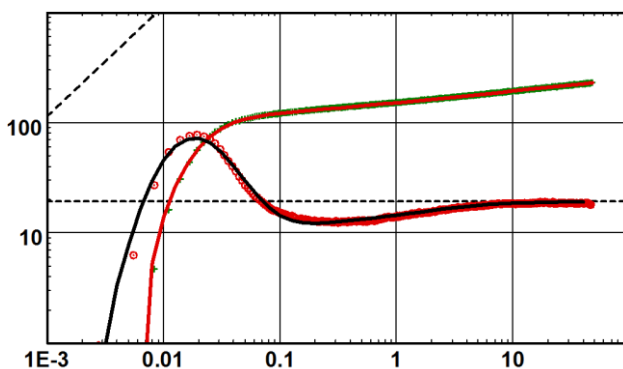


Fig. 6.H.16 – Horizontal well:
Negative geometrical skin

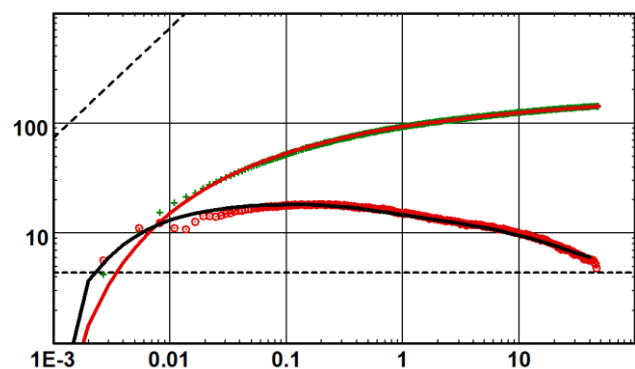


Fig. 6.H.17 – Horizontal well:
Positive geometrical skin

6.I Slanted wells

As with horizontal wells, slanted wells are designed to increase productivity by maximizing reservoir contact. In fact the horizontal well is just a subset of the generalized slanted well solution.

We have seen in low vertical permeability formations that horizontal wells are not very efficient.

An answer to this problem is the slanted well which maximizes the communication length with the formation while crossing it totally. Even zero vertical permeability formations are connected to the well over the complete thickness.

Generating analytical solutions to simulate and study such wells is quite easy. The challenge is to select the adequate model and to define the various corresponding parameters.

Common questions are: “my well is deviated, do I have to consider it as a slanted well?” or “my well is sub-horizontal, do I analyze it as a horizontal or slanted well?”, and then the series of questions: “Which thickness do I use if my formation is not horizontal, do I use the measured depth or the true vertical depth?” In addition the slanted well can either be fully penetrating or with a selected interval perforated or open to flow. The well will invariably cross different layers so this will also have to be considered in the solutions.

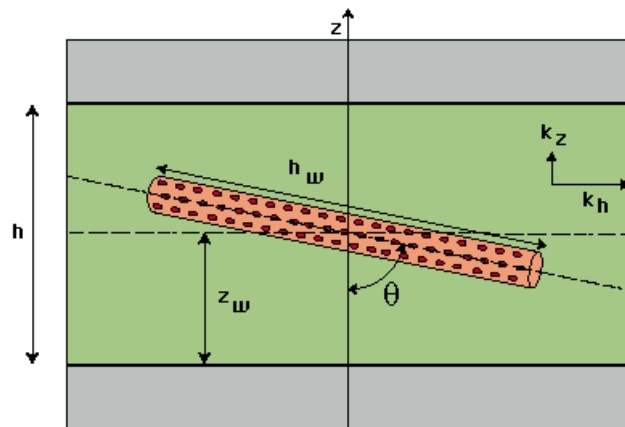


Fig. 6.I.1 – General slanted well

The answer to these questions is simple after understanding that we do not analyze the formation geometry but the pressure behavior, therefore the parameters or the criteria we use are the parameters influencing this behavior. The selection of the model is imposed by the shape of the pressure curve, not by the geometries.

Of course, the diagnostic will not tell you if the well is vertical, slanted or horizontal, you are already aware of that (hopefully). It will tell you how it behaves and how it has to be treated.

The following sections illustrate the typical sequences of flow regimes and pressure behaviors that characterize the different well types.

Analytical solutions respect certain assumptions such as the negligible effect of gravity on fluid flow. This means that the analytical slanted well model describes the cases of slanted wells in a horizontal formation, or if you want, a vertical, slanted or a horizontal well in a slanted multilayer formation. The parameter to consider is the angle between the well and the main flow direction.

Initially the impact of this geometry description is on h and h_w :

- h is the net drained thickness, perpendicular to the flow direction (not systematically TVD or MD).
- h_w is the contributing producing well length.

6.I.1 Behavior

There are, like in the horizontal well, some main flow regimes that can develop. If the angle with the vertical is large, the well is approaching a horizontal well. The dip of the layer is such that the well follows the formation stratigraphically, then the equivalent behavior will be that of a horizontal well and three distinct flow regimes may develop.

'Early time' radial flow in the plane normal to the well, this regime is usually masked when the slant is such that the well is close to a vertical well. Wellbore storage will also in most cases mask this behavior.

Linear flow between an upper and lower boundary if the well angle approaches the horizontal.

Reservoir radial flow if the test is long enough.

The below figure illustrates the loglog behavior of a real slanted well where all the main flow regimes have developed.

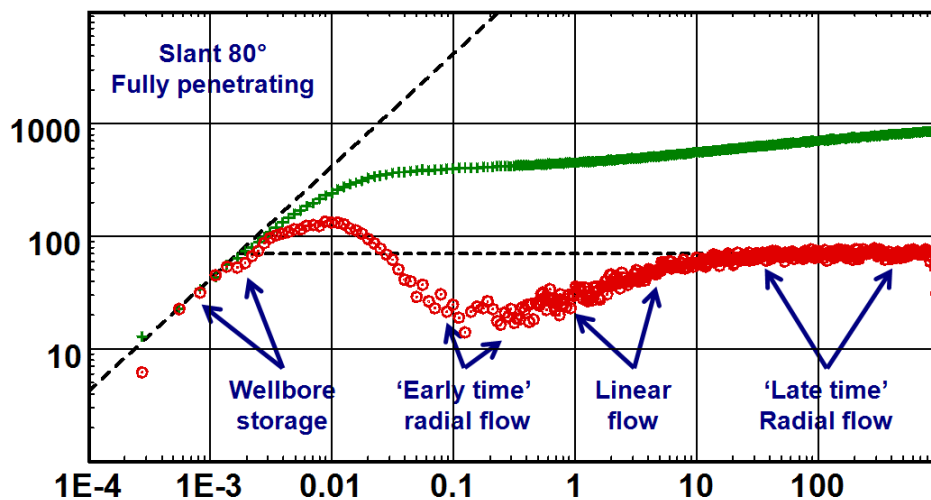


Fig. 6.I.2 – Slanted well response

6.I.2 Sensitivity to different parameters

To illustrate the response of the slanted well various models were generated with various scenarios. None of the scenarios are intended to reflect a real well but are run to see the response to various situations of some interest. The comparison to the horizontal well response is shown in various settings.

The below figure illustrates the response of a fixed contributing length of a fully penetrating vertical well, the same penetration at an angle of 45 degrees and the equivalent horizontal well response. One can easily see that the horizontal well with the same penetration length as the vertical well is a poorer well due to the anisotropy.

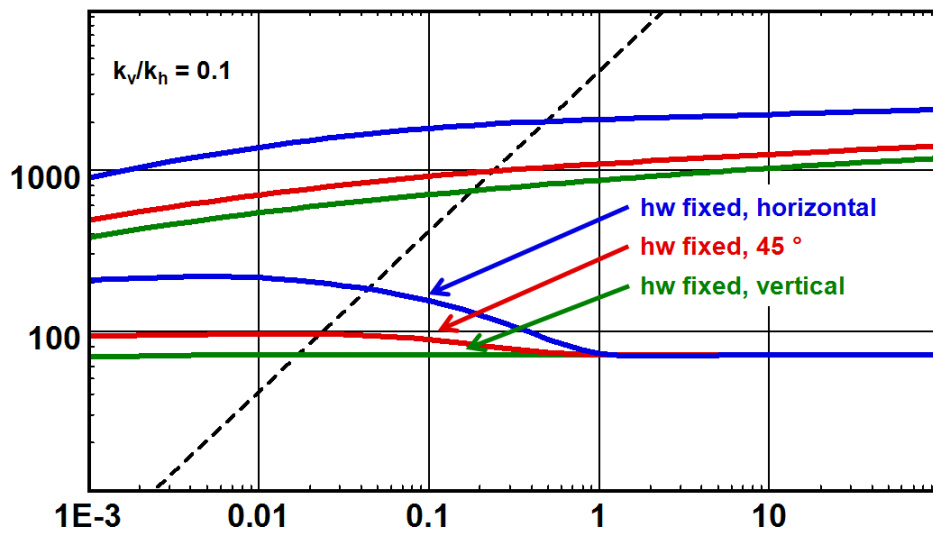


Fig. 6.I.3 – Slanted well fixed penetration

The next figure illustrates the behavior when the well is fully penetrating from top to bottom boundaries with various inclination angles. The reservoir in this case is isotropic. It is possible to observe the phenomenon caused by the end effects; flow at the extremities of each of the slanted wells, as well as the 'early time' radial flow $h_w \sqrt{k_r k_v}$ equivalent to the response in a pure horizontal well.

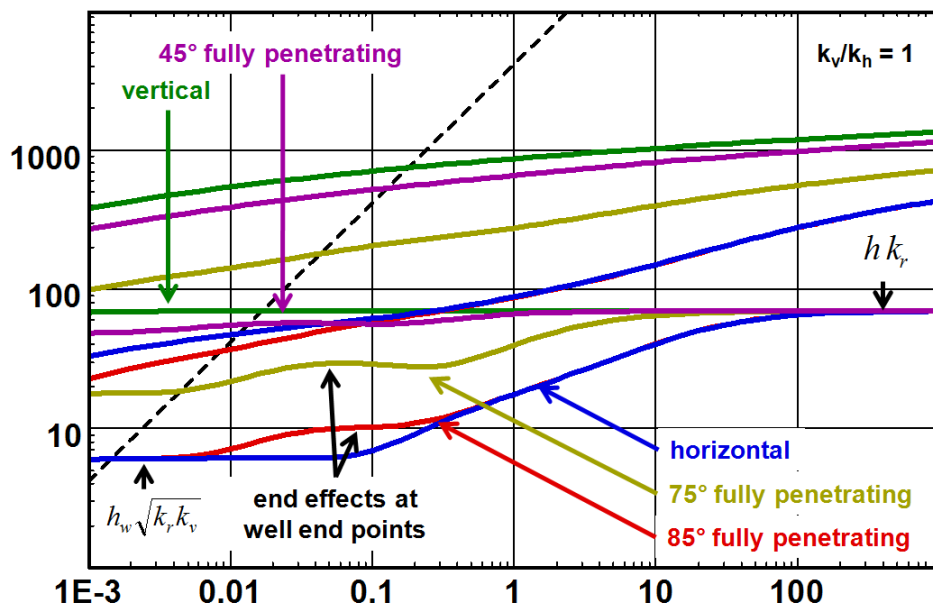


Fig. 6.I.4 – Slanted well variable penetration

The following is a comparison of a horizontal well in a highly anisotropic rock with various slanted wells, all with the same contributing length. It can be seen that crossing the reservoir with a well at an angle is advantageous because of the anisotropy.

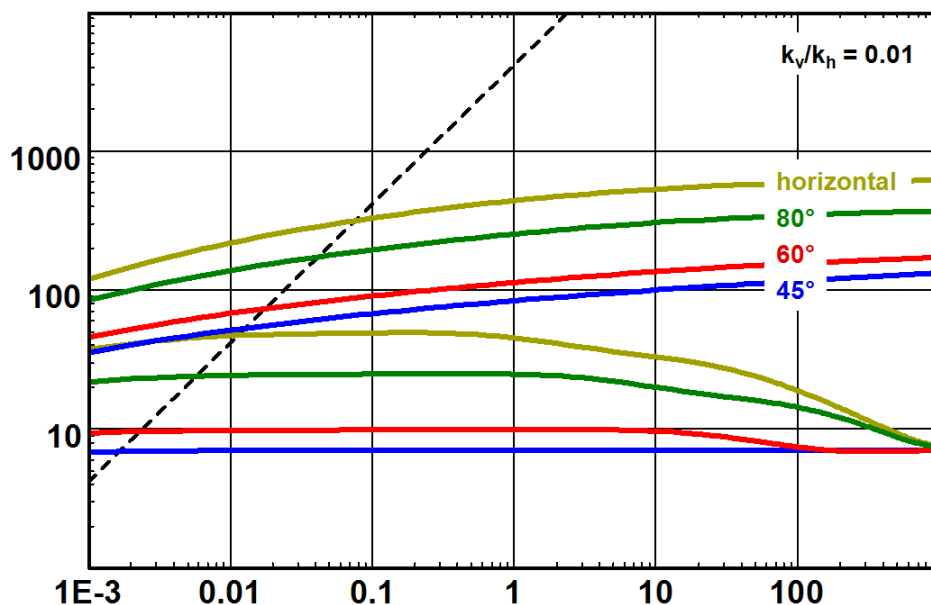


Fig. 6.I.5 – Slanted well, high permeability contrast

As the permeability contrast increases the efficiency of the well decreases. The figure below shows a slanted well with increasing permeability contrast.

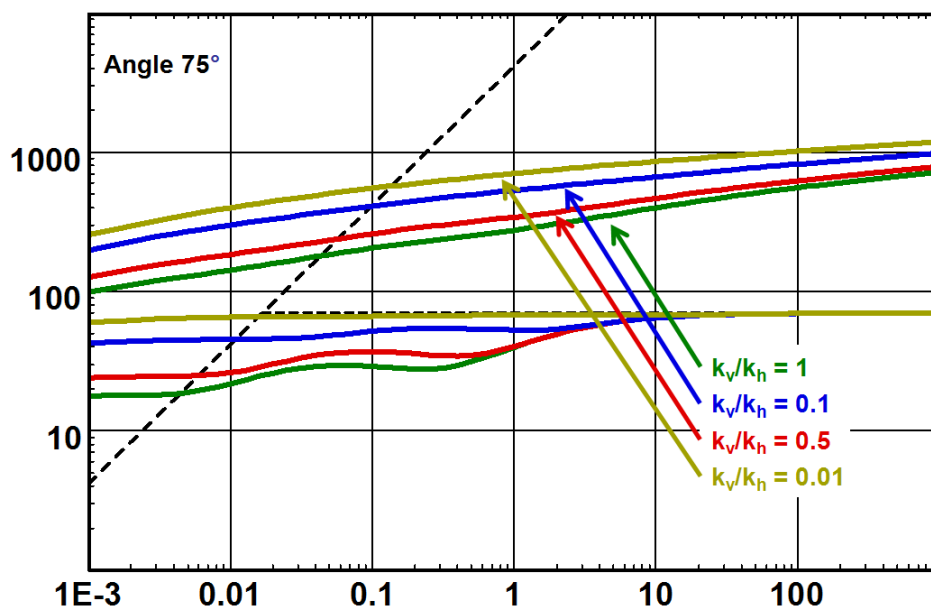


Fig. 6.I.6 – Slanted well, increasing permeability contrast

Finally we show a limited entry well with various inclinations, due to the anisotropy the vertical well is the best choice. Spherical flow develops in all the wells, and lasts longer as the inclination approaches the horizontal well.

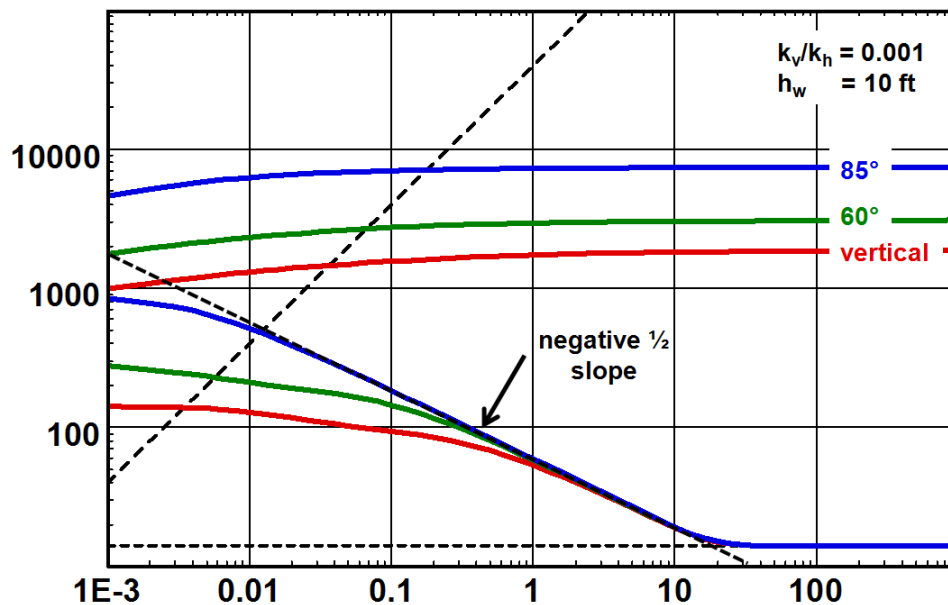


Fig. 6.I.7 – Limited entry well

6.I.3 Adding wellbore storage

Wellbore storage will affect the early time data and mask any 'early time' radial flow and the characteristic end effects of the slanted well. See the below figure.

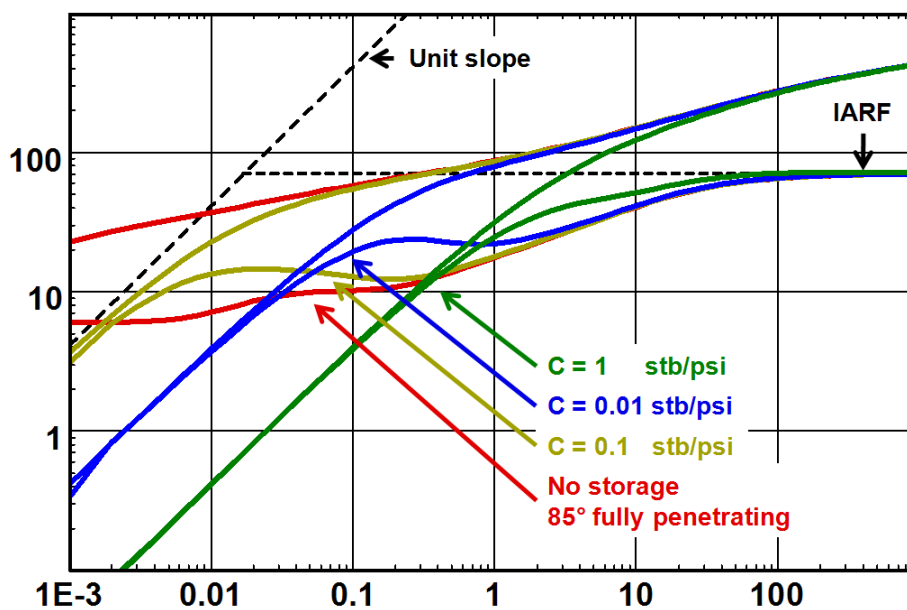


Fig. 6.I.8 – Wellbore storage influence

6.I.4 Skin

The skin has no effect on the derivative so none of the features (shapes) particular to the slanted well is lost. This is of course in practice not true as most wells will also be influenced by wellbore storage, and worse still changing wellbore storage and/or phase segregation in the wellbore.

Nevertheless, below is illustrated the effect of skin only on the slanted well.

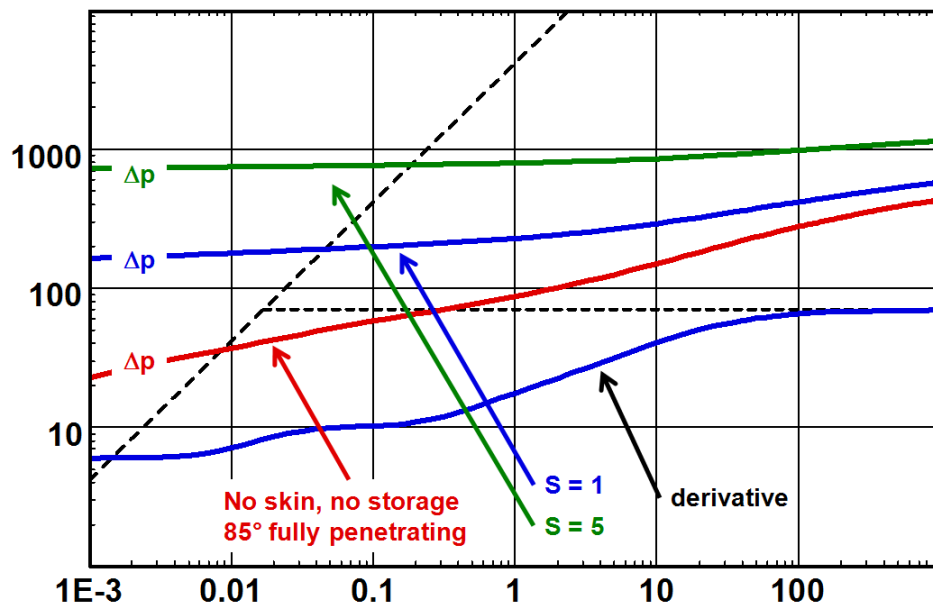


Fig. 6.I.9 – Influence of skin

6.I.5 Slanted well multilayer

6.I.5.a Hypothesis

The model simulates the behavior of a slanted well crossing multiple layers. The layers are strictly horizontal; however the model can easily predict the behavior of horizontal wells crossing slightly dipping layers.

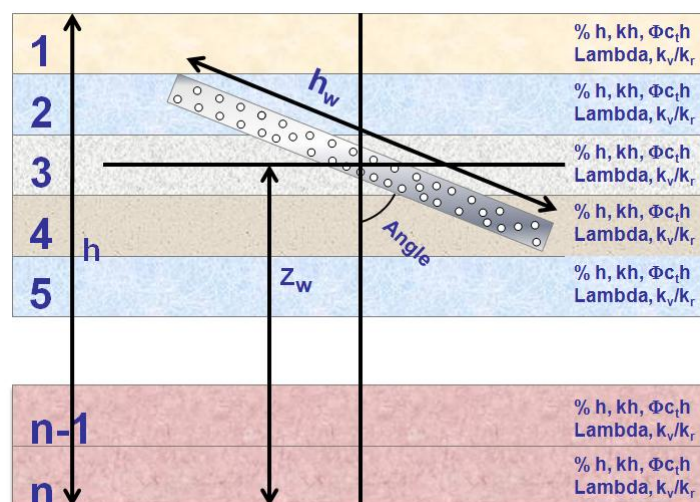


Fig. 6.I.10 – Slanted well multilayered

The individual layer parameters are defined by a fraction of the total thickness h , the permeability thickness product, kh and the storativity, $\Phi_c h$. The anisotropy is also specified for each layer.

The interlayer crossflow is determined by the Lambda value, which can be automatically calculated.

Thus the model caters for layers with or without crossflow.

6.I.5.b Behavior

The following figure illustrates the classical behavior of the double permeability response but using this model (see the chapter on 'Reservoir models'). The fully penetrating slanted well model at 80° is compared to the vertical well. The longer slanted well is of course the best producer. The reservoir is isotropic.

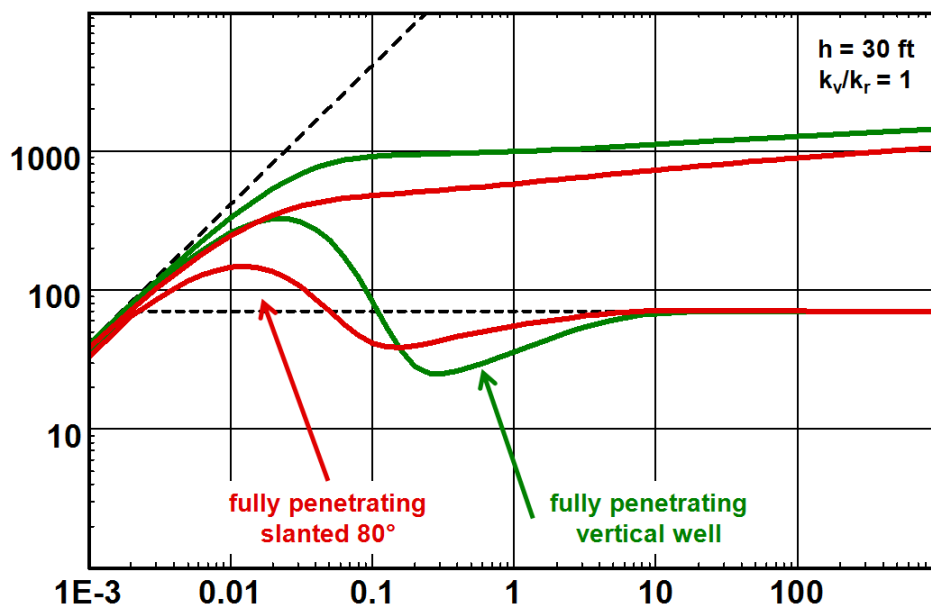


Fig. 6.I.11 – Slanted well, two layers with cross flow

The following figure illustrates the response of a three layered reservoir; the well is fully penetrating, vertical and slanted at 80° . The reservoir is isotropic. The double feature of the transition due to unequal heterogeneity parameters in the different layers can easily be seen in the fully penetrating vertical well. This is masked with the slanted well fully penetrating at 80° .

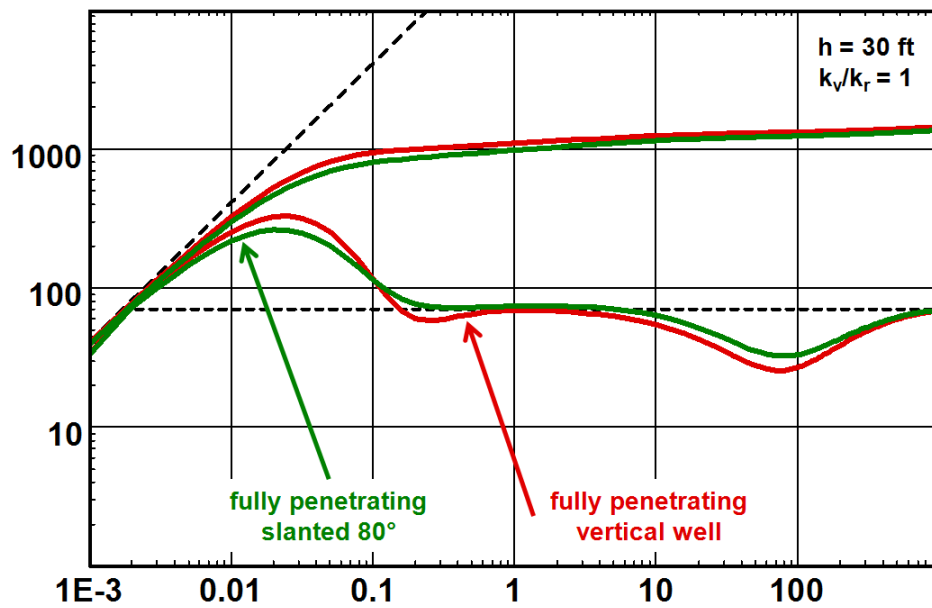


Fig. 6.I.12 – Slanted well, three layers, cross flow

The following figure show the responses with a horizontal well placed in a high permeability layer communicating with a low permeability layer and the well placed in the low permeability layer communicating with the high permeability layer. It is evident that placing the well in the high permeability layer is an advantage to the short term production.

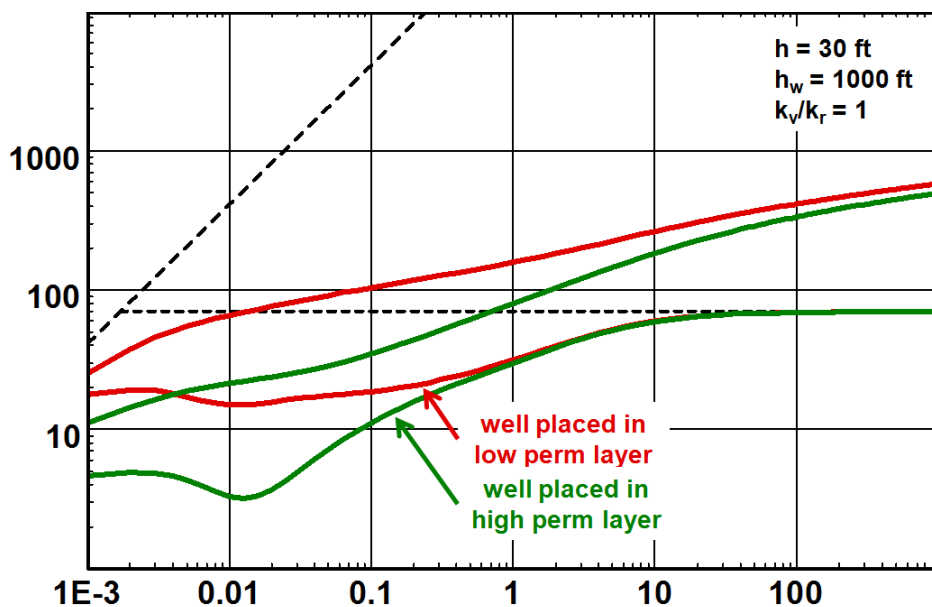


Fig. 6.I.13 – Well placement

We know that in general the horizontal wells are not strictly horizontal and in real life invariably the wells will cut through various layers on its way through the reservoir. This is just a fact of life and a problem the interpretation engineer is faced with constantly. Very often he will find to his dismay that the interpreted horizontal contributing length is much shorter than what had been predicted and even measured by production logging and that the anisotropy does not make any sense at all.

This could very well be caused by the fact that the well is in fact cutting through distinct layers and cannot be analyzed as if the horizontal well drained one single homogeneous medium.

To illustrate this we have generated the slanted well model traversing various non communicating layers. It can be easily seen from the below figure that if the response from several layers is interpreted using the classical horizontal well model draining one single layer, the interpreted contributing length (h_w) would be too small, and the anisotropy would probably show a vertical permeability larger than the horizontal.

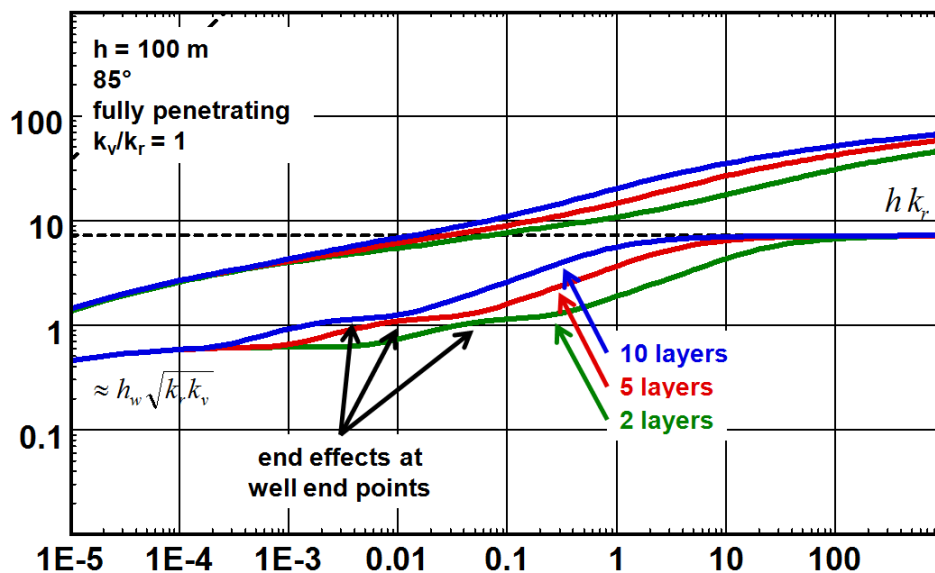


Fig. 6.I.14 – Influence number of layers

6.J Multilateral wells

6.J.1 Hypothesis

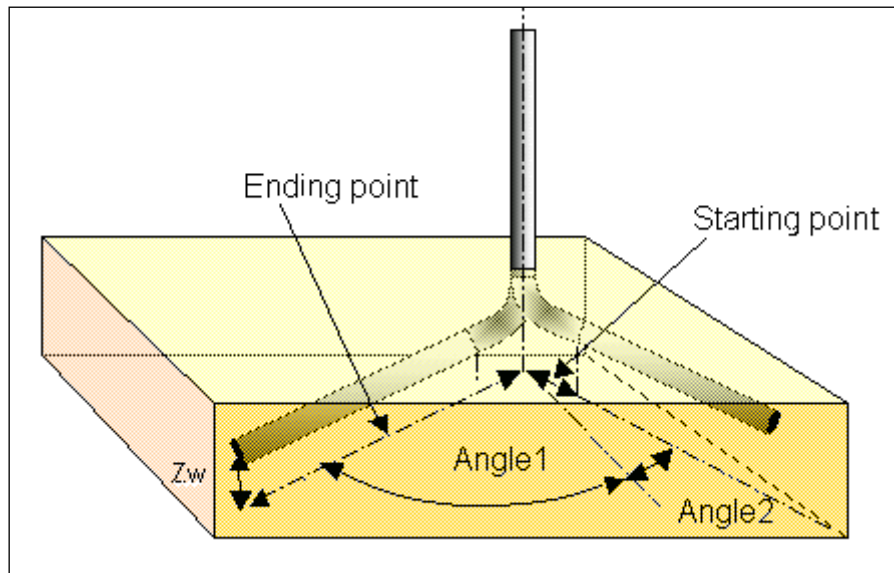


Fig. 6.J.1 – Multilateral schematic

Another answer to the quest for better productivity and sweep are the multilateral maximum reservoir contact wells. They consist of multiple drain holes, each drain can be aimed at a specific layer. For this purpose the drain holes may be drilled at different elevations and directions.

This is the production engineer's dream and the reservoir engineer's nightmare. If 'smart well completions' have not been installed only total well pressure is available, reflecting the 'average' behavior of all the drains/layers. The determination of the individual layer and drain characteristics is therefore impossible through a single information source.

6.J.2 Behavior

Specific cases may allow analysis and the diagnostic of well-known behaviors. As an example; the pressure behavior of two lateral drains at 180° is similar to the behavior of a horizontal well of length equal to the sum of the two drains. The classical sequence (see horizontal wells) can be observed: infinite acting radial flow in the vertical plane, linear flow then, at late time horizontal radial flow.

The below figure illustrates the response of three different multilateral configurations.

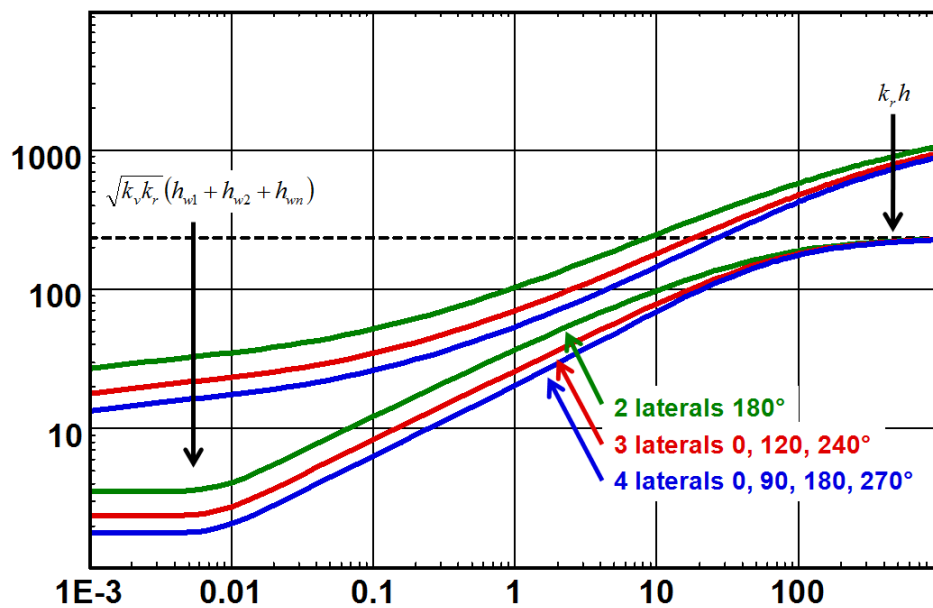


Fig. 6.J.2 – Multilateral well responses

In fact, the analytical model for multilateral wells simulates perfectly the sum of each drain behavior, but it does not permit a diagnostics that could be useful to understand detailed drain properties.

Testing lateral drains individually would permit the determination of individual drain properties. Aggregating this discrete information to simulate the global behavior is one possible approach.



7.A Introduction

In Pressure Transient Analysis (PTA), reservoir features are generally detected after wellbore effects and well behavior have ceased and before boundary effects are detected. This is what we might call an intermediate time response. In Production Analysis (PA), reservoir behavior will be detected when a change in the production sequence is clear enough to produce transients before Pseudo-Steady State is reached. So for the production analyst, reservoir behavior will relatively be an early time effect that may or may not be seen.

The main parameter we are looking for is the mobility of the fluid in the reservoir, k/μ . When there is a doubt about the effective reservoir thickness, the parameter calculated is kh/μ . When the fluid viscosity is known and assumed to be constant we can calculate the permeability-thickness product kh . Whatever the variant, and whether we are performing pressure transient or production analysis, this result will be quantified by the pressure match on the loglog (both PTA and PA) and Blasingame (PA) plots. This result will be common to all models described below, whether they are homogeneous or heterogeneous.

In PTA, some well configurations will allow reservoir characterization even at the early time of the pressure response. Early time behavior of limited entry wells will be a function of an equivalent spherical permeability that in turn will depend on the reservoir vertical anisotropy. Also the early time response of a horizontal well will involve an X-Z permeability which in turn also depends on the reservoir horizontal anisotropy. Fractured well early time behavior will depend on both fracture length and conductivity and so on.

The second factor will be the reservoir storativity $\phi c_t h$. Generally this parameter will be an input, but in the case of an interference test this will be a result of the interpretation process, generally giving the porosity and assuming the other two factors as 'known'.

Finally, one will want to characterize the reservoir heterogeneities by using and matching heterogeneous models. Such heterogeneities can be local, for example the double-porosity case, vertical as in layered reservoirs, or areal, in the case of composite systems and any combination of these. It is possible to input heterogeneities such as porosity, permeability and thickness maps into a numerical model, or generate and upscale a geostatistical model. In this case, quantifying the heterogeneities will be useful to correct our assessment of the long term reservoir potential.

7.B Homogeneous reservoir

The homogeneous reservoir is the simplest possible model assuming everywhere the same porosity, permeability and thickness. The permeability is assumed isotropic. That is, the same in all directions.

The governing parameters are:

- kh Permeability-thickness product, given by the pressure match.
- $\phi c_t h$ Reservoir storativity, input at the initialization of a standard test or as a result in interference tests.
- S Skin

At early time the pressure response is dominated by the well models described in the chapter on 'Well models', the most common early time responses are thus:

Wellbore storage, linear flow (high conductivity fracture), bilinear flow (low conductivity fracture), spherical flow, horizontal well (linearity after early time radial flow). These regimes are coupled with a hump caused by the storativity and the skin.

In addition we have the line source well with no skin or wellbore storage used for the analysis of interference tests.

In fact, the reservoir response in a homogenous reservoir is simply the linearization of the pressure with respect to the logarithm of time, infinite acting radial flow (IARF) is established and the Bourdet derivative stabilizes and is flat at a level related to the permeability.

The below figure shows a schoolbook example of the response of a wellbore storage and skin homogeneous model in an infinite reservoir. If this was a common behavior the task of the PTA engineer would have been easy indeed.

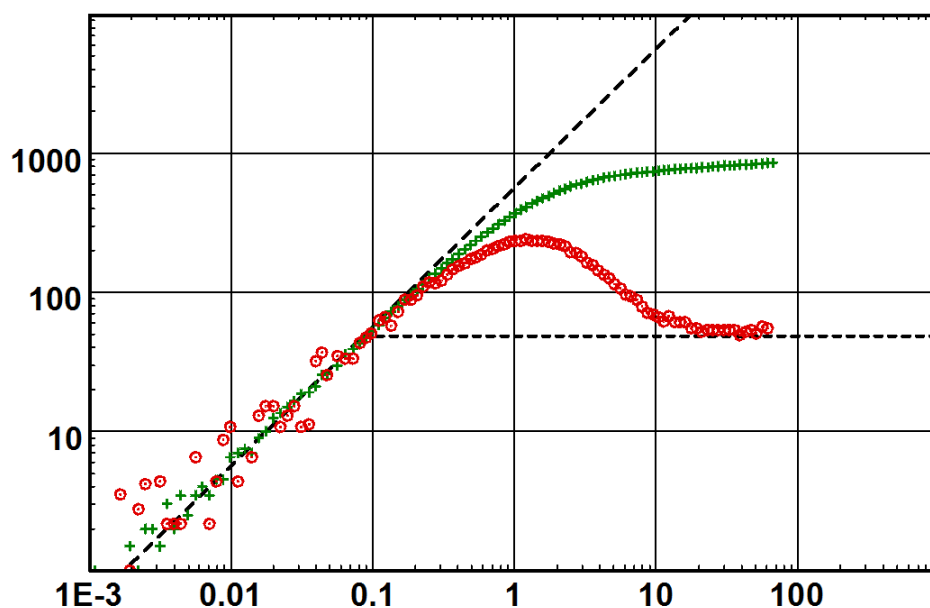


Fig. 7.B.1 - Schoolbook response

The below figures illustrates the various homogenous behaviors on a loglog plot commonly seen in pressure transient analysis. The line source solution is also shown.

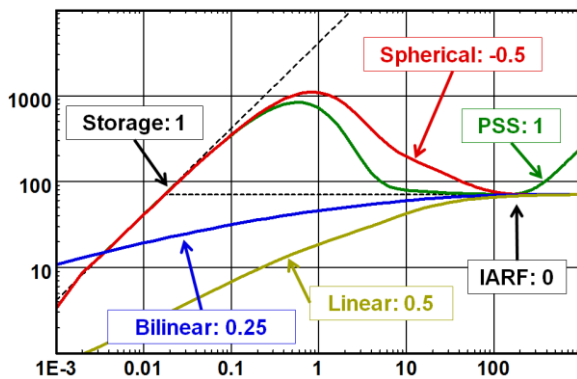


Fig. 7.B.2 – Homogeneous loglog plots

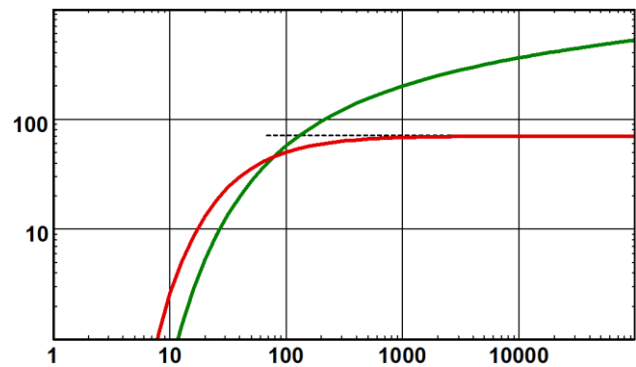


Fig. 7.B.3 – Line source

And following we illustrate the semilog behavior of wellbore storage and skin in a homogeneous reservoir.

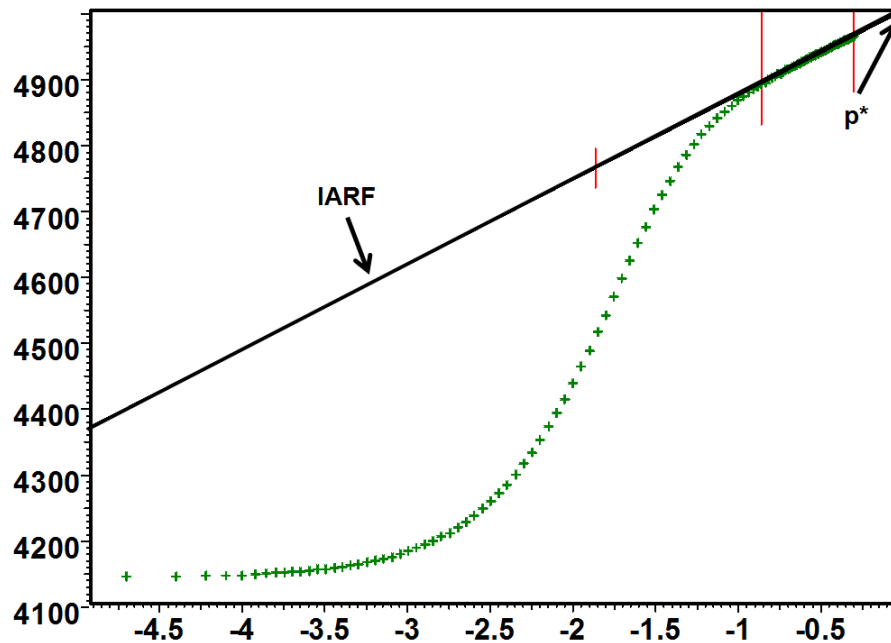


Fig. 7.B.4 – Homogeneous semilog plot

7.B.1 Homogeneous Sensitivity to parameters

7.B.1.a Skin

Below is shown the response with a variable skin. Values for skin are -3, 0, 2, 5 and 10.

Storage: Skin does not change the position of the early time unit slope (pure wellbore storage) but affects the amplitude of the hump. A larger skin will produce a larger hump, hence delaying the time at which Infinite Acting Radial Flow is reached.

IARF: Once IARF is reached, the skin has no effect on the vertical position of the derivative, but has a cumulative effect on the amplitude of the pressure.

PSS: Skin does not have an effect on the time at which PSS is reached or on the derivative response at the end. However the cumulative effect on the pressure remains and all responses 'bend' and remain parallel when PSS is reached (see history plot below).

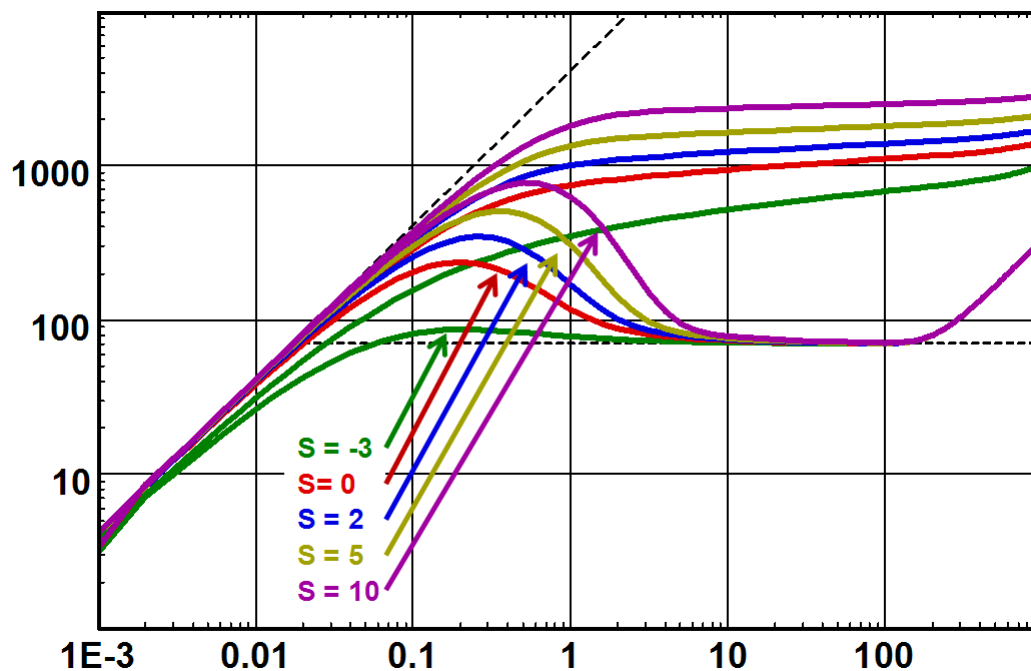


Fig. 7.B.5 – Effect of skin, loglog plot

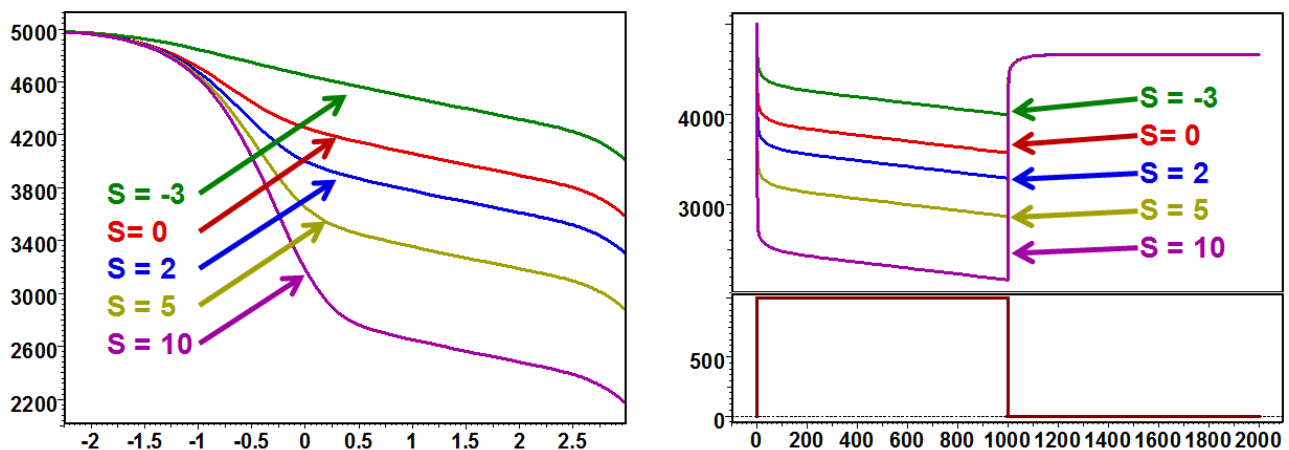


Fig. 7.B.6 – Effect of skin, semilog and history plot

7.B.1.b Permeability

The figure below presents the response with a variable permeability. Values for k are 2, 5, 10, 20 and 50 mD.

Storage and IARF: The derivative responses have the same shape but they are translated along the wellbore storage line of unit slope. When the permeability is higher, the reservoir reacts faster and deviates earlier from pure wellbore storage. The level of stabilization of the derivative, i.e. the slope of the semilog plot, is inversely proportional to k . For this reason the responses diverge on the semilog plot, the different slopes being inversely proportional to k .

PSS: At late time all derivative signals merge to a single unit slope. This is linked to the fact that permeability has no effect on the material balance equation.

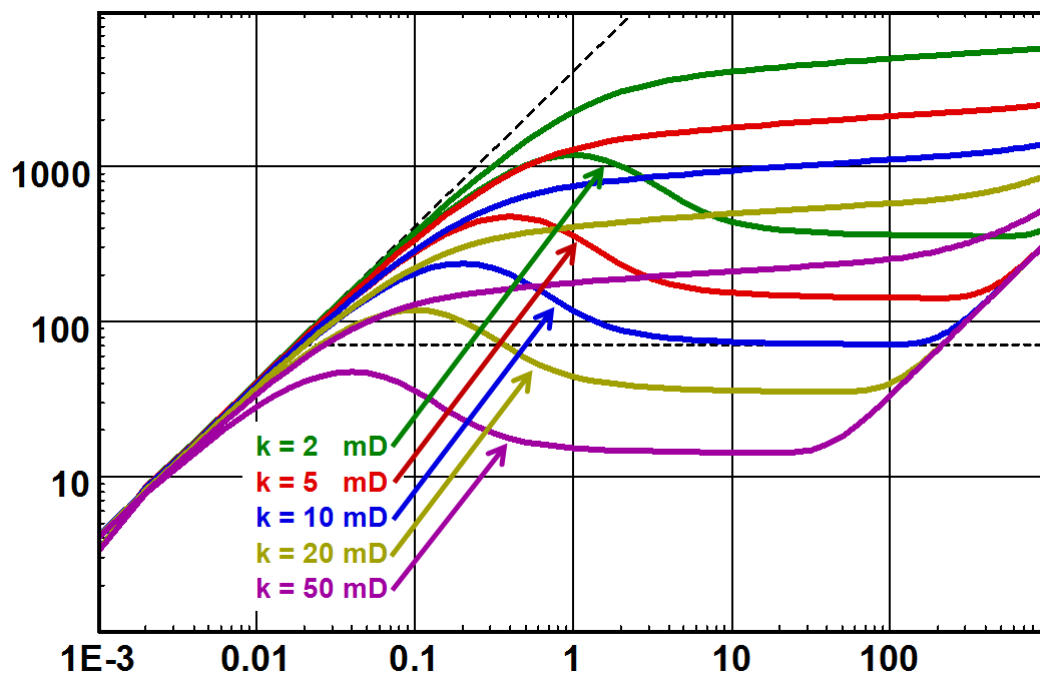


Fig. 7.B.7 – Influence of the reservoir permeability, loglog plot

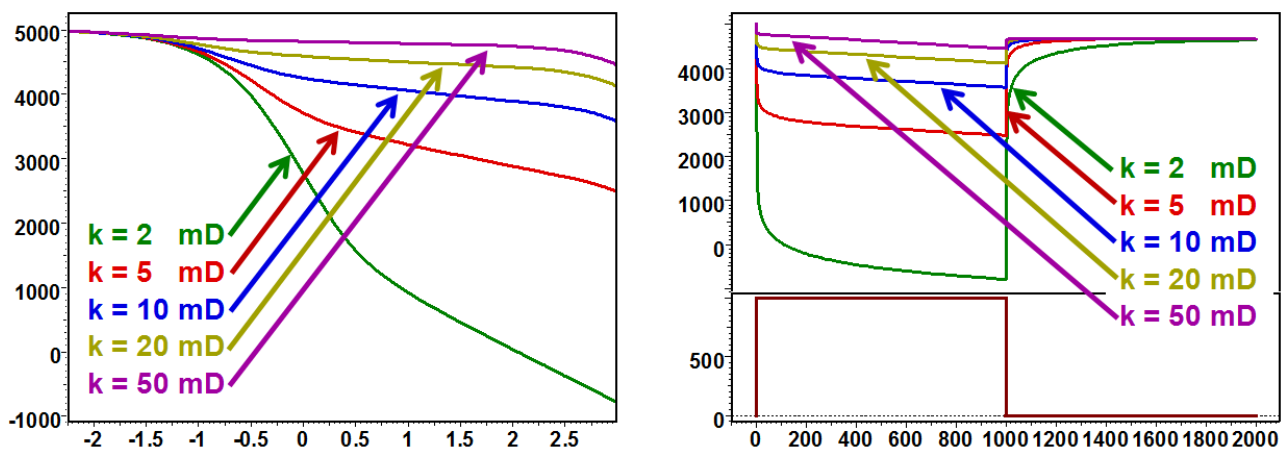


Fig. 7.B.8 – Influence of the reservoir permeability, semilog and history plot

7.B.1.c Wellbore radius

The response with varying wellbore radius is illustrated below. Values of r_w are 0.1, 0.3, 1 and 3 ft.

The effect of a change in the wellbore radius is strictly the same as the consequence of a skin change: Early time amplitude of the derivative hump, no middle time and late time effect on the derivative, but a shift in the pressure that stays constant once wellbore storage effects are over. The equivalence between wellbore radius and skin is hardly a surprise, as skin can also be defined with respect to an equivalent wellbore radius. The well response is in fact a function of the equivalent wellbore radius $r_{we} = r_w \cdot e^{-S_{kin}}$.

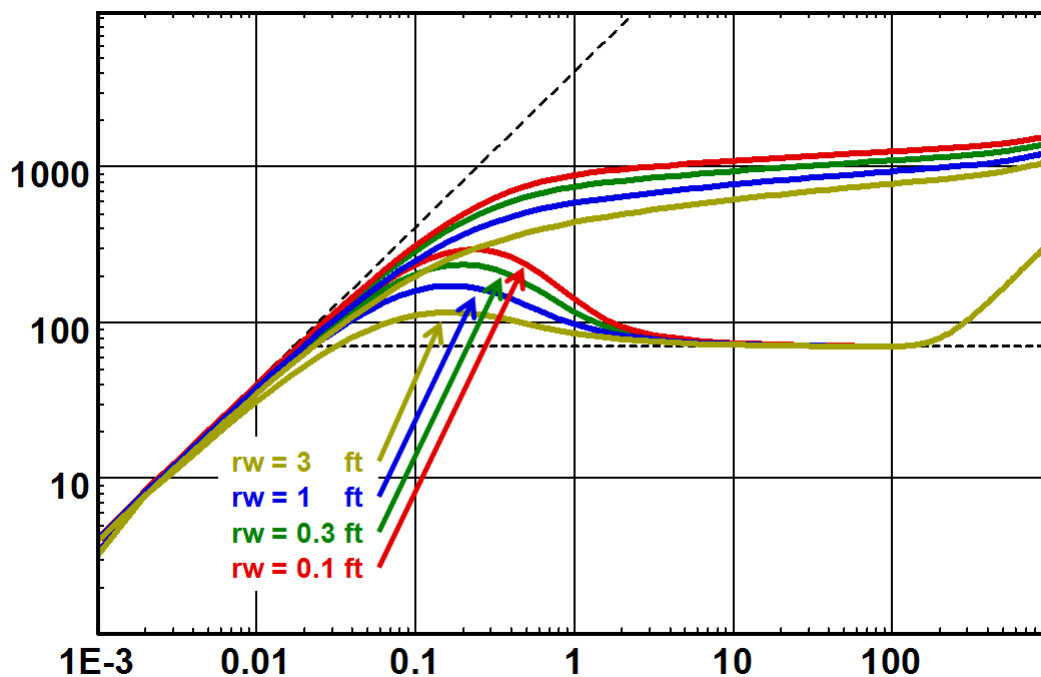


Fig. 7.B.9 – Effect of wellbore radius r_w , loglog plot

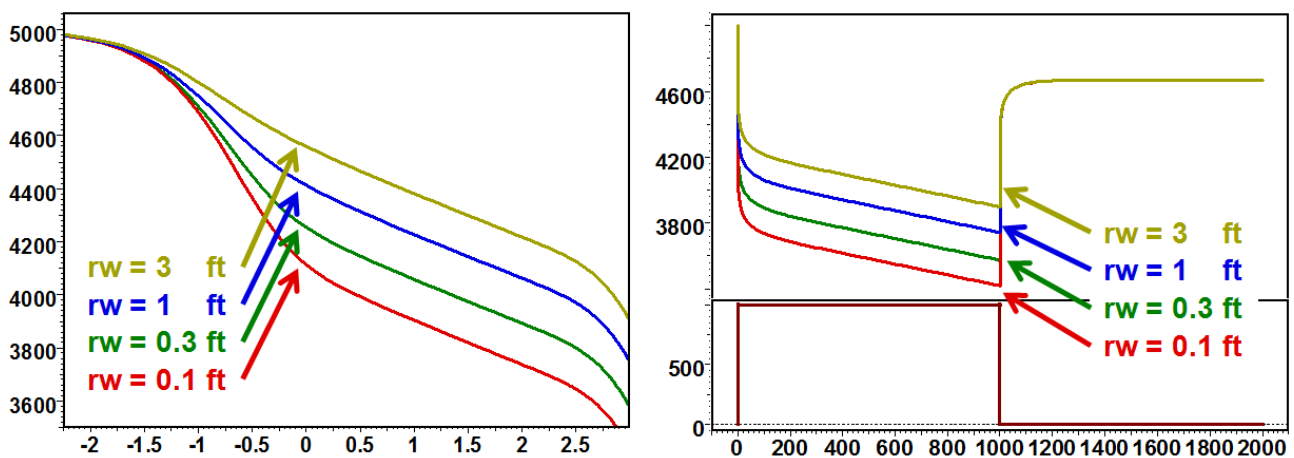


Fig. 7.B.10 – Effect of wellbore radius r_w , semilog and history plot

7.B.1.d Porosity

The figure below presents the response by varying the porosity. Values for ϕ are 3%, 10% and 30%.

Storage and IARF: Porosity behaves like the skin or the well radius. A smaller porosity produces a higher hump on the derivative but does not change the derivative IARF level. The equivalence between porosity and skin is used in two different areas. In Interference tests the Skin has a marginal influence, and the pressure amplitude is used to assess the porosity.

Hydrogeology: Hydrogeology will assess a value of skin (generally zero) and use the absolute value of the pressure change to assess the Storativity S , i.e. the porosity.

For a given reservoir size, the time for PSS is proportional to ϕ . Underestimating the porosity by 10% will provide an overestimation of the reservoir bulk volume of 10%, and therefore an overestimation of the boundary distance. The total pore volume will remain correct.

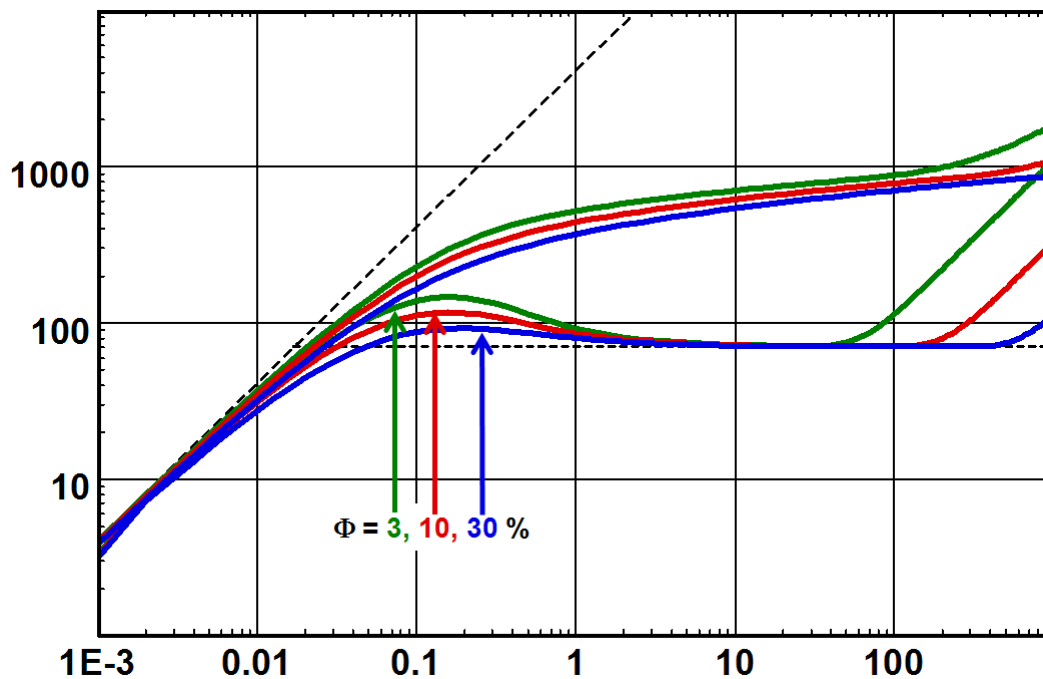


Fig. 7.B.11 – Effect of the reservoir porosity, loglog plot

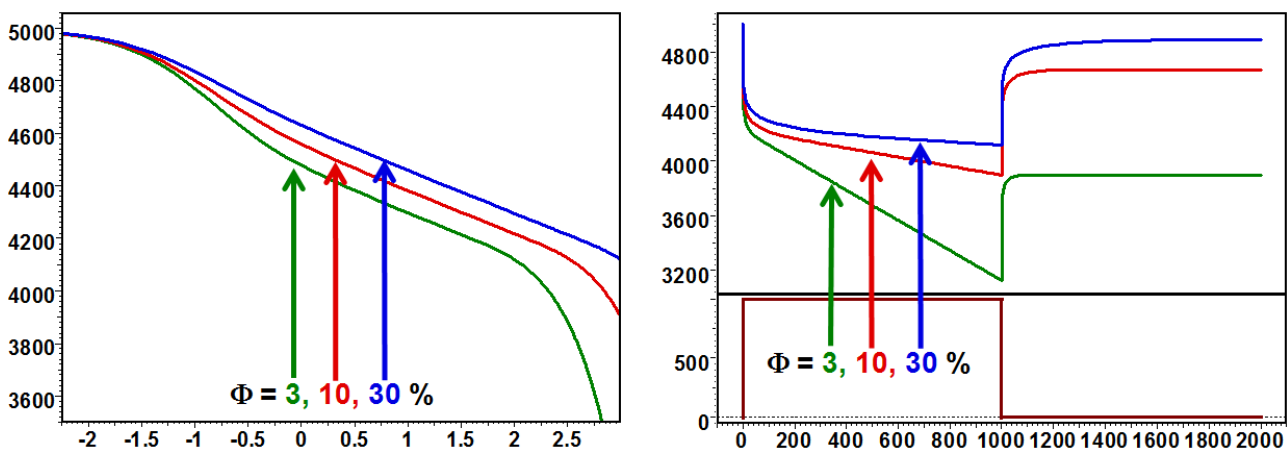


Fig. 7.B.12 – Effect of the reservoir porosity, semilog and history plot

7.B.1.e Total compressibility

Illustrated below is the response computed by varying the total compressibility. Values for c_t are $3 \cdot 10^{-6}$, $1 \cdot 10^{-5}$ and $3 \cdot 10^{-5}$ psi⁻¹. The sensitivities at Early Time (Storage), Middle time (IARF) and late time (PSS) are strictly the same as for the porosity: A smaller compressibility produces a higher hump of the early time derivative. Compressibility does not affect the derivative level when IARF is reached but has a cumulative effect on the pressure. At late time, compressibility affects the time at which the boundary is detected and the material balance equation. As for porosity, under-estimating c_t by 10% will provide an over-estimation of the reservoir size by 10%, and therefore an over-estimation of the boundary distance. In fact, on all parts of the response, the influence of porosity and compressibility will be a function of their product $\phi \cdot c_t$.

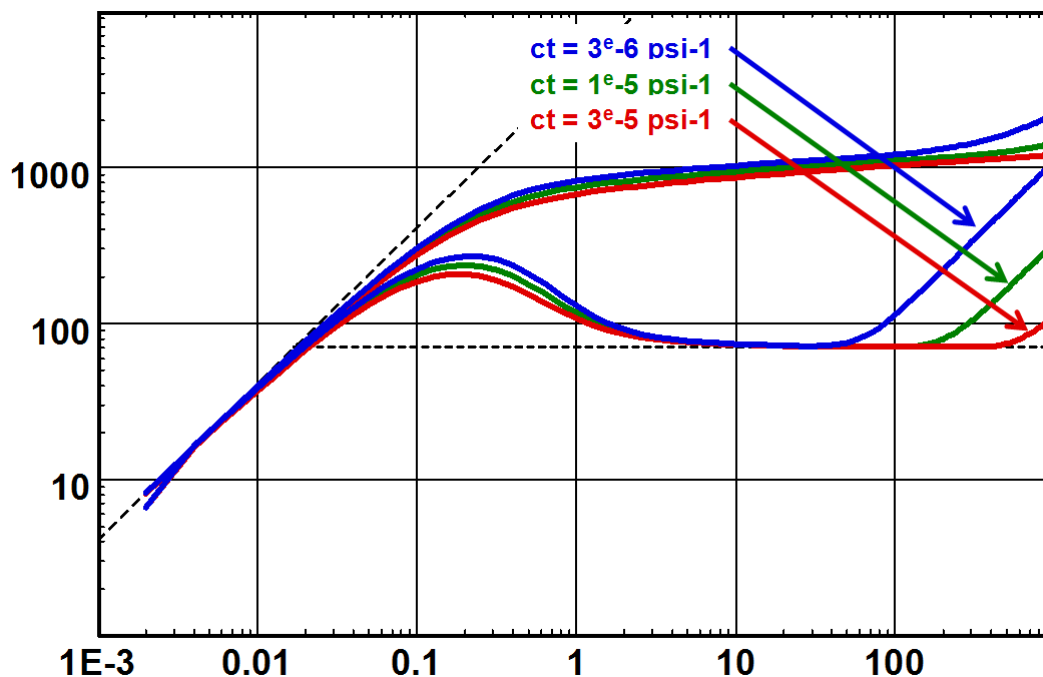


Fig. 7.B.13 – Effect of total compressibility, loglog plot

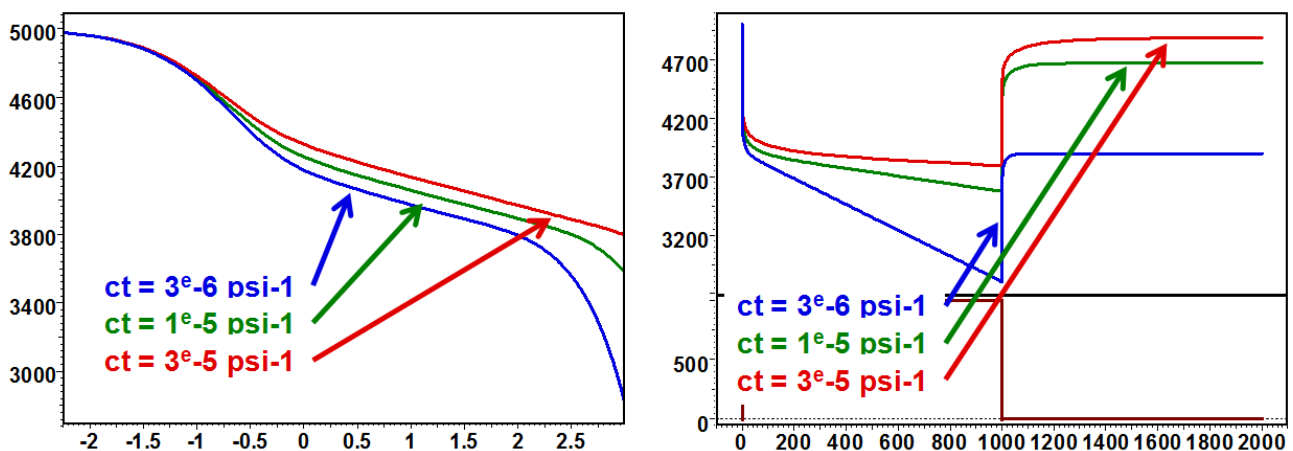


Fig. 7.B.14 – Effect of the total compressibility, semilog and history plot

7.B.1.f Viscosity

The next figure illustrates the response with variable fluid viscosity. Values for μ are 0.2, 0.5, 1, 2 and 5 cp. If we compare the response with the Fig. 2.H.8 illustrating the effect of a permeability change (above), we see that the sensitivity to viscosity is exactly opposite to the sensitivity to permeability. At early time (Storage) and middle time (IARF), the derivative responses have the same shape but translated along the wellbore storage line of unit slope. When the viscosity is lower, the reservoir reacts faster and deviates earlier from pure wellbore storage. The levels of stabilization of the derivative and the semilog slopes are proportional to μ . At late time all derivative signals merge to a single unit slope. In other words, the sensitivity on $1/\mu$ is the same as the sensitivity to k on all parts of the response. This means that we have another governing group with k/μ , also called the mobility.

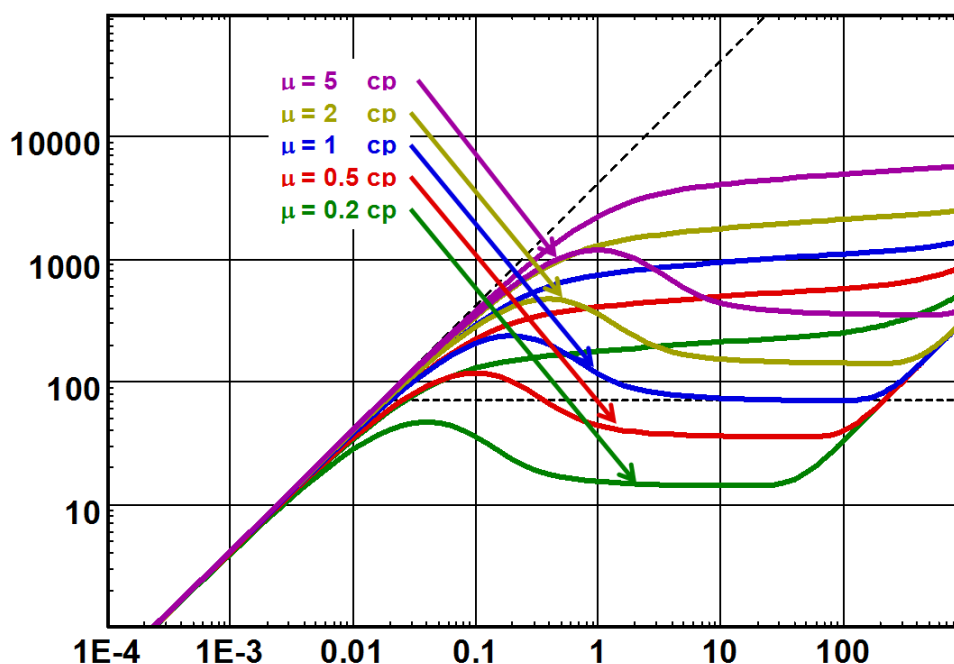


Fig. 7.B.15 – Effect of the fluid viscosity, loglog plot

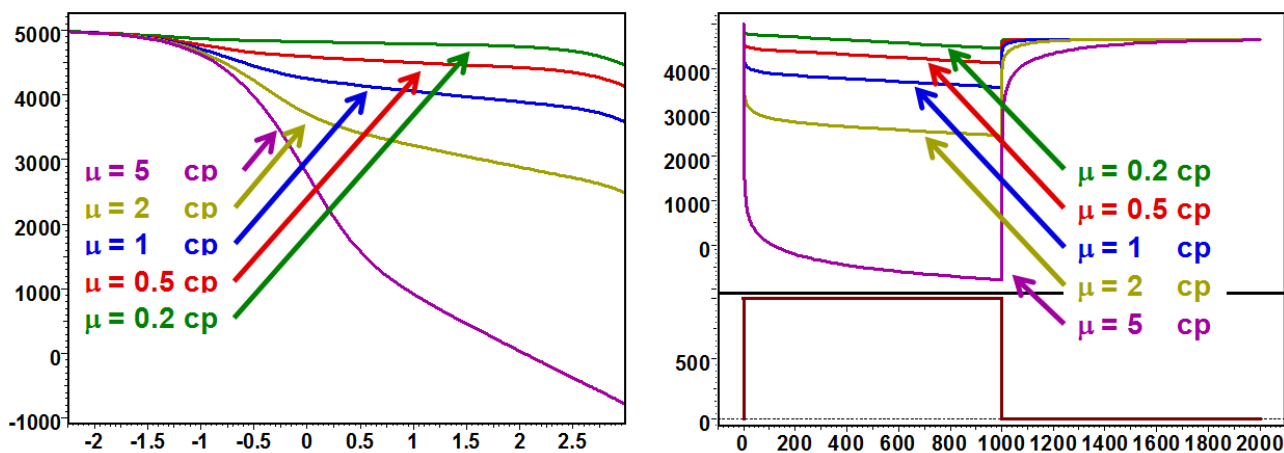


Fig. 7.B.16 – Effect of the fluid viscosity, semilog and history plot

7.B.1.g Thickness

Illustrated below is the response computed with a varying net drained thickness. Values for h are 20, 50, 100, 200 and 500 ft.

Storage and IARF: Changing the thickness has a similar effect to changing the permeability and an effect opposite to changing the viscosity. In other words, the governing group that defines the early time response, apart from wellbore storage and skin, is kh/μ .

PSS: Unlike permeability and viscosity, the reservoir thickness also has an effect on the late time material balance calculation. Also, the time at which the derivative deviates from IARF towards PSS does not change, and therefore the influence of the thickness on the position of the PSS straight line is similar to the sensitivity to the reservoir porosity or the compressibility.

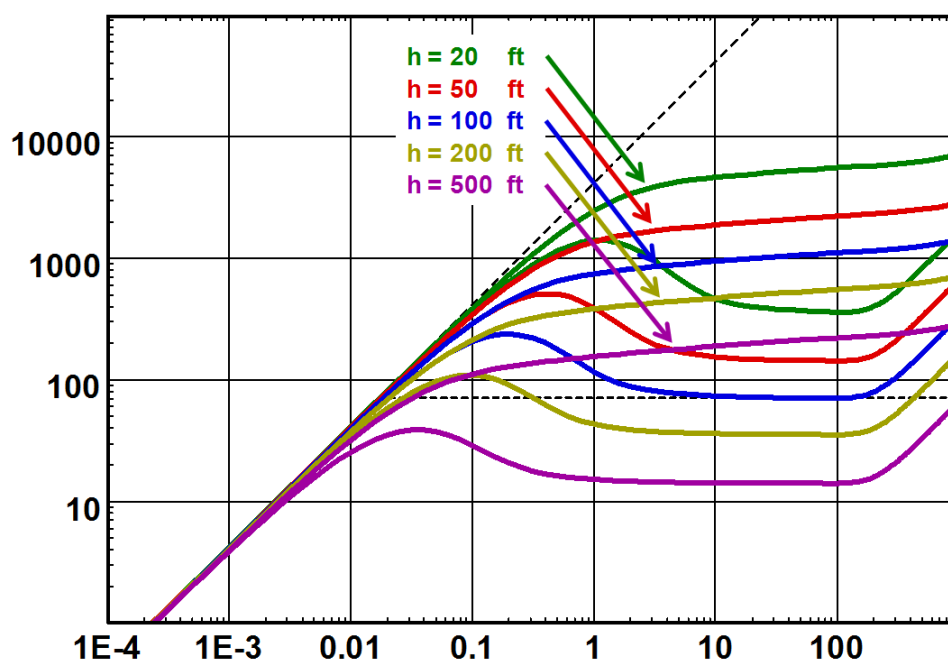


Fig. 7.B.17 – Effect of the reservoir thickness, loglog plot

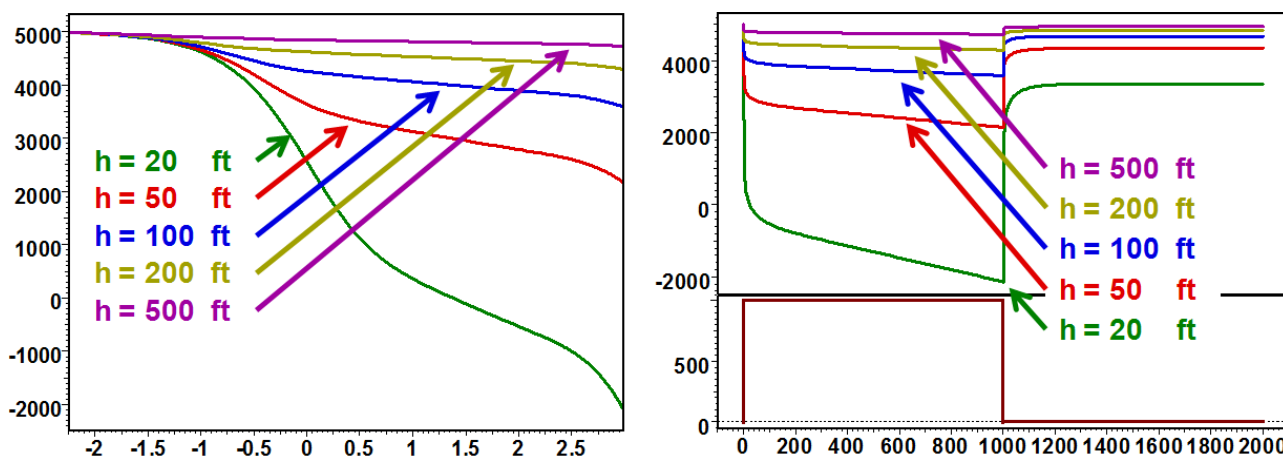


Fig. 7.B.18 – Effect of the reservoir thickness, semilog and history plot

7.B.1.h ... and how about rates?

We are not referring to superposition effects, but to the plain value of the rate, i.e. the effect of a systematic error on the rate values and/or the formation volume factor B.

Fig. 2.H.22 figure below illustrates the response with a variable rate for each simulation. Values for $q.B$ are 600, 800, 1000, 1200 and 1400 rb/d.

The result of varying $q.B$ corresponds to a straight multiplication of the pressure change from p_i . The loglog response is shifted vertically, and the semilog and history plots are vertically compressed or expanded, the fixed point being the initial pressure.

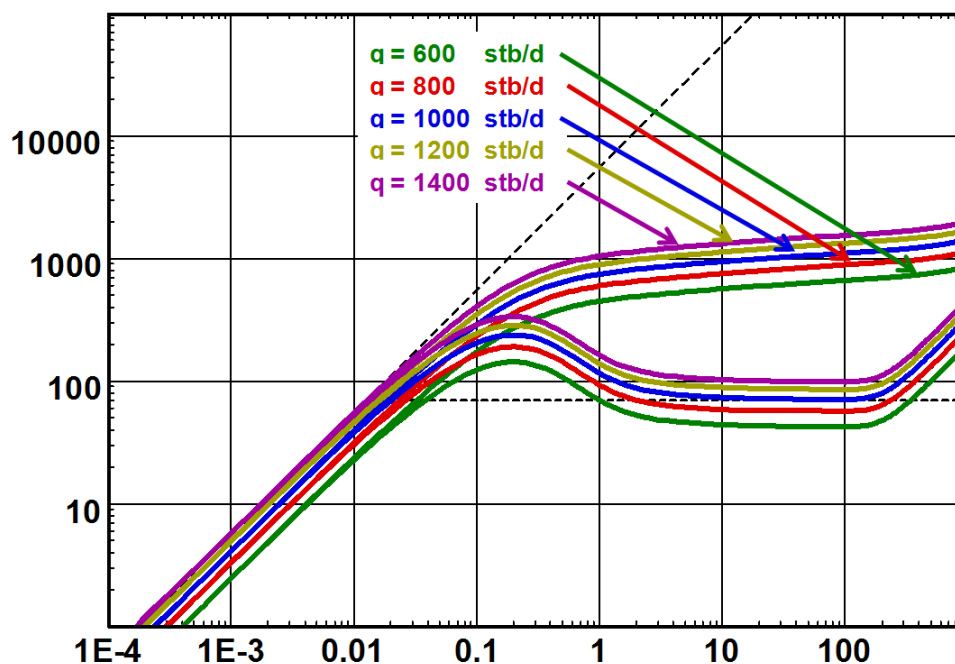


Fig. 7.B.19 – Effect of the rate– $q.B$, loglog plot

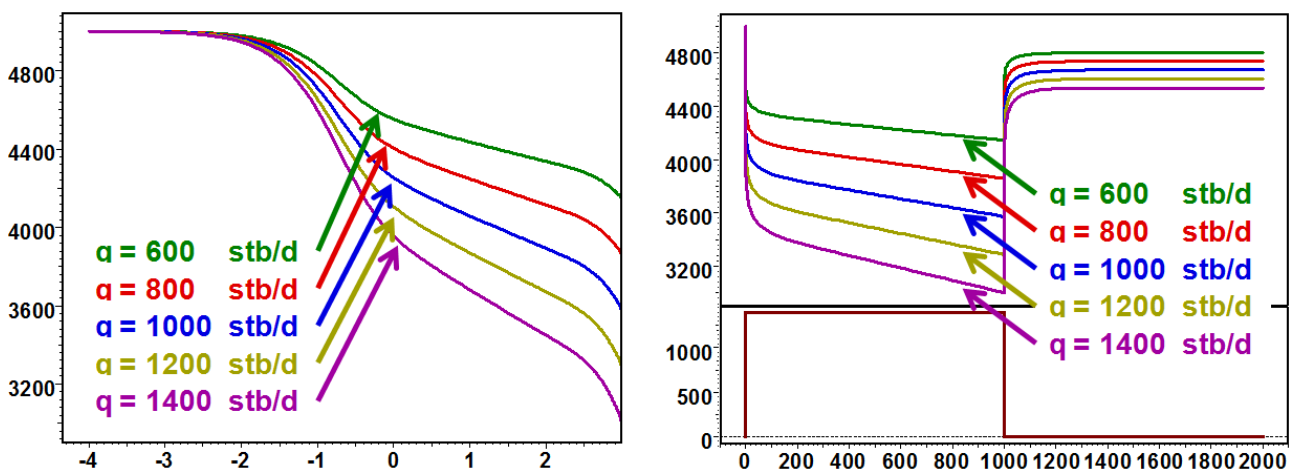


Fig. 7.B.20 – Effect of the rate– $q.B$, semilog and history plot

7.C Double-porosity reservoir

7.C.1 Hypothesis

The double-porosity (2Φ) models assume that the reservoir is not homogeneous, but made up of rock matrix blocks with high storativity and low permeability. The well is connected by natural fissures of low storativity and high permeability. The matrix blocks cannot flow to the well directly, so even though most of the hydrocarbon is stored in the matrix blocks it has to enter the fissure system in order to be produced.

The double-porosity model is described by two other variables in addition to the parameters defining the homogeneous model: ω is the storativity ratio, and is essentially the fraction of fluids stored in the fissure system (e.g. $\omega=0.05$ means 5%).

ω , storativity ratio:

$$\omega = \frac{(V\Phi c_t)_f}{(V\Phi c_t)_m + (V\Phi c_t)_f}$$

λ is the interporosity flow coefficient that characterizes the ability of the matrix blocks to flow into the fissure system. It is dominated by the matrix/fissures permeability contrast, k_m/k_f .

λ , the interporosity flow parameter:

$$\lambda = \alpha r_w^2 \frac{k_m}{k_f}$$

When the well is first put on production, after any well dominated behavior, the first flow regime to develop is the fissure system radial flow, i.e. the fissure system is producing as if this system was there alone, and there is no change in the pressure inside the matrix blocks.

This first flow regime is typically over very quickly, and is frequently masked by wellbore storage. If not, it will develop as an IARF response and the pressure derivative will stabilize horizontally.

Once the fissure system has started to produce, a pressure differential is established between the matrix blocks and the fissures. The matrix is still at initial pressure p_i , and the fissure system has a pressure p_{wf} at the wellbore, the matrix blocks then start to produce into the fissure system, effectively providing pressure support, and the drawdown briefly slows down as this extra energy tends to stabilize the pressure, thus a transitional dip in the derivative is created.

The total system radial flow (IARF) is established when any pressure differential between the matrix blocks and the fissure system is no longer significant, and the equivalent homogeneous radial flow response is observed. A second IARF stabilization in the pressure derivative is therefore developed after the transitional dip, called by some the derivative valley. According to the mathematics, this takes place when the pressure inside the matrix blocks is the same as in the fissure system however; this can never be true at all points in the reservoir, as there would be no production into the fissure system.

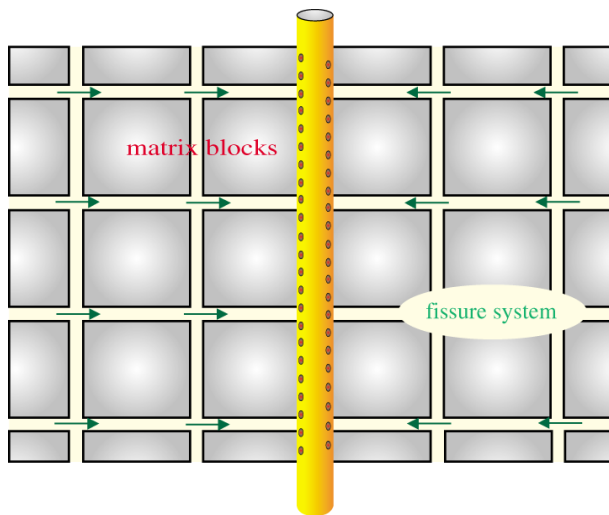


Fig. 7.C.1 – Fissure system production

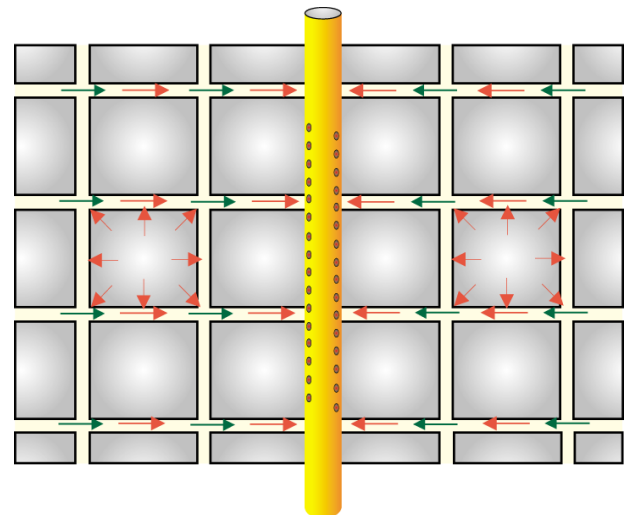


Fig. 7.C.2 – Total system production

7.C.2 Loglog behavior

Pseudo-Steady State (PSS) interporosity flow

In this case it is assumed that the pressure distribution in the matrix blocks is uniform, i.e. there is no pressure drop inside the matrix blocks. A physical explanation for this might be that the matrix blocks are small, so that any pressure drop inside them is insignificant compared to the pressure diffusion in the reservoir away from the wellbore. The entire pressure drop takes place at the surface of the blocks as a discontinuity, and the resulting pressure response gives a sharp dip during the transition.

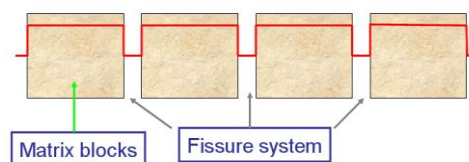


Fig. 7.C.3 – Pressure cross section

A real buildup from a double porosity reservoir is illustrated below.

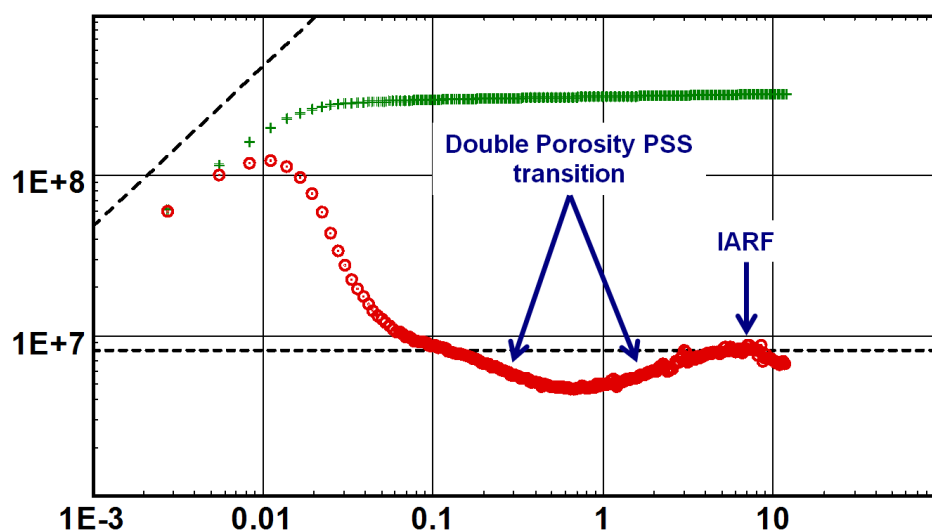


Fig. 7.C.4 – Double porosity loglog plot, PSS

ω is the fraction of interconnected pore volume occupied by the fissures. It determines the depth of the dip. For small ω values, corresponding to a very high proportion of the hydrocarbon stored in the matrix system, the support during the transition is substantial, and the dip is deeper and longer. The figure below illustrates the influence of the value of ω .

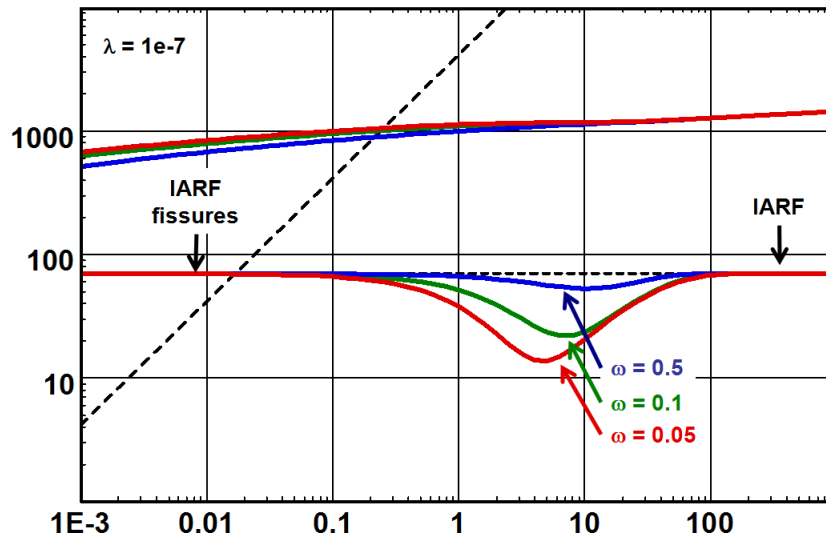


Fig. 7.C.5 – Influence of ω

λ describes the ability of the matrix to flow to the fissures, and is a function of the matrix block size and permeability. It determines the time of start of transition and controls the speed at which the matrix will react, therefore the total time of the transition. For a high λ , the matrix permeability is comparatively high, so it will start to give up its fluid almost as soon as the fissure system starts to produce. Conversely a low λ means a very tight matrix, and more drawdown will have to be established in the fissured system before the matrix blocks will appreciably give up any fluid, and the transition starts later. This is illustrated in the following figure.

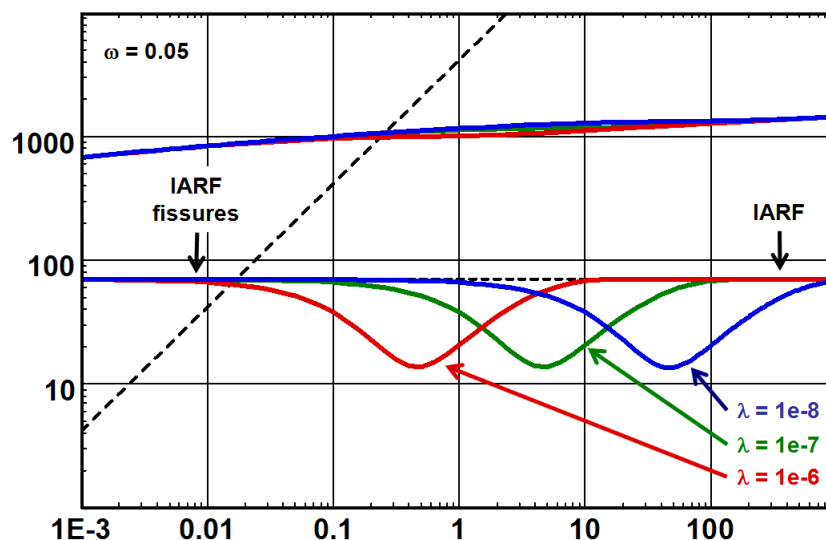


Fig. 7.C.6 – Influence of λ

Transient interporosity flow

This model assumes that there is a pressure gradient and therefore diffusivity, within the matrix blocks. If the pressure profile inside the blocks is significant, then the shape of the blocks has to be taken into consideration, and for this reason there are 2 models available, each corresponding to different matrix block geometries.

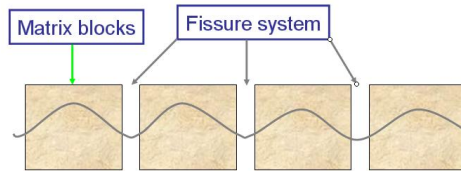


Fig. 7.C.7 – Pressure cross section

The 'slab' geometry model assumes rectangular matrix blocks, which is what we have been considering so far with the double-porosity PSS models. The 'spheres' model, physically realistic or not, represents another simple geometry with which to define the boundary conditions for the mathematical solution. It is difficult to visualize a reservoir consisting of spherical matrix blocks, but perhaps due to fluid movements over geological time the fissure network can become 'vuggy' and the edges of the matrix blocks rounded. Double-porosity data sets sometimes match the 'spheres' model better than any other. As before, our mathematical models may not be an accurate representation of what nature has provided in the reservoir, but the performance from these models is very close to the measured pressures from these wells. Below is a loglog plot of a buildup in a double porosity transient behavior reservoir. Unfortunately the test stopped in the middle of the transition.

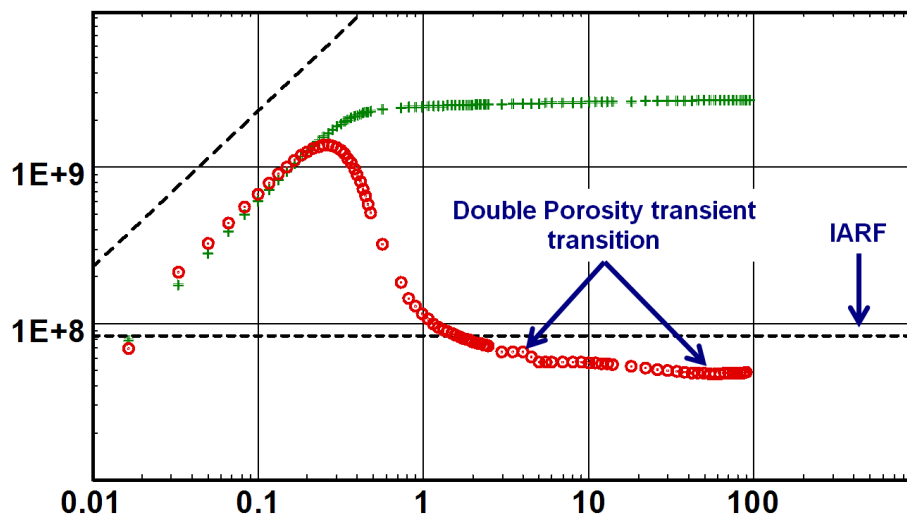


Fig. 7.C.8 – Double porosity transient behavior

The following figure illustrates the difference between the 'slab' and 'sphere' blocks, the difference is small.

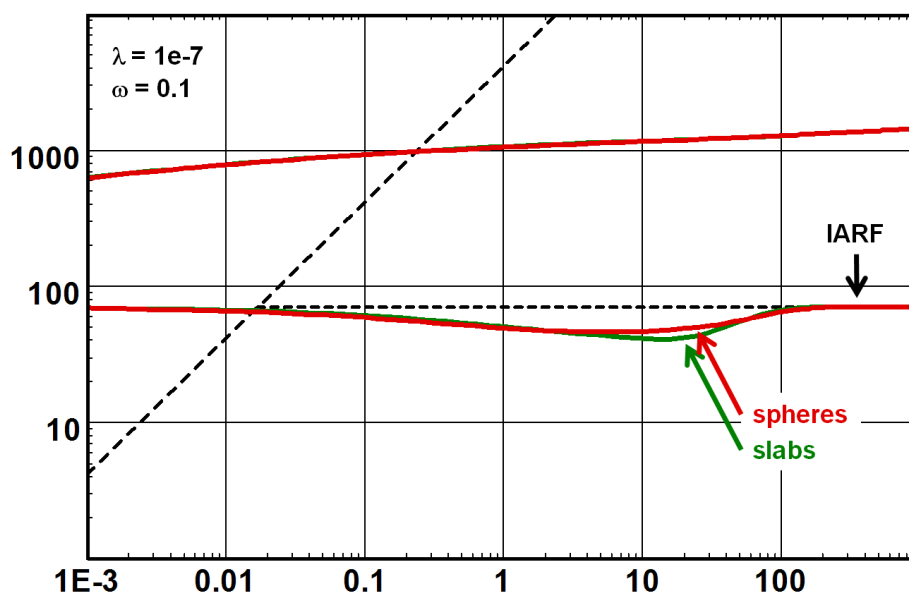


Fig. 7.C.9 – Slab/Sphere matrix blocks

As shown in the following plots, the fissure system radial flow is very short-lived, and in practice is not seen. At the deepest point in the transition, the semi-log slope/derivative value is half of the total system radial flow value. ω in this model has a more subtle effect on the shape of the derivative, and λ defines the time at which the response transitions to total system IARF.

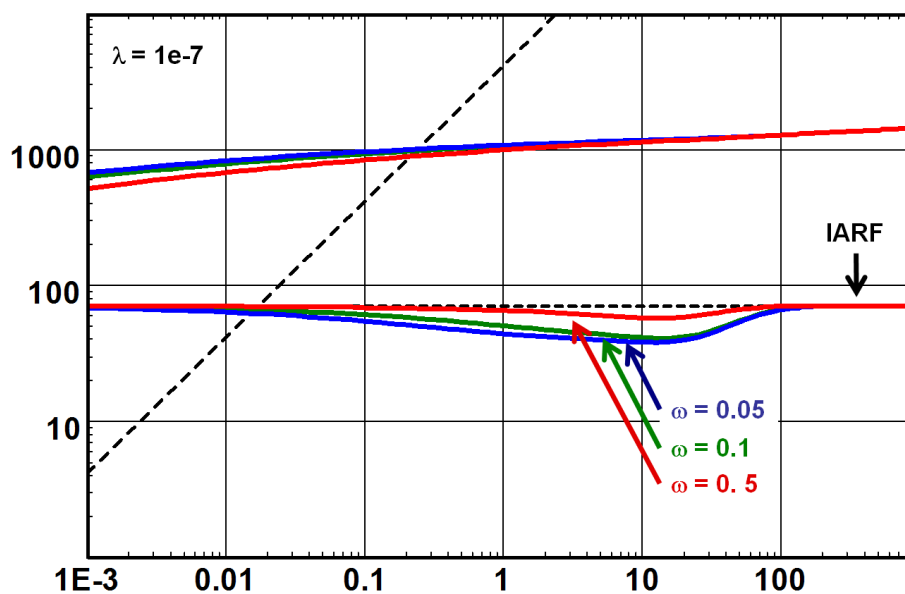


Fig. 7.C.10 – Slab matrix blocks influence of ω

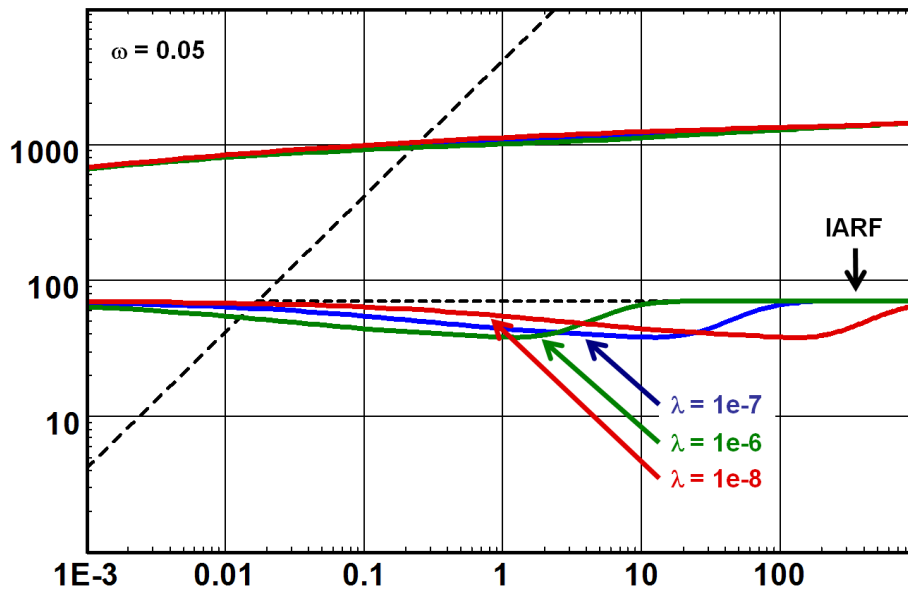


Fig. 7.C.11 – Slab matrix blocks influence of λ

7.C.3 Specialized analysis

There are theoretically two IARF stabilizations on the pressure derivative, hence two parallel straight lines on the semilog plot; the first is almost invariably obscured by wellbore storage.

If seen, the two lines would each correspond to $k_f h$, radial flow in the fissure system, as in the first case only the fissure system is producing. In the second case, although the total system is producing, any pressure differential between the matrix blocks and the fissure system is now negligible, and the only pressure drop in the system is in the fissures, as fluids flow to the wellbore. Imagine a droplet of oil in a matrix block 50 meters from the wellbore; it lazily travels a few centimeters to enter the fissure system, expelled by a negligible Δp , and then travels 50 meters through the fissure network, accelerating as it approaches the wellbore as the pressure gradient increases and flow area decreases. It is this pressure gradient, in the fissure system that creates the measured wellbore response.

In case the two straight lines are seen in the response, semilog specialized analysis can also yield information about ω and λ . ω is evaluated using the vertical separation of the two straight lines;

$$\omega = 10^{\frac{\Delta p}{m}}$$

and λ is evaluated using the time of the middle of the straight line through the transition;

$$\lambda = \frac{\omega \ln \frac{1}{\omega}}{0.000264k} \frac{\Phi \mu c_r r_w^2}{\Delta t}$$

An example of this type of analysis, easily performed using Saphir, is illustrated below.

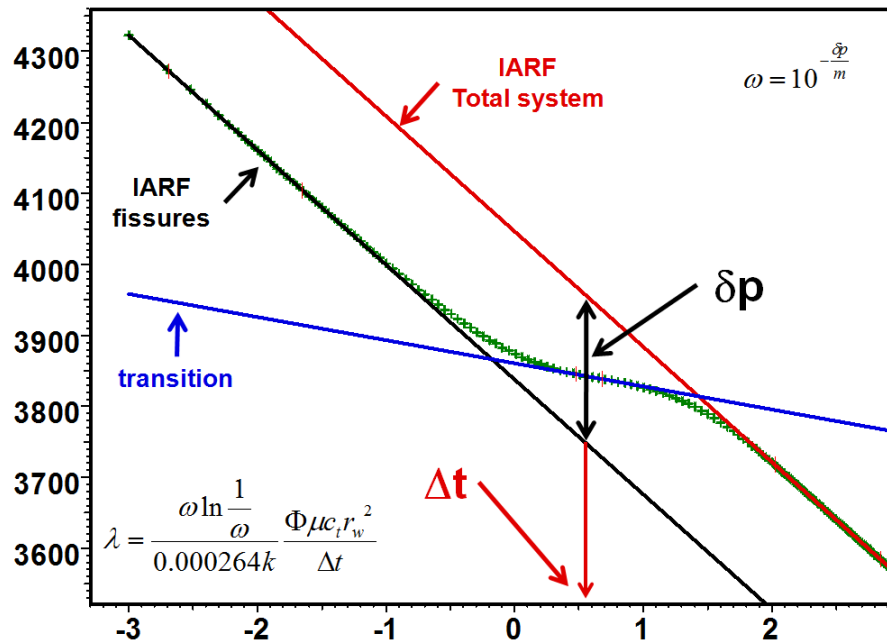


Fig. 7.C.12 – Double porosity PSS semilog analysis

7.C.4 Effect of wellbore storage

Wellbore storage will invariably mask the fissure response in the double porosity reservoir. The transition can thereby easily be misdiagnosed and the whole interpretation effort can be jeopardized. However, there are some lifelines that can save the day.

Typically there will be a negative skin associated with the double porosity reservoir where no negative skin was expected. The wellbore storage constant also tend to show a value which is unusually high and reflects the increase in the wellbore volume that the direct communication to the fissures and fractures sets up.

Illustrated below is a plot that demonstrates how the early time fissure response and transition is affected by an increasing wellbore storage coefficient. At higher wellbore storage coefficients even the whole transition period may be lost.

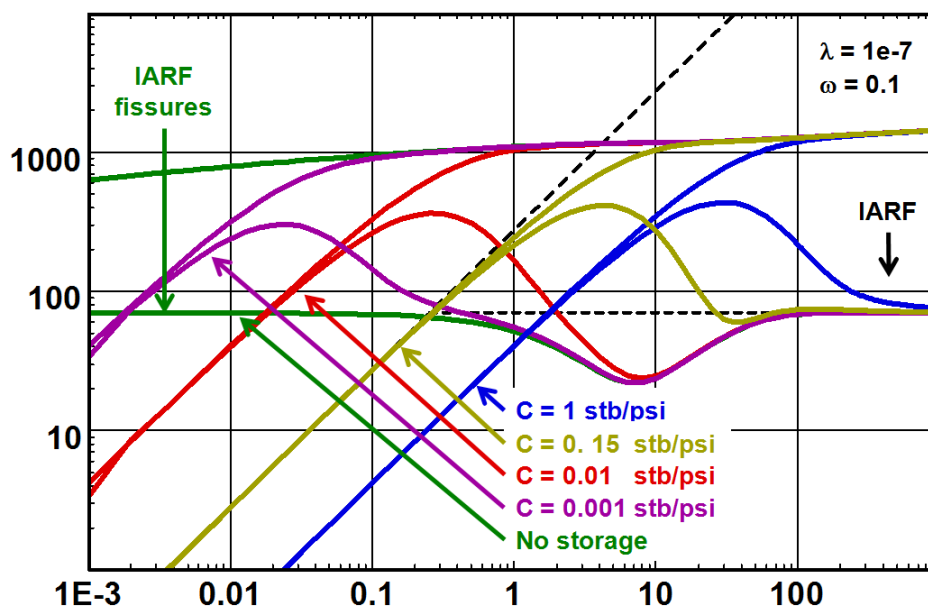


Fig. 7.C.13 – Double porosity PSS, influence of wellbore storage

7.C.5 Skin

Positive skin has no influence on the derivative and hence no influence on the transition thus no diagnostic feature is lost.

Highly negative skin will distort the early time response of both the derivative and the pressure change, the response approaches that of an infinite conductivity and linear flow can be seen to develop before the fissure system is in infinite acting radial flow.

See the below figure.

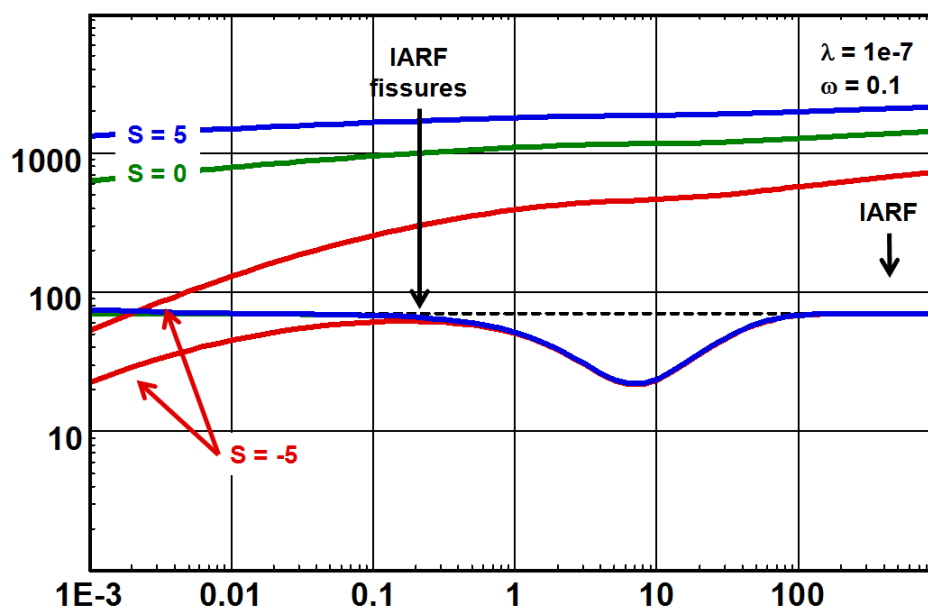


Fig. 7.C.14 – Double porosity, influence of skin

7.D Extensions of the double-porosity reservoir

7.D.1 Multiple porosities

The two families of double-porosity models are very different in behavior. The Pseudo-Steady state behavior starts with pure fissure flow, followed by an abrupt transition between the fissure and the total flow, characterized by a valley in the derivative response. The transient flow behavior (slab or sphere) will move immediately into transition, and this transition will be relatively smooth. In many cases, the behavior of naturally fractured formations, when seen, will be intermediate between the sharp and the smooth versions of these models. This is why several attempts were made to smooth the PSS model or sharpen the transient models.

7.D.2 Hypothesis

Pseudo-Steady State with multiple porosities

To extend the double porosity PSS solution one can consider matrix blocks of different sizes. In the following case we will consider only two different matrix blocks.

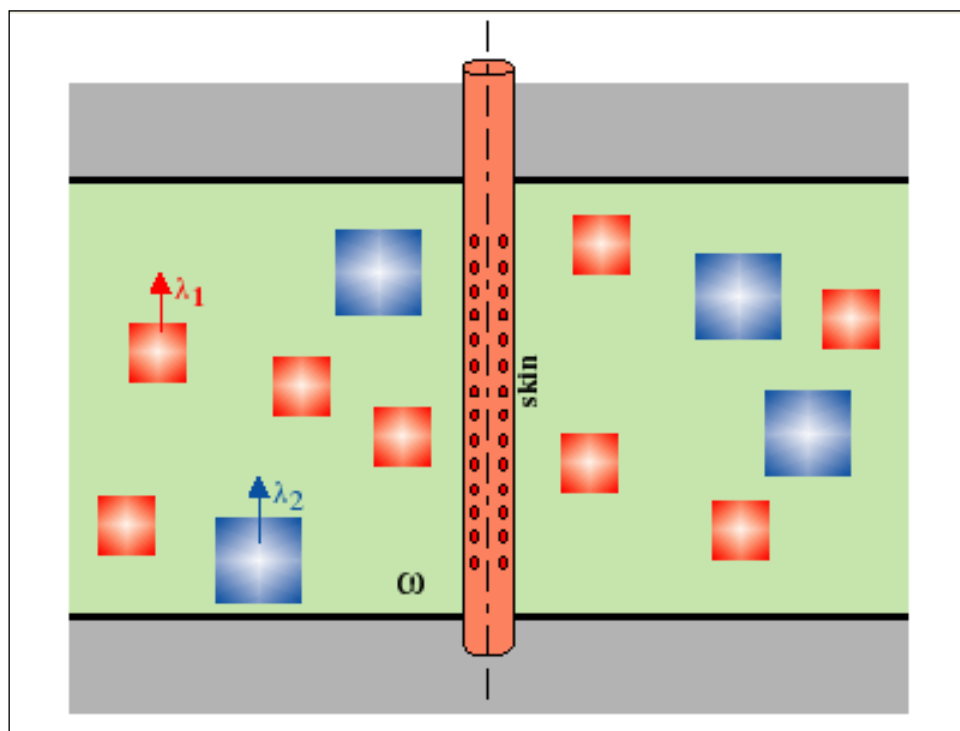


Fig. 7.D.1 – Triple porosity PSS

ω is still defined as the fraction of the interconnected pore volume occupied by the fissures. Each series of matrix blocks has its own value of λ (i.e. λ_1 and λ_2), corresponding to different transition times, and each subtype of blocks will occupy a different fraction of the total matrix pore space. We will define δ_1 the fraction of the matrix pore space occupied by the first series of blocks with respect to the total block storativity:

$$\delta_1 = \frac{(\Phi V c_t)_1}{(\Phi V c_t)_{1+2}} \quad \text{and} \quad \delta_2 = 1 - \delta_1$$

Transient double porosity with skin

An extension to the double porosity transient flow model is to add skin to the matrix face. The notion of spheres and slabs is still valid and ω and λ have the same definitions as before. The below figure illustrates the schematic of the model.

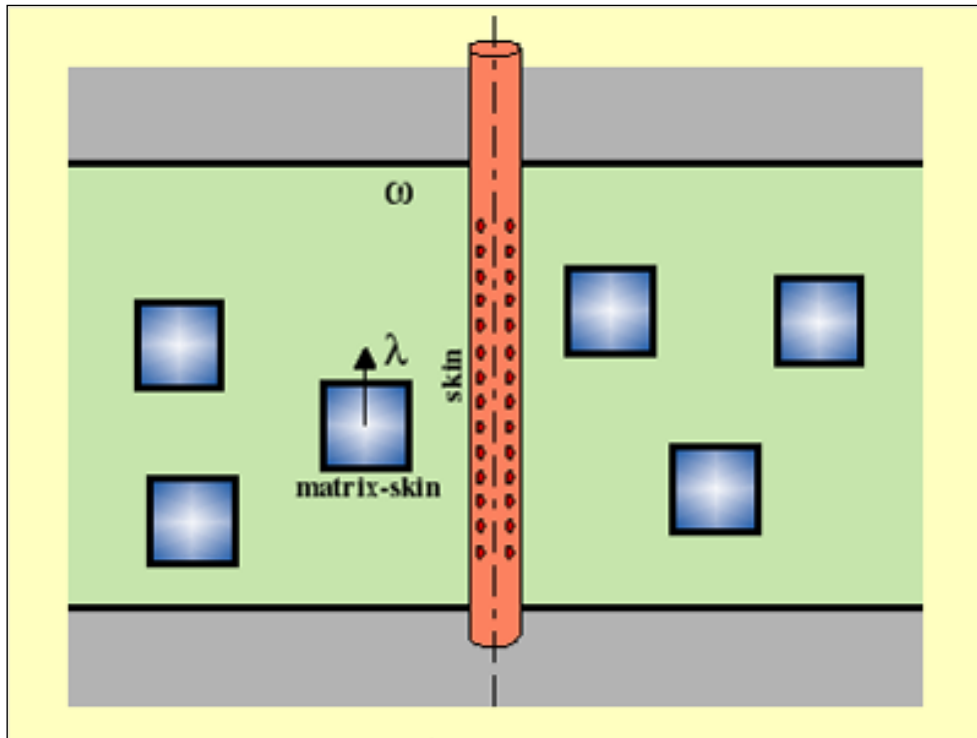


Fig. 7.D.2 – Transient model with matrix block skin

7.D.3 Loglog behavior

The following figure shows a typical response on the loglog plot. If an appropriate choice of the parameters and parameter ratios has been made it will allow the observation of a triple heterogeneous behavior. The first dip in the derivative is caused by the transition from the smaller sized block system to the fissures. The second dip in the derivative is only seen if the contrast of the interporosity flow coefficients of the two block systems is large enough.

For a constant ω value, the smaller the δ_1 value, the smaller the first dip and the greater the second.

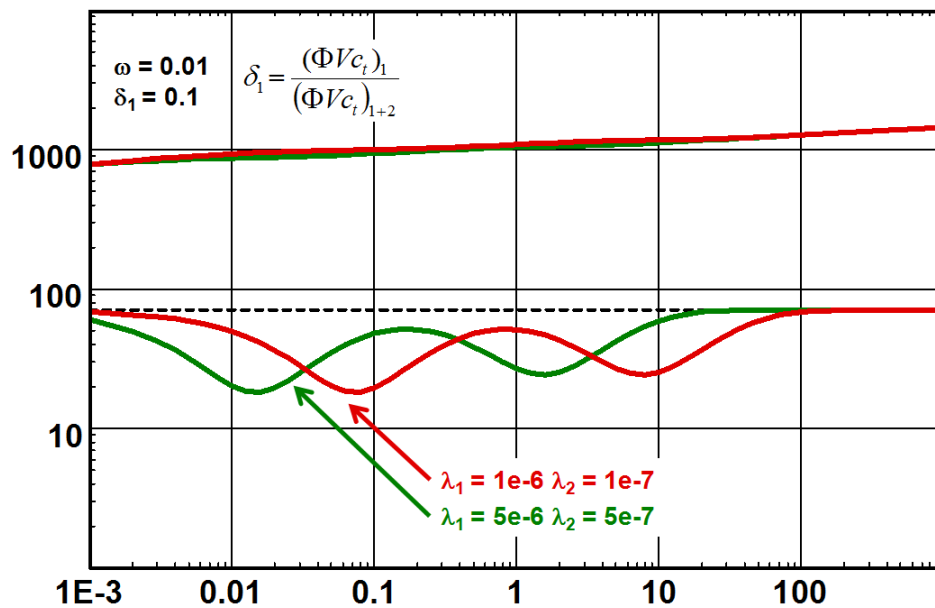


Fig. 7.D.3 – Triple porosity PSS response

Although this geological setting can easily be observed in real life the parameters governing this model is usually such that the two distinct transitions and valleys are not observed, in most cases only one transition valley is seen.

The following figure illustrates that adding skin to the matrix face the transient solution approaches that of the PSS double porosity response.

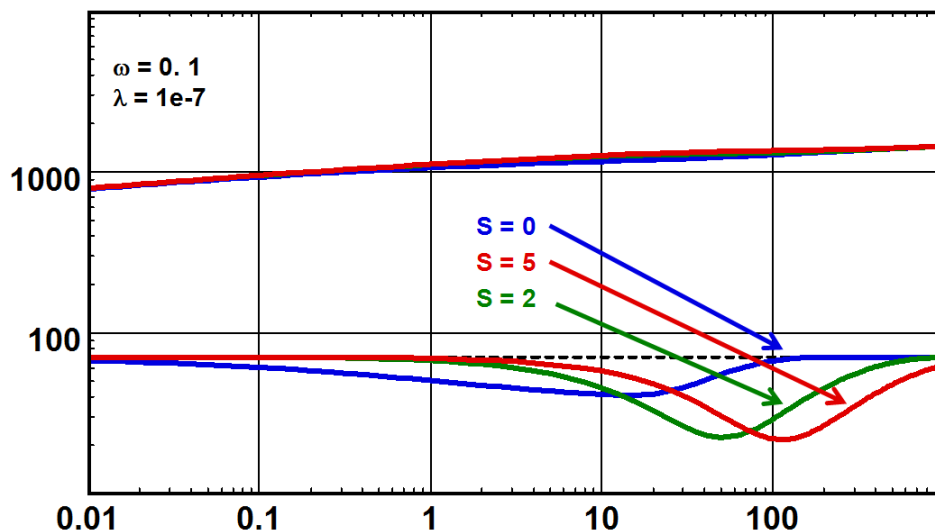


Fig. 7.D.4 – Transient double porosity, matrix blocks skin

7.D.4 Effect of wellbore storage

In the PSS model any wellbore storage will mask the first transition; as some wellbore storage is invariably present this means that in practice the first transition in such a system will very rarely be observed. See the following figure.

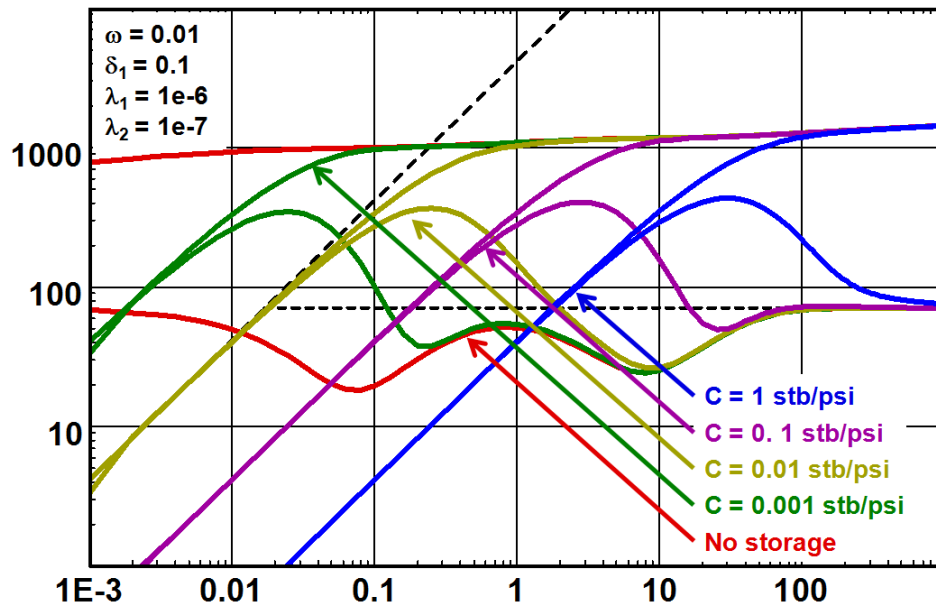


Fig. 7.D.5 – PSS influence of wellbore storage

The transient model with matrix skin will only be affected by significant wellbore storage which is illustrated by the following figure.

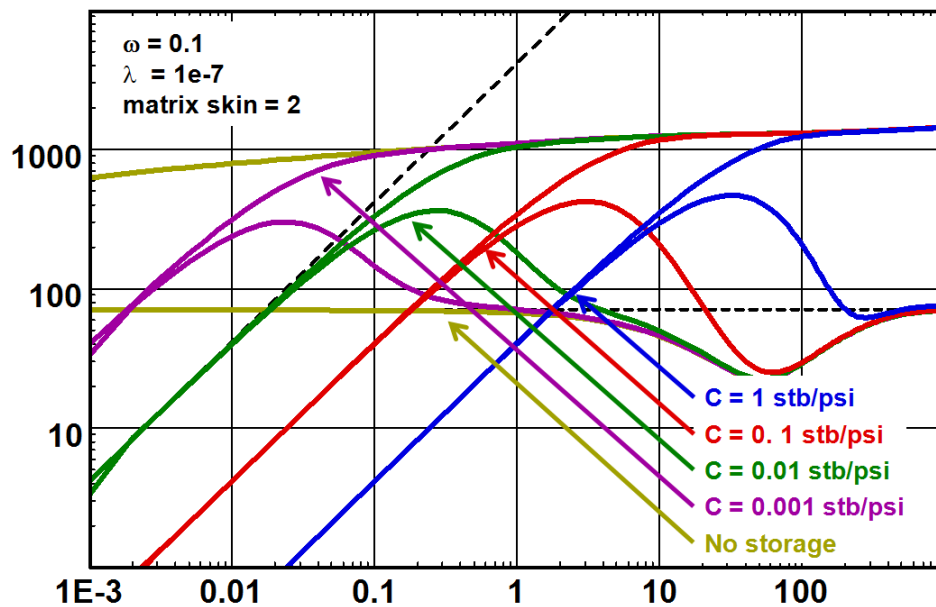


Fig. 7.D.6 – Transient, influence of wellbore storage

7.D.5 Effect of skin

The Bourdet derivative is not affected by the skin, except at very early time when the skin becomes very negative. In this case the behavior is similar to that of a fracture and linear flow in the fissure system may develop.

The below figure illustrates the model behavior with different skin values for the 'triple porosity' PSS reservoir.

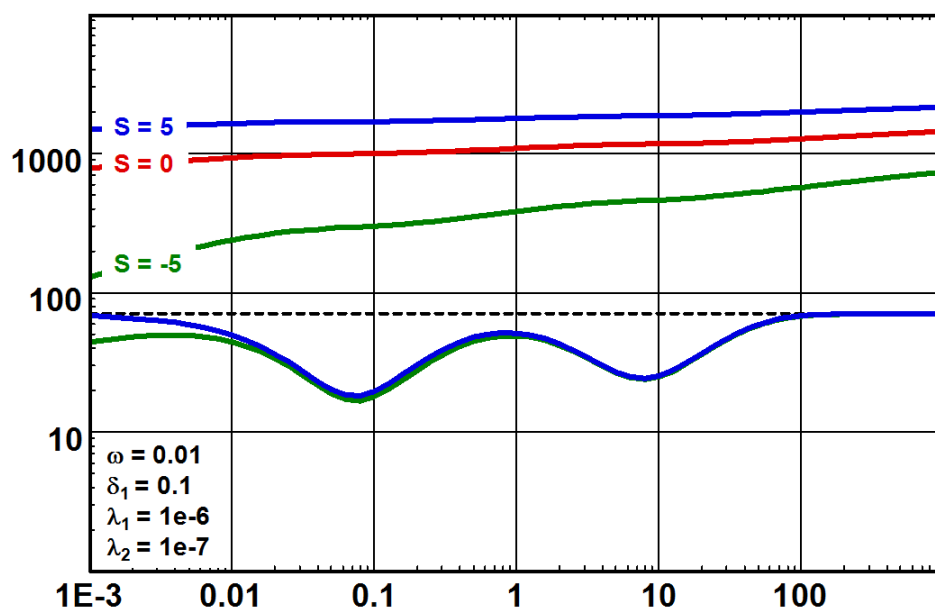


Fig. 7.D.7 – PSS influence of skin

Following we show the influence of the model skin (the skin acting between the well and the fissures) on the transient model with a constant matrix skin of 2 (the skin acting between the matrix blocks and the fissures).

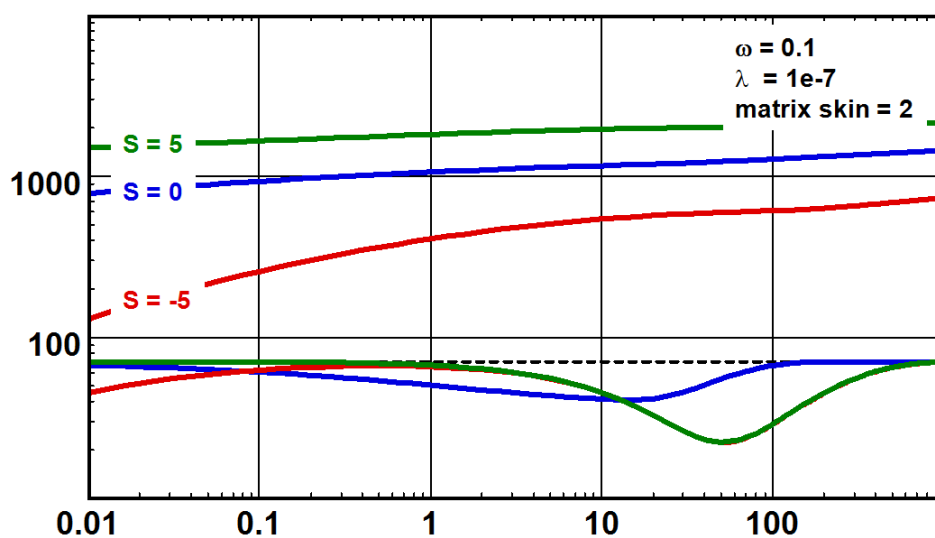


Fig. 7.D.8 – Transient, influence of skin

7.E Double-permeability reservoirs

7.E.1 Hypothesis

When is a layered reservoir not a layered reservoir? When each layer has the same properties, in which case the behavior of the system will be the equivalent behavior of the summed interval, it is homogeneous. However, the most pertinent question to ask is probably: "Does a homogeneous reservoir really exist? Just by the nature of the deposits would not most reservoirs be layered?"

Fortunately we know how to deal with layered systems.

In the double-permeability (2K) analytical model assumption the reservoir consists of two layers of different permeabilities, each of which may be perforated (contributing) or not. Crossflow between the layers is proportional to the pressure difference between them.

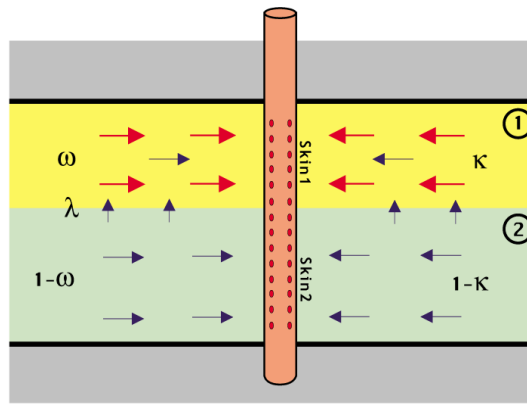


Fig. 7.E.1 – Double permeability reservoir

Making the comparison with the double-porosity PSS model, ω and λ have equivalent meanings. Adding one more leading parameter will describe the analytical model:

$$\omega = \frac{(V\Phi c_t)_1}{(V\Phi c_t)_1 + (V\Phi c_t)_2} \quad \lambda = \alpha r_w^2 \frac{(kh)_1}{(kh)_1 + (kh)_2}$$

ω , layer storativity ratio, is the fraction of interconnected pore volume occupied by layer 1, and λ , inter-layer flow parameter, describes the ability of flow between the layers. In addition another coefficient is introduced: κ is the ratio of the permeability-thickness product of the first layer to the total of both:

$$\kappa = \frac{(kh)_1}{(kh)_1 + (kh)_2}$$

Generally the high permeability layer is considered as layer 1, so κ will be close to 1. At early time there is no pressure difference between the layers and the system behaves as 2 comingled homogeneous layers without crossflow. As the most permeable layer produces more rapidly than the less permeable layer, a pressure difference develops between the layers and crossflow begins to occur. Usually the semi permeable wall hypothesis is applied and λ is dependent upon the thickness of the wall, its vertical permeability and the individual vertical permeability of the layers:

$$\lambda = \frac{r_w^2}{kh} \frac{2}{2 \frac{h'}{k_z} + \frac{h_1}{k_{z1}} + \frac{h_2}{k_{z2}}}$$

Assuming that the vertical permeability in the layers is the same, if no semi permeable wall or skin is present then:

$$k_z = kh \frac{\lambda}{r_w^2} \frac{h}{2}$$

Eventually the system behaves again as a homogeneous reservoir, with the total kh and storativity of the 2 layers.

A transitional dip is governed by ω and λ , which have the same effect as in the double porosity models, and κ , which reduces the depth of the dip as κ decreases. If $\kappa=1$ then $k_2=0$ and the properties of the low permeability layer is equivalent to that of the matrix blocks of a double porosity system and can only be produced by cross flowing to the high-permeability layer, equivalent to the fissure system in the double porosity model PSS.

7.E.2 Loglog behavior

The below figure illustrates the response in a well tested in a two layered system.

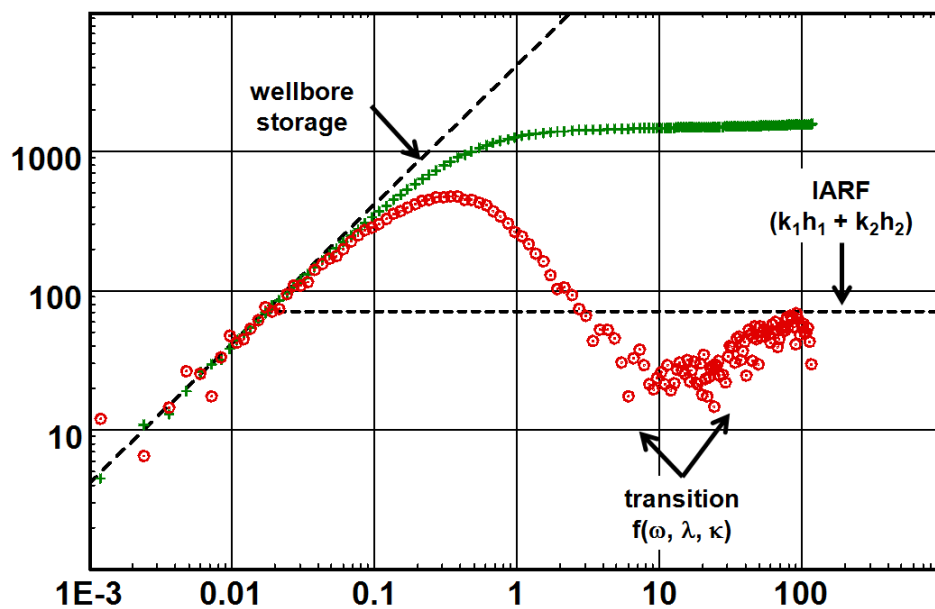


Fig. 7.E.2 – Loglog plot

The following figures illustrate the sensitivity to the parameters ω , λ and κ . Both layers are perforated and can produce to the well.

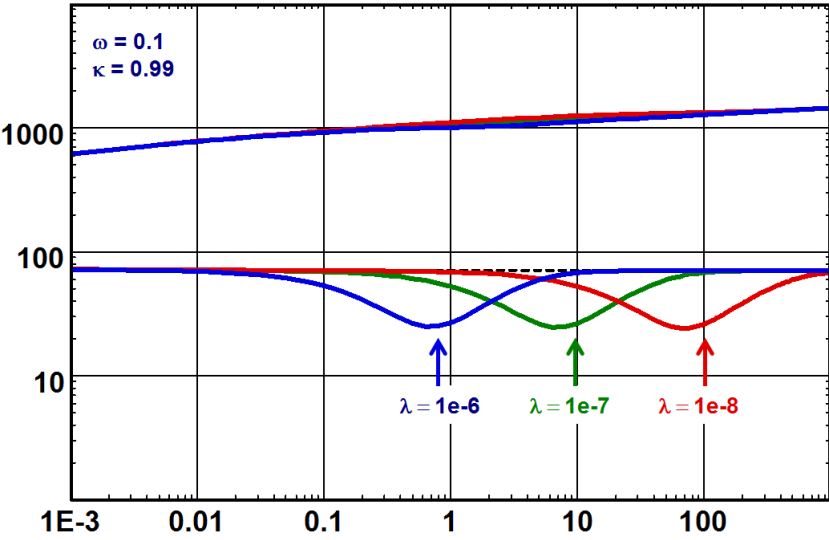


Fig. 7.E.3 – Influence of λ

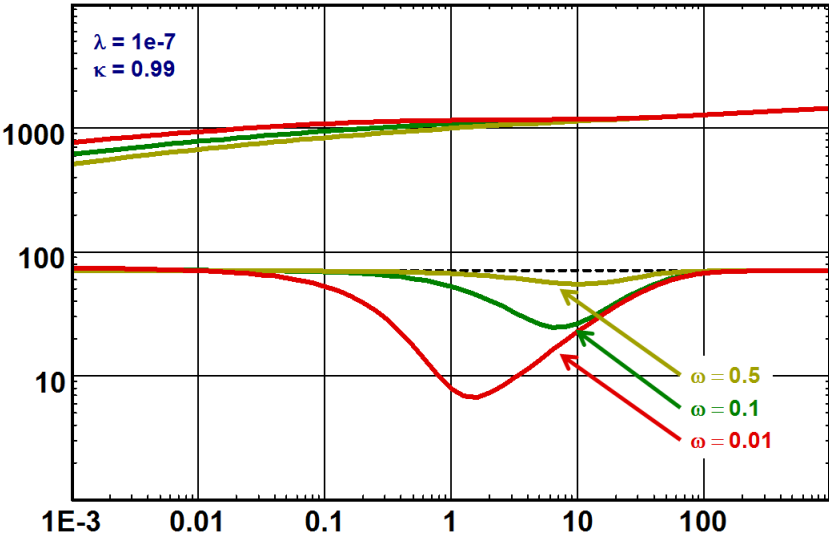


Fig. 7.E.4 – Influence of ω

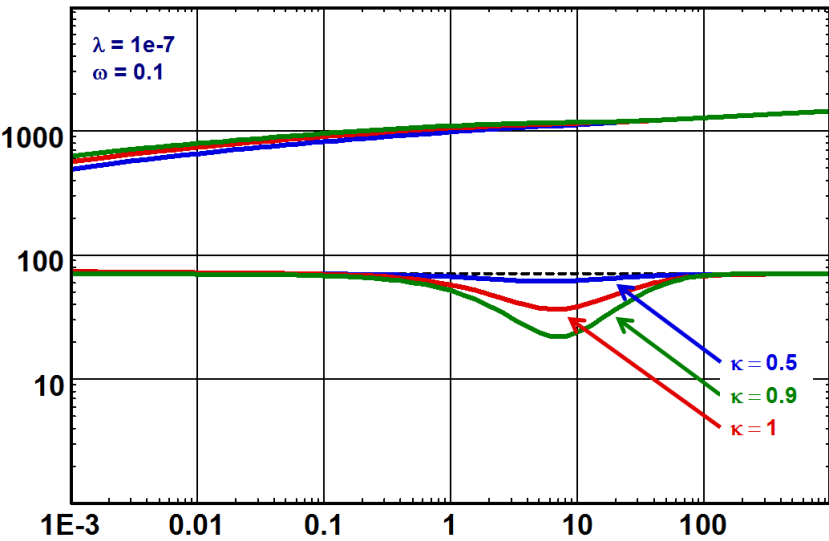


Fig. 7.E.5 – Influence of κ

7.E.3 Effect of wellbore storage

Wellbore storage will mask the transition. This is illustrated in the following figure.

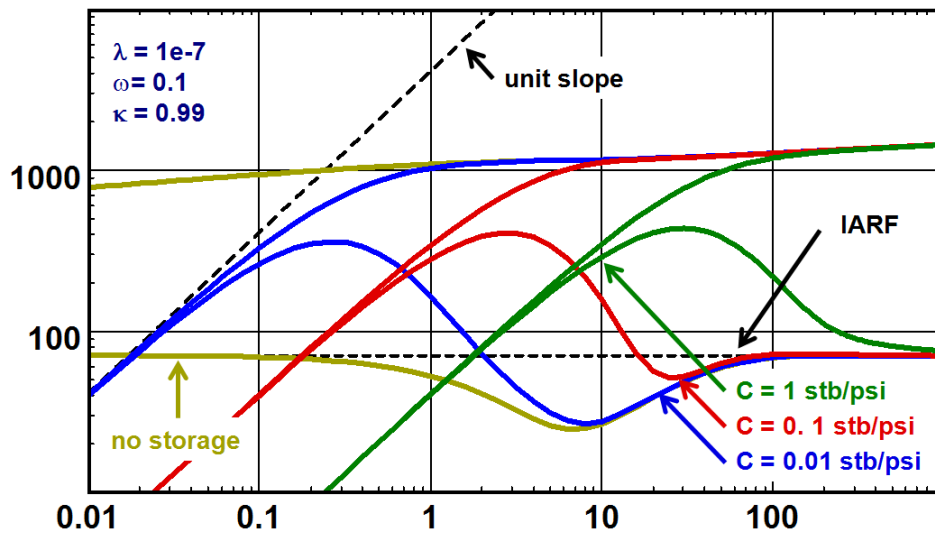


Fig. 7.E.6 – Influence of wellbore storage

7.E.4 Skin

Varying the skin in layer 2 has little or no impact on the model behavior as illustrated below.

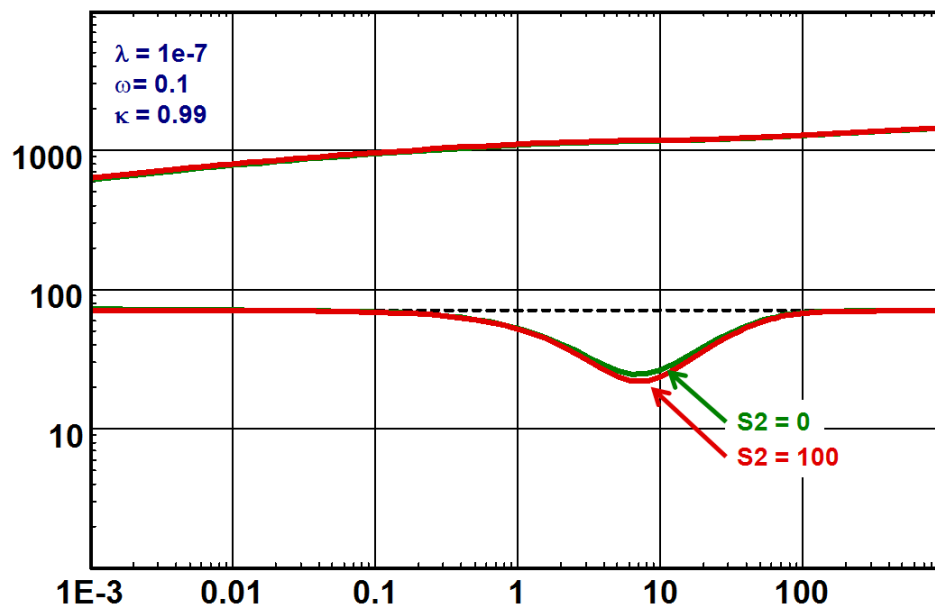


Fig. 7.E.7 – Influence of skin (S2)

However varying the skin in the high permeability layer sets up a totally different response and describes a different well configuration by using a reservoir model. The well could be perforated in the low permeability layer only or the high permeability layer could have been plugged at the well inducing a considerable skin. In this way the high permeability layer can only contribute to the production through reservoir cross flow to the lower permeability layer.

This is a scenario similar to that of limited entry or partial penetration, but in this case spherical flow will not quite develop. This well and reservoir configuration can easily be analyzed using the double permeability model by increasing the skin in layer 1 to simulate the high skin, plugging or non perforation of this layer. The below figure illustrates the behavior of the model as the skin in the high permeability layer increases.

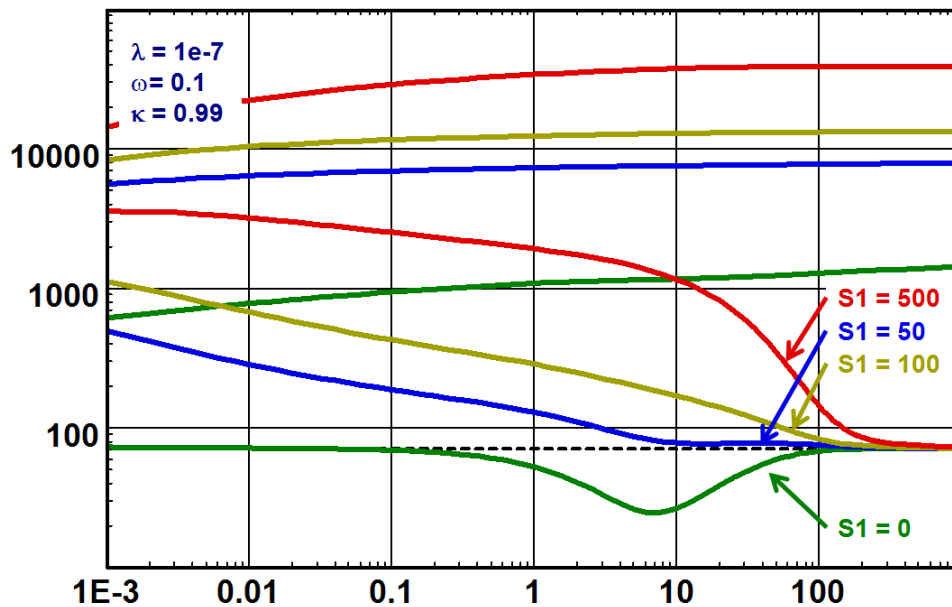


Fig. 7.E.8 – Influence of skin (S_1)

7.E.5 Field examples

To illustrate two real examples and their model match we present a classical double permeability response and a real example where the higher permeability layer was plugged. Later this diagnostic was confirmed by a production log and remedial action was successfully taken.

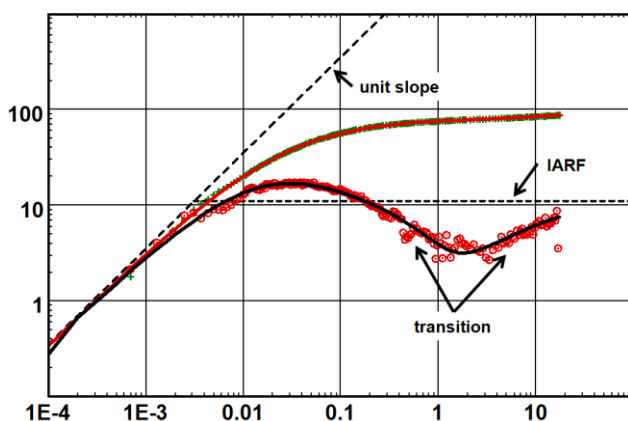


Fig. 7.E.9 – Classic double permeability

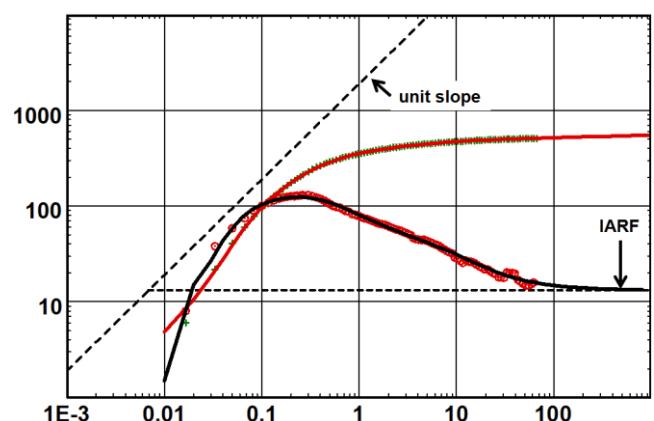


Fig. 7.E.10 – Double permeability layer 1 damaged

7.F Extension of double-permeability reservoirs

7.F.1 Multiple layers

The double permeability model can easily be extended to n-layers.

The two layer model can be applied to many cases in the measure that it is frequently possible to split a multilayer formation into two packs of layers and treat this as an equivalent two layer system. However, this may become an oversimplification and the use of more layers in the model can be necessary.

The same principle used in the double permeability solution can be directly extended to more than two layers.

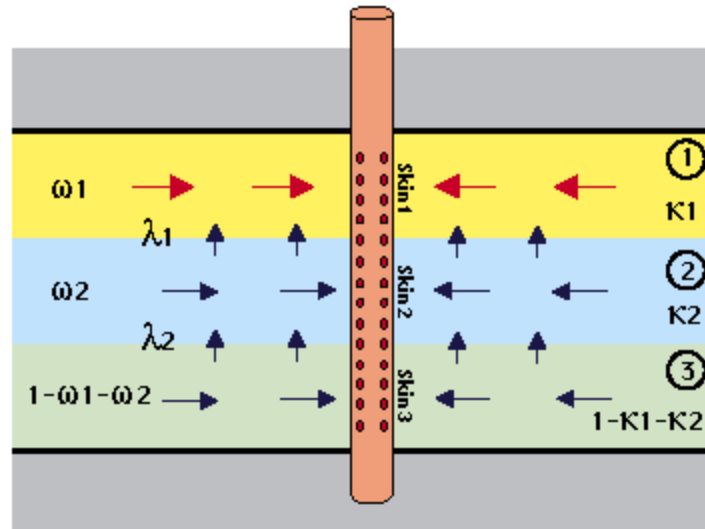


Fig. 7.F.1 – Three layers

The parameters already defined for the two layer case are extended to layer i :

ω_i , layer storativity ratio, is the fraction of interconnected pore volume occupied by layer (i) with respect to the total pore volume

$$\omega_i = \frac{(V\Phi c_t)_i}{\sum_j (V\Phi c_t)_j}$$

λ_i , inter-layer flow parameter, describes the ability of flow between the layer i and $i+1$:

$$\lambda_i = \alpha r_w^2 \frac{(kh)_i}{(kh)_i + (kh)_{i+1}}$$

κ_i is the ratio of the permeability-thickness product of the layer i to the total layers kh :

$$\kappa_i = \frac{(kh)_i}{\sum_j kh_j}$$

In this type of multi-permeability system one can expect to see as many heterogeneous responses as we have dual systems. This is as long as the parameters governing the heterogeneity are sufficiently different to not mask one another.

The below figure illustrates the behavior of a three layered model with cross flow. At early time, the layers are producing independently and the behavior corresponds to three layers producing without crossflow. When the first interlayer crossflow starts (interface with the greater λ value), a transition period is observed, shown by an inflection in the pressure response and a valley in the derivative.

After this first transition, the derivative comes back to its IARF stabilization and then exhibits a second transition. After all the transitions the reservoir acts as a homogeneous medium with total kh and storativity.

In the example only one parameter ω_2 , changes the overall shape of the response as an increase in ω_2 implies a decrease in ω_3 , therefore an inversion of contrast.

$$\omega_3 = (1 - \omega_1 - \omega_2) \text{ and } \kappa_3 = (1 - \kappa_1 - \kappa_2)$$

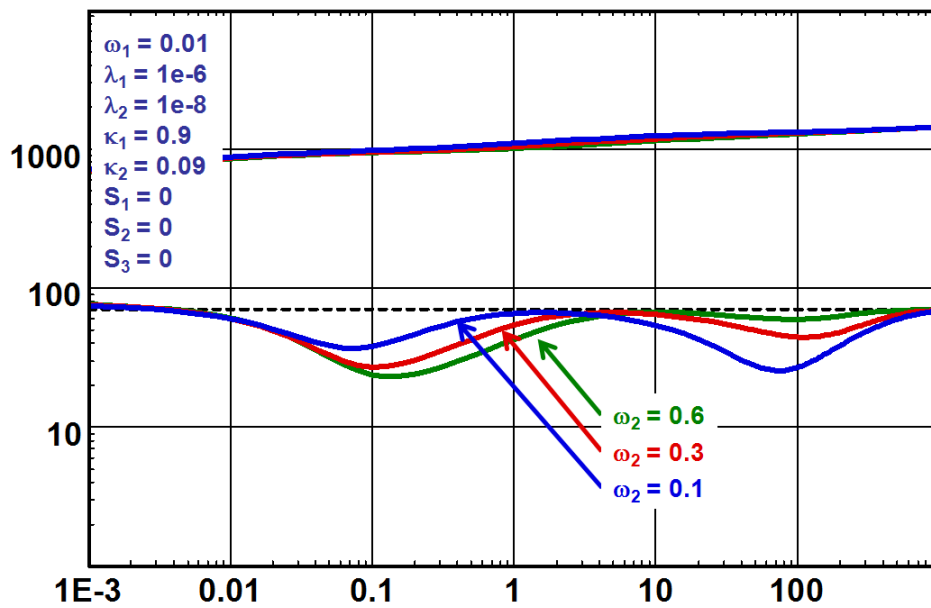


Fig. 7.F.2 – Three layers

The three layered model demonstrated here is part of the Saphir external model library. In this library also exists a 4 layered model with cross flow.

7.F.2 Numerical double permeability

The analytical double permeability model can easily be reproduced by a numerical multilayer model allowing cross flow. It suffices to define a leakage factor between the layers. The layers are isotropic and the vertical permeability is equivalent to the harmonic average of the layer permeabilities:

$$k_z = \frac{(h_1 + h_2)}{\left(\frac{h_1}{k_{z1}} + \frac{h_2}{k_{z2}} \right)}$$

And the relationship with λ is:

$$k_z = kh \frac{\lambda}{r_w^2} \frac{h}{2}$$

The leakage factor has a value between 1 (full leakage) and 0 (no cross flow).

The use of numerical models to simulate complex layered formations is detailed in the chapter 'Multilayered models'.

Each layer can produce to the well or be completely blocked off thus only producing through cross flow.

The below figures illustrates the response of the numerical simulator with two layers with various leakage factors and the response when the high permeable layer has been selectively shut off (this is a feature of the numerical multilayered model, one can selectively shut off or open individual layers for flow to the well).

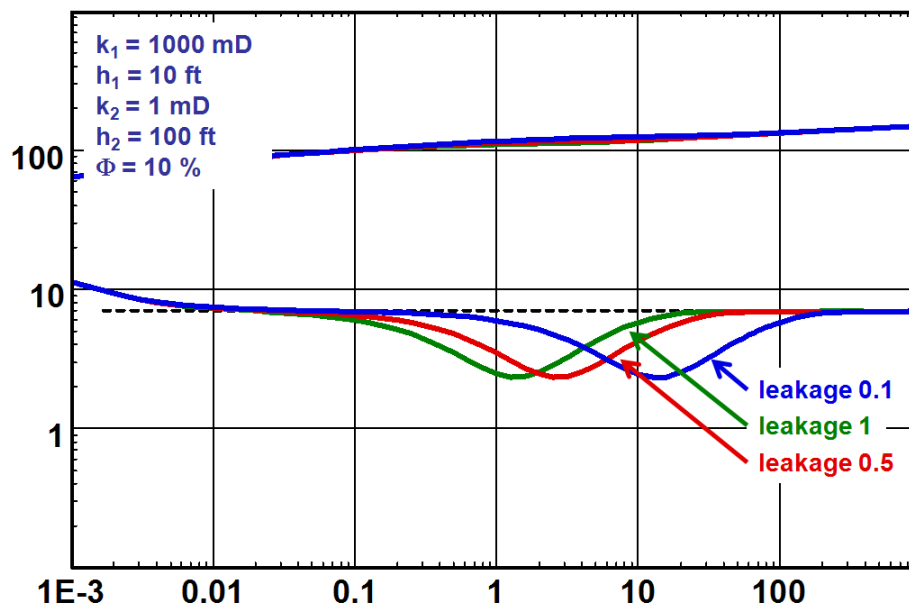


Fig. 7.F.3 – Numerical two layers both producing to the well

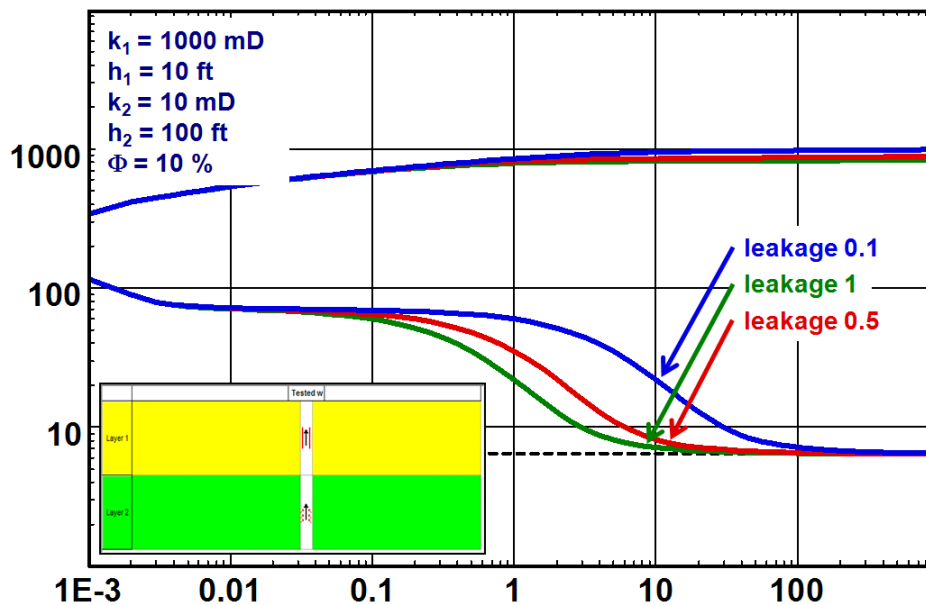


Fig. 7.F.4 – Numerical two layers, high permeability layer shut off

7.G Multilayered reservoirs

In this section we will present the multilayered analytical model and briefly describe the multilayer numerical solution available in the KAPPA suite of programs. As opposed to the double permeability solution presented earlier in this chapter, the multilayer analytical model assumes that the layers produce comingled to the well without any reservoir cross flow. This assumption is crucial and fundamental and leads us immediately to kill one of the biggest myths in well testing of multilayered reservoir:

If the layers are homogenous and infinite and even if the initial pressures of each layer is different we will not be able to differentiate the behavior of each layer in the common pressure response measure in the wellbore. The response measured at the pressure gauge is simply the global response.

Now, any text book with some respect for itself will invariably present a pressure response that wonderfully show the behavior of at least two and sometimes several layers. And this is possible if one or several of the layers are bounded. The boundaries are described in more detail in the chapter on 'Boundary models', however we show below the response of a two layered system where one layer is infinite and the other layer is just a small sand lens. And, yes, the first stabilization of the derivative corresponds to the total kh , the second level corresponds to the permeability thickness product of the infinite layer. The unit slope response in the middle of this buildup reflects the bounded layer and the distance (to the boundaries) can be deduced. This type of behavior can also easily be described by a composite model as it is a limiting case of the radial composite model, so the reader be aware.

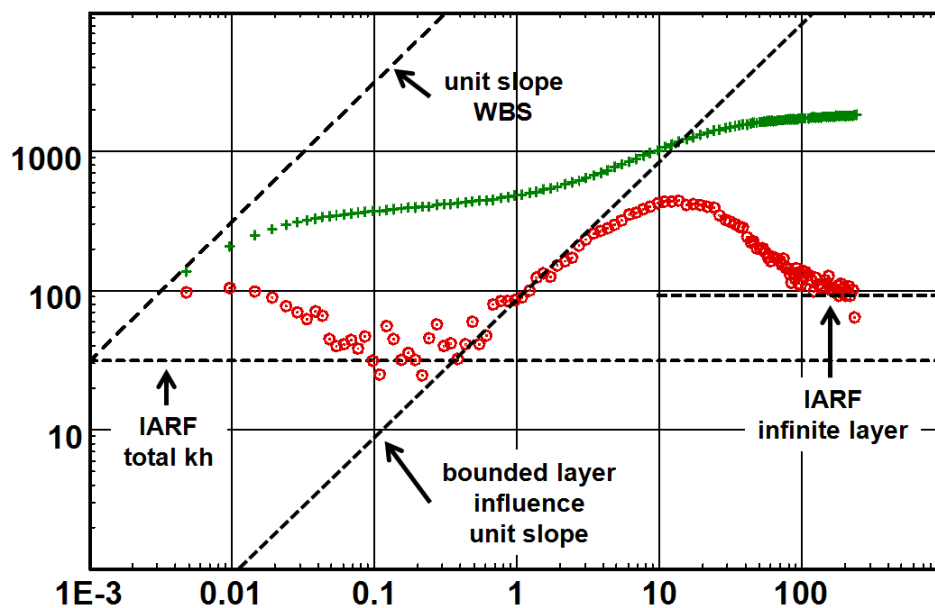


Fig. 7.G.1 – Two layers, one layer bounded the other infinite

To reiterate on the above observations, the behavior of any multilayered system as long as each layer is homogeneous and infinite acting, the model response will be an equivalent global response with early time wellbore storage and a global stabilization at the level of total kh ;

$$(kh)_{total} = \sum_{i=1}^n k_i h_i$$

With total skin

$$S_T = \sum_{i=1}^n \frac{S_i k_i h_i}{(kh)_{total}}$$

7.G.1 Hypothesis

The reservoir has n layers; each layer can have a well model as the well models already described in the chapter on 'Well models'. The reservoir model of each layer can be any of the reservoir models already presented in this chapter and each layer can have boundary configurations as those presented in the chapter on 'Boundary models'. The initial pressure P_i can be different from layer to layer.

The analytical model does not allow any cross flow between the layers in the reservoir thus the production to the well is comingled. Cross flow between layers is allowed in well.

The total behavior of each model will be a superposition of each layer behavior, thus it is far too complex to generalize the model behavior in a similar manner compared to that done with the other reservoir models described elsewhere in this chapter.

The concept of pattern recognition and the identification of the different flow regimes during a flow period to be analyzed is no longer a straight forward task. The notion of solving the 'inverse' problem is no longer an issue. In order for the engineer to come up with a plausible answer to the problem he has to rely more heavily on other results and measurements done in the well. Open hole logging, cores and seismic are some of the data that will and has to influence the model choice and the final interpretation.

And finally, the layer contributions; this can be the individual rate of each layer or a combination of rates at different stations in the wellbore. Without the layer rates the engineer is faced with a task he can rarely win.

But we are the bearer of good news; the multilayer model can include the individual layer rates or a combination of different layer contributions. And the best news is that the layer rates or transient layer rates can be taken into account when optimizing the solution with non linear regression. In fact the only way to give a solution a proper chance is to include the layer rates in the object function thus optimizing with the layer rates becomes a part of the method for solving the multilayer transient test problem.

So, the bad news is that without production logging, PTA with the objective to assign individual reservoir characteristics and skin to each layer is virtually impossible with any confidence. Not knowing the layer contributions will open a 'Pandora box' that is so full of different models and leading parameters of which any combination can produce the same response, that it may become impossible to make a reasonable choice.

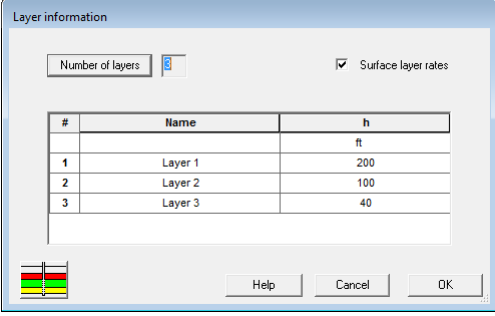
In fact the problem is expanded to what we are often up against with even simpler models; the solution is very far from unique.

As already stated the model response will be a superposition of the different well and reservoirs models assigned to each layer thus it is impossible to describe this in any detail over a few pages. The model response of the various well models is covered in the chapter on 'Well models', the reservoir responses are covered in this chapter, and the boundary responses are covered in the chapter on 'Boundary models'.

We will however, in the following section, describe how we build a multilayer model in the PTA (Saphir) or PA (Topaze) KAPPA suite of programs.

7.G.2 How to build a multilayer model

The first task is to define the number of layers and their thickness. At the same time one can define if the layer rates or the layer contributions are reported at surface or downhole conditions. A word of advice here; in the KAPPA suite of software (Topaze and Saphir) the layer contribution is identical to the individual layer rate and layer rates are the rates measured at the top of each layer i. e. the depth cumulative rate.



Layer information

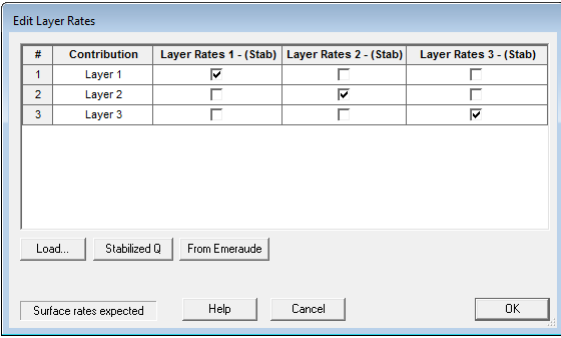
Number of layers: 3 ☒ Surface layer rates

#	Name	h
		ft
1	Layer 1	200
2	Layer 2	100
3	Layer 3	40

Help Cancel OK

Fig. 7.G.2 – Defining the geometry and flowrate conditions

The layer rates will have to be loaded either as a compatible file, from Emeraude or by hand. The rate is usually measured during production logging and can be transient stationary rates versus time or is the result of a production log versus depth interpretation, such as provided using Emeraude.



Edit Layer Rates

#	Contribution	Layer Rates 1 - (Stab)	Layer Rates 2 - (Stab)	Layer Rates 3 - (Stab)
1	Layer 1	<input checked="" type="checkbox"/>	<input type="checkbox"/>	<input type="checkbox"/>
2	Layer 2	<input type="checkbox"/>	<input checked="" type="checkbox"/>	<input type="checkbox"/>
3	Layer 3	<input type="checkbox"/>	<input type="checkbox"/>	<input checked="" type="checkbox"/>

Load... Stabilized Q From Emeraude

Surface rates expected Help Cancel OK

Fig. 7.G.3 – Defining the layer rates

The next step is to define the layer's well, reservoir and boundary model and the layer characteristics.

The Multi-Layer Model dialog box is shown with the 'Layer properties' tab selected. It displays a global reservoir model with three layers: Layer 1 (yellow, 200 ft), Layer 2 (green, 100 ft), and Layer 3 (red, 40 ft). The 'Wellbore model' is set to 'Constant wellbore storage'. The 'Individual layer model' is set to 'Layer 1' with 'W. Vertical', 'R. Homogeneous', and 'B. Infinite' options. The 'Wellbore & other reservoir parameters' table is also visible.

Parameter	Value	Unit
Layer 1		
Skin	5	
k	12	md
h	200	ft
Phi	0.1	
Layer 2		
Skin	0	
k	3	md
h	100	ft
Phi	0.1	
Layer 3		
Skin	7	
k	260	md
h	40	ft
Phi	0.1	
Wellbore & other reservoir parameters		
Pi	5000	psia
C	0.001	bb/psi

Fig. 7.G.4 – Defining the model and characteristics

Layer name	h	k	kh	Phi	Phi.Ct.h	% k.h	% Phi.Ct.h
	ft	md	md.ft		ft.psi-1		
Layer 1	200	12.2084	2441.69	0.1	6E-5	19.2859	58.8235
Layer 2	100	5.46416	546.416	0.1	3E-5	4.31591	29.4118
Layer 3	40	241.81	9672.38	0.1	1.2E-5	76.3982	11.7647
All Layers	(total)	(average)	(total)	(average)	(total)	(total)	(total)
	340	37.2367	12660.5	0.1	1.02E-4	100	100

Fig. 7.G.5 – List of layer characteristics

Generate the model and adjust the parameters by hand or run the improve option. To add the layer rates in the objective function of the nonlinear regression the optimization is carried out on the history (simulation) plot.

The Multi-layer improve dialog box is shown with the 'Improve Settings' tab selected. It displays a global reservoir model with three layers: Layer 1 (yellow, 200 ft), Layer 2 (green, 100 ft), and Layer 3 (red, 40 ft). The 'Improve Settings' section shows 'Improve on' set to 'simulation' and 'include layer rates' checked. The 'Parameter' table shows the minimum, value, and maximum for each parameter.

Parameter	Minimum	Value	Maximum
Layer 1			
Skin	-10	5.22526	10
k	3.16423	12.2084	316.423
Layer 2			
Skin	-10	5.05802	10
k	3.16423	5.46416	316.423
Layer 3			
Skin	-10	5.91699	10
k	3.16423	241.81	316.423
Wellbore & other reservoir parameters			
Pi	494.827	5000	49482.7
C	1.11475E-4	0.00102215	0.011147

Fig. 7.G.6 – Running improve including layer rates

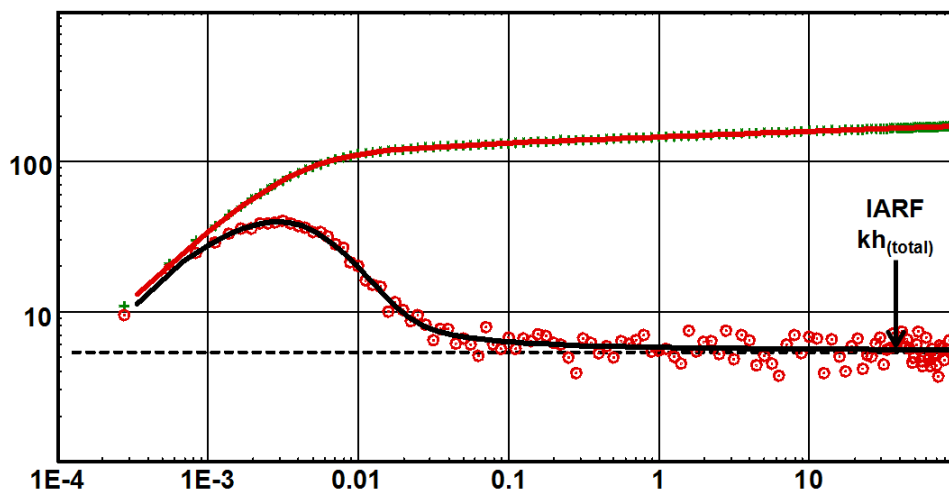


Fig. 7.G.7 – Multilayer model match

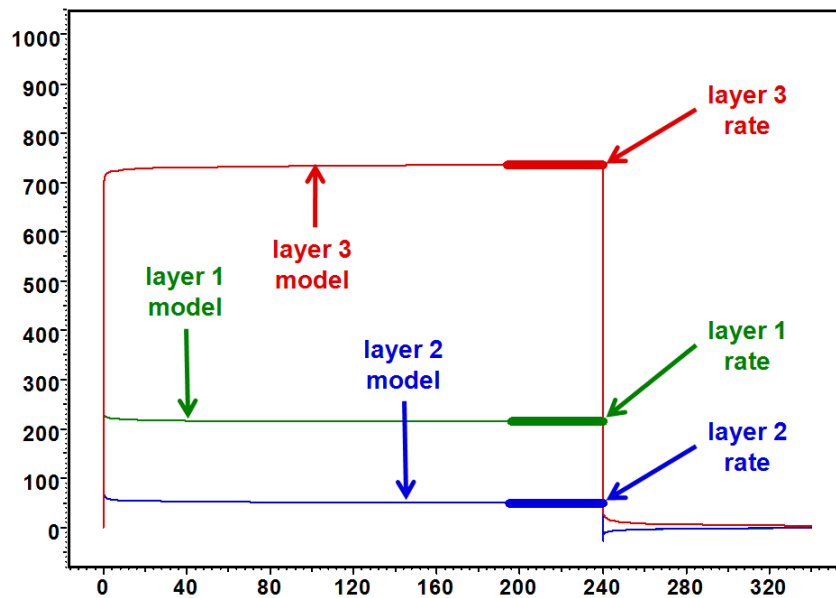


Fig. 7.G.8 – Layer contribution match

A numerical multilayer model is also available. The numerical model is more flexible and allows cross flow in the reservoir. This is defined either as a leakage factor, an equivalent vertical permeability or the classical lambda coefficient of a double permeability reservoir. Each layer can also be specified as perforated (communicating with the well) or not.

There are various multilayer tests subject to pressure transient analysis; all of the tests involve in a form or another, the use of production logging tools to capture the production of the layers. These tests and their analysis approach is cover in the chapter on 'PTA – Special test operations'.

7.H Composite reservoirs

7.H.1 Hypothesis

Up to this point the models assumptions were uniform with constant saturations, mobility and effective permeability. In most cases this assumption is valid within the time limits of a well test and radius of investigation. However, in some cases it will be necessary to consider a variation in the mobility in the lateral direction.

The most common cases where one can observe a change in mobility in the reservoir area are:

- Injection of a fluid different to the reservoir fluid
- Change in saturation due to an aquifer
- Change in saturation due to a gas cap
- Change in lateral saturation due to production below bubble or dew point
- Compartmentalization
- Facies changes
- Actual changes in reservoir characteristics (k , Φ)

The analytical solutions which model these cases are called composite models. Their geometry is quite straightforward and they are governed by two simple parameters.

The most common analytical composite models are the radial and the linear composite. The radial composite geometry is centered at the well, and r_i is the radius of the inner compartment.

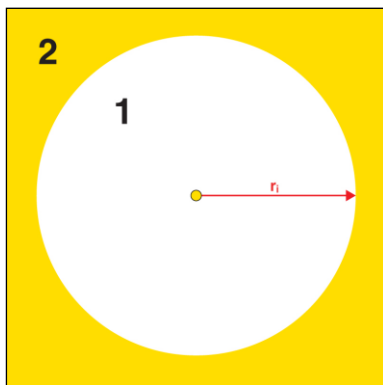


Fig. 7.H.1 – Radial composite reservoir

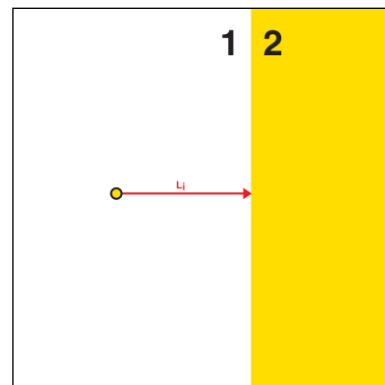


Fig. 7.H.2 – Linear composite reservoir

For the linear composite reservoir (of infinite extent), the corresponding parameter will be L_i , the distance from the well to the mobility change.

When one reference is chosen, the properties of the other compartment are calculated from the first using two parameters:

The mobility ratio $M = (k/\mu)_1 / (k/\mu)_2$

The diffusivity ratio $D = (k/\Phi\mu c_t)_1 / (k/\Phi\mu c_t)_2$.

It is interesting to introduce the ratio $M/D = (\Phi c_t)_1 / (\Phi c_t)_2$.

We see that the ratio M/D represents the compressibility ratio which is often taken, as a first approximation, equal to 1 when both fluids are of the same.

Below we illustrate the pressure profile for a radial and a linear composite reservoir. At the composite interface, there is no pressure loss but a change in the pressure gradient. The flux on both sides is the same, but because the mobility is different Darcy's law will give two different pressure gradients.

At early time, the pressure will diffuse in compartment 1 only, and the behavior will be homogeneous. When the composite limit is detected, there will be a change of apparent mobility and diffusivity.

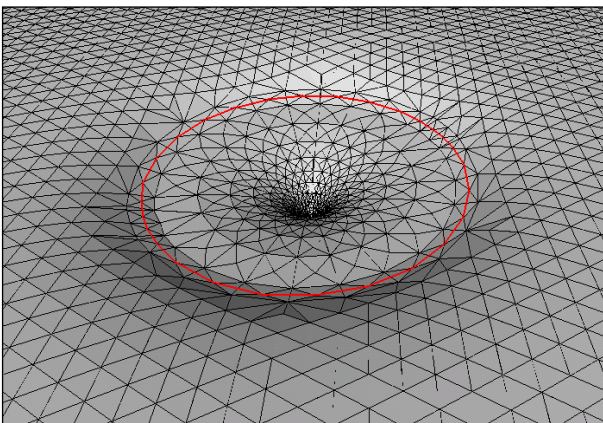


Fig. 7.H.3 – Radial composite pressure profile

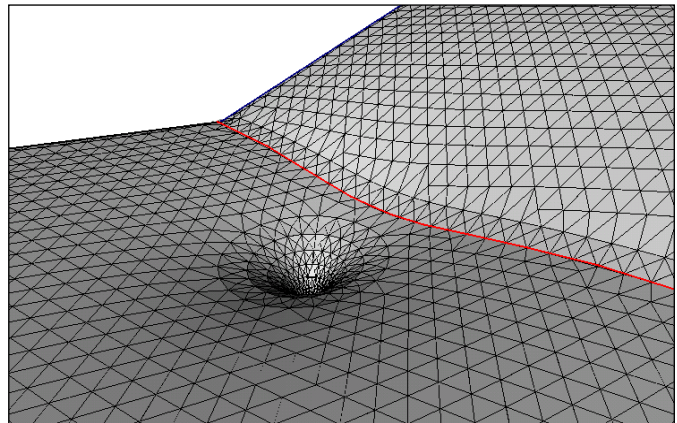


Fig. 7.H.4 – Linear composite pressure profile

With the radial composite reservoir, the apparent mobility and diffusivity will move from the inner values (compartment 1) to the outer values (compartment 2), the final mobility will be that of compartment 2. For the linear composite reservoir, after the transition, the final apparent mobility and diffusivity will be the average of compartments 1 and 2.

7.H.2 Loglog behavior

The following figure illustrates the response (buildup) of a typical well in a (radial) composite reservoir.

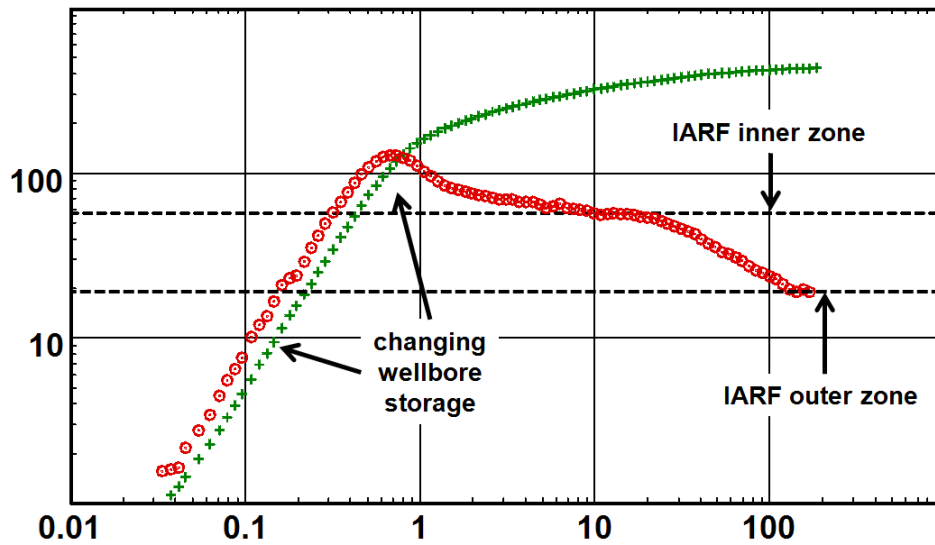


Fig. 7.H.5 – Radial composite buildup response

The following figures show the loglog response of a radial composite reservoir with constant distance to the interface and several values of $M=D$. The time at which the derivative deviates from the initial IARF (compartment 1) to the final IARF (compartment 2) is linked to r_i with the same relation as for a sealing or constant pressure boundary. The ratio between the final and initial derivative level will be that of the ratio between the initial and the final mobility, equal to M . When $M=D=1$, the response is obviously homogeneous.

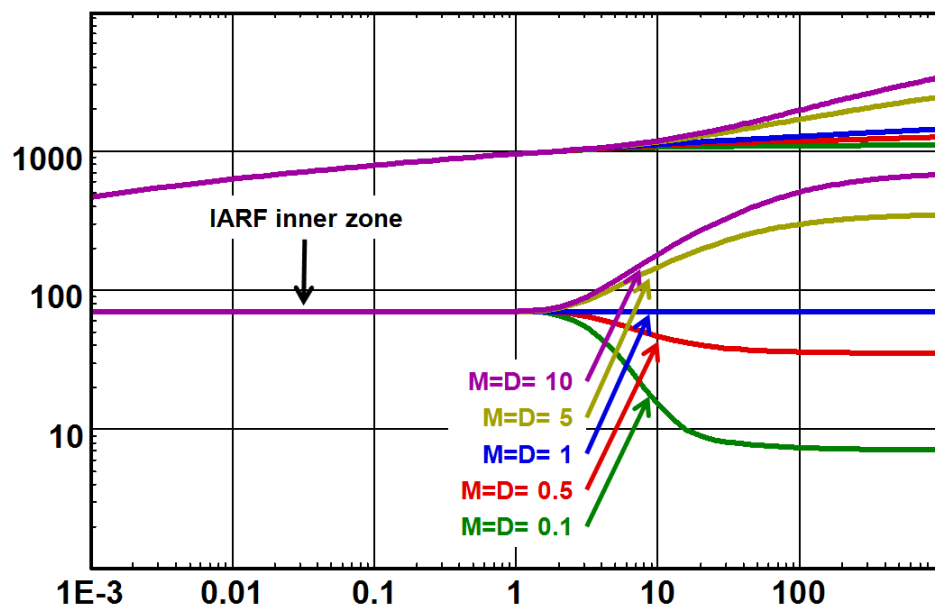


Fig. 7.H.6 – Loglog response, radial composite

Below is the loglog responses for the same parameters, but now in a linear composite reservoir. The final stabilization corresponding to the average of compartments 1 and 2, the transition will be smoother, and it is easy to show that the ratio between the final and initial derivative level will be $2M/(M+1)$.

When M tends to infinity, i.e. the permeability of the outer compartment tends to zero; this ratio will tend to 2. This corresponds to the particular case of a sealing fault. When M tends to zero, the permeability of the outer compartment tends to infinity and the pressure will be sustained at initial pressure at the boundary. This is the particular case of a constant pressure linear boundary.

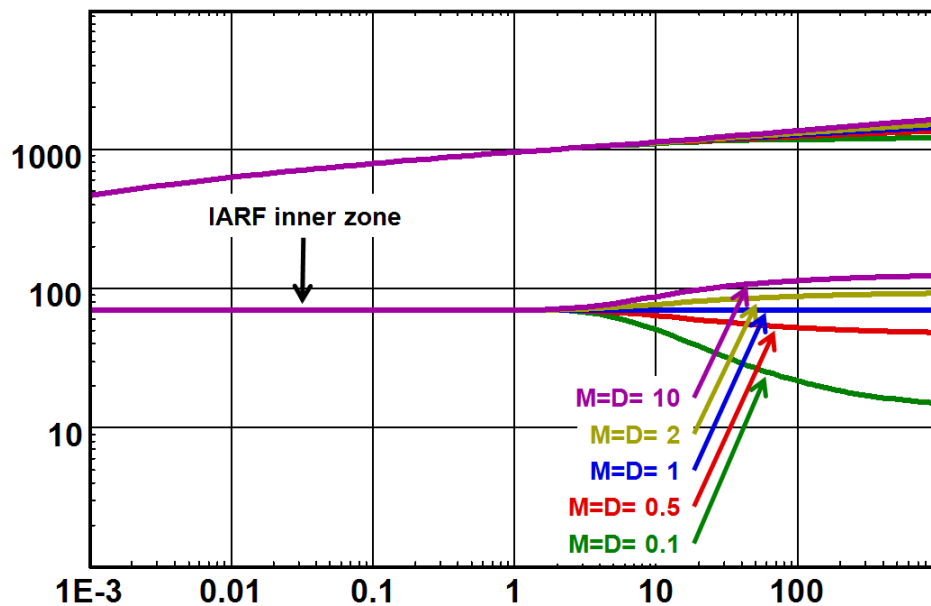


Fig. 7.H.7 – Loglog response, linear composite

To illustrate the behavior of the model when mobility and diffusivity is no longer equal we have generated the radial composite model under different scenarios.

Following is a figure where the mobility M is kept constant and varying the diffusivity ratio D .

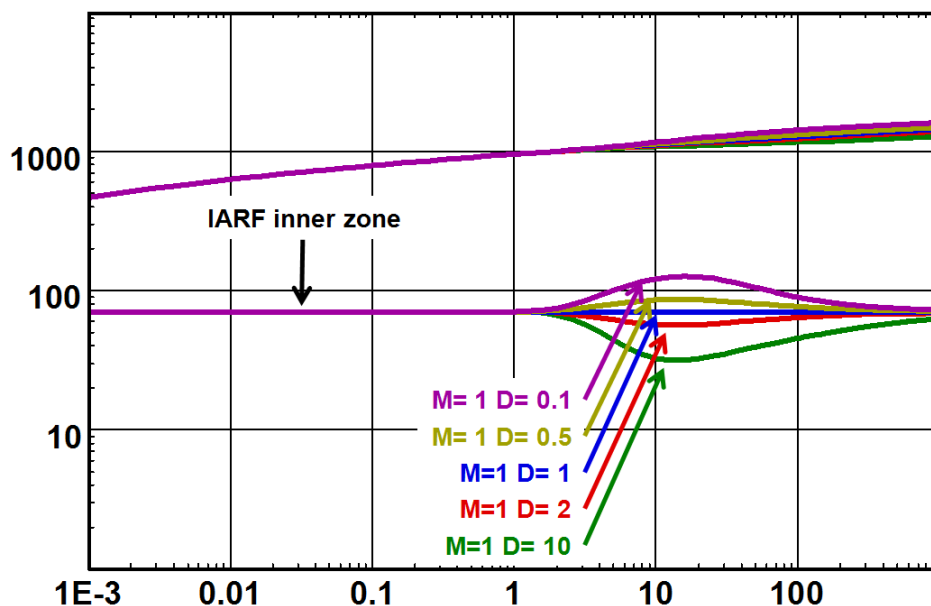


Fig. 7.H.8 – Loglog response, radial composite $M \neq D$

Depending on the value of D , the derivative will deviate upwards ($D < 1$) or downwards ($D > 1$). The response with a valley is qualitatively close to a double-porosity behavior. The difference in shape comes from the fact that this change of storativity occurs in compartment 2 only, while in the double-porosity model it occurs everywhere.

In the general case where M and D are different, the derivative will go from the IARF level of the inner zone to the final level being a function of M only. There will be an upwards transition when $D < M$ and a downwards transition when $D > M$.

7.H.3 Specialized analysis

Theoretically the semilog plot will exhibit two straight lines, the first line corresponds to the mobility in the inner zone, the second to the outer zone if the system is radial composite or the average of the two zones in the case of linear composite. The ratio of the slopes will give M (radial) or $2M/(M+1)$ (linear). For buildups the intercept of the second line can be extrapolated to p^* , while the skin will be given by the first straight line (inner zone) analysis.

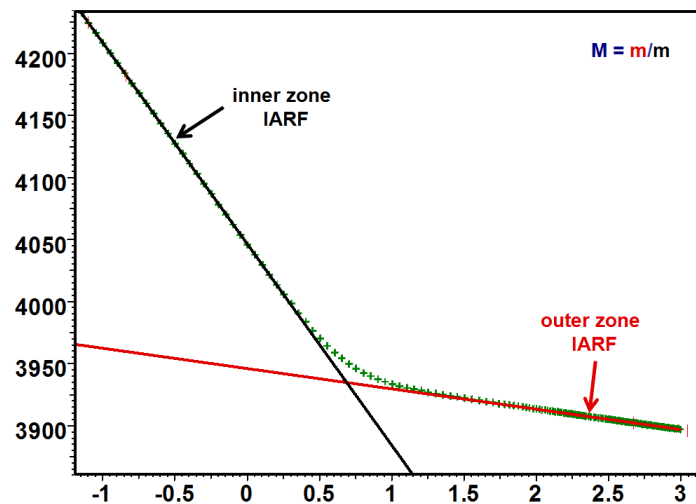


Fig. 7.H.9 – Semilog plot, radial composite

7.H.4 Effect of wellbore storage

Increasing the wellbore storage will mask the inner radial flow. The effect on the outer IARF is negligible as this is a flow regime that happens at relative late time. See the below illustrations.

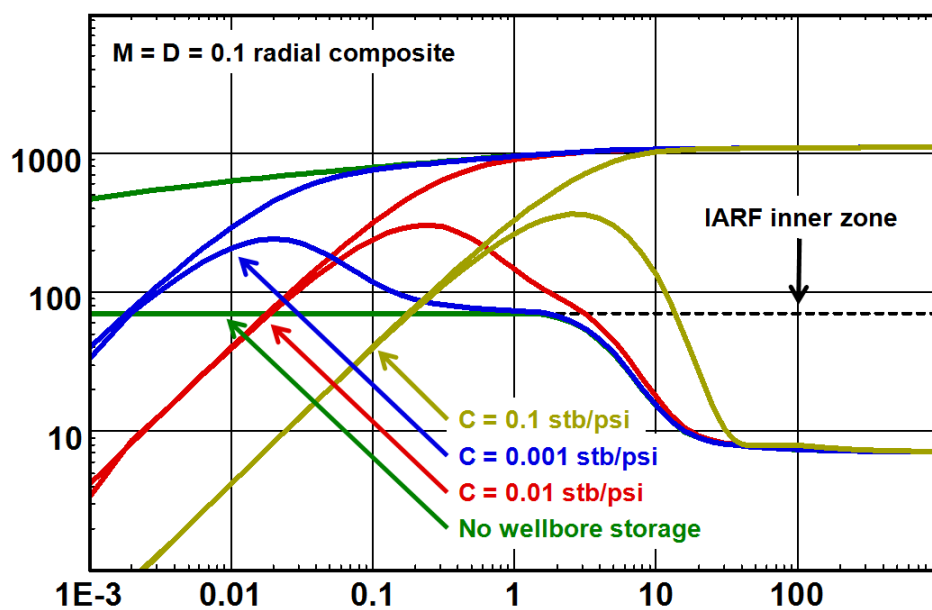


Fig. 7.H.10 – Influence of wellbore storage

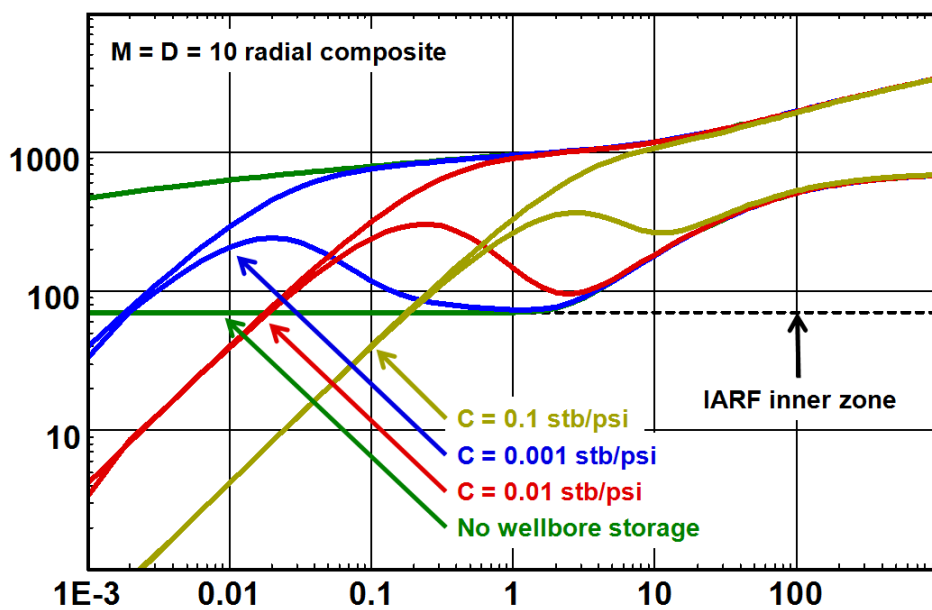


Fig. 7.H.11 – Influence of wellbore storage

7.H.5 Skin

The skin can be evaluated using the classical semilog methods. The 'inner zone' radial flow will give the well skin and the 'outer zone' radial flow will return a 'total skin'. This 'total skin' is defined by the two components:

$$S_T = \frac{1}{M} S_{(inner\ zone)} + \left(\frac{1}{M} - 1 \right) \ln \frac{r_i}{r_w}$$

When $M < 1$ we say that the mobility increases at some point further away from the well and often we consider that the inner zone as being damaged by invasion or other causes. This gives rise to the concept of a skin with 'dimensions'. The literature contains many examples of this behavior, whether due to actual damage or some other phenomena such as changes in fluids or geological facies. What the literature is missing is actual proof that remedial action can in fact connect the better mobility reservoir directly to the well thus bypassing the 'block' and increase the well performance. See the section in this chapter on "When should we use a composite model?".

The following figure illustrates the model behavior with a changing well skin with $M < 1$. A positive skin has no influence on the Bourdet derivative. A negative skin will affect both the derivative and the pressure change as the early time behavior approached the behavior of a fracture.

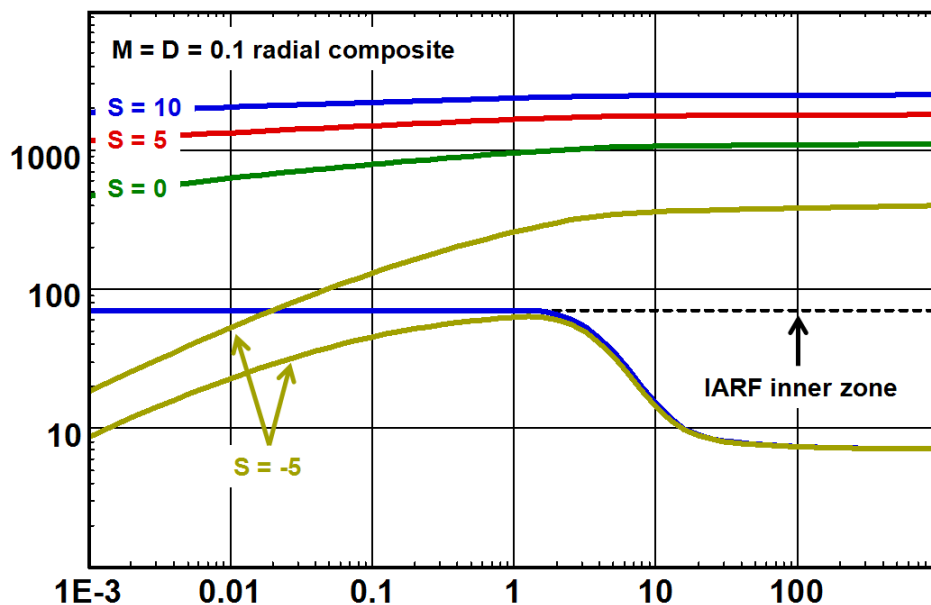


Fig. 7.H.12 – Influence of skin, $M < 1$

Below we show the skin behavior when $M > 1$.

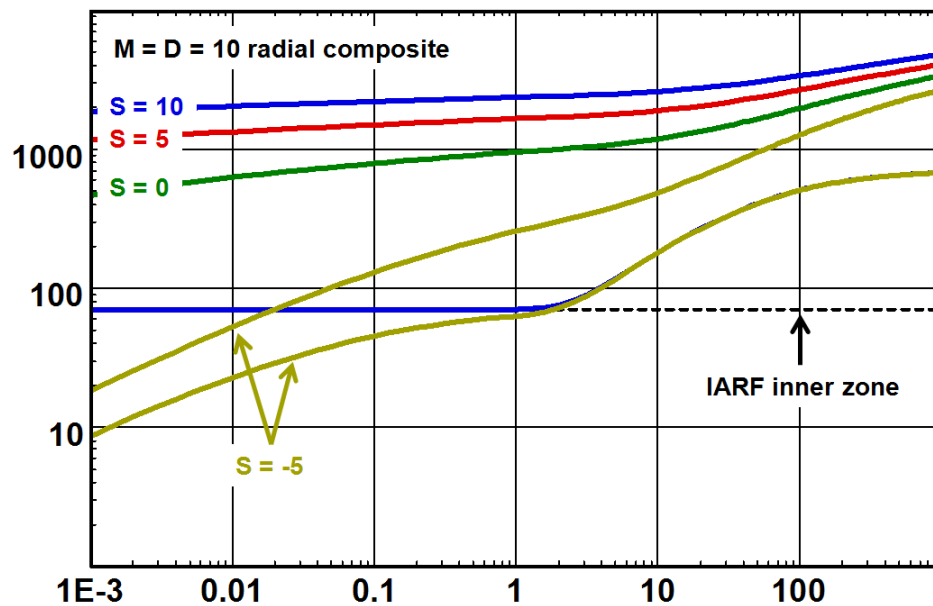


Fig. 7.H.13 – Influence of skin, $M > 1$

7.H.6 Extensions of the composite reservoir

The above composite models are used as simplified approaches to simulate fluid saturation variations, facies changes and damage.

In some cases these assumptions may be too simplistic; e. g. when a producing well is surrounded by multiple fluid annuli, due to particular PVT characteristics creating gas blocking or condensate banks. There may be more than one distinct change in the facies properties. In these cases several condition changes can take place close to the well and will require a multiple radial change model.

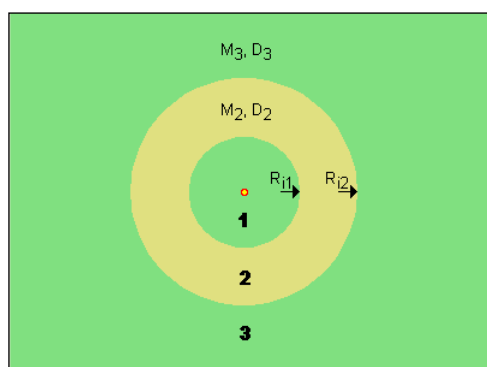


Fig. 7.H.14 – 3 zone radial composite

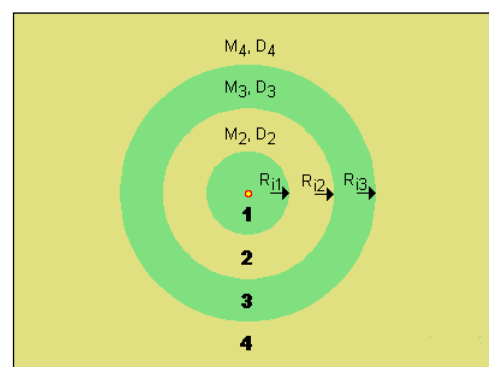


Fig. 7.H.15 – 4 zone radial composite

The parameters M_i and D_i in the model have respectively the same definition as in the simple model described above. The below figure illustrates the response where a four zone radial composite model has been used.

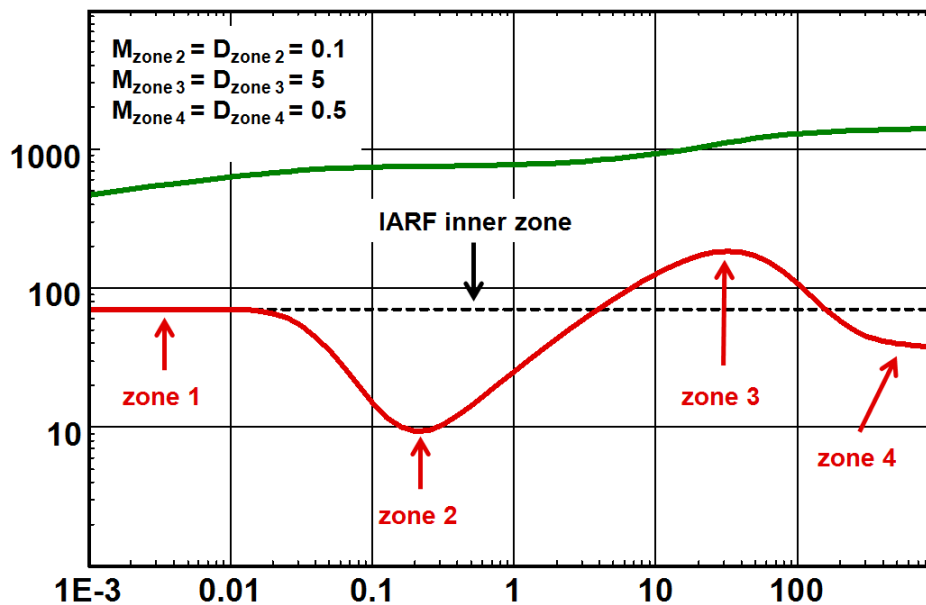


Fig. 7.H.16 – 4 zone radial composite

Now the question is, are these models really useful? Jumping forward and bearing in mind the paragraph on 'When should we use a composite model?' in this chapter, the answer is yes, but not in the hands of a novice interpreter. These models are certainly not to be used as a last resort just to obtain a match for the sake of making the match only and ignoring the physical implications that comes with the description of the model.

The obvious draw back that can make its use dubious is the fact that strictly speaking everything has to be perfectly radial which in real life is clearly not the case. However, we have to understand that when we use such models, and any analytical models for that matter, we are looking for an equivalent behavior. These models are particularly useful to describe changes in fluid banks close to the well. Production can be close to or below the bubble point pressure in a bubble point fluid and the gas saturation can vary radially away from the well. Thus there can be zones with both movable and immovable gas governed by the critical saturation. This can give rise to various zones of different mobilities and even gas blocking.

In a dew point type of fluid, different saturation fluid banks may build up around the well and again give rise to a variation of the mobility.

The physical properties may very well change and even gradually change as the distance increases from the well, thus a composite behavior is not only possible but common.

The below figures illustrates the changing mobility of a 'gas block' matched with a multiple zoned radial composite analytical model. The other figure illustrates the match of a response cause by condensate 'banking' around the well.

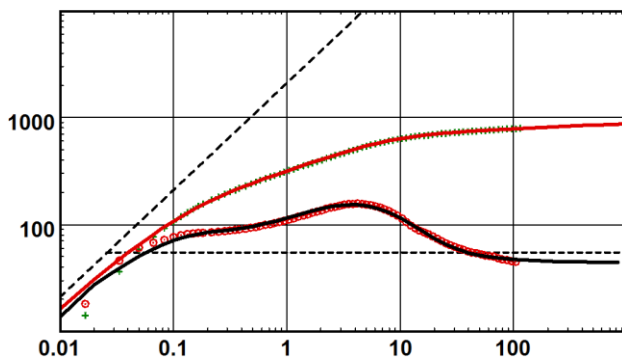


Fig. 7.H.17 – Gas blocking

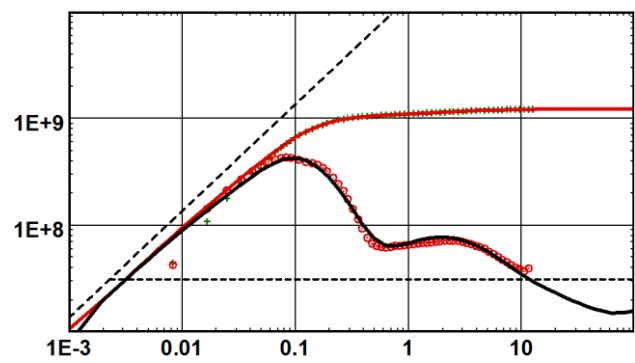


Fig. 7.H.18 – Condensate bank

7.H.7 Numerical models

Composite numerical models can be built easily and will, in most cases, represent real life better than the analytical models. To many engineers the fact that a more real type of model is used is more convincing than using the composite analytical models. The use of numerical models to simulate complex composite reservoirs is detailed in the chapter on 'Numerical models'.

Following we show a typical numerical model with an unstructured Voronoi grid. The colors indicate composite zones where the mobility ratio M , and diffusivity ratio D can be defined. The loglog response is also illustrated.

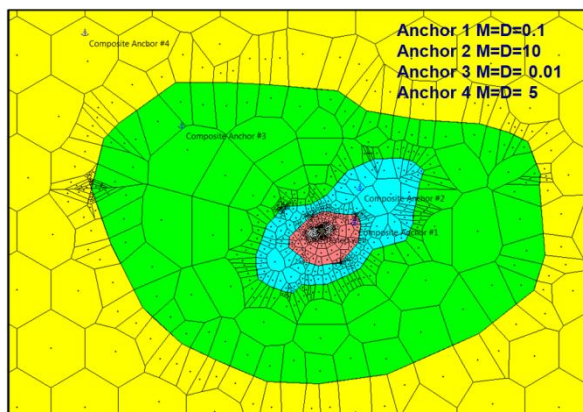


Fig. 7.H.19 – Numerical model

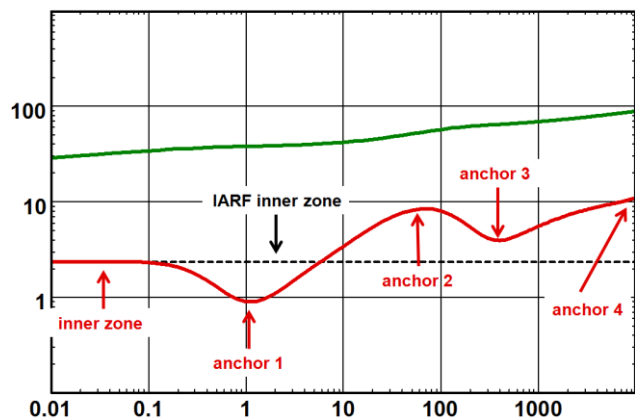


Fig. 7.H.20 – Response

7.H.8 When should we use a composite model?

7.H.8.a Changes of reservoir properties

In this case, the main physical changes are in the permeability and the porosity. M will reflect the permeability ratio, and D the porosity ratio. An example of such a model is the numerical simulation of the geological facies of the reservoir determined by geostatistics.

The use of the radial composite model can always be criticized as it is always highly unlikely that the well has been drilled smack in the middle of a circular reservoir.

7.H.8.b Fluid front

The simplest case is the water injector. When the well is shut-in the pressure response can behave as a radial composite reservoir, corresponding first, to the diffusion in water, then in the original reservoir fluid. M and D can be adjusted to the changes in relative effective permeability, viscosity and compressibility between water and the original fluid. The use of a radial composite model is valid during the shut-in phase, where the phase front is stable. During injection phases, the front is moving and the behavior will be different. The injection response will behave like a homogeneous reservoir with water only, i.e. the displacement of the phase front will mask the well from the original reservoir fluid.

7.H.8.c Gravel packs and the invaded zone

In such a scenario the classification of the composite model as a boundary effect is not proper, the inner zone can correspond to the packed zone or the gravel pack, while the outer zone represents the actual reservoir.

7.H.8.d Match any old weird response

Composite models are probably the most overused and misused models in the industry of well testing. Because of its remarkable flexibility in matching just about any derivative signature, the radial composite model, when combined with a changing wellbore storage model, is the ultimate weapon to get rid of any tough interpretation problem by generating the perfect match that will please everybody that knows nothing or too little about pressure transient analysis. Worse, multiple composite models, where changes in diffusivities and mobilities can be allocated at different distances, hence act at different times, gives no limit to our ability in matching any response. If this is the way the model is used it is nothing more than fudging and cheating. It just amounts to matching the transient well productivity index, and it is no better than doing this with a simple spline.

Composite models only make sense if all parameters such as the location of the interface, mobility change and diffusivity change are within acceptable ranges and can be explained. The decision to use these models is the knowledge of the actual real conditions where composite responses are expected, not that the data cannot be matched with other less flexible models.

7.I Reservoir anisotropies

In the past reservoir anisotropy was seldom considered in pressure transient analysis. As the inclusion of these limiting effects in the analytical model is relatively simple, today most analysis software have the option to include both horizontal and vertical anisotropy for applicable models.

During infinite acting radial flow (IARF) the slope of the semilog plot and the level of the pressure match in the loglog plot yields $h\sqrt{k_x k_y}$.

7.I.1 Vertical anisotropy

Vertical anisotropy typically comes into play in horizontal and limited entry wells. Vertical anisotropy also affects the behavior of multilayered systems with cross flow in the reservoir. Below is illustrated the sensitivity to the ratio of k_v/k_r in a limited entry, or partially penetrating, well. Following we show the sensitivity of horizontal well behavior to vertical anisotropy.

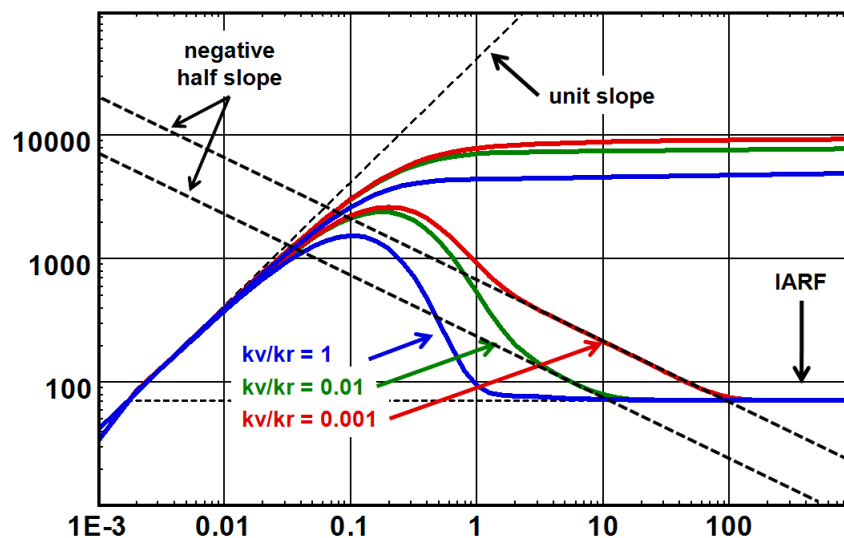


Fig. 7.I.1 – Limited entry well

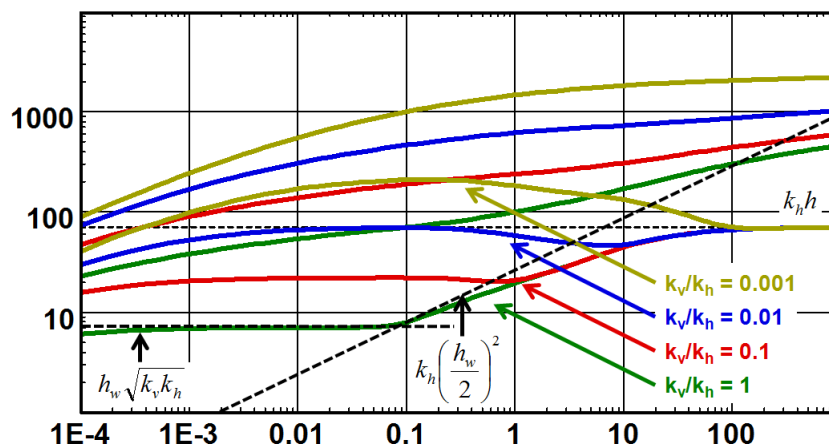


Fig. 7.I.2 – Horizontal well

7.I.2 Horizontal anisotropy

In a horizontal well the response will be dependent on the areal distribution of the permeability. The effect is illustrated below where it can be easily seen that the ideal permeability distribution is when the best permeability is perpendicular to the horizontal well. In this case the permeability in the x direction is along the well and the highest productivity is obtained when $k_x/k_y < 1$.

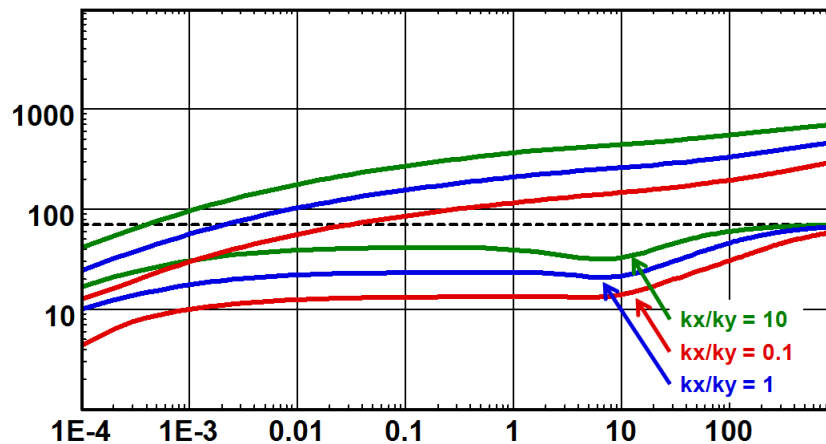


Fig. 7.I.3 – Horizontal well areal anisotropy

When the reservoir system is bounded, the time to 'see' a fault depends upon the directional permeability. In the below example the one single fault that is simulated, is by default parallel to the x direction in the reservoir (this default can be modified in the model dialog). An increase in the y direction permeability (decrease of the ratio k_x/k_y) will decrease the 'time' necessary to 'see' the fault.

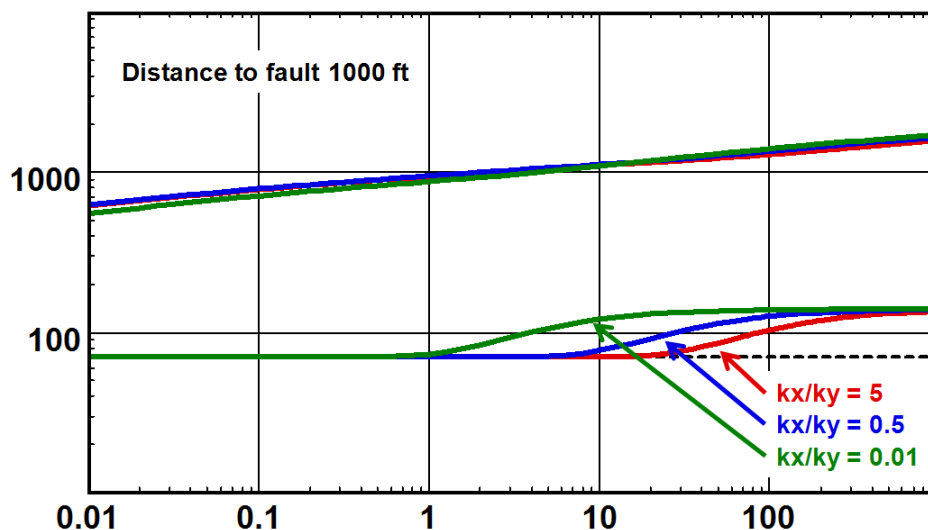


Fig. 7.I.4 – Model response single fault with horizontal anisotropy

7.J Analytical combinations of reservoir models

The heterogeneous models individually described in the previous sections can be combined in a single analytical model. Not surprisingly, the resulting behavior will be a combination of the individual behaviors, and may occur at completely different times if the parameters so dictate.

With respect to the KAPPA software suite, some model combinations were implemented as external DLL's that may be connected to the applications on a needed basis. The reasons that they were not made a part of the standard model catalog are summarized below.

- These are delicate models to use. They have so many leading parameters that, without paying attention to the physics it is possible to force a match to do anything. Delivering the solutions as external models allows client companies to control their distribution.
- The solutions are more complex and more rarely used and tested. They are therefore less stable than simpler models that are part of the built-in capabilities of the applications.

7.J.1 Double permeability radial composite

Below we show the schematic and an example of the behavior for the combination of two layers with cross flow in radial composite system. An example of the use of the model is a reservoir with two zones that are hydraulically separated at the level of the well but connected at a distance.

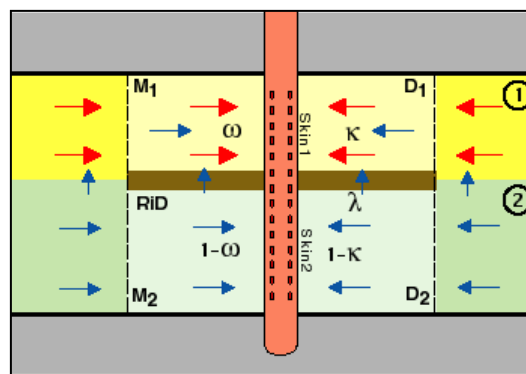


Fig. 7.J.1 – Double permeability radial composite

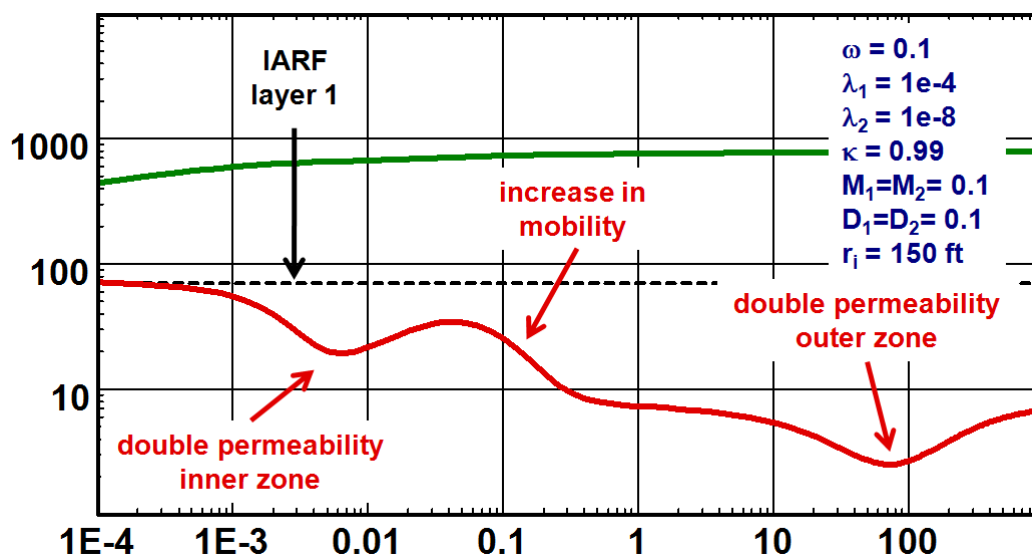


Fig. 7.J.2 – Double-permeability reservoir with radial composite zones

7.J.2 Double permeability double porosity layers

The below figure show the schematic of double-porosity layers in a double permeability reservoir, followed by the theoretical loglog response.

These models are only relevant if we know beforehand, from the petrophysics, that part or all of the layered and composite system is naturally fractured and fissured.

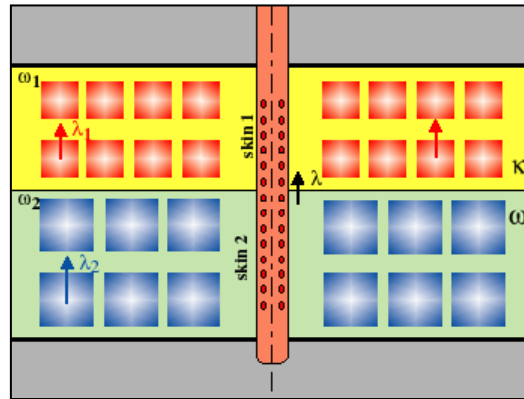


Fig. 7.J.3 – Double permeability double porosity

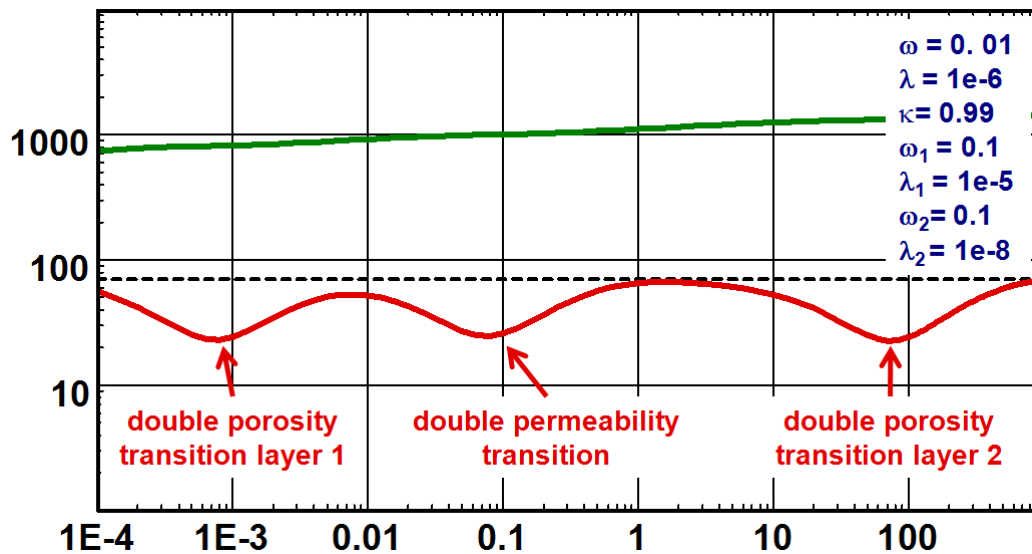


Fig. 7.J.4 – Double-permeability reservoir with double-porosity layers

7.J.3 Double porosity radial composite

The below figure show the schematic of the hypothesis and an example of a calculated response with the pressure change and the Bourdet derivative in the loglog plot.

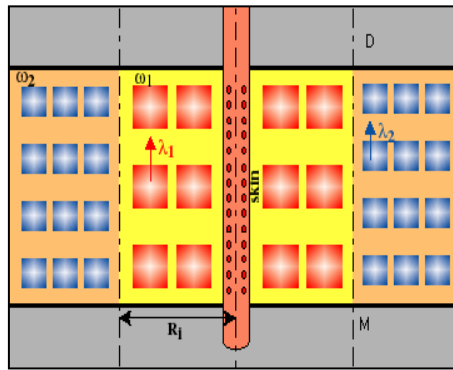


Fig. 7.J.5 – Radial composite double porosity

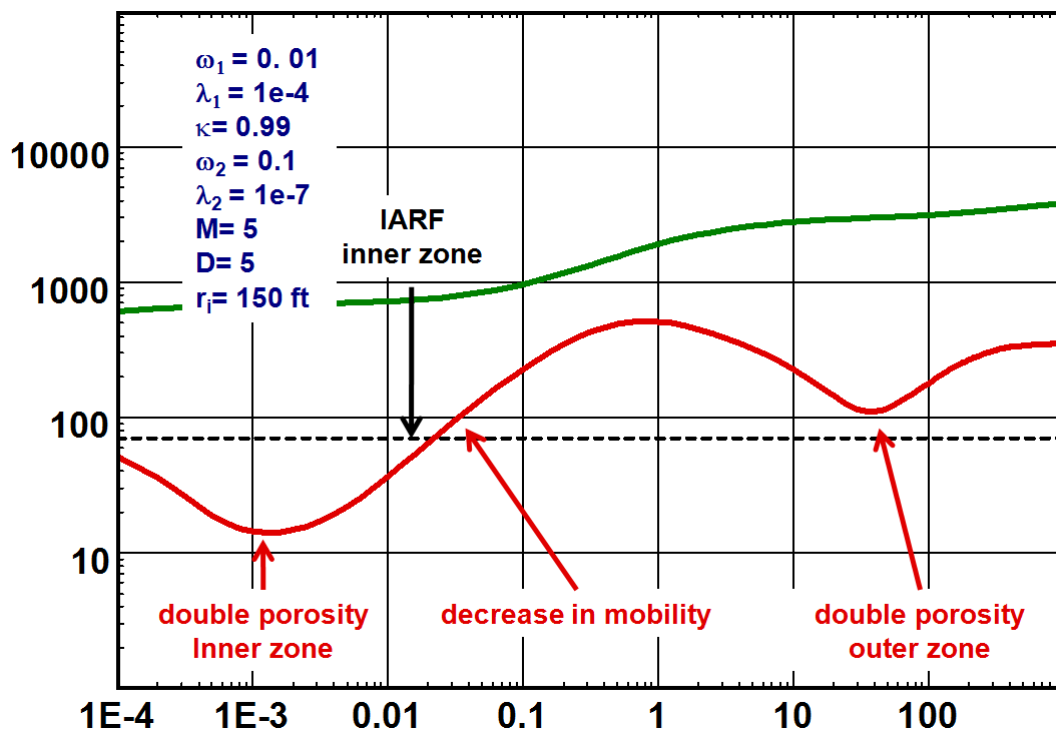
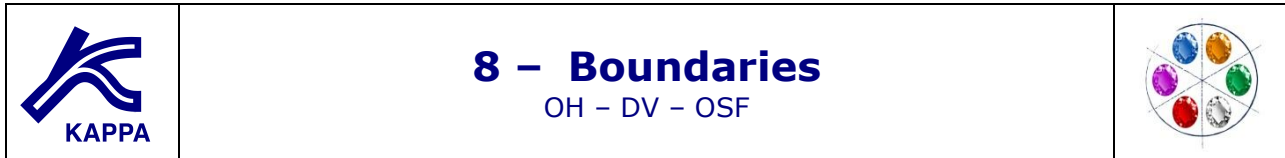


Fig. 7.J.6 – Radial composite reservoir with double-porosity

7.J.4 Just a comment on the above described models

Such models should never be used just for the sake of matching any strange looking response. There must be some evidence, some knowledge of the formation and fluids that would justify such a choice. One should also not forget that there are far too many leading parameters in the models so the concept of a solution to the 'inverse' problem is lost.



8.A Introduction

In most well tests, and with most models used in pressure transient analysis, the first part of the pressure response is dominated by wellbore effects and flow diffusion immediately around the well. If the well is not fully penetrating the reservoir or not vertical, the early time response is also affected by vertical flow from the top and bottom parts of the producing interval. Then in most cases, but not always, the middle and/or late time pressure response will be dominated by Infinite Acting Radial Flow (IARF), characterized by a stabilization of the Bourdet derivative, where the average reservoir mobility (k/μ) and the global well productivity, total apparent Skin, may be assessed. In many well tests, the analysis will stop there and IARF will be the final detected behavior.

But, should the reservoir be small enough, and should the test be long enough boundary effects will be encountered during the test. This encounter may be accidental, deliberate, as in reservoir limit testing, or inevitable in the case of long term production data.

This chapter covers the different types of boundaries, their respective pressure and derivative behaviors and corresponding analysis methods. It also shows how apparent boundary effects may be, in fact, be something else.

We will only consider boundaries that produce deviations from IARF, and we will not consider the vertical limits of the producing interval. Physically this is a questionable option, as these are boundaries too but for our methodology it makes sense. Upper and lower boundaries will generally be considered in well models involving vertical flow, such as limited entry and horizontal wells, where the early time response will involve a vertical diffusion until these limits are reached. Paradoxically the analyses involving top and bottom boundaries is associated to well models and developed in the corresponding chapter.

We have also excluded composite limits. Though their detection and analysis process are similar to what is done for boundaries, they will be assimilated to reservoir heterogeneities, and treated in the chapter dedicated to reservoir models.

Finally we will also look at the way recent developments on the deconvolution allow boundaries to be assessed while not being detected in any individual build-ups.

8.B Different types of boundaries

8.B.1 Description of a boundary behavior

A boundary is a surface Σ located at a distance from the tested well where a change in the flowing property occurs. A typical boundary effect is shown below where the example used is a single sealing fault. We will start dealing with no flow boundaries.

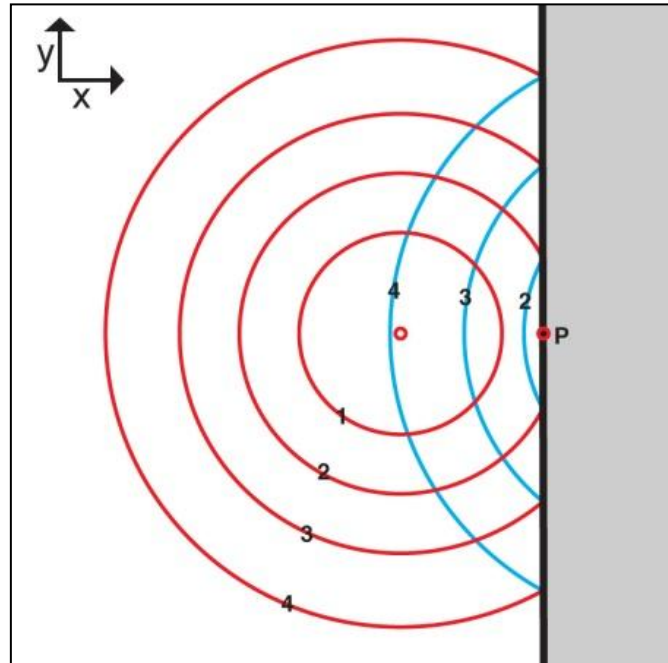


Fig. 8.B.1 – X-Y representation of the additional pressure drop (blue) due to a boundary (example of a sealing fault)

The figure above does not represent a 'wave' but the points at which the pressure drop reaches a given value (e.g. 1 psi) at different times (1, 2, 3, 4). The red circles represent the influence of the well production itself if it was producing in an infinite reservoir. The blue circles represent the additional pressure drop **due to the boundary** at the same times.

This requires a physical explanation: The well production creates a pressure drop around the well that diffuses within the reservoir. As long as the boundary influence is negligible the diffusion will be radial and the 'radius of investigation' (red circles) will be proportional to the square root of time.

When a boundary is present, there will be no pressure support beyond the boundary, and there will be an additional pressure drop compared to an infinite configuration. This pressure drop (blue circles) will affect the pressure profile and will also diffuse.

At a time the amplitude of this additional pressure drop will be picked up by the gauge in the well, and the boundary is detected. This will only occur if the test is long enough and the gauge is sufficiently sensitive to pick up the signal.

The pressure derivative deviates from IARF at the time when the influence of the closest boundary becomes noticeable. The derivative then takes a shape that will depend on the type and shape of the boundary, the flow period of interest, if it is a flow or shut-in, and in some cases the well production history.

We will consider four types of boundaries and their typical behavior, alone or combined with other boundaries. These are no flow, constant pressure, leaky and conductive.

8.B.2 No flow boundaries

No fluid will pass in any direction through a no flow boundary Σ . The mathematical formulation of this condition is given by Darcy's law, applied at zero rate at the boundary, in a direction orthogonal to this boundary:

$$\left[\frac{\partial p}{\partial \vec{n}} \right]_{\Sigma} = 0$$

This equation means that the pressure profile is flat when arriving orthogonally to the boundary. The vertical cross-section below shows the pressure profile from the well to the boundary.

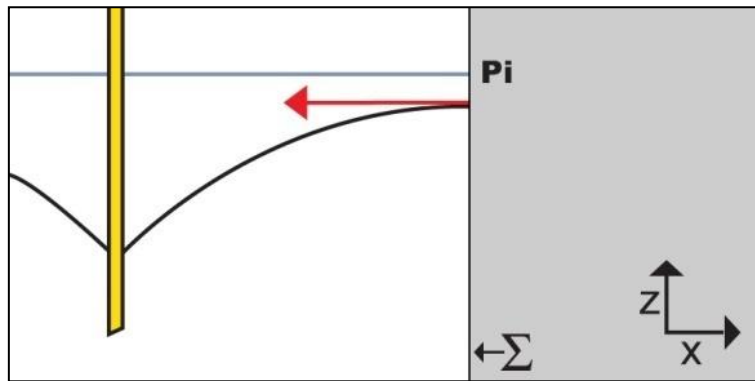


Fig. 8.B.2 – Profile near a no-flow boundary

The figure below is a 3D display of the pressure profile due to a well producing near a no-flow boundary. We are representing here a 2D problem, and the z axis represents the pressure. The pressure at the boundary is not uniform. The pressure change is larger at the point of the boundary than it is the closest to the well. But looking at every line orthogonal to the boundary it becomes flat at the boundary. This is simply Darcy's law for no flow in one direction.

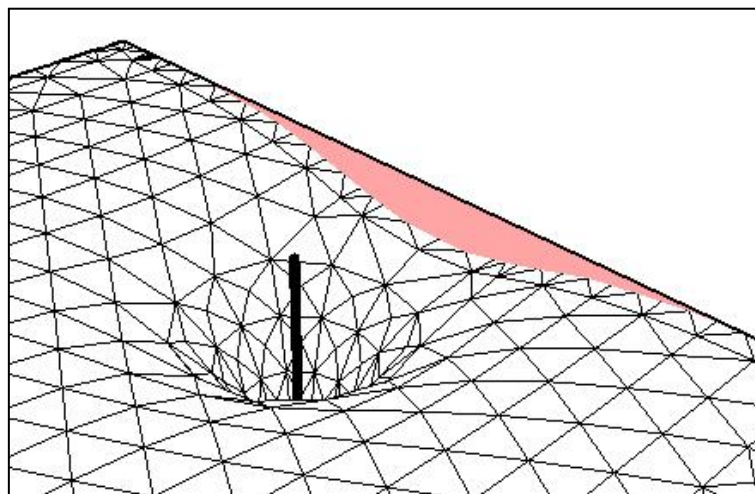


Fig. 8.B.3 – 3D representation of the pressure profile
Between a producer and a no-flow boundary
Pressure, in the z axis is a function of x and y

8.B.3 Constant pressure boundaries

A constant pressure boundary is a surface beyond which there is sufficient pressure support to keep the pressure at the boundary constant, generally at reservoir initial pressure:

$$[p]_x = p_i$$

The figure below shows a vertical cross-section of the pressure profile from the well to the boundary. The slope at the boundary will correspond to the fluid flux required to keep the pressure constant.

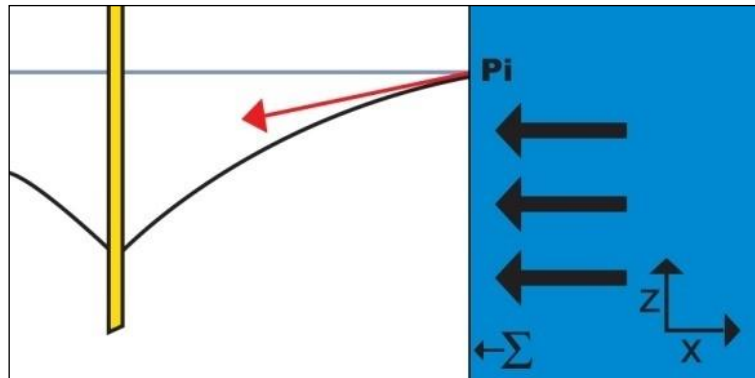


Fig. 8.B.4 – Profile near a constant pressure boundary

8.B.4 Aquifers

The constant pressure boundary above is the only pressure support model which can be easily modeled analytically, using the method of image wells. This implies that the pressure support is very strong and that multiphase flow effects can be neglected. This approximation works generally quite well for gas caps. In the case of water drives such approximation may not work, and aquifer models may be used.

Aquifers are generally modeled analytically. They require a choice of model, that will define the aquifer strength, and a relatively permeability table to model the sweeping of the hydrocarbon by the water phase.

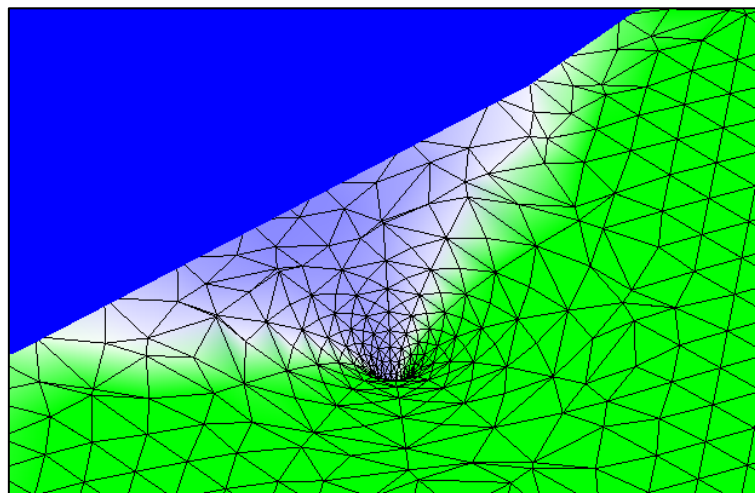


Fig. 8.B.5 – Numerical Aquifer

8.B.5 Leaky boundaries

A leaky boundary is a reservoir inner boundary through which a pressure drop occurs. As for a wellbore skin, the pressure drop at a point of the boundary will be, typically, proportional to the flux through the leaky fault at this point. The vertical cross-section below shows of the pressure profile from the well to the boundary.

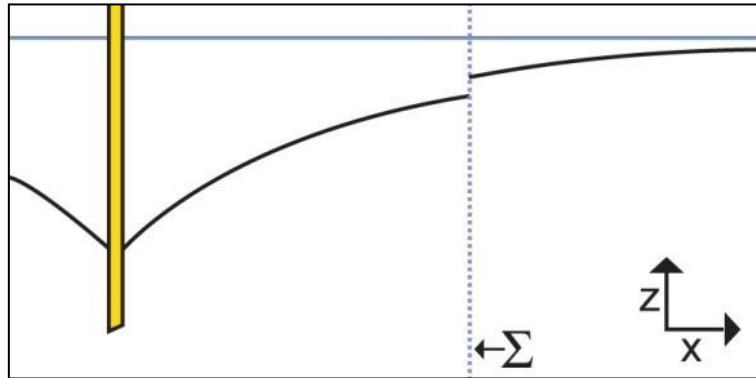


Fig. 8.B.6 – Profile near a leaky boundary

8.B.6 Conductive boundaries

Conductive faults (boundaries) can be modeled numerically or analytically. In this section we will use the analytical model which is part of the Saphir external model suite to illustrate its use and pressure response.

It solves for the pressure behavior at a well near a non-intersecting finite conductivity fault or fracture. The solution includes an altered zone around the fault across which it is possible to add Skin. The reservoir properties on either side of the fault can be different.

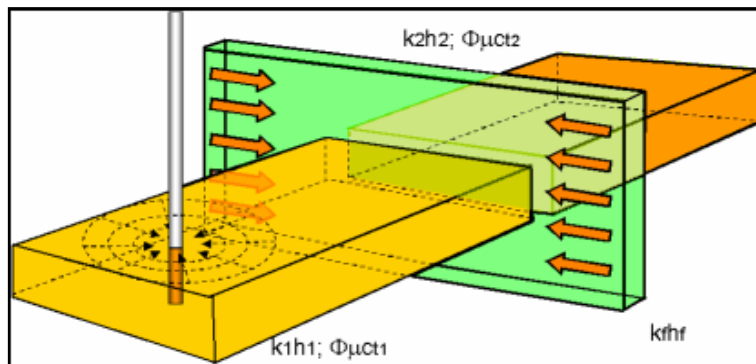


Fig. 8.B.7 – Conductive fault

8.C Single sealing fault

The simplest model for a no flow boundary is a single linear sealing fault of infinite extent. This configuration is easily modeled analytically using an image well (see the section 'Superposition in space of analytical models' in the 'Theory' chapter). The effect of a sealing fault is equivalent to adding a symmetric well with exactly the same production history. This will create an additional pressure drop that will assure that no flow occurs orthogonally to the fault.

In the case of more complex well models (fractures, horizontal wells, etc), to ensure that the model is valid, one has to add an image well of the same geometry, the position being the symmetric to the real well. To enforce symmetry, wellbore storage must also be added. In some cases however it will be possible to get a good approximation of the response using a simple line source solution with no wellbore storage.

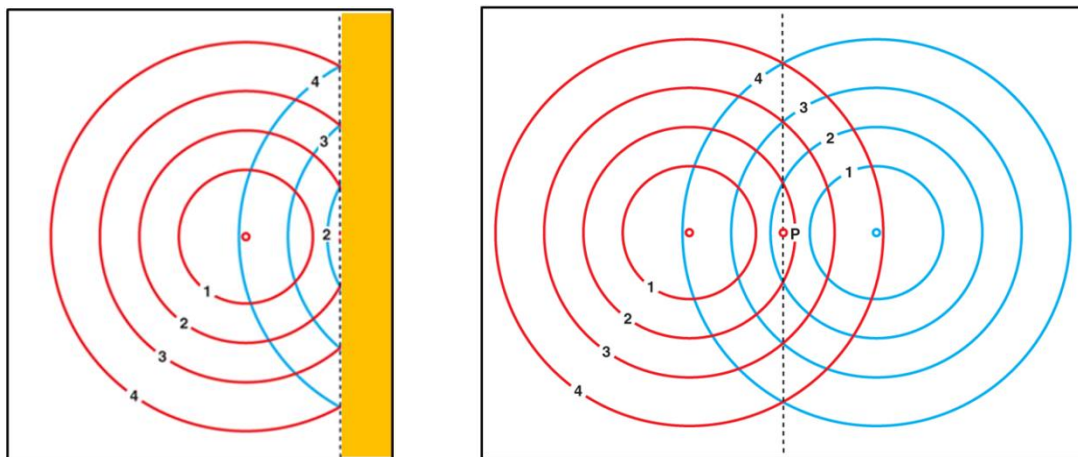


Fig. 8.C.1 - Single fault and equivalent image well.

8.C.1 Behavior

Before the additional pressure dropped due to the boundary is picked up by the pressure gauge, the system behaves as if the reservoir was of infinite extent in all directions.

When the boundary is detected, the response deviates from infinite acting radial flow until it doubles. If one considers the physical reservoir, the well has received the information that the reservoir is actually twice smaller than in the infinite case. After the sealing fault is detected, only half of the originally planned reservoir is now available, and therefore the speed of the pressure drop doubles. If one considers the equivalent image well, after the detection there are two wells producing instead of one, and for the same reason we have a doubling of the speed of the pressure drop.

8.C.2 Semilog analysis

The initial IARF is characterized by an apparent linearity on the semilog plot. Drawing the corresponding semilog straight line will give both kh and the total apparent Skin. A sealing fault will be characterized by a deviation from this initial straight line and a transition towards another semilog straight line with twice the original slope. From the time of intersection of the two straight lines, we can get the boundary distance:

$$L = 0.01217 \sqrt{\frac{k\Delta t_{\text{int}}}{\phi\mu c_t}}$$

Boundary distance:

8.C.2.a Drawdown response

As for infinite reservoirs, the semilog plot of choice during a constant rate production will be the MDH plot. Starting from initial pressure, the pressure response will follow a first straight line when IARF is reached, and until the sealing fault is detected. The pressure response will then deviate before stabilizing towards a second straight line, that we call below 'half radial flow'. The slope of this line is twice the slope of the original IARF line.

As in the infinite case, the permeability and skin will be given using the slope of the IARF line. The time of intercept between the IARF line and the half radial flow line will give the boundary distance using the equation above.

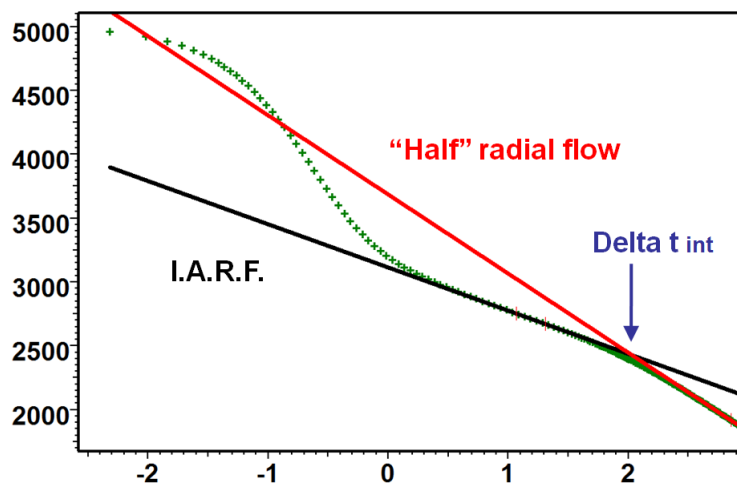


Fig. 8.C.2 - semilog plot for a sealing fault

8.C.2.b Build-up response

In the case of a shut-in following a single production period, the MDH plot is replaced by the Horner plot. In the case of a more complex production history the semilog plot of choice will be the superposition plot, though the Horner plot is also used for complex shut-ins, provided that a sound value of production time is used.

The behavior is the same as for drawdowns, with an initial IARF line, a second line with twice the slope for half radial flow, and a boundary distance related to the time of intercept of these two straight lines. The only difference is that, in the case of shut-ins the intercept of the half radial flow line (and NOT the IARF line) will be the one used to calculate p^* .

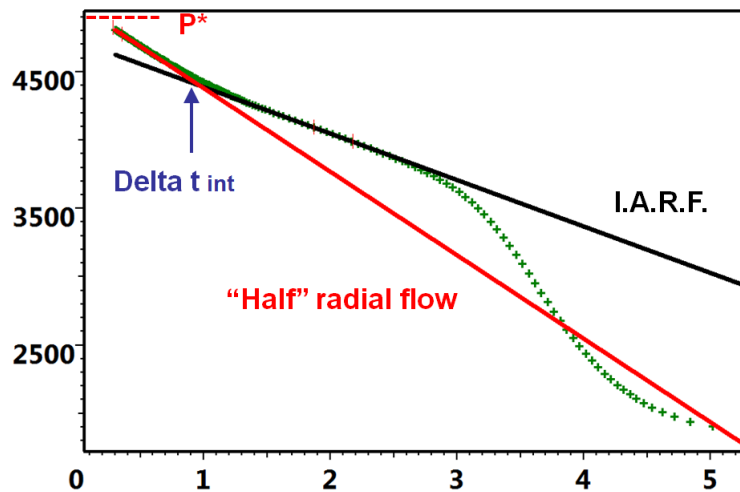


Fig. 8.C.3 - Horner plot or Superposition plot for a sealing fault

8.C.3 Loglog analysis

On a loglog plot, the derivative will initially follow an infinite response, and the derivative will stabilize to a level corresponding to IARF. When the boundary is detected the derivative will deviate upwards, then tend to stabilize again towards a level twice of the original IARF.

The easiest technique to match such response is to first focus on the early and middle part of the data, matching this part with an infinite model. This may include an initial nonlinear regression on all the points before the deviation from IARF. In the case of a vertical well in a homogeneous reservoir this will fix C , kh and S_{kin} .

In a second stage the boundary effect is added, and the first estimation of the distance will be obtained from the semilog analysis or, preferably, an interactive Saphir / Topaze feature where the time of deviation is picked by the user. After initial simulation the parameters, especially the boundary distance, will be improved from nonlinear regression, this time on all data points.

In case of poor data quality, if the nonlinear regression fails it is possible to correct the boundary manually using the following rule of thumb: If we multiply the boundary distance by 2 we multiply the boundary time by 4. For small corrections, adding $X\%$ to the boundary distance will add $2 \cdot X\%$ to the boundary time.

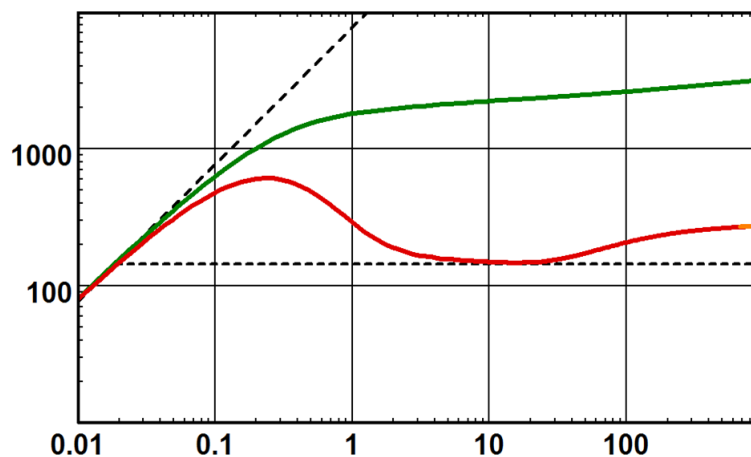


Fig. 8.C.4 - Loglog response for a sealing fault

8.C.4 Influence of the boundary distance

The figure below shows the sensitivity of the response to the boundary distance. As for any radial diffusion problem, the governing group is t/r^2 . Doubling the boundary distance will multiply by four the time at which this boundary is detected. This relation is valid for all boundary models discussed in this chapter.

If the boundary is very close to the well (e.g. 100 ft in the example below), IARF may not develop before the fault is detected. For very nearby boundaries the pressure response could look like a homogeneous infinite response with an apparent kh equal to half the true kh .

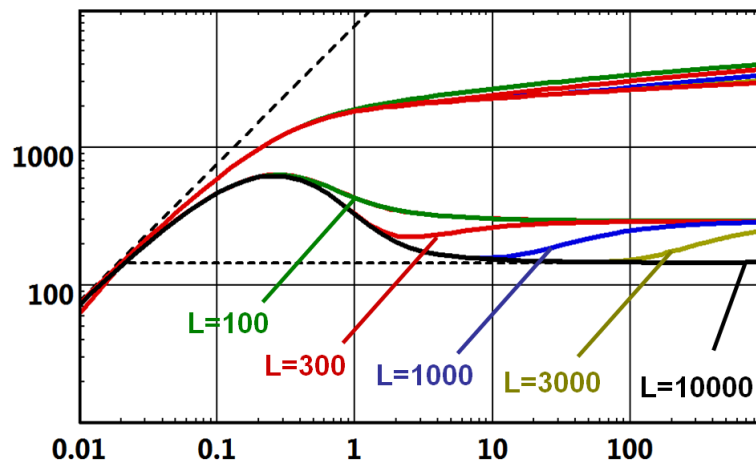


Fig. 8.C.5 - Influence of the boundary distance

8.C.5 The case of shut-ins after a short production time

The Bourdet derivative responses for single sealing faults are similar for drawdowns and shut-ins. In most cases the build-up response will actually match the drawdown response.

However the shape the Bourdet derivative may be distorted in the case of shut-ins following a very short production. In this case the initial effect of the boundary due to the opening of the well will be detected during the build-up, creating a temporary down trend before the effect of the shut-in on the same boundary is detected.

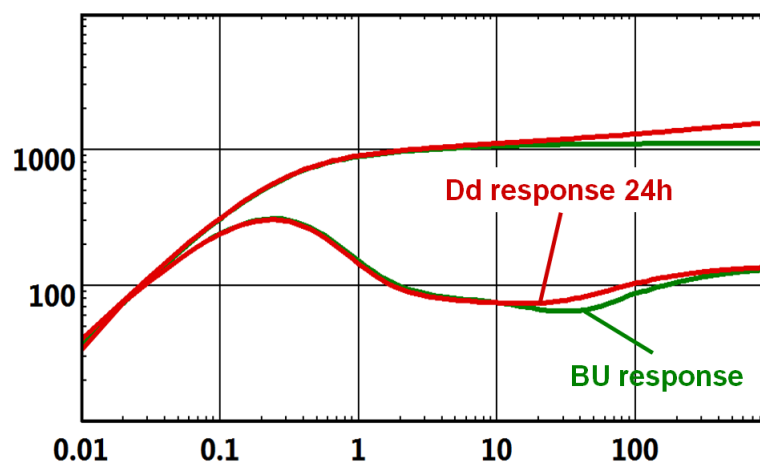
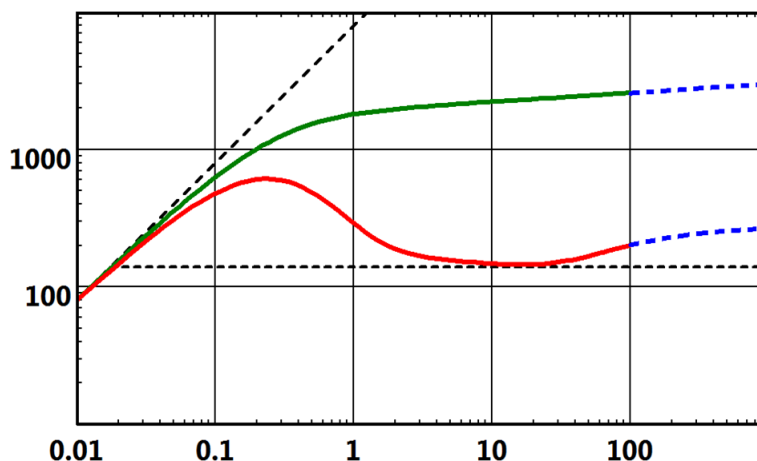


Fig. 8.C.6 - Shut-in after a short production time

8.C.6 Remarks on the sealing fault model

A full doubling of the slope is seldom seen on real data. It requires almost one and half log cycles in time after the initial deviation from IARF, i.e. over a period 30 times longer than what it took to initially detect the boundary. You are likely to see other boundaries before the doubling of the slope occurs. In addition, tests are rarely long enough to provide the opportunity for such a doubling to take place, and shutting the well in one or two more days will not be worth the additional information.



*Fig. 8.C.7 - Loglog response for a sealing fault
Incomplete response with no doubling of the slope*

The single fault model will be used when the slope is less than double because it is just the simplest boundary model that allows the association between a time and a distance. If we see a deviation from IARF, and IF we think this deviation is due to a boundary, the sealing fault model will provide a good estimate of the distance from the well to such boundary. From this distance we will decide if the hypothesis of a boundary is reasonable.

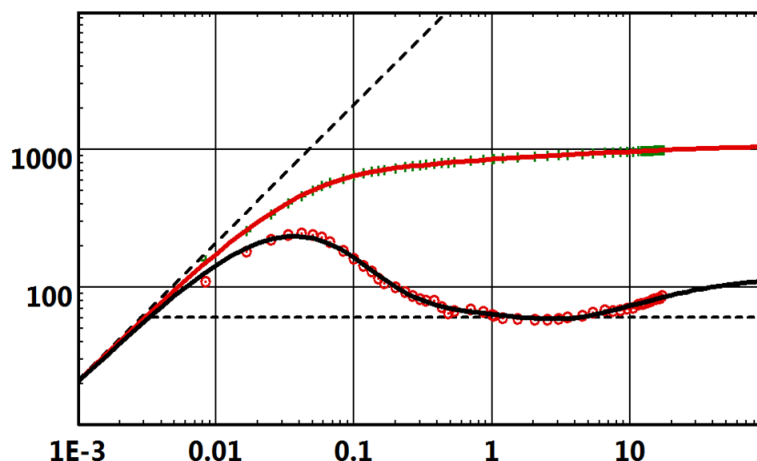
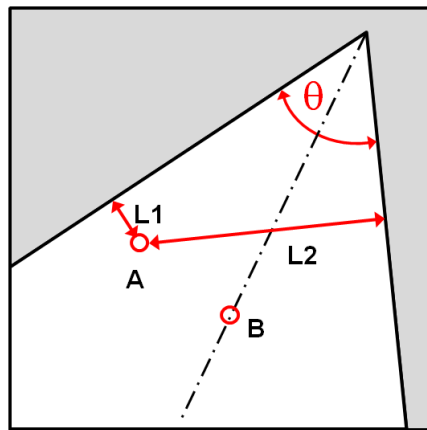


Fig. 8.C.8 - Example of sealing fault match

8.D Intersecting faults

8.D.1 Description

The simple single fault model described in the previous section is the simplest way to relate the time of detection of a boundary and its distance to the well. As stated above, it is rare to see a full doubling of the slope, as after a while the nonlinearity of the single fault, or other faults will be detected. Eventually the full extent of the reservoir is seen; see in 'Closed systems' section further. One of the main analytical models used to model these complex, but still open, systems is the intersecting faults model shown in figure below.



*Fig. 8.D.1 – Schematic of intersecting faults
point A is closer to one fault, with point B at the bisector*

The well is located between two intersecting linear boundaries of infinite extent. θ is the angle between the faults, $L1$ and $L2$ are the orthogonal distances between the well and the two faults. A particular case is when the well is located on the bisector of the faults ($L1=L2$).

8.D.2 Behavior

If the well is significantly closer to one of the boundaries (point A), the initial behavior is the same as for a single sealing fault. When the second fault is detected, the response enters its 'final' behavior. If the well is fairly equidistant from the two faults, the response goes straight from IARF into the 'final' behavior.

The 'final' behavior is semi-radial flow restricted to the quadrant delimited by the two faults. If θ is the angle between the two faults, the actual reservoir size is smaller than an infinite reservoir by a factor of $2\pi/\theta$; hence the pressure drop is $2\pi/\theta$ larger to produce the same fluid to the well.

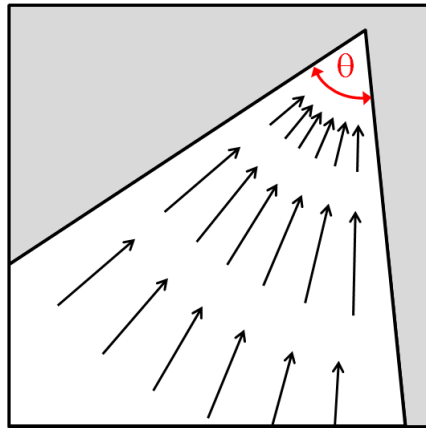


Fig. 8.D.2 – Schematic of intersecting faults wider view showing final semi radial flow

We use the term 'final' in parentheses as, clearly, there would be a time when further boundaries would be detected if the test was continued.

8.D.3 Semilog analysis

On a semilog plot, this will be characterized as a second straight line with a slope $2\pi/\theta$ greater than the initial IARF line slope. As for a single fault, k_h and s_{kin} will be calculated from the first straight line. The angle θ between the faults, will be $2\pi / (m_{final} / m_{initial})$.

8.D.3.a Drawdown response

As for infinite reservoirs, the semilog plot will be the MDH plot. Starting from initial pressure, the pressure response will follow a first straight line when IARF is reached, and until the faults are detected. The pressure response will then deviate before stabilizing towards a second straight line corresponding to the closest limit and eventually a third straight line that we call below 'final radial flow'. The slope of this last line is $2\pi/\theta$ the slope of the original IARF line.

In most of the cases the second straight line caused by the closest limit is very brief and masked by the effect of the second one.

As in the infinite case, the permeability and skin will be given using the slope of the IARF line. The time of intercept between the IARF line and the half radial flow line will give the boundary distance using the equation above.

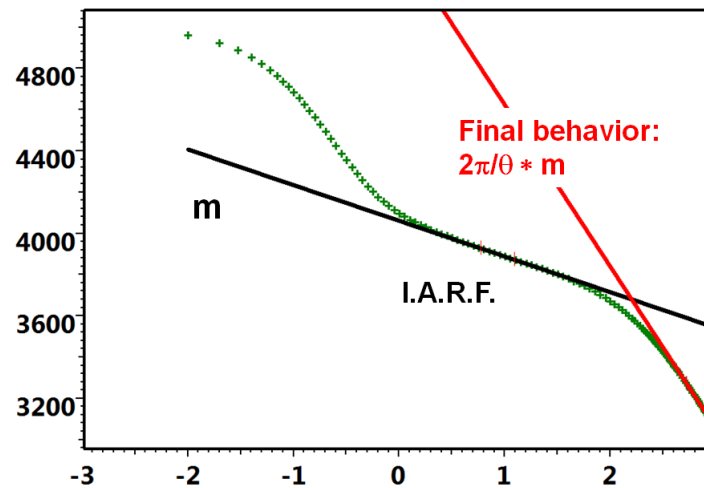


Fig. 8.D.3 – MDH plot for intersecting faults – point B

8.D.3.b Build-up response

As for a single limit, in the case of a shut-in following a single production period, the MDH plot is replaced by the Horner plot and the case of a more complex production history it is replaced by the superposition plot.

The behavior is the same as for drawdowns, with an initial IARF line, a second line with twice the slope for the first limit could be briefly seen then, when the second limit effect appears a third straight line called 'final radial flow' and the slope of this last line is $2\pi/\theta$ the slope of the original IARF line. The only difference is that, in the case of shut-ins the intercept of the 'final radial flow' line (and NOT the IARF line) will be the one used to calculate p^* .

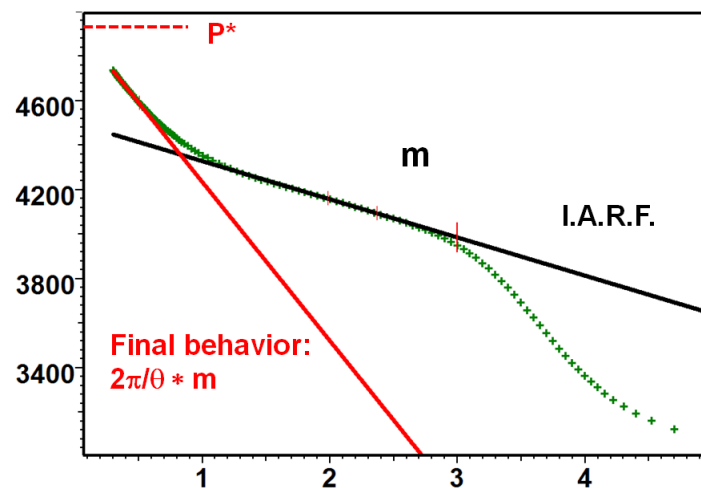


Fig. 8.D.4 – Horner plot for intersecting faults – point B

8.D.4 Loglog analysis

On a loglog plot, the response will be characterized by a final stabilization of the pressure derivative at a level $2\pi/\theta$ times above IARF. In other words, the stabilization level will provide an estimate of the fault angles, while the time at which the derivative levels off from IARF, and eventually (well A) levels off from the sealing fault line, will provide an estimate of the boundary distances.

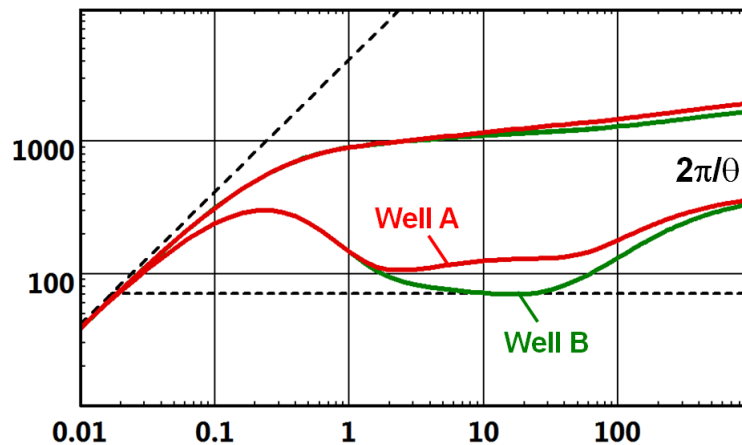


Fig. 8.D.5 – Loglog plot for intersecting faults – wells A & B

8.D.5 Remarks on the intersecting faults model

The single sealing fault is a particular case of intersecting faults where $L_1=L_2=L$ and $\theta=\pi$

When intersecting faults are generated using image wells the interpreter has to choose the angle θ only within a discrete range of values, corresponding to integer fraction of π or 2π . Image wells are very easy to implement and very fast to calculate on a computer or a hand-calculator. But geometrically they require the angle to be an integer fraction of 2π if the well is situated on the bisector (well B), and an integer fraction of π if the well is located anywhere else (well A). The major limitation is that we will generally not match exactly the final stabilization level, and θ will not be accessible as a nonlinear regression parameter.

Conversely, methods using integral solutions will simulate the response for any angle at a higher, but now acceptable, CPU cost. These models will even allow θ to be higher than π , and go up to 2π . We then end up with a half fault that may be described later as an incomplete boundary. Integral solutions also allow regression on θ .

8.D.6 Example of intersecting faults match with field data

In spite of the acquisition noise, the diagnosis of intersecting limits is perfectly accessible:

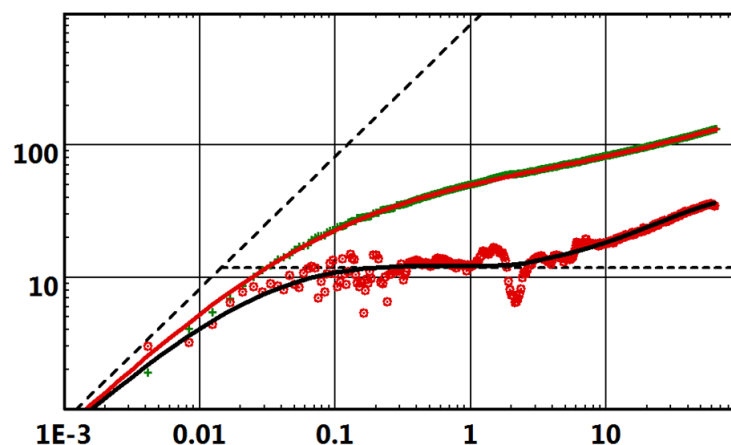
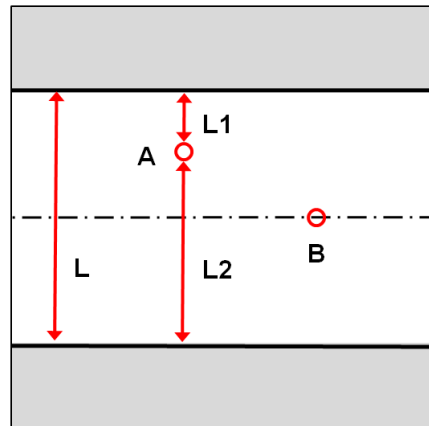


Fig. 8.D.6 – Example of intersecting faults match

8.E Two parallel faults

8.E.1 Description

This solution is also sometimes referred to as a channel reservoir. The well is located in a channel limited by two parallel sealing faults. We will call $L1$ and $L2$ the orthogonal distances between the well and the two boundaries. $L = L1 + L2$ is the width of the channel. As was the case for intersecting faults, we will consider the situations where the well is much closer to one boundary or in the middle of the channel.

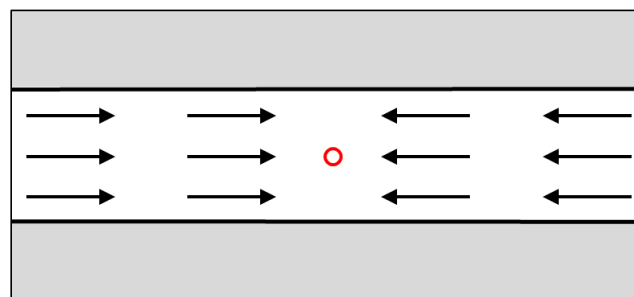


*Fig. 8.E.1 – Schematic of parallel faults
A closer to one fault with B central*

8.E.2 Behavior

If the well is significantly closer to one of the boundaries (well A), the initial behavior will be the same as a single sealing fault response. When the second fault is detected, the response will enter its 'final' behavior. If the well is at fairly equidistant from the two faults (well B), the response will go straight from IARF into the final behavior

The final behavior is linear flow along the channel. Again we should refer to the term 'final' in parentheses as, obviously, there will come a time when the last outer boundaries will be detected if we wait long enough.



*Fig. 8.E.2 – Schematic of parallel faults
wider view showing the 'final' linear flow*

Linear flow, or more generally the flow of fluid through a constant cross-section, is encountered in several well test models, such as fractures at early time after storage, horizontal wells at intermediate times, after the top and lower boundaries have been reached (see 'Well models' chapter), and parallel faults at late time. In each case, the flow is characterized by linearity between the pressure change and the square root of the elapsed time:

$$\Delta p = A\sqrt{\Delta t} + B$$

$$\Delta p' = \Delta t \cdot \frac{\partial \Delta p}{\partial \Delta t} = \frac{1}{2} A\sqrt{\Delta t}$$

8.E.3 Semilog analysis

Semilog plots are of little help in diagnosing or quantifying, parallel faults. After IARF, the pressure response will continuously increase.

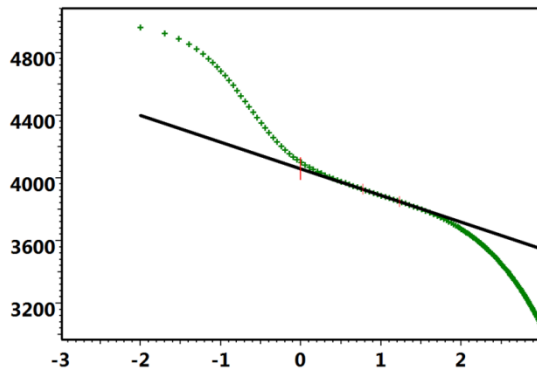


Fig. 8.E.3 – MDH plot for parallel faults – point B

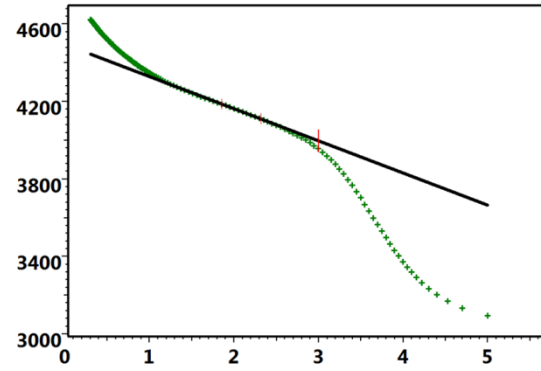


Fig. 8.E.4 – Horner plot for parallel faults – point B

In case of build up the adequate plot would be the Horner plot or a Superposition plot, but in no case it could be used to extrapolate to a p^* since the final pressure behavior do not reveal any straight line on a semilog plot.

8.E.4 Loglog analysis

We will first consider the case of a production phase. After a possible single fault response (point A), the response will reach linear flow. As soon as linear flow is reached, the pressure derivative will follow a half slope on the loglog plot, while the pressure change, because of the constant term B in the equation, will only tend to a half slope. If the pressure half slope is clearly established, there will be a ratio of two between the pressure and the derivative half slope lines.

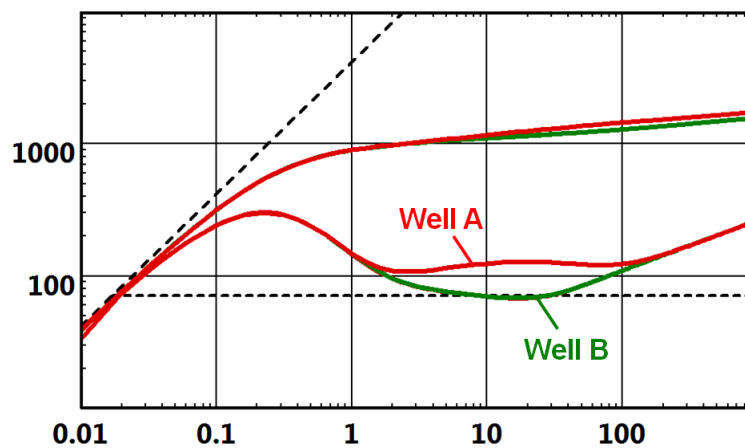


Fig. 8.E.5 – Loglog plot for parallel faults points A & B - drawdown only

The behavior above is only strictly valid for production. In the case of a build-up or complex production in theory, nothing guarantees that a specific behavior will occur on the loglog plot. In reality, the loglog plot is also usable for shut-ins.

Strictly speaking, only the derivative of the production period will follow a half slope. For any practical purpose, especially considering the noise of real data, all flow periods will show a derivative with a slope oscillating around 0.5. The pressure response itself will bend down during build-ups and will not show any specific behavior.

Practically, the interpretation engineer will require the program to generate the pressure response from the usual relation between mobility, time of departure from IARF and boundary distance. The model will be generated taking into account the well production. Any deviation from the strict half slope will also be simulated by the model. Then a nonlinear regression on the boundary distances will correct any initial error in the estimate of these boundary distances due to this superposition effect.

8.E.5 Specialized analysis

As an alternate to the model optimization method above, one can use a specialized analysis involving the square root of the time. For a drawdown, a plot of Δp vs $\sqrt{\Delta t}$ will exhibit linearity. The same plot will be used for the analysis of early time fractures, intermediate time horizontal well and late time channel responses. For parallel faults, the slope will provide an estimate of $k.L^2$, hence of L if the IARF has been clearly identified.

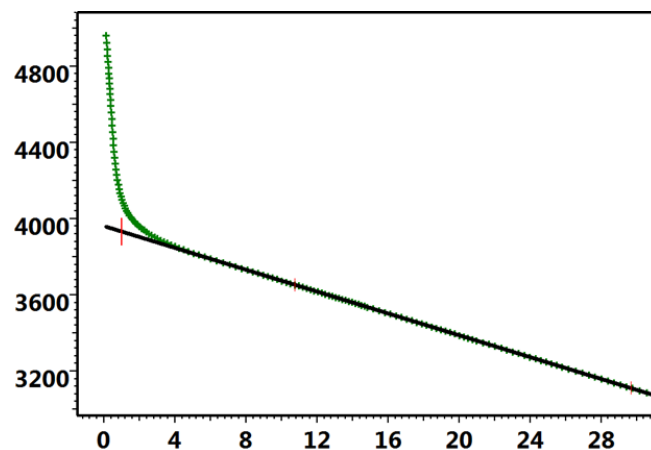


Fig. 8.E.6 – Square root plot for parallel faults point B - production period

For shut-ins and complex production histories, fracture, horizontal well and parallel faults will diverge in the choice of the superposition function. As the linear flow is the 'final' behavior of the channel response, if the considered shut-in has reached linear flow, all component functions used in the superposition will be in linear flow, and the time scale to use is the multirate superposition of the square-root.

For a simple build-up following a unique production, the tandem square root function $[\sqrt{(t_p + \Delta t)} - \sqrt{\Delta t}]$ will be used. For more complex production, the superposition of the square root function will apply. For a shut-in, the extrapolated pressure corresponding to infinite shut-in time will be the right estimate of p^* .

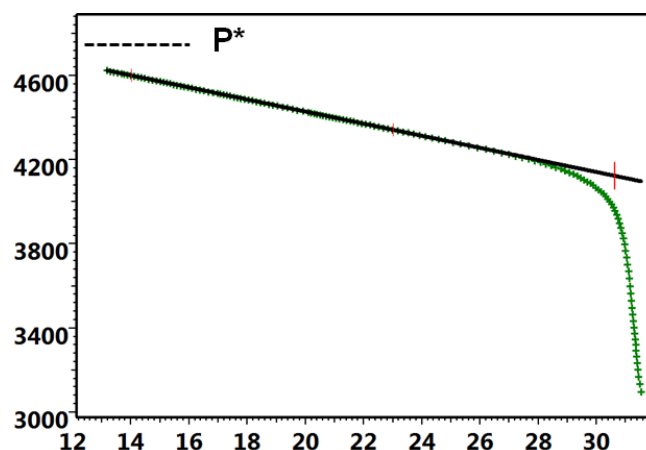
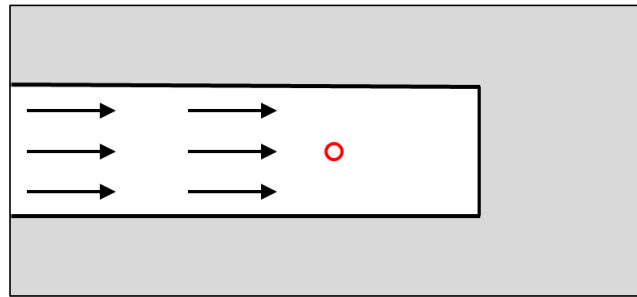


Fig. 8.E.7 – Tandem square root plot for parallel faults

8.E.6 U-Shape reservoir

The U-shape reservoir model, where parallel faults are limited on one side, exhibit at late time, a similar linear behavior to the above, but this time in only one direction.

The early time transient will depend on the distance between the well and the now three sealing faults. This will not be discussed in detail here, and we will only consider the case of a point at equidistant from the three boundaries. The solution is compared with the parallel fault solution, i.e. in the absence of the third boundary.



*Fig. 8.E.8 – Schematic of a U-shape reservoir
Wide view showing the 'final' linear flow*

The two responses are similar and the U-shape reservoir produces a late time half slope. Compared to the parallel fault solution, the final behavior is shifted upward by a factor of two on the loglog plot. This shift is coherent with the fact that the U-shape reservoir is half the size of the corresponding complete channel.

Specialized analysis will also provide an estimate of $k.L^2$. The software will need to know that it is a U-shape reservoir, in order to apply the correction by two in the line calculation.

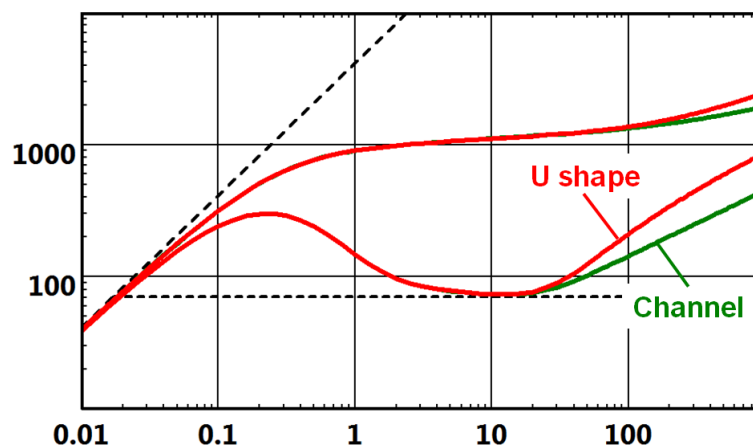


Fig. 8.E.9 – Parallel faults vs U-shape – loglog plot

8.E.7 Remarks on the parallel faults model

The response of the parallel fault model is not related to the fact that the boundaries are straight lines. A channel type reservoir, of any shape but of constant width, would have strictly the same response, as in the figure below. This is why this solution is also called a channel reservoir.

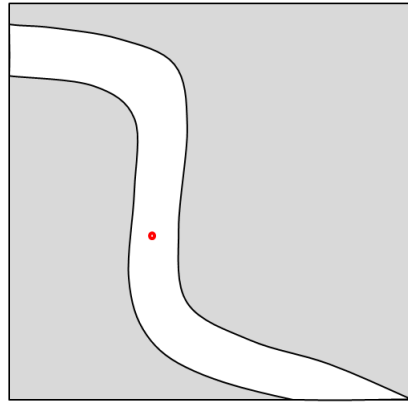


Fig. 8.E.10 – Channel reservoir

8.E.8 Field example

An analytical model for two parallel faults is used to match the field data below.

Even if the reality is not strictly two linear parallel faults but non regular limits close to to be parallel, this model gives a very satisfactory approach before going to more sophisticated models.

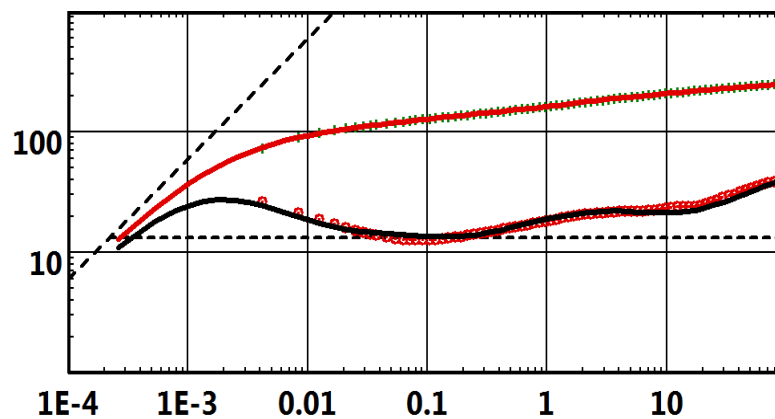


Fig. 8.E.11 – Example of parallel faults match

8.F Closed systems

In the previous sections, the reservoir was still considered to be of 'infinite volume'. What we mean by this is that, at least in one direction, the total extent was not detected during the pressure survey. As a result, the pressure would return to initial pressure at infinite shut-in time.

Conversely, a closed system will be modeled when the test is long enough, or the reservoir is small enough, to detect the whole extent of the reservoir. This will be characterized by at least one of the following behaviors: (1) during the production, we will see linear depletion, (2) at shut-in the pressure will stabilize at a pressure lower than the initial reservoir pressure.

8.F.1 Description

The most common and easiest way to model closed system is the circular model. It assumes that the tested well is located at the center of a reservoir of circular shape.

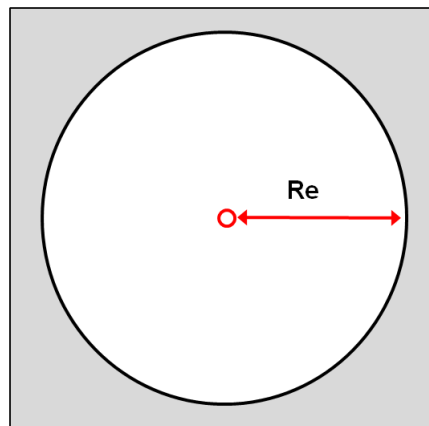


Fig. 8.F.1 – Circular reservoir

This model is unlikely to reflect the exact reservoir geometry and the well location. However it is useful and fast when depletion is detected. But the geometry is unknown and the response does not exhibit any intermediate boundary behavior.

The second most popular closed system model is the rectangular reservoir. Using the principle of image wells, this solution allows us to define an aspect ratio between the reservoir and the position of the well at any point in the rectangle. From the well point of view, it means that the four boundaries may be positioned at any distance. When all four distances are equal, the well is at the center of a square, which is practically identical in response to a circular solution with the same area.

Another advantage of this model is that it can easily be extended to multiwell solutions where contributions of interfering wells can be added. This possibility is critical to properly address material balance issues.

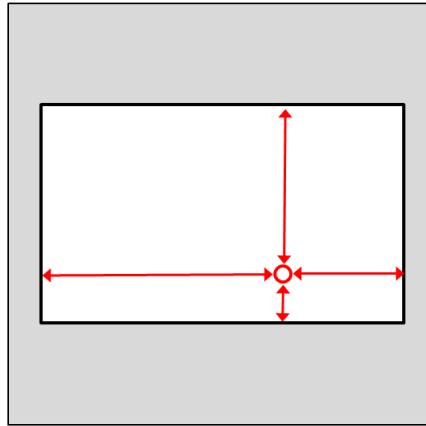


Fig. 8.F.2 – Rectangular reservoir

Numerous other models of closed systems have been published and used. Complex shapes can be modeled using boundary elements or numerical models, and can also be extended to multiple wells.

8.F.2 Behavior

In the illustrations below, we will show the response of a circular reservoir and a rectangle. The shape of the rectangle and the position of the well is illustrated in the figure above. Both rectangle and circle will have the same area.

Unlike the open systems described in the earlier sections, the behavior of closed systems is radically different between production, or injection, and shut-in periods.

During production, or injection, the pressure information will diffuse and reach boundaries sequentially. When the last boundary is reached, the pressure profile will stabilize and then drop uniformly. This particular phase of flow is called Pseudo-Steady State (see chapter 'Theory - Outer boundaries'). It is characterized by linearity between the pressure drop and the time.

$$\Delta p = A \cdot \Delta t + B$$

$$\Delta p' = \Delta t \cdot \frac{\partial \Delta p}{\partial \Delta t} = A \cdot \Delta t$$

For the circle, the response will go straight from IARF to PSS. For the rectangle, closer boundaries will be detected beforehand.

When the well is shut-in, there will be a transfer of fluid back to the well zone, until the pressure stabilizes back to the average reservoir pressure.

8.F.3 Semilog analysis

As for the parallel faults, the semilog plot will not act as a tool to quantify the boundary effects. During the production, the semilog plot will deviate from IARF and tend to an infinite slope. For the shut-in, the pressure response will go horizontal, stabilizing at average reservoir pressure.

The figures below illustrate the stabilization, the model is closed circular.

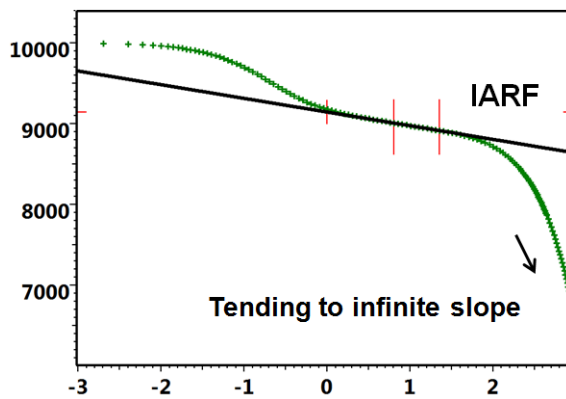


Fig. 8.F.3 – Production semilog plot, circular reservoir

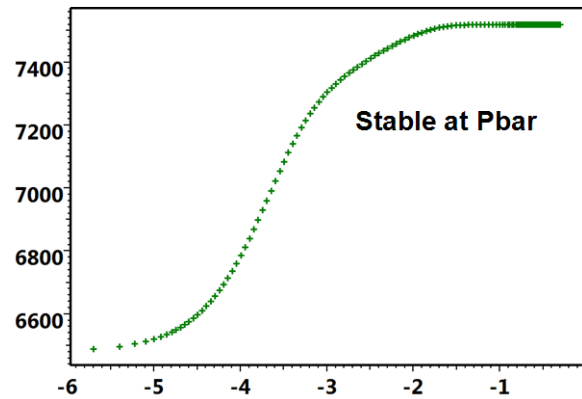


Fig. 8.F.4 – Build up semilog plot, circular reservoir

8.F.4 Loglog analysis

During the production or injection phase, PSS will be characterized by a late time unit slope, first on the derivative, then ultimately on the pressure response.

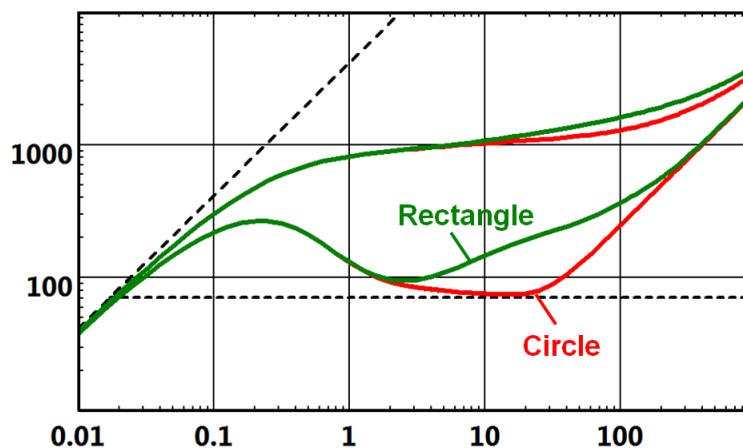


Fig. 8.F.5 – Circle and Rectangle solutions
Production period, loglog plot

For the shut-in the pressure will stabilize at average reservoir pressure, the derivative will 'dive' towards zero. It would not be correct to imagine that because a system is closed, the shut in derivative will only behave this way and only 'dive'. For the rectangular model or any model with closer boundaries, intermediate boundary effects will be detected with the derivative going up before the final dive.

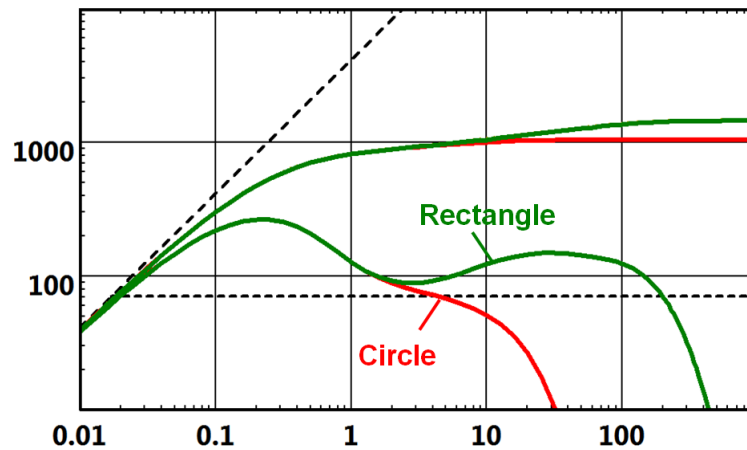


Fig. 8.F.6 – Circle and Rectangle solutions
Shut-in period, loglog plot

8.F.5 Specialized analysis

The PSS response will follow a straight line on a linear plot. The slope m will give the size of the reservoir. The intercept will be the cumulative effect of the well damage, ie: Skin factor and an additional pressure drop due to the transition between IARF and PSS. This pressure drop, linked to the shape of the reservoir and the position of the well, is generally linked to a parameter named the shape factor, CA . The higher the shape factor, the lower the pressure drop. The model with the highest shape factor is the circle, as there is a straight transition between IARF and PSS.

Today the contribution of the shape factor to the pressure drop at PSS is implicitly calculated by the model.

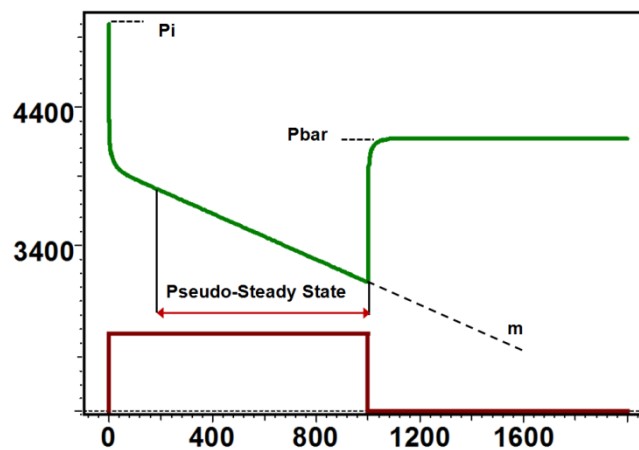


Fig. 8.F.7 – Linear plot of a closed system response

The slope of a linear plot of the flowing pressure versus time is:

$$m = 3.36.10^6 \frac{qB\mu}{Ah\phi c_t}$$

8.F.6 Closed system versus drainage area

This is a subject of frequent confusion. In a producing field, when production is stable, the drainage area of a well will be the zone in which the fluid will flow towards this well rather than an offset well. It is not a physical but a mathematical boundary built from the equilibrium of production between the wells. In the absence of injectors, each drainage area will be limited by a curve where the pressure profile is flat. When a well production rate is changed, the limits will move and the drainage areas will change.

It is perfectly correct, over the production period, to work as if the drainage area was the limit of a small reservoir with one well only (left side figure below). This is what average pressure calculation, AOF and IPR curves are designed for. But the limit of a drainage area is in no way a hydraulic boundary as those described in this chapter and the analogy ceases as soon as we start dealing with a build-up. When the well is shut-in (central figure below), the drainage area will very quickly shrink, taken over by nearby wells. Ultimately another set of drainage areas will stabilize (right side figure). So a closed system model can NOT be used during a build-up.

We observe on the build-up the shut in effect superposed to the depletion effect due to the other wells production.

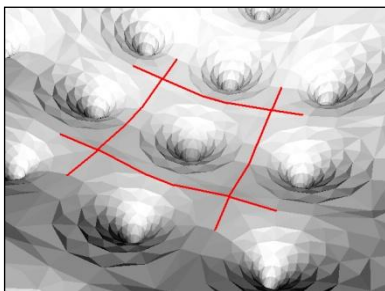


Fig. 8.F.8

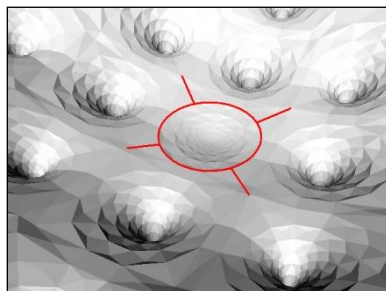


Fig. 8.F.9

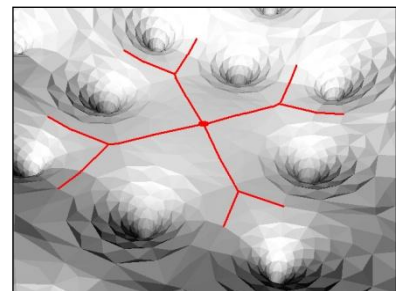


Fig. 8.F.10

Drainage area: Evolution when a well is shut in

8.F.7 Other remarks on the closed systems

One typical mistake with novice interpreters is the expectation that a build-up response in a closed system would follow a unit slope on the derivative. This is wrong, as this would mean that pressure potentially goes 'back' to infinity. But this triggers a question: why are drawdown and build-up responses so different while other models show equivalent derivative behaviors in both?

Actually, what is surprising is that most other models do show equivalent derivative behaviors during productions and shut-ins. We have already seen that it was not strictly true for parallel faults although close enough. The derivative is calculated with respect to superposition time, which itself was designed to handle one, and only one behavior; IARF. Calculations were done for the superposition derivative to stabilize when all components of the production history reach IARF. The wonderful surprise is that, indeed, the derivative carries the signature of numerous well, reservoir and boundary models, and in most cases these signatures survive the superposition process.

However there is no surprise with single faults and intersecting faults, because the long term behavior is IARF multiplied by a fixed factor. It just happens that, numerically, when the models are of infinite extent, i.e. the pressure returns to the initial pressure at infinite shut-in time, the derivative behavior is only marginally affected by the superposition.

But this is not the case for closed systems. When PSS is reached, we are no longer in the usual diffusion process. The reservoir behaves like a depleting tank, and all that survives from the diffusion is a steady pressure profile. When the well is shut-in, the diffusion process will regain its territory until, again, all boundaries are reached. Because the reservoir acts like a tank, as there is no longer any production, the pressure stays constant and uniform and at average reservoir level. This is why the behaviors are so different. On a large time scale, we have a straight material balance behavior, only perturbed by transient diffusion effects whenever rates are changed.

8.F.8 Example of matches with field data

On the production period data the derivative, after exhibiting the various limits effects, tend to a unit slope characteristics of the PSS.

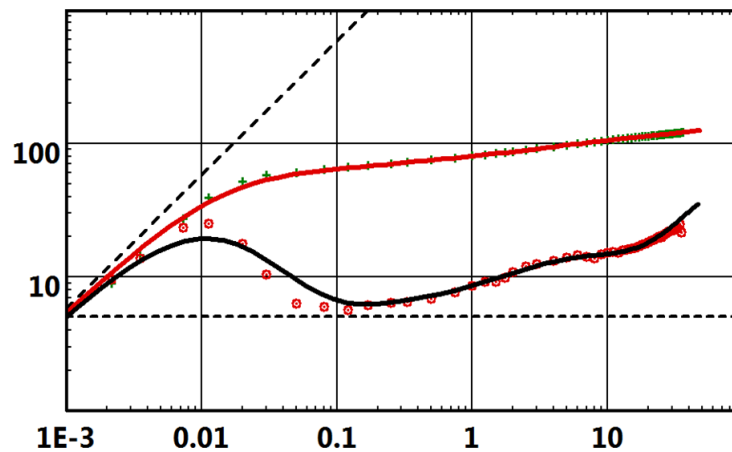


Fig. 8.F.11 – Match with the closed system, production field data

On the shut-in period data the derivative can also show the various limits effects but will drop down characterizing a stabilized pressure.

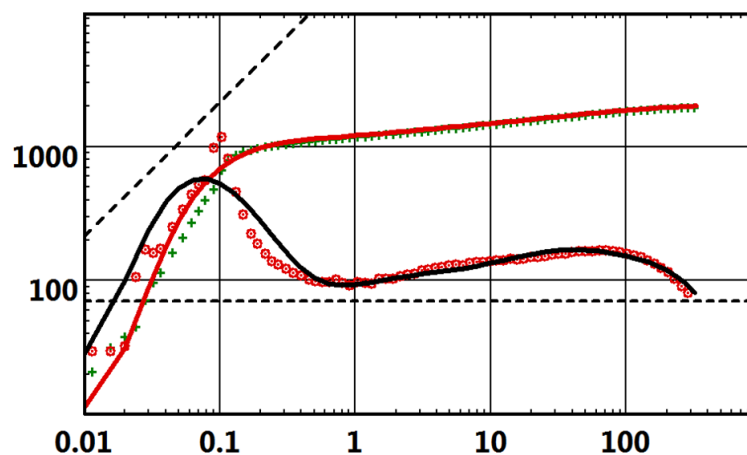
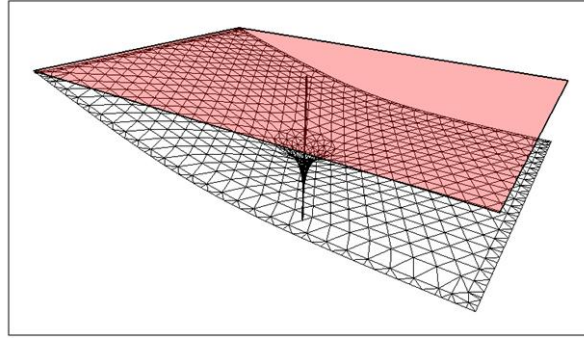


Fig. 8.F.12 – Match with the closed system, shut-in field data

8.G Constant pressure boundaries

8.G.1 Description

Constant pressure boundaries may be the only boundary effect in the model, or may be complemented by sealing boundaries. Most solutions involving boundaries account for sealing or constant pressure boundaries, and any combination when applicable.



*Fig. 8.G.1 – Flow profile in a rectangle with three sides sealing and one at constant pressure
In red the original pressure plan, in black the pressure plan after production*

The combinations are potentially unlimited, but we will illustrate constant pressure behavior by the two simplest, pure, constant pressure boundaries using three examples. These are the linear, ie the constant pressure equivalent of the sealing fault, the circular; the constant pressure equivalent of the closed circle, and a rectangular model where one side is at constant pressure. We will use the geometry described below, and consider the west boundary to be at constant pressure.

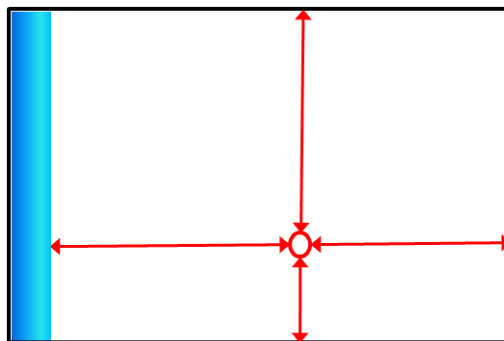


Fig. 8.G.2 – Rectangular reservoir, with a constant pressure west limit

8.G.2 Behavior

As soon as the constant pressure boundary is reached, it will provide the necessary volume of fluid to charge the boundary pressure to its original value to flow into the reservoir. The pressure will stabilize and the derivative will dip. The speed of this dip will depend on the boundary geometry.

8.G.3 Semilog analysis

As for the bounded reservoir models where the final behavior is not a radial flow, the semilog plot does not act as a tool to quantify the constant pressure boundary effect. During the production, the semilog plot will deviate from IARF and will tend to a constant flowing pressure line. For the shut-in, the pressure response will stabilize at average reservoir pressure.

The figures below illustrate this stabilization, the model is constant pressure circular.

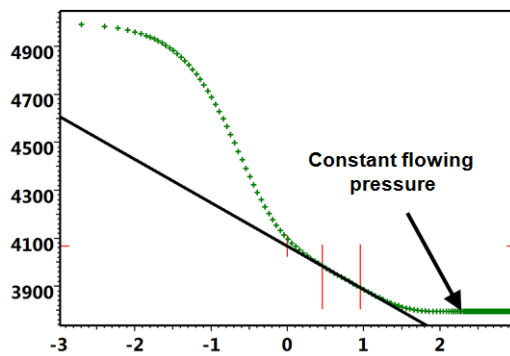


Fig. 8.G.3 – MDH for a production period

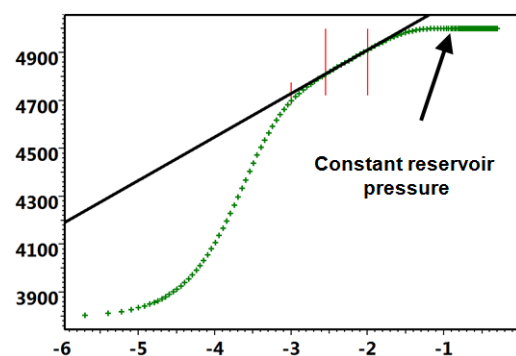


Fig. 8.G.4 – Horner for a Shut in period

8.G.4 Loglog analysis

8.G.4.a Drawdown response

Below, the response of a linear and a circular constant pressure boundaries, for a drawdown, is displayed and compared to their sealing counterpart. The circular boundary derivative response will exponentially dip down, while the response for a linear boundary will dip down with a negative unit slope.

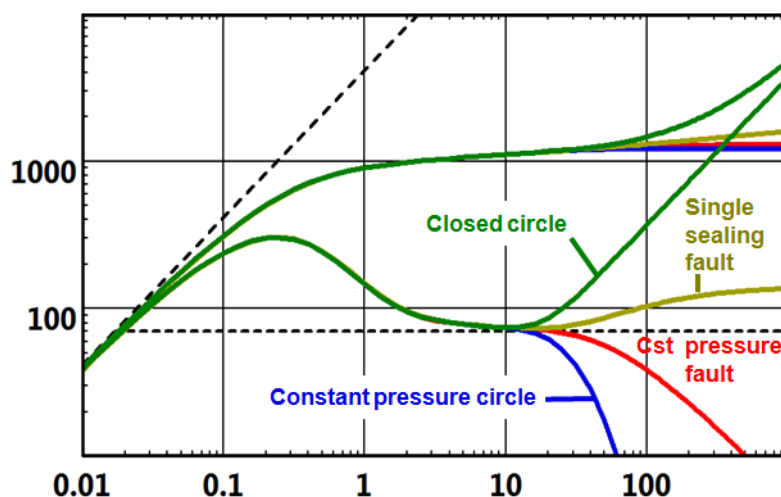
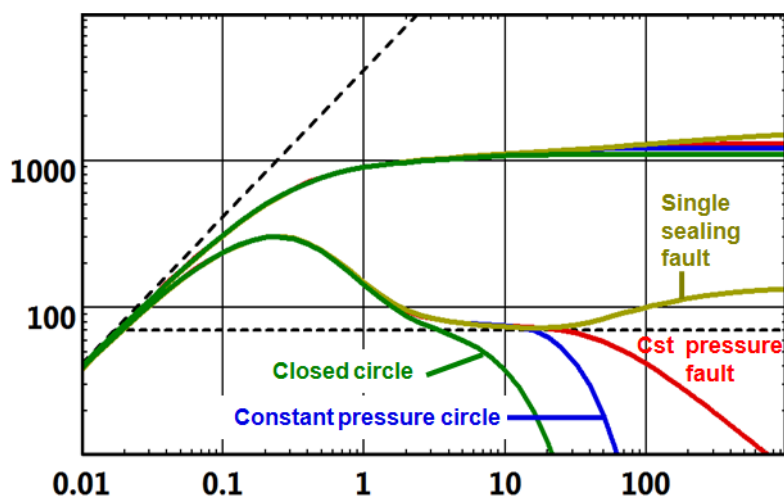


Fig. 8.G.5 – Ct pressure, flowing
Linear and Circular boundaries
Comparison with sealing equivalents

8.G.4.b Build up response

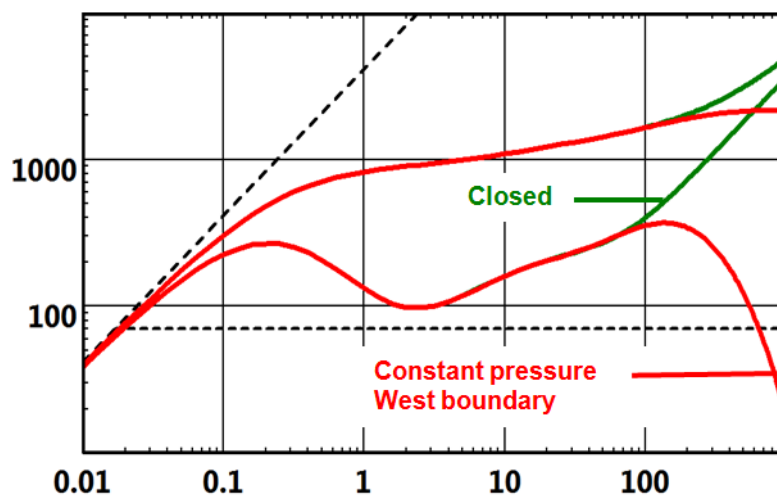
The same responses are shown below and compared for a build-up. In this example, both constant pressure models behave the same way as in the producing phase. This will not always be the case if the producing time is very short and the boundaries are not seen during the drawdown. Then transition effects will be seen during the build-up.

There may also be a slight difference in the shape of the response, due to the fact that the superposition time is used to calculate the derivative. In the case of constant pressure boundaries, it is preferable to use the drawdown derivative, and not the superposition derivative, to get a derivative response matching exactly the shape of the drawdown. But the difference is in, any case, small. And, if the model derivative is calculated the same way as for the data, either option in the derivative calculation will provide reliable and equivalent results after nonlinear regression.



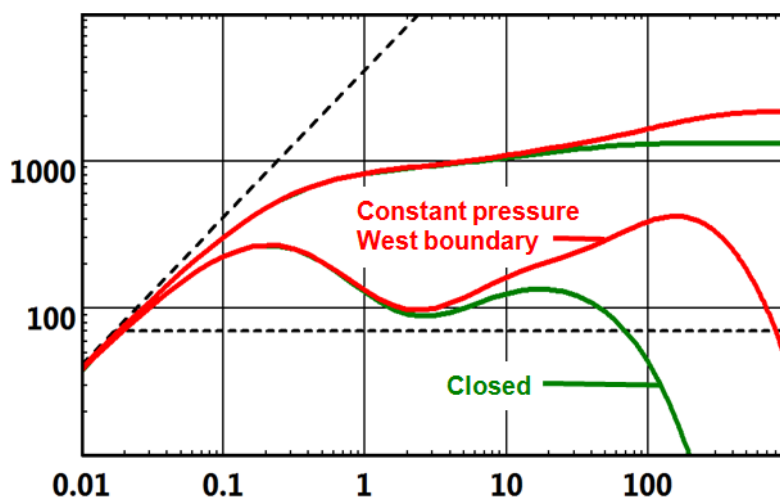
*Fig. 8.G.6 – Ct pressure, shut-in
Linear and Circular boundaries
Comparison with sealing equivalents*

In the figure below we see the response of the rectangular model during drawdown, with and without a constant pressure west boundary. Both responses match until this last boundary is seen. At this point, the closed system will reach PSS displaying unit slope of the derivative, while the derivative of the rectangle with a constant pressure boundary will go down and pressure will stabilize.



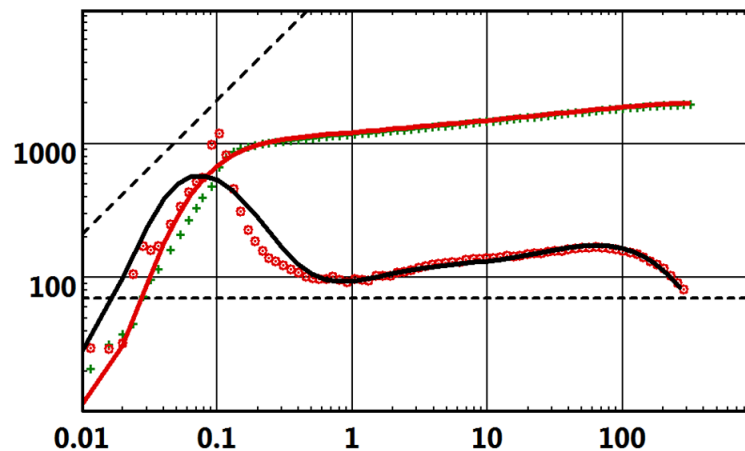
*Fig. 8.G.7 – Rectangle, production
Last boundary sealing or constant pressure*

Now, the same rectangular responses are compared for the shut-in. The closed system derivative response inverts its behavior and dives quickly, while the mixed boundary response shows a very similar behavior. Again, this may not be strictly true if the production time is very short.



*Fig. 8.G.8 – Rectangle, shut-in
Last boundary sealing or constant pressure*

The figure below shows a field example, where the plunging derivative is interpreted as a constant pressure boundary. The same example as illustrated below can also be matched with a closed system model.



*Fig. 8.G.9 – Closed system shut-in
Interpreted with a constant pressure boundary*

8.G.5 Constant pressure vs. closed system

For production responses, there is a clear difference between sealing boundaries that will produce a rise of the derivative, and the constant pressure boundaries that will produce a stabilization of the pressure, hence a fall of the derivative. Unfortunately, for shut-in responses, both closed systems and constant pressure boundaries will show a fall of the pressure derivative. As an illustration the plots below show excellent matches of the same data, with these two very different models.

The loglog plot shows a comparison of this set of data, with two rectangular solutions, one with only sealing faults, one with combinations of sealing and constant pressure boundaries. Again, the quality of the match is excellent, and the slight differences alone would not permit us to discriminate between the choice of models.

There is no answer if all we have is the build-up response. But generally, the uncertainty will be lifted by looking at the rest of the well test, and in particular the starting pressure. When a constant pressure boundary is involved, the final shut-in pressure will invariably revert to the initial pressure.

For a closed system, the final shut-in pressure will be the average reservoir pressure, derived from the initial pressure with a straight material balance calculation. So the starting point of the simulation will be very different from one model to the other.

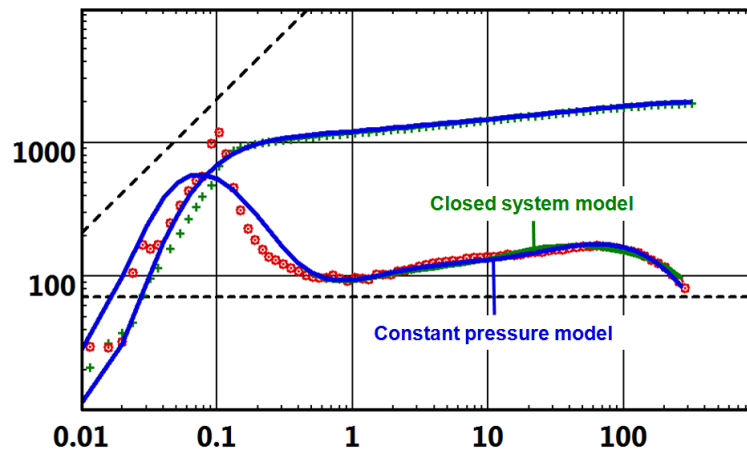


Fig. 8.G.10 – Loglog match of a shut-in
With both constant pressure and closed system models

The history plot below shows the comparison between the two options on the whole production history, showing that the constant pressure system model is absolutely not a realistic option, even if it perfectly matches the build-up response. Unfortunately, the choice is not always that simple.

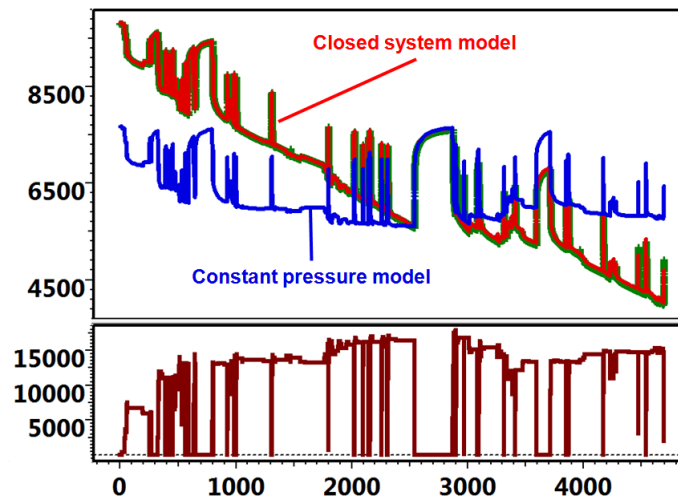
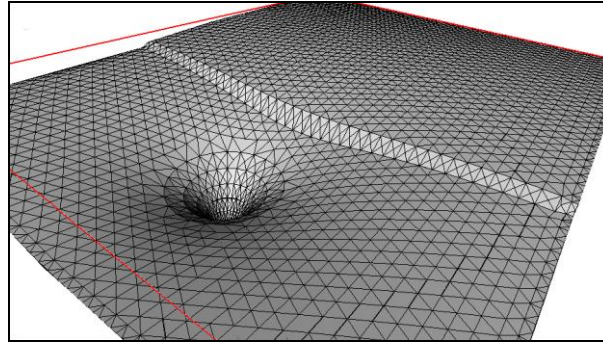


Fig. 8.G.11 – History match with both
constant pressure and closed system models

8.H Leaky and incomplete boundaries

Leaky and incomplete boundaries share similar behaviors, even though the assumptions are different.

Below, a leaky fault: the leakage allows some flow to pass through the fault.



*Fig. 8.H.1 – 3D pressure profile with a leaky fault
The red lines correspond to the level of p_i*

Here below, an incomplete fault: the flow will pass around it.

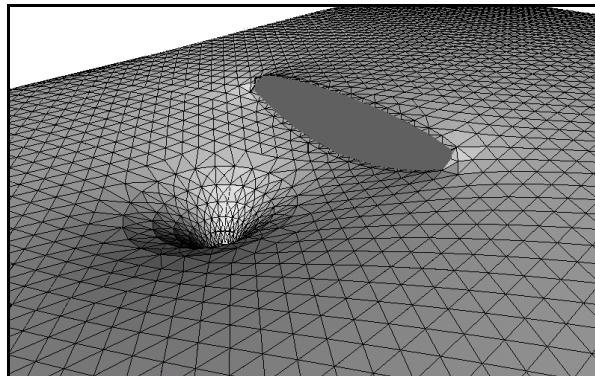


Fig. 8.H.2 – 3D pressure profile with an incomplete fault

In both cases, it is an obstacle that still allows the part of the reservoir beyond the boundary to contribute to the flow. The models will be characterized by a deviation from IARF, then a progressive return of the derivative to the same level.

8.H.1 Leaky fault

8.H.1.a Behavior

Leaky boundaries may be modeled numerically or analytically. We will illustrate the behavior of leaky boundaries with the simplest analytical model, i.e. a single leaky linear boundary of infinite extent. The compartment on the other side of the boundary may have different properties. In the following we will assume it is the same reservoir. If it is not, the behavior described below will have to be combined with a linear composite response.

The boundary is defined by a leakage coefficient α , also called transmissibility ratio. $\alpha=0$ will correspond to a sealing fault, $\alpha=1$ will correspond to an infinite reservoir, i.e. no boundary.

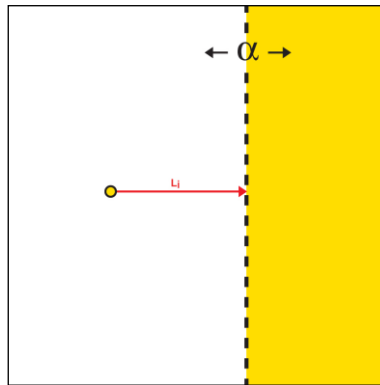


Fig. 8.H.3 – Schematic of a leaky fault

8.H.1.b Semilog analysis

The semilog plot exhibits a first straight line corresponding the IARF in well side of the reservoir then a drop, or increasing slope, describing the restriction to the flow, and finally the plot goes back to straight line parallel to the first one, because the reservoir is identical on the other side of the fault:

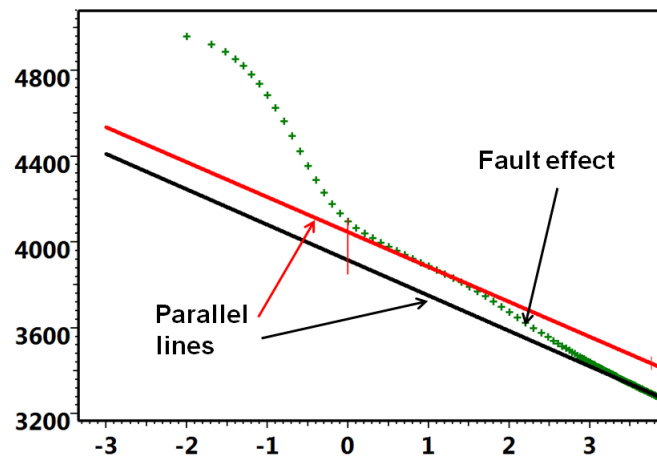


Fig. 8.H.4 – Semilog plot, leaky fault in a homogeneous reservoir

The amplitude of the drop, therefore the distance between the two straight lines depend on the α value. A very small value of α would make the drop to last longer and the distance between the lines to increase.

The behavior that we can observe on a Horner or a superposition plot for a build up is similar and, as mentioned before for other limit effects, the first line is used for the IARF calculation and it is the second one that is extrapolated to get the P^* .

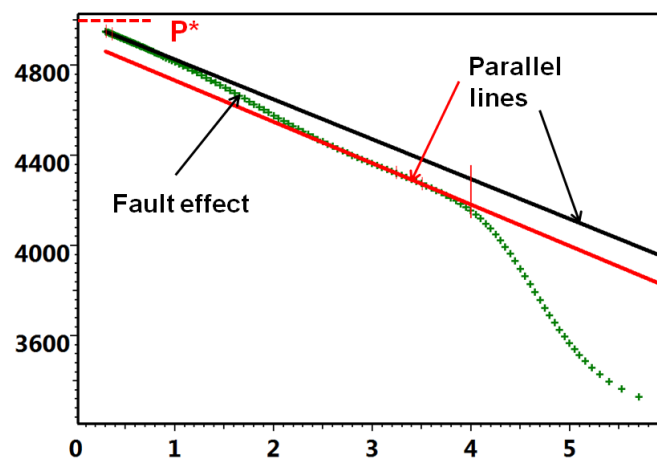


Fig. 8.H.5 – Horner plot, leaky fault, homogeneous reservoir

8.H.1.c Loglog analysis

The figure below shows the loglog response for several values of α . When the fault is detected, the derivative will deviate from IARF as for a sealing fault, albeit with a smoother behavior depending on the value of α . Then the pressure drop through the leaky fault will start to stabilize and the derivative will, progressively, return to IARF provided the reservoir has the same property on the other side of the fault.

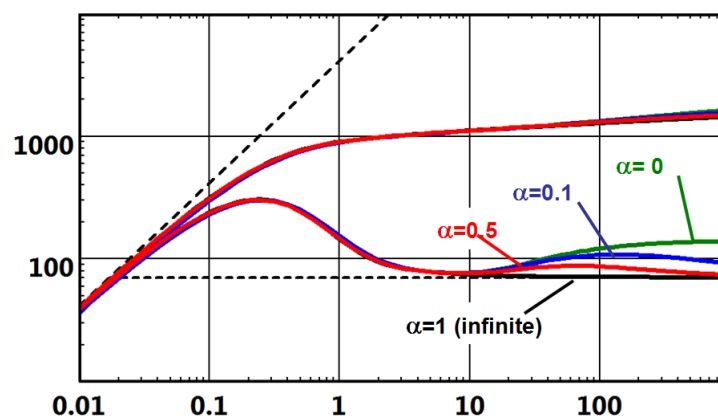


Fig. 8.H.6 – Loglog plot, leaky fault, homogeneous reservoir

It does not mean that when the derivative has returned to IARF the effect of the fault is over. In fact it is not IARF, and there is a cumulative effect on the pressure response, corresponding to the stabilized pressure drop through the fault as illustrated below on the isobar map generated with a numerical model:

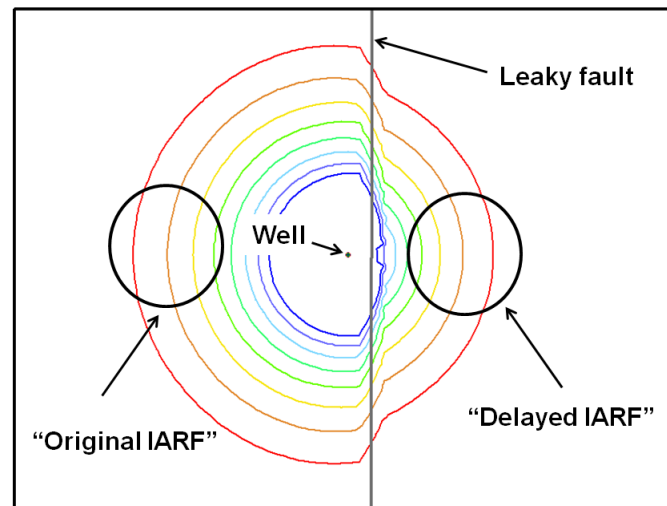


Fig. 8.H.7 – Isobar map showing the pressure drop at the fault

Each color line corresponds to a certain pressure value but it can also be interpreted as an investigation or influence zone at a certain time.

The blue represents the early time influence zone, the green to yellow the intermediate time and the red the late time.

We see on the map that the radial flow goes on the other side of the fault but with a certain delay. That corresponds to an additional pressure drop at the well compared to the infinite system.

8.H.2 Incomplete boundary

8.H.2.a Behavior

Incomplete boundaries are easily modeled numerically. To illustrate the behavior we will use an incomplete fault with various positions of its end with respect to the well as shown below.

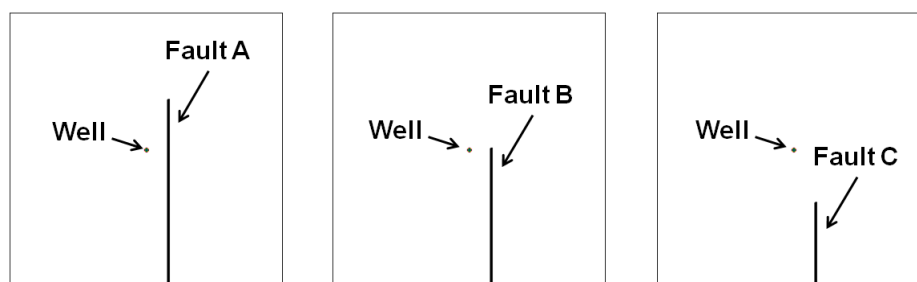


Fig. 8.H.8 – Half fault in positions A, B, C

The presence of the fault influence temporarily the pressure behavior, it creates a deviation from the IARF but when the pressure signal 'turns around' the fault, the complete reservoir contributes then to flow and the behavior goes back to IARF. It just remains a partial restriction to the drainage, creating an additional pressure loss.

The time when the fault effect is observed depends on the distance to the fault. Its amplitude depends on its position: the more the fault is in front of the well, the higher is the amplitude (case A).

8.H.2.b Semilog analysis

The semilog plot shows first an IARF straight line then a drop, or increasing slope, due to the obstacle created by the fault, then the plot show a second straight line parallel to the first one, corresponding to the complete drainage of the reservoir.

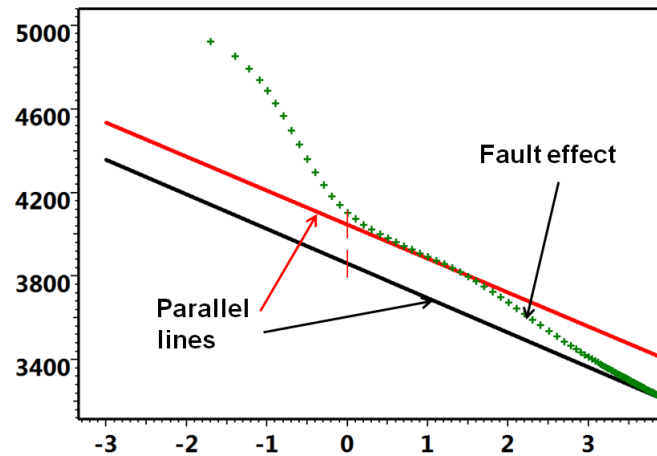


Fig. 8.H.9 – Semilog plot behavior for a incomplete fault

The build up behavior is identical. The first line is used for the IARF calculation and the second one to extrapolate to P^* .

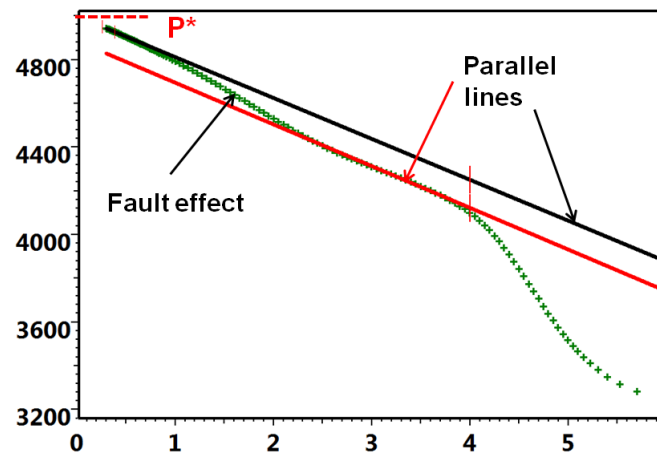


Fig. 8.H.10 – Horner plot, behavior for a incomplete fault

8.H.2.c loglog analysis

The figure below shows the loglog behavior for these different cases. The response corresponding to the fault B is already very close to infinite behavior, and fault C case would show absolutely no boundary effect.

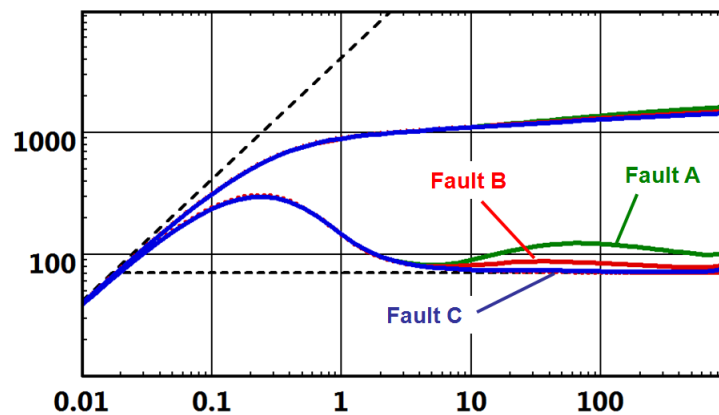


Fig. 8.H.11 – Loglog response of a incomplete fault in positions A, B, C

Below, the isobar maps plotted for a certain time of production illustrates very well the influence of the position of the incomplete fault on its effect on the pressure behavior.

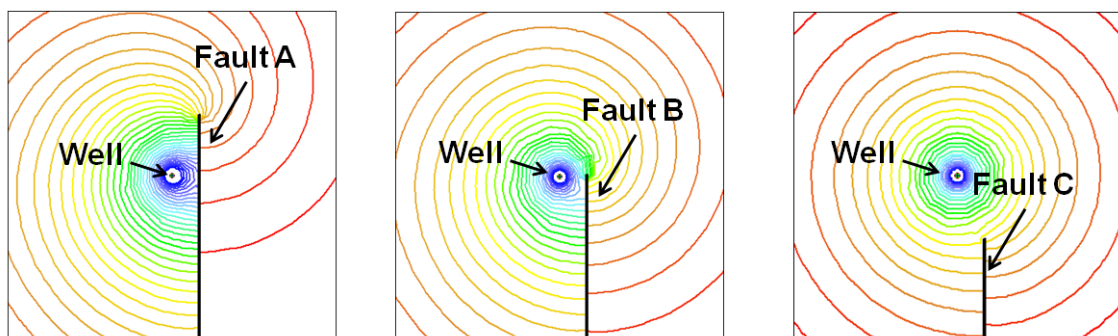


Fig. 8.H.12 – Isobar maps for three positions of an incomplete fault

For the fault B case, the early time and the intermediate time are influenced but the late time get very close to the classic circle of an Infinite Acting Radial Flow.

In the case C, the early and intermediate time are in infinite acting radial flow and the fault is hardly influencing the late time isobar lines.

8.I Conductive faults

Conductive faults can be modeled both numerically and analytically. In this section we will use the analytical model which is part of Saphir external models to illustrate its use and pressure response. We will use the numerical model for its display facilities.

This model solves for the pressure behavior at a well near a non-intersecting finite conductivity fault or fracture. The solution includes an altered zone around the fault with the possibility to add skin across it. The reservoir properties on either side of the fault can be different.

3D schematic of the model:

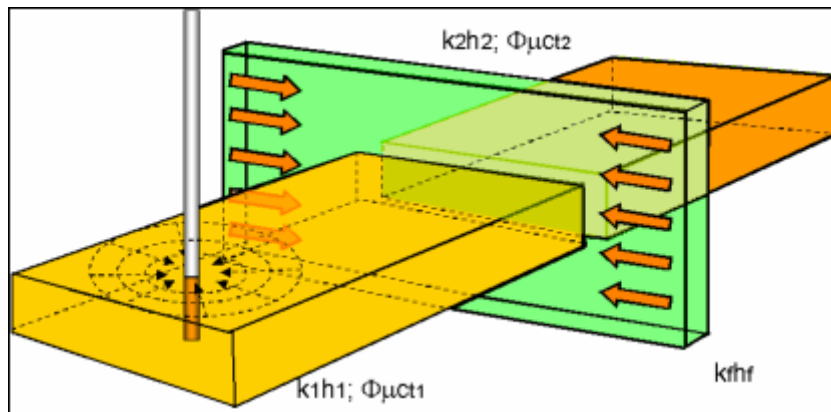


Fig. 8.I.1 – Conductive fault model schematic

The model needs the following parameters:

kh and skin of the well side, the distance to the fault or the fracture, the conductivity and skin of the same and the mobility, M and diffusivity, D ratios defined as the ratio of the well side parameters divided by the parameters of the reservoir on the other side of the fault or fracture:

$$\text{Mobility ratio: } M = \frac{(k/\mu)_{\text{well side}}}{(k/\mu)_{\text{other side}}}$$

$$\text{Diffusivity ratio: } D = \frac{(k/\Phi\mu c_t)_{\text{well side}}}{(k/\Phi\mu c_t)_{\text{other side}}}$$

8.I.1 Behavior

After wellbore storage, the next flow regime would be, typically, IARF reflecting the permeability and skin of the reservoir around the well. This would be followed by the influence of the fault seen as an increase in mobility, then by a linear flow corresponding to the drainage of the reservoir by a linear source. When the investigated reservoir area is large enough and the fracture flow is not anymore dominating a final IARF can be observed

An isobar map, generated after a certain of production can help to visualize the type of behavior due to a conductive fault.

Each color line corresponds to a certain pressure value but it can also be interpreted as an investigation or influence zone at a certain time.

The blue represents the early time influence zone, the green to yellow the intermediate time and the red the late time.

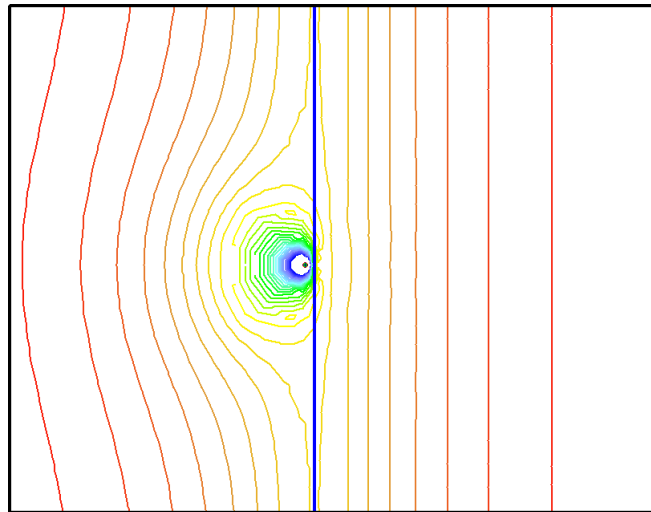


Fig. 8.I.2 – Isobar map conductive fault

We can observe in blue and green the early IARF before any fault effect.

At early time, on the well side, the radial flow is influenced by the uniform pressure imposed by the conductive fault while, that create the derivative dip.

On the other side of the fault, the parallel isobar lines characterize a linear flow which dominates at late time, until a larger zone is interested and a final radial flow is established.

8.1.2 Semilog analysis

The semilog plot can be used, when the fault is far enough and when the IARF can be observed before the conductive fault effect. The challenge is to detect the time interval where to draw the semilog straight line, it is recommended to determine it from the loglog derivative.

This limitation makes the semilog plot of not much interest in this case:

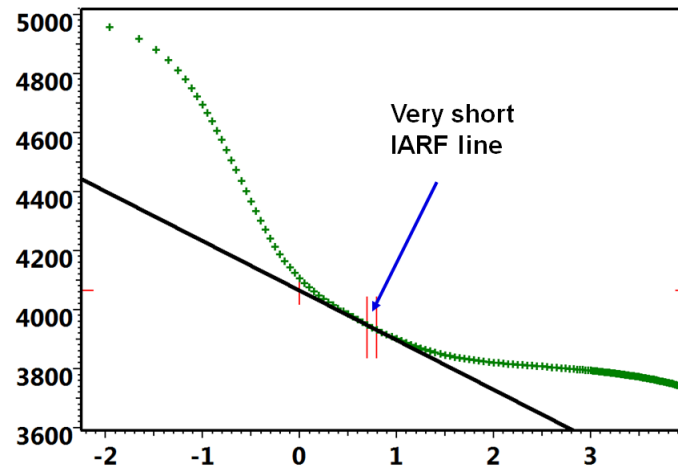


Fig. 8.1.3 – MDH plot for a conductive fault behavior

8.1.3 Loglog analysis

A first derivative stabilization corresponding to the initial IARF in the reservoir around the well can be observed before the fault effect. Then the derivative drops until bilinear/linear or linear flow develops in the fault (fracture) and the derivative follows a positive $\frac{1}{4}$ / $\frac{1}{2}$ or $\frac{1}{2}$ slope. The $\frac{1}{4}$ slope, or bilinear flow, is evidence of finite conductivity in the fault or the fracture, the $\frac{1}{2}$ slope (linear flow) alone is a sign of infinite conductivity.

Finally a homogeneous global behavior should be observed with IARF stabilization at a level governed by the mobility ratio M .

The figure below illustrates the effect of the distance to a low conductivity fault or fracture (100 mDft). It can be seen that the transition through the fault ends with a $\frac{1}{4}$ slope (bilinear flow) before reaching the second IARF stabilization (M and $D = 1$). When the fault is far enough it can be observed an IARF on the well side before the fault effect.

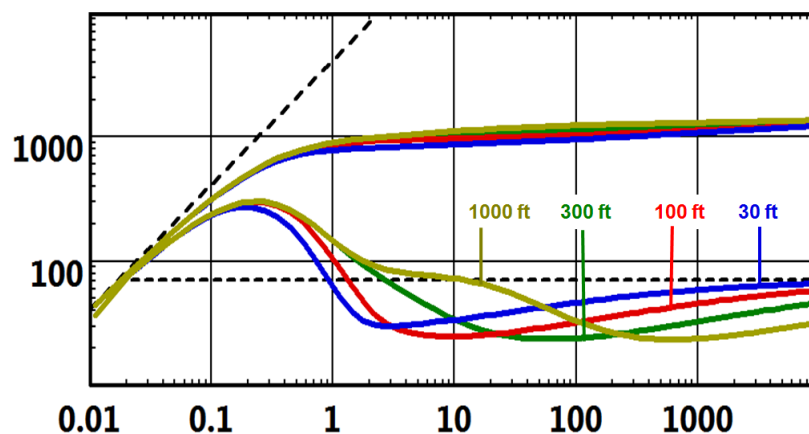


Fig. 8.1.4 – Effect of distance to fault

The figure below illustrates the effect of the distance to a high conductive fault (100000 mDft). In this case the transition through the fault is much deeper and ends with a $\frac{1}{2}$ slope (linear flow) before reaching the second IARF stabilization (M and D= 1).

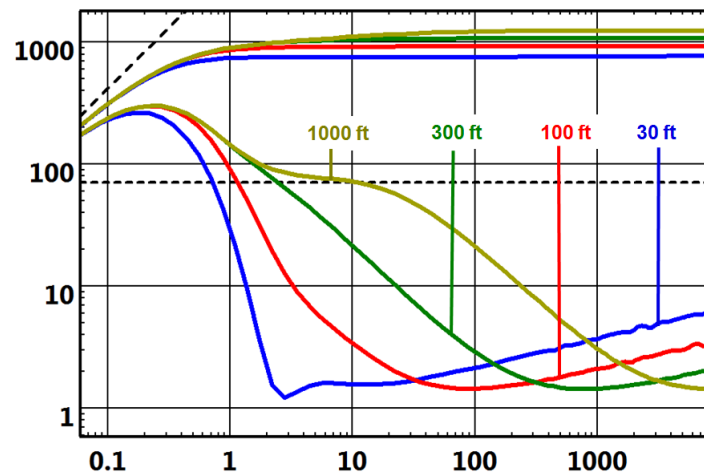


Fig. 8.I.5 – Effect of distance to fault

The figure below illustrates the effect of a change in the fault skin. The damage at the fault creates a hump on the derivative and the transition through the fault happens later as the skin increases. The distance to the fault is 1000 ft and the fault conductivity is 1.e5 mDft, M and D=1.

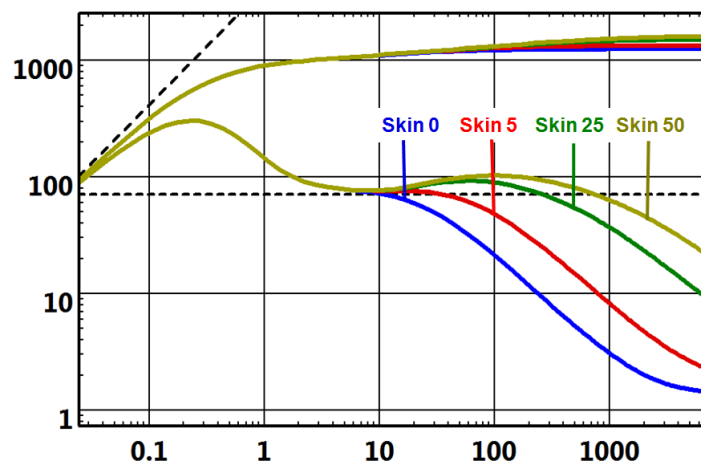


Fig. 8.I.6 – Effects fault skin

The below figure shows the influence of a change in mobility. The conductive fault has a permeability thickness product of 1000 mDft, the distance to the fault is 1000 ft, the fault skin is zero and the permeability thickness of the well side of the reservoir is 1000 mDft.

What is important to note here is that when the mobility increases the tell-tale bilinear and linear flow is largely masked.

The mobility ratio changes the level of the second level of IARF (final stabilization = first stabilization $\times 2 / (1 + 1/M)$).

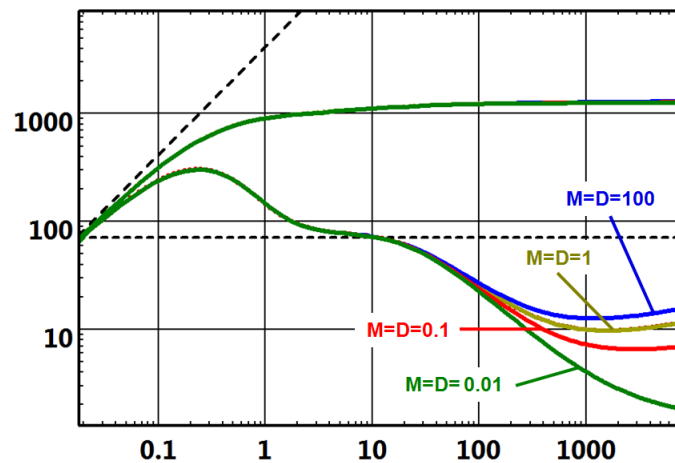


Fig. 8.I.7 – Effects of mobility changes

Note that when M tends to infinity (ie with no 'other side of the fault' conductivity) the second stabilization is twice that of the first IARF level; equivalent to a single sealing fault. Equally, when M tends to zero, the response is equivalent to a constant pressure fault. This is in line with the response of the linear composite reservoir model. However, for intermediate increases and decreases in mobility the conductive fault model retains the diagnostic sign of the presence of the fault or the fracture rather than the linear interface assumption used in the linear composite reservoir model. The figure below illustrates this.

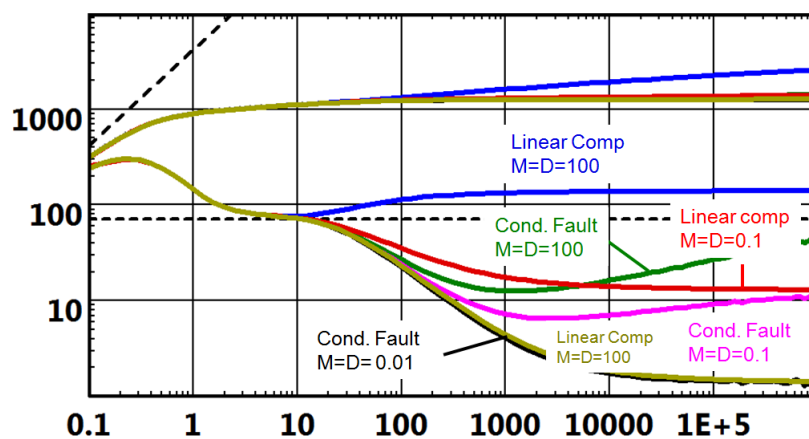


Fig. 8.I.8 – Comparison Conductive Fault and Linear Composite

8.J Combination with other reservoir and well models

All boundary models described above have been presented assuming a fully penetrating vertical well, with constant wellbore storage and skin, in a homogeneous reservoir. In real life, we will have to combine a wellbore, a well, a reservoir and boundary models, each of them having its own signature.

In an ideal world, one behavior will occur after the other, and logic dictates that we see first wellbore effects, then the well geometry, then IARF and/or reservoir heterogeneities, and then finally boundary effects. The figure below shows such a simulated combination. In this case, discriminating all behaviors would require six logarithmic cycles, provided that the parameters are such that one behavior starts exactly where the previous ends. In the case shown below, with IARF occurring after one hour, this means a test duration of 10,000 hours. So in real life this will not happen, and these different behaviors will often occur at the same time. Sometimes, and to make matters worse, they will not occur in their logical order, and a reservoir heterogeneity may, for instance, occur after the first boundary is seen.

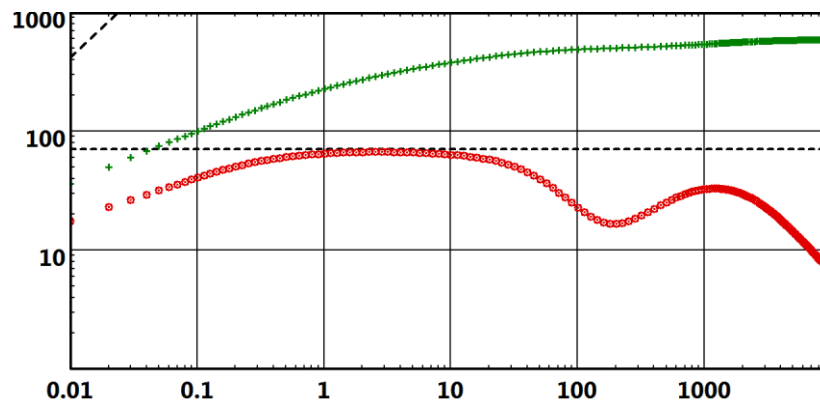


Fig. 8.J.1 – Fractured well in a double-porosity reservoir and a constant pressure linear boundary analytical simulation over six log cycles

The name of the game is common sense. In general, these behaviors will aggregate, or one will override the other. When the engineer has a good knowledge of how individual features will show up on the derivative, he/she will easily figure out, qualitatively at least, what the resulting combination may look like. But there may be 'numerical' surprises, and only the generation of the model will confirm this guess.

The above is a general comment. What is specific to boundaries is that they occur at late time and are numerically even more sensitive to errors and residual behaviors.

8.K Assessing boundary effects

In the previous sections we have described how the different boundary models will behave. Assuming that the boundary is the last behavior in the derivative response, the principle will be first to match the early and middle time behavior with the right wellbore / well / reservoir model, or alternatively in the situation where the data appears to be of poor quality, figure out why we cannot match the early time and at least get a fair estimate of the mobility, i.e. the pressure match, in order to gain a realistic relationship between the boundary distance and the time at which it is detected.

If this is done, the initial estimate of the boundary parameters will be relatively easy. The mobility and the identification of the time of deviation from IARF will give the distance(s), and various specialized analyses or interactive pick options will allow us to assess the other parameters. For example the angle between intersecting faults will be obtained by indicating the level of the second derivative stabilization by the click of the mouse.

After the initial model generation, and assuming that we think this is the right model, the principle will be to adjust the boundary parameters. This will be done manually and/or by nonlinear regression.

Manual improvements will be very effective to correct the initial gross mistakes, as the rules of thumb are pretty straightforward. For the distances, the basic rule is that for a given mobility the governing group is t/r^2 . In other words, if we see that the model is showing the boundary behavior at the 'wrong' time, multiplying the boundary distance by two will multiply the time of occurrence by four. More realistically, for small multipliers $(1+\xi)$ where ξ is small, it means we get a time of occurrence $\xi\%$ longer, we will need to set a boundary distance $(\xi/2)\%$ further away. There are also software related 'tricks' that correct the boundary distance by sliding the match, but that will not be detailed here.

Using nonlinear regression to improve the boundary parameters will require a little more caution. Because the boundary effects are a late time behavior identified on a relatively small pressure change, the match will be very sensitive if the early time of the response has not been correctly matched. If one runs an optimization on all parameters; kh , skin and boundary distance, starting from an initial model where the infinite acting part is not matched, typically, the boundary distance will go bananas. Advanced software features, such as genetic algorithms, are improving the process, but these are not really needed if the engineer knows what he/she is doing.

The recommended procedure is to get a match first on the early part of the response. This will be done, for example, using an infinite model and optimizing all parameters on the part of the response that is not influenced by the boundary effect. Then, the boundary will be added, and generally the remaining work will be to regress on the boundary parameters, keeping the other parameters, especially the mobility, constant. Sometimes, adding the boundary will have a small effect on the match, and it might be necessary to allow the mobility to vary, or make a small correction to the mobility before running the regression.

The above is only valid if a good early time match is possible. Sometimes it will not be, because early time data is messy, or the combination of wellbore / well / reservoir / boundary models is just not available. It will still be possible to use optimization on the boundary distance if the following rule is followed. 'However nasty your early time match, the important thing is that the simulated pressure, at the time where the derivative deviates from IARF, is spot on'. This can be achieved by making a first optimization on skin only, the target being this particular point in time from which IARF will deviate. Then, if we keep all parameters not related to boundary, including the skin, constant, and if optimization is only performed on points after IARF, this will work.

Last but not least, there is information on boundary effects that may be obtained beyond the signature of the build-up derivative. This was already shown in section H, where the simulation match could discriminate between a no-flow and a constant pressure boundary. This is what we call the 'missing boundary'. If we consider a closed system, we may only assess one or two distances from the build-up response. The principle then is to add the missing boundaries at a distance large enough to be unnoticed in the build-up, and then run a nonlinear regression on the total production history, keeping all parameters that ensure the quality of the build-up match constant, in order to improve the objective function. This may not always work, but if there has been depletion during the production, matching the initial pressure will at least provide a rough estimate of the reservoir size, even if individual boundaries are not calculated.

8.L Radius of investigation vs minimum reserves

One of the most abused results in well test interpretation is the radius of investigation. By itself it is a harmless relation between time and distance for a given mobility. The most common definition of the radius of investigation is linked to the circular area where flow would reach PSS at a given time:

$$r_D = 0.029 \sqrt{\frac{kt}{\Phi \mu c_t}}$$

This definition is harmless as long as it is not used. But the trouble starts when somebody else with no well test background takes this number, calculates the corresponding pore volume, assigns a recovery factor and uses this number to assess minimum proven reserves. This is, of course, completely erroneous, and for several reasons:

1. This definition assumes that the flow is radial homogeneous. This definition will lose its meaning when we are confronted by complex configurations that might include fractures, horizontal wells, lateral boundaries, composite zones and heterogeneous formations. So we should speak about area of investigation, or better still, the volume of investigation.
2. This definition does not take into account the gauge resolution and the overall quality and noise of the pressure response, which may or may not allow us to detect the boundary effect.
3. What time are we talking about? In the case of a build-up, is it the duration of the shut-in, or the duration of the test? After all, as shown in the previous section, it is possible to get some information from the history match.

It is indeed possible to obtain a decent estimation of minimum reserves, but certainly not using the radius of investigation. This can be achieved using boundary models as follows:

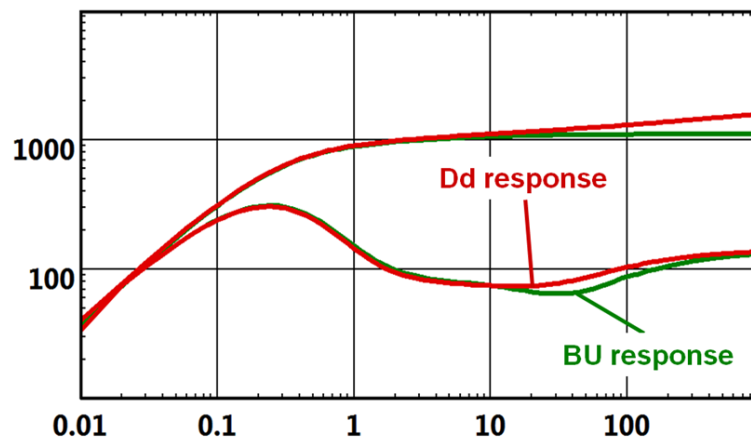
1. If you have diagnosed a closed system and managed to identify all limits, the problem is over, and the reserve estimates will correspond to the pore volume of your reservoir times a recovery factor.
2. If you have not diagnosed a closed system, and even if you have only used an infinite model, the principle is to find the minimum size of the reservoir that is consistent with your well test response. If you have diagnosed an infinite reservoir you will take the same model and start with an arbitrarily large circular or square reservoir. If you have identified some, but not all, boundaries you will complement and close the system with additional, arbitrarily far boundaries. Then, in both cases, you shrink the reservoir model as much as you can, to get to a point where, if the reservoir was smaller, you would have detected and diagnosed the additional boundaries during the test. This is of course a much more subjective approach than a simple equation, but, from an engineering point of view, it is the only one that makes sense.

8.M Superposition effects

8.M.1 Can we see a fault in a build-up and not in the drawdown?

Theoretically, nothing prevents us from detecting the reflection of the pressure signal of the boundary after the well was shut-in, even if this was not detected during the drawdown. In practice, it is a matter of the amplitude of the signal, resolution of the gauges and background noise. More generally, if we consider a given production, the shut-in will be interpretable as long as the amplitude of the residual pressure signal is within the gauge capabilities, and the background noise does not jam this residual signal. Under these conditions, the initial duration of the production is not an absolute limit for the duration of an interpretable build-up. So it is possible, and routinely happens that we investigate during the build-up, a larger area than what was seen during the drawdown. The rules of thumb relating the production time and shut-in time were set at a time when the quality of the measurements was much lower. That said, they are not so bad, and should be overridden only after a careful test design.

There is even an extreme behavior that may be seen under exceptional conditions. In the case of a short production time, as mentioned in a previous paragraph, the reflection of the production information on the boundary may not have reached the boundary before the well was shut-in. So this information will reach the well after the shut-in, followed by the reflection of the shut-in itself. When the reflection of the production reaches the well, the derivative will go down, then back up when the shut-in information bounces back. The derivative will then look as below. It requires an exceptionally good signal and gauge, but it is seen from time to time. The presence of a slight valley in the derivative should not be, of course, systematically interpreted as such an effect, as the amplitude of the pressure signal is very small. But, in the case of a short production time, if the model also exhibits such transition behavior, this will be the explanation, and actually a sign of very good data quality.



*Fig. 8.M.1 – Loglog response for a sealing fault
Drawdown response vs. shut-in for a short production time*

8.M.2 Superposition effect consequence on the boundaries diagnosis

The above signalled effect can be observed in case of multiple limits at different distances and therefore different times. i.e. A nearby fault can be observed during the production while a further limit could not have been detected but its effect will appear during the build up.

It results that the multiple limit behaviour observed on a build up can be quite different from the expected behaviour that was described for a production period.

It is a reason why the 'typical derivative behaviour' catalogs have a limited interest as long as they represent drawdown behaviour, excluding any superposition effects and we usually interpret build data.

The figures below show not only how the build up response can differ from the drawdown response but also how the same short production duration can have a different influence on different intersecting faults geometry.

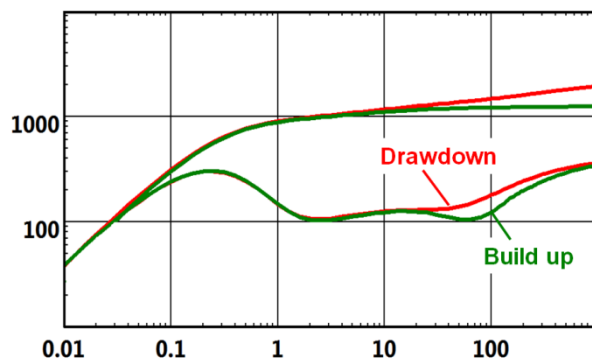


Fig. 8.M.2 – BU response after a short production on intersecting faults

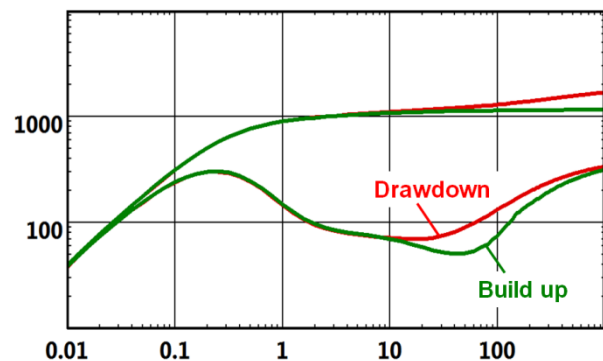


Fig. 8.M.3 – BU response after the same short production on different geometry intersecting faults

The same is observed in case of parallel faults: even the position of the half unit slope differs on the build up, that limits the quantitative result validity of the conventional '1/2 unit slope straight line' drawn on the derivative.

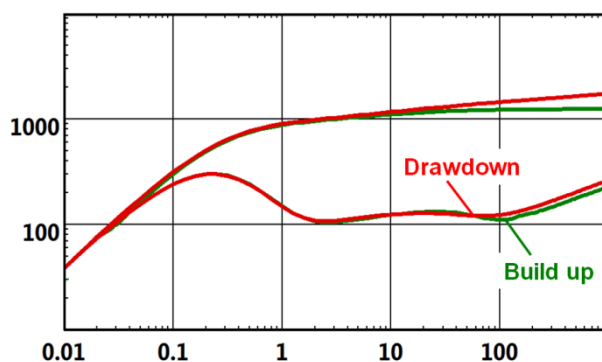


Fig. 8.M.4 – BU response after a short production on parallel faults

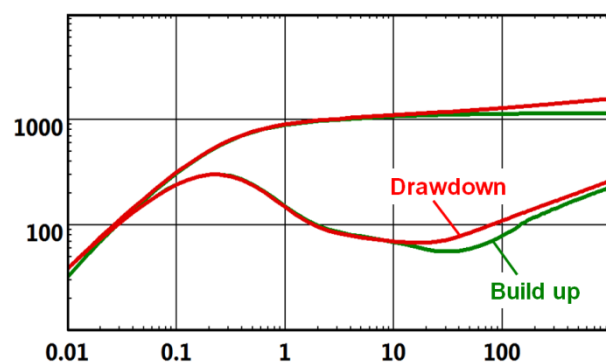


Fig. 8.M.5 – BU response after the same short production on different parallel faults

When dealing with a closed system the superposition and the build up effects cumulate and they become more crucial.

In the figure below we compare the drawdown derivative shape with two build ups after a long and a short production period.

It was already known that the drawdown and build up behaviour are systematically different in case of Pseudo Steady State but it also shows clearly that the two build up derivatives are also different and could lead to misinterpretation.

The long production duration build up derivative (in green) dips at the P.S.S.

The short production duration build up derivative (in blue) dips also but additionally it is subject to a deviation at intermediate time.

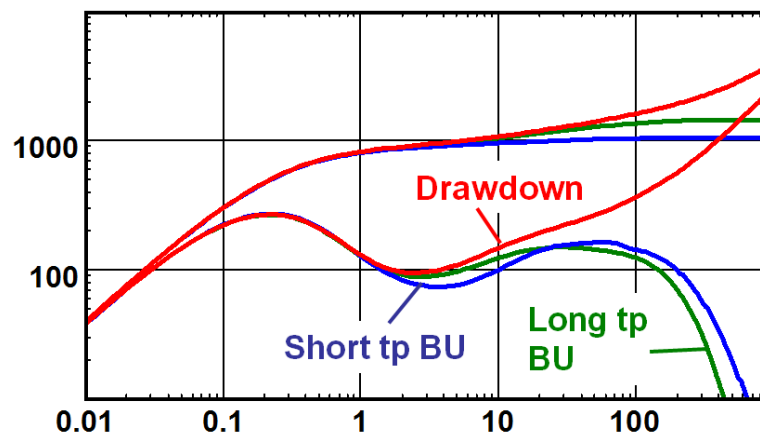


Fig. 8.M.6 – BU response after short and a long production on the same closed system

The diagnosis of multiple boundaries on build up data is not as straight forward as it appears if we only rely on the drawdown typical derivative behavior. The shape is highly influenced by the previous production history and only a model derivative taking into account the various superposition effects must be used for a final match with the data.

8.M.3 Conclusion

The only pure conventional boundaries effect can be observed on the production period data, assuming a constant production rate but the production period data are usually noisy due to rate instabilities.

The build up data, supposed to be more stable, are therefore classically used for analysis purpose, and their sensitivity to the superposition effect makes the diagnosis more difficult, it requires more experience and impose the used of software based on the model matching method.

A simpler answer could be brought if the build up data, victims of the superposition, could be 'de-superposed' in order to appear as a drawdown response to a constant rate, this is called the Deconvolution method and it will be developed in the next chapter.

8.N Typical errors diagnosing a boundary effect

Boundary effects are typically diagnosed from a derivative trend at the end of a build-up, when the pressure approaches stabilization. The derivative is a magnifying glass and a lot of importance is given to a signal of very small amplitude. The derivative may pick up a signal that has nothing to do with boundaries, or errors somewhere else may have an effect on the pressure, or on the superposition time from which the derivative is calculated. This may result in the improper diagnostic of a boundary effect. We will list below the most common mistakes.

8.N.1 Incorrect production history

This is certainly the most commonly known problem, but it is still, also, the main source of misinterpretations. The derivative calculation corrects the pressure scale in order to account for the details of the well production history. If this history is taken into account in the superposition time, the IARF behavior will result in a stabilized derivative. Conversely, if some relevant rates are not taken into account, or wrongly estimated, this will result in an artificial late-time trend in the derivative. Considering the wide range of models and behaviors described above, there will be no difficulty in finding several boundary models to match this trend.

In the figure below, on the left, a partial production history (last 60 hours well test data) was used to generate the loglog plot of a field data set. The derivative exhibits a clear 'boundary effect': it is actually the result of a false superposition calculation with a too short production time.

The right side plot shows the result when using the complete production history (adding 440 hours of previous production): no more boundary effect can be too 'easily' diagnosed.

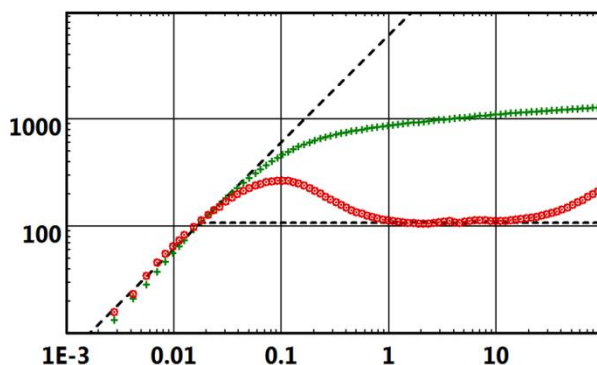


Fig. 8.N.1 – Loglog field data response with IARF using incomplete production duration

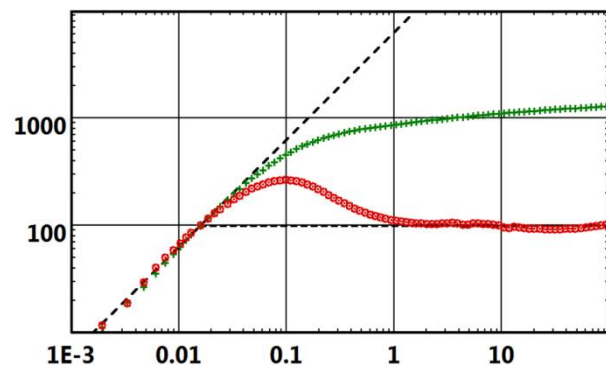
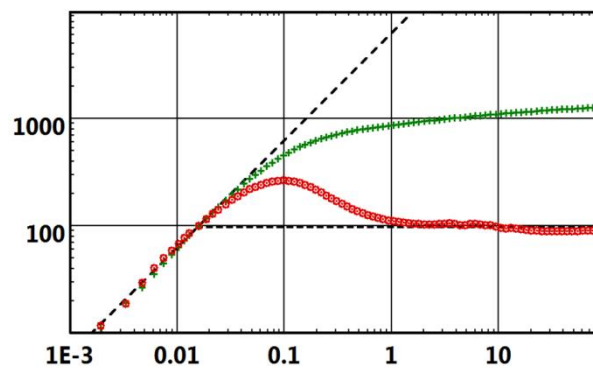


Fig. 8.N.2 – Loglog field data response with IARF using correct production history

Using a false too long production history (1000 hours more) can also have an incidence on the derivative shape. The resulting curve, below, does not really show a boundary effect, but the apparent mobility will be over-estimated. In other cases the response will display an artificial constant pressure boundary.



*Fig. 8.N.3 – Loglog field data response
With over-estimated production time*

Generally speaking, this rule of thumb works: when you under-estimate your production time you under-estimate your reservoir, i.e. your kh will be too low or you will see a no-flow boundary that does not exist. When you over-estimate your production time you over-estimate your reservoir, i.e. your kh is too high or you will see a constant pressure boundary that does not exist.

8.N.2 End effect in the derivative calculation

The derivative, which is the slope of the semilog plot displayed on the loglog plot, is numerically calculated from the data. At a given point, the derivative generally comes from a 3-point central calculation process. The central point is the considered pressure point, the choice of the left and right points will depend on the smoothing.

Most algorithms take a superposition time window around the considered point, the smoothing being the distance between the point and each window limit. The program then selects, to the left and the right, the first points outside the window, and with these two additional points, makes a 3-point central calculation of the slope.

In the middle of the pressure response there is no problem. But, towards the end of the response the last point will be systematically used as the right point in the derivative calculations of all the data within the smoothing window. If this last point is wrong, and it may not even be displayed on the loglog plot, it will induce a trend in the smoothing that may be confused with a boundary effect.

Even if the way to calculate the derivative is different, an incorrect end point will generally create this sort of error.

The best way to avoid this problem is to properly set and synchronize the rate and pressure histories. But if this is overlooked, one way to check this sort of problem is to change the derivative smoothing. If the late time, boundary looking behavior changes with the smoothing, then the engineer will have to look for a possible erroneous point.

8.N.3 Gauge drift

If a gauge is drifting, it will add an artificial linear function of time to the pressure response, systematically creating a pseudo-boundary effect as soon as the slope of this drift becomes non-negligible compared to the effective change of pressure. The drift will affect the whole pressure response, but will only affect the shape of the derivative at the end of the response, hence creating this apparent boundary response.

When several gauges are run it is easy to identify drifting gauges if proper Quality Control is performed. If only one gauge is run, then one should select a type of gauge that will be unlikely to drift within the expected test duration.

The loglog plot below shows a comparison between two gauges used for the same test. Before deciding which gauge was correct, it was necessary to make a basic calibration check (i.e. at atmospheric pressure). In this case a 9 psi indicated pressure increase was found on the 'guilty' gauge, between before and after the measure.

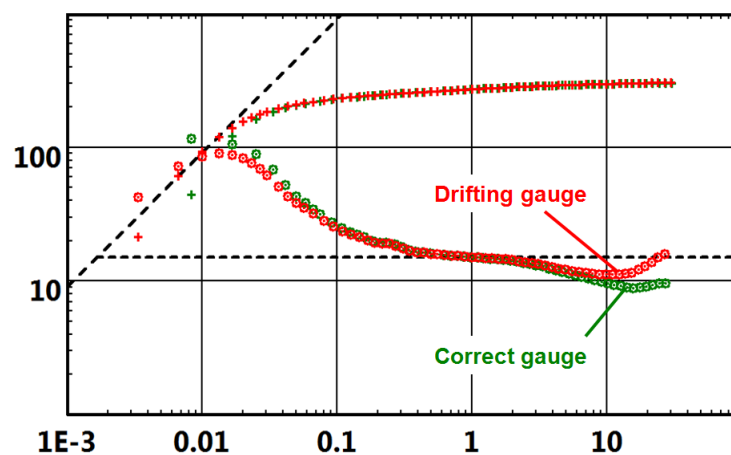


Fig. 8.N.4 – Gauge drift effect on the derivative shape

8.N.4 Reservoir trends

Reservoir trends will have the same effect as a drift. A producing reservoir may have a trend. For example, if an injection campaign was started recently the trend may be upward. Conversely the reservoir may have a depleting trend. When we run a well test we are applying a disturbance and observe the reaction to this disturbance. As the reservoir trend has nothing to do with this disturbance, it is perfectly justified to correct the pressure response by the observed trend. The principle is to run the gauge and monitor the pressure response for some time before starting anything related to the well test. The slope of this trend may then be used to correct the pressure data. We will then not interpret the pressure response but the corrected pressure, i.e. the pressure that would be, hopefully, observed if there was no reservoir trend.

8.N.5 Interference from other wells

If boundary effects can be modeled using virtual image wells, one can guess that the interference of real wells may induce virtual boundaries. The best example of a virtual boundary is the limit of the drainage area.

In a producing well, when you shut a well in and have not done anything recently on the nearby wells, the residual transient signal due to these wells will be negligible for the duration of the test. But for long term testing, or if the production of the nearby wells has changed, they may induce false boundary effects.

The author recalls an interpretation he had to do on a producing well on which a simple build-up survey was run. The response showed a constant pressure boundary that was making absolutely no sense. After (too) much time the author discovered that, in order to assure constant production, the production of the closest well had been temporarily increased simultaneously with the shut-in, hence creating an opposite image well, hence creating a ghost boundary at half the distance between the two wells.

When the engineer is in doubt about the influence of nearby wells, the best thing is to run a first interpretation without the wells, then run a second model adding the interference of nearby wells. If the difference between the two models is negligible, the engineer may return to the simpler interpretation and ignore the effect of interference.

That can be illustrated by a field example.

Below left is the pressure response acquired during the final build up of a well test, it can be adjusted with an analytical multilayer model. But if we compare this response with the one given during the previous build up it reveals an inconsistency see on right side plot.

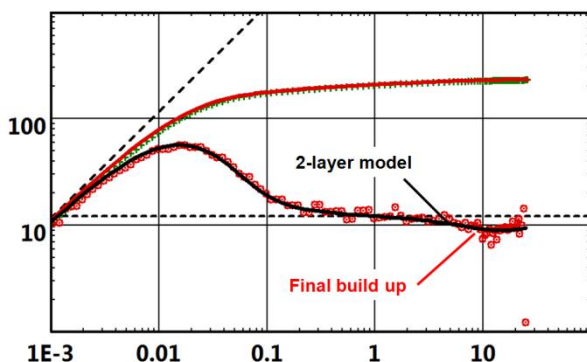


Fig. 8.N.5 – Build up raw data matched with a 2-layer model

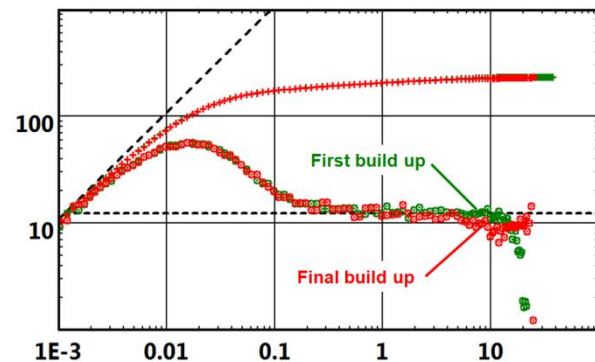


Fig. 8.N.6 – Comparison between two build ups Loglog plot response

In fact a nearby well (2200 ft distance) was opened for 50 hours and then closed during this test, creating interferences. Another well test performed in quiet conditions no other well was opened or closed but just left in their status reveals the truth, an homogeneous behavior:

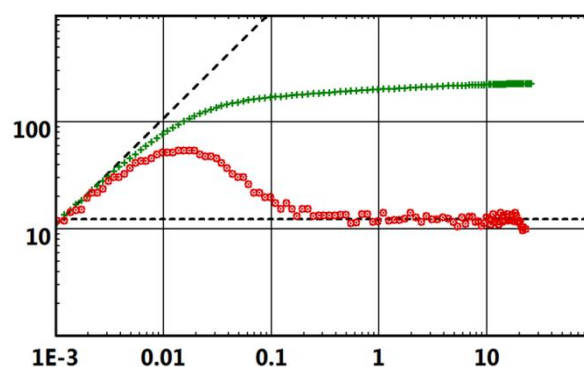


Fig. 8.N.7 – Pure build up response without any other well interference

8.0 Deconvolution

As already mentioned above, the analyses are generally performed on the build up data for acquisition and stability reasons. Unfortunately these periods are limited in time and most of the information is contained in the 'noisy' production periods. Another fact, in addition to the short duration the build up data are subject to the superposition effect influences and the boundaries diagnosis become more difficult.

One solution is to get rid of the superposition effect and to take advantage of the long duration of the production periods. This solution passes through the technique called deconvolution: in few words it transform a limited duration build up into a drawdown pressure response with a duration equal to the considered production history, consequently, it makes possible to detect boundary effects in a test signal when the individual flow period was too short to detect said boundaries.

This approach is covered in detail in Chapter PTA.

A fied example illustrates the approach below.

We get a complete rate history but the pressure history data is poor and only the detailed acquisition for the last build allows an analysis:

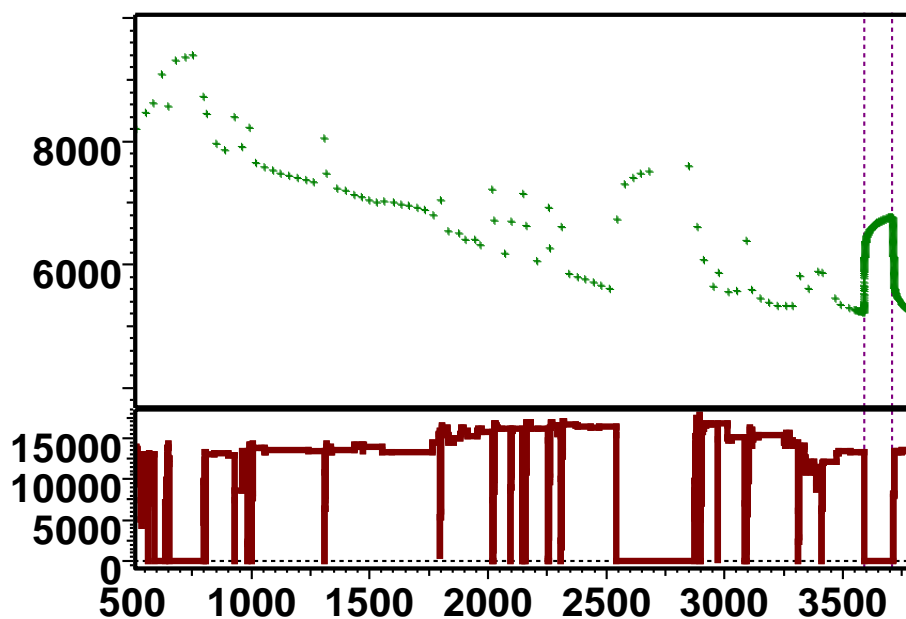


Fig. 8.0.1 – Production and rate history

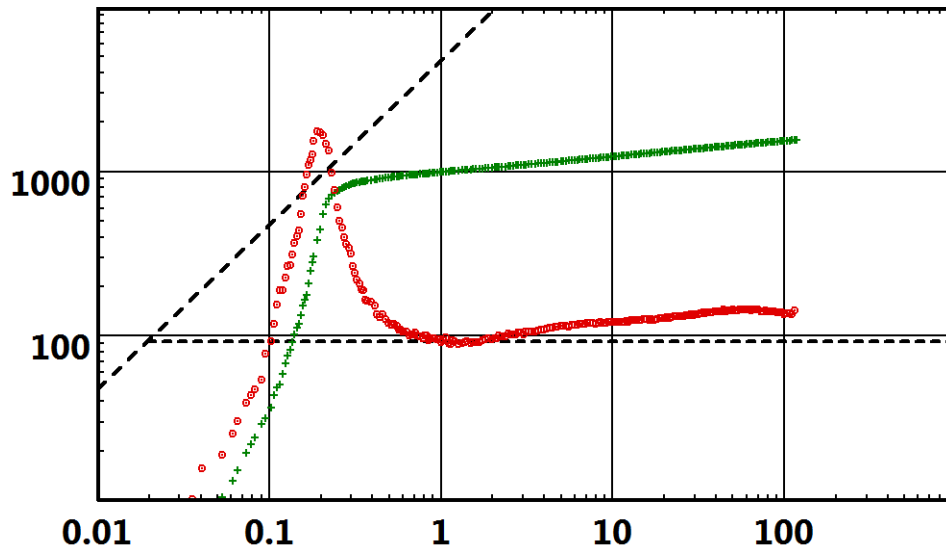


Fig. 8.O.2 – Single build up loglog plot

Although the build up data have a good quality, its relatively short duration (110 hours) limits the depth of the analysis to the observed boundaries.

If we use the build up pressure data and the complete previous production history for a deconvolution we get the loglog plot shown below:

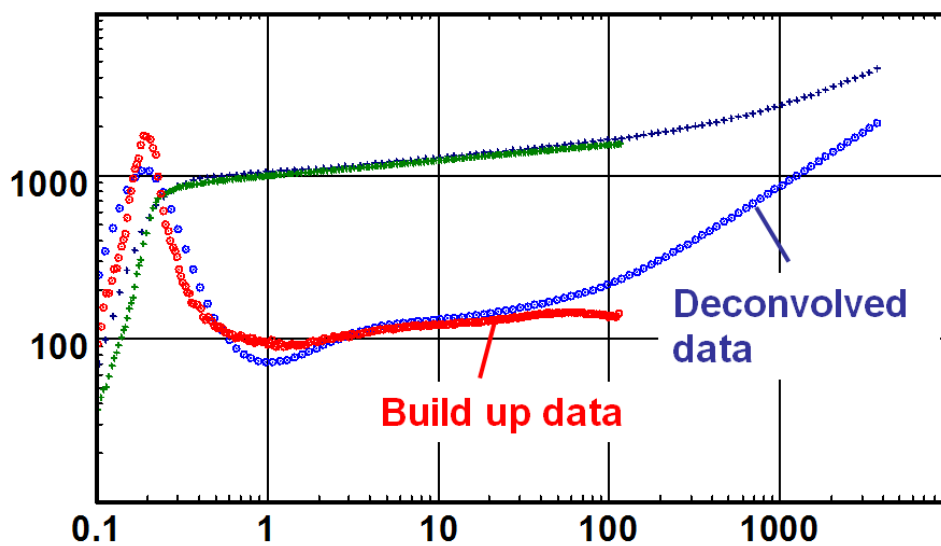


Fig. 8.O.3 – Loglog plot of build up and deconvolved data

Advantages:

- The deconvolved data exhibit the drawdown behavior shape.
- It makes the diagnosis easier, (i.e. making easy the distinction between closed system and constant pressure limit).
- Its duration corresponds to the total history length (3800 hours vs 110 hours).
- Consequently the investigation radius is increased (here it is multiplied by 5.8).

8.P Conclusion

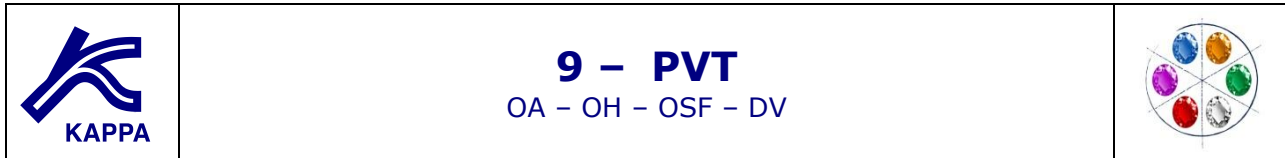
Boundary effects are not systematically detected during a well test, but the identification of boundaries is one of the most important results of Pressure Transient Analysis. Such identification provides valuable information on proven volumes and reservoir geometry.

Even the lack of boundary effects is information by itself. The smallest closed system that can reproduce the infinite looking, or only partially sealing, response will produce a much more reliable estimate of the minimum reservoir size; far more reliable than using an equation of 'radius of investigation'.

The limits of the well drainage area may be reservoir boundaries or 'virtual' boundaries coming from the production equilibrium with other wells. They may be encountered in the producing phase of very long tests, or when using permanent downhole gauge (PDG) data. Production Analysis is also a good candidate to interpret this data.

When analyzing a build-up, boundaries are generally detected at the end of the test by identifying deviations of the Bourdet derivative from Infinite Acting Radial Flow. A significant deviation of the derivative may correspond to a very small deviation of the original pressure signal. Numerous different causes, unrelated to reservoir limits, may incorrectly mimic the response of a boundary effect: for example, incorrect rate history, gauge drift, reservoir trends and interference from other wells.

Before rushing into the diagnostic of a reservoir limit, the pressure transient analyst must to check that there is no other explanation. The sensitivity to the well production history, and its integration in the calculation of the Bourdet derivative, is a critical point to consider. The boundary distances must also be compatible with prior knowledge of the reservoir. Talking to the geologist is a key to gaining confidence in the boundary diagnostic.



9.A Introduction

Pressure-Volume-Temperature, PVT, is the study of the physical behavior of oilfield hydrocarbon systems. Information on fluid properties such as volumes and phases, and how they change with temperature and pressure, is essential to many aspects of Dynamic Data Analysis.

The need for valid PVT data cannot be over-stressed. Reservoir fluid sampling should be a major objective of any test, particularly during drill-stem testing, as PVT analysis should be performed as early as possible in the life of the field. Once production has started, it may never again be possible to obtain a sample of the original reservoir fluid, which may be continually changing thereafter.

For the PTA or PA interpretation engineer, PVT will be used to:

- Assess which fluid phases are present at sandface and at surface
- Calculate fluid phase equilibrium and phase compressibility to correct produced volumes from surface to sandface
- Calculate fluid phase equilibrium and phase gravities to correct pressures to datum
- Calculate fluid viscosity to get from mobility to permeability
- Calculate pseudopressures and pseudotime to linearize the equations in order to use analytical models
- Input PVT properties in a numerical model

The present book is not aimed at teaching PVT, which is an 'art' in itself. However the validity of PTA / PA diagnostics and results is largely dependent on the knowledge of the fluid PVT. It is difficult to assess where we should start this subject. So, we will assume nothing and start from scratch, with our humble apologies to those who have read this a hundred times before.

9.B Phase equilibrium

9.B.1 Single-component fluids

Hydrocarbon fluids can exist in two or more separate phases, typically gaseous and liquid, which have different properties. Water may also be present as a separate phase in the reservoir. Reservoir types are classified by their phase behavior, which depends upon the composition, the pressure and temperature. It is the phase behavior that determines the economic recovery in most cases, that makes fluid sampling difficult, and that can sometimes complicate Dynamic Data Analysis.

The simplest form of phase behavior is for a pure substance, such as methane or water, and it can be represented on a simple 2-dimensional graph of pressure versus temperature in the figure below:

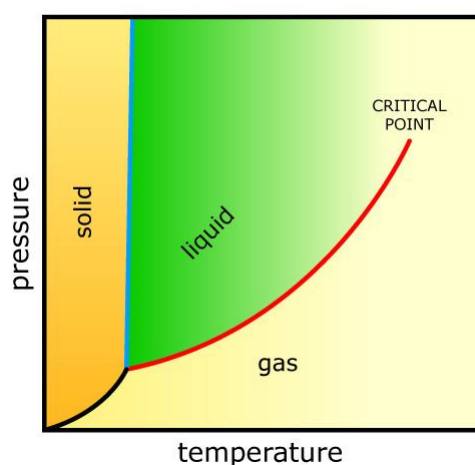


Fig. 9.B.1 – Pure component P-T behavior

The boundary lines between the solid, liquid and gas phases represent values of pressure and temperature at which two phases can exist in equilibrium. Crossing the liquid-gas curve from left to right at constant pressure, by increasing the temperature, corresponds to heating the liquid to its boiling point and boiling it off as gas or vapor.

If the gas is then cooled in the reverse process, it will condense at the same temperature. There is no upper limit to the solid-liquid equilibrium line, but the liquid-gas line or vapor pressure curve, terminates at the **critical point**. At pressures or temperatures above this point only one phase can exist, referred to only as fluid because it has properties similar to both gas and liquid close to the critical point.

For a pure component, the typical Pressure-Volume behavior at constant temperature is shown above. Starting in a single-phase liquid state, the volume is increased which causes a sharp pressure reduction due to the low liquid compressibility. The point at which the first gas bubble appears is the **bubble point**. When the volume is further increased the pressure remains the same until the last drop of liquid disappears; this is the **dew point**. Past that point, only gas exists and as the volume increases, the pressure is reduced. By comparison not as quickly as with the single phase liquid, because of the higher compressibility. The following right figure brings together the P-V and P-T behaviors into a 3-dimensional surface.

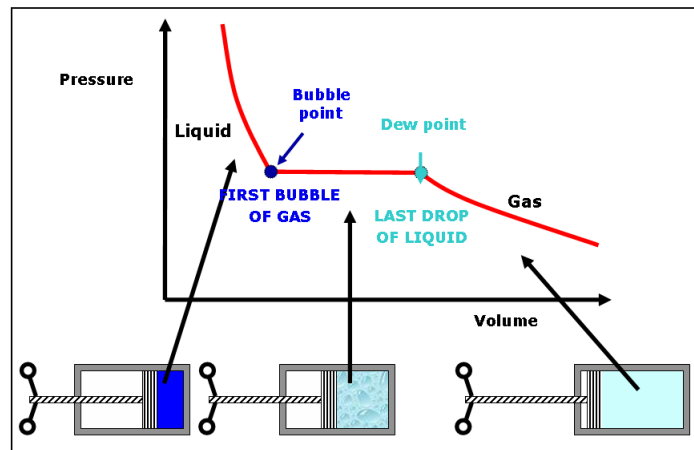


Fig. 9.B.2 – Single component P-V behavior

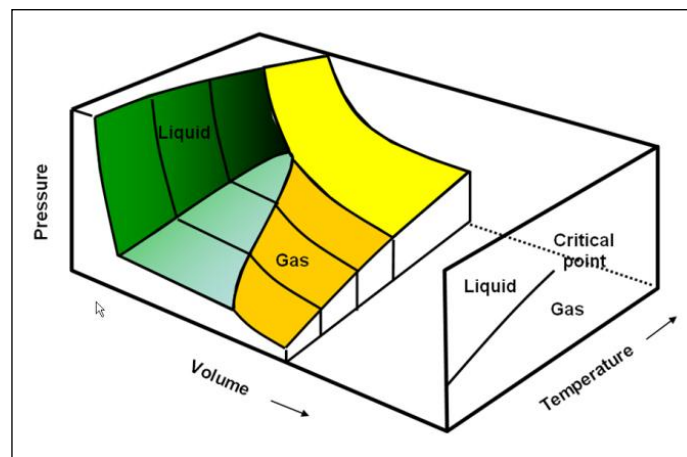


Fig. 9.B.3 – Single component P-V-T behaviour

9.B.2 Multi-component fluids

As soon as a mixture of at least two components is considered, phase boundaries become areas rather than lines, due to the combination of the physical properties of two components with different compositions.

Instead of a single vapor pressure curve there are separate lines to represent the bubble points and dew points of the mixture. The two-phase boundary of the system can extend beyond the critical point, i.e. above the critical pressure or the critical temperature. The critical point lies at the intersection of the bubble and dew-point curves, and no longer serves to identify where the single phase region begins.

With most reservoir systems it is normal to concentrate only on the liquid-gas equilibrium behavior, although some hydrocarbons do exhibit solid phases, such as wax precipitation (solid-liquid) and gas hydrate formation (solid-gas). Natural hydrocarbon fluids can contain hundreds of different pure substances, and the multiple interactions may lead to a great number of phase loops where liquid and gas phases can exist in equilibrium over a wide range of pressures and temperatures.

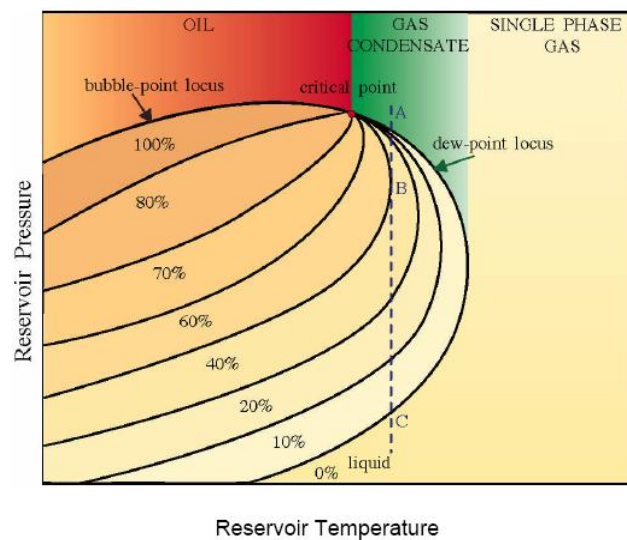


Fig. 9.B.4 – Generalized phase-diagram

The behavior of an oil reservoir with decreasing pressure would be as follows: At reservoir temperatures below the critical point, the two-phase region is entered via a bubble point, where there is initially 100% liquid. As pressure continues to fall, gas is liberated and the system reaches the 20% gas / 80% liquid line, and so on.

When it is above the bubble point, the oil is said to be **under-saturated**. At the bubble point, or anywhere in the two phase region, the oil is said to be **saturated**.

For a fluid above the critical point at 'A', pressure reduction will pass through a dew point with initially 0% liquid. Continued pressure reduction condenses more liquid through the 10% and 20% curves. It is this 'reverse' behavior, of pressure reduction condensing gas to liquid, which has led to the term retrograde. Below a maximum liquid percentage, at 'B', re-evaporation begins (normal gas-condensate behavior) and the system can go through a second dew-point at 'C', if the original fluid composition has not changed.

9.C Classification of reservoir fluids

The phase diagram is a function only of the reservoir fluid composition. The reservoir fluid behavior is determined by the shape of the phase diagram, in particular the position of the critical point, and the relative position of the reservoir temperature. It is actually possible to have the same fluid in two different reservoirs, and in one case it will be oil, while in the other, at higher temperature, it will be a gas. In rare cases this can happen even within a single reservoir, if it is near the critical temperature and has a significant temperature gradient. The main fluid types are:

- **Oil:** When the reservoir temperature is below the critical point, the fluid behaves as oil and shows a bubble point.
- **Retrograde gas condensate:** Between the critical temperature and the upper temperature limit of the two phase region, the fluid will be a retrograde gas condensate, and exhibit a dew-point.
- **Single phase gas:** If the reservoir temperature is above the upper temperature limit of the two phase region, the fluid will be a single phase gas.

The three main fluid types can be further subdivided:

- Oil reservoirs can be classified as **volatile** (high shrinkage) or **non-volatile** (low shrinkage).
- Retrograde gas condensates can be **rich** or **lean**
- Single phase gas reservoirs can be **dry gas** or **wet gas**, depending on whether liquid is collected in surface separation facilities.

Divisions between the sub-types are not clearly defined, except in the case of single-phase gas, but usually give a good idea of the behavior of the fluid.

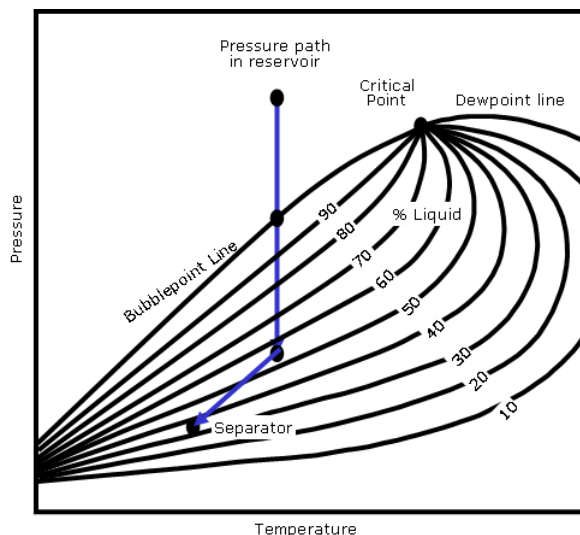


Fig. 9.C.1 – Non-volatile oil

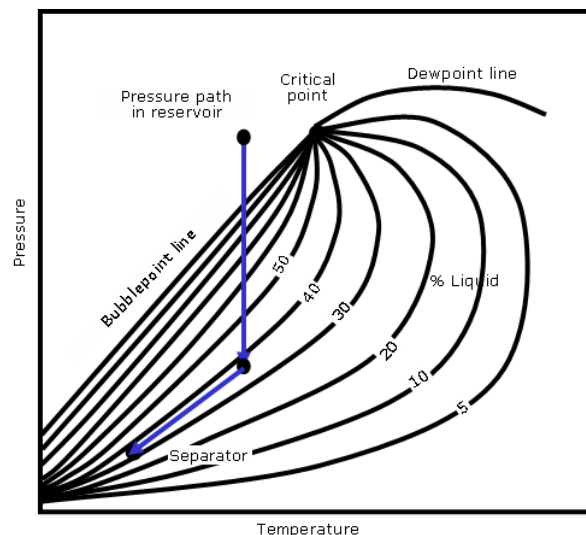


Fig. 9.C.2 – Volatile oil

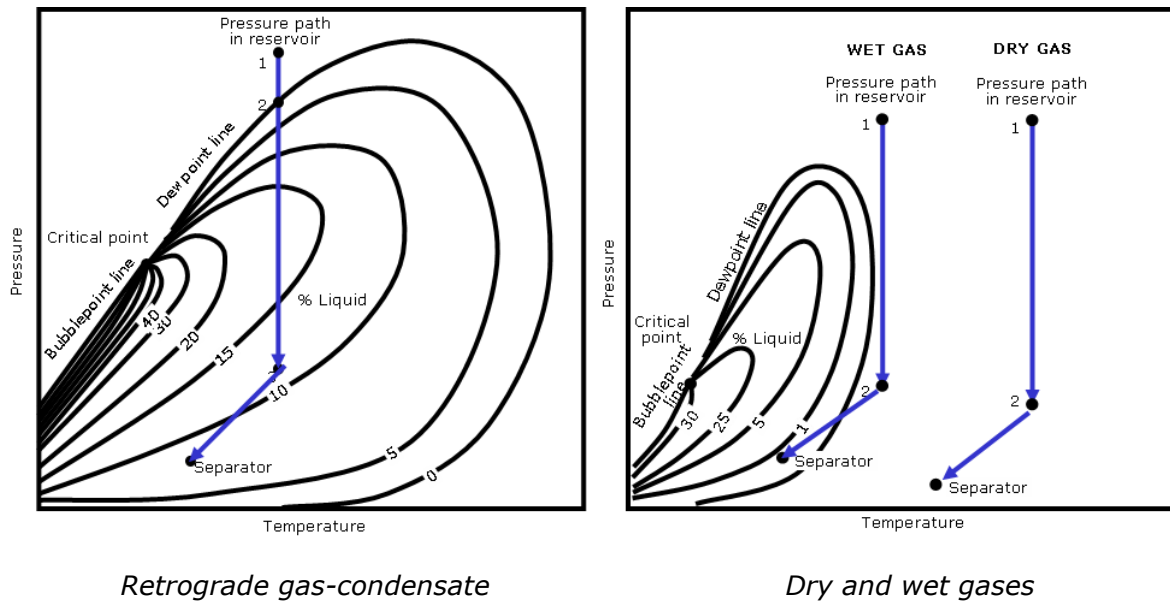


Fig. 9.C.3 – The 5 reservoir fluid types

Field classification can be based on a few quantities:

- Initial Producing GLR = Initial producing Gas Liquid Ratio at surface conditions
- Initial oil API gravity;
$$^{\circ}API = \frac{141.5}{\gamma_o(60^{\circ}F)} - 131.5$$
- Shrinkage @ P_b = reduction in the liquid volume from bubble point to surface

	Non Volatile Oil	Volatile Oil	Condensate	Wet Gas	Dry Gas
Initial producing GLR, scf/stb	< 2000	2000–3300	3300–50,000	> 50,000	> 100,000
Initial API	< 40	40-50	50-70	60-70	No liquid
Color	Very dark	Colored	Lightly colored	-	-
Shrinkage@ P_b	< 2	> 2	-	-	-

9.D Phase description

9.D.1 Oil - Classical Black-Oil (BO) formulation

The main assumption of the Black Oil formulation, sometimes referred to as the β -formulation, is that the reservoir fluid is made of two surface components resulting from the production process: stock-tank oil, and total surface gas. It is further assumed that the properties of the surface gas and stock-tank oil do not vary during reservoir depletion. The traditional BO properties characterize the volumetric behavior and the distribution of the surface components as a function of pressure.

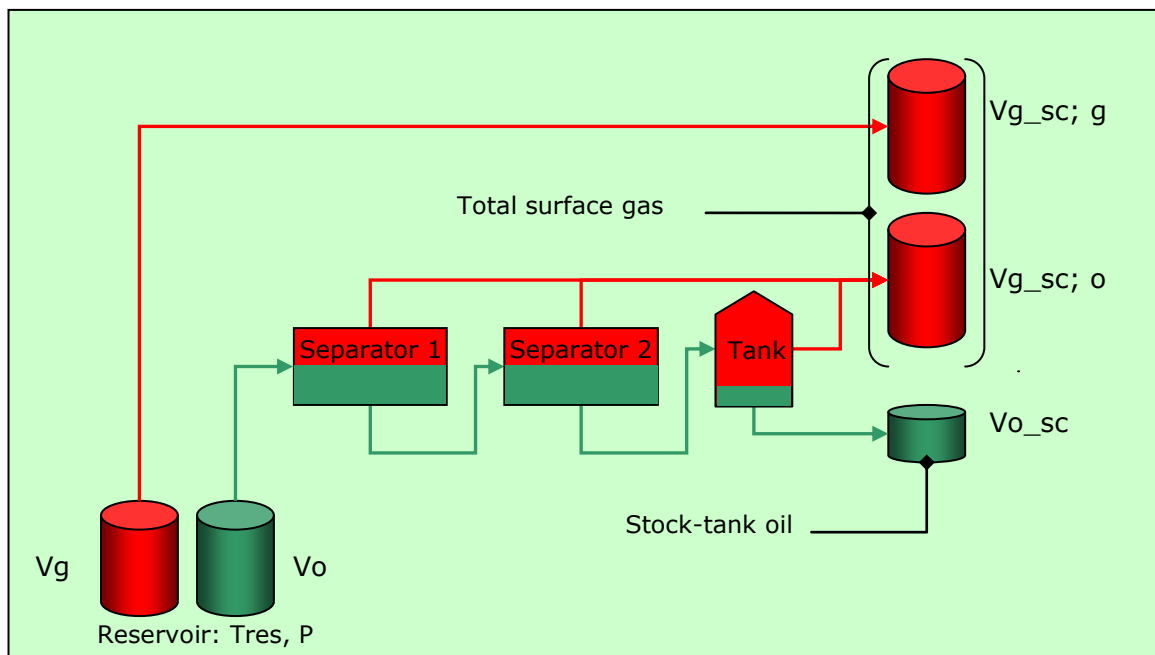


Fig. 9.D.1 – Black Oil volume definition

We consider the situation described above where reservoir gas and oil at some pressure P are brought to surface. The oil goes through a series of separation stages. The volumes are noted as follows:

- V_g = gas volume at reservoir conditions
- V_o = oil volume at reservoir conditions
- $V_{g_sc;g}$ = volume of surface gas produced from the reservoir gas
- $V_{g_sc;o}$ = volume of surface gas produced from the reservoir oil
- V_{o_sc} = volume of stock-tank oil

It is assumed that no liquid evolves from the gas when it is brought to surface; *the Modified Black-Oil accounts for this situation – see the Wet gas section.*

With the above definitions and assumptions the usual Bo properties are given:

- Solution Gas Oil Ratio, R_s :
$$R_s = \frac{V_{g-sc;o}}{V_{o-sc}}$$
- Oil Formation Volume Factor, B_o :
$$B_o = \frac{V_o}{V_{o-sc}}$$
- Gas Formation Volume Factor, B_g :
$$B_g = \frac{V_g}{V_{g-sc;g}}$$

Entailing the following relation between surface and downhole volumes:

$$V_{o-sc} = \frac{V_o}{B_o}; \quad V_{g-sc} = \frac{R_s \times V_o}{B_o} + \frac{V_g}{B_g}$$

B_o , B_g and R_s , are functions of pressure and temperature. They can be obtained from correlations or laboratory studies.

We write $R_{sb} = R_s(P_b)$, $B_{ob} = B_o(P_b)$. If we consider the separation process, it is important to realize that R_{sb} and B_{ob} do depend on the separator(s) conditions. A typical behavior is shown below with varying separator pressure.

The selected separator process should be the one providing the minimum R_{sb} .

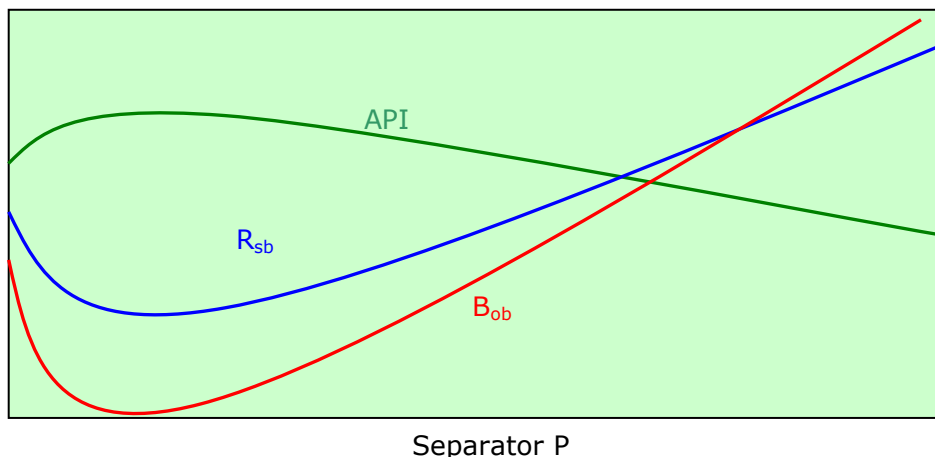


Fig. 9.D.2 – Influence of separation pressure

9.D.2 Wet gas

When dealing with wet gas it is common to calculate the reservoir gas gravity from the surface effluents. We assume that there is one separator stage before stock-tank conditions as pictured below:

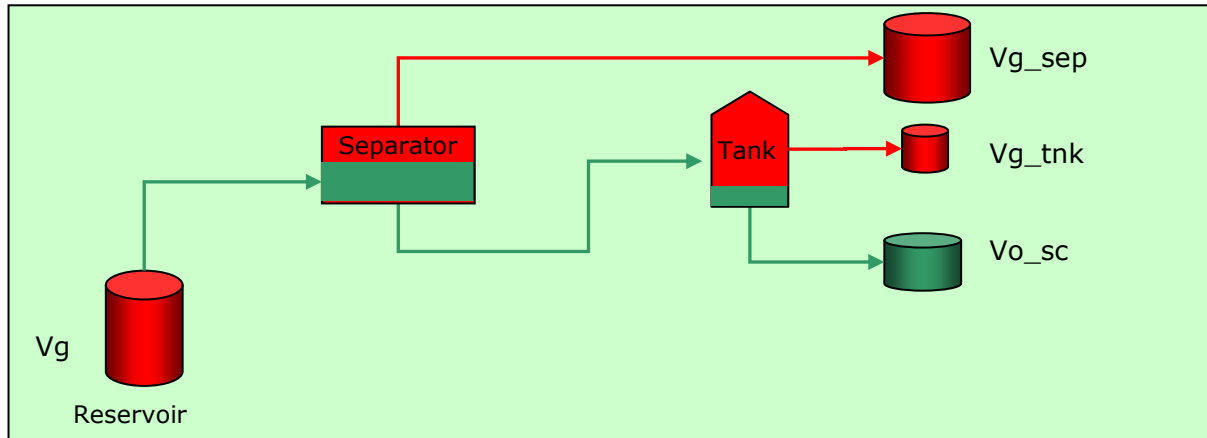


Fig. 9.D.3 – Wet gas production

The volume, at standard conditions, and the specific gravity of the gas produced at the separator and the tank are measured. The corresponding gas-oil-ratios, referenced to the stock tank oil volume are calculated:

$$R_{sep} = \frac{V_{g_sep}}{V_{o_sc}} ; \quad R_{tnk} = \frac{V_{g_tnk}}{V_{o_sc}} ; \quad \text{and the total gas-oil ratio is: } R = R_{sep} + R_{tnk}$$

9.D.3 Modified Black Oil (MBO) PVT Formulation

The modified formulation accounts for liquid condensation from the gas. The properties are defined from the volumes in the following schematic.

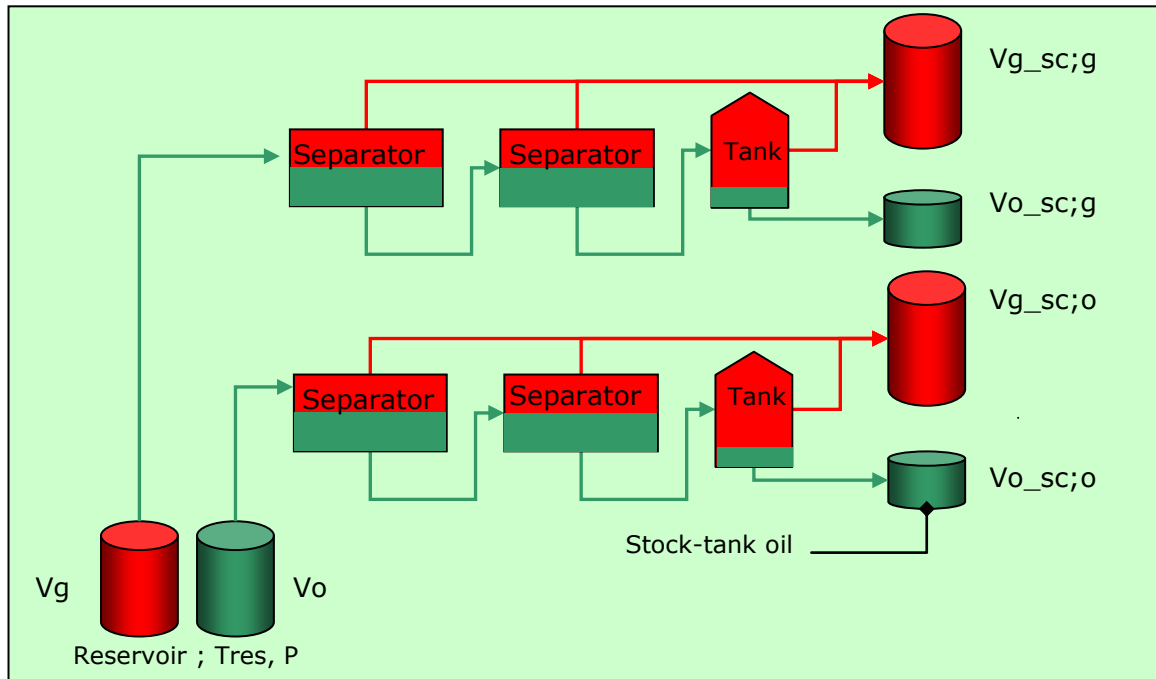


Fig. 9.D.4 – Modified Black Oil formulation: volume definition

The volumes are noted as follows:

- V_g = gas volume at reservoir conditions
- V_o = oil volume at reservoir conditions
- $V_{g_sc;g}$ = volume of surface gas produced from the reservoir gas
- $V_{g_sc;o}$ = volume of surface gas produced from the reservoir oil
- $V_{o_sc;g}$ = volume of surface oil produced from the reservoir gas
- $V_{o_sc;o}$ = volume of surface oil produced from the oil

The usual parameters are modified as follows:

- Solution Gas Oil Ratio, R_s :
$$R_s = \frac{V_{g_sc;o}}{V_{o_sc;o}}$$
- Oil Formation Volume Factor, B_o :
$$B_o = \frac{V_o}{V_{o_sc;o}}$$
- (Dry) Gas Formation Volume Factor, B_g :
$$B_g = \frac{V_g}{V_{g_sc;g}}$$

A new parameter is added to quantify the oil produced from the gas:

- Solution Oil Gas Ratio, r_s :
$$r_s = \frac{V_{o_sc;g}}{V_{g_sc;g}}$$

The relation between reservoir and surface volumes is thus expressed:

$$V_{o_sc} = \frac{V_o}{B_o} + \frac{V_g \times r_s}{B_g}; \quad V_{g_sc} = \frac{R_s \times V_o}{B_o} + \frac{V_g}{B_g}$$

Most MBO formulations assume that all surface oils are the same. In other words the gravity of the oil produced from the reservoir oil and the one produced from the reservoir gas are assumed to be the same. A similar assumption is made for the surface gases.

9.D.4 Water production

In the case where the reservoir production includes water, an extension of the above definitions is made introducing a water formation volume factor B_w , and possibly water gas solubility, R_{sw} :

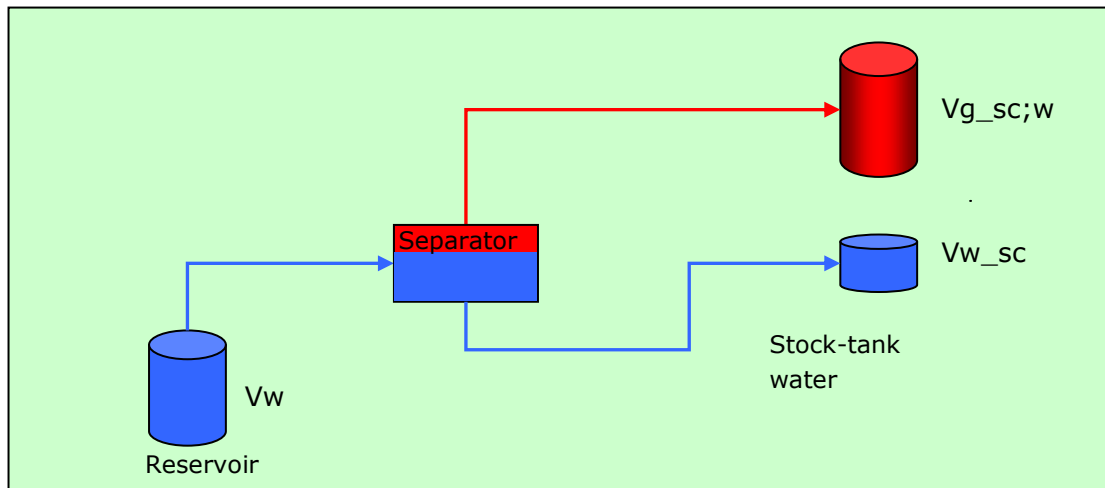


Fig. 9.D.5 – Black Oil property definitions for water

- $V_{g_sc;w}$ = surface gas produced from the reservoir water
- V_{w_sc} = surface water (produced from the reservoir water)

- Water gas solubility, R_{sw} :
$$R_{sw} = \frac{V_{g_sc;w}}{V_{w_sc}}$$

- Water Formation Volume Factor, B_w :
$$B_w = \frac{V_w}{V_{w_sc}}$$

9.E Fluid properties

In addition to the Black Oil properties described in Phase description section, the following are of interest to Dynamic Data Analysis: density, isothermal compressibility, viscosity, gas compressibility factor. This sections review them in detail for each phase. PVT studies, Correlations, and EOS are discussed later in their corresponding sections.

9.E.1 Gas properties

For Dry gas

Specific gravity: Ratio of the gas density at standard conditions, with air density at standard conditions.

$$\gamma_g = \frac{(\rho_g)_{sc}}{(\rho_{air})_{sc}}$$

Z factor: By definition of the real gas law $PV = ZnRT$

Can be obtained from a correlation or a PVT study, or from B_g if given from a PVT study.

Formation volume factor: relates the volume in the reservoir to the volume at standard conditions; defined by Z.

$$B_g = \frac{V_{res}}{V_{sc}} = \frac{Zp_{sc}T}{pT_{sc}}$$

Coefficient of isothermal compressibility: relative change in volume with pressure; given by Z.

$$c_g = -\frac{1}{V} \left(\frac{dV}{dP} \right)_T = -\frac{1}{B_g} \left(\frac{dB_g}{dp} \right)_T = \frac{1}{p} - \frac{1}{Z} \left(\frac{dZ}{dp} \right)_T$$

Gas viscosity: measure of the resistance to flow. Difficult to obtain from measurement, usually determined from correlations.

Gas density: given by Z.

$$\rho_g = (\rho_{air})_{sc} \times V_{sc} \times \frac{p\gamma_g}{ZRT}$$

where V_{sc} = volume of one gas mole at standard conditions: 379.4 scf

The plots below show some typical behaviors.

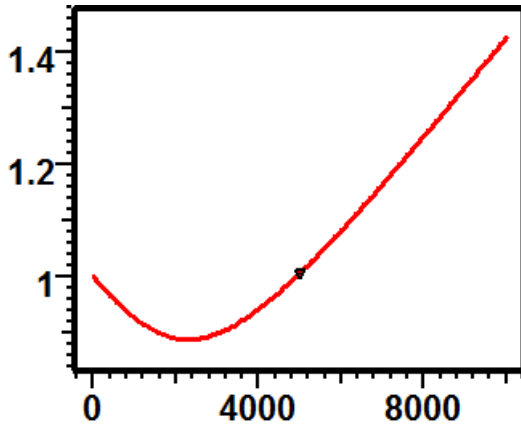


Fig. 9.E.1 – Z factor vs. p [psia]

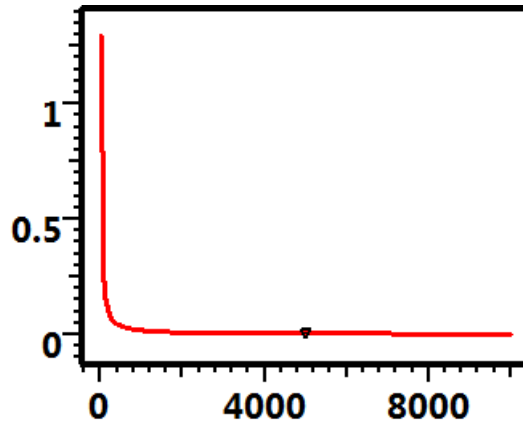


Fig. 9.E.2 – B_g [scf/rcf] vs. p [psia]

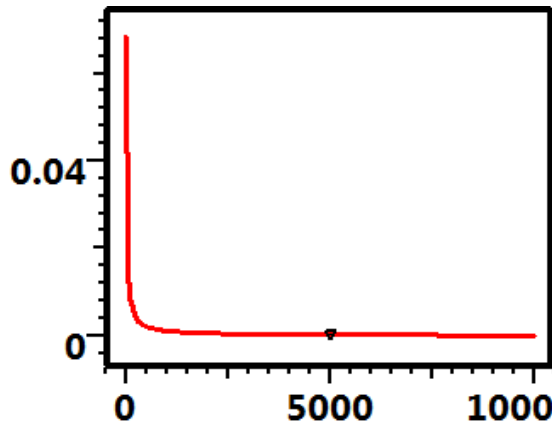


Fig. 9.E.3 – c_g [psi^{-1}] vs. p [psia]

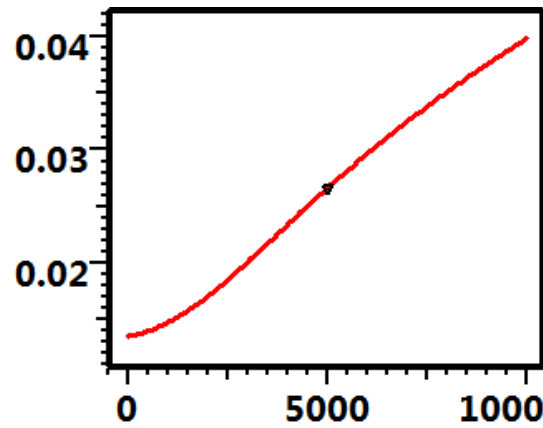


Fig. 9.E.4 – μ_g [cp] vs. p [psia]

For Wet gas

With the measurement of the two specific gravities γ_{g_sep} and γ_{g_tnk} , we define the average surface gas gravity as:

$$\gamma_g = \frac{R_{sep} \times \gamma_{g_sep} + R_{tnk} \times \gamma_{g_tnk}}{R}$$

And the specific gravity of the reservoir gas is then given by (R in scf/STB):

$$\gamma_{gr} = \frac{R \times \gamma_g + 4,600 \times \gamma_o}{R + 133,300 \frac{\gamma_o}{M}}$$

With γ_o the stock tank oil gravity, M_o the condensate molecular weight.

This can be calculated from:

$$M_o = \frac{42.43}{1.008 - \gamma_o}$$

All reservoir gas properties are then estimated using the reservoir gas gravity.

9.E.2 Oil properties

Specific gravity:

$$\gamma_o = \frac{(\rho_o)_{sc}}{(\rho_{water})_{sc}}$$

Recall also the definition of API gravity defined by $^{\circ}API = \frac{141.5}{\gamma_o (60^{\circ}F)} - 131.5$

Formation volume factor: Reservoir oil / surface oil. Obtained from lab study, or from a correlation.

Coefficient of isothermal compressibility: Calculated from B_o and R_s .

$$c_o = -\frac{1}{V} \left(\frac{dV}{dP} \right)_T ;$$

Above P_b : $c_o = -\frac{1}{B_o} \left(\frac{dB_o}{dp} \right)_T$; Below P_b : $c_o = -\frac{1}{B_o} \left[\left(\frac{dB_o}{dp} \right)_T - B_g \left(\frac{dR_s}{dp} \right)_T \right]$

Solution gas-oil ratio: gas dissolved in oil; lab study result or from correlation.

Viscosity: measured or from correlation.

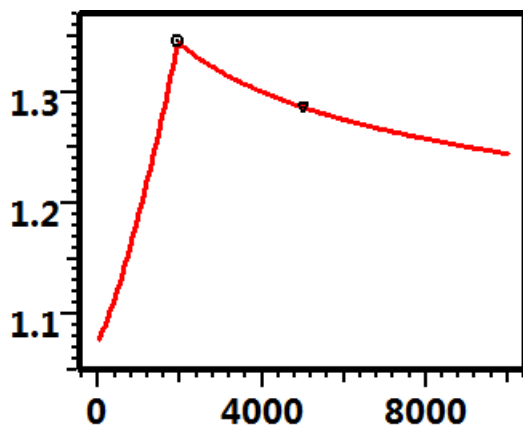


Fig. 9.E.5 – B_o [rb/STB] vs. p [psia]

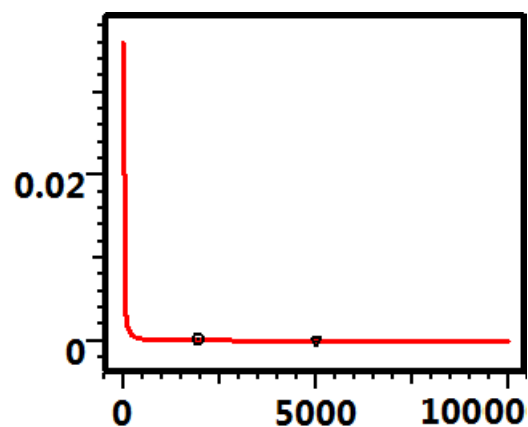


Fig. 9.E.6 – c_o [psi-1] vs. p [psia]

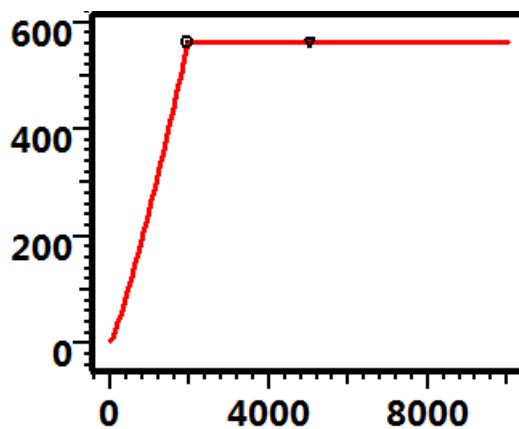


Fig. 9.E.7 – R_s [scf/STB] vs p [psia]

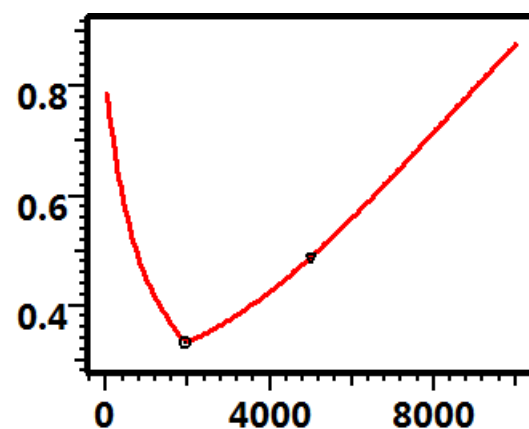


Fig. 9.E.8 – μ_o [cp] vs p [psia]

Oil density: calculated

$$\rho_o = \frac{(\rho_w)_{sc} \cdot \gamma_o + (\rho_{air})_{sc} \cdot \gamma_g \cdot R_s}{B_o}$$

9.E.3 Water properties

All formation water contains dissolved solids, primarily sodium chloride, NaCl. For this reason, the formation water is often called brine or salt water. The amount of dissolved solids is usually expressed in ppm; parts per million = grams of solids per million grams of brine. This is called water salinity and is a key input in estimating the water properties.

In addition, when gas is present, it may dissolve in the water leading to the consideration of R_{sw} Gas solubility.

Specific gravity: This is usually estimated from the measured salinity:

$$\gamma_w = 1 + 7.8216 \times 10^{-6} \times \text{Salinity}_{ppm}$$

Density: The density at any condition is obtained by dividing the standard condition density by B_w . The effect of dissolved gas on the density is usually ignored.

$$\rho_w = \frac{(\rho_w)_{sc}}{B_w}$$

Formation volume factor: Reservoir water / surface water. Several effects are involved: evolution of dissolved gas from the brine as P and T change, the contraction of the brine. Obtained from correlation.

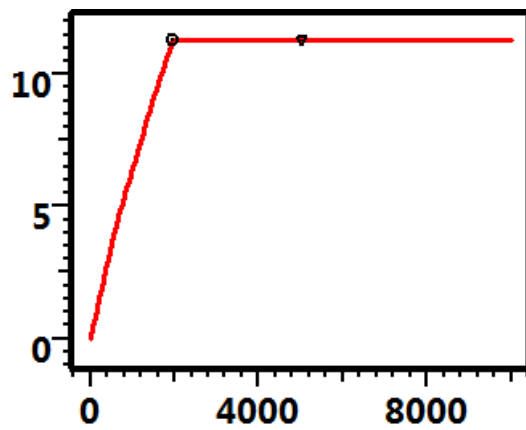
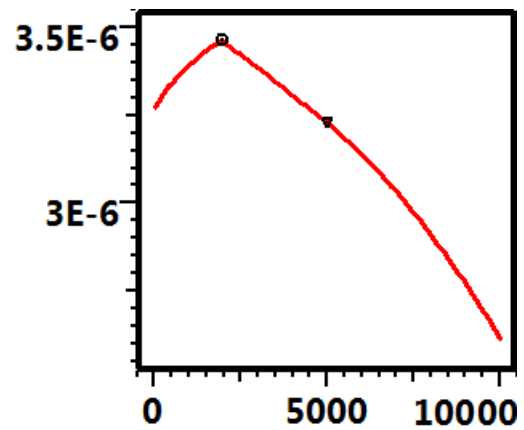
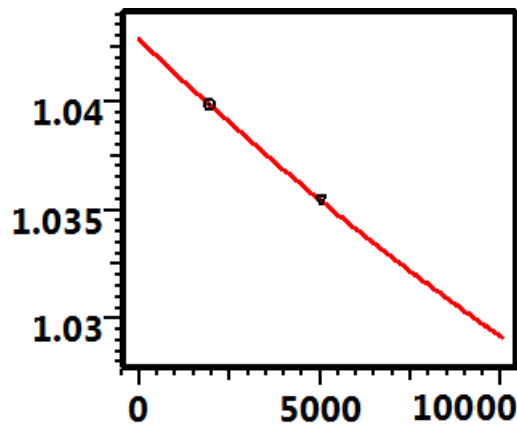
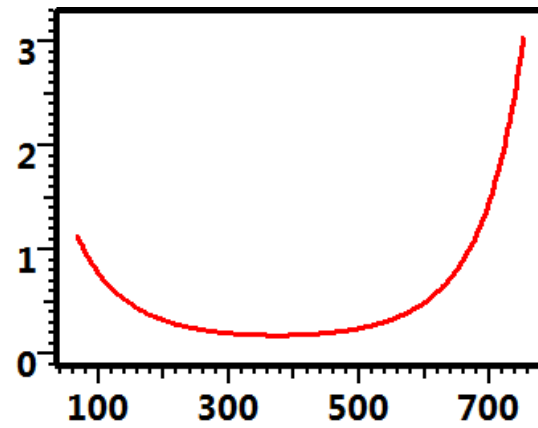
Gas-solubility: correlation value.

Coefficient of isothermal compressibility: calculated from B_w and R_{sw} .

$$c_w = -\frac{1}{V} \left(\frac{dV}{dP} \right)_T$$

$$\text{Above } P_b: c_w = -\frac{1}{B_w} \left(\frac{dB_w}{dp} \right)_T; \text{ Below } P_b: c_w = -\frac{1}{B_w} \left[\left(\frac{dB_w}{dp} \right)_T - B_g \left(\frac{dR_{sw}}{dp} \right)_T \right]$$

Viscosity: correlation value.

Fig. 9.E.9 – R_{sw} [scf/STB] vs. p [psia]Fig. 9.E.10 – c_w [psi⁻¹] vs. p [psia]Fig. 9.E.11 – B_w [rb/STB] vs. p [psia]Fig. 9.E.12 – μ_w [cp] vs T [deg F]

9.F Use of PVT data in DDA (oil)

For historical and practical reasons, a significant part of DDA relies on using analytical solutions to a linearized diffusivity equation. To produce the required linearity, PVT properties are at times assumed constant, at other times encapsulated in a pseudo function that adequately transforms the problem. The various cases are covered here. An alternative to this approach is to solve the problem numerically. The complete PVT behavior is then required and non-linearities can be handled directly. A multiphase simulator can either use a Black Oil or compositional PVT. In the first case, we will see in the section 'Compositional' PVT from BO (and MBO) model how the problem can be formulated in terms of the mass fraction of the surface oil and gas in order to account for varying bubble point.

In a fully compositional simulator, the mass fractions of individual components such as methane, ethane, etc would be considered and PVT properties estimated using EOS.

Even though the problem is not different from what is done in other fields such a full-field reservoir simulation, a numerical model turns out to be inadequate to simulate short transients in a bubble point or dew point system. This is not linked to the PVT representation but rather to the way of estimating mobilities from average cell saturations. This aspect is not covered in this chapter. Instead we focus on the classical analytical approaches.

Oil reservoir treatment in DDA can be made in different ways: single phase oil, Perrine, or using an oil pseudo pressure.

9.F.1 Single-phase oil

The assumption is that only oil is flowing to surface, and the reservoir pressure is above the bubble point. The diffusivity equation introduced in the Chapter 'Theory' involves two PVT parameters: total compressibility c_t , and oil viscosity. In addition, the surface volumes need to be converted to downhole conditions and this requires the knowledge of the oil formation volume factor B_o .

Total compressibility is defined as:

$$c_t = c_f + S_o c_o + S_w c_w + S_g c_g$$

Assuming no gas in the reservoir the last term can be removed. The influence of connate water may be considered.

In the simplest situation, DDA treats the three parameters c_t , μ_o , and B_o as constants. They are estimated at the reservoir temperature and a given reservoir pressure.

9.F.2 Perrine

The Perrine method considers multiphase flow using a single mixture fluid downhole and treats this fluid as a liquid analogue. The PVT properties involved (FVF's, solution gas-oil ratio, etc), are estimated once and for all for the reservoir temperature and some given reservoir pressure.

The total downhole rate is calculated from surface rates as:

$$q_o \times B_o + q_w \times B_w + (q_g - q_o \times R_s) \times B_g$$

Internally a surface oil equivalent can be used, defined as the above expression divided by B_o .

$$q_t = \frac{q_o B_o + q_w B_w + (q_g - q_o R_s) B_g}{B_o}$$

This is the surface oil rate that would give the same downhole total rate.

In order to define the total compressibility, fluid saturations in the reservoir are needed, and they are assumed constant.

Total compressibility is calculated from:

$$c_t = c_f + S_o c_o + S_w c_w + S_g c_g$$

Then, a single phase liquid analysis is conducted, on the basis of total mobility:

$$\lambda_t = \frac{k_o}{\mu_o} + \frac{k_w}{\mu_w} + \frac{k_g}{\mu_g}$$

In Ecrin an oil equivalent permeability k_{o_equ} is defined, which is the total mobility, multiplied by the oil viscosity:

$$k_{o_equ} = \lambda_t \times \mu_o$$

The main assumption of the Perrine method is that the ratio of the fluid mobilities is equal to the ratio of the downhole productions. This can be used to express the effective permeabilities as follows:

$$\frac{k_o}{\mu_o} = \lambda_t \times \frac{q_o B_o}{q_t B_o} ; \quad \frac{k_w}{\mu_w} = \lambda_t \times \frac{q_w B_w}{q_t B_o} ; \quad \frac{k_g}{\mu_g} = \lambda_t \times \frac{(q_g - R_s q_o) B_g}{q_t B_o}$$

If the relative permeabilities are known the value of the absolute permeability can be calculated with:

$$k = \frac{k_o}{k_{ro}} = \frac{k_w}{k_{rw}} = \frac{k_g}{k_{rg}}$$

Two major assumptions of the Perrine's approach are that (1) reservoir saturations are constant (2) the ratios of mobilities are equal to the ratios of the downhole productions. By combination, those assumptions should entail that the production ratios are also constant. In fact, Perrine's method is usually applied on a given build-up, and only the last rates before this build-up are considered. The implementation in Ecrin is an extension that should be used with care should the production ratios vary significantly.

9.G Use of PVT data in DDA - continued (oil)

9.G.1 Single phase oil pseudopressure

An alternative to the assumption that the PVT properties are constant with pressure is to replace P by a pseudopressure defined as:

$$m(P) = (B_o \mu_o)_{res} \int_0^P \frac{dP}{B_o \mu_o}$$

The integration of the viscosity and formation volume factor in the pseudo pressure permits a consistent analysis where the pressure and thus the PVT properties vary significantly over a period of time. This is provided that one considers periods where the pressures are above the bubble point. Typically a series of build-ups over a long history, each one being at pressure levels above the bubble point, will give consistent kh's. Note however that if the FVF and viscosity are assumed to vary, the change in compressibility is not captured by the pseudo pressure, so the pseudo pressure is only applicable for getting adequate permeability. Estimates of sizes, boundary distances with a varying PVT will not be reliable.

9.G.2 Multiphase pseudopressure

In order to linearize further in the case of multi-phase flow, pseudo functions have been proposed of the form below, for solution gas drive, as well as gas condensate reservoirs.

$$m(p) = \int_0^p \left(\frac{k_{ro} \rho_o}{\mu_o} + \frac{k_{rg} \rho_g}{\mu_g} + \frac{k_{rw} \rho_w}{\mu_w} \right) dP$$

To evaluate the above expression a relation must be formulated between pressure and saturation. A common assumption is that of steady state, predicting that the sandface saturations can be calculated using the production ratio. More precisely, we can write the steady-state assumption here for oil / gas):

$$\frac{k_{ro}}{k_{rg}} = \frac{\rho_g \mu_o L}{\rho_o \mu_g V}$$

Where L and V are respectively the mole fractions of Liquid and Vapor.

If we know the relative permeabilities as a function of saturations, and if we have, or we can calculate, the quantities L and V from the PVT, then we can get the saturation corresponding to a given pressure and the full m(p) can then be obtained.

There are several potential problems with this approach. The relative permeabilities must be known and they will have a direct and important impact of the shape of the pseudo-pressures, and thus on the diagnostic made from looking at the response in terms of m(p). The necessary relation between saturation and pressure is typically based on a near wellbore behavior and this may not be valid elsewhere in the reservoir. For closed systems in particular, it has been shown that the pseudo-pressure will not provide an analogy with the liquid case in pseudo-steady state. Finally, in cases where the pressure in the reservoir varies significantly it is also necessary to worry about the variation of the total compressibility. Pseudo-time functions can be considered but again the saturations are part of the equations and this approach relies (as with m(p)) on the assumption of some relation between pressure and saturations, with the same potential dangers.

9.H Use of PVT data in DDA (gas)

Gas was covered in precedent chapters. As shown, the conventional approach is to try and linearize the diffusivity equation and to solve the gas problem as a liquid analogue. This is done replacing pressure and possibly time by pseudo functions.

9.H.1 Dry gas

Only gas is flowing to surface and inside the reservoir. The usual approach replaces pressure by the gas pseudo pressure, see *Chapter Theory - The case of dry gas*.

$$m(p) = 2 \int_0^p \frac{p}{\mu Z} dp$$

Using pseudo-pressure alone assumes that the viscosity - compressibility product is constant. When this assumption is not valid, time may be replaced by a pseudo-time, see Chapter 'Theory - The case of dry gas'.

$$(\text{Normalized version}) \quad t_{ps}(t) = \int_0^t I(p_{wf}(\tau)) d\tau \quad \text{where} \quad I(p) = \frac{(\mu c_t)_{ref}}{\mu c_t}$$

We saw also in precedent chapters that an equivalent function can be defined in order to correct for material balance, see Chapter 'Theory - The case of dry gas'.

9.H.2 Wet gas and condensate single phase analog

The approach is similar to that of dry gas, using the reservoir gas gravity, and correcting the rates. Recall from section Fluid Properties – Gas properties that the reservoir gas gravity is obtained from:

$$\gamma_{gr} = \frac{R \times \gamma_g + 4,600 \times \gamma_o}{R + 133,000 \frac{\gamma_o}{M}}$$

Corrected rates qt are used in the analysis and defined as: $q_{geq} = q_g (1 + 133,000 \frac{\gamma_o}{M_o \cdot R})$

When dealing with gas-condensate, the same approach is often used even though the single phase m(p) is not strictly applicable within the reservoir. The formation of condensate within the reservoir will result in varying saturations and thus mobilities. This may be revealed on transient responses as radial composite reservoirs and analyzed as such. Some studies suggest that close to the well the fluid velocity may sweep the condensate more efficiently thereby causing a three mobility zones. Specific models have been developed for this situation.

9.I Use of PVT data in DDA - continued (gas)

9.I.1 Multiphase pseudopressures for condensate

The general form is the same as given earlier for oil:

$$m(p) = \int_0^P \left(\frac{k_{ro}\rho_o}{\mu_o} + \frac{k_{rg}\rho_g}{\mu_g} + \frac{k_{rw}\rho_w}{\mu_w} \right) dP$$

And the same steady-state assumption relating production and saturations is usually made:

$$\frac{k_{ro}}{k_{rg}} = \frac{\rho_g \mu_o L}{\rho_o \mu_g V}$$

As stated before there are a number of potential problems with this approach, starting with the validity of the steady-state assumption. The pseudo pressure shows two distinct sections, below and above the dew point, with two distinct slopes. This change in slope which is supposed to correct the distortions due to the presence of condensate, and its effect on mobility, can produce such corrections that may create erroneous responses.

As in the oil case, pseudo pressure may work for the sake of a getting kh from a semilog analysis during a given flow period. Beyond that, their use is limited and dangerous.

9.J Getting properties from PVT studies

The objective of this section is to describe the main study types and to see in particular how their results relate to the usual Black-Oil properties. Apart from the compositional analysis, three main experiments are reviewed:

- Constant Composition Expansion (CCE)
- Differential Liberation Expansion (DLE)
- Separator Tests

In addition to measuring the physical properties of the reservoir fluid, PVT laboratories also determine the chemical composition. Because of the enormous number of individual components present in most hydrocarbons it is not possible to identify them all, and similar components are grouped together. Typically, individual measurements are given for the non-hydrocarbons; nitrogen, carbon dioxide and hydrogen sulphide, and for the hydrocarbon groups of primary paraffins, methanes to butanes. Heavier hydrocarbons are then grouped according to the number of carbon atoms, and a final fraction groups all the unidentified heavy components.

9.J.1 Constant Composition Expansion (CCE)

Also called Flash vaporization

In a CCE experiment, a reservoir sample is placed in a cell at a pressure greater than or equal to the reservoir pressure, and at reservoir temperature. Pressure is successively reduced by modifying the cell volume. The total hydrocarbon volume V_t is noted and plotted versus Pressure.

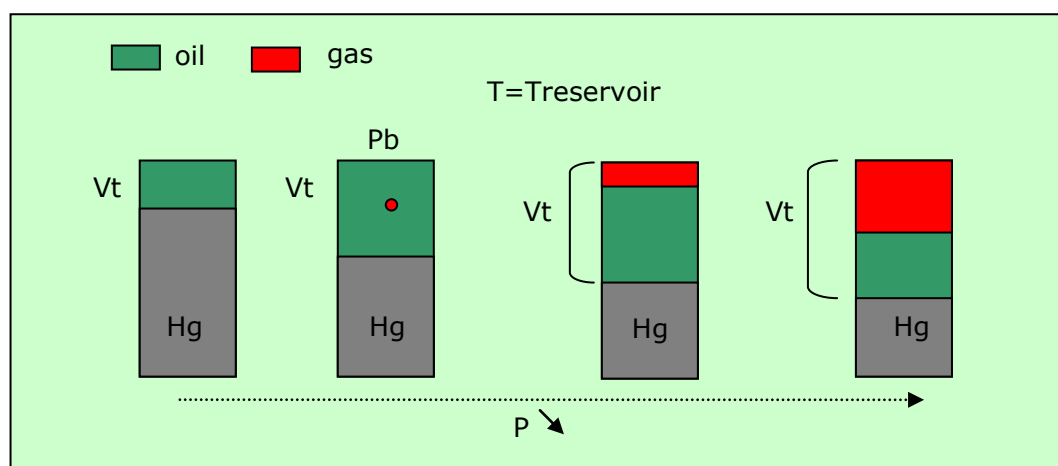


Fig. 9.J.1 – CCE schematic

With a fluid showing bubble point behavior, there is a dramatic change of slope as the first bubble of gas forms and the gas phase compressibility dominates the two-phase behavior.

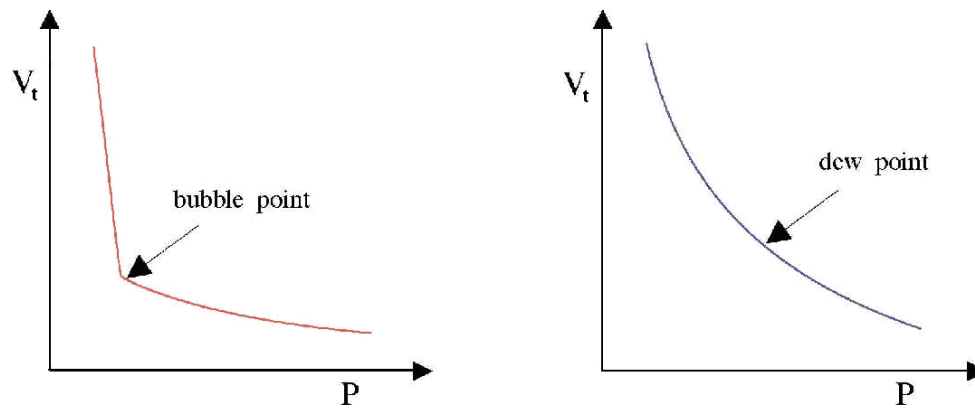


Fig. 9.J.2 – Total volume V_t versus P

In contrast, for gas condensates at the dew point pressure the first drop of liquid that forms has a negligible effect on the overall compressibility, and there is no identifiable change in slope. This curve will also be seen for single phase gases, and some volatile oil fluids near the critical point, where gas and oil phases have similar properties. In these cases laboratory studies are performed in a 'window cell', where the formation of a drop of liquid or a bubble of gas can be physically observed. This need for visual inspection is a major handicap in trying to identify samples at the wellsite.

9.J.2 Differential Liberation Expansion (DLE)

Also called Differential Vaporization.

The DLE experiment is designed to represent the depletion process within the reservoir. A sample of reservoir fluid is brought to reservoir T and bubble point pressure. The pressure is reduced by changing the cell volume. Gas is expelled while maintaining constant pressure. The gas volume ΔV_g and gravity are measured, as well as the oil volume. The step is repeated until atmospheric pressure P_{sc} is reached. The temperature is then reduced to 60°F and the residual oil volume is measured, V_{or} .

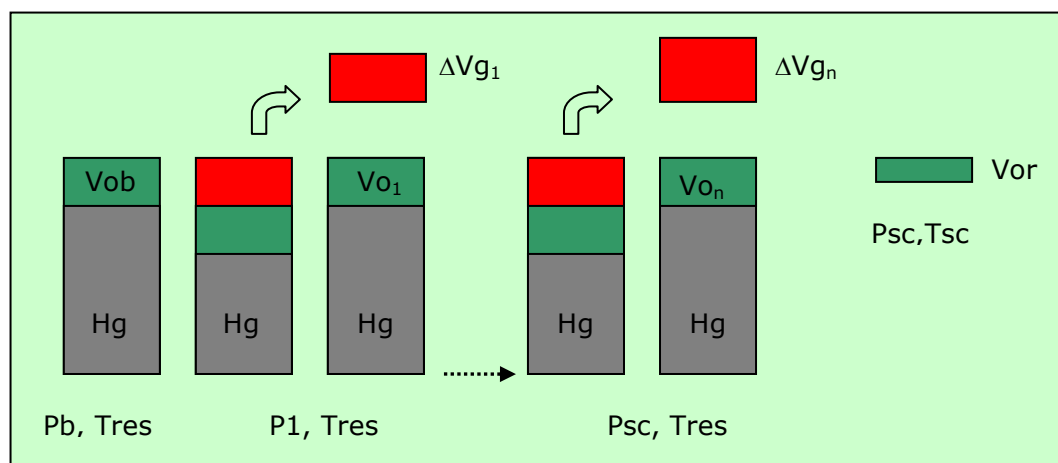


Fig. 9.J.3 – DLE schematic

The following quantities can be determined for the DLE experiment:

- Gas Z factor
- Differential solution gas-oil ratio R_{sD}
- Differential oil FVF B_{oD}

The Differential qualifier, and the 'D' trailing character on the properties, is introduced because the volumes determined in the DLE experiment are referenced to the residual oil volume V_{or} . This is different from the reference stock-tank oil volume obtained when going through different surface separator stages. The conversion of the DLE results to the usual BO properties is explained in section Converting Fluid Study Results.

At any step R_{sD} and B_{oD} are calculated from:

$$R_{sD}(P_k) = \frac{\sum_{i=k}^n \Delta V_{g_i}}{V_{or}} ; \quad B_{oD}(P_k) = \frac{V_{o_k}}{V_{or}} ;$$

9.J.3 Separator Tests

The main objective of the test is to obtain values to convert the DLE results from a residual oil to a stock-tank oil basis. A sample of reservoir fluid is initially set at reservoir temperature and bubble point pressure. It is then brought to the conditions of the first separator stage. The gas volume and gravity are measured. This is repeated until a last step to bring the sample to standard (stock tank) conditions.

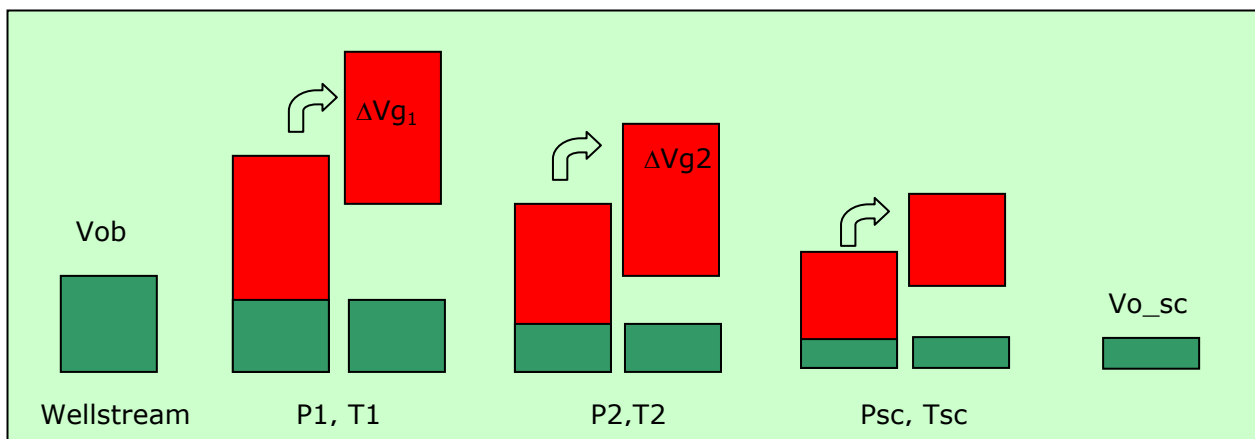


Fig. 9.J.4 – Separator test schematic

The following properties are obtained:

- R_{sSb} where the subscript 'S' indicates that this is from a separator test and 'b' indicates that the original sample pressure is bubble point pressure.
- Similarly a value of oil FVF is obtained: B_{oSb} .

The gas volumes expelled from the various separator stages are expressed at standard conditions. The above properties are then calculated as:

$$R_{sSb} = \frac{\sum_i \Delta V_{g_i}}{V_{o_sc}}; \quad B_{oSb} = \frac{V_{ob}}{V_{o_sc}}$$

9.J.4 Converting Fluid Study Results

Recall the results from the various tests:

- CCE: V_t = total (oil + gas) volume at P ; and V_b = oil volume at P_b
- DLE: solution gas-oil ration $R_{sD}(P)$, oil FVF $B_{oD}(P)$
- Separator test: R_{sSb} , B_{oSb}

At pressures below the bubble point it is assumed that the process in the reservoir is represented by the DLE, and the process from bottomhole to the surface is represented by Separator Tests.

We note $R_{sDb} = R_{sD}(P_b)$ and $B_{oDb} = B_{oD}(P_b)$. The DLE values are corrected using the separator test values as follows:

$$P < P_b \Rightarrow B_o(P) = B_{oD}(P) \frac{B_{oSb}}{B_{oDb}}; \quad R_s(P) = R_{sSb} - (R_{sSb} - R_{sD}(P)) \frac{B_{oSb}}{B_{oDb}}$$

At pressures above the bubble point, properties are obtained from a combination of CCE and Separator tests.

$$P > P_b \Rightarrow B_o(P) = \frac{V_t(P)}{V_b}; \quad R_s(P) = R_{sSb}$$

9.K Obtaining properties from PVT correlations

Correlations are empirical relationships between properties which have no simple inter-dependence, for which some apparent relationship has been identified. Charts and monographs have been in use in the oil industry for a long time, and have proved useful for providing values where measurements were not feasible, in extrapolating from measured values at different conditions, and for checking the consistency of measurements. Although most correlations are simple to use, they are often based upon data from limited geographical areas, especially those within North America. Also the precision of the correlation is rarely referred to, even in relation to the data on which it is based.

With the evolution of computers in the oil industry, many commonly-used correlations have been converted into equation form to facilitate their use. However, the equations are never a perfect fit to the original graphical relationship, so additional errors are incurred. For example, the Dranchuk and Abou-Kassem equations for the Standing-Katz Z chart add an average error of 0.3% to the values. Similarly, equations used to represent the Carr et al gas viscosity correlation introduce an average error of 0.4%. In most cases such additional errors are acceptable, but much larger than average errors do occur, particularly as the correlations can be used outside their acceptable range of application. Some more recent correlations have been developed directly in equation form, which avoids the additional fitting error.

Correlations are invaluable to the industry, but experimental data should be obtained wherever possible. If a choice between correlations has to be made, the ideal approach is to make comparisons with real PVT data on a number of similar fluids, to identify the most suitable correlation and to obtain an idea of the likely errors involved. If this is not possible, it is best to use the correlation derived from data of similar fluid type and geographical origin. It may also be advisable to compare results obtained from different correlations, to see if any key parameters are particularly sensitive to this choice. In the following sections we are providing some information that may be relevant in the selection.

9.K.1 Gas correlations

9.K.1.a Z factor

The existing correlations are representations of the Standing and Katz Z-factor chart, relating Z to reduced pressure and temperature.

The reduced pressure and temperature are defined as $P_r = \frac{P}{P_c}$; $T_r = \frac{T}{T_c}$; where P_c and T_c are the pseudo-critical pressure and temperature. Recall from the beginning of this chapter the definition of critical point for a pure component. The pseudo-critical properties are the mixture equivalent and they are obtained either by mixing rule or correlation.

A correlation by Standing gives the pseudo-critical properties from the gas specific gravity. A correction is required when sour gases are present (CO₂, N₂, H₂S), and this is based on a correlation by Wichert and Aziz.

Three classical representations of the Standing and Katz chart are:

- Dranchuk and Abou-Kassem
- Hall and Yarborough
- Beggs and Brill

The first two are the most accurate in representing the chart. Beggs and Brill is limited in range so the others should be preferred.

9.K.1.b Gas viscosity

As previously mentioned, gas viscosity is usually estimated from correlation since it is difficult to measure it in the PVT lab.

- Carr et al: gives a table for $\mu_g(T,P)/\mu_{g_sc}(T,P)$ and a way of obtaining the standard conditions viscosity from T_r, P_r , and the amount of sour gases.
- Lee et al: used by most PVT laboratories reporting gas viscosity, relates μ_g to molecular weight, density, and temperature.

These correlations predict gas viscosities with an error of about 3% in most cases. When the gas gravity increases about 1, i.e. with rich gas condensate, the error can increase to 20%.

9.K.2 Oil correlations

Oil correlations have been developed for bubble point pressure, B_o , solution GOR, viscosity, and compressibility. They predict properties from the surface oil and gas properties, and total solution gas-oil ratio.

9.K.2.a P_b and R_s

The correlations typically give a relation between bubble point pressure, solution gas-oil-ratio, oil and gas gravities. When using the total GOR as an input, the correlations provide P_b . Conversely, when using any pressure below P_b , they give $R_s(P)$. Below is the list of correlations used in Ecrin.

- Standing (based on California crudes)
- Lasater (based on samples from Canada, US, and South America)
- Vasquez and Beggs (based on data from commercial laboratories)
- Glaso (based on North Sea samples)
- Petrosky and Farshad (based on samples from the Gulf of Mexico)

No significant difference should be expected between those correlations for most cases. Standing and Lasater correlations are recommended for general use. Correlations developed for a particular region should probably be used in that region.

9.K.2.b Oil FVF

The available correlations in Ecrin are:

- Standing (based on California crudes)
- Vasquez and Beggs (based on data from commercial laboratories)
- Glaso (based on North Sea samples)
- Petrosky and Farshad (based on samples from the Gulf of Mexico)

As for P_b and R_s , the estimates are based on total solution GOR, oil and gas gravities. The prediction of the above are in most situations fairly close.

9.K.2.c Oil viscosity

The determination of oil viscosity by correlation typically involves 3 successive steps:

1. Determination of the dead oil viscosity, μ_{oD} correlated in terms of gravity and temperature.
2. Correction of μ_{oD} based on R_s .
3. In the under-saturated section, correction (usually based on P alone).

There exist different correlations for those steps. In Ecrin three methods are offered generically called 'Beal', 'Beggs and Robinson', and 'Glaso'. They correspond to the following combination:

- Beal: 1=Beal, 2=Chew and Connally, 3=Beal
- Beggs and Robinson: 1 = Beggs & Robinson, 2=Beggs & Robinson, 3=Vasquez and Beggs
- Glaso: 1=Glaso, 2=Chew and Connally, 3=Beal

The estimate of dead-oil viscosity by correlations is very unreliable. Lab values should be preferred whenever available.

9.K.2.d Oil isothermal compressibility

Oil compressibility can be calculated from the knowledge of R_s and B_o . Direct correlations exist. In Ecrin the following is offered:

- Vasquez and Beggs: Actually combines a correlation by McCain below P_b and Vasquez and Beggs above P_b .
- Glaso: combination of McCain below P_b and Glaso above.
- Petrosky and Farshad: combination of McCain below P_b and Petrosky and Farshad above.

9.K.3 Water correlations

Following is the list of correlations available in Ecrin.

9.K.3.a Water FVF

- Gould
- McCain
- Meehan and Ramey

9.K.3.b Water Compressibility

- Dodson and Standing
- Osif

9.K.3.c Gas solubility

- Katz
- Meehan and Ramey

9.K.3.d Water Viscosity

- Van-Wingen and Frick
- Helmholtz
- Meehan and Ramey

9.K.4 Correlation: feeding and matching

It is always desirable to adjust the prediction of fluid properties obtained from correlations. On-site measurements can be used for that purpose or else values resulting from PVT studies. In the latter case however if a full PVT study is available this should be used rather than the correlations.

When correlations are applied with known values, the modification made to the properties is usually linear using a factor and a shift. The two fitting parameters can be obtained by running a non-linear regression on any number of constraint points. *For some properties, the modification is different as reference values must be preserved. This is the case for formation volume factors or gas Z-factor, with $B(P_{sc})=1$ and $Z(P_{sc})=1$.*

In the Black Oil model, we have seen that the oil and gas properties are obtained as a function of the surface component gravities, and the solution GOR. There is a one-to-one relation between total GOR and bubble point.

This can be considered as the definition of the fluid composition, as explained in the next section.

For given surface gravities, the effect of varying the GOR is shown below. The saturated sections up to the bubble points are the same, whereas a funnelling is seen above P_b .

The saturated section is therefore a function of the surface component gravity only, and the value of any property at a particular pressure requires only the additional knowledge of the GOR, or equivalent P_b .

When using match values, those values may characterize a fluid with a GOR different from the one under consideration. If this is the case then it may not be relevant to compare those values and the values predicted by the correlation. Only if the GOR is the same can values be compared for any pressure.

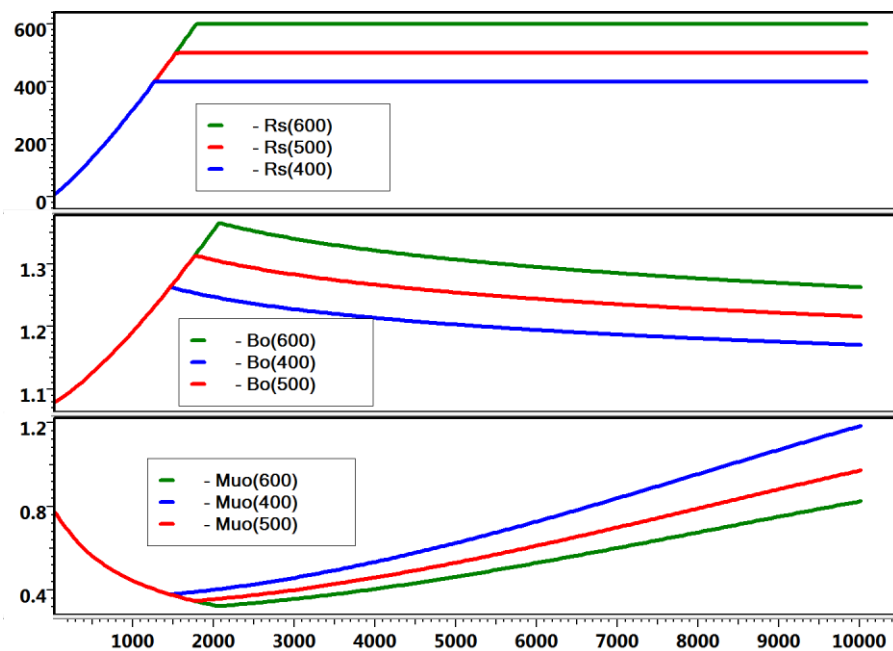


Fig. 9.K.1 – Effect of changing the total GOR

As a rule, the input to correlations should be the latest set of consistent production GOR, and surface oil and gas gravities. When constraining this PVT with values originating from lab studies of some initial fluid with GOR_i and P_{b_i} , beware that undersaturated values cannot be matched if the GOR has significantly evolved. For the saturated section, values can be matched only for pressures below $\min(P_b, P_{b_i})$.

9.L 'Compositional' PVT from BO (and MBO) model

We consider as multi-component model, with three components named *water*, *oil* and *gas*. The *water* component exists only in the Water phase. The *gas* component exists in the Gas and Oil phases. The *oil* component exists only in the Oil phase for the BO model, and in both Oil and Gas phase for the MBO model. This can be summarized with the following tables.

BO	component		
phase	w	o	g
W	x		
O		x	x
G			x

MBO	component		
phase	w	o	g
W	x		
O		x	x
G		x	x

The *oil* and *gas* components are the stock tank oil and total separator gas, as defined in the previous sections. All reservoir fluids are a mixture of these components. The phases can be characterized by their composition, fraction of each component expressed in a conservative quantity, for instance the mass. So the phases are defined by their **mass composition** C_o , C_g and C_w . We write C_p^k the fraction of component k in phase p . The compositions add up to unity: $\sum_k C_p^k = 1$.

9.L.1 2-Phase envelope

The phase envelope of the Gas-Oil equilibrium for a real mixture of two components similar to a reservoir sample can be plotted on a Pressure-composition plot as shown below. The plot considers a general MBO situation where oil can exist in both oil and gas phases, and similarly for gas.

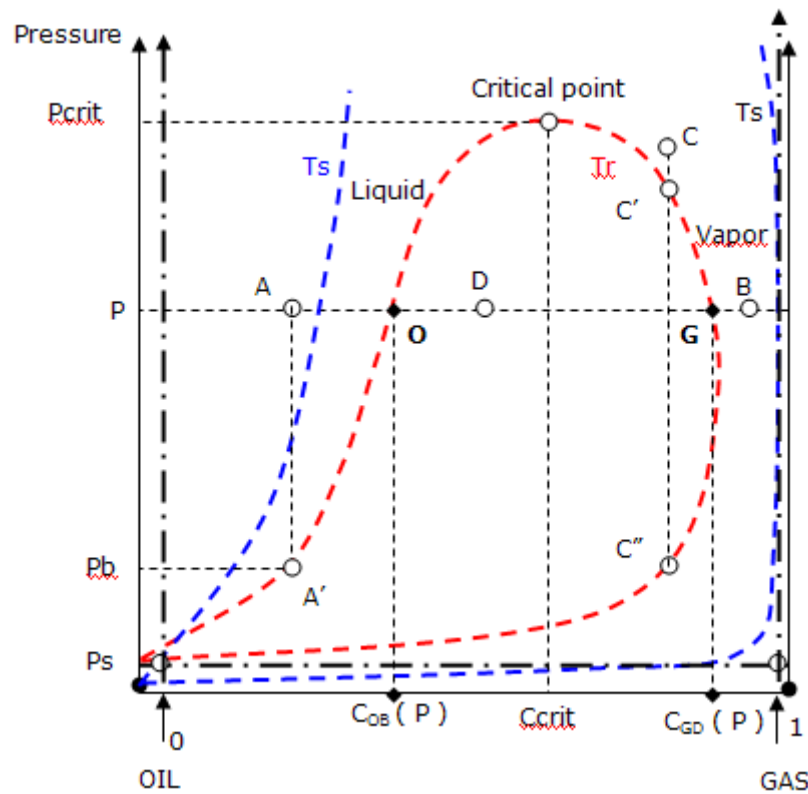


Fig. 9.L.1 – Pressure/Composition diagram of binary mixture

Two curves have been plotted: in **red**, for reservoir temperature T_r in **blue** for standard temperature T_s . Each mixture of known composition at a given pressure is represented by a point on this graph.

- The D mixture at pressure P is inside the envelope: it is the 2-phase region. The 2 phases are characterized by the points O and G, of compositions $C_{OB}(P)$ and $C_{GD}(P)$. The mass fraction of each component in each phase is given by:

For the oil phase, point (O):

- mass fraction of oil $C_O^o = (1 - C_{OB}(P))$

- mass fraction of gas $C_O^g = C_{OB}(P)$

For the gas phase, point (G):

- mass fraction of oil $C_G^o = (1 - C_{GD}(P))$

- mass fraction of gas $C_G^g = C_{GD}(P)$

- The A mixture is an undersaturated liquid, whose bubble point pressure P_b corresponds to the point A' of same composition on the Liquid curve.
- The C mixture is an undersaturated gas which has at reservoir temperature a retrograde dew point C', and a direct dew point C''.
- The B mixture is a dry gas which has no dew point at reservoir temperature, but has 2 dew points at standard temperature T_s .

The critical pressure P_{crit} at reservoir temperature is the maximum pressure where both phases can exist. The corresponding composition C_{crit} is the critical composition at T_r . As we assume that the components are the phases at standard conditions, the components used in the model are the Oil phase in standard conditions, called **oil**, and the dryer gas phase at T_s , called **gas**.

The same diagram can be plotted in the ideal case for the BO and the MBO models. In the BO model, the gas phase always contains only gas.

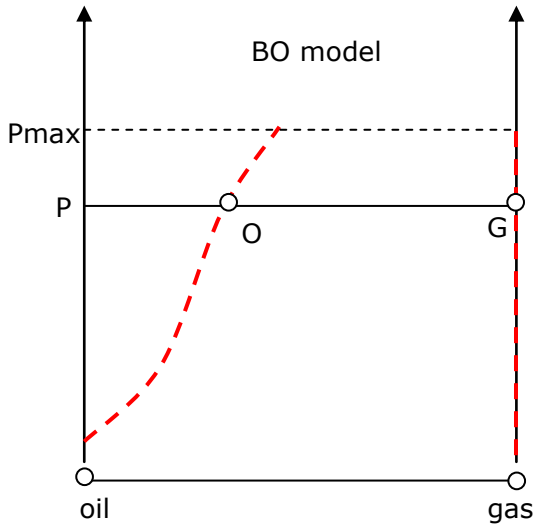


Fig. 9.L.2 – Pressure/Composition diagram of BO

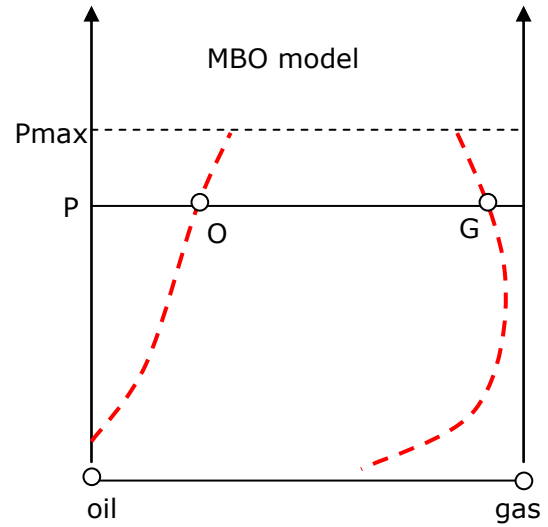


Fig. 9.L.3 – Pressure/Composition diagram of MBO

The composition at bubble point of the oil phase, and at dew point of the gas phases, can be obtained from the Black Oil properties and the oil and gas densities at standard conditions.

$$R_s(P_b) = \frac{C_o / \rho_{gsc}}{(1 - C_o) / \rho_{osc}} \quad \text{with } C_o = C_{OB}(P_b) \Rightarrow C_o = \frac{1}{1 + \frac{\rho_{osc}}{R_s(P_b) \times \rho_{gsc}}}$$

Similarly with the Modified Black Oil:

$$r_s(P_d) = \frac{(1 - C_G) / \rho_{osc}}{C_G / \rho_{gsc}} \quad \text{with } C_G = C_{GD}(P_d) \Rightarrow C_G = \frac{1}{1 + \frac{\rho_{osc} \times r_s(P_d)}{\rho_{gsc}}}$$

As illustrated in the previous section, this indicates that once the surface gravities are known, the fluid is defined by the knowledge of the function $R_s(P_b)$, which is the same as the undersaturated gas-oil ratio (and $r_s(P_d)$). Visualizing the problem in terms of compositions makes it easier to consider mixture of varying compositions for which the bubble point and/or dew points can be readily obtained on the $C_{OB}(P)$ or $C_{GD}(P)$ curves. For other properties in the 2-phase region, all that is required is the knowledge of $\rho_o(P_b)$ and $\mu_o(P_b)$ for the expected range of bubble points. In the single phase region (undersaturated case) an assumption can be made to estimate the properties. A common hypothesis is that of constant slope, ie the derivative of the particular property with pressure.

This is the basis for the multi-phase numerical model of Ecrin. This model can be fed with a set of correlations, or may use tabulated properties resulting from a PVT study.

9.M Equations of State

Equations of State (EOS) are models predicting the phase behavior and properties from the fluid composition obtained from the laboratory analysis of the reservoir fluid. Most EOS have developed from early attempts to correct for behaviour of gases which deviated from the ideal gas law. The general form is a cubic equation usually expressed in terms of $Z = PV/RT$:

$$Z^3 + A_2 Z^2 + A_1 Z + A_0 = 0$$

Van der Waals proposed the equation:

$$P = \frac{RT}{V-b} - \frac{a}{V^2}$$

in which b represented the volume of individual molecules, and a was the inter-molecular attraction.

The two most common equations of state used in PVT calculations are:

- Soave-Redlich-Kwong (SRK):
$$P = \frac{RT}{V-b} - \frac{a}{V(V+b)}$$
- Peng-Robinson (PR):
$$P = \frac{RT}{V-b} - \frac{a}{V^2 + 2bV - b^2}$$

Equations of State are used in compositional simulators, as opposed to Black Oil, and they are a *sine qua none* condition for considering such problems as CO₂ flooding, mixture of several reservoir fluids, etc.



10.A Introduction

Numerical models are becoming increasingly popular in well test analysis, mainly because they address problems far beyond the reach of analytical and semi-analytical models. The two main areas of usage of numerical models are nonlinearities, such as multiphase or non-Darcy flow, and complex reservoir or well geometries. Numerical models can also be used to replace rate by pressure constraints when the well flowing pressure goes below a certain point, hence avoiding the embarrassing negative pressures often generated by analytical models.

The first attempts at numerical well testing were done ad hoc across the industry by engineers using standard reservoir simulators with local grid refinement. In the early 1990's, the first industrial project involved pre-conditioning of an industry standard simulator using PEBI gridding. Since then, several technical groups have been working on numerical projects dedicated to transient analysis.

In recent years, improvements in automatic unstructured grids and the use of faster computers have allowed such models to be generated in a time that is acceptable to the end user. The change has been dramatic, the time required to calculate the solution has decreased from days to hours, then to minutes, and now, for linear diffusion problems, to seconds. Using gradient methods even nonlinear regression is possible, and improved well-to-cell models allow simulation on a logarithmic time scale with little or no numerical side effects. Last, but not least, automatic gridding methods allow such models to be used without the need for the user to have a strong background in simulation.

The main goal of numerical models is to address complex boundary configurations, but this part of the work is actually easily done by any simulator. The problem is to also address what is easily done by analytical models, i.e. the early time response and the logarithmic sampling of the time scale. This requires, one way or the other, to get more grid cells close to the well, and this has been done using three possible means: local grid refinement of cartesian grids, unstructured (Voronoi, PEBI) gridding, or finite elements. These different options, shown below, have their pros and cons that are beyond the scope of this book.

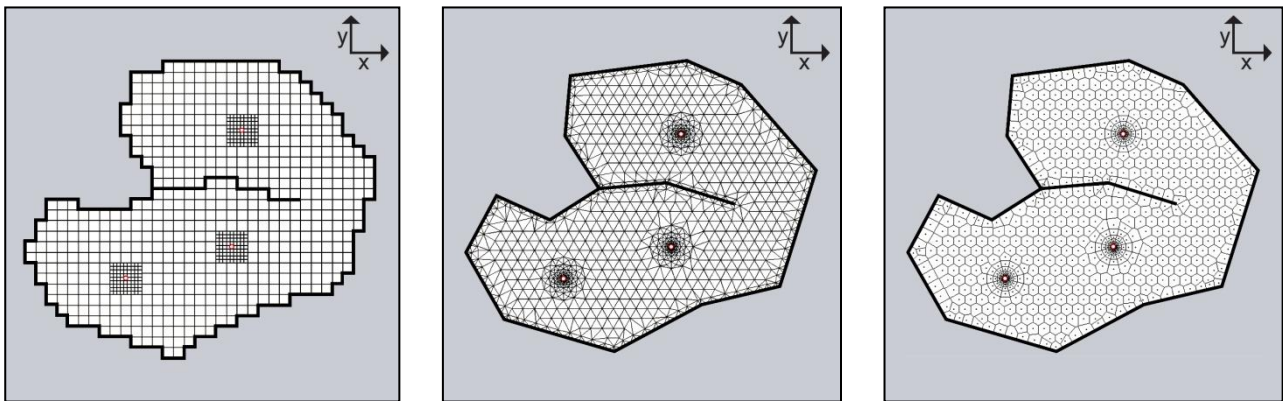


Fig. 10.A.1 – Cartesian, Finite elements and Voronoi/PEBI grid

Warning: KAPPA has taken the option to develop a numerical model using the Voronoi grid. This chapter describes this option only, and as such is far more software related and vendor specific than the rest of this book.

Numerical models adapted to DDA include an interactive process to define the geometry, an automatic grid builder and a simulator. The simulator will typically have a linear and a nonlinear solver.

When the diffusion problem to model is linear, taking the same assumption as in an analytical solution, the process only requires one iteration of the linear solver for each time step. The solution is very fast and the principle of superposition can be applied. In this case, the numerical model acts as a 'super-analytical-model' which can address geometries far beyond those of an analytical model. This is developed in Section 'Handling linear problems'.

When the problem is nonlinear the numerical module is used more like a standard simulator, with 'just' a grid geometry adapted to a logarithmic time scale. The nonlinear solver is used, iterating on the linear solver. Nonlinearities are developed in Section 'Handling Non-linear problems'.

A numerical model can also be used to change the well constraint in time. For each well, a minimum pressure is set, below which the simulator changes mode and simulates the well production for this minimum pressure. This is also developed in Section 'Handling Non-linear problems'.

10.B Building complex geometries

10.B.1 Building a 2D model

To start a bitmap (BMP, JPG, etc) representing the reservoir is loaded (Figure below). The engineer first defines the scale by using a known distance between two points. Once these dimensions are known, the tested well is positioned and the reservoir outer limits described as a closed polygon.

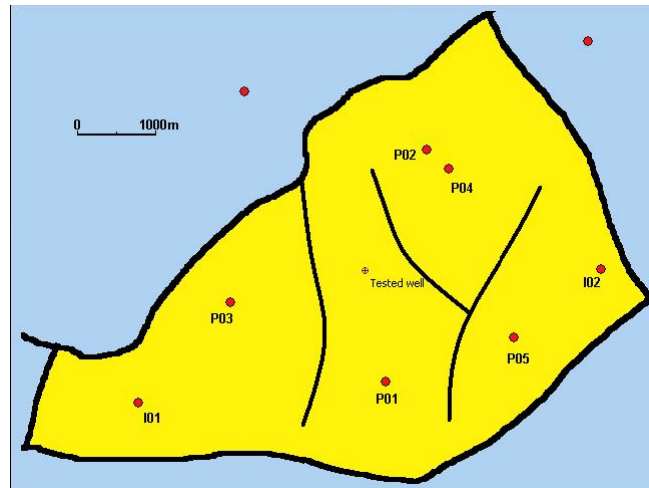


Fig. 10.B.1 – Bitmap of field

Any segment of this polygon may be set as a sealing or constant pressure boundary. If inner boundaries are present, any number of polyline faults may be drawn with control of individual fault transmissibility. Individual wells (vertical, horizontal and/or fractured) may be created and positioned, and their corresponding production history entered. Later, when the model is defined, vertical and fractured wells may be individually specified as fully penetrating or of limited entry. Once the geometry of the problem is defined, the display of the original bitmap is turned off and the 2D Map displays a vector description of the problem:

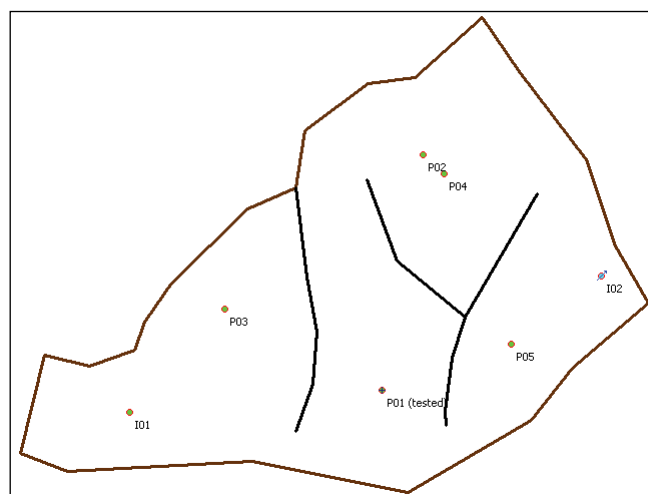


Fig. 10.B.2 – Vector description of the problem

Fault polylines may also be used to delimit composite zones where separate mobilities and diffusivities may be defined. Additional composite zones may also be added around each well, the figure below illustrates this with two radial composite wells and a different western reservoir compartment.

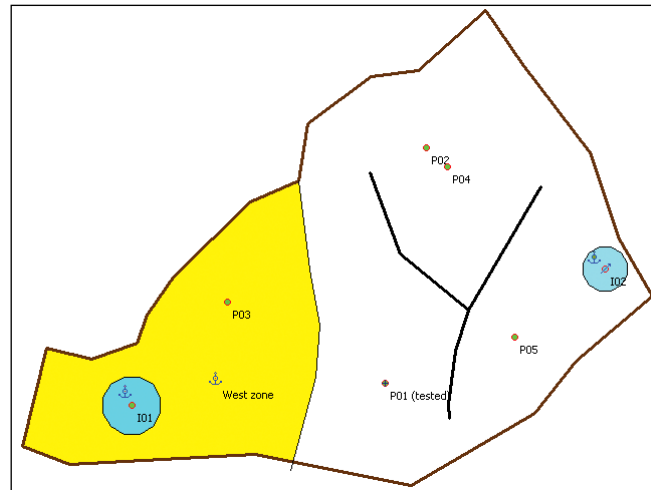


Fig. 10.B.3 – Composite zones added

Porosity, thickness or permeability fields may also be defined, either interactively or by importing an ASCII file. Kriging and other interpolation / extrapolation algorithms are used to populate these properties at each cell:

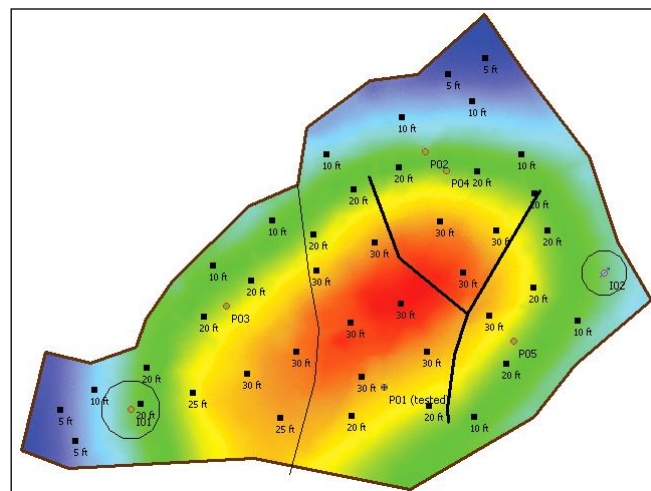


Fig. 10.B.4 – Thickness map

The model can display the automatic gridding, adapted to honor the reservoir contour, inner faults and wells:

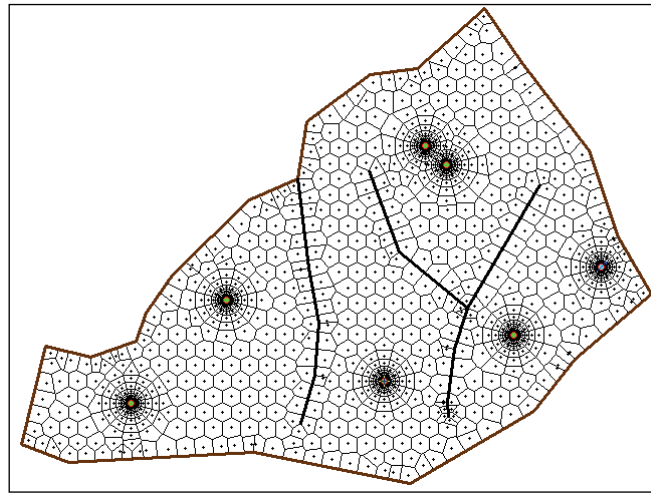


Fig. 10.B.5 – Unstructured Voronoi grid

The default is recommended but specialists may modify the basic grid geometry, size, main directions, and the local grid refinement around each well:



Fig. 10.B.6 – Customized grid

10.C Principles of Voronoi / PEBI gridding

10.C.1 What is a Voronoi grid

The basis of Voronoi gridding is to generate a series of carefully located points called 'grid nodes'. Individual grid nodes can be specified anywhere inside the domain regardless of the position of any other node. It is therefore impossible to identify a grid by a series of indices (i,j) in 2-D and (i,j,k) in 3-D. This is why a Voronoi grid is qualified as 'unstructured'.

A Voronoi cell is defined as the region of space that is closer to its grid node than to any other grid node. A key property of the Voronoi grid is that the contact segment (also called contact face) between two neighboring cells is the bisector of the segment linking the cell nodes.

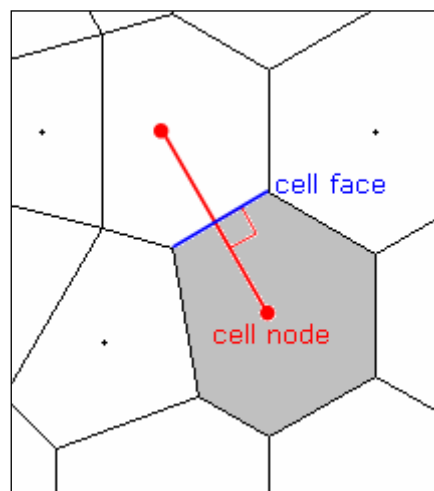


Fig. 10.C.1 – Property of Voronoi grid

The Voronoi grid is closely related to the Delaunay triangulation. In fact the Delaunay facets are obtained by linking the Voronoi cell nodes together. The most important geometrical property of the Delaunay triangulation is that each triangle verifies the empty circle condition, i.e. each triangle's circumcircle does not enclose any other point of the point set:

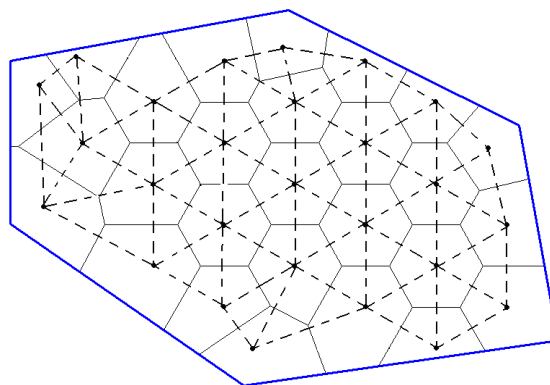


Fig. 10.C.2 – Voronoi grid and Delaunay triangulation (broken lines)

10.C.2 Building the Voronoi grid

The grid is built by superposition of simple modules. A module is a set of sites associated to a reservoir element. The main module types are presented in the three figures below:

- Base, or background, modules, which may be rectangular or hexagonal.
- Segment module introduced in order to respect constraint lines such as the reservoir contour and faults.
- Corner modules introduced at corners of the constraint lines.
- Well modules, which are radial for vertical wells but present more complex shapes for fractured (2-D), horizontal and limited entry wells (3-D).

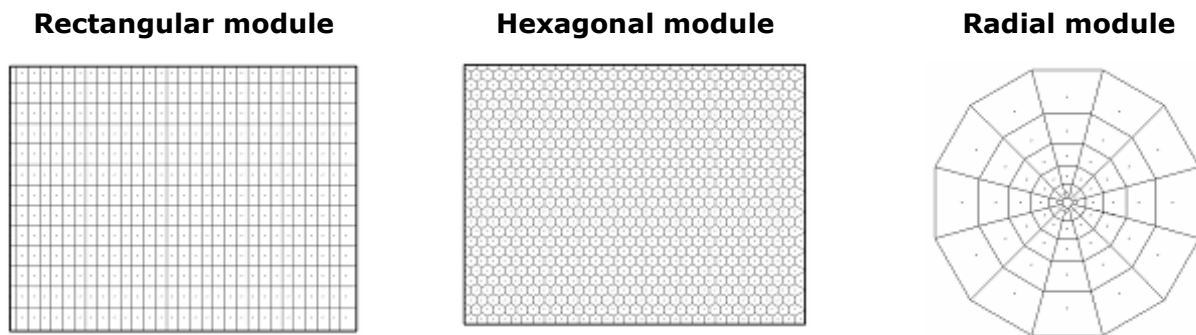


Fig. 10.C.3 – Base modules used in the Voronoi grid construction

A short description of how to build a complete Voronoi grid is presented below. We will however not detail here all steps that are necessary to do so. In particular we will skip the somewhat tedious treatment of interference between modules.

Everything starts with a vector representation of the problem and particularly with a contour, wells and inner boundaries:

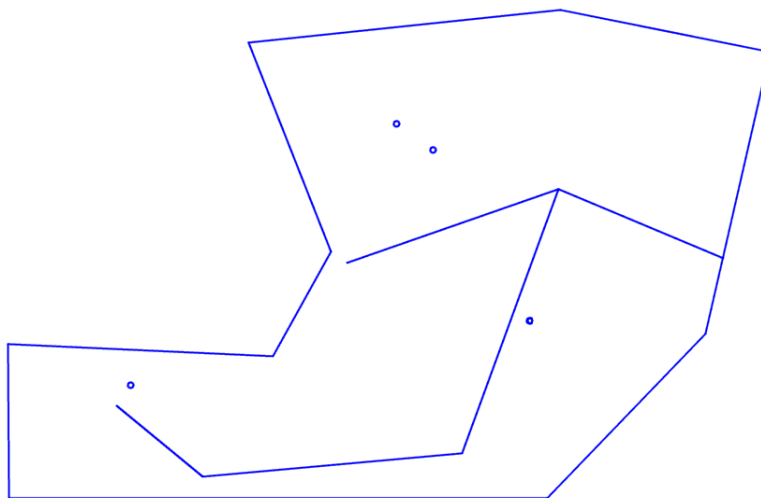


Fig. 10.C.4 – Vector representation of the problem: contour, faults, vertical wells

The base module is built as in the figure below. In this figure the points that would be overlapping with other modules have already been removed.

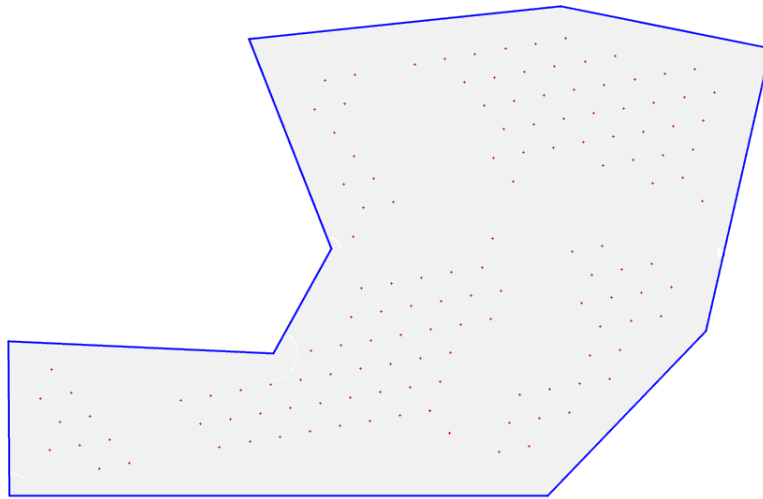


Fig. 10.C.5 – Base module nodes for a hexagonal grid

The radial modules are built around the wells. Fig. 10.C.6 shows the new modules truncated by interference and the nodes remaining after processing:

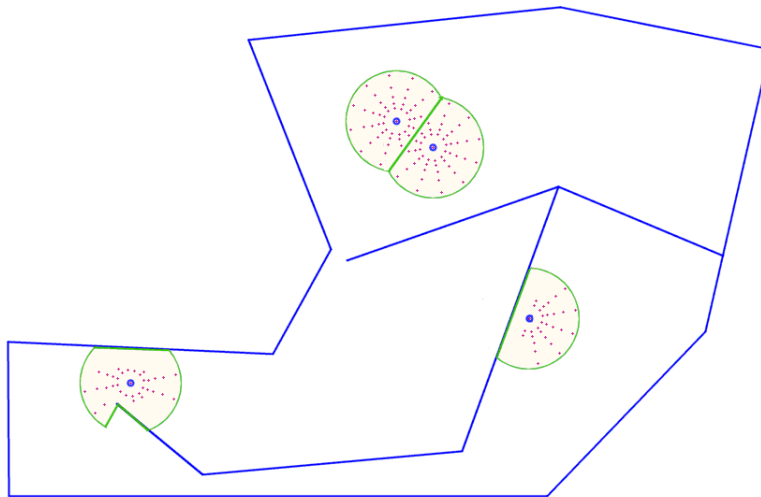


Fig. 10.C.6 – Radial modules around wells

The segment modules are built around the faults and the contour. In the diagram below the corresponding nodes remaining after processing:

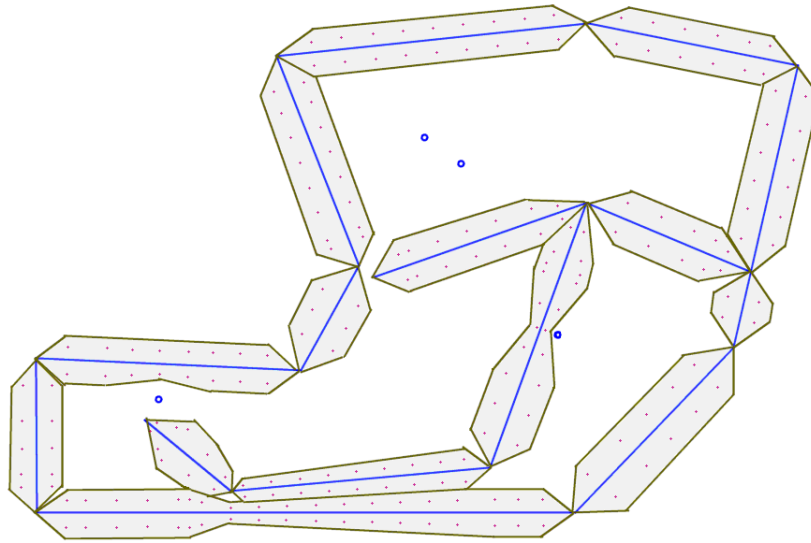


Fig. 10.C.7 – Segments modules around faults and contour

The corner modules are built. They constitute a local refinement that ensures that the shape of the Voronoi grid will exactly follow the angles of the contour and inner fault polylines.

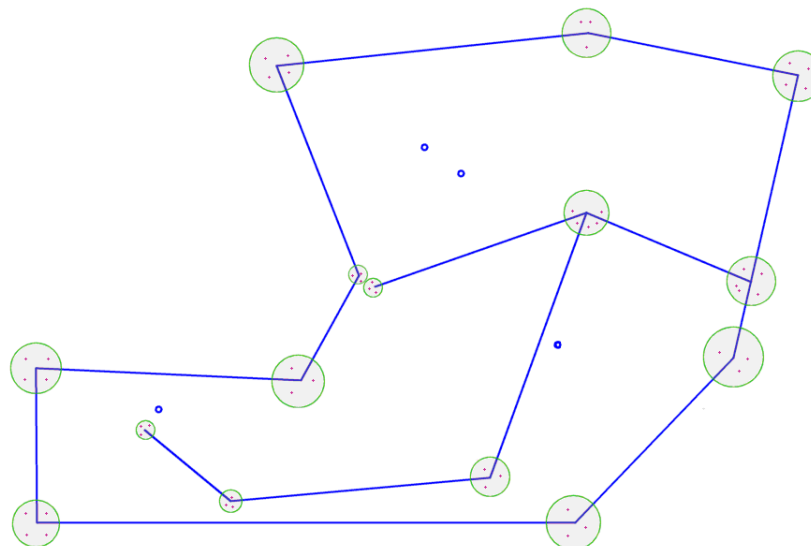


Fig. 10.C.8 – Corners modules around faults and contour angles

The figure here shows the final superposition of all modules leads to the representation below, in which the main interferences are indicated (S=segment, R=radial, C=corner):

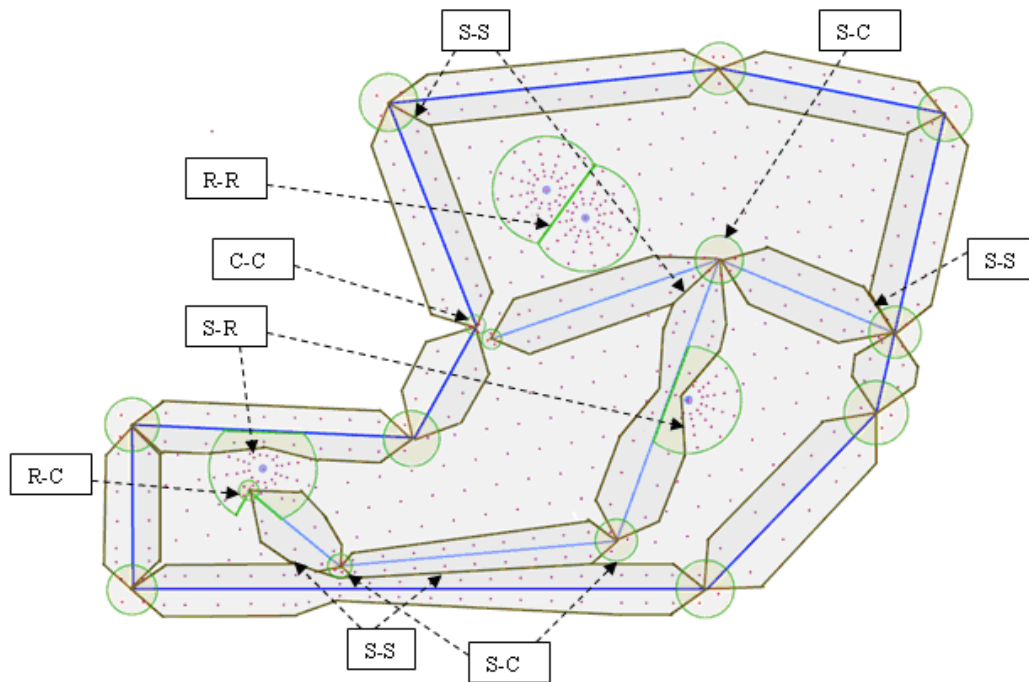


Fig. 10.C.9 – Final superposition

Finally, the triangulation is performed and the resulting Voronoi grid is shown here:

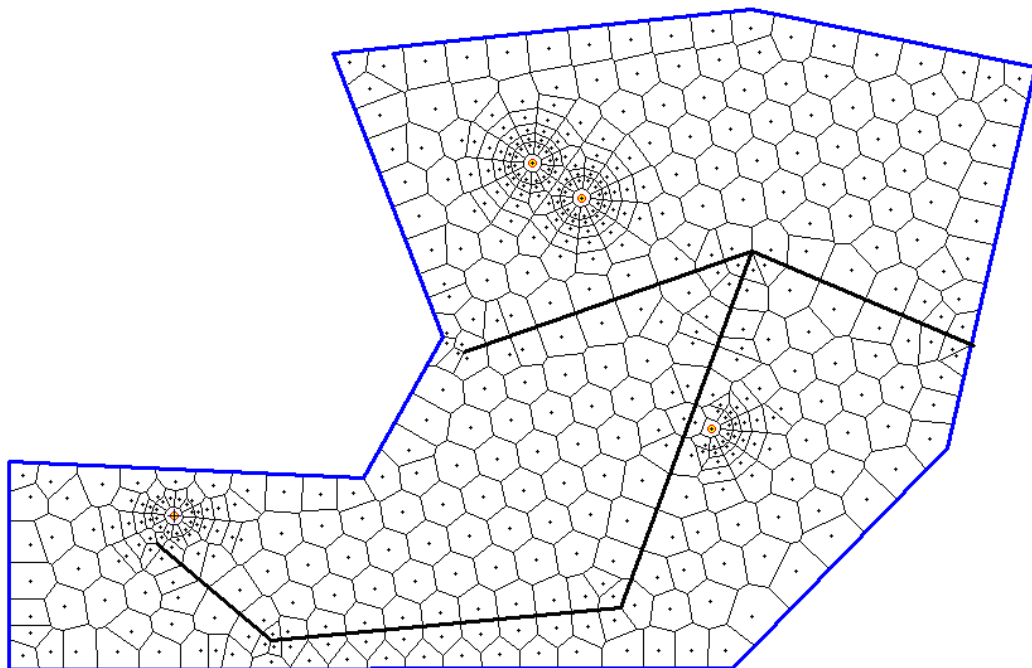


Fig. 10.C.10 – Final Voronoi grid

This result is to be compared with the composite image below showing the specific influence of each module on the final result:

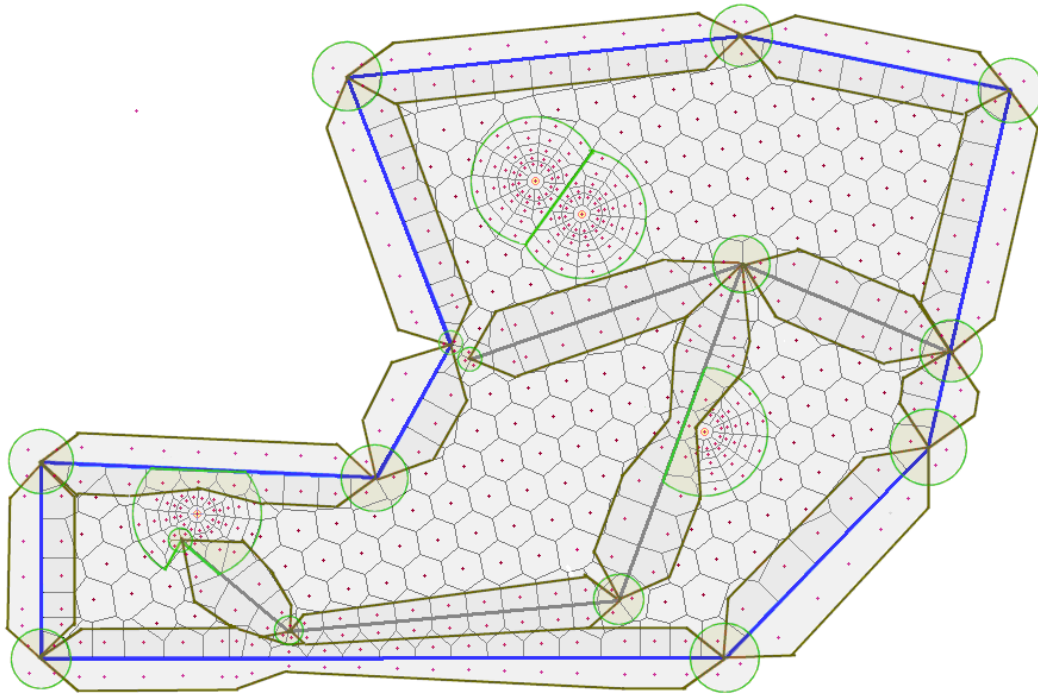


Fig. 10.C.11 – Final Voronoi grid and modules areas of influence

10.C.3 Local 3D refinement for specific well geometries

The example detailed in the previous paragraph addresses only vertical fully penetrating wells, but beyond those simple well geometries the numerical module should also account for fractured, partially penetrating, limited entry fracture and horizontal wells. Whenever needed the 2D reservoir module around the well is replaced by a 3D unstructured grid refinement.

10.C.3.a Vertical wells

Because the well is vertical and fully penetrating a 2D gridding module is sufficient to capture the radial flow. Circular rings are constructed following a geometric series. The other well gridding controls are the bounding radiuses of the module (R_{min} , R_{max}) and the number of sectors (12 here below).

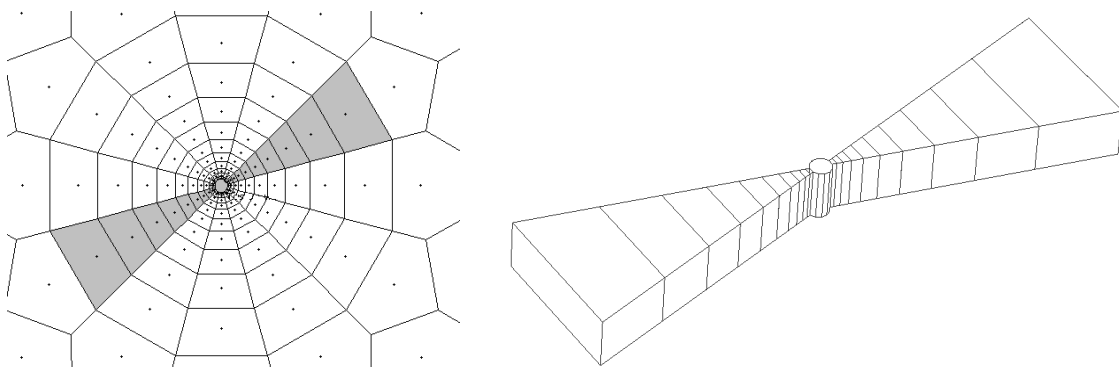


Fig. 10.C.12 – Vertical well gridding: 2D view and 3D display of the highlighted (gray) sectors

10.C.3.b Fractured (fully penetrating) wells

As before, a two-dimensional grid is sufficient because both well and fracture are fully penetrating. As a result fluid flow towards the wellbore is two-dimensional. The gridding module must be designed to follow the fluid flow characteristics in such a case: linear flow at early time, followed by radial flow at later time. The fracture itself has a grid constructed when it presents finite conductivity behavior. In addition to the number of sectors and the bounded radii the module is characterized by the number of linear segments (N_{dx}) used to grid the fracture – reservoir interface (10 segments in the example below).

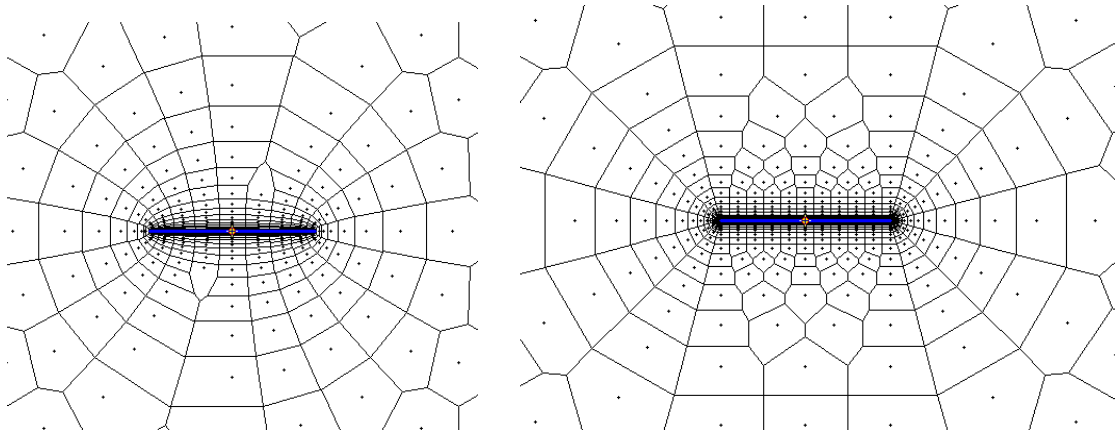


Fig. 10.C.13 – Two possible gridding modules for a fractured well: elliptic (left) and pseudo-radial (right).

10.C.3.c Limited entry wells

The well gridding must be tri-dimensional because of the necessity to reproduce early time hemispherical flow. A 3D Voronoi unstructured module is inserted in the 2D background grid. This module may be distorted by vertical anisotropy as necessary. The number of vertical cells N_z and 10 in the example below, now appear as an additional gridding parameter.

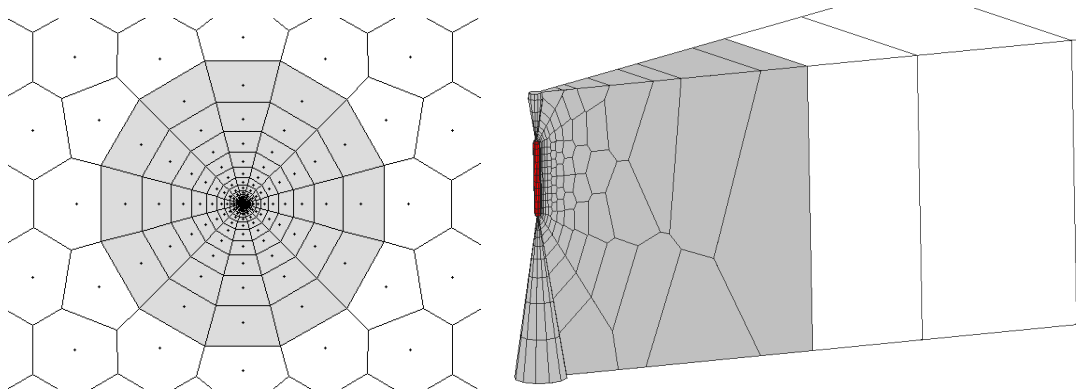


Fig. 10.C.14 – Limited entry gridding module: 2D display (the 3D module is highlighted in gray) and 3D view (the well is highlighted in red).

10.C.3.d Limited entry fractured wells

As before, the well module must be tri-dimensional. The resulting unstructured 3D module is obtained by combining the limited entry with the fully penetrating fracture module. Hence, the defining parameters are now: R_{min} , R_{max} , number of sectors, N_{dx} and N_z .

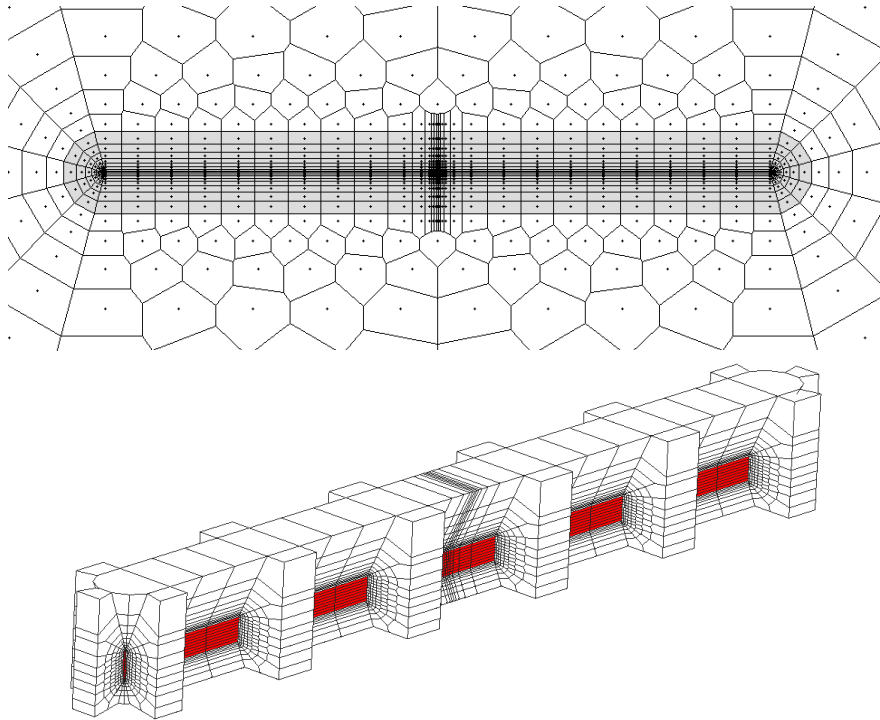


Fig. 10.C.15 – Limited entry fracture gridding module: 2D display (the 3D module is highlighted in gray) and 3D view (the fracture is highlighted in red).

10.C.3.e Horizontal wells

The well module is 3D in order to capture early time spherical and vertical radial flows. The resulting 3D unstructured module may be distorted if vertical anisotropy is introduced. It is controlled by the following parameters: R_{min} , R_{max} , number of sectors and N_{dx} .

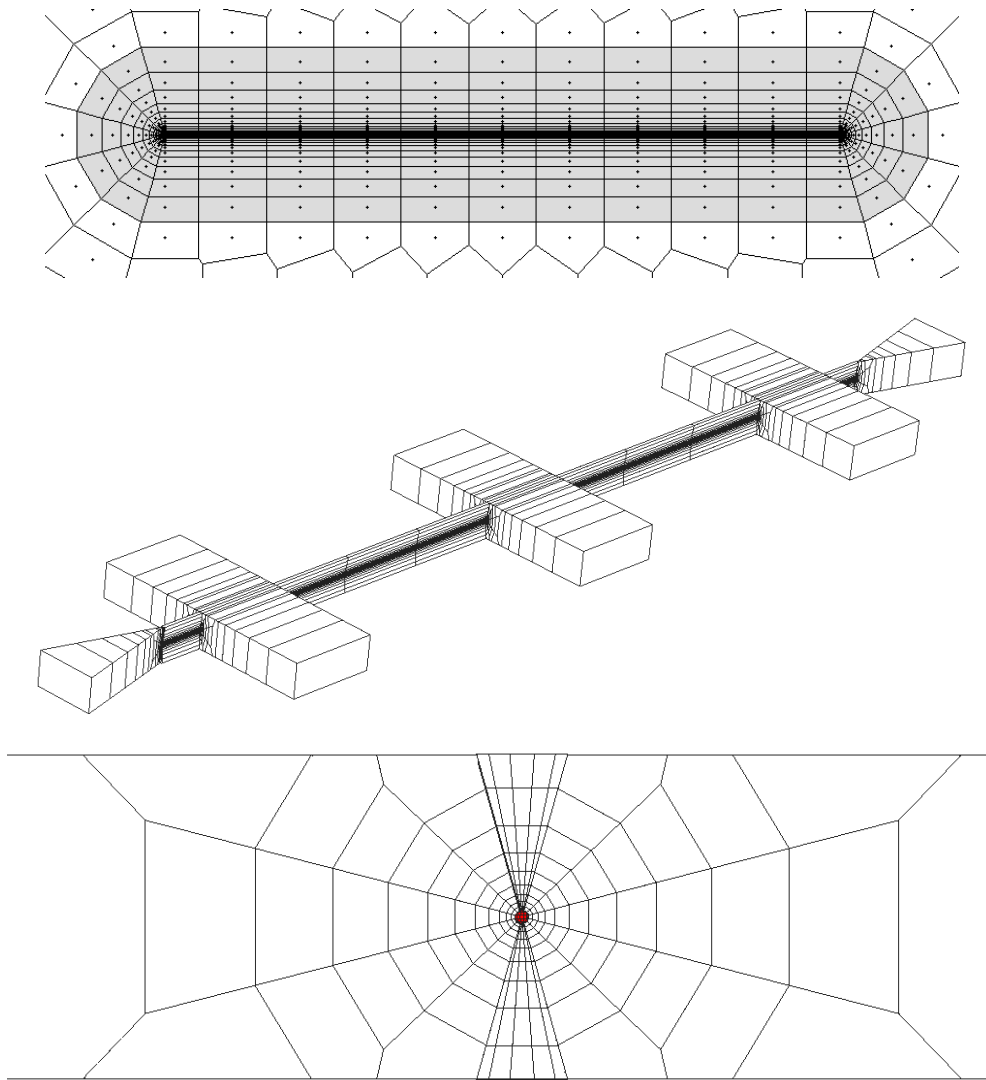


Fig. 10.C.16 – Horizontal well module: 2D display (the 3D module is highlighted in gray), 3D view and vertical cross-section (the well is highlighted in red).

10.D Handling Linear Problems

10.D.1 A 'super-analytical model'

When solving linear diffusion problems, we may consider the numerical simulator as a super type-curve generator.

One typical application of this is numerical solutions for gas flow in which pressure dependence of the gas properties is, in part, handled by the classical pseudo-pressures. In which case the numerical simulator is solving its system of equations for $m(P)$, instead of P . This approach allows us to easily obtain solutions that would be out of reach to analytical solutions (the two figures below). Even more important, in some situations the numerical (linear) simulator provides a solution faster than analytical solutions on equivalent geometries, considering its simplicity and the somewhat complex form that the later can take.

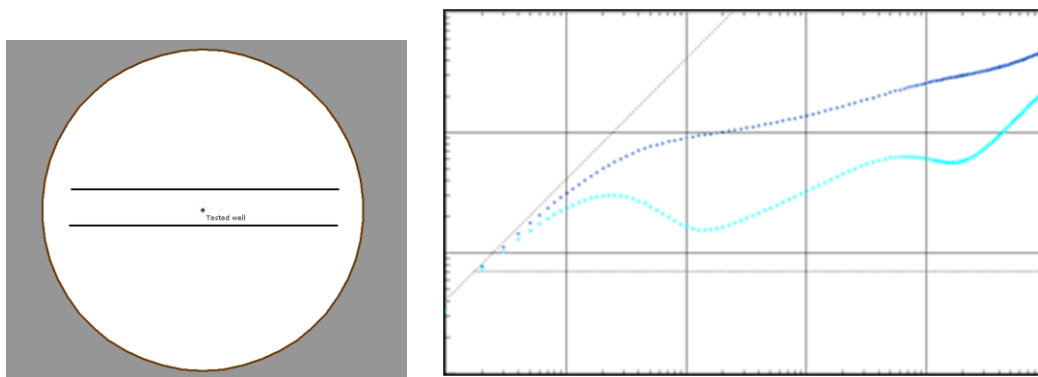


Fig. 10.D.1 – Circular reservoir with two parallel faults, and its corresponding numerical type curve. One can see the transition from linear flow, due to the faults, to pseudo-steady state flow that is due to the circular boundary.

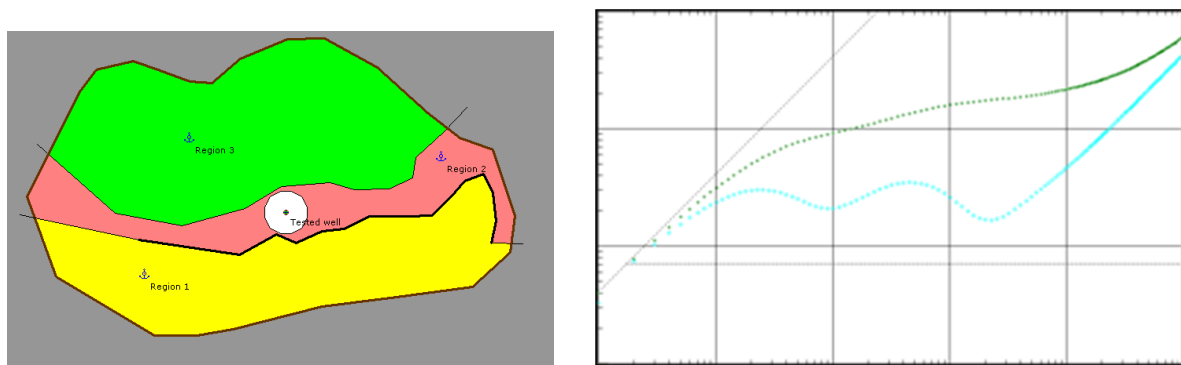


Fig. 10.D.2 – Complex composite reservoir (3 zones)

Naturally, in this application the solution obtained numerically is based on the usual assumptions and limitations for analytical solutions: single phase flow of a slightly compressible fluid, constant rock properties, etc. Hence it will lead to the same approximations and possibly the same errors:

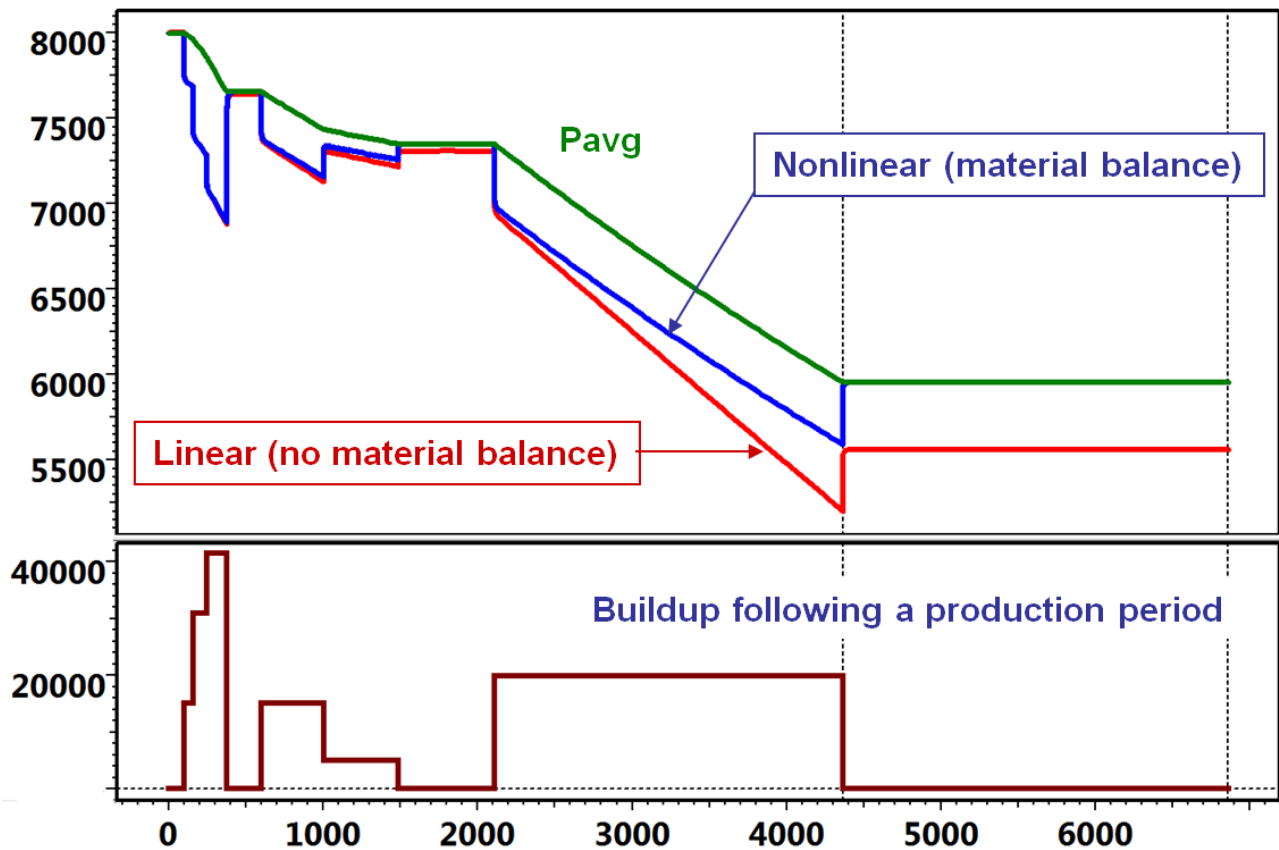


Fig. 10.D.3 – Buildup following a production period. Both solutions are numerical, but the linear curve (in red) does not take gas material balance into account, whereas the full nonlinear solution (in blue) does so: it is in agreement with the average pressure (in green).

10.D.2 Formulation

The numerical resolution of the partial differential equations ruling fluid flow in reservoirs consists in replacing those equations by difference equations where space and time are discretized. We have seen in the previous paragraphs how space is discretized into grid cells and grid nodes. Time discretization implies that the simulator will not provide a continuous solution (As, say, the cylindrical source solution computed analytically for a vertical well in an infinite reservoir), but will instead provide a discrete series of pressures P at given time steps $\{t_1, \dots, t_N\}$.

When the reservoir (e.g., rock compressibility, permeability) and the fluid parameters (e.g., viscosity) can be considered constant in time the problem becomes linear: the reservoir state at time t_i does not depend on the parameters we are looking for, that is usually the pressure. This simplification reduces quite considerably the complexity and CPU time needed to numerically solve the given problem.

Single phase incompressible flow through a homogeneous porous media Ω is described by Darcy's law and the mass conservation law:

$$\vec{V} = -\frac{k}{\mu} \nabla P$$

$$-div(\rho \vec{V}) = \frac{\partial(\rho \phi)}{\partial t}$$

Considering gridding of the reservoir, the material balance of the cell (i) is expressed at a given time as:

$$e_i = \sum_{j \in J_i} T_{ij} \cdot \lambda_{ij} (P_j - P_i) - \frac{\partial}{\partial t} \left(\frac{V_i \cdot \Phi_i}{B_i} \right) - q_i$$

Where e_i is the material balance difference in the cell (i), J_i all cells connected to cell (i), V_i the cell volume, and λ_{ij} the transmissivity coefficient at connection (ij). The additional term q_i refers to the eventual presence of a well in cell (i).

This equation is discretized in time. Over the time interval $\Delta t = [t^n, t^{n+1}]$ one can write:

$$e_i^{n+1} = \sum_{j \in J_i} T_{ij} \cdot \lambda_{ij}^{n+1} (P_j^{n+1} - P_i^{n+1}) - \frac{V_i}{\Delta t} \left[\left(\frac{\Phi_i}{B_i} \right)^{n+1} - \left(\frac{\Phi_i}{B_i} \right)^n \right] - q_i^{n+1}$$

If we assume that the coefficients in e_i^{n+1} do not depend on the pressure the equation above can be written in terms of $F(P)=0$, with

$$P = [P_1, P_2, \dots, P_N]^t \text{ and } F = [e_1, e_2, \dots, e_N]^t, \text{ where } P_i \text{ is the pressure at cell (i).}$$

Iterative solver methods (BiCGStab, GMRES, etc...) are coupled with matrix pre-conditioners (ILU, SSOR, etc...) to solve this linear system for P .

10.E Handling Linear problems (Advanced)

10.E.1 Modeling composite zones

Linear numerical models are not limited to the treatment of complex boundaries and faults. It is possible to define regions of enhanced or reduced mobility and/or storativity without a penalty in CPU time, since in any case the simulator computes transmissivities at every grid node. Hence it is possible to reproduce analytical solutions for composite systems (see below) – and to compute some solutions on composite systems that are not so easy to obtain analytically (2nd figure below).

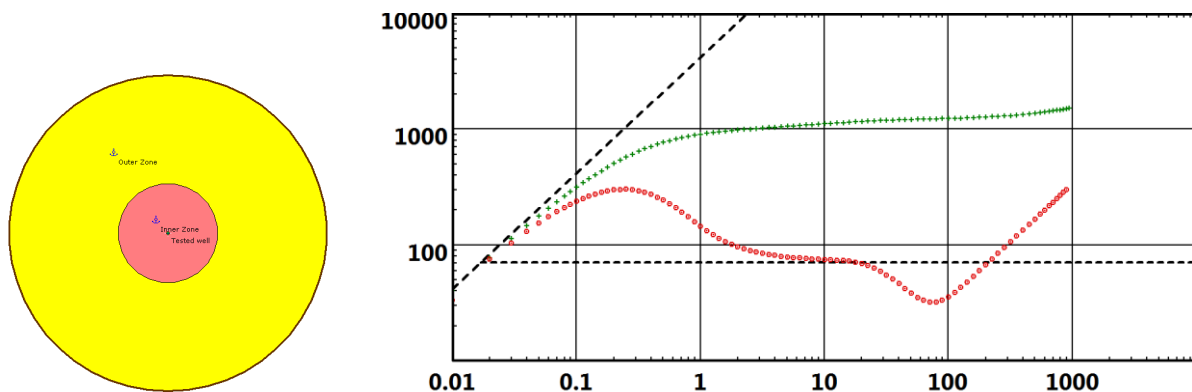


Fig. 10.E.1 – Numerical solution for a radial composite system in a closed circular reservoir. The outer zone (in yellow) presents a higher mobility.

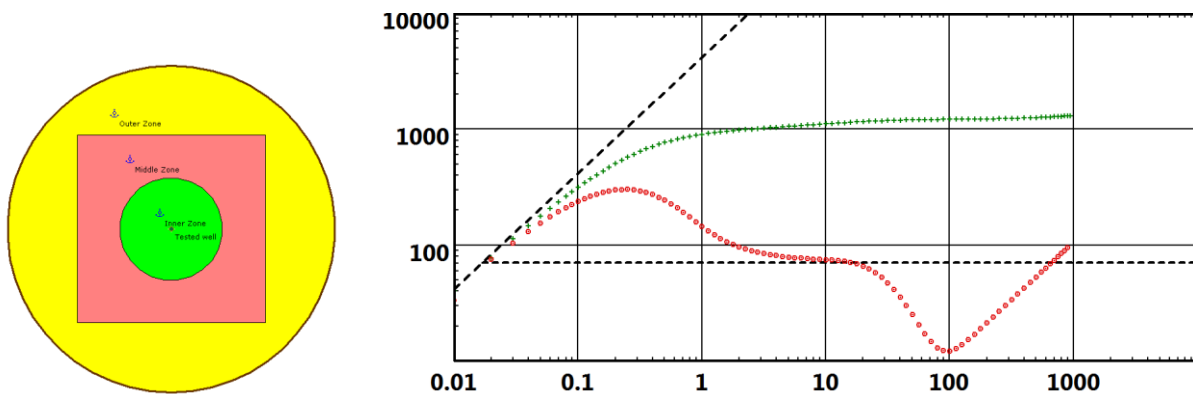


Fig. 10.E.2 – There is now one more composite zone, for which there is no simple analytical solution for this (unrealistic) geometry.

Composite zones are particularly useful to model a transition between fluids such as water around an injector. But from the simulator point of view it is just a matter of different rock properties assigned to the grid cells.

10.E.2 Using field data

It is of course possible to go one step beyond and to define specific rock properties for each cell. For instance it may be possible to make a numerical simulation based on permeability and porosity maps, as shown below.

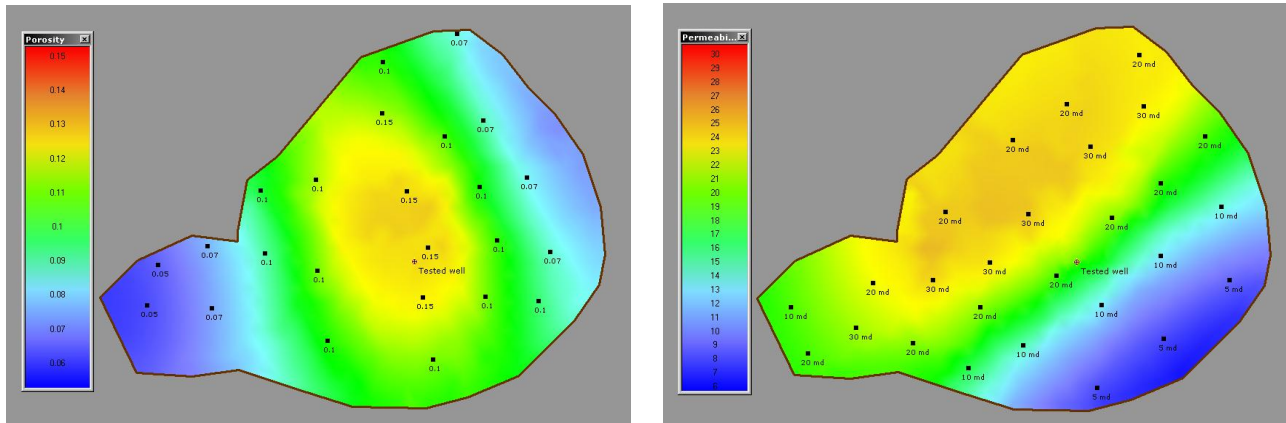


Fig. 10.E.3 – Interpolated porosity (left) and permeability (right), and the point data used to generate their corresponding maps.

The representation of petrophysical properties displayed in the above figure is the final result of a two-dimensional interpolation of input data which are represented by the black data points.

Three interpolation algorithms are available in Ecrin:

- Inverse distance weighting, where the power parameter n (typically, $n=2$) is the power to which each distance is elevated in the weighting process. The smaller n , the smoother the final interpolated surface.
- Linear interpolation, where the surface is assumed to be linear by parts. In this case the interpolation is performed on the Delaunay triangulation.
- Kriging, where the interpolated surface is obtained from a variogram (inverted covariance) fit on the data points.

The three options along with their leading parameters permit a wide spectrum of possible interpolation results, illustrated here:

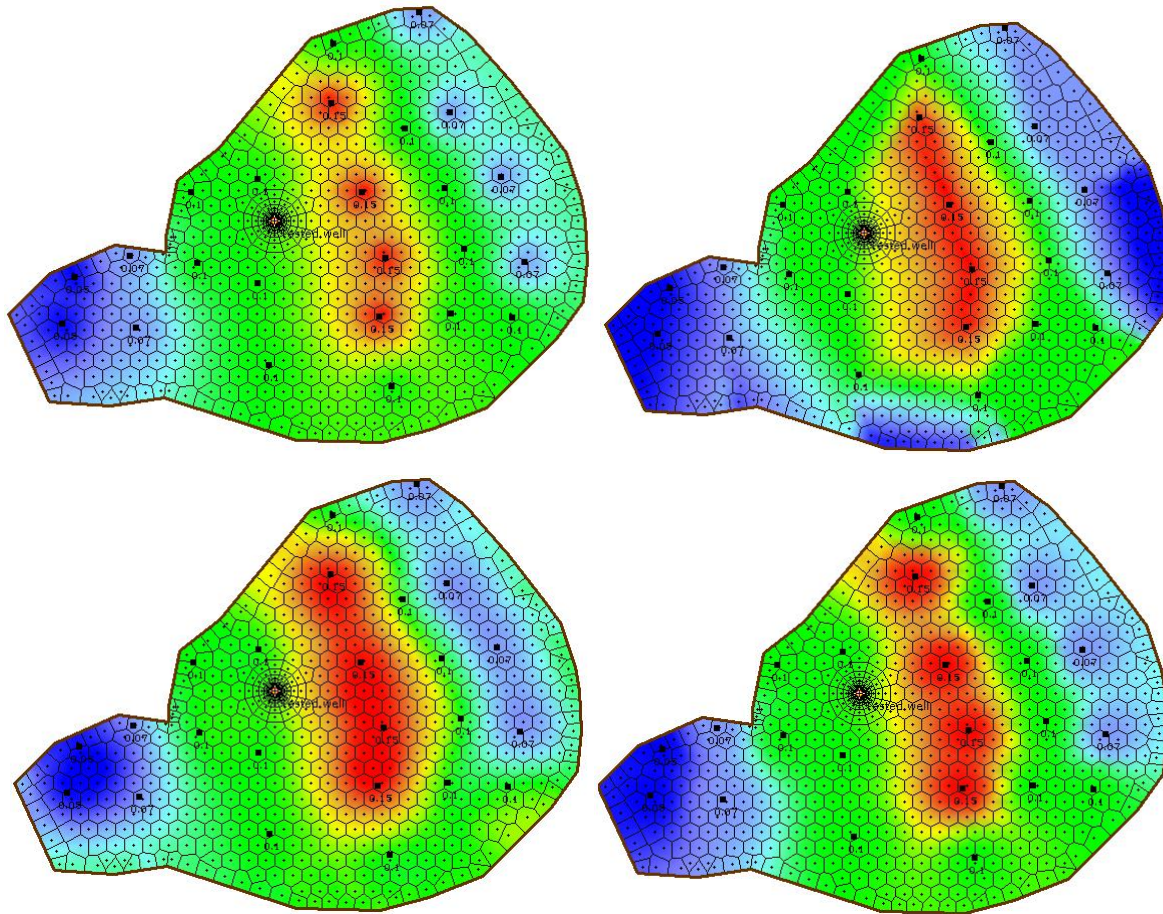


Fig. 10.E.4 – Four different interpolated fields obtained from the same input (porosity) data. From top-left to bottom-right: inverse distance weighting (n=2), linear interpolation, kriging with a range of 1500 ft, kriging with a smaller range of 750 ft.

The data subject to interpolation may be classified into two categories: the data that affects the reservoir geometry such as horizons and thickness. And the data describing the fluid and rock properties. Concerning the reservoir geometry, only the layer thickness presents a significant importance in well test analysis, since gravity effects are usually neglected. With the fluid and rock properties, the main data of interest are usually porosity and permeability. The interpolated fields for the two last parameters are radically different in one respect: the average reservoir porosity can be easily calculated from the interpolated field values, however there exists no rigorous approach to compute the average permeability equivalent to a permeability field such as the one shown in the figure below.

In fact, the best approximation consists in evaluating the effective average permeability as a result of the numerical simulation. In such a case the pressure match line on the loglog plot is no longer an input but a simulation result. This match line may still be moved up and down if one introduces a 'fudge factor' k/k_{field} , i.e. a global multiplier applied to the entire interpolated permeability field when a simulation is performed.

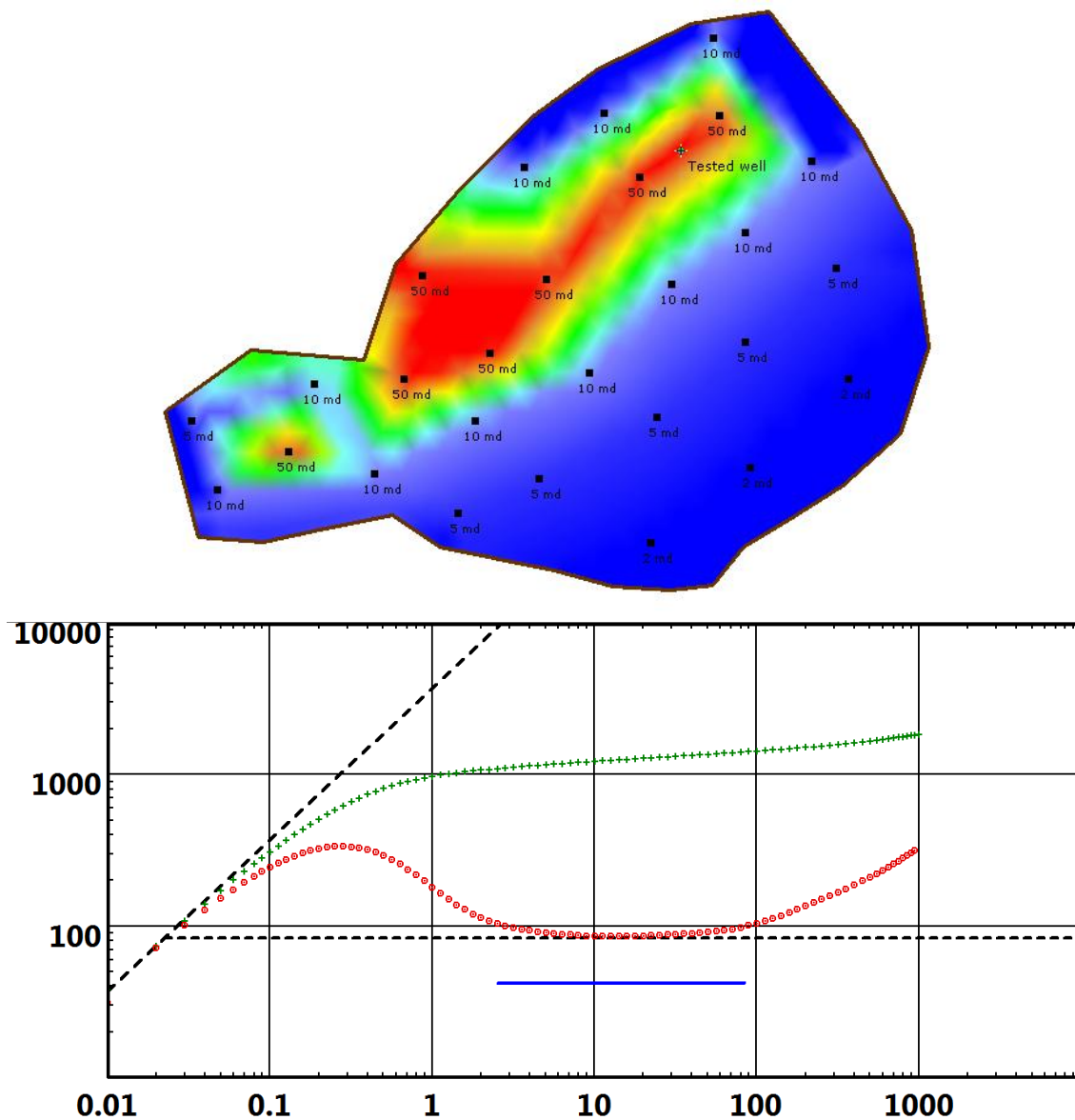


Fig. 10.E.5 – Permeability field and corresponding simulation: although the tested well is in a 50 mD 'channel' (the red zone in top figure), the effective simulation permeability is more than 40% lower (when comparing the pressure match line to the 50 mD blue IARF line).

10.E.3 Double-porosity reservoirs

The numerical model can simulate a double porosity medium by splitting each grid cell into two: the first half represents the fissure and the second the matrix. Each sub-cell will occupy the same geometrical volume and the same location. Hence the gridding is not affected. In the simulation, the pore volume and the transmissivity of each fissure and matrix sub-cell is computed using the model storativity ratio (ω) and interporosity flow parameter (λ). Furthermore, the matrix sub-cell is only connected to its corresponding fissure sub-cell. In other words, the model input permeability k is the fissure permeability.

The reservoir cell characterized by a pore volume V and a permeability k is split into a fissure sub-cell f with a pore volume V_f and a matrix sub-cell m with a pore volume V_m . V_f and V_m are computed from the storativity ratio ω :

$$V_f = V \cdot \phi \cdot \omega$$

$$V_m = V \cdot \phi \cdot (1 - \omega)$$

Where ϕ is the porosity. The transmissivity T_{fm} between the fissure and the matrix sub-cells is defined using the interporosity flow parameter λ :

$$T_{fm} = k \cdot \lambda \cdot \frac{V}{r^2}$$

Where r is a characteristic length of the matrix-fissure interface.

To sum-up, double-porosity reservoirs in numerical models may be described with identical parameters as for analytical solutions. We may use the same basic procedures to graphically estimate ω and λ as in the analytical case, as shown in here:

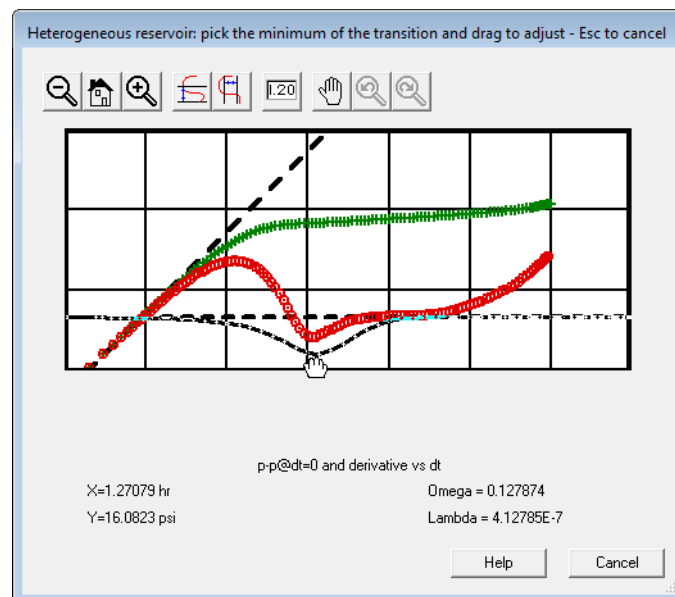


Fig. 10.E.6 – Estimating ω and λ by pick in the definition of a double porosity numerical model.

The numerical simulation of double porosity behavior may be combined with more complex geometries and heterogeneities, hence providing far more flexibility in terms of problem definition than can be found in analytical solutions. It is even possible to consider the combination of different defined double porosity within different composite zones, as shown in here:

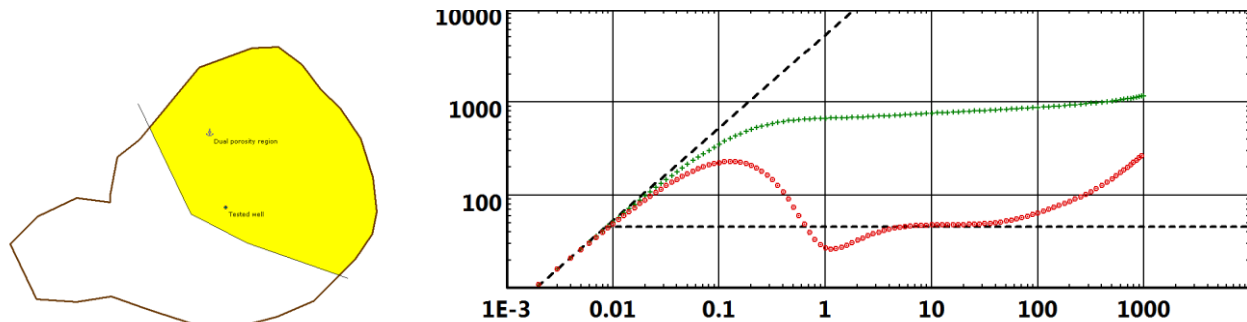


Fig. 10.E.7 – Yellow zone only defined as double porosity.

10.E.4 Modeling permeability anisotropy

When an horizontal permeability anisotropy is defined the Voronoi grid is internally deformed (figure just below). However, the deformed grid is no longer a Voronoi grid, as it does not respect the orthogonal condition between node segments and cell faces. In fact, the problem is solved on an equivalent isotropic grid displayed in the second figure below. Similar situations and grid deformations are encountered in the case of vertical anisotropy and 3D gridding modules.

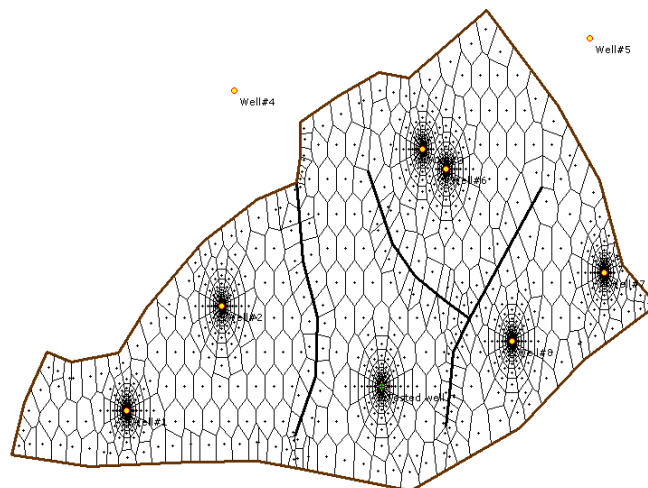


Fig. 10.E.8 – 'Voronoi' grid for an anisotropic reservoir ($k_x/k_y=0.2$)



Fig. 10.E.9 – Equivalent Voronoi grid for an anisotropic reservoir ($k_x/k_y=0.2$)

To sum up, horizontal and vertical anisotropies affect the grid construction phase but the other simulation steps such as the matrix system to be solved, are not affected. This simple treatment is only possible when the anisotropy is constant, that is, when the grid may be entirely deformed using a unique anisotropy tensor.

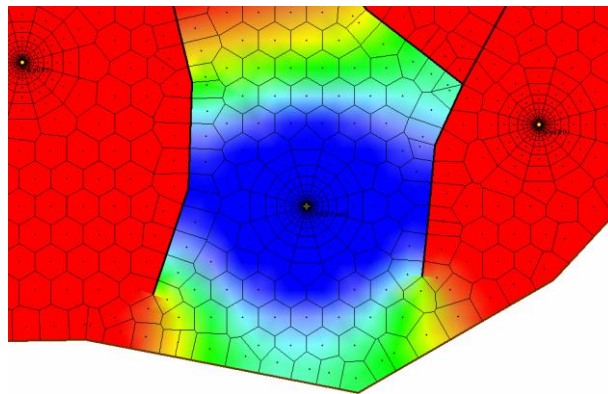


Fig. 10.E.10 – Pressure field around producer, isotropic reservoir

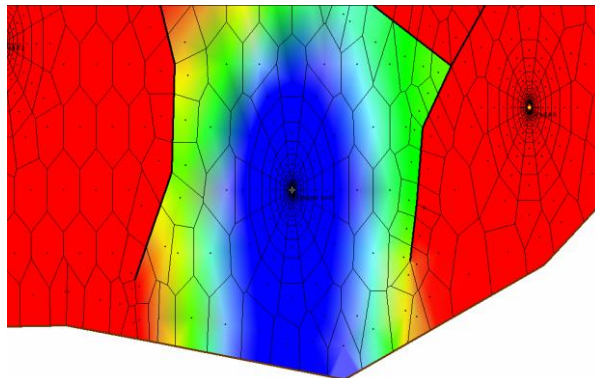


Fig. 10.E.11 – With anisotropy ratio k_x/k_y of 1/5.
Obviously the faults are seen much later than in the isotropic case.

10.E.5 Modeling multi-layer reservoirs (with or without cross-flow)

Extending the numerical model to multi-layer reservoirs can be made in a very simple way if we limit ourselves to vertical wells and if the contour / faults are handled as vertical walls intersecting all layers identically. In this case the 2D single layer grid merely needs to be replicated n times for n layers, as shown here:

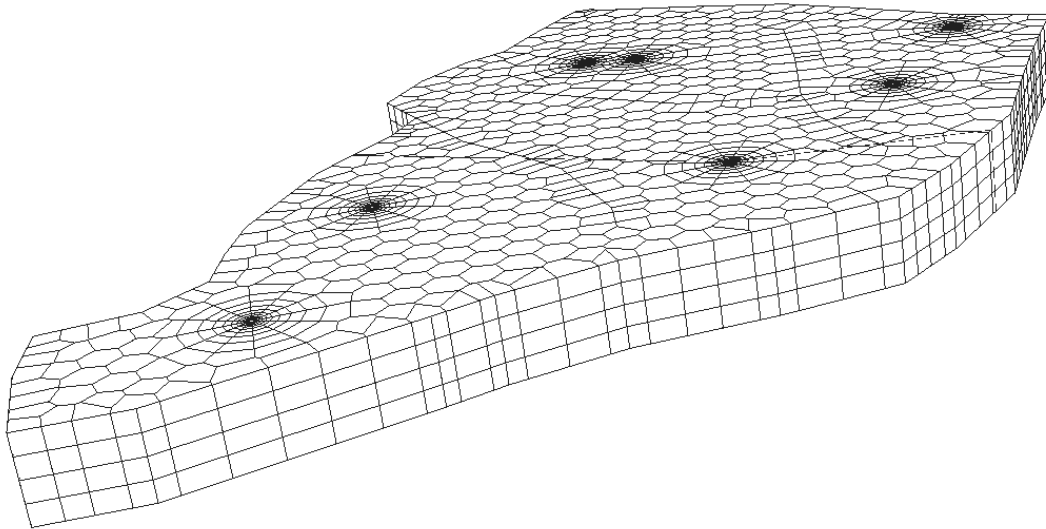


Fig. 10.E.12 – 2D grid piled up to simulate a 4 layer system

The reservoir geometry is somewhat restricted with this configuration: the layers cannot be disconnected and the layer horizons are constant. In fact this limitation is acceptable as long as single phase flow without gravity effects is simulated. Other than that, the layered system may be commingled with no hydraulic communication between layers, or there may be some crossflow between layers, as shown below:

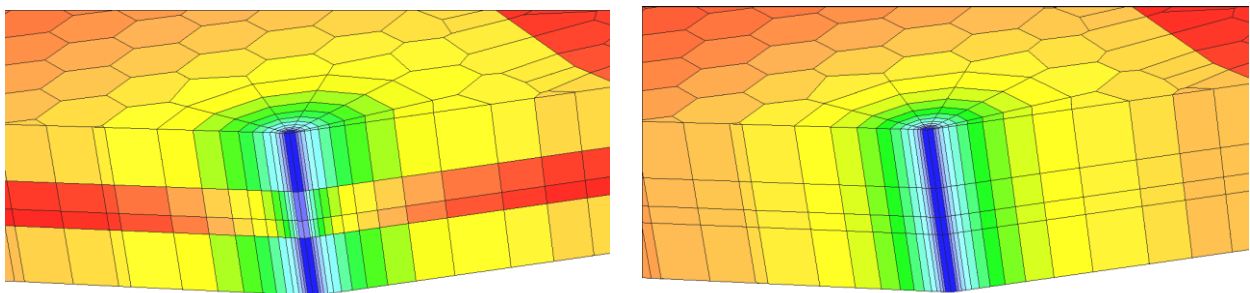


Fig. 10.E.13 – Pressure field around a well producing in a four layer system, without and with vertical crossflow between layers. (left and right respectively). The top and bottom layer have been defined with equal permeability. Middle layers with lower permeability.

Multi-layered systems give more degrees of freedom concerning the well perforations. Instead of perforating the well over the complete reservoir it is possible to open individual perforations of each layer (figure below). Note however, that with the 2 ½ D gridding used the early time spherical flow that should theoretically appear due to the partial completion does not do so, as the specified vertical permeability in the model only applies at the interface between the layers. The layers themselves are isotropic.

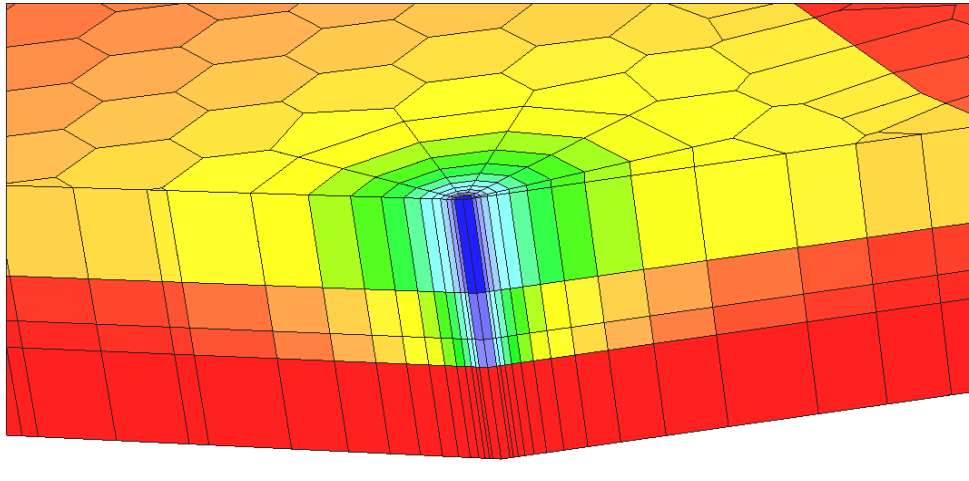


Fig. 10.E.14 – Pressure field around a well producer in a (commingled) four layer system. The bottom layer is not perforated (compare with Fig. 10.E.13).

In multilayer simulations it is also possible to compute and output layer rates at the wellbore, i.e. individual layer, bottom hole, contributions. This output facility is particularly useful in identifying potential crossflow in the wellbore during shut-in periods, as displayed below.

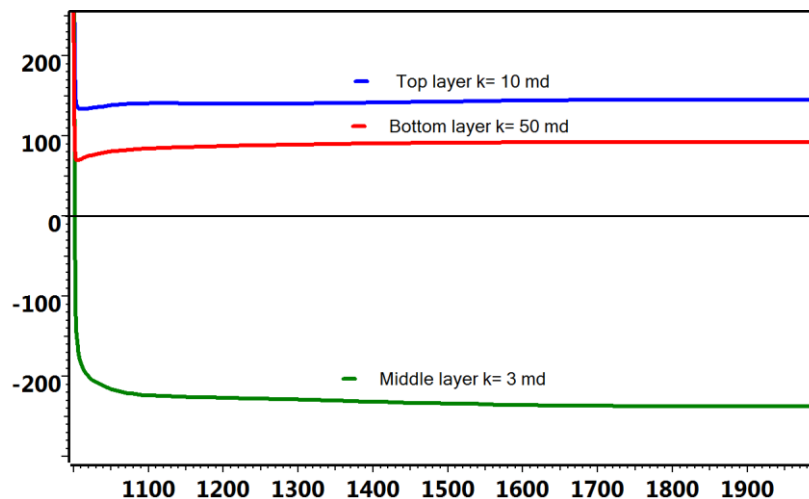


Fig. 10.E.15 – Three layer system, layer contributions simulated at the well during a build-up following a production period. Because the pressure drop is less important in the middle, high permeability, layer at the end of the production, crossflow occurs in the wellbore until the pressure reaches equilibrium.

10.F Handling nonlinear problems

In situations where the pressure, hence time dependency of the reservoir and fluid parameters, can no longer be ignored, the numerical problem to be solved becomes non-linear. We have no other choice but to iteratively linearize this non-linear system within a non-linear root finding algorithm. The Newton-Raphson technique is broadly used in this situation.

If we recall the discretized material balance equation in the cell (i) over the time interval $\Delta t = [t^n, t^{n+1}]$ obtained in section Handling Linear Problems (Basic):

$$e_i^{n+1} = \sum_{j \in Ji} T_{ij} \cdot \lambda_{ij}^{n+1} (P_j^{n+1} - P_i^{n+1}) - \frac{V_i}{\Delta t} \left[\left(\frac{\Phi_i}{B_i} \right)^{n+1} - \left(\frac{\Phi_i}{B_i} \right)^n \right] - q_i^{n+1}$$

The system $F(P)=0$ is now non-linear because the components in the e_i^{n+1} term depend on pressure. It can be solved with an iterative Newton-Raphson method, in which a linearized approximation of the solution for the non-linear iteration can be written:

$$F^{l+1} = F^l + J \cdot \Delta P \text{ where } J = \left[\frac{\partial F}{\partial P} \right] \text{ is the Jacobian matrix and } \Delta P = (P^{l+1} - P^l).$$

The linearized system $P^{l+1} = P^l - J^{-1} \cdot F^l$ can now be solved for P^{l+1} , using the same techniques as in the linear case.

At each time step, the Newton-Raphson algorithm iterates until an acceptable minimum is obtained. This will happen until the next iteration point gets too close to the current solution. In this process the CPU time clearly depends on the precision sought, as can be seen in the table below.

	Number of linear iterations/time step	Material balance error (%)	CPU ratio
Linearized problem (m(p))	14	--	0.9
Nonlinear, residual=1E-3	14.5	5.0E-12	1
NL, residual=1E-5	15.5	1.8E-12	1
NL, residual=1E-8	30	1.1E-12	3
NL, residual=5E-9	102	1.5E-14	13.4

The above numbers were obtained simulating a single gas well producer in a rectangular, homogeneous reservoir. Various runs were compared; a linear case where the simulator solves a problem made linear after the introduction of pseudo-pressures, and four non-linear cases with increasing restrictions on the non-linear loop convergence criterion (the 'residual'). The non-linear loop introduces only a small overhead in this example because the problem remains only slightly non-linear. More so because the dependency of the gas PVT on the pressure variable remains relatively smooth. It will be shown in the sections below that the additional CPU time can be far more important when strong non-linearities are introduced. It can also be demonstrated that forcing the convergence criterion to very small values is particularly useless. The only effect being to make the CPU time explode, for a slight gain in precision before reaching the limit of the machine.

10.F.1 Non-Darcy flow

See also section of dry gas considerations for PTA.

Darcy's equation is only valid for laminar flow but in some situations fluid flow in the reservoir can become turbulent. For example, in a reservoir in the vicinity of high rate gas producers. In fluid mechanics the transition from laminar to turbulent flow is characterized by the Reynolds number Re :

$$Re = \frac{\rho v L}{\mu} = \frac{\text{Inertial forces}}{\text{Viscous forces}}$$

Laminar flow occurs at low Reynolds numbers ($Re < 2000-3000$), in which case fluid flow is a constant and smooth fluid motion. When inertial forces ($Re > 4000$) dominate fluid flow becomes turbulent, producing random vortices and other fluctuations.

Because turbulence usually occurs in the vicinity of the wells a classical way to handle this involves introducing a pseudo-skin parameter D so that the total skin S' becomes: $S' = S_0 + Dq$, where q is the well flowrate. This simplified approach can of course be used as-is in numerical simulations. However numerical simulation makes it possible to incorporate the non-Darcy flow effects at an upper level, through the introduction of the Forchheimer factor β in a generalized Darcy's equation.

The classical Darcy's law:

$$-\nabla P = \frac{\mu}{k} \cdot \vec{u}$$

is replaced by its generalized form:

$$-\nabla P = \frac{\mu}{k} \cdot \vec{u} + \beta \cdot \rho \cdot |\vec{u}| \cdot \vec{u}$$

In which β is the Forchheimer factor. β has the dimension L^{-1} , that is m^{-1} in SI system. If we introduce the notions of Darcy velocity u^D (grossly speaking, the velocity given by laminar flow) and non-Darcy velocity u , we can obtain the following relationship:

$$u = f^{ND} u^D \quad \text{with} \quad f^{ND} = \frac{2}{1 + \sqrt{1 + 4 \cdot \beta \cdot k \cdot \lambda \cdot u^D}}$$

Where k is the permeability, and $\lambda = \rho/\mu$ is the inverse of the kinematic fluid viscosity.

In fact it can be shown that both approaches (pseudo-skin and Forchheimer factor) are equivalent when the kinematic fluid viscosity (μ/ρ) is held constant. In practice, both approaches provide results that are comparable:

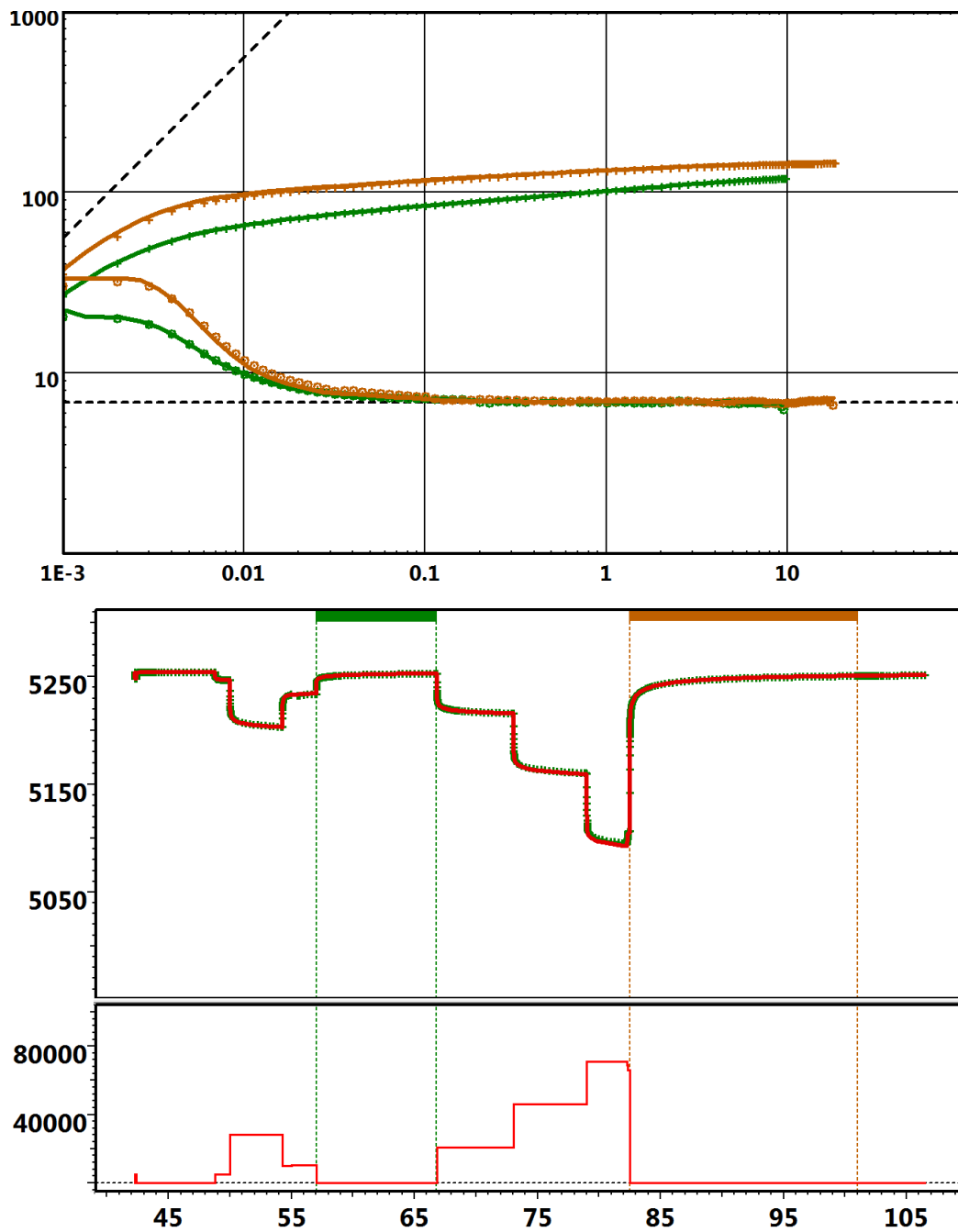


Fig. 10.F.1 – Non-Darcy flow around a gas producer, successive buildups following constant, and increasing, rate production periods. The crosses and dots are simulated using the Forchheimer equation, whereas the plain curve is obtained using an equivalent pseudo-skin factor D .

However there are situations in which the pseudo-skin factor D leads to a somewhat incomplete modeling of the problem and it is better to replace this by the generalized Darcy equation.

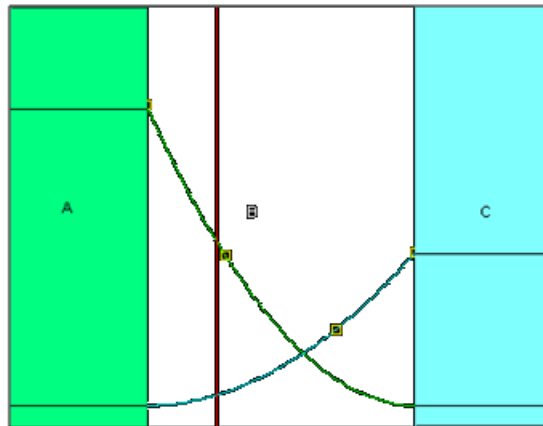
10.F.2 Flow with Water and Hydrocarbons (Oil OR Gas)

The numerical simulator is not limited to single phase flow. We will consider dead oil + water and dry gas + water, situations without phase exchange between the components, no dissolved gas in the oil phase, no vaporized oil in the gas phase. Capillary pressures are neglected.

In that case relative permeabilities must be introduced and total mobility becomes:

$$\left(\frac{k}{\mu}\right)_t = \left(\frac{k_p}{\mu_p}\right) + \left(\frac{k_w}{\mu_w}\right) = k \cdot \left(\frac{k_{rp}(S_w)}{\mu_p} + \frac{k_{rw}(S_w)}{\mu_w}\right)$$

Where p refers to oil or gas and S_w is the water saturation. Contrary to the assumptions that have to be made in analytical methods (Perrine), the water saturation is not held constant in time or in space. Relative permeability curves define regions of phase mobility, as shown in the figure below.



*Fig. 10.F.2 – oil (green) and water (blue) relative permeability curves. In the saturation region (A) water is not mobile and maximum oil relative permeability is reached.
In region (C) oil is not mobile.*

Hence, the stabilization of the derivative on the loglog plot depends not only on the bulk permeability, but also on the dynamic phase mobilities induced by the distribution of fluid saturations.

Let us consider the example of a water injector in an oil reservoir (following figure):

- During the injection phase the pressure match line is based on the total mobility with maximum water saturation since we inject only water.
- The fall-off however sees different effective permeabilities induced by varying water saturation. This is at a maximum close to the well and a minimum further away in the reservoir.
- The effective two-phase mobility can take values in the range of 'minimum water saturation (the green line)' and 'maximum water saturation (the blue line)'.

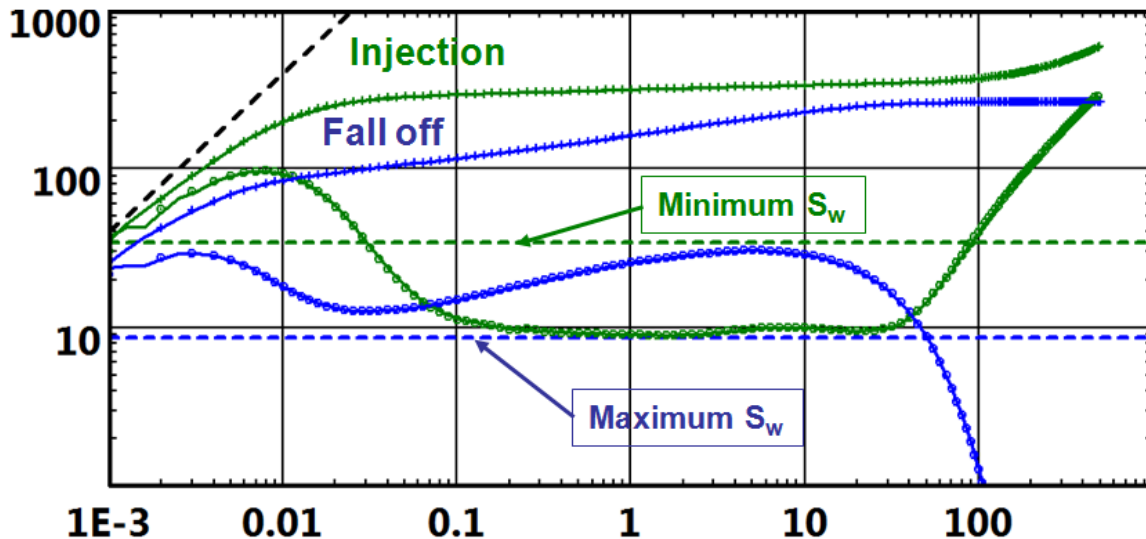


Fig. 10.F.3 - Fall-off following a water injection in an oil reservoir

10.F.3 Unconsolidated formations

In unconsolidated formations porosity and permeability depend on the internal stress of the formation. When there is no overburden isostatic pressure, this stress is directly related to the difference between external and internal fluid pressure, so we may model porosity and permeability as decreasing functions of the pressure drop ($P_i - P$) occurring in the reservoir. That is the porosity and permeability decrease as the reservoir deplete:

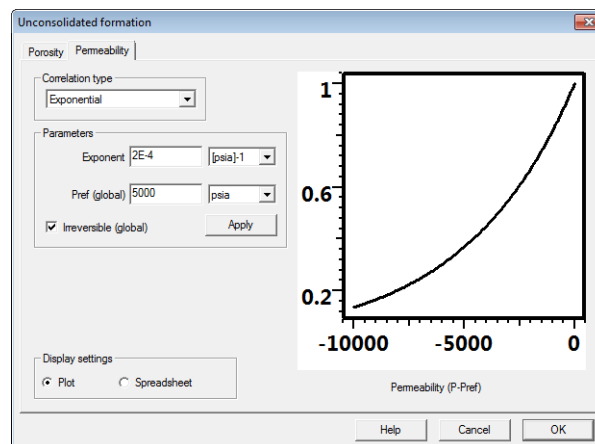


Fig. 10.F.4 – Defining the $k(P-P_i)$ function for an unconsolidated formation

In an isotropic, linear, elastic reservoir we model the rock deformation through a relationship between porosity, permeability and the average internal stress σ_m :

$$\phi = \phi_0 \cdot (1 - a \sigma_m)$$

$$k = \begin{cases} k_0 \cdot (1 - b \sigma_m) & (1) \\ k_0 \cdot \exp(-b \sigma_m) & (2) \\ k_0 \cdot \left(\frac{\phi}{\phi_0}\right)^n & (3) \end{cases}$$

Where k is defined by the equation (1), (2) or (3) depending on the rock type. In the absence of overburden isostatic pressure, we introduce the following relationship between σ_m and the pressure drop $P_i - P$:

$$\sigma_m \equiv \frac{1}{3}(\sigma_x + \sigma_y + \sigma_z) = (P_i - P)$$

Hence, k and ϕ are directly related to the pressure drop $P_i - P$.

Porosity and permeability reduction may or may not be irreversible, in the sense that the model can authorize (or not) the model parameter to recover its initial value when the pressure drop decreases (see figures below). The effective permeability is lower here during the two production phases (blue and red), and reverting to its initial value during the build-ups, as the model permeability is reversible.

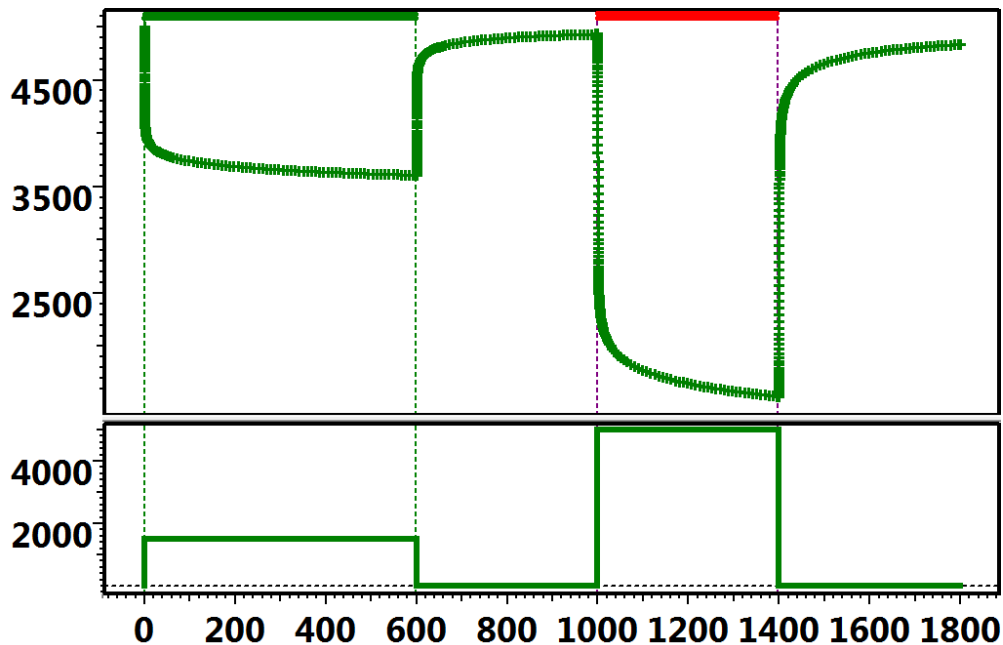


Fig. 10.F.5 – Simulation of two production and build-up sequences in an unconsolidated reservoir: History plot

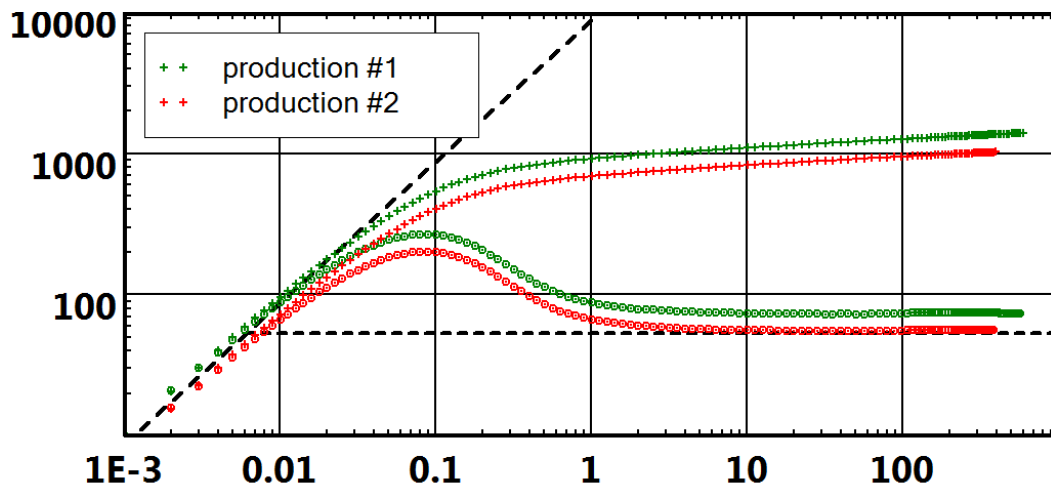


Fig. 10.F.6 – Simulation of two production and build-up sequences in an unconsolidated reservoir: Loglog plot

Introducing pressure dependency on porosity and permeability renders the problem highly nonlinear. This makes it awkward to use and to interpret considering the difficulty in gathering valid data to build the $\phi(\Delta P)$ and $k(\Delta P)$ curves, and the strong dependency of the simulated pressure to these curves. A 5% error on $k(\Delta P)$ can easily induce a 50% error on the simulated pressure.

10.F.4 How about three-phase flow?

Numerical simulation applied to well test analysis is almost identical to 'classical' reservoir simulators, except that the models have to be simulated on a much smaller time-scale that is minutes and seconds instead of days. They also have to be viewed on a loglog plot; to be examined through the Bourdet derivative 'magnifying glass'.

With the simulation of three-phase flow problems we reach the limits of our current capabilities in terms of numerical well test modeling. The ruling equations and the solution methodologies are well known and in essence three-phase flow is merely an extension of the dead oil and water or dry gas and water problems we have already described. Unfortunately one unexpected problem arises, as can be seen in the figure below.

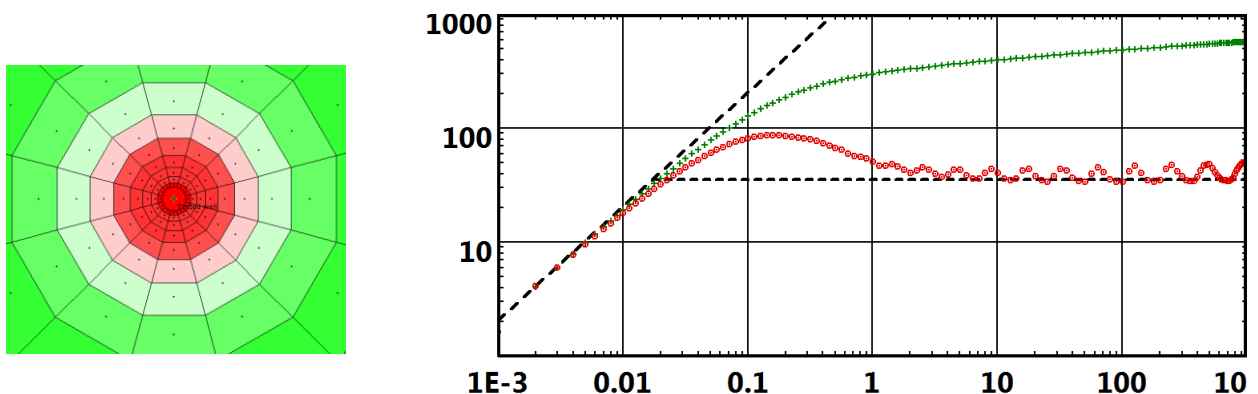


Fig. 10.F.7 – Simulation of a producer in a saturated oil reservoir: left: the gas saturation at the end of the production, right: the resulting simulation on a loglog plot.

In the illustrated example, the erratic behavior of the semilog derivative is due to the successive appearance of free gas, cell ring by cell ring, around the well as the depletion occurs and the cell pressure drops below the fluid bubble point.

This appearance is not controlled by the relative permeabilities (free gas can appear before it reaches a saturation high enough to be mobile) but by thermodynamic equilibrium. Successive cell rings can be flooded by free gas within a few time steps, hence changing considerably the effective permeability, and thence inducing the erratic behavior on the loglog plot.

Unfortunately, changing the grid cell size is not sufficient to get rid of the problems. This just changes the frequency of the humps and bumps on the loglog plot.

10.F.5 Changing well controls

With numerical modeling combining constant rate and constant pressure well controls becomes relatively straightforward. It is possible to impose a pressure constraint in addition to the rate target. This constraint takes the form of a pressure interval within which the simulated well sandface pressure must remain, as shown in the figure below. The pressure interval lower limit may be reached by producing wells, whereas the upper limit may be reached by injectors.

Parameter	Value	Unit
X	0	ft
Y	0	ft
rw	0.3	ft
Pwf min	14.7	psia
Pwf max	7900	psia

Fig. 10.F.8 – Throughout its production history the well pressure must remain above 14.7 psia ('pwf min') and below 7900 psia ('pwf max').

When the bounding pressure values are reached, the well is switched from rate-controlled to pressure-controlled production. It may switch back again to rate-controlled production when the simulated pressure re-enters the permitted limits. Such a case is shown in Fig. 10.F.9: during the first production phase the well pressure reaches a minimum and switches to constant pressure production. Later it reverts back to variable rate production.

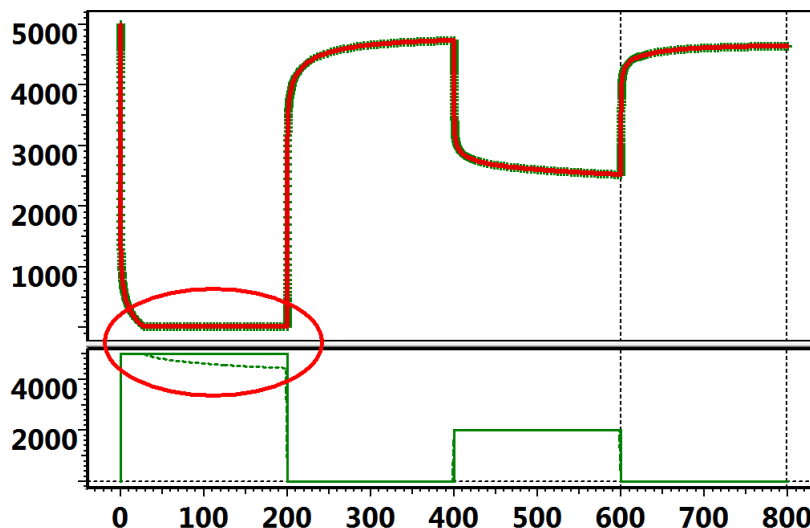


Fig. 10.F.9 – The minimum bounding pressure is reached during the first production

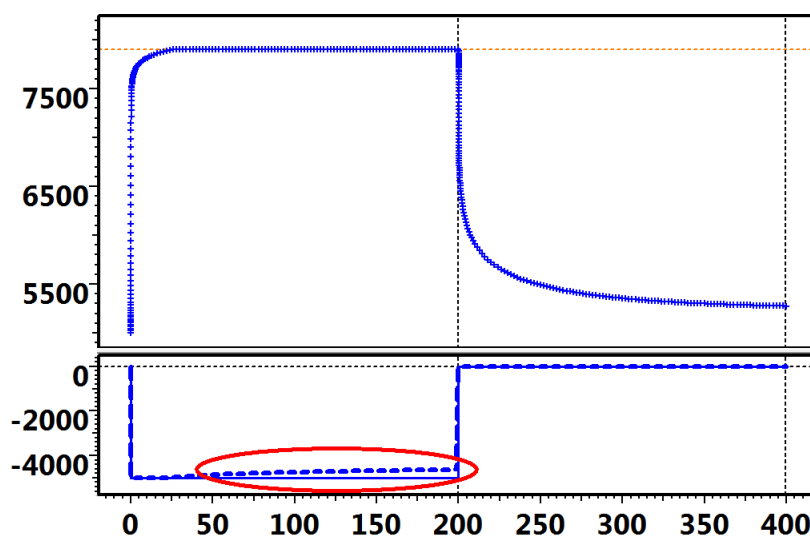


Fig. 10.F.10 – This water injector reaches its maximum pressure (orange dotted line) and is then switched to constant pressure injection. Later, the injection target rate is lowered and the well can switch back to constant rate injection.



11.A Introduction

In a *standard test* we put the well in production and we monitor the pressure build-up. We use the single total production rate in the same well to correct the pressure model by superposition. As long as we neglect the difference of fluids, injection / fall off tests can also be considered standard tests. *Special tests* are just whatever is not standard. In this version of the book we will detail four different types of special tests.

Formation tests

When looking at the pressure response at the producing probe or packer, a formation test can be considered to be a standard test using a very specific well geometry. The methodology will be strictly the same. The difference will be when using multi-probe tools, where one has to integrate the standard pressure response of the producing probe and the different vertical / lateral interferences observed at the other probes. This is where the methodology and the models will diverge. In fact we are today at the starting point of KAPPA's specific work on formation tests. Later developments (Generation 5) will include a specific software module, and probably a dedicated chapter in this DDA book.

Slug tests

In most DST's the early part of the well production will see no flow at surface and a rise of the liquid column. This will proceed until the liquid level eventually reaches the surface. 'Slug' pressures vs. time will be used to quantify the sandface production, which then can be used as the input rate history for the build-up analysis. However there are some techniques that allow the transient pressure response of the slug to be analysed independently. This specific processing will be demonstrated in this chapter.

Multilayer tests

One will perform a standard test in a multilayer formation if we produce the whole reservoir and just acquire the pressure and total producing rates. There are analytical models in Saphir / Topaze which will account for layering, such as the double-permeability model. We will call a multilayer test an operation where we will adjust the test sequence or add measurements to discriminate the different layer contributions. This can be done by producing the layers successively or in different combinations, or by adding production log measurements.

Interference tests

In any test we can add the interference of the other wells in the Saphir analytical and numerical models. Despite this model refinement we will still consider that we are in a standard test if the reference production history and the pressure are taken at the same well. In a proper interference test the pressure that we interpret was acquired in an observation well, i.e. not in the well from which the reference rates were recorded. This will generally imply that the observation well is not producing and that most of the amplitude of the observed pressure change is, precisely, this interference.

11.B Formation Tests

The initial formation tests were designed to find static pressures and multiple stations would provide an initial static pressure gradients and initial fluid contacts. The last generation of formation testers is much more sophisticated. It allows to take multiple PVT samples in a flow sequence that is a good candidate for Pressure Transient Analysis. Multiple observation probes allow a vertical understanding of the system but require specific processing and modeling.

11.B.1 Tool description

There are two main tools for the production/buildup mode that is analyzed by conventional or specific PTA methods:

- Single active probe tool with pressure measurements at the probe
- Multiple packer tool with pressure measurements between packers

Both tools are illustrated in the schematic below with the leading parameters of a conventional or formation tester specific PTA model indicated.

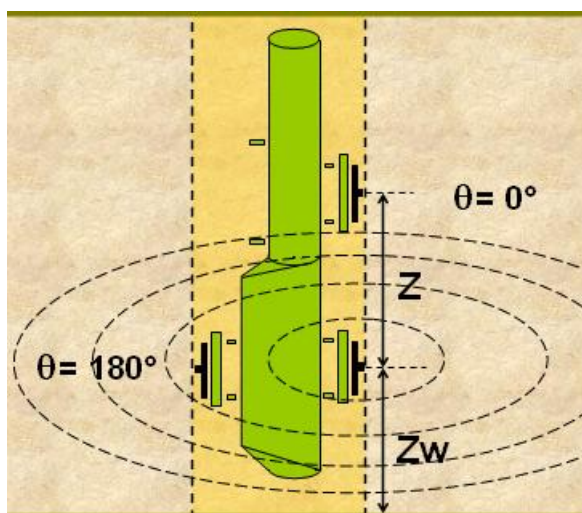


Fig. 11.B.1 – Multi probe WFT tool

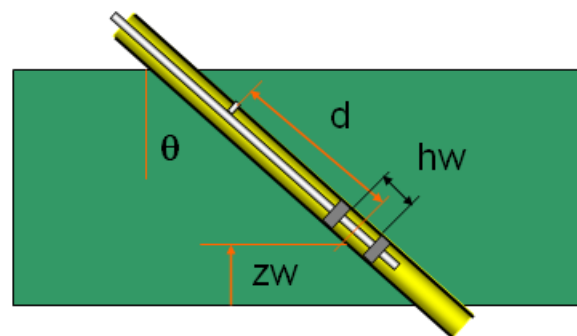


Fig. 11.B.2 – Multi packer WFT tool

The probes of the probe tool will actually penetrate into the formation and is usually sealed off with a pad/packer.

Both tools can have multiple pressure and temperature 'observer' probes spaced in the tool string vertically. The probe tool can also have an observer probe at any angle with respect to the active probe and at the same level as the active probe; this is illustrated in the above left figure where an extra observer probe has been placed in the tool string at the opposite side of the active probe (180°). The advantage of the multiple probe tools is that it allows the detection of vertical communication between the active probe and the observing probes. Multiple probes can also sometime allow the differentiation of changing anisotropy.

The tool is designed to control the withdrawal of fluid from a probe or between packers. The measurement of pressure and the sampling of formation fluids involves the withdrawal of fluid through a probe penetrating through to the formation, or a pad set on the formation wall and

thus induce a 'drawdown' in the vicinity of the probe (pad) as fluid is being withdrawn into a sample chamber or is pumped through by the tool. This period is followed by a 'shut-in' period to let the pressure build up to static conditions for the measurement of the 'virgin' pressure of the formation at this fixed depth. The transient pressures are increasingly used for interpretation of reservoir parameters, mainly permeability. Early permeability estimates promote greater confidence in test design or in the decision process of whether further well testing can be skipped or not. The use of formation test straddle packers for DST-type tests is also increasingly being used.

Besides yielding a value for permeability, single probe data can identify or confirm thin flow units within reservoir sections, where it may not otherwise be clear that vertical barriers are present. The ultimate goal of such formation tests is to reduce the use of conventional well testing with all the downhole and surface hardware this require and thus increase safety by avoiding any flow of live reservoir fluids at surface. Such tests will also complement conventional well testing when testing every zone or layer is not possible, and thus enable more detail in the vertical reservoir characterization.

11.B.2 Test sequence

A formation tester typical test sequence is described below and illustrated in the following figure.

Mud pressure, the hydrostatic pressure of the fluid in the well before the probe/pad or the packers is set.

Pretest, the pressure recorded after setting the tool.

Sampling, the pressure recorded as the fluid of the formation is allowed to flow or being pumped to or through the tool.

Buildup, the shutin pressure.

Mud pressure, the pressure returns to the hydrostatic pressure of the fluid in the well after the tool has been unset.

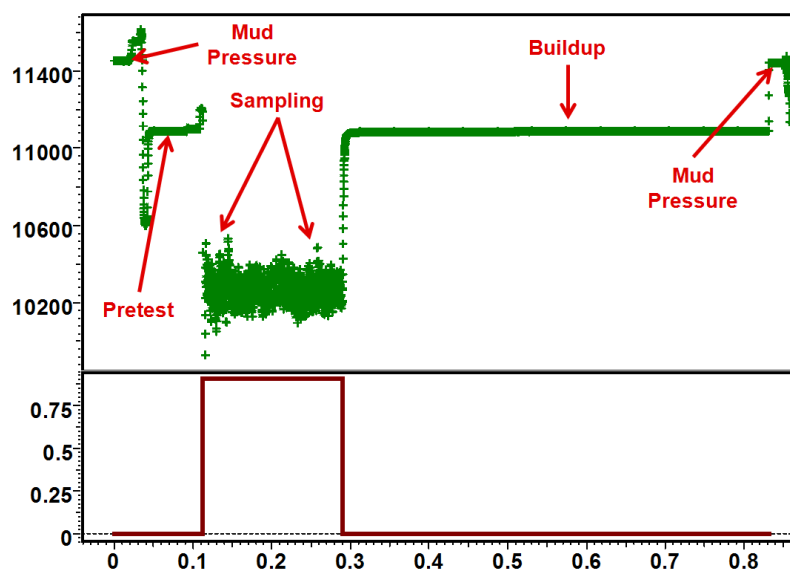


Fig. 11.B.3 – WFT typical test sequence

11.B.3 Standard Pressure Transient Analysis

In view of the probe configuration which is relatively small and in the majority of cases also very small compared to the effective bedding thickness that can be up to several meters thick, depending of course of the distribution of vertical no permeability seals, the pressure behavior will invariably show spherical flow before the possible onset of classical infinite acting radial flow. Thus the pressure behavior can easily be modeled with the limited entry well model of classical well testing (PTA). There are several studies in the well test literature that has clearly showed that in most practical cases the use of this model gives satisfactory results and by that eliminating the old straight-line analysis developed before such analytical models became available.

A schematic of the theoretical flow regimes is illustrated in the below figure:

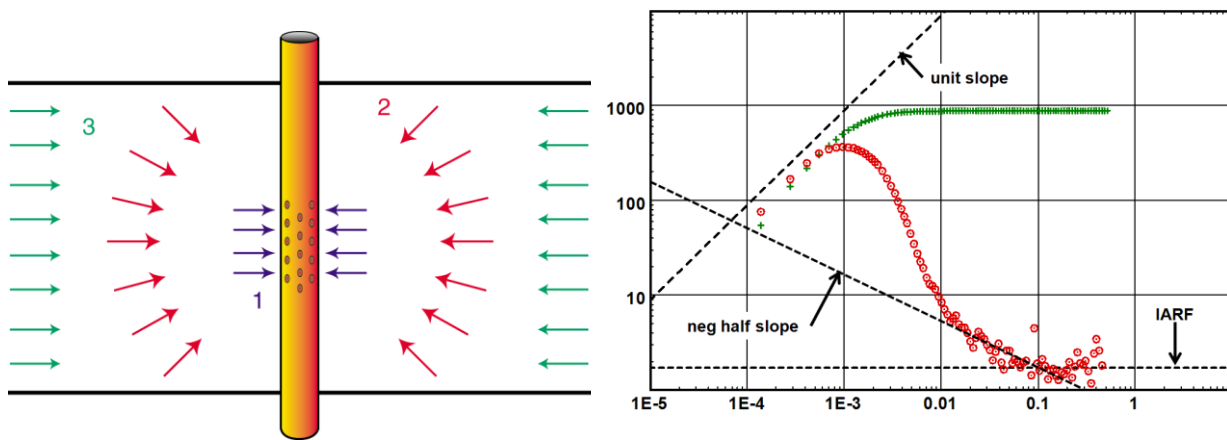


Fig. 11.B.4 – Limited entry flow regimes

In flow regime '2' there is a vertical contribution to flow, and if the perforated interval is small enough, which it invariably will be using a small probe of limited dimension, a straight line of slope $-1/2$ (negative half slope) will develop in the Bourdet derivative, corresponding to spherical or hemi-spherical flow. The pressure is then proportional to $\frac{1}{\sqrt{\Delta t}}$.

The relation of the pressure change and the 'one over the square root' of the elapsed time is:

$$\Delta p = \frac{70.6qB\mu}{k_s r_s} - \frac{2453qB\mu\sqrt{\phi\mu c_i}}{k_s^{3/2}} \frac{1}{\sqrt{\Delta t}}$$

$$\text{With: } k_s = (k_r^2 k_v)^{1/3}$$

The pressure change during spherical flow is:

$$\Delta p = m \frac{1}{\sqrt{\Delta t}} \quad \text{where} \quad m = \frac{2453qB\mu\sqrt{\phi\mu c_i}}{k_s^{3/2}}$$

$$\Delta p' \approx \frac{d\Delta p}{d \ln(\Delta t)} = \Delta t \frac{d\Delta p}{d\Delta t} = \Delta t \frac{m}{-2\sqrt{\Delta t}} = -\frac{1}{2} m \sqrt{\Delta t} = -\frac{1}{2} \Delta p$$

The characteristic flow regime is spherical flow until upper and lower vertical flow boundaries have been reached and then followed by classical radial flow, IARF in the reservoir.

The interesting flow regime here is spherical flow during which the pressure change is proportional to $\frac{1}{\sqrt{\Delta t}}$, the Bourdet derivative will follow a negative half unit slope straight line.

From this flow regime it is possible to determine the anisotropy $\frac{k_v}{k_r}$.

11.B.4 Specific Formation Test Analysis

The formation test option in Saphir is a standalone analysis option that the interpreter chooses at startup of a new project. This option is currently available in the latest version of Ecrin but KAPPA is developing, and will soon release, a formation tester module that will integrate this feature with specific analysis options and the study and interpretation of the reservoir pressure versus depth for gradient determination, fluid contacts, compartmentalization and correlation both vertically and laterally.

The formation test option allows the inclusion of any number of observation probes in the test setup and the study of the vertical response to the disturbance caused by the active probe.

It is possible to load in one session one active probe pressure measurement and as many observation probes pressure channels as necessary.

The rate history can be loaded as classic flowrate versus time (downhole or surface rates) but it is also possible to load downhole pump or chamber volumes and convert this to the appropriate rate history within the module.

Once the data is loaded the classic workflow of conventional pressure transient analysis is followed. The extract option can extract all gauges, active and observers, simultaneously.

Prior to the extraction the interpreter will define the tool configuration and assign each pressure channel to its appropriate probe.

The next figure illustrates the loglog plot of the buildups recorded, after tool pump through, of the pressure response of each probe.

We can see that the active probe and all the observers appear to have a common stabilization at later time thus indicating common kh. The active and the nearest observer probes have largely a common derivative behavior indicating no vertical changes of the reservoir characteristics. The observer probe furthest away from the active probe is recording close to its gauge resolution.

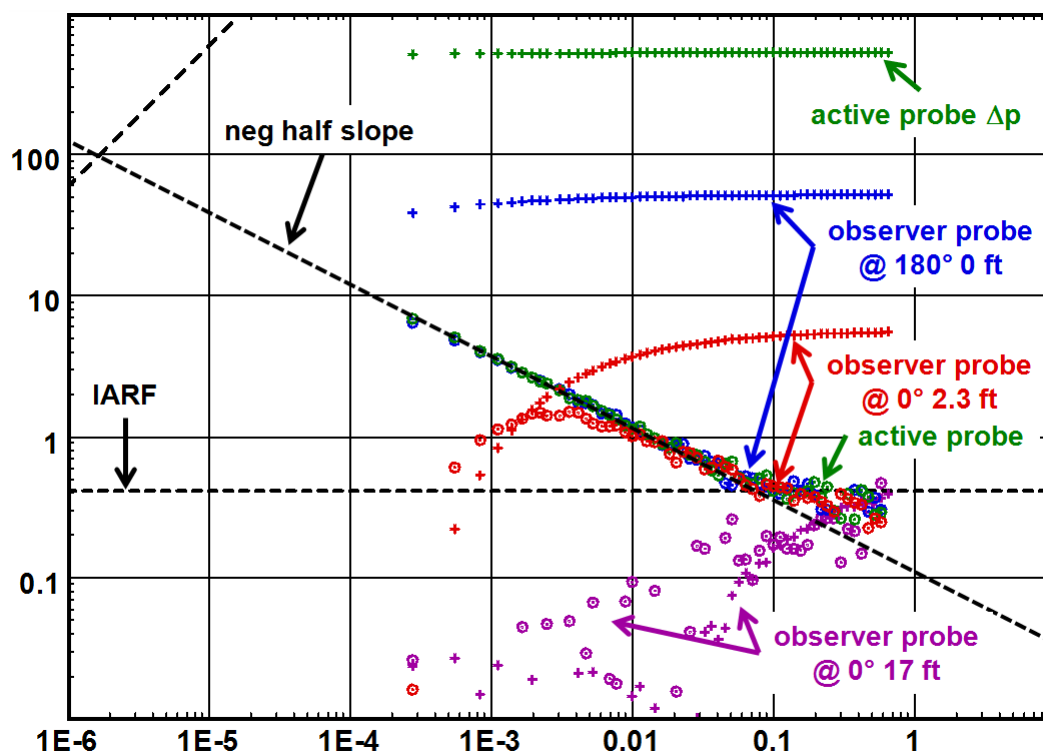


Fig. 11.B.5 – Loglog plot of 4 WFT probes

There is no model catalogue as such in the WFT module. The model is either for the probe or packer configuration of the tool. We illustrate the two model dialogs below.

Model

Analytical

Wellbore model: No wellbore storage

Well model: Vertical

Reservoir model: Homogeneous

Boundary model: Infinite

Parameter	Value	Unit	Pick
Probe 1 - Active (single probe)			
Skin	0		
Zw	15	ft	
Pi	4900.01	psia	
kz/kr	1		
Probe 2			
Delta-Pi	0	psia	
kz/kr	1		
Probe 3			
Delta-Pi	0	psia	
kz/kr	1		
Probe 4			
Delta-Pi	0	psia	
kz/kr	1		
Reservoir & Boundary parameters			
h	30	ft	
k	27.6546	md	
Top	No flow		

Schematic

keep opened Time Help Cancel Generate

Fig. 11.B.6 – Model dialog probes

Model

Analytical

Wellbore model: No wellbore storage

Well model: Vertical

Reservoir model: Homogeneous

Boundary model: Infinite

Parameter	Value	Unit	Pick
Probe 1 - Active (packer)			
Skin	0		
hw	3	ft	
Zw	15	ft	
Delta-Pi	0	psia	
Probe 2			
Delta-Pi	0	psia	
Probe 3			
Delta-Pi	0	psia	
Probe 4			
Pi	4900.01	psia	
Reservoir & Boundary parameters			
h	30	ft	
k	27.6546	md	
kz/kr	1		
Top	No flow		
Bottom	No flow		

Schematic

keep opened Time Help Cancel Generate

Fig. 11.B.7 – Model dialog packer

The well can be vertical, slanted or horizontal and the reservoir homogeneous, double porosity or composite. It is also possible to combine the models with outer boundaries.

Below we illustrate the final model match with the WFT probe model with no anisotropy.

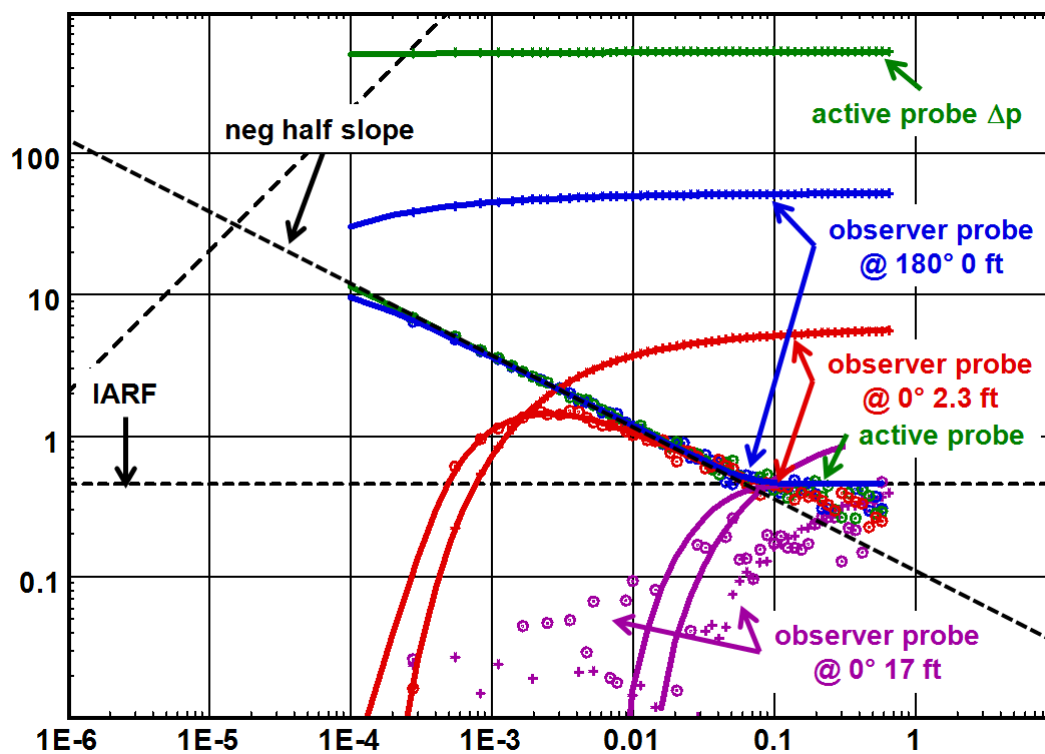


Fig. 11.B.8 – WFT model match

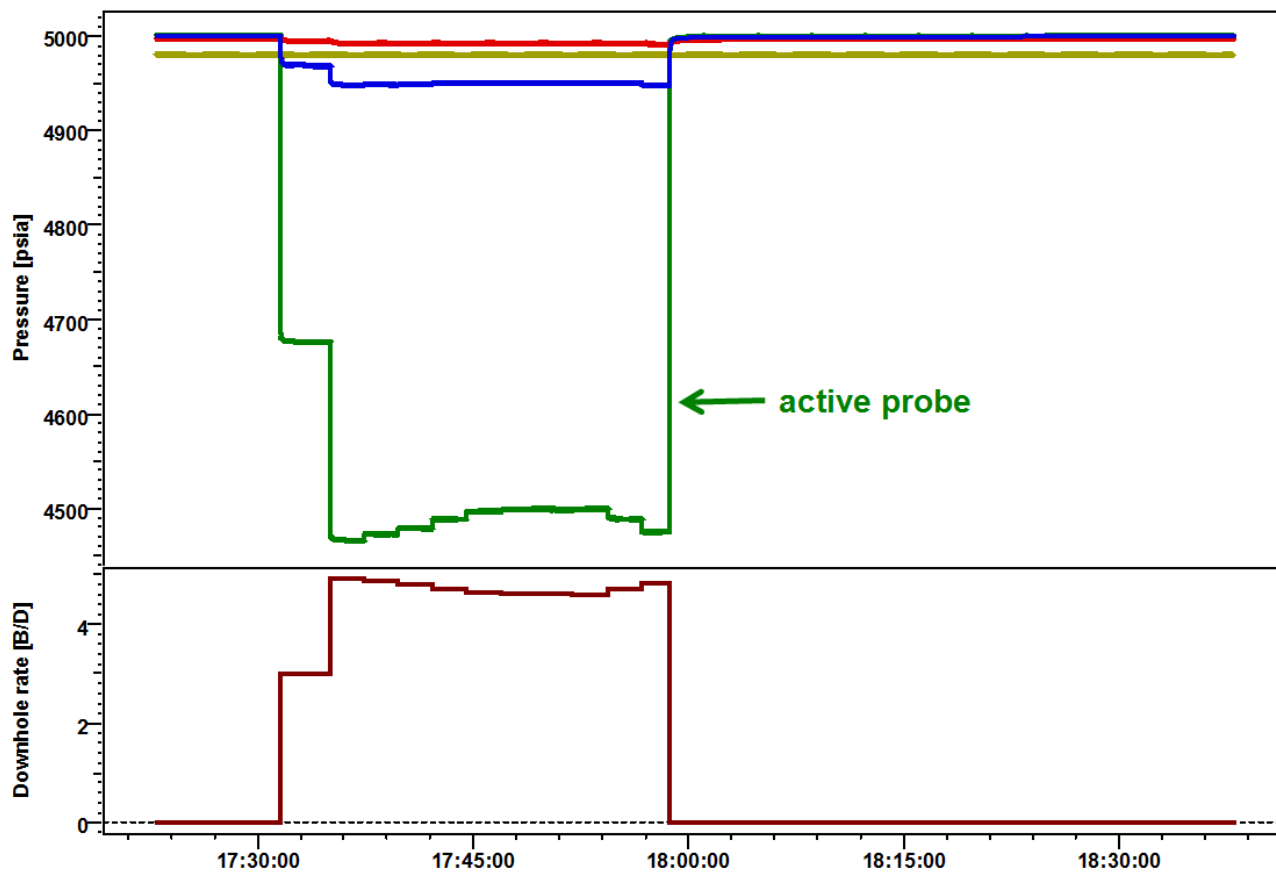


Fig. 11.B.9 – WFT History match

11.C Slug Tests

Slug tests correspond to the initial flow of a Drill Stem Test (DST). This period can be used to define the flow rates in order to analyse the following buildup, or it can be analysed by itself using the method presented in this section.

11.C.1 Test sequence

We will not explain what a DST is, the types of tools that are run downhole, etc. There are plenty of other places to learn this. We describe the DST from the point of view of the analyst.

The downhole pressure recording of a typical DST is shown in the figure below. During this operation the well is open and closed with a downhole valve. The pressure sensor is positioned below the downhole valve to follow the reservoir pressure when the well is shut in.

We start at initial pressure p_i . Before the well is open downhole an initial static column of fluid, typically a cushion of diesel or water, may or may not be placed above the downhole valve.

During this operation the surface valves remain open to flow to bleed the air.

The test starts by opening the downhole valve. The pressure instantaneously switches from p_i to the initial static pressure p_0 . If the well is not flowing the pressure will remain stable or will change very little, and the test will be over.

If we have a producer and if p_0 is less than p_i the fluid starts to flow from the reservoir to the well, the static column rises and so does the pressure. This is the beginning of the slug test. It will last until the fluid eventually reaches surface. The well is shut in and we have our first buildup. While the well is shut in the static column will remain stable, but it will not be recorded by the pressure gauge which is on the other side of the valve.

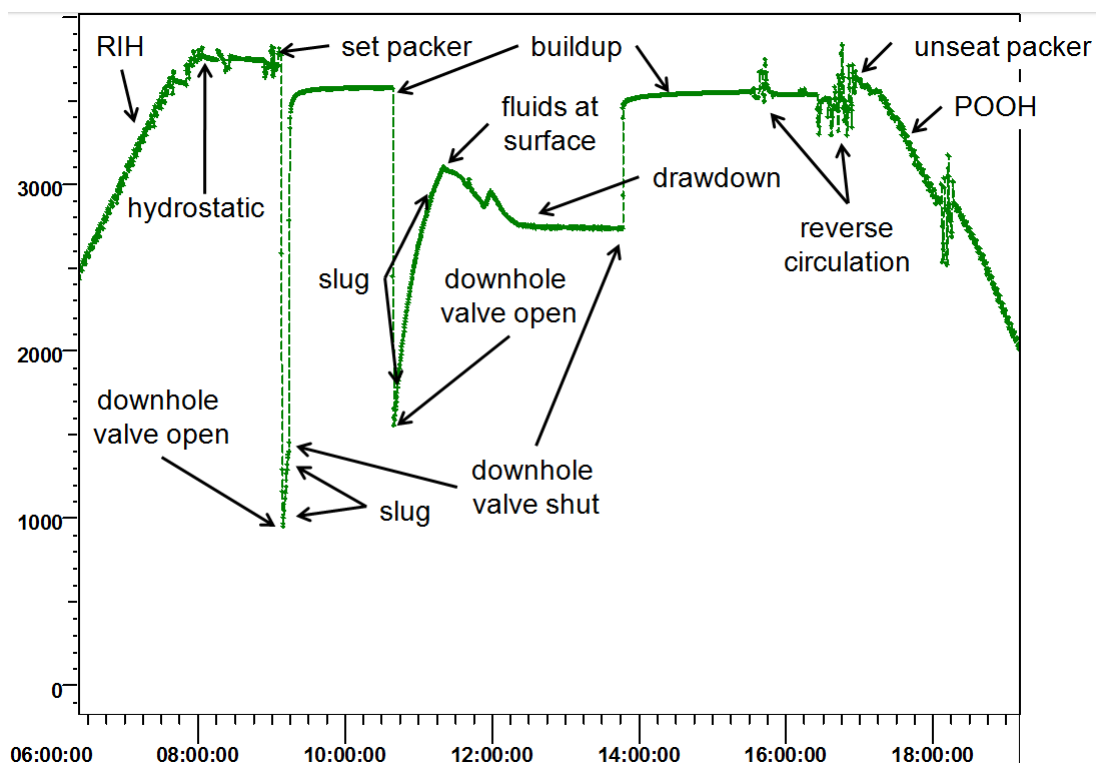


Fig. 11.C.1 – Conventional DST

When we open the well again we restart at the previous level of the static column and the slug resumes. At this stage several scenarios can happen:

- The system does not have enough energy and the slug dies. Throughout the test there is no flow to surface.
- The system has enough energy and the fluid breaks at surface. At this stage the pressure starts to decrease again and we are back to the conditions of a standard test. After stabilization the fluid is flowed through the separator, surface rates and samples are taken until a final buildup is run. This standard scenario is the one shown in the figure above.

11.C.2 Buildup analysis using slug rates

Before we go into the specifics of the slug analysis we will look at the 'standard' analysis of the buildup data following the slug. To analyse this buildup we need to know the flow rates before shutin. As no separator measurements were possible at this stage we use the fact that the recorded downhole pressure reflects the rise of the static column. From this rise we can assess the volume of fluid produced at sandface, hence the rate.

If we cut the slug sequence into a discrete series of intervals we get the following equations:

Slug rates from slug pressures:

$$q(t_i) = C \times \frac{p(t_i) - p(t_{i-1})}{t_i - t_{i-1}} = 80.5 \frac{r_w^2}{\rho} \times \frac{p(t_i) - p(t_{i-1})}{t_i - t_{i-1}}$$

The rates are calculated using the internal diameter of the effective well and the fluid density to obtain a wellbore storage coefficient that is then used to calculate the rates.

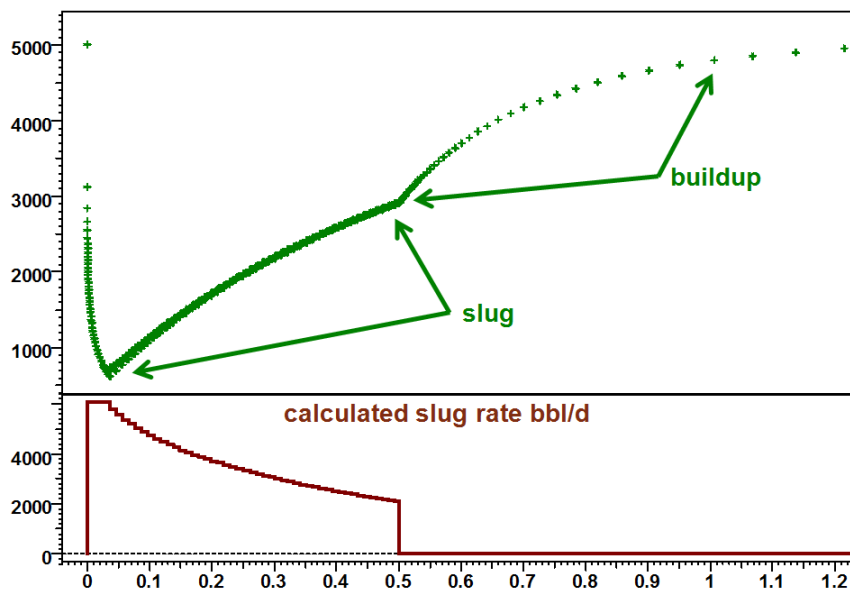


Fig. 11.C.2 – History plot

The figures below show the buildup loglog and history match. The trick here is to use a changing well model and the changing wellbore storage option. There are two statuses; the first during the slug will have a wellbore storage of 0 and the buildup whatever is appropriate.

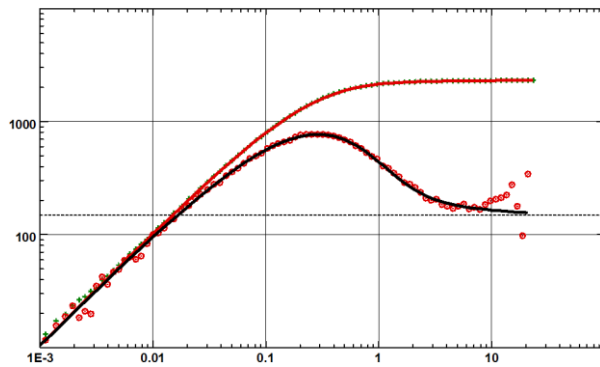


Fig. 11.C.3 – Buildup loglog match

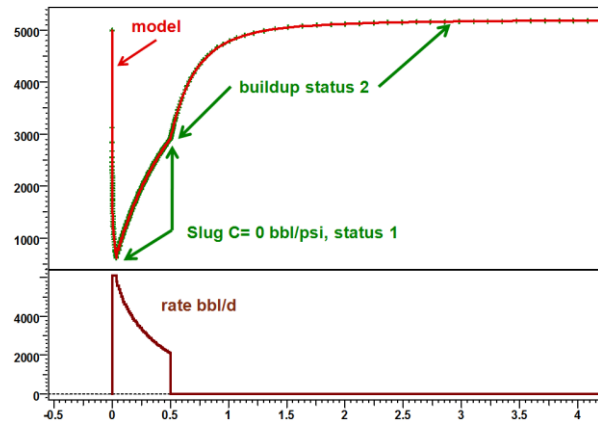


Fig. 11.C.4 – History match

11.C.3 Slug test analysis

In the previous section we have used the pressures recorded during the rise of the static column to build a rate history and analyse the following buildup in a standard way. The Slug test analysis is about considering the rise of the column itself, independently of the buildup.

In a standard test we have two separate sets of data: the rates and the pressures. In PTA one will try to interpret the pressure response using the rate history to correct for the superposition effects. In Production Analysis it will do more or less the opposite. What is puzzling at first glance in slug test analysis is that the pressure, by differentiation, also gives the rate. So here we have a single transient signal that is supposed to give all information at the same time, and from which we are expected to make an analysis. How come?

Mathematically, a slug is the answer to an instantaneous production with wellbore storage. The volume of the instantaneous production corresponds to the initial static column, i.e. the internal cross-section of the tubing at the liquid interface multiplied by the height of the difference between the initial static column ($p_{sf}=p_0$) and a virtual stabilized static column ($p_{sf}=p_i$). This is virtual as the height of the stabilized column could exceed the internal volume of the completion if the well / reservoir system has enough energy to flow to surface.

So to make a parallel with a standard test the pressure remains the pressure but the rate is replaced by the value of this virtual volume.

The slug test is mathematically equivalent to a close chamber test, even if the volumes are calculated differently. The hydro-geologists have been doing this sort of test for a long time. In the very low permeability formations for nuclear waste disposals, they pressure up a fixed volume of water and watch the relaxation. They call these tests impulse tests, which should not be confused with the trademarked impulse test by Schlumberger.

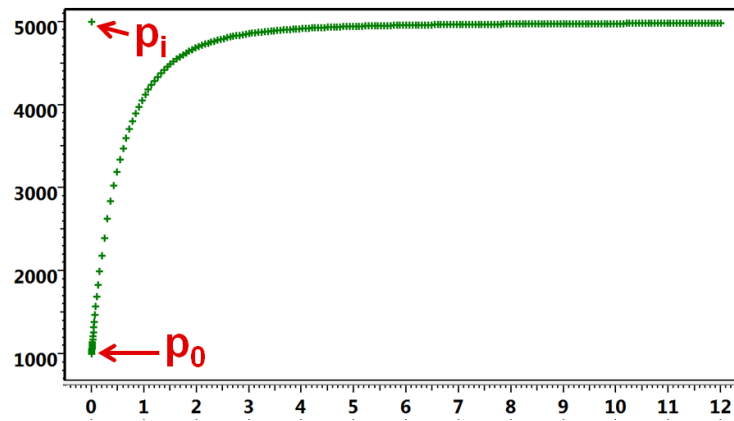


Fig. 11.C.5 – Slug schematic

In 1975 Ramey et al published a set of loglog type-curves showing the slug test responses, in dimensionless terms, for various values of the usual dimensionless parameter $CDe2S$. These type-curves were starting with a horizontal behavior and finish with a negative unit slope. The pressure data would be matched on the type-curve after the following transformation

Ramey's slug transform:
$$p_D(t) = \frac{(p_i - p(t))}{(p_i - p_0)}$$

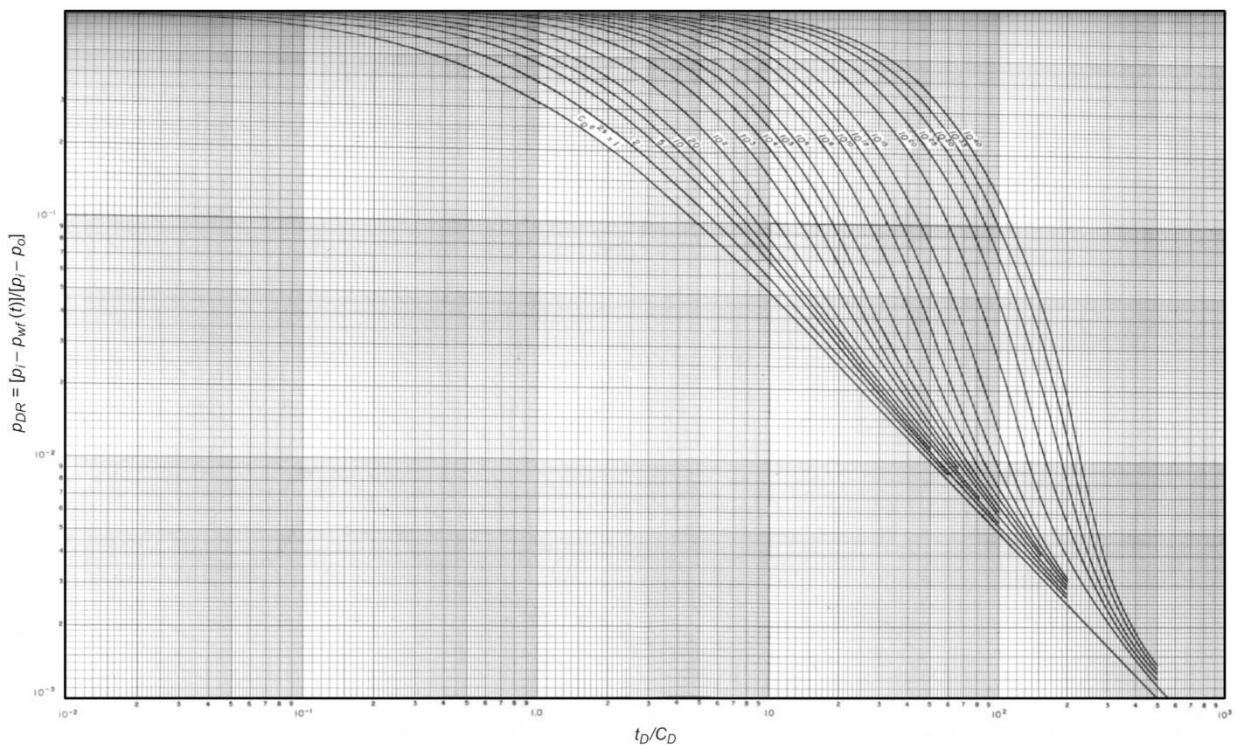


Fig. 11.C.6 – Ramey's type-curves

In 1995 Houzé and Allain had to adapt Saphir for ANDRA (French nuclear wastes agency) in order to implement hydro-geologist's impulse tests for very low permeability formations. This is when they realized that multiplying the 1975 Ramey's type-curves by Δt we would get... the dimensionless derivatives (in red below) in the 1983 Bourdet derivative type-curves.

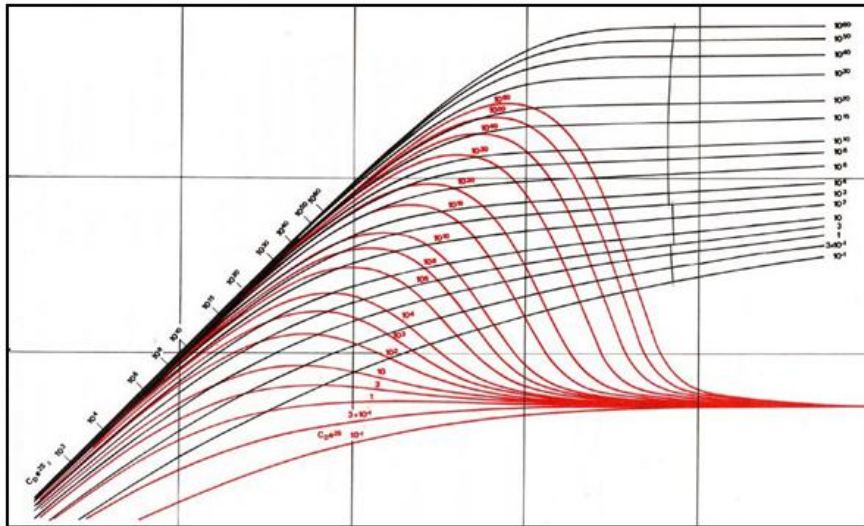


Fig. 11.C.7 – Bourdet derivative type-curve

So, in order to match the analytical models the modified Ramey transform will be:

$$\text{Modified Ramey transform} \quad \frac{(p_i - p)}{(p_i - p_0)} \Delta t = \frac{3389 C \mu}{k h} p'_D (T_{match} \times \Delta t)$$

Where p'_D is the Bourdet derivative of the corresponding dimensionless model. Another way to present this (initially surprising) observation is that:

After the modified Ramey transform, the pressure response to an instantaneous (Dirac) production matches the derivative of the constant rate response for the same system.

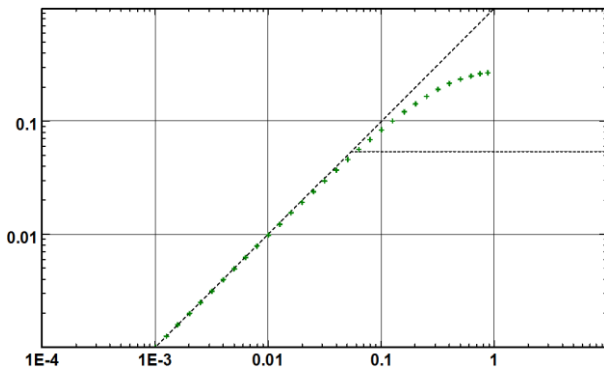


Fig. 11.C.8 – Typical duration Slug: Loglog plot

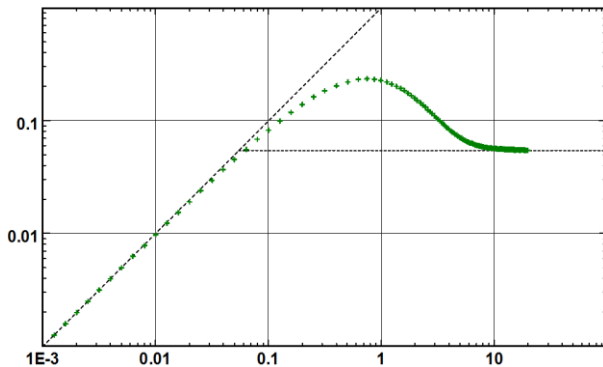


Fig. 11.C.9 – Extended duration Slug: Loglog plot

To perform the analysis the values of p_i and p_0 must be input. The wellbore storage coefficient can be calculated from the tubing diameter and the wellbore fluid density. It is assumed that the inner diameter is constant. If changes occur there will be a corresponding change in the wellbore storage coefficient.

With a fixed storage and a loglog response like the one displayed above on the left one can see immediately that it is not possible to get both skin and kh with any confidence from the analysis. This is illustrated in the figures below with two different diagnostics. In the first we have the skin set to 0, in the second the skin is set to 10. A regression was run on kh for each case and the values are respectively 1740 and 4610 mDft.

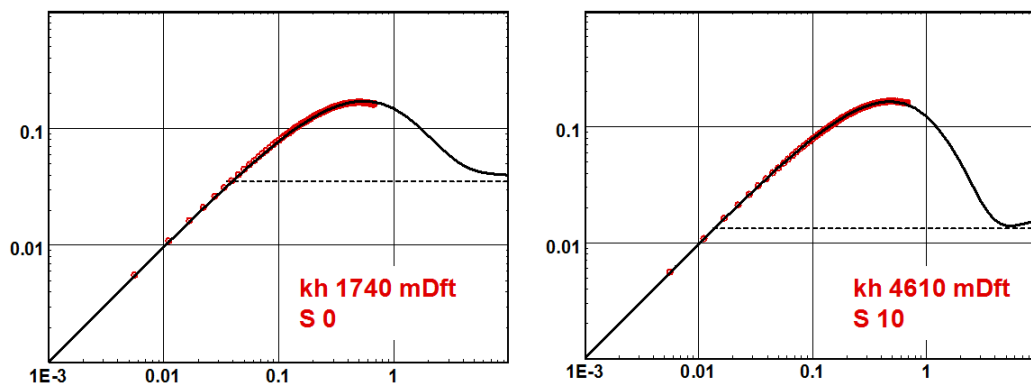


Fig. 11.C.10 – Slug Loglog matches

In the worst case we can only establish a relationship between the permeability and skin.

However, in the oil industry most slug tests are followed by a downhole shutin. The pressure slug can also be used to calculate the downhole flowrate as we have illustrated in a previous section, as long as we have a reasonable idea of the fluid density. It goes without saying that we know the hardware we have put in the well, so we know dimensions such as internal diameter and if there are any diameter changes in the well. We also know what fluid has been put in the pipe above the tester valve, so P_0 is known and acts as a check.

The figures below show the slug match versus the buildup match. Due to the length of the buildup, the pressure and time match becomes 'unique' with high confidence in analysis results.

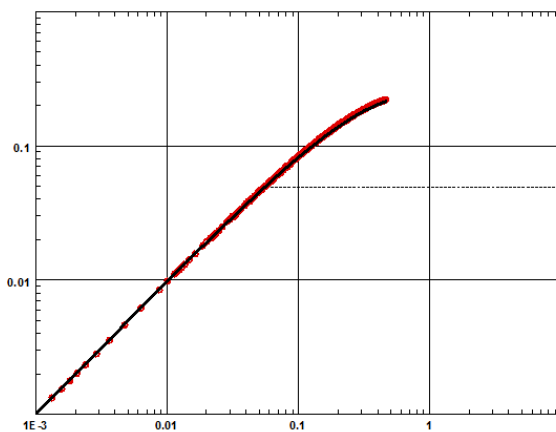


Fig. 11.C.11 – Slug match

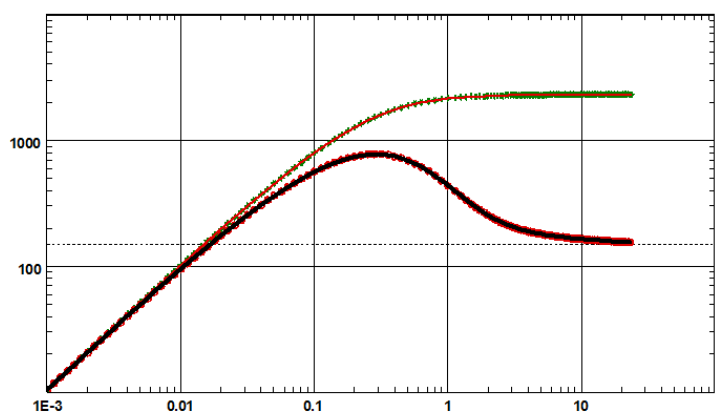


Fig. 11.C.12 – Buildup match

11.D Multilayer tests

11.D.1 Introduction

Most reservoirs have a commingled production from multiple zones. These zones may or may not be from the same geological formations, and they may or may not be communicating at the level of the formation. In most cases we perform a Pressure Transient Analysis considering the reservoir as a single global contributor.

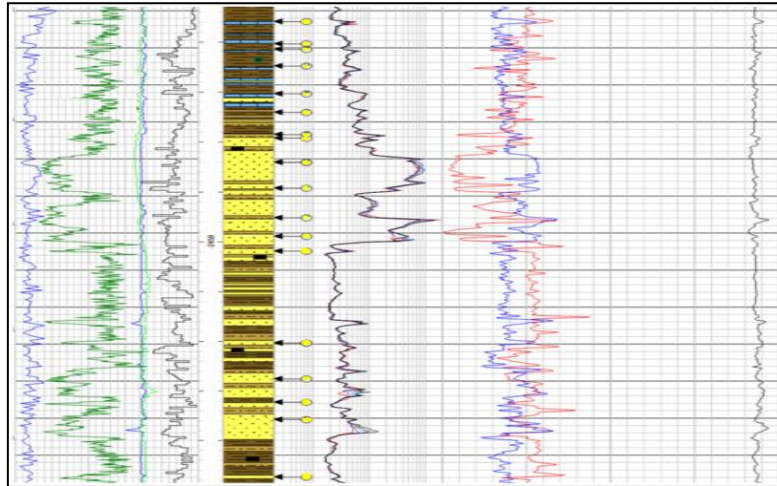


Fig. 11.D.1 – Log of a multi-layer formation

However we want to get a better understanding of the vertical distribution of the production, hence the contribution and characteristics of individual layers, or selected groups of layers. We will execute a multilayer test and perform a multilayer analysis. The challenge is to see if we can discriminate the layers with the standard information we have, or to add measurements and/or specific test sequences to allow this discrimination.

Analyzing a multilayer reservoir may be eased if there is a 'multilayer behavior' and the pressure response that cannot be matched with a homogeneous model. However this is not required. Even multilayer formations showing a global homogeneous behavior in terms of pressure-rate response can be subject to multilayer tests and analyses if we decide to add measurements or adjust the test sequences in order to isolate individual contributions.

11.D.2 Available models

In order to simulate multilayer responses modern software offer 3 types of models. All these models are able to provide the global pressure response and individual layer rates:

- **Analytical models:** The first and most common model is the double-permeability reservoir, which has now been around for thirty years. It has been extended to three, four and more layers, and recent developments can model the response of complex slanted and multilateral wells, all allowing crossflow between the layers.

- **Analytical commingled multilayer models:** A mathematical trick allows the simulation of the pressure and rate response for any number of layers, provided that there is no reservoir crossflow between these layers. Each such layer may correspond to any analytical model, including the multilayer analytical models presented before.

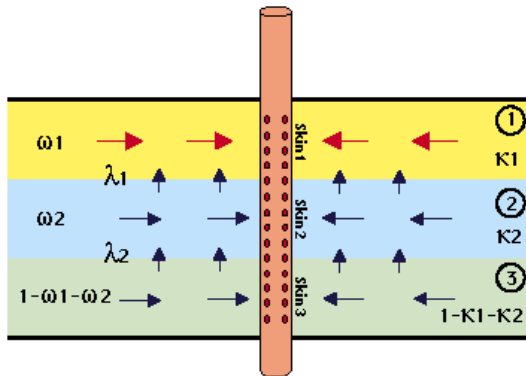


Fig. 11.D.2 – Schematics of a 3-permeability model

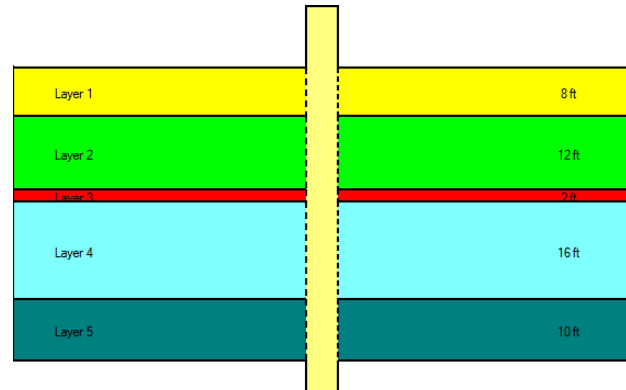


Fig. 11.D.3 – Schematic of a generic multilayer analytical model

- **Numerical models:** A multilayer numerical model with cross flow in the reservoir can be easily built by defining vertical leakage governing the flow at the interface between each layer. The anisotropy defined here is not the anisotropy of the layers but of the semi-permeable wall between the layers.

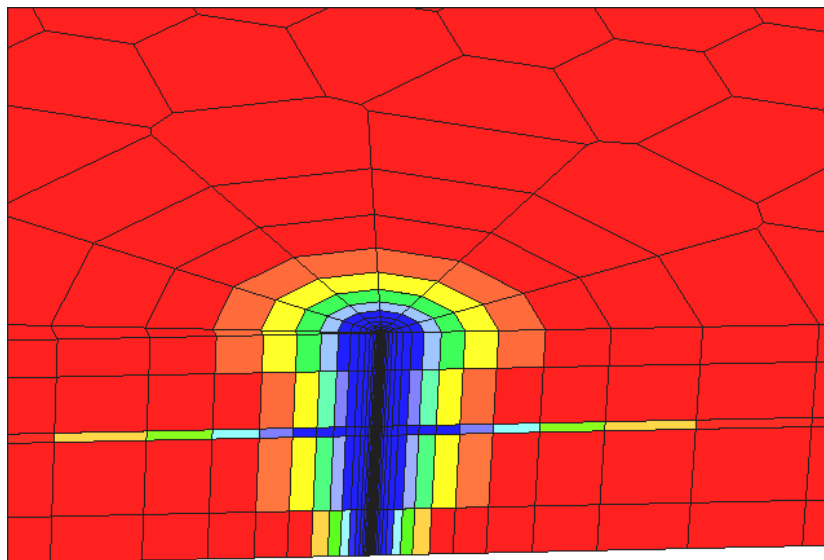


Fig. 11.D.4 – Multilayer numerical model

11.D.3 Standard tests

A standard well testing acquisition provides only the total production rates and bottom hole pressure channel; they represent the global behavior and cannot give direct access to individual layer properties. So the layered nature of the formation will be characterized only if the Bourdet derivative exhibits a heterogeneous behavior.

The typical analytical model used to perform such standard analysis is the double-permeability model, which assumes that the reservoir is constituted by two layers that may or may not be producing to the well, and that may or may not be communicating at the level of the reservoir.

The simplest homogeneous reservoir model will have 3 parameters: C , kh and $skin$. The double-permeability model will have 7: C , total kh , skin to layer 1, skin to layer 2, ω (porosity ratio), λ (cross-flow connectivity) and κ (permeability ratio). This is described in details in the Reservoir Models chapter.

Incidentally the name of KAPPA Engineering comes from the parameter κ .

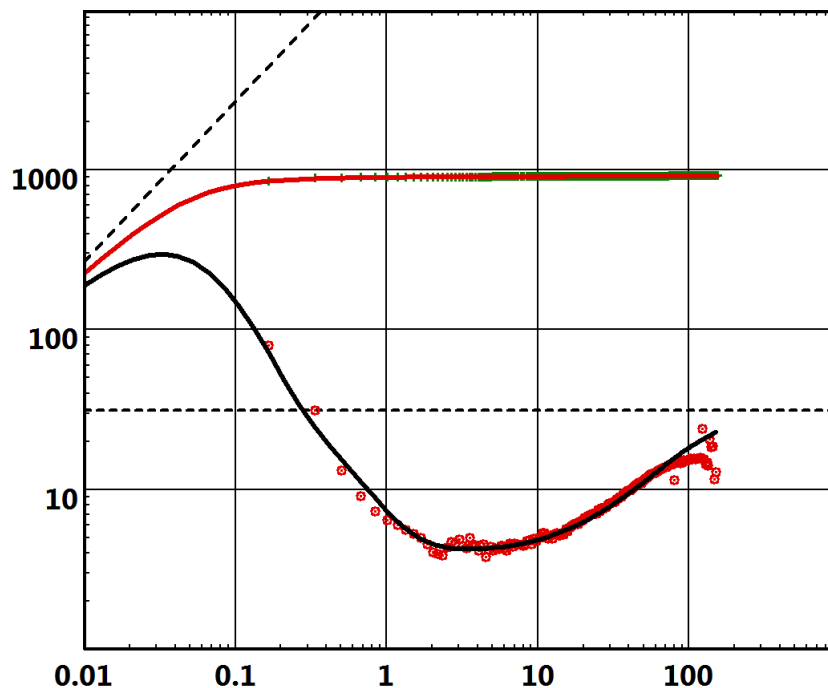


Fig. 11.D.5 – Loglog match with a double-permeability model

There are more complex analytical models available that model layered formations: three layers, four layers, and generic models allowing the combination of as many comingled layers as we want with separate well, reservoir and boundary models. However in a standard test we match models on a single, global Bourdet derivative response. Matching and identifying the seven parameters of the double-permeability model is already an act of faith, and will already require strong contrast between layer properties to show any specific behavior. Matching even more complex models without any strong information to constrain them is simply ridiculous.

So if we want to go further we need to change the test sequence or acquire additional information.

11.D.4 Using Production Logs

11.D.4.a Stabilized rate acquisition

The pressure and fluid velocity and density measurements are performed under stabilized rate conditions during runs up and down at several constant cable speeds.

The production logging data analysis can give access to rate versus depth logs, therefore to the individual layer rate and contribution.

It is necessary information for the determination of certain layer properties.

- The layer static pressure: using selective inflow performance analysis.
- The respective layer permeability by using the adequate multilayer model which calculates the individual layer contribution.

Note: We shall call in the following pages:

- Layer rate: the production rate measured above a layer, it is the sum of the production of all the layers below.
- Layer contribution: the individual production of a single layer.

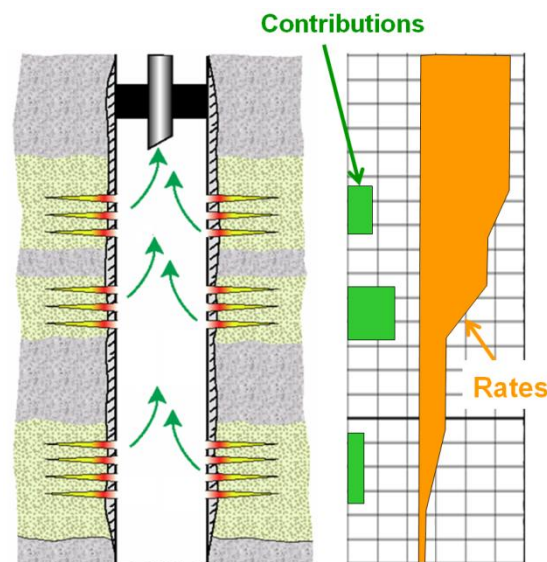


Fig. 11.D.6 – Layer rates and contributions

11.D.4.b Transient rate acquisition

The pressure and fluid velocity and density measurements can also be made versus time at constant depth and during the transient behavior due to a production rate change.

The objective is to acquire and observe the transient behavior of the layer rate, and then to intent to analyze it to get the individual properties by:

Either, analyzing globally the layer system and describing it in detail with a multilayer model matching

Or processing the data in order to extract the individual behavior and then to analyze separately the various layers using a classical single layer model.

11.D.5 Designing a multilayer test

We have seen above, that various types of measurement can be performed. Each type of acquisition provides different class of data that will be used in the adequate analysis.

The objective of a Multilayer Test is to gather the maximum information in a single well test therefore the design must offer all necessary circumstances to a complete acquisition.

The base of a multilayer test design is a multirate test, and the sequence of PLT operations allows the acquisition of both Static measurements of transient rate versus time and measurement of stabilized pressure.

A first step is to define the possible Static survey points, according to the openhole logs and/or the perforation. At this level logic and realism are the key points for a necessary simplification:

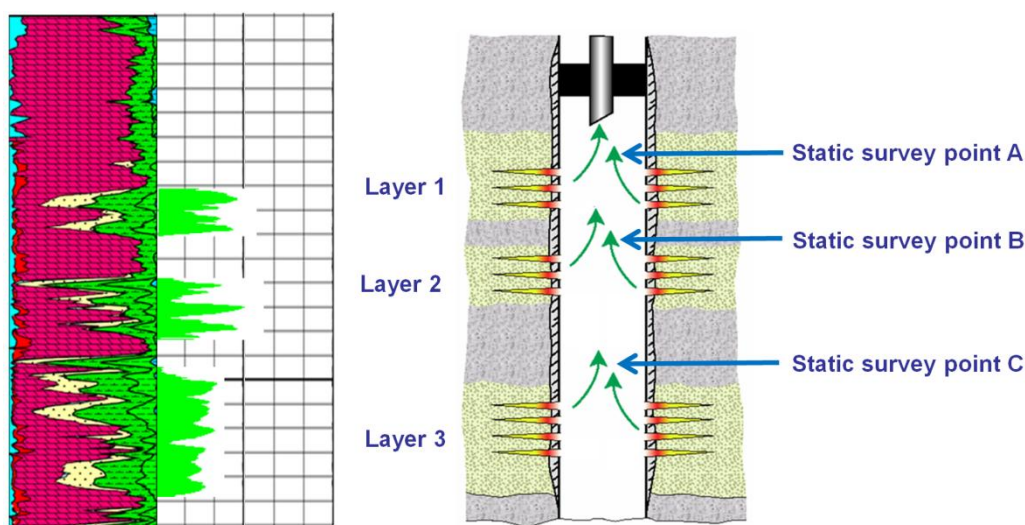


Fig. 11.D.7 – Survey location determination: simplification of the reality

Then to program the operation to acquire static and versus depth measurements, i.e.:

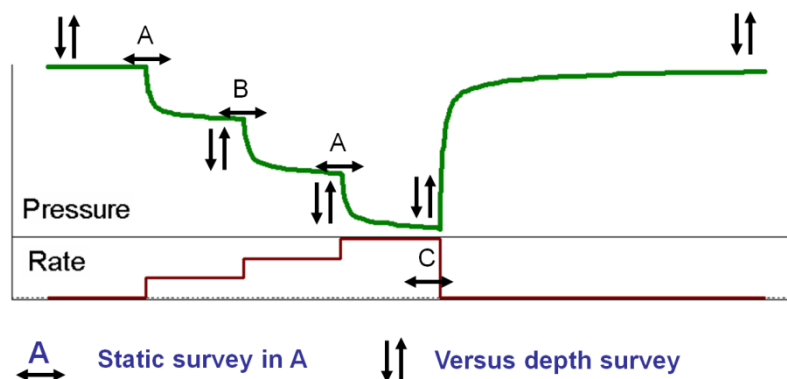


Fig. 11.D.8 – Example of testing sequence of events

This sequence includes the stabilized rate versus depth acquisition under various flowing and shut in conditions and also the transient rate static acquisition at the key points under various rate changes.

11.D.6 Multilayer analysis workflow

The method is based on the model matching, but not only the measured pressure but also the individual measured rate using the adequate analytical or numerical multilayer models.

Both versus depth and versus time acquisition can be used, but each one presents its own interest and provides certain information with more or less success:

- The rate versus time acquisition measures the transient rate behavior, its analysis gives better information on early time behavior (well conditions) and for late time behavior (limit conditions). Its weakness: it is easily subject to the noisy acquisition conditions.
- The rate versus depth acquisition measures the stabilized rate. It is more adequate for the IARF period (permeability and skin determination). Its weakness: it is a constant value ignoring any unstable behavior.

The model optimization is global and aims the adjustment of the complete set of parameters. This method, compared to other methods, sequential and iterative, presents the advantage not to accumulate the uncertainty at each step: when analyzing layer 1, then 1+2, then 1+2+3...

These methods show their limits above three layers.

The field data analysis presents several difficulties and pitfalls that can be avoided by following an adequate work flow.

11.D.6.a Preparation of the data

- The layer geometry must be simplified and clearly defined:

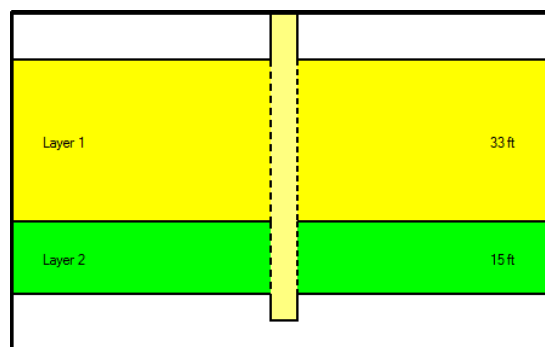


Fig. 11.D.9 – Layers geometry

- The pressure data must be first corrected at the same depth when the transient behavior was recorded at several depths.

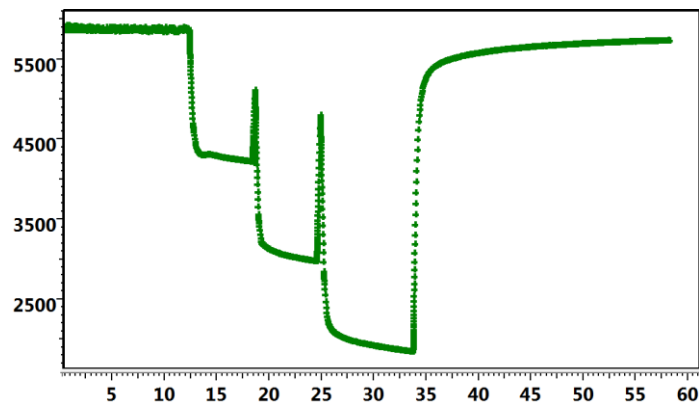


Fig. 11.D.10 – Pressure history

- The stabilized rate and/or contribution data must be calculated with the adequate software from the Production Logging measurements.
- The transient rate data must be extracted and set in a proper format files then synchronized with the pressure data.

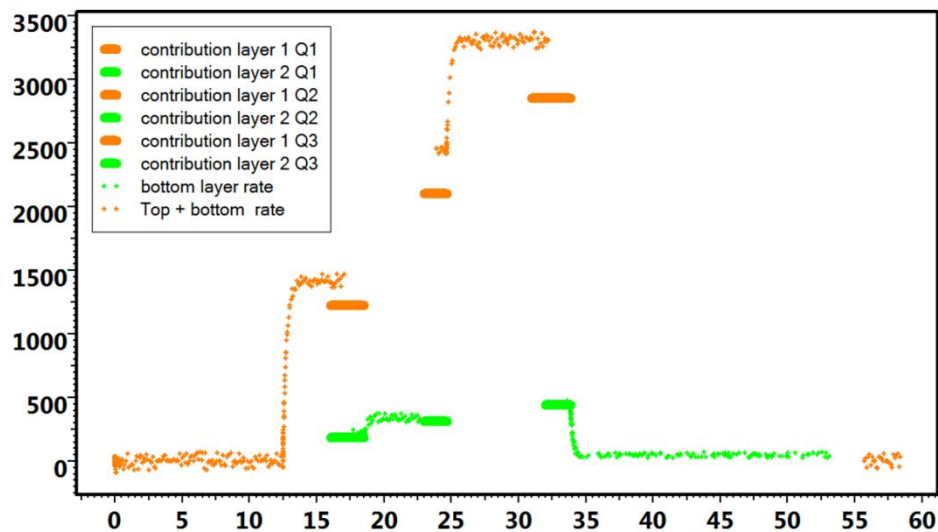


Fig. 11.D.11 – Rate and contribution history

Note: the pressure and rate model matching method used for this multilayer analysis does not requires specifically the rate data to be under the 'rate' or the 'contribution' format since, the model is able to provide the simulated individual production under any format.

11.D.6.b Getting the global results

In order to get a starting point for the model definition, it is necessary to perform first a standard analysis of the multirate test data. That provides the main parameter values for the global behavior: total permeability-thickness product, global skin, limit effect diagnosis.

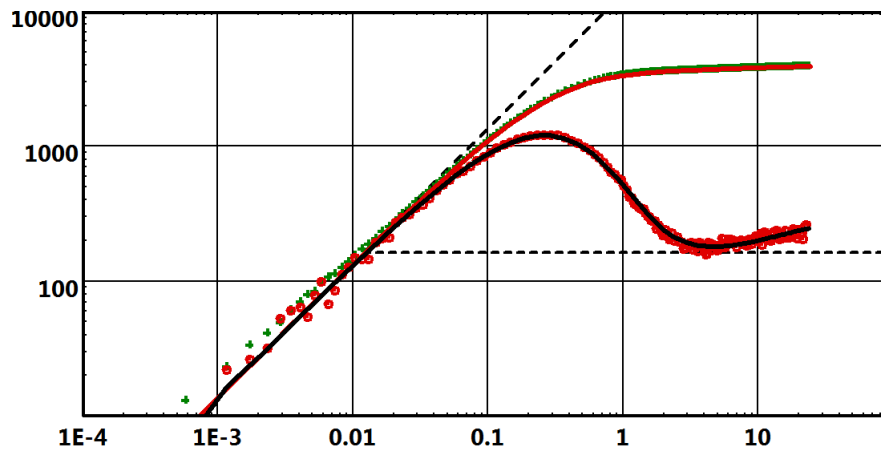


Fig. 11.D.12 – Single layer global match

- The total kh value will be kept in the rest of the analysis as a constraint for the global regression.
- The static pressure, found at 5869 psia will be also kept in the continuation of the analysis as a constraint as long as no 'layered pressure' hypothesis is considered.
- The wellbore storage value will also be kept since it is a well characteristic.
- The limit diagnosis is here a single fault at around 500 ft.

11.D.6.c Multilayer model building and first run

The layer geometry is defined, then, the layer rates and contribution are input.

The first multilayer model parameter definition is, by default uniform permeability, equal skin and boundaries conditions are taken identical to the standard analysis results.

Parameter	Value	Unit
Layer 1		
Skin	2.5	
k	26.017	md
h	33	ft
Phi	0.1	
L	No flow	500
		ft
Layer 2		
Skin	2.5	
k	26.017	md
h	15	ft
Phi	0.1	
L	No flow	500
		ft
Wellbore & other reservoir parameters		
Pi	5869	psia
C	0.00933634	bb/psi

Fig. 11.D.13 – Initial multilayer parameters table

The result of this first run confirms the global pressure behavior:

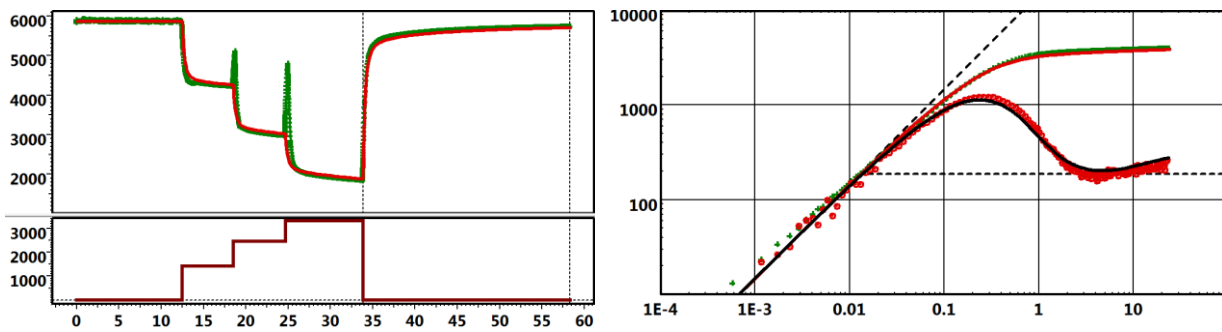


Fig. 11.D.14 – Initial history and log log match

But the non-matching simulated layer rates and contribution reveals clearly the permeability contrast consequence on the individual contributions:

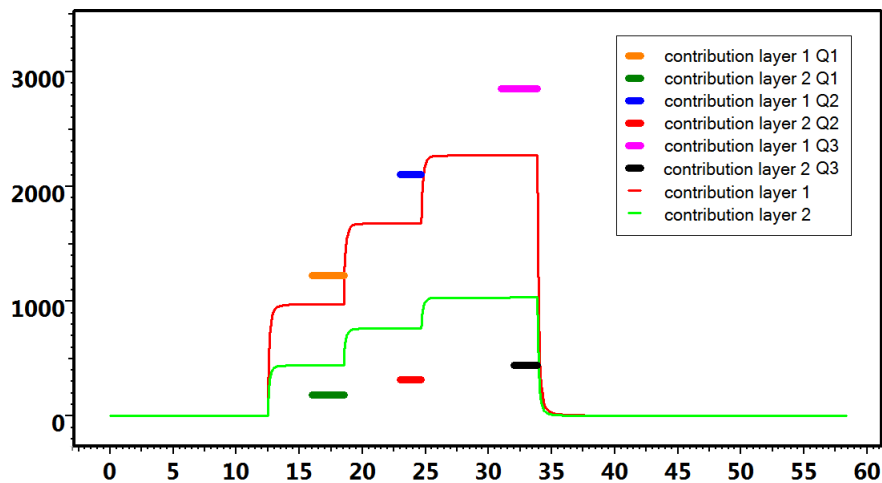


Fig. 11.D.15 – Initial layer rate match

11.D.6.d First improve of the model

The individual permeability values will be adjusted by performing a nonlinear regression on the pressure and rate values with only the permeability and the skin as adjustment parameters. The constant total kh has to be set as constraint.

This has to be done on the complete pressure history and by selecting the stabilized rate values adjustment as objectives.

For the sake of the efficiency it is absolutely compulsory to select the most adequate regression point on the history plot, taking care to eliminate the 'abnormal' pressure behavior like phase segregation effects or operational errors, i.e.:

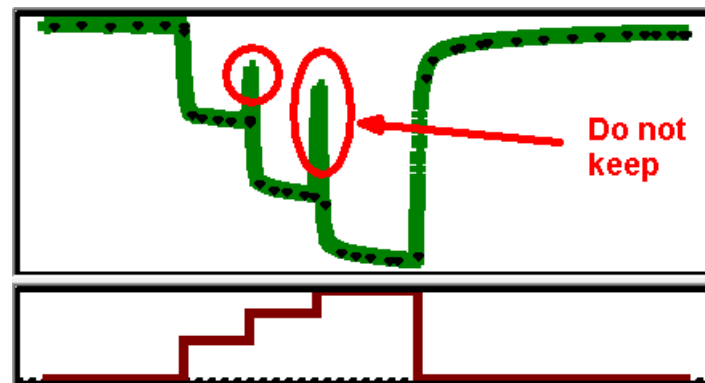


Fig. 11.D.16 – Regression point selection

The effect of the nonlinear regression on the contribution and rate matching is immediate:

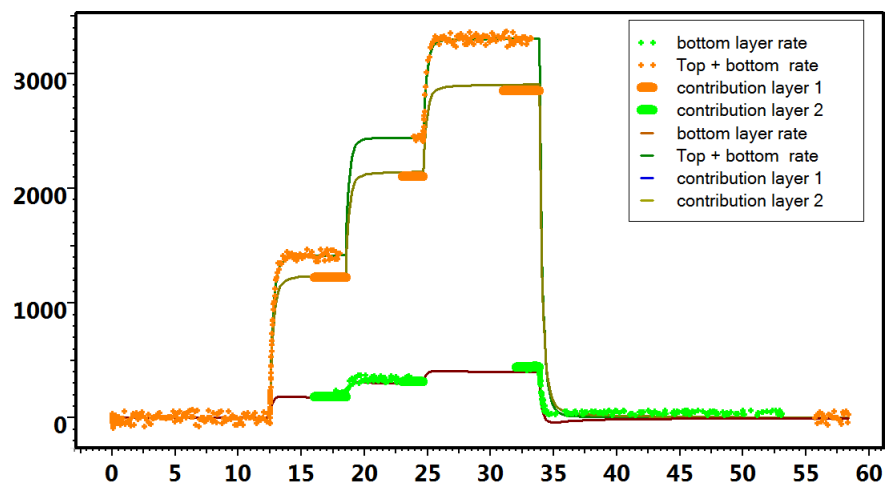


Fig. 11.D.17 – Layer rate match after regression

It is the result of the adjusted permeability and skin values:

Layer 1			
Skin		4.2	
k		38.5067	md
h		33	ft
Phi		0.1	
L	No flow <input type="button" value="v"/>	500	ft
Layer 2			
Skin		3.1	
k		11.4146	md
h		15	ft
Phi		0.1	
L	No flow <input type="button" value="v"/>	500	ft
Wellbore & other reservoir parameters			
Pi		5869	psia
C		0.010468	bb/psi

Fig. 11.D.18 – Multilayer parameters table after regression

The quality of the pressure match on the loglog and history plot is maintained:

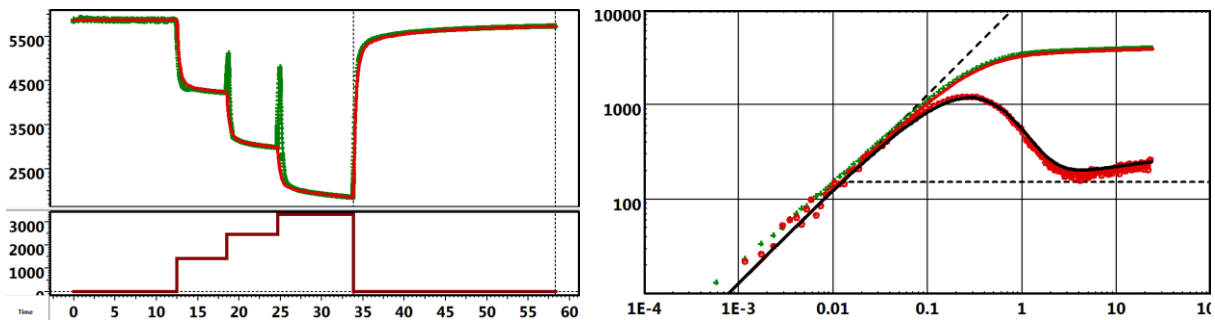


Fig. 11.D.19 – History and log log match after regression

11.D.6.e Final model adjustment

Once the main parameters are determined and considered as reliable, the additional parameters, like the boundary geometry, can be then adjusted.

The same process is used, with the nonlinear regression, to adjust the limit distance:

- The permeability, the skin, the wellbore storage and the initial pressure values are removed from the regression parameters list.
- More weight is given to the transient rate measurement matching.

The final model parameters values:

Layer 1			
Skin		4.2	
k		38.5067	md
h		33	ft
Phi		0.1	
L	No flow	626.97	ft
Layer 2			
Skin		3.1	
k		11.4146	md
h		15	ft
Phi		0.1	
L	No flow	1657.61	ft
Wellbore & other reservoir parameters			
Pi		5869	psia
C		0.010468	bbI/psi

Fig. 11.D.20 – Final multilayer parameters table

Provide a match satisfying:

1) Pressure history matching:

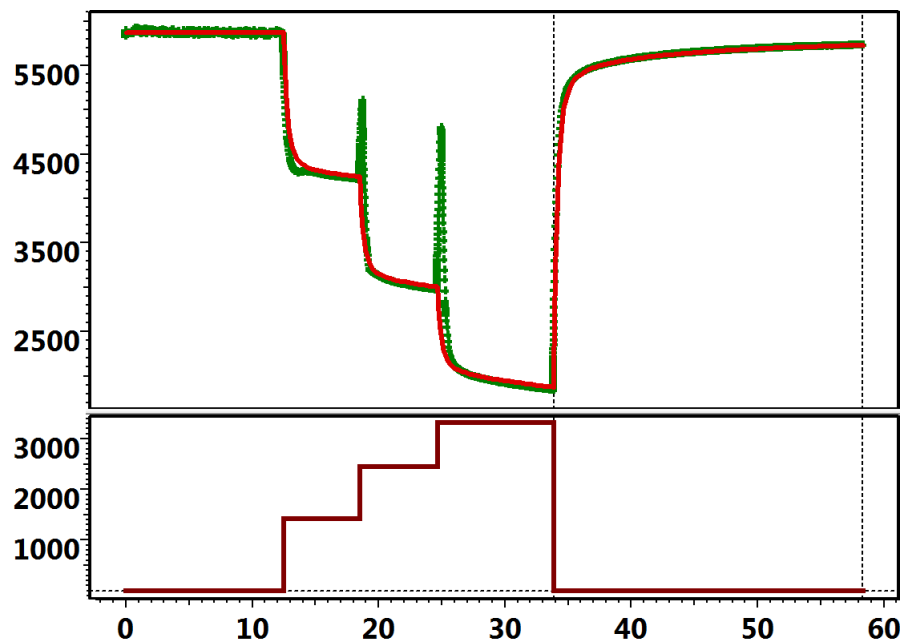


Fig. 11.D.21 – Final pressure history matching

2) Pressure and derivative loglog:

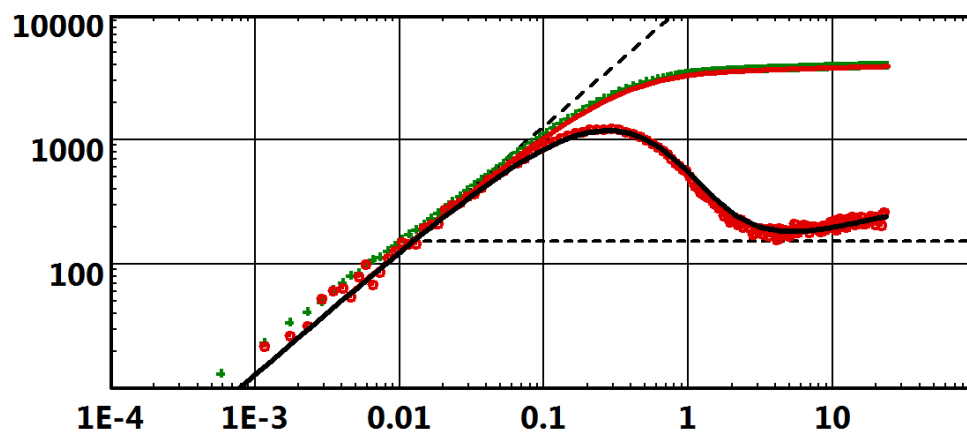


Fig. 11.D.22 – Final pressure and derivative loglog

3) The production rate and contribution:

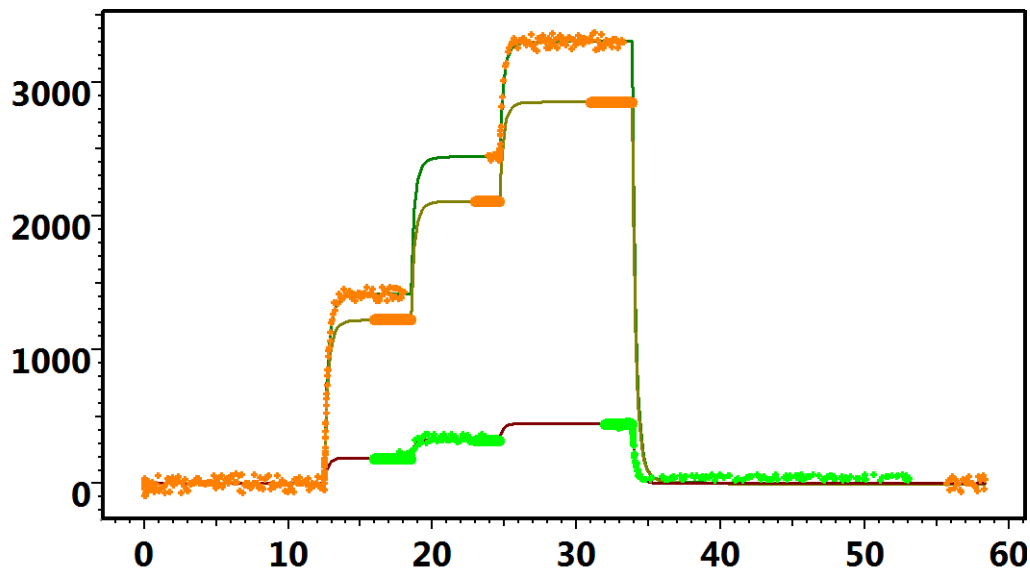


Fig. 11.D.23 – Final production rate and contribution match

11.D.6.f The solution uniqueness

We are dealing here, in this specific case, with a 12-parameter system to be adjusted to match three data channels, one pressure and two layer production rates.

It would be presumptuous to pretend that this solution is unique since we are looking for the minimum of three values (the average distance between simulated and measured pressure and rates) in a 12 dimensions space. This complex space certainly contains multiple areas where the searched minimum is approached (local minimum), and a unique one which is the absolute minimum.

It is certain that other sets of slightly different parameters could give equivalent satisfaction in term of pressure and rate matching, but any result has to be guided and eventually chosen according to other external information coming from geology, geophysics or just the logic.

This method remains, by its principle and its flexibility, a perfectly adequate tool to help us in this search and to check the validity of the results.

11.E Interference Tests

Under the umbrella of multiple well, well testing comes the classic and theoretically simplest (and oldest) of all pressure transient tests, the interference test. Pulse testing is just another variety of the interference test that was devised to avoid the long disruption of production that a typical interference test sometimes was causing. It was also devised to avoid natural phenomena such as tide effects and reservoir noise that could sometimes make the interference test difficult to analyse.

C. V. Theis developed the interference test for hydrogeology (1935). Johnson, Greenkorn and Woods devised the pulse test and Kamal and Brigham perfected and developed a special analysis procedure using type curves to facilitate the analysis by hand. None of the old analysis techniques are relevant today, thus we will not repeat what is already abundant in the old literature on well testing but concentrate on the modern methods of analytical and numerical modelling.

Interference testing involves at least two wells but the test can easily be extended and analysed today with any number of wells present in the interference test scenario. Simply put, the interference test involves the withdrawal or injection of (reservoir) fluids from/into one well while measuring the resulting response in another. So we have the concept of an "Active well" and an 'Observation well'. It is the well response in the 'Observation' well that is subject to analysis and since this well is (hopefully) at static conditions the concept of skin and wellbore storage is eliminated. Thus, in the majority of cases, the Line source solution (or the Theis' solution) as presented in the chapter on 'Theory' can be used directly to analyse the observation well pressure response.

The solution, at any point and time, for a Line Source well producing a homogeneous infinite reservoir, is given by the following:

$$p(r,t) = p_i - \frac{70.6qB\mu}{kh} \left[-E_i \left(-\frac{948.1\Phi\mu c_i r^2}{kt} \right) \right]$$

A typical line source response is displayed in the figures below, on loglog (with the Bourdet derivative) and semilog scale.

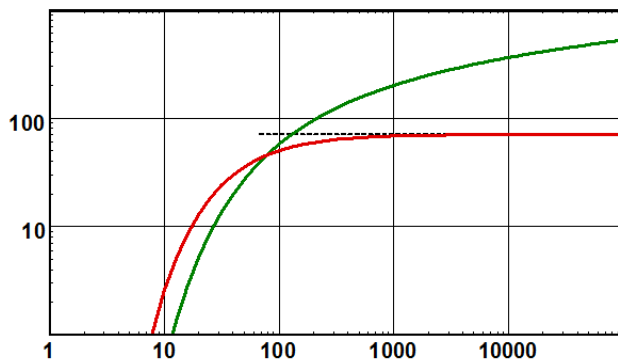


Fig. 11.E.1 – Line source loglog plot

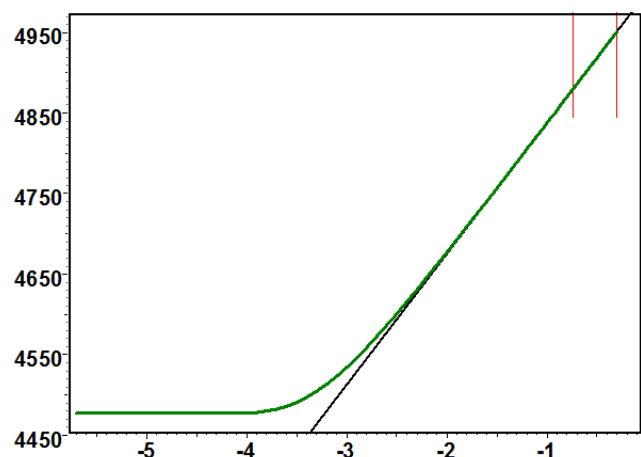


Fig. 11.E.2 – Line source semilog plot

As demonstrated in the chapter on 'Theory', there is a value of time above which the Line Source Solution reaches a 'regime' where one can use an approximation of the highest interest to the well test interpretation engineer. It is the semilog approximation and this regime is called **Infinite Acting Radial Flow**, or **IARF**.

$$\text{IARF: For } t \geq \frac{379200\Phi\mu c_i r_w^2}{k} \quad p(t) \approx p_i - \frac{162.6q\mu}{kh} \left[\log(t) + \log\left(\frac{k}{\Phi\mu c_i r_w^2}\right) - 3.228 \right]$$

The workflow involved in the analysis of the observation well pressure response is thus largely the same as that of conventional well testing. Both loglog and semilog analysis is used and can be valid, and the Line source and wellbore storage and skin models are available to analyse and model the response.

Heterogeneities such as layering, double porosity and permeability and outer boundaries can also be applied analytically.

The figure below illustrates the response in an observation well at static conditions resulting from a simple constant rate production of the active well.

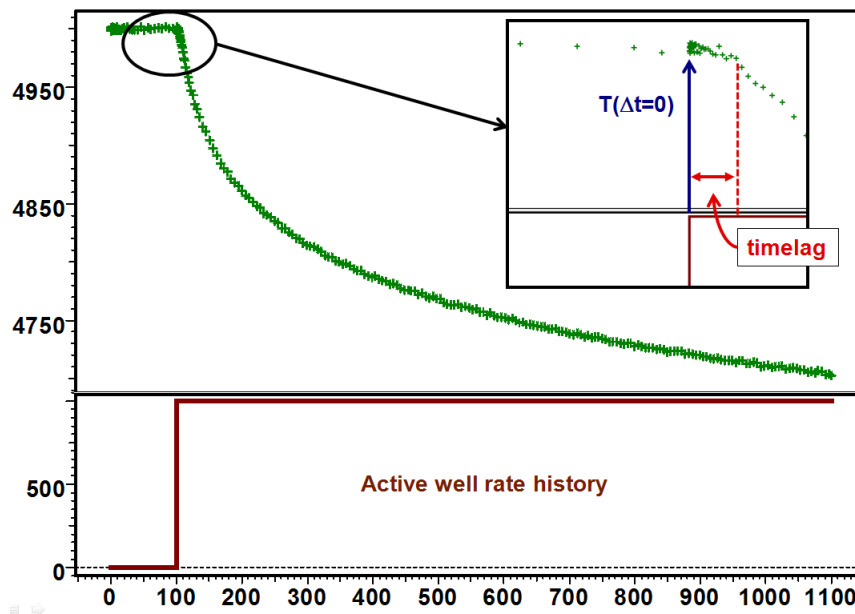


Fig. 11.E.3 – Interference response

As illustrated in the figure above there is a delay (time lag) before the pressure gauge can start to see the response in the observation well. The loglog plot below is constructed as the pressure change from time $T(\Delta t=0)$ thus it can be seen that the first points before there is an actual detectable response in the pressure signal has to be ignored.

Below is the response plotted in loglog coordinates as the pressure change and the Bourdet derivative.

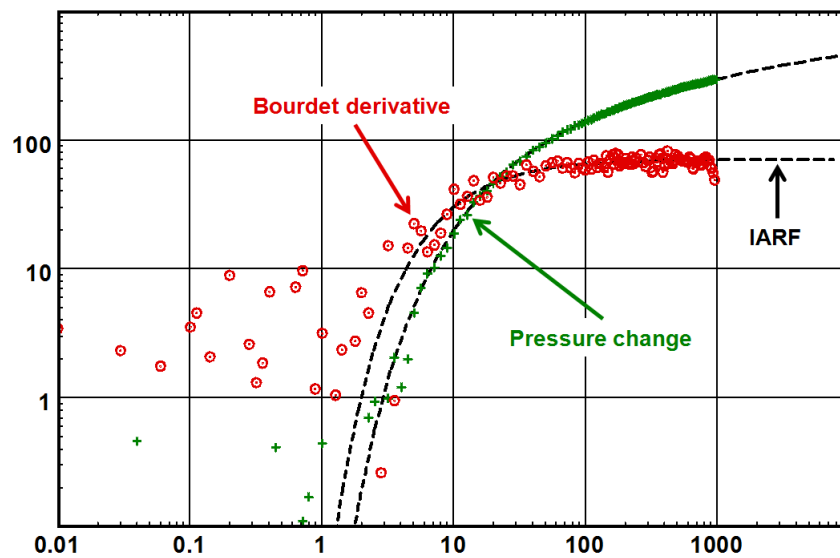


Fig. 11.E.4 – Loglog plot of observation well response

11.E.1 Homogeneous, sensitivity to parameters

The governing parameters are:

kh Permeability-thickness product.

$\phi c_t h$ Reservoir storativity.

Both are results from the analysis. It is said that the only way to get a reliable value for rock compressibility is through an interference test. Of course this assumes that you know the fluid saturations, and the individual fluids compressibility and the porosity. Normally, however, it is the ϕc_t product that is posted as the result with the permeability vector k .

The following figures illustrate the sensitivity to the porosity Φ .

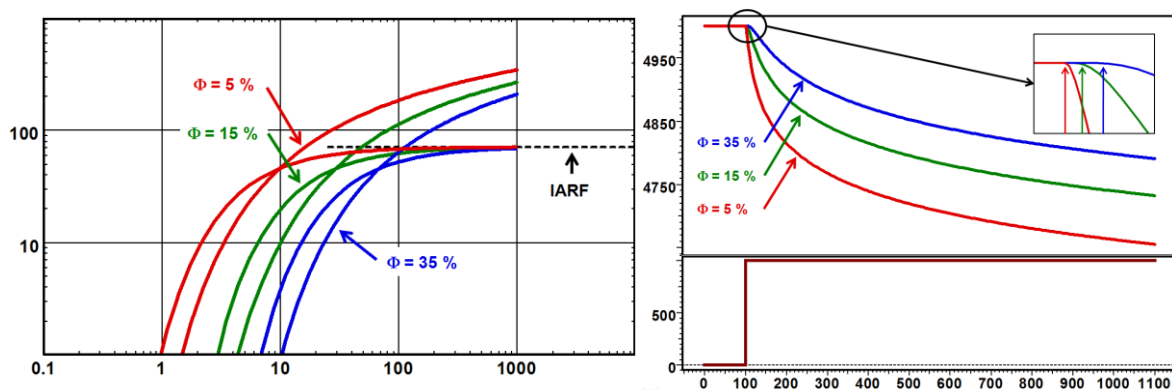


Fig. 11.E.5 – Sensitivity to the porosity, Φ

And below we illustrate the sensitivity to the permeability thickness product, kh .

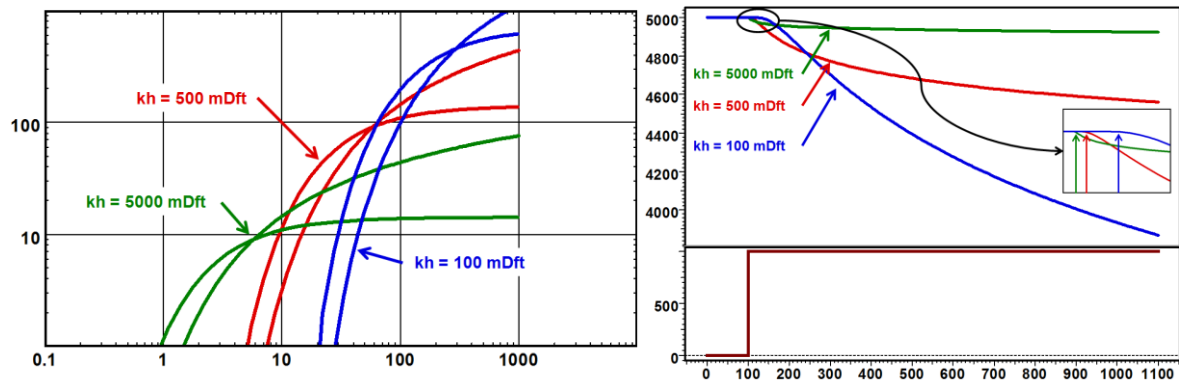


Fig. 11.E.6 – Sensitivity to permeability, kh

Not surprisingly, we observe that the lower the porosity and higher the permeability, the disturbance caused by the active well travels faster to the observation well. The lower the permeability and the porosity the higher is the response amplitude in the observation well.

Actually the original leading parameters can be seen in the line source equation and the exponential function argument:

$$p(r,t) = p_i - \frac{70.6qB\mu}{kh} \left[-E_i \left(-\frac{948.1\Phi\mu c_t r^2}{kt} \right) \right]$$

On the time scale, determining the time lag, it is the diffusivity group: $\frac{\Phi\mu c_t}{k}$

On the pressure scale, determining the pressure amplitude, it is the transmissivity group: $\frac{kh}{\mu}$

11.E.2 Influence of wellbore storage and skin

Ignoring wellbore storage in the active well can lead to underestimation of kh and an over estimation of the porosity Φ . Wellbore storage and skin will increase the time lag and decrease the amplitude in the observation well, it acts as a delaying effect at the active well and this effect is increased by the skin damage.

Below we have illustrated the response in the loglog plot of two different cases of wellbore storage and skin and compared this to the line source solution. The figure to the right illustrates the increase in time lag and the decrease in the amplitude of the response.

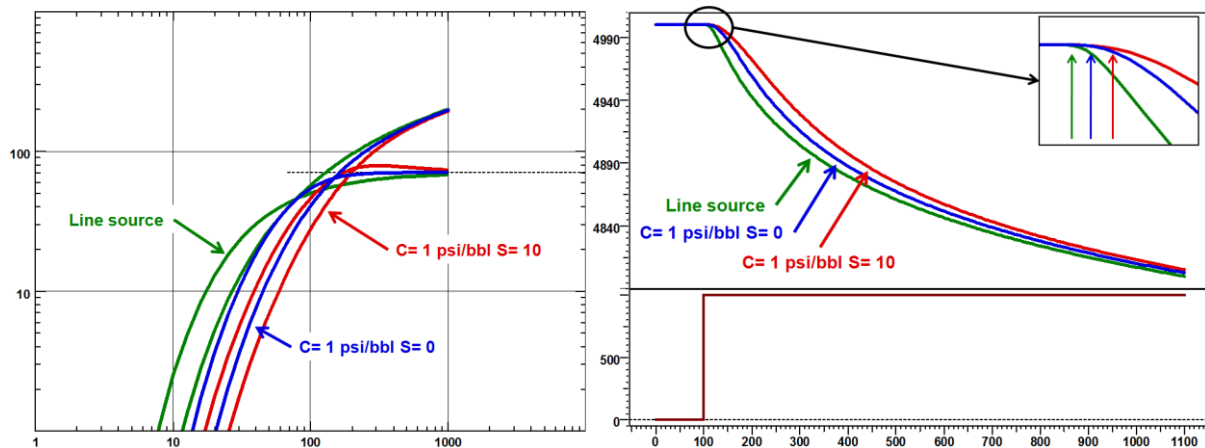


Fig. 11.E.7 – Sensitivity to wellbore storage and skin

Note that the wellbore storage coefficient value used in this simulation is taken very large to make the effect more visible. It is certain that a normal wellbore storage value would have a lot less effect.

11.E.3 Multilayer numerical: An overview

The interference problem can easily be solved numerically with any number of layers, with or without cross flow. It would be beyond the scope of this document to present all possible scenarios in a multilayer situation so we are just presenting an appetizer of what can be done using a numerical linear solution to the problem. It would be up to you, the user, to apply what is outlined here to your own particular problems.

In order to keep it simple and in line with what was discussed in the foregoing section on double permeability, we will only consider a system of two layers with cross flow.

The figure below illustrates the simulated loglog response of a two layered system with the following characteristics matched with the analytical double permeability model for comparison.

Layer name	h	k	kh	Phi	Phi.Ct.h	% k.h	% Phi.Ct.h
	ft	md	md.ft		ft.psi-1		
Layer 1	15	66	990	0.017	7.65E-7	99	10.1796
Layer 2	15	0.66666	9.9999	0.15	6.75E-6	0.99999	89.8204
All Layers	(total)	(average)	(total)	(average)	(total)	(total)	(total)
	30	33.3333	1000	0.0835	7.515E-6	100	100



Fig. 11.E.8 – Numerical layer properties

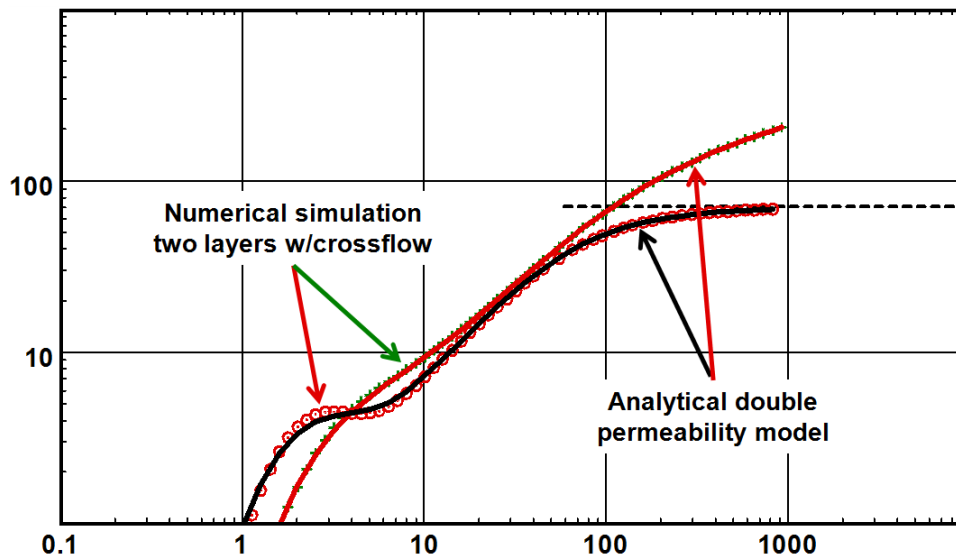


Fig. 11.E.9 – Simulated numerical and analytical model match

One can also open and close perforations of the layers in the observation well of the example. If the high permeability and low storativity layer is turned off the pressure gauge in the observation well will only record the pressure interference through the lower low permeability layer. One can see the comparison of the response in the observation well with the upper layer closed and the response with both layers open. One can indeed conclude that the effect of the active well will induce cross flow from the lower to the upper layer in the observation well. See the figure below.

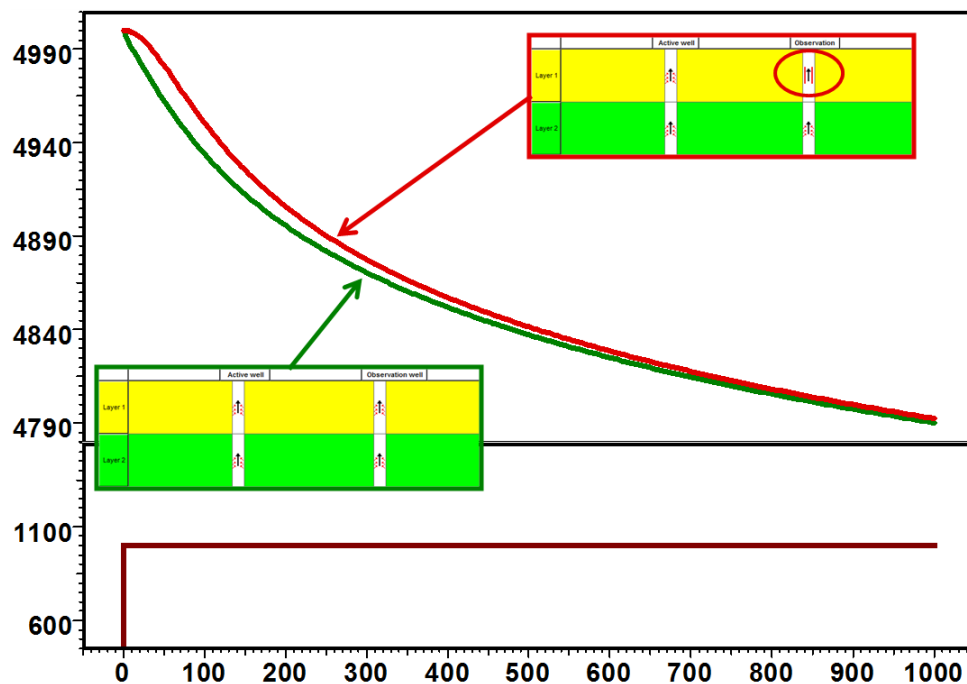


Fig. 11.E.10 – Comparison of response with dominating interfering layer closed off

11.E.4 Other application of the numerical model

The analytical models are limited with respect to the well models of the active well. However, using the numerical model the active (and the observation) well can be any type of well. Naturally fractured (infinite conductivity), induced finite conductivity fracture, limited entry, slanted and horizontal wells. Horizontal fractured wells can also be defined. The well model of the active well can and will in some cases have a direct influence upon the response measured in the observation well thus it makes sense to take this into account in any analysis or design work carried out.

The figure below illustrates the response in a vertical observation well caused by production of a vertical, and two differently configured horizontal wells. The horizontal well at 0° has the toe pointing to the active well in the X direction and the well at 90° has the heel and toe parallel to the Y direction.

Not surprisingly, one observes that the response caused by the horizontal active well with the tip pointing towards the observer is 'seen' by the observer earlier than the interference caused by the horizontal well which points in the Y direction.

Another interesting observation is that the response amplitude caused by the vertical active well is higher than the horizontal well at 90°, and the amplitude caused by the horizontal well placed in the X direction, pointing towards the observer is causing the highest delta p.

From this follows naturally, the fact that it should be possible from these observations to identify areal anisotropy that can also be used in the numerical models.

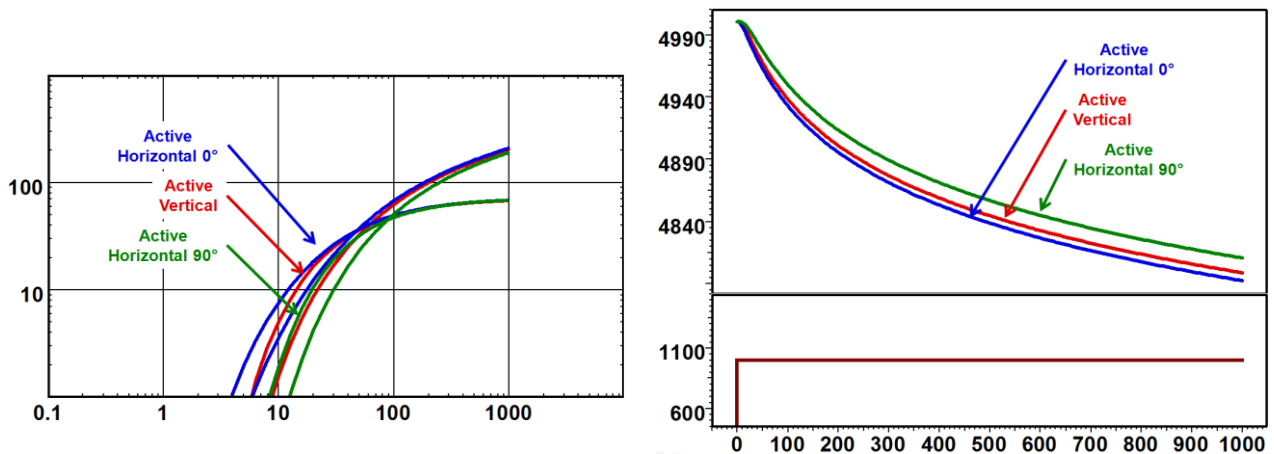


Fig. 11.E.11 – Vertical observer horizontal active well: Loglog and history plot

The numerical model will also take care of reservoirs that are not handled analytically. Composite reservoirs can easily be modelled using the numerical model. Variable data fields such as thickness, porosity and permeability can be modelled.

Below we illustrate the use of the numerical model on fake reservoir with variable permeability. The distance between the observation and the active well is some 12500 ft as the 'crow flies', however the actual distance the diffusion has to travel before a response is seen in the observation well is a lot more tortuous because of the faults. The active well is producing for a month followed by a two months shut-in of the active well. The observation well is at static conditions throughout the interference test. It is possible to extract both the production and the shut-in and display the derivative and the pressure change in the loglog plot. However it can be immediately be seen in the simulated pressure history that even after two months of shut-in the effect has not yet been detected in the observation well thus the loglog plot will be empty and no diagnostics can be done. In fact in this case the diagnostic plot becomes the history plot and the interpreter will thus just try to match a model to the history response. See the next section on 'Interference testing and real life'.

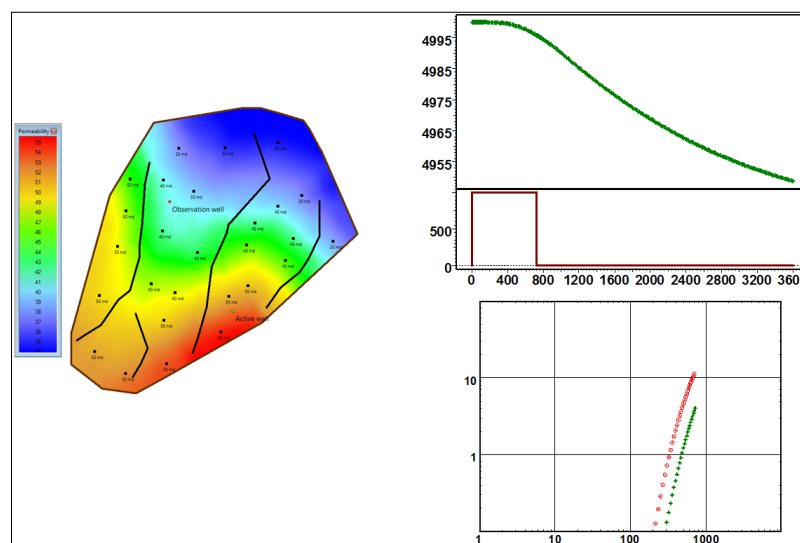


Fig. 11.E.12 – Simulated numerical interference response

11.E.5 Interference testing and real life

11.E.5.a The signal

In an interference test we measure a signal in one or several wells caused by a change in conditions in one or more active wells. The pressure signal can have a short term changing amplitude with a certain value or the pressure signal is the result of more long term and larger changes. It is important to realize that a signal can only become detectable by the pressure gauge in the observation well(s) if it induces a break in the latent response that may already be present due to natural or other foreign causes.

The signal in itself must be measurable by the pressure instrument, thus the resolution of the tool is an issue that cannot be overlooked. This was in particular critical in the past when the quality of the measuring tools was average and the best pressure gauges were not readily available, and when they were, at an exuberant price. Today (2010) this is no longer an issue as most pressure and temperature sensor, at least those based on quartz technology, are readily available and at an affordable price. Even permanent downhole gauges are today of such a quality that they can easily be used for interference testing where only minute pressure changes are necessary in order to detect a signal through the reservoir.

The most common natural signal present in static pressure measurement is the Tide; the combined effect of the gravitational forces exerted by the Moon, the Sun and the rotation of the earth. This effect is not only seen in pressure measurements in offshore fields, but is also common in the middle of the desert or in the middle of a rain forest. To enable the detection of a manmade signal it must therefore be possible to distinguish this signal from the tide signal. A pulse test would never be designed in such a way that the pulse period would correspond to the natural tide period.

The below figure illustrates the tides signal measured in a static observation well during a long term interference test in some part of the world.

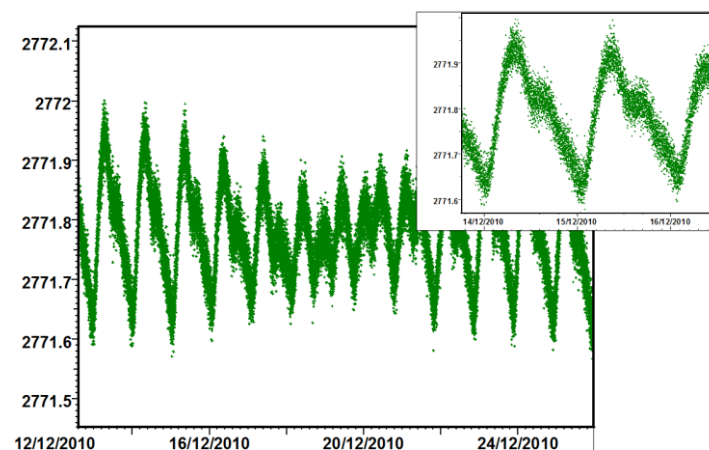


Fig. 11.E.13 – Tides

There is no response in the signal other than the tide effect so there is no other external influence on the measurements. We are 'seeing' no interference i. e. there is no 'break' in the signal. To illustrate that we have indeed a 'break' we are looking at the same signal but some three months later on in the history of the measurements. There is definite a 'break' that can be explained by the interference from a nearby injector.

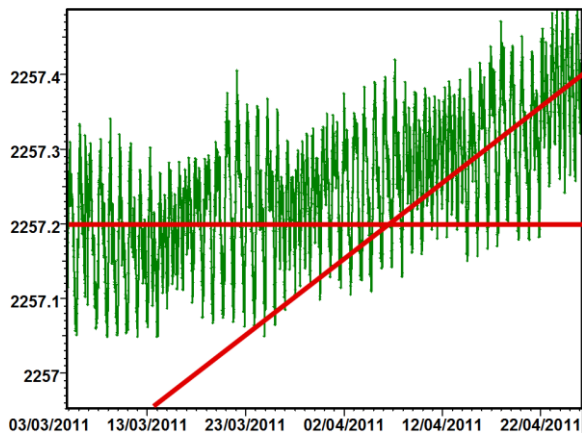


Fig. 11.E.14 – 'Break' detected

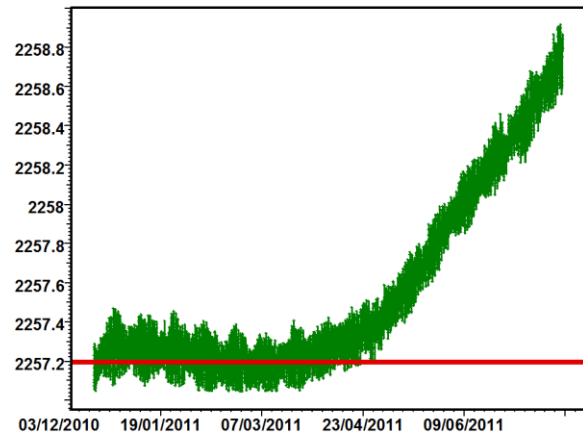


Fig. 11.E.15 – The whole story

Although the 'break' is small to start with we can definitely see that there is an interference response in the well which was caused by a nearby injector when we look at the 'whole' story.

The tide signal oscillates with a Δp of about 0.3 psi, the 'break' is achieved by a total Δp of about 1.5 psi.

The following figure illustrates the response in a well where the pressure rises linearly over time; in this pressure response there is no 'break' thus no interference response. In fact the pressure gauge is 'drifting' with a drift of about 0.03 psi/day.

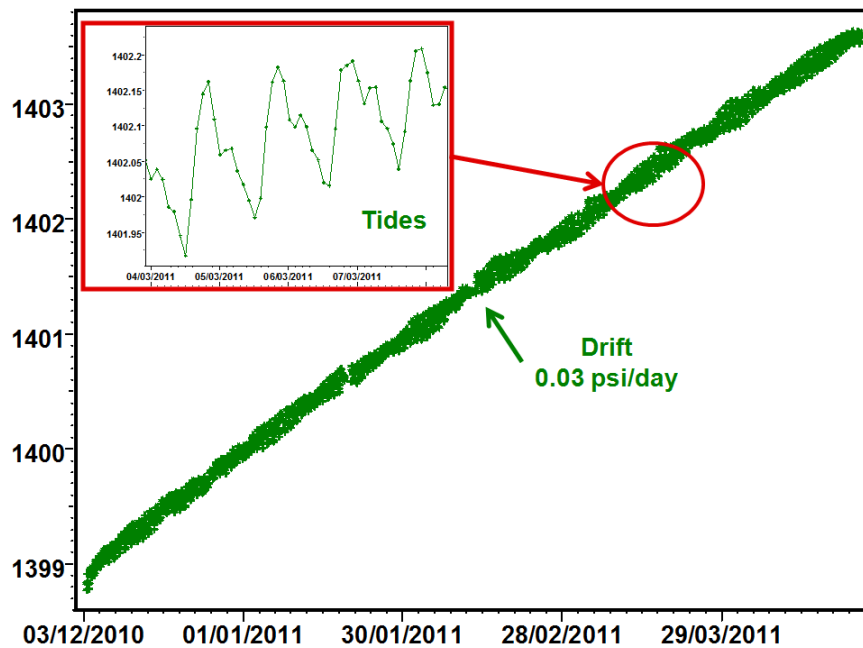


Fig. 11.E.16 – No interference response, drifting gauge

11.E.5.b The tests

One of the pitfalls with interference and pulse testing is that they are so easy to design using the relatively simple theory. This will sometimes backfire and become a problem. The theory can in most cases show that whatever scenario you choose with as many wells that you select as observers or active wells, the theory says that you will get a detectable response every time (as long as you're not testing tombstone and the distance between the wells is not too big). You can even have producers or injectors as the observer wells, the theory will show that this works. Experience shows us that this is more often than not a myth in real life.

The workflow is based upon the same principle as conventional PTA where a diagnostic plot is generated and plotted in loglog coordinates with the pressure change and the Bourdet derivative plotted versus the elapsed time. If the workflow is adhered to it is an easy task to differentiate the shapes and thus the different reservoir and boundary models and deduce all pertinent parameter associated with this and that model. Therefore the requirement is that some 'clean' periods are built into the test design. By clean periods we mean periods of constant flowrate, be it shutin, injection or production periods.

Unfortunately experience show that although these 'clean' periods may have been built into the design, they are often too short so there is not sufficient time to see in the pressure response the actual influence of these 'clean' periods, thus any extraction to the loglog plot is not possible. In real life the production or injection is never totally stable, and the flowrate is variable, and on top of this, may not have any 'built-in' clean periods at all, so the interpreter is left with an empty loglog plot and is reduced to the task of blindly matching a pressure history.

The below figure illustrates a typical long term interference test where the active well is just following the normal operation of production of the active well with all the day to day incidents that always happens to disturb this production, such as unscheduled shutins, changes in rate, perturbations due to normal and daily operation etc. In fact the interference design here is just the ramp-up of production at the end of November 2001 which we can see has little noticeable effect on the pressure response in the observation well.

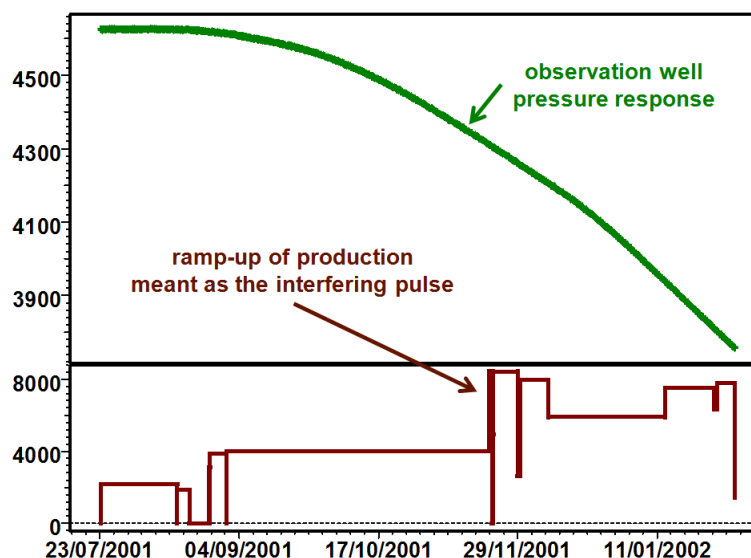


Fig. 11.E.17 – Interference test

We lose the diagnostic power of the loglog plot.

By artificially adding a clean period to the production history of the previous example, a shutin at the end, and generating the model to 5000 hrs shutin time (some 200 days) we can easily observe that the period of buildup has to be a minimum of some 100 days long to give a reasonable response at the observation well and allow the extraction of a loglog plot for diagnostic purposes. Not an easy task to sell to the management. See the illustration below.

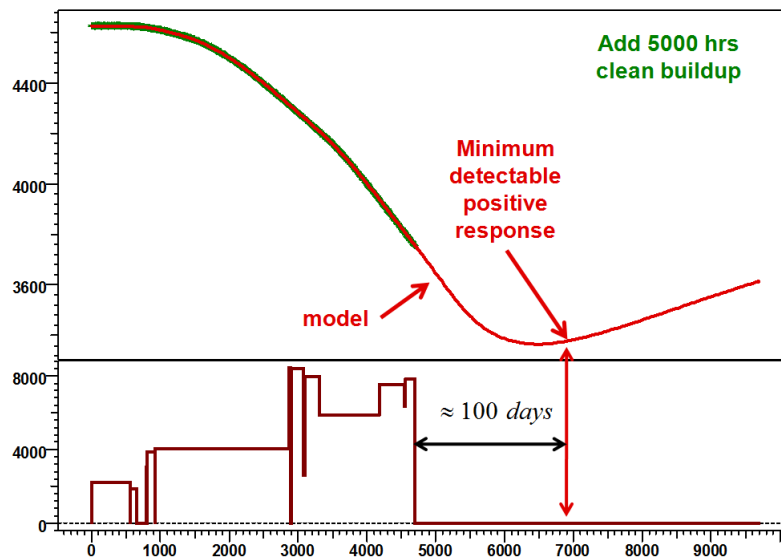


Fig. 11.E.18 – Clean period design

The only diagnostic we can exercise here is to blatantly state that, yes, there is a response in the observation well and the reservoir in between the wells is in communication. Using the history and the simple homogeneous model will (hopefully) give a match, thus a value for permeability kh , and the storativity product Φc_t . Assigning any parameters to heterogeneities would be pure speculation.

Very often we are actually only looking for a yes or a no answer. If no communication is detected this is also valuable information to the practicing reservoir engineer.

Interference testing in producing fields is possible and can be very successful. The times it does not work it is usually due to the under design of the desired minimum pulse amplitude and the lack of the induction of 'breaks' that can be recognized and distinguished from the background noise and trend in the observers.

The ideal interference test is of course carried out in a reservoir that is at rest, but we all know that this would be a costly affair in a producing field....

11.E.6 Pulse tests

The pulse test was first developed when the first high sensitive mechanical pressure gauges became available in the 1960-70's. Since these gauges could measure a small pressure change the pulse test was designed so that the active well flowrate rate was alternating between short flow or injection periods and equally timed shut-in periods. The idea was to be able to shorten the traditionally long duration of an interference tests.

As high sensitive pressure gauges were both expensive and not readily available, they were often reserved for this kind of test.

Later high accuracy electronic gauges became common and cheaper and consequently the argument of the pulse test to enable the shortening of the classical interference test did no longer hold.

However, the pulse test still has an application when the background trend and noise in the reservoir is such that a small response of the interference test can be difficult to detect and find in the pressure history. It is easier to recognize the pulsing behaviour resulting from a pulse test and is not easily lost when the time lag of the response is long.

If one is planning and programming a pulse test one should be aware that there is a phenomenon that can easily perturb the results. Many reservoirs are under the influence of tide effects which overall resembles the response from a pulse test. Therefore it is important to remember the tide influence on the background trends and noise and we need to know the tide amplitude and frequency. The pulse test must be programmed to be 'out of phase' with the tides and the response amplitude must be such that the two signals can be differentiated.

The early studies of the pulse tests proposed methods for manual analysis. At the time the proposed method turned out to be the best advantage of the pulse test compared to conventional interference testing. The method was based on the 'tangent method' and is illustrated in the below figure.

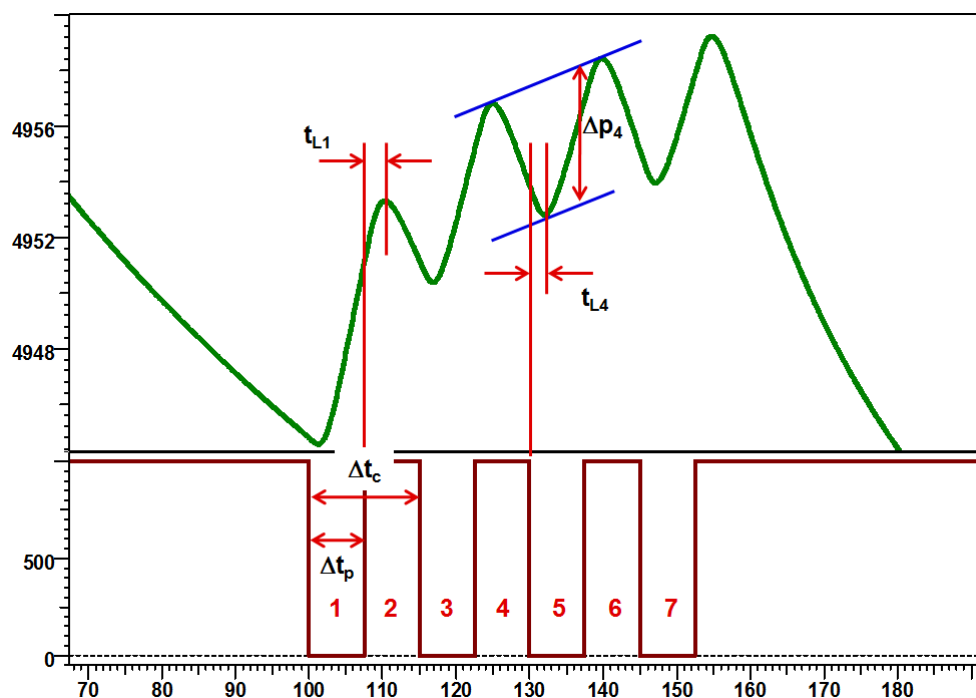


Fig. 11.E.19 – Pulse test tangent method

11.E.6.a The old stuff

Kamal and Brigham presented correlation curves for the manual analysis of pulse tests (1976); these were later modified by Al-Khalifa (1985). The pulses were split between odd and even pulses. The curves for the first even and odd pulse are different, for all other even and odd pulses the correlation charts are the same.

The correlation charts were developed for a homogeneous infinite reservoir with line source wells.

The leading parameters in the correlation charts based on the parameters defined in the 'tangent' approach as defined above:

$$F' = \frac{\Delta t_p}{\Delta t_c} \quad \text{cycle time divided by pulse time}$$

$$(t_L)_D = \frac{t_L}{\Delta t_c} \quad \text{dimensionless time lag}$$

$$(\Delta t_c)_D = \frac{k\Delta t_c}{948.3\mu r^2\Phi C_t} \quad \text{dimensionless cycle time}$$

$$\Delta p_D = \frac{kh}{70.6qB\mu} \Delta p \quad \text{dimensionless pressure}$$

The correlation charts are not shown in this book as these charts are seldom used nowadays as these methods have been replaced by a new modern approach (the right stuff). However, older textbooks on pressure transient analysis will carry these charts so they are readily available to the users.

11.E.6.b The right stuff

Today the manual approach has been replaced by proper modelling of the pressure history using available analytical and numerical models. Due to the lack of an appropriate diagnostic plot the problem is often reduced to matching the pressure history of the observation well. Thus, in most cases the analysis is obtained through non linear regression and seeking interpretation results that are in line and consistent with data from other sources.

The example below illustrates a history match of a pulse test where the pressure response is influenced by tide effect.

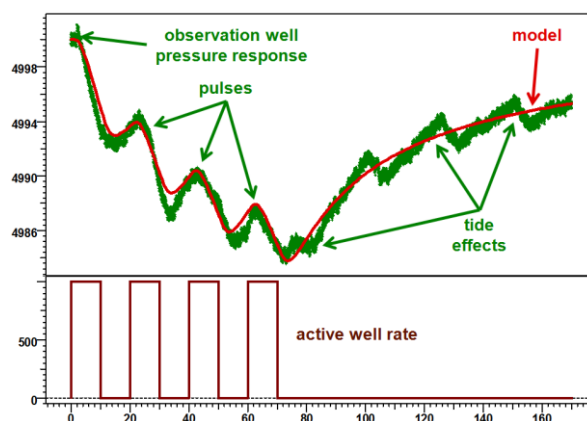


Fig. 11.E.20 – Pulse test

11.E.7 Vertical interference tests

The vertical interference or pulse test is designed to determine the vertical communication in the reservoir or simply to prove that vertical barriers exist to flow.

The figure below illustrates the typical geometric scenario of a vertical interference test.

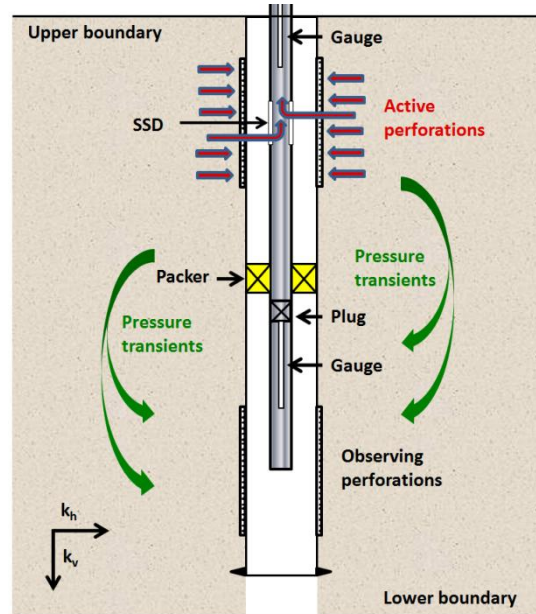
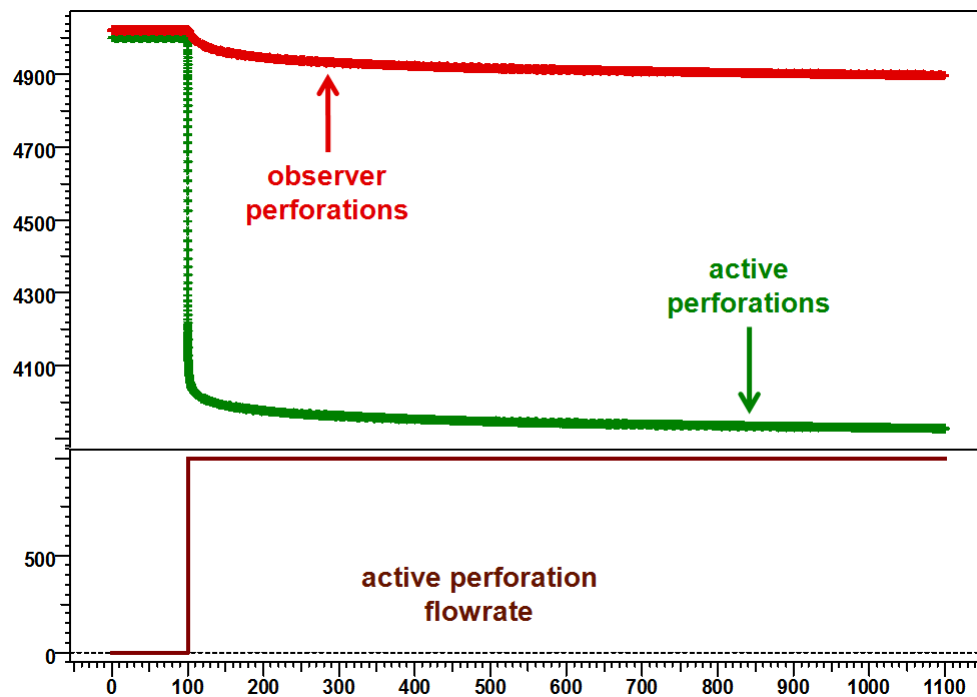
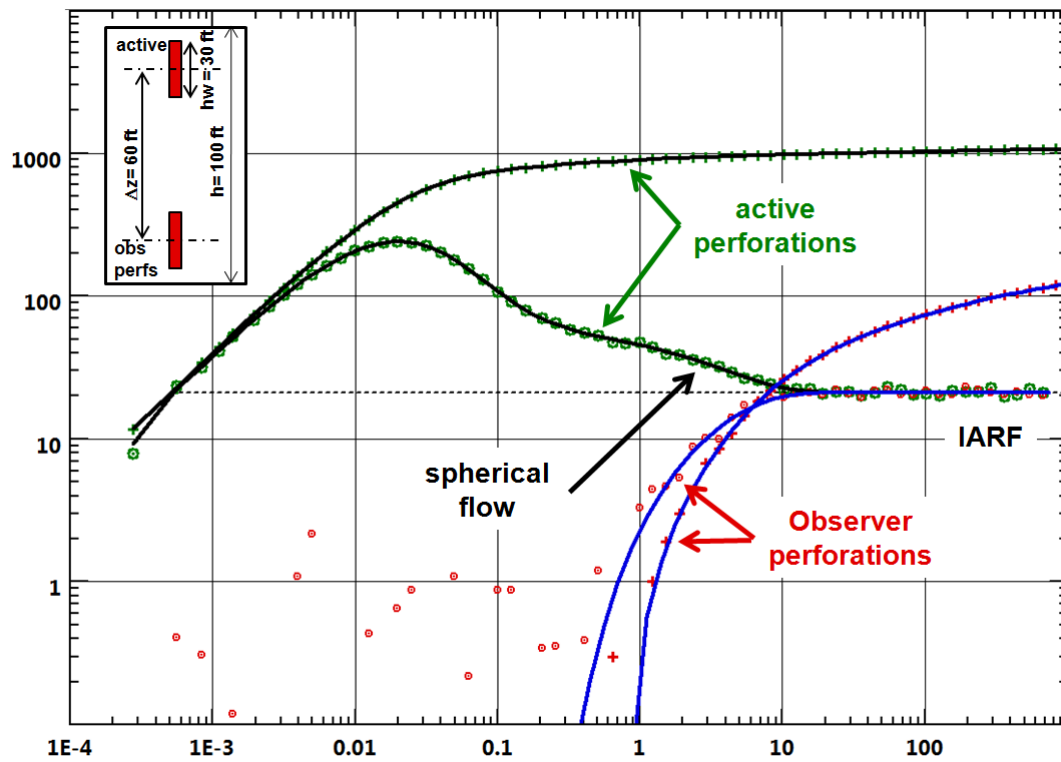


Fig. 11.E.21 – Vertical interference test

Type curves were developed to allow conventional analysis by hand in the 1980's (Kamal). The curves had to be developed for a number of geometrical situations as both the active and observer perforations have to be identified and appropriately placed with respect to each other and the upper and lower boundary. Using the type curves it was possible to estimate both horizontal and vertical permeability.

Today we use modelling as the analysis method. We can apply directly the models developed for the formation tester tools and can thus determine all the pertinent parameters of the reservoir including the vertical permeability.

Below is illustrated the model match of a vertical interference test in a homogeneous infinite reservoir with vertical anisotropy. The response and the model match of the active and observer perforations are shown in the same graphic.





12.A Introduction

The objective of any dynamic data analysis is the best possible understanding of the system 'Reservoir / Well'. To achieve that, it is absolutely necessary to dissociate the respective influences of the reservoir side and of the well side. Not only the performance of the system depends on both, but also the analysis of the reservoir requires being able to correct the data for the wellbore effect in order to extract the pure reservoir response.

The following paragraph will deal with the 'well modeling', necessary to correct the pressure data for depth and to include the wellbore effects in the reservoir analysis.

12.B Inflow Performance Relationship and A.O.F.

The goal of an Inflow Performance Relationship (IPR) is to establish a relation between the flowing pressure and the flowing rate. The Absolute Open Flow (AOF) uses this IPR in order to estimate the maximum possible rate when the flowing pressure is as low as possible, i.e. at atmospheric pressure.

Objection: Needless to say the idea of IPR and AOF is an anathema to the purist Pressure Transient Analyst. Everyone knows that, even in the optimistic case of an infinite reservoir, the pressure will continue drawing down when we are at constant rate, and the rate will keep declining when we are at constant flowing pressure. So, from a well testing point of view, this makes as little sense as the notion of a productivity index.

Objection to objection: Of course this objection is not completely correct. There is a regime where there is such a relationship and that is Pseudo-Steady State. When PSS is reached the shape of the pressure profile stabilizes and moves downwards. A relation between the production and the difference between the average pressure and the flowing pressure can be established.

Objection to objection to objection: Unfortunately we generally do not wait for PSS to be reached before performing an IPR, and the conditions under which the data is acquired are, generally, transient. We therefore look for changes that become small enough to be ignored. This complete process is therefore not strictly correct.

Objection to objection to objection to objection: This will not be too far out and, in any case, it has proven to work relatively well in the past, especially for gas reservoirs. In addition, IPR from PSS models are the best we have to simulate production networks and input in reservoir simulators where the details of the transient responses are not this important. IPR / AOF are useful because they give accurate ideas of the performance of the wells, and they are really the least bad thing to use when we optimize reservoir production.

12.B.1 The IPR types

Any available method is based on an equation which links the rate and the flowing pressure drawdown values.

These equation parameters can either be determined by adjusting the IPR curve to measured well test data set or they can be calculated using empirical equations.

12.B.1.a Straight line Constant IPR:

The constant productivity index (P.I.), only used in oil wells, was during a long time the only approach to oil IPR. Nowadays this is applicable to undersaturated oil only.

It is the simplest inflow performance relationship where the inflow is directly proportional to the drawdown.

$$PI = \frac{Q}{P_r - P_{wf}}$$

Where:

P _{wf}	flowing wellbore pressure	P _r	reservoir average pressure
Q	liquid flow rate		

It just requires a minimum of two measured rate and pressure values under flowing conditions.

12.B.1.b Darcy Equation

The Darcy IPR describes a linear relationship, where the parameters are calculated from the reservoir properties. Its equation results directly from the solution of a radial flow around a well within a circular drainage area of constant external boundary pressure, assuming a laminar flow.

It requires the knowledge of the well and reservoir drainage area parameters.

Oil case

$$P_r - P_{ws} = Q141.2B\mu \left(\ln re/rw \right) - 0.75 + sCA + s \big/ (kh)$$

Where:

Q	liquid flow rate	k	permeability
h	net formation drained thickness	rw	wellbore radius
S	skin	m	viscosity
P _{ws}	flowing sandface pressure	P _r	reservoir average pressure
sCa	shape skin	s	mechanical skin

Gas case

The equation is expressed in terms of Pseudo pressure $m(p)$:

$$m(P_r) - m(P_{ws}) = ((1.42248e + 6)TQ(\ln(re/rw) - 0.75 + sCA + s) + QDg) / kh$$

Where:

Q	gas flow rate	$m(p)$	pseudo pressure
sCa	shape skin	Dg	Drainage area factor
k	permeability	hw	perforated interval
h	net formation drained thickness	A	drainage area
rw	wellbore radius	gg	gas specific gravity
S	skin	m	viscosity
T	reservoir absolute temperature (° R)		

12.B.1.c C&n IPR

Several approaches were made to add the turbulent or the diphasic flow influences, among which is the C&n approach.

It was first used in gas cases, where the turbulent flow cannot be ignored or neglected, then it was extended to oil cases.

The measured production rates and their corresponding flowing pressure values are used to determine the C & n coefficients values.

Gas case

In 1936, Rawlins and Shellhardt published the IPR equation:

$$q = C(\bar{p}^2 - p_{wf}^2)^n$$

Where:

C	is the performance coefficient
n	the turbulent flow exponent, equal to 0.5 for fully turbulent flow and equal to 1 for laminar flow.

Oil Case

In 1973 Fetkovich demonstrates that the same can be used for oil wells.

The effect of the reservoir turbulences can be modeled with the use of the back pressure equation:

$$Q = C(\bar{p}^2 - p_{wf}^2)^n$$

$$Q_{\max} = Q_b + \frac{PI \times P_b}{1.8}$$

Where:

Q	Total liquid rate flow rate	Q _{max}	Maximum flowrate
Q _b	Rate at bubble point pressure	P _r	Average reservoir pressure
P _{wf}	Bottom hole flowing pressure		

The method consists in using pressure and production data to determine the P_i, then the Q_{max} value.

12.B.2 Different types of multirate tests

The IPR equations assume stabilized rate and flowing pressure conditions, the most basic multirate test design is the back pressure test also called the flow after flow test which is a sequence of flow periods long enough to reach stabilized conditions originally proposed by Rawlins et al in 1936.

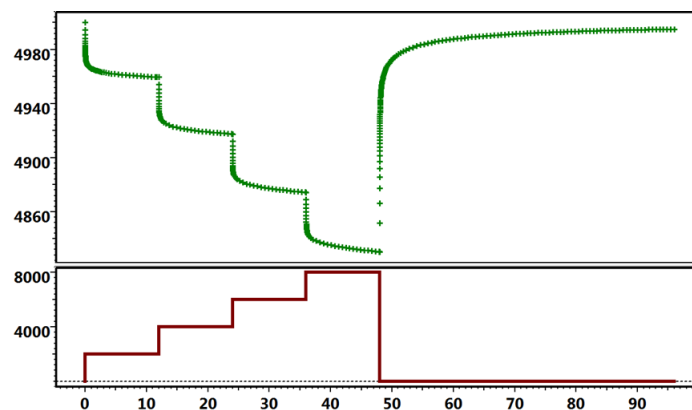


Fig. 12.B.1 – Back pressure (Flow after Flow) test

A second approach is based on the fact that only the laminar coefficient of the equations depends on the flow duration, the NonDarcy coefficient remains independent.

The test design includes short flow periods of equal duration, not necessarily stabilized, at various rates followed by shut-ins of equal duration until stabilization which are not necessarily the same duration as the drawdowns. The resulting values are used to determine the NonDarcy flow coefficient.

An extended flow period until stabilization allows determining the correct laminar coefficient.

This is the isochronal test proposed by Cullender in 1955.

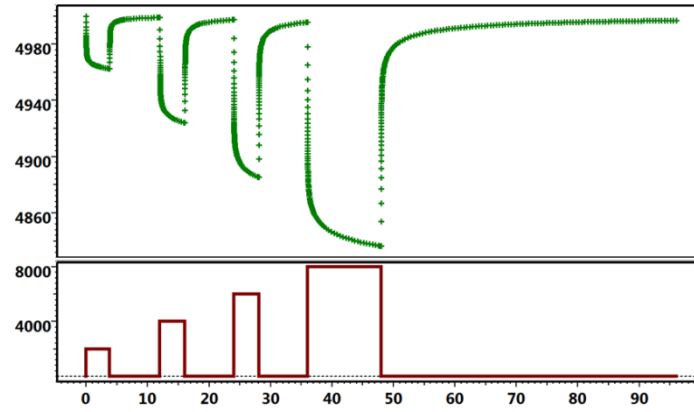


Fig. 12.B.2 – Isochronal test

The flowing pressure drawdown values are calculated from the initial average pressure.

The modified isochronal test, proposed by Katz et al in 1959, is characterized by short shut-ins between production periods, of equal duration, with neither of the periods necessarily stabilized. The final flow to stabilization is followed by a final long shut-in.

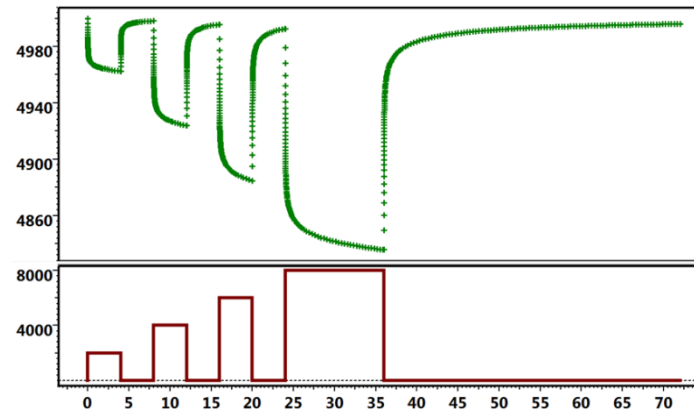


Fig. 12.B.3 – Modified isochronal test

The flowing pressure drawdown values are calculated from the previous last shut in pressure.

12.B.3 Different IPR/AOF calculation methods

12.B.3.a The Rawlins and Shellhardt method (C&n)

It can use either the p^2 valid for Oil or Gas:

$$q = C(\bar{p}^2 - p_{wf}^2)^n$$

Or, for gas only, the pseudo pressure $m(p)$:

$$q = C(m(\bar{p}) - m(p_{wf}))^n$$

The pressure and rate data are plotted on a log-log scale:

$$\log(\bar{p}^2 - p_{wf}^2) \text{ versus } \log(q)$$

Or

$$\log(m(\bar{p}) - m(p_{wf})) \text{ versus } \log(q)$$

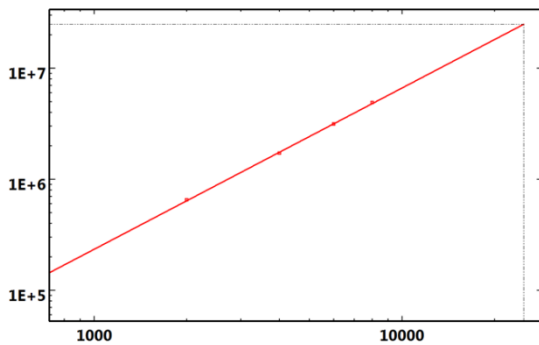


Fig. 12.B.4 – Back pressure test

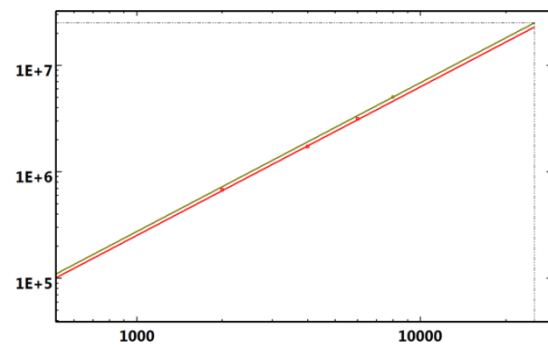


Fig. 12.B.5 – Isochronal test

The n value is calculated from the slope, C from the line intersect.

Then:

$$AOF = C(\bar{p}^2 - (p_{atm})^2)^n$$

Or

$$AOF = C(m(\bar{p}) - m(p_{atm}))^n$$

12.B.3.b The LIT Method

Developed specifically for gas, it is based on the equation:

$$m(\bar{p}) - m(p) = aq + bq^2$$

The pressure and rate data are plotted:

$$\frac{m(\bar{p}) - m(p_{wf})}{q} \text{ versus } (q)$$

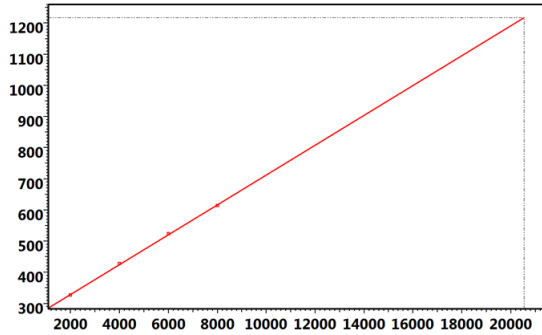


Fig. 12.B.6 – Back Pressure test

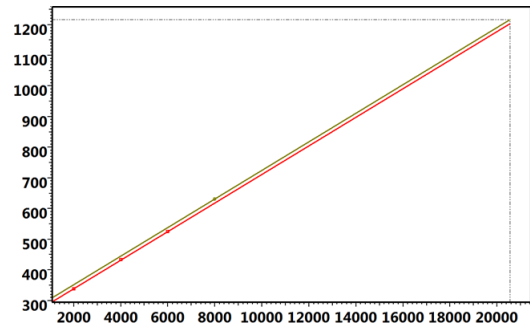


Fig. 12.B.7 – Isochronal test

The b value is calculated from the line slope and the "a" value from the intersect:
The AOF is then:

$$AOF = \frac{-a + \sqrt{a^2 + 4b[m(\bar{p}) - m(p_{atm})]}}{2b}$$

12.B.3.c Jones method

The method is also based on the equation suggested by Jones, Blount and Glaze in 1976 to account for turbulences in a producing oil well:

$$Pr - P_{wf} = aQ + bQ^2$$

Where a and b parameters are calculated from empirical equations:

Oil case

The equation:

$$Pr - P_{wf} = aQ + bQ^2$$

With:

$$a = (141.2B\mu(\ln(re/rw) - 0.75 + sCA + s) / kh$$

$$b = \frac{1.4352 \times 10^{-12} \gamma_l \beta B^2 \left(\frac{1}{r_w} - \frac{1}{r_e} \right)}{hw^2}$$

SCA Shape skin (from Dietz shape factor)

hw perforated interval

γ_l liquid specific gravity

h net formation drained thickness

k permeability

B formation volume factor

β turbulence coefficient

re drainage radius

rw	wellbore radius	S	skin
μ	viscosity		

Gas Case

The same principle equation, using $m(p)$ is:

$$m(\bar{p}) - m(p) = aq + bq^2$$

But the parameters a and b are estimated from the following empirical equations:

$$a = \frac{1495.6T \left(\log \frac{A}{r_w^2} + \log \left[\frac{2.2458}{C_A} \right] - 0.87s \right)}{kh}$$

$$b = \frac{1299.15TD}{kh}$$

$$D = \frac{0.00003gg}{\mu h r_w k^{0.333}}$$

Where:

Ca	Dietz shape factor	D	Turbulence factor (1/ft)
k	permeability	hw	perforated interval
h	net formation drained thickness	A	drainage area
rw	wellbore radius	gg	gas specific gravity
S	skin	μ	viscosity
T	reservoir temperature (deg R)		

Other similar methods exist for various well geometries, the difference remains in the empirical equations.

12.C Intake models in PTA and PA

12.C.1 Classic pressure correction

The fact that the pressure gauges sensing points are seldom at the level of the sandface is most often overlooked by the interpretation engineer.

Classically, the static pressure (p_i , p^* , p_{bar} , final build-up pressure) are corrected:

- from the gauge depth to the sandface using the static well static gradient.
- from the sandface to a common reservoir datum using the reservoir gradient taking into account any gradient changes if it is necessary to move through a fluid contact in the reservoir.

This correction is usually done manually and is essential to establish reservoir pressure trends, declines and depletion rates.

The resulting corrected static pressure maps can be used to study:

- The effectiveness of artificial or natural pressure maintenance.
- It can also reveal reservoir compartmentalization.

It is an essential part of material balance studies and full field simulations.

Little attention has been put on the correction of flowing pressures and the fact that the skin calculation returned by Pressure Transient Analysis is in fact at the gauge level, therefore it includes the pressure loss due to friction between the sandface and the gauge.

In that way, the skin, and specially the rate dependant skin, can be considerably over evaluated. We are only interested in sandface values but this problem has largely been ignored by the well test community until recently.

Most Pressure Transient and Production Analysis software packages include such corrections. This can be a correction of the model to simulate the pressure at a given depth, or to correct, a priori, the pressure history from the gauge depth to sandface.

12.C.2 Correction methods

It is necessary to evaluate the pressure profile and lift curve of the well under flowing and shut-in conditions.

The pressure profile is defined by:

- A temperature profile;
- A flow correlation or a lift curve;
- PVT definitions;
- The completion configuration including deviation.

The below figure shows a 'Vertical intake curve'; pressure vs. rate at a selected well depth using a fixed GOR and water cut.

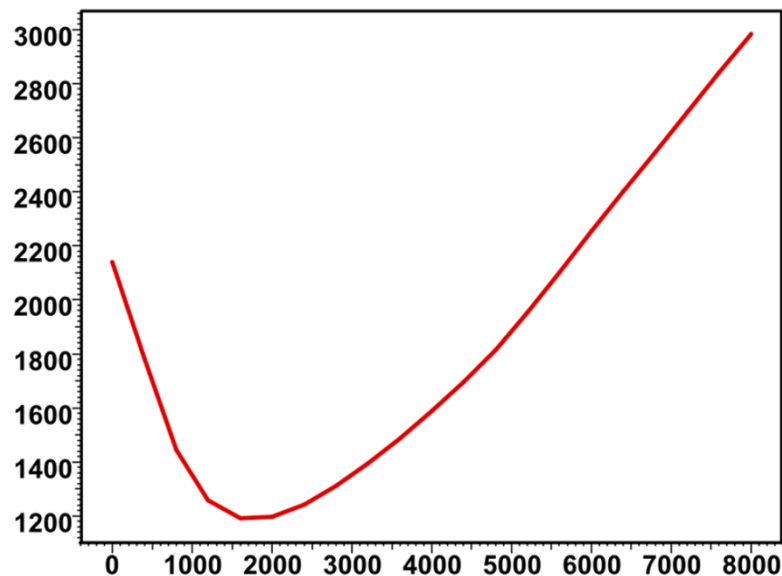


Fig. 12.C.1 – Vertical intake curve, flowing pressure vs. rate

12.C.2.a Flow correlations for oil

Duns-Ross: The result of laboratory work where liquid holdup and flow regimes were observed. This utilizes a flow pattern map to determine the slip velocity, and consequently liquid holdup, and friction factor. This correlation is recommended for wells where high GLRs and flow velocities have induced flow regime behavior.

Orkiszewski: Developed using work from both Duns & Ross and Hagedorn & Brown. It uses the Griffith and Wallis method for bubble flow, a new method for slug flow, and Duns and Ross for transition and mist flow.

Hagedorn-Brown: Developed experimentally using a 1500ft test well with 1", 1.25", and 1.5" tubing. The correlation is used extensively throughout the industry and is recommended in wells with minimal flow regime effects.

Beggs-Brill: This correlation was developed experimentally using 1" and 1.5" pipe, inclined at several angles. Correlations were made to account for the inclined flow. The correlation is recommended for deviated or horizontal wells.

Mukherjee-Brill: Developed experimentally using 1.5" steel pipe inclined at several angles. This includes downhill flow as a flow regime. This is recommended for inclined or horizontal wells.

Dukler-Eaton: Based on 2600 laboratory and field tests to generate an expression for frictional pressure losses along pipelines. It can be used for horizontal flow.

12.C.2.b Flow correlations for gas

Cullender & Smith: This correlation is based on gas properties as defined by the PVT, and a general friction factor calculated using the Colebrook and White equation. Note that when handling a condensate case with equivalent gas gravity and total rates, the proper gradient and rates are used in Cullender and Smith to account for the presence of condensate. The presence of water can be accommodated, based on a constant water to gas production ratio.

12.C.2.c Lift curves

The interpretation engineer can input lift curves generated by third party programs such as Amethyste, Eclipse and Prosper. The lift curves are usually imported in Eclipse format.

Lift curves usually provide the pressure drop between the well head and lift curve depth. However, it can happen that they correspond to a pressure drop between a given depth that is different from the well head and the lift curve depth.

External lift curves are discrete data. When using them the pressure drop calculations are performed by interpolations in the lift curve table in each of the required dimensions. Therefore it is recommended to provide as many lift curves as possible to cover the widest possible range of situations such as varying rates, phase ratios and well head pressures.

12.C.3 General calculation method

In vertical multiphase flow calculations the pipe is divided into small depth increments. The pressure loss in each increment is determined in a reiterative process using average pressure and temperature values to calculate fluid properties. This is necessary as flow regimes and subsequent fluid and flow properties continually change through the pipe. As a result, a computer solution is almost mandatory.

Multiphase cases are treated using multiphase flow correlations. In the event that the interpreter has identified more than one phase rate, Perrine's method is usually used and the phase ratios are calculated at each step from the loaded measured multiphase rates and used in the intake calculator for the pressure depth correction.

If a non-linear numerical model is used the numerical model output will provide sandface phase rates. The phase ratios are calculated at each step from the simulated multiphase rates and used in the intake calculator for the pressure depth correction.

Pressure drop correlations are valid under dynamic conditions only, not during build-ups or fall-offs. To ensure continuity of the corrected pressure, the limit of the pressure drop when the flowrate tends to zero is used during shut-ins. With the flow correlations, this amounts to dividing the tubing into small segments where each contains phase rates corresponding to the amount given by the flash PVT, and consequently the deduced holdups.

12.C.4 Correcting gauge data vs. correcting model

Correcting the data: In production analysis, Topaze, when the intake pressure model has been defined, the interpretation engineer will decide during extraction to make the pressure correction to whatever depth is desired. There is an option to create a new pressure gauge with the corrected pressure. In Saphir it is possible to transform the pressure data to whatever depth at any time.

Correcting the model: In Saphir, when the intake pressure model has been defined, the interpretation engineer will decide that when generating the model the model response will be corrected to gauge depth.

The downhole rates are calculated by the model and will therefore incorporate wellbore storage effects. This ensures that, with significant friction, there will be no discontinuity in the corrected model when the surface rate changes.

The model match will now return results at sandface.



13 – Permanent Gauges & Intelligent Fields

OH – OSF – DV



13.A What PDG data can bring

Historically the pioneers in the deployment of PDG were large operators wishing to implement real time reservoir surveillance on a few high profile wells or field development projects. The use of PDG is increasing constantly. By 2010, however, the spread was still very unequal from one country to another and from one operating company to the next.

However the trend seems irreversible. Unit prices are falling, and reliability is increasing, and the installation cost for a permanent gauge in a new development well is now marginal compared to the overall cost of a brand new well.

When they are placed in the hole, PDG have already been sold for the sake of reservoir surveillance and the wish to know what is happening in real time. Any additional use of this data, as presented in this chapter, can be considered as the icing on the cake, although there are some additional steps to take in the acquisition, storage and retrieval of the data in order to properly fit our needs.

The interest in PDG data goes beyond the simple knowledge of pressure and temperature at any given time. The combination of the well production, when known, and this pressure data is a good candidate for mainly two types of analyses and for real time rate allocation. Fig. 13.A.1 shows a typical set of permanent downhole pressure data. The period covered is approximately three months. With an acquisition rate of one point every five seconds, this corresponds to around 1,500,000 raw data points.

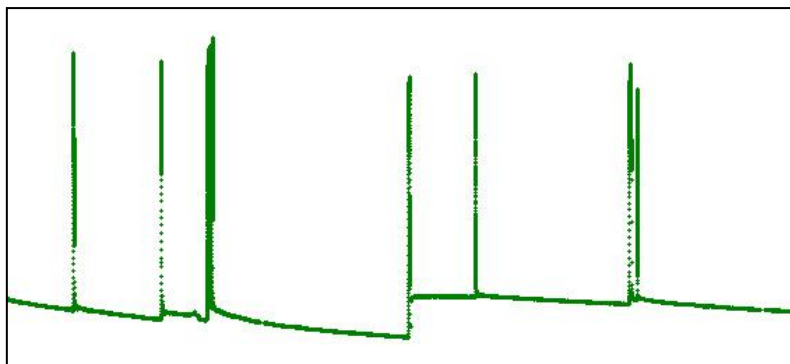
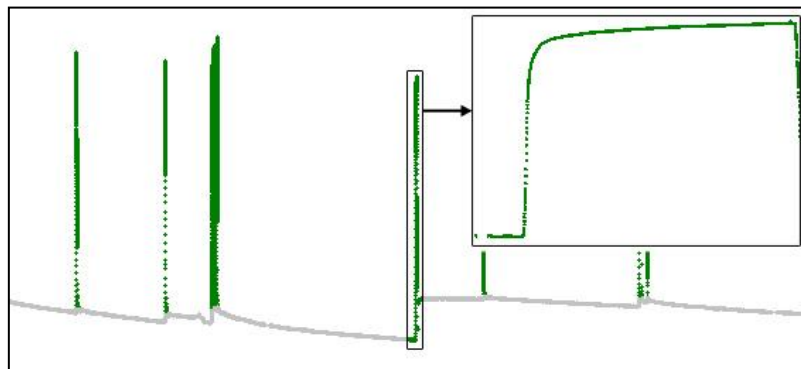


Fig. 13.A.1 – Example of permanent pressure gauge data three months of data - downhole pressure vs. time

This data carries two types of information:

Each peak in the data is a shut-in. The following figure shows an expanded version of one of these peaks. If we have a fair idea of the producing rates, and this may in itself be an issue, each peak is a good candidate for Pressure Transient Analysis (PTA). It is potentially the equivalent of a free, but not designed well test. In addition, comparing these successive build-ups in time will provide information on how the well and the reservoir within the well drainage area have evolved between these build-ups.

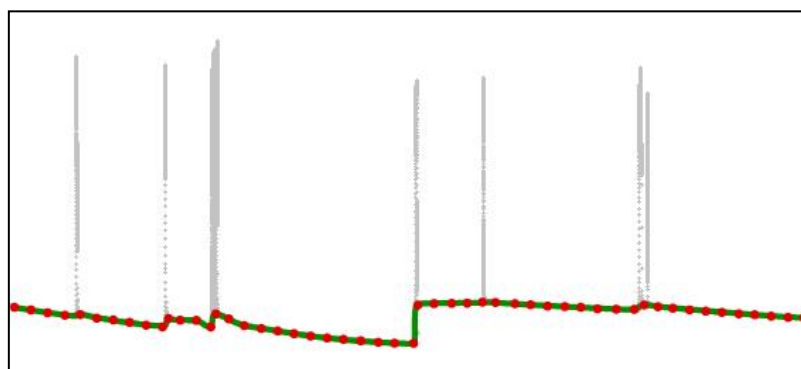
In order to get a reliable last flowing pressure and analyse the early time of each build-up we will use the smallest time steps, i.e. the highest frequency we can get, on repeated but relatively short time ranges.



*Fig. 13.A.2 – Example of permanent pressure gauge data
High frequency signal for Pressure Transient Analysis*

On the other hand, in the following figure we have ignored the peaks and focussed on the producing pressures, as a low frequency signal over the whole time range of the permanent gauge survey. These pressures, combined with the production rates, may be used for Production Analysis (PA) if, again, we have some idea of the well production.

In order to use these data, we need a low frequency extraction of the producing pressures over a relatively large time range.



*Fig. 13.A.3 – Example of permanent pressure gauge data
Low frequency signal for Production Analysis*

13.B Challenges of PDG data

The main challenge with continuous information is the enormous mass of data that is involved.

The usage of permanent gauge data presented in the previous section and developed later in this chapter is possible only because we are getting data at a high acquisition rate AND over a large time interval. If we multiply high frequency by large durations, crudely, we end up with a huge number of data points.

For an acquisition rate of every 5 seconds over a period of 3 years, we get 20 million data points per channel. Acquisition rates and durations vary, but 20 million is a reasonable geometric average, with a range (in 2010) typically between tens of millions and a few hundred million data points per gauge channel, sometimes referred to as **tags** in the storage databases. And with the life expectancy of the permanent installations increasing all the time, this number just grows to mind-boggling values.

13.B.1 Storage and access

When visiting operating companies, the following questions often generate embarrassed answers, or no answer at all. Sometimes, a fight breaks out:

- Where is your PDG data stored?
- What is stored? (acquisition rate, storage duration, interpolation, filtration, etc)
- How can I access this data right now and from here?

Answering these questions is generally half of the work. Historically, storage and access options would be decided by the people that purchased the gauges and essentially 'just' saw them as a real time surveillance tool. Getting back to ALL the raw data from the beginning of the acquisition was not really top of the agenda. But we will see in the following that this is precisely what is needed; ALL data, since the beginning, with NO prior editing.

13.B.2 Smart reduction

We need to have access to ALL the data in order to ensure that no processing has been done that could reduce the value of this data in the analysis processes. However it does not mean that we need all data for such analysis; it is the analyst that decides what data to use:

- Low frequency data (PA): Considering that rates are typically given daily, 1 pressure point per hour is more than enough. For a 10-year survey, we need less than 100,000 points.
- High frequency data (PTA): Considering we will typically find 100 or less relevant build-ups, and considering that 1,000 points extracted on a logarithmic time scale will be suitable for analysis, we need another, albeit different, 100,000 points.

So even for the largest data sets 200,000 points are sufficient to satisfy our processing needs. This is around 100 times less than the median size of a raw data set. Unlike the number of raw data, this reduced number is also well within the memory and processing capability of today's (2010) PCs.

The challenge is how to get to this reduced number of *relevant* points. The answer lies in applying a 'smart' filter that picks and selectively reduces both low and high frequency data. Then we need to be able to transfer the filtered data to the different analysis modules. The work flow is shown in the following figure.

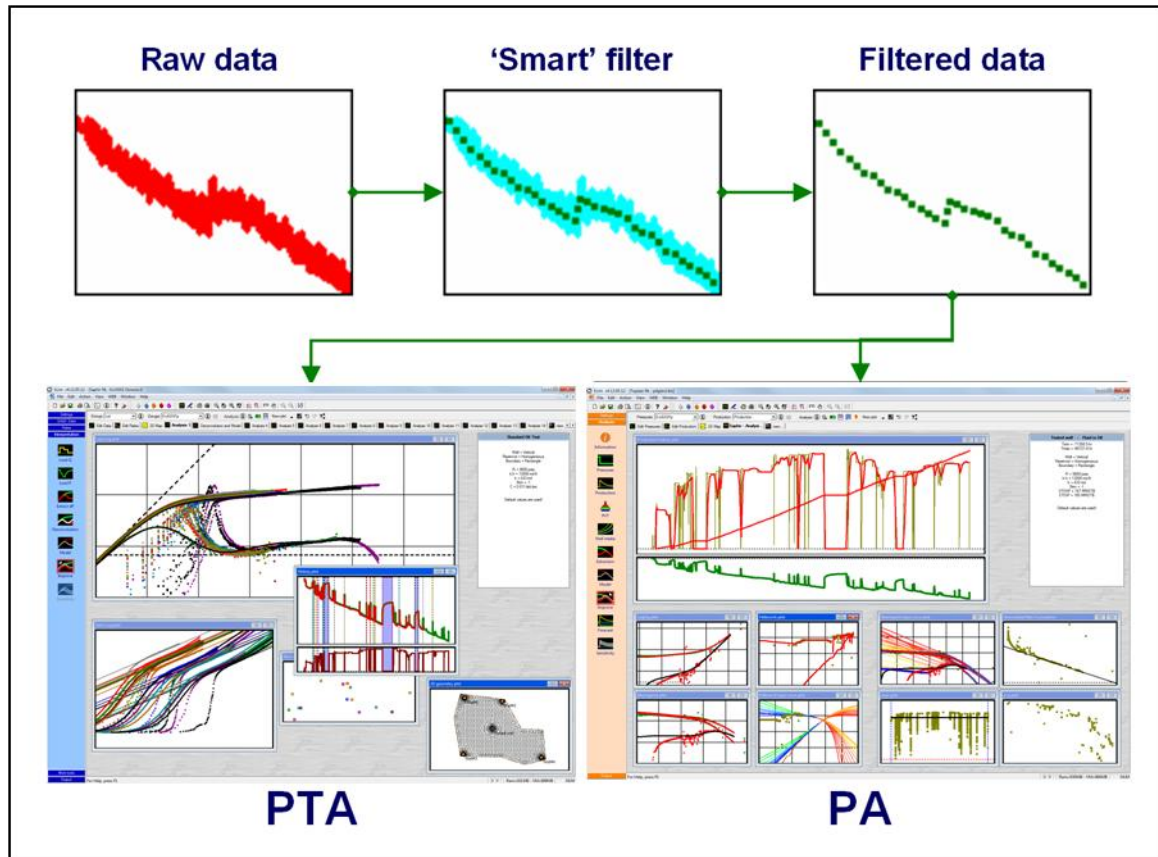


Fig. 13.B.1 – Permanent gauge data: storage, filtering and access

13.C Wavelet filtration – an overview

The main challenge in the processing of permanent gauge data was to implement a 'smart' filter that would drastically reduce the number of data points without losing either high frequency or low frequency data.

Permanent gauge data is naturally noisy. For the low frequency information, i.e. the production period, an efficient reduction requires some de-noising before the reduction in number of points. This is the typical task of a low pass filter.

The problem is the opposite when we want to keep the high frequency data. Whenever we have a shut-in, we do not want the break in the pressure response to be masked by a low pass filter. At the time of the shut-in, we want a high pass filter.

So, depending on the part of the information we are interested in, we need a low pass filter or a high pass filter. The 'magic' solution would be a filter that identifies the relevant break of high frequency data, acts as a high pass filter on these breaks to keep them intact, but acts as a low pass filter anywhere else, in order to smooth producing phase responses and allow an efficient data reduction. This must be done based on the pressure data only, without knowing, a priori, the well producing history.

This specification is successfully met by wavelet algorithms. For the engineer it acts as a filter with a threshold. Any noise below a certain level is considered as noise and is filtered out. This will be, hopefully, the case for most noisy signals during the producing phase. On the other hand, any noise above a certain level of threshold will be considered as a representative break in the data and will be preserved. This will be, hopefully, whenever the well is shut in. The break in the pressure data will act as local, high level noise.

Before we get into the (optional) theory of the next section, the below figure shows the different steps of the wavelet filtration process, from the 'user's point of view.

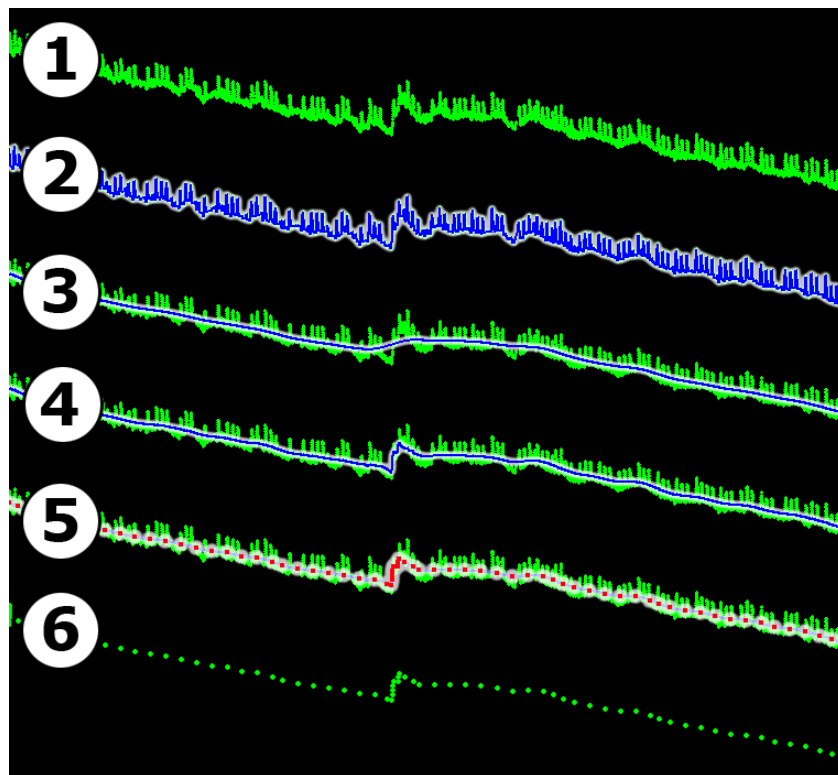


Fig. 13.C.1 – The steps of wavelet filtration

Curve 1 shows a set of raw data corresponding to 12,000 points over a period of 5 days. The noise level is high, and we see that a change in the trend occurs in the middle of the display window.

Curve 2 shows the wavelet filtered signal with a low threshold. With such a setting the significant break and a lot of noise is considered significant.

Curve 3 shows, conversely, the result with a very high threshold. All features in the response, including the break, are below threshold, and the wavelet acts as a standard low pass filter.

Curve 4 shows the result for an intermediate value of threshold that clears most of the noise but keeps the break intact. We will use this setting.

Once the correct threshold is set, we still have the same number of points but it is now possible to reduce them using simple post-filtration, which is typically a combination of time intervals and maximum pressure change.

Curve 5 in Figure above shows the suggested result of this post-filtration.

Curve 6 shows the filtered data, with only 70 points remaining.

13.D Wavelet filtration - Theory

13.D.1 Wavelet and scaling functions

Wavelet algorithms are multi-frequency processes. We will start by showing what happens on one given frequency, corresponding to a time period 'a'.

We use two basic tools: a normalized **scaling function** ϕ used to define a low pass filter, and a corresponding **wavelet function** ψ used to define a high pass filter. These functions must respect the following conditions:

$$\int_{-\infty}^{\infty} \phi(x) dx = 1 \quad \text{and} \quad \int_{-\infty}^{\infty} \psi(x) dx = 0$$

A simple example for functions ϕ and ψ is shown in the following figure. In reality the functions are a little more complex in order to avoid numerical effects, we will see this in a later section discussing wavelet processing.

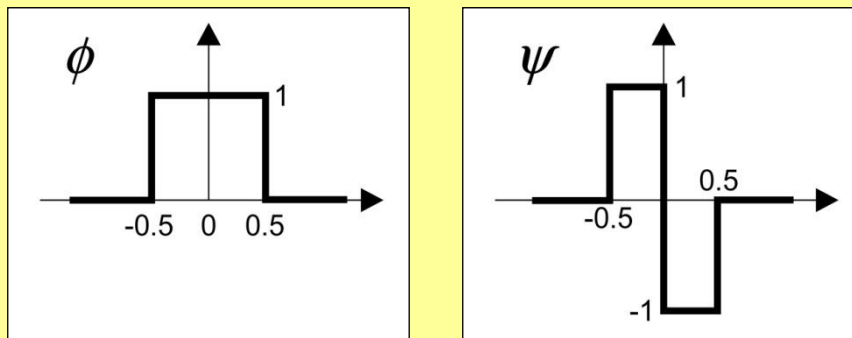


Fig. 13.D.1 – Simplest example of scaling and wavelet functions

These functions are used to decompose a given signal (our original data or some transformed data) into two component signals: the complementary transform C_a and the wavelet transform W_a , by respective convolution of the original data with the scaling and wavelet functions.

$$C_a(t) = \frac{1}{a} \int_{-\infty}^{\infty} f(x) \phi\left(\frac{x-t}{a}\right) dx$$

$$W_a(t) = \frac{1}{a} \int_{-\infty}^{\infty} f(x) \psi\left(\frac{x-t}{a}\right) dx$$

If we consider our example functions, the complementary transform $C_a(t)$ is the average of the signal f on the segment $[t-a/2, t+a/2]$. This is our 'low pass' filter.

Understanding the wavelet transform $W_a(t)$ is less immediate:

- If the signal is constant or slowly changing over the interval $[t-a/2, t+a/2]$, the wavelet transform is zero, or very close to zero.
- If the signal is random, or oscillating at a much higher frequency, the wavelet transform will also be very close to zero.
- It is only if substantial variations occur at the scale of a , for example, if the signal has a shape like ψ over this interval, then the wavelet transform will be positive or negative.

- If there is a break of the signal at time t , one can expect that the wavelet transform, whatever the considered frequency, is likely to be strongly positive (break downwards) or negative (break upwards).

One remarkable property of these transforms is that there is a numerical way to make these transformations reversible. If we decompose a signal into a wavelet transform and a complementary transform, we will be able to re-create the original signal from these two transforms by a reverse operation. So this dual transforms act as a 'projection' of the signal into two complementary spaces. This is only possible because the operators ϕ and ψ have been carefully chosen. One operator ϕ will correspond to one operator ψ , and reverse.

13.D.2 Wavelet filtration with a single frequency

The process for a single frequency is schematized in the following figure. The numerical implementation of this algorithm requires that original data are evenly sampled in time, the time interval being a .

Important: Original raw data is generally not evenly sampled. The required initial interpolation may have a large impact on the process, as any information in the raw data lost in this initial interpolation will be lost for good. This is why the frequency choice is important.

The transforms given in the equations above are replaced by numerical algorithms on discrete, regularly sampled data sets. They will not be detailed here.

The function $W_a(t)$ depends on the level of noise of frequency $1/a$ around time t . If the noise is high, or if there is a break in the data at time t , the value of $W_a(t)$ will be strongly negative or positive. We select a threshold value THR , which defines the value of W_a above which we consider the signal should be kept. We define then a modified wavelet function:

$$|W_a(t)| > THR \Rightarrow W'_a(t) = W_a(t)$$

$$|W_a(t)| \leq THR \Rightarrow W'_a(t) = 0$$

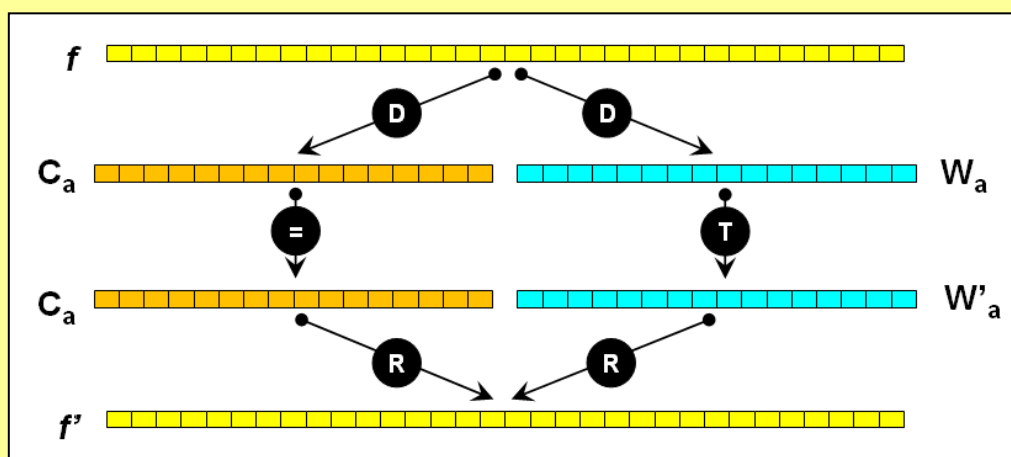


Fig. 13.D.2 – Schematic of a single frequency wavelet algorithm
 D = Decomposition ; T = Threshold ; R = Recombination

Instead of recombining $C_a(t)$ with the original wavelet transform $W_a(t)$ and arriving back at the original signal, we recombine $C_a(t)$ with the **modified** wavelet transform $W'_a(t)$.

When the noise level corresponding to the frequency $1/a$ is small, i.e. when the wavelet transform is **below threshold**, the function $W'_a(t)$ is set to zero, and after recomposition the data will have been smoothed out. When the wavelet transform is **above threshold**, the function $W'_a(t)$ is not truncated, and after recomposition the noise/break is kept.

If we had N evenly sampled data points on the original signal f , after decomposition we now have $N/2$ evenly sampled data points in each of the transforms. The total number of points remains N , but as we have two signals the time interval is now $2a$.

13.D.3 Wavelet filtration with multiple frequencies

Comprehensive wavelet de-noising is a multiple frequency process as shown in the following figure. In this example there are four such frequencies. This is a parameter that will be controlled in the filtering application.

The process must first interpolate (I) the raw data to start with a set of points C_a with a uniform time spacing a . The choice of a is discussed in a later section.

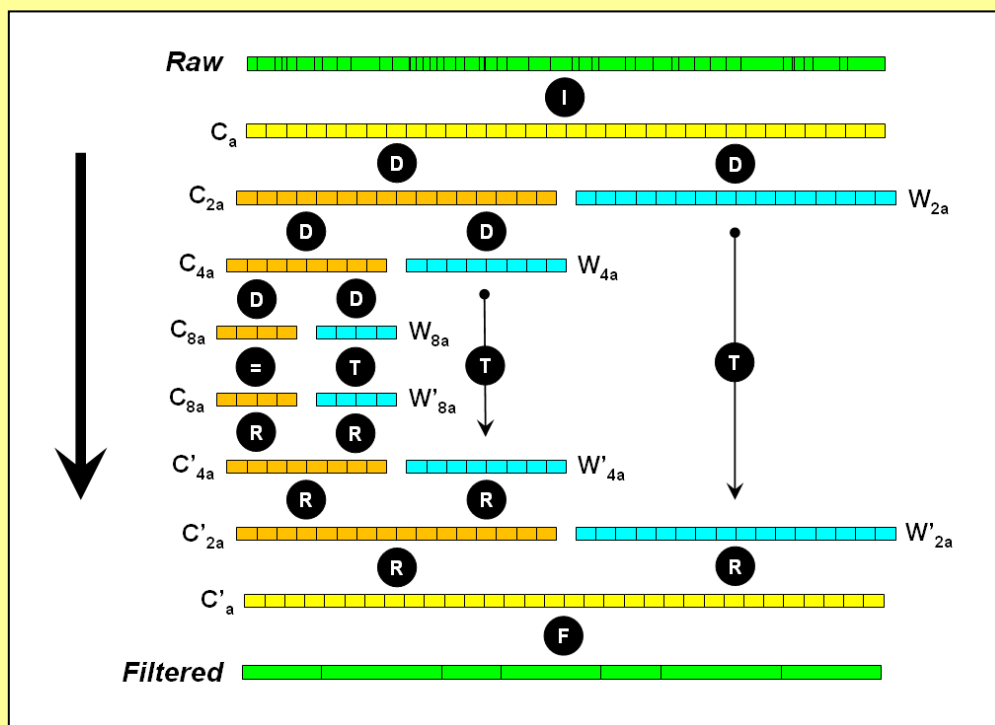


Fig. 13.D.3 – Schematic of complete wavelet algorithm
 (I) = Interpolation; (D) = Decomposition; (T) = Threshold
 (R) = Recombination; (F) = Post-Filtration

The filter will not interpolate and process ALL raw data in a single run. This would be far beyond the computing power of today's (2010) computers. The idea is to take windows of typically 100,000 to 1 million data points, and work successively on overlapping windows in order to avoid end effects.

The signal C_a is decomposed (D) into a complementary transform C_{2a} and a wavelet transform W_{2a} . The total number of points remains the same, half with C_{2a} and half with W_{2a} . The time spacing for each of these series is $2a$, and the frequency is now half the original. The signal C_{2a} is in turn decomposed into C_{4a} and W_{4a} , C_{4a} is decomposed into C_{8a} and W_{8a} , until the desired number of decomposition levels is reached. Here we will stop at C_{8a} .

At this stage, the original interpolated signal C_a was decomposed into four series: C_{8a} , W_{8a} , W_{4a} and W_{2a} , representing the same total number of points as C_a . If we were recombining these components in the reverse process, we would return to our original signal C_a .

The data is de-noised by applying the Threshold (T) to the different wavelet transforms. The new signal C_a' will be created by successively recombining (R) C_{8a} with the modified wavelet transforms W_{8a}' , then recombining the resulting C_{4a}' with W_{4a}' , and finally recombining the resulting C_{2a}' with W_{2a}' .

We now end up with the same number of points, but this time large sections of the data, the producing part, will be smoothed, and this will allow data elimination with simple post-Filtration (F).

In order to avoid any fatal improvement due to the filtration, the process will typically store the break points, i.e. the points at which the wavelet functions had exceeded the threshold, and instruct the filtration process to keep them no matter what.

On a typical set of permanent gauge data, the ratio between the number of raw data points and the number of filtered points will range between 100 and 1000.

13.D.4 Parameters controlling wavelet processing

The functions ϕ and ψ presented in Fig. 13.D.1 are the simplest case and were presented to illustrate the process. Functions used on real data are smoother in order to avoid numerical effects. The following figure shows another set of functions, more likely to be used on real life data. Similarly, the threshold algorithm presented in the wavelet function is too abrupt. Threshold filters used in real life are continuous.

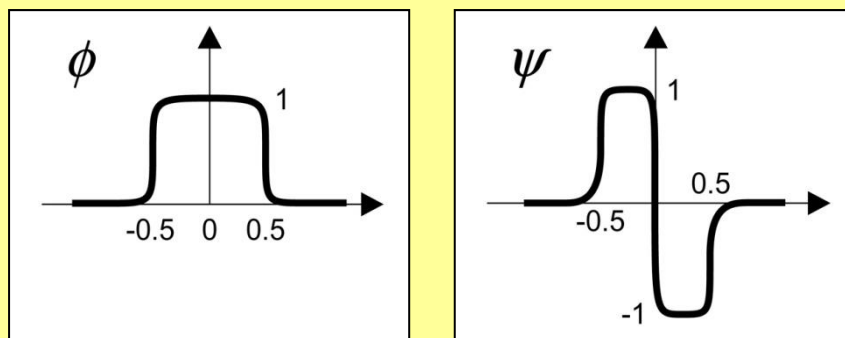


Fig. 13.D.4 – Real scaling and wavelet functions

The parameters that define the wavelet process may be automatically set or controlled by the engineer performing the filtration. In the following list we specify the parameters that will generally be automatic or controlled, and the following sections will describe the influence of the controlled parameters.

- Scaling and wavelet functions ϕ and ψ (automatic)
- Starting data frequency $1/a$ (controlled)
- Number of decomposition levels (automatic)
- Choice of threshold function (controlled)
- Threshold value (controlled)
- Post-filtration parameters (controlled)

13.D.5 Selection of the initial time step / frequency

The initial time spacing a is very important. $1/a$ will be the highest frequency handled by the wavelet algorithm, and behaviour with a higher frequency will be lost in the initial interpolation.

Selecting the smallest time interval between consecutive raw data is not a solution as acquisition times are not regular, and it will not guarantee that the raw data points are taken.

The highest possible frequency, i.e. the smallest possible a , (e.g. the resolution of the time information) does not work either as the amount of interpolated data would be unmanageable.

Filtration with an initial interpolation sampling of one tenth of a second would guarantee that we will not miss anything, but it would involve one or several billion points.

Furthermore, starting with a very high frequency has a major drawback. For each additional level of decomposition there is only a doubling of the time stepping. As the number of these decomposition layers is limited, we might miss the frequency of the real noise.

The solution is to select an initial time stepping that fits the engineer's needs. A time stepping of 1 second will work but will involve CPU demands that may not be worth it, and the de-noising of the production data may be insufficient. If the interest is not at all in high frequency data, a time step of one minute will be more than enough and very fast. When one wants to pick the high frequency at a reasonable expense, a time step of 10 to 20 seconds will be a good compromise. The exact point of shut-in may not be spotted exactly, but still the data will be usable for pressure transient analysis, and it will be possible to return to the raw data and selectively reload specific sections of interest.

13.E Wavelet filtration - Practice

The following wavelet filtration work flow is presented as it is implemented in Diamant or Diamant Master; the KAPPA workstation and client / server solutions dedicated to the processing of PDG data. At this stage we do not focus on where the raw data comes from, how it is accessed and where the filtered data is stored. We only focus on the filtration itself and the kind of interface required for the engineer to properly control this process.

The first thing that one has to do when 'connecting' to a PDG data tag is to have an idea of what the data looks like globally. Having a quick preview of the data seems to be an obvious task, but this is not the case when one has to connect to 300,000,000 data points on a slow server. To do this, the process will request, when possible, the total number of data points and request to send one data every n (typically 1,000 to 10,000) in order to get a fast preview of a few thousand points. Such a preview is shown below.

This may be the time for a surprise. In many cases the data were stored and never looked at again. Here are some of the typical, irreversible problems that may be encountered at this stage:

- No data! Data was stored over time, never checked and we only have zeros.
- Buffered data! Only the last, say, three months are present. The data historian was programmed to only buffer the data for so long. Data older than the buffer were irreversibly erased or massively decimated.
- Bad data! Data are very noisy and scattered and hardly usable.
- Massaged or pre-filtered data! In the interest of saving storage or data transmission bandwidth the data has been filtered from one per second to one every fifteen minutes.

Other issues may be detected and addressed:

- Slow access! The time to get this initial preview takes forever. One may analyse the process to get the data or improve the bandwidth between the machine and the data historian. There may also be too many simultaneous accesses to the same historian. This problem will generally be addressed by mirroring the data from the historian to the engineer's machine (Diamant local) or the dedicated server (Diamant Master).
- Apparently buffered data! On the face of it this is the same symptom as the buffered data, except that fortunately, in this case, the data is stored. The problem is that the setting of the data historian is such that older data is not accessible to the client unless the historian setting is changed.
- Partly irrelevant data! For whatever reason there were some times when the gauge failed, or was turned off, or for whatever reason gave irrelevant readings. The engineer may then wish to graphically select a data range out of which data will just be ignored.

After the preview, and unless an irreversible problem was detected, the engineer may proceed to set the wavelet filter and post-filtration. At load time the wavelet will be applied on consecutive packs of data of a given buffer size. The first pack of points, within the load range, is loaded and displayed. The typical size of a buffer will be 100,000 points but this can be changed by the engineer. 100,000 points corresponds to six days of data stored once every five seconds.

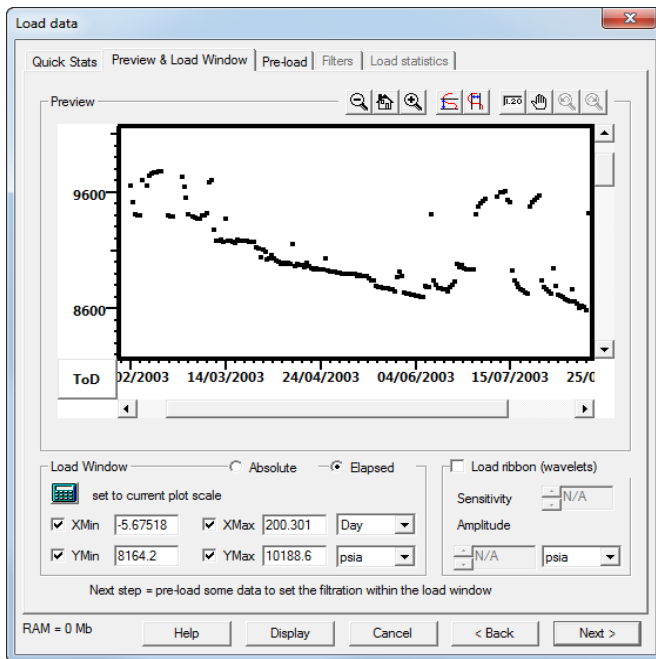


Fig. 13.E.1 – Data preview

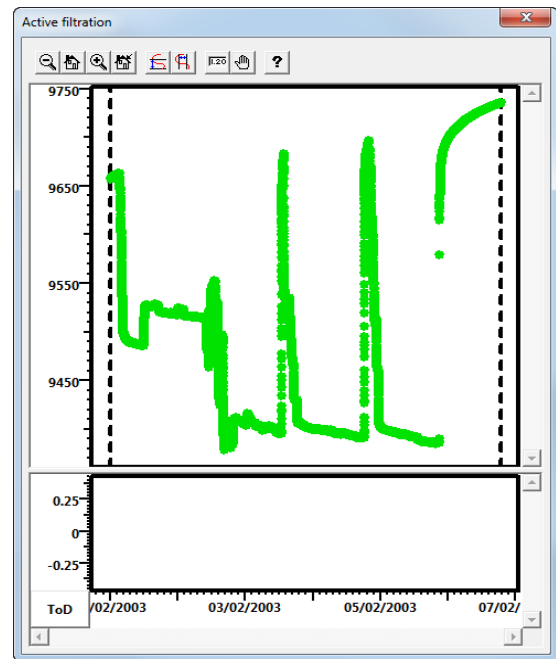


Fig. 13.E.2 – Selecting the first buffer of points

The engineer will then specify the wavelet and the post filtration. At this stage it is the engineer's decision to set the different parameters, zoom on some parts of the data (shut-ins, noisy sequences, etc) in order to ensure that the data reduction does not affect the information we want to keep in the de-noised signal. An example of wavelet setting is shown below. The process will also show the difference between the original data and the de-noised signal.

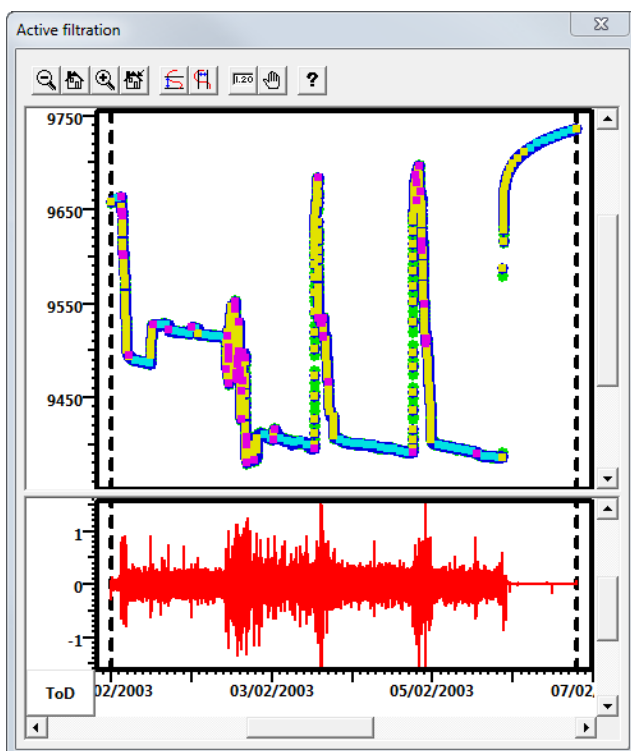


Fig. 13.E.3 – Setting the wavelet filtration

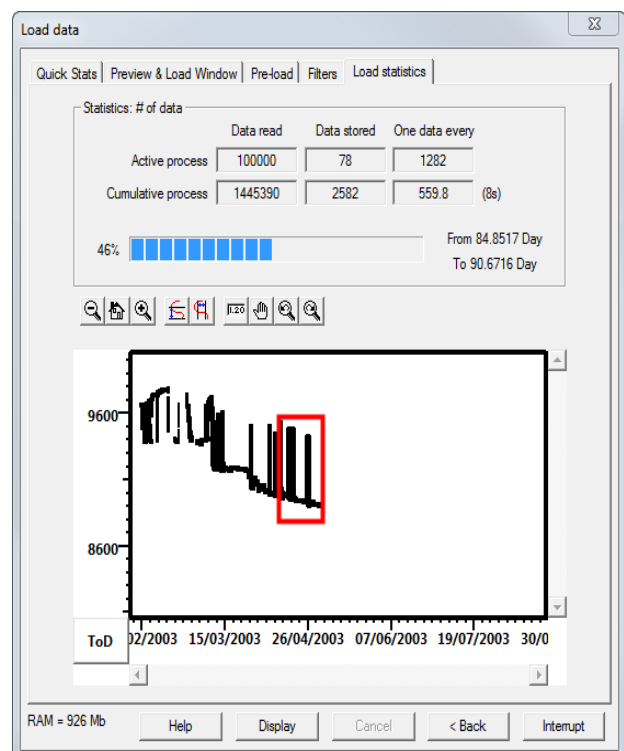


Fig. 13.E.4 – Global view of the load

Once the engineer is satisfied by the filter the real load can start. The process takes raw data by packs corresponding to the size of the buffer. In order to avoid tail end effects, the different packs will overlap and the first / last de-noised points will be systematically ignored. The process will typically show the global load, i.e. where the current buffer stands in the overall data history and a local view of the buffered data with both raw and de-noised data. At this stage the engineer may stay and watch. If the data is locally mirrored, the process takes around one second of CPU per buffer of 100,000 points.

During the load the engineer may realize that the filter setting is incorrect. The load can be interrupted and the settings modified and tried. Once the setting is modified the load can be restarted again, or the new setting may take over the old setting from a time selected by the engineer.

Once the load is over, i.e. when all data currently stored in the data historian have been treated, the process stops and statistics are displayed.

At this stage, the application has maintained a persistent link with the data historian and will know how to get the new incoming data. With a time set by the engineer, typically one week, or on the engineer's direct request, the same process will re-establish connection to the data historian, get the new raw data and apply the wavelet filter to this new data to increment the filtered data set. At this stage the engineer probably has better things to be getting on with as the refreshing and updating of data becomes an automatic process.

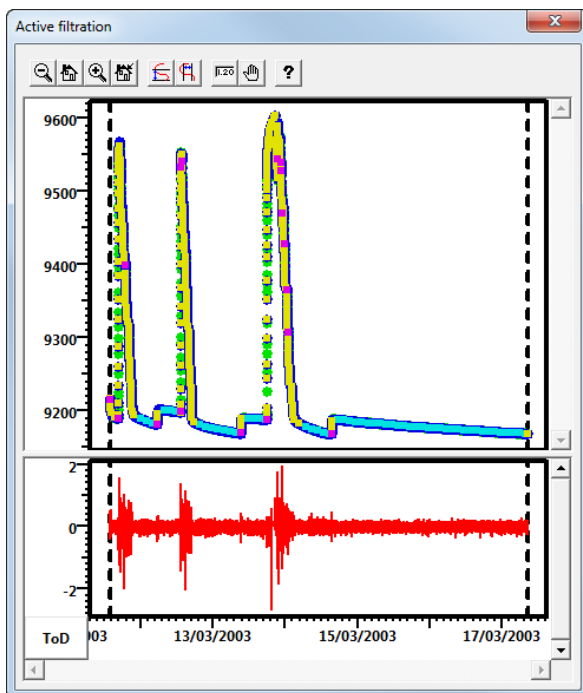


Fig. 13.E.5 – Local view of the load

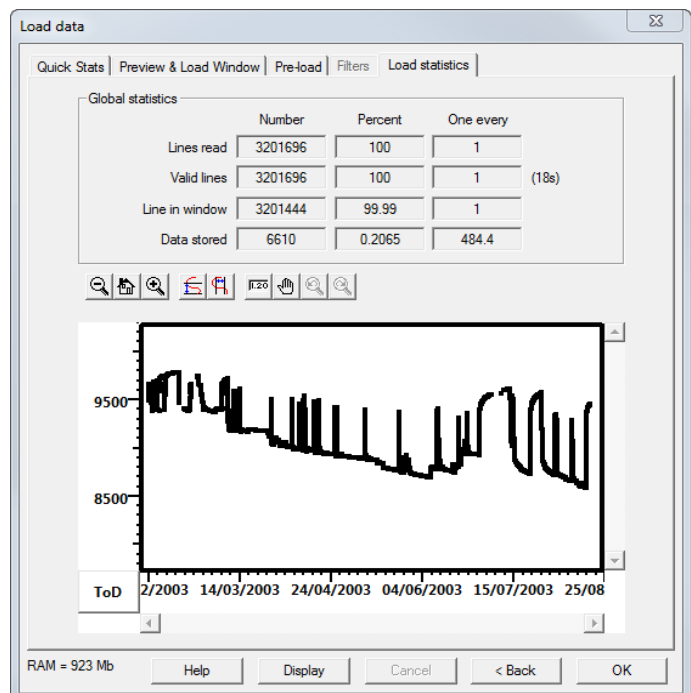


Fig. 13.E.6 – Load finished – Display and stats

13.F Pressure Transient Analysis of PDG data

The figure below shows PDG pressure and flowrates data coupled over several months of production, after filtration in Diamant. The rate history originates from another permanent measurement and was simplified. Buildup periods were defined using the automatic buildup detection functionality available in Diamant local or Diamant Master.

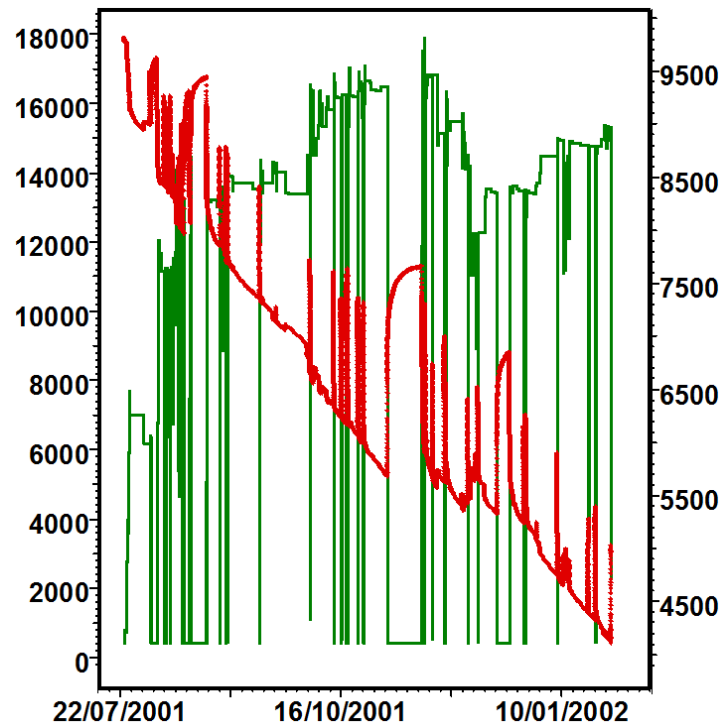


Fig. 13.F.1 – Several months of PDG data - 20 build-ups

Most aspects of Pressure Transient Analysis developed in this document are relevant to interpret buildups recorded by PDG i.e.: there is nothing specific in the methodology itself.

However, the process will have to be adapted to the origin of the data, its volume and its signature. The main differences with a standard well test are the following:

- In most cases, the rate information is the daily reallocated production. Rates are generally not synchronized with pressures. Though it will not be detailed here, with rare exceptions the creation of the rate history will be the main source of trouble after the link with the data historian and the filtration is established. Furthermore, it is now possible to perform the synchronization automatically using Diamant, in case that this might be an issue.
- There are not one or two shut-ins, but typically 20, 50 or more. Because no engineer will have a spare three months to interpret this data, productivity tools have been developed to process all the buildups in a single work flow.
- Many of these shut-ins are 'free', however they are rarely designed on purpose: they can come from unscheduled automatic safety shut-downs of the wells, well operations or well maintenance. Some of the shut-ins will be too short to carry any relevant information, or they will follow a production phase that may not be stabilized and for which we may not have any rate value. As a consequence, only part of the recorded build-ups will be valid and useable.

- The shut-ins are spread over the life of the well, and one cannot assume that the well model, or at least the skin factor, will be constant throughout PDG recordings. However, the succession of buildups will be an opportunity to study the evolution with time of the well productivity, in particular the skin.

The loaded data is sent from the data module (Diamant Master) to the PTA module (Saphir) by drag-and-drop or transferred seamlessly by a click of the mouse. All build-ups are extracted and shown on the loglog plot. Typically, an option will allow the engineer to select only build-ups of a certain minimum duration. The resulting history and loglog plots are illustrated below.

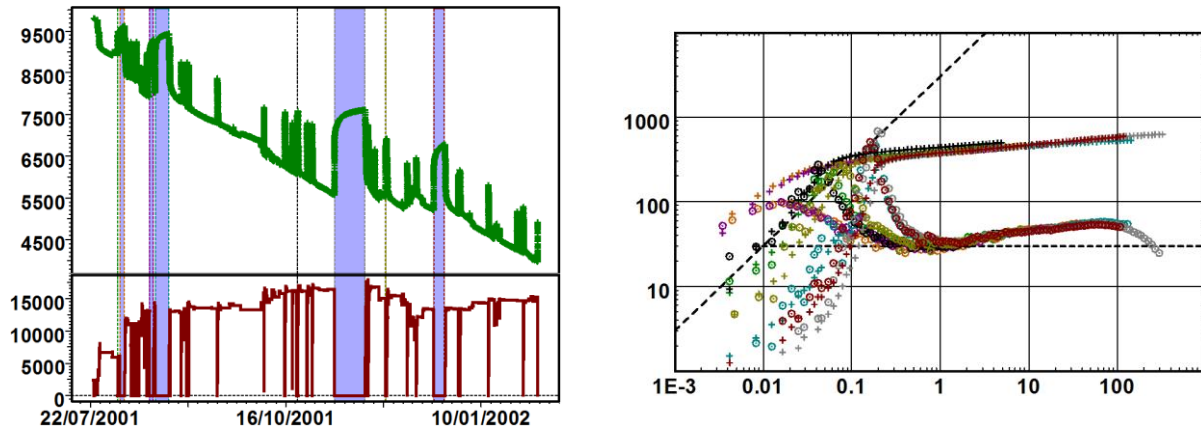


Fig. 13.F.2 – Transfer to PTA software and extraction of the build-ups

The main problem when obtaining 20 to 100 build-ups, is that we certainly do not want to extract and interpret all of them, one after the other. In order to face this problem (too much data!) we need to use productivity tools that will run statistics and qualify the build-ups on which we are ready to spend some time.

One 'low tech' way to do this is to return to IARF (yes, the old stuff). An example of this method is, on the loglog plot, to select the time of stabilization of the majority of the derivatives and draw a series of semilog straight lines from this. An option could be to set a vertical range of acceptable permeabilities, only keep the build-ups which calculated k within this range, then run a global regression where the unknown is one single value of k and one skin value per build-up. The resulting straight lines and evolution of skin in time is shown below.

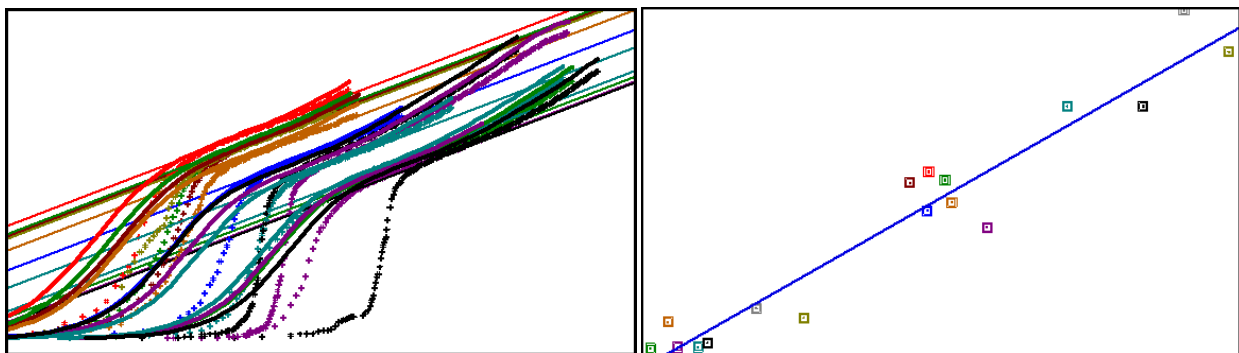


Fig. 13.F.3 – Multiple line analysis with the same k (left) and plot of skin vs. time (right)

Another way to use this information is to select consecutive quality build-ups that tell, more or less, the same story. We can then use recent work on deconvolution to end up with a response that will be longer and may provide more information on the reservoir boundaries and/or the drainage area of the well. This tool must however be used with care. The extracted build-ups and deconvolved responses are shown below.

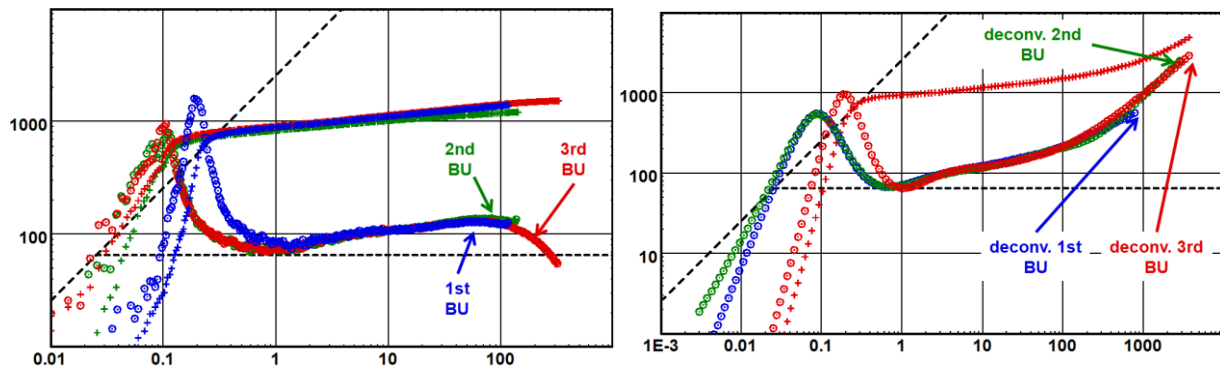


Fig. 13.F.4 – Extraction of three build-ups and simultaneous deconvolution

Once the engineer has focussed on a few build-ups of interest, it may be wise to return to the raw data and reload some of these. After all, what we have loaded so far is the result of a careful but not fool proof filtration. Because the data module (Diamant Master) maintains the link with the data historian, it may be possible to re-visit this raw data and, for the time range, corresponding to the build-ups of interest, reload the raw data with a different filter or none at all. The originally filtered data will be replaced by the reloaded data on this time range only. New data will still be loaded with the default wavelet setting.

The original filtered data and the reloaded data are compared in the figures below. In most cases, the wavelet filtration will not have affected the response and could have been used for analysis, but the advantage of the reload is that we are now absolutely sure the signature was maintained.

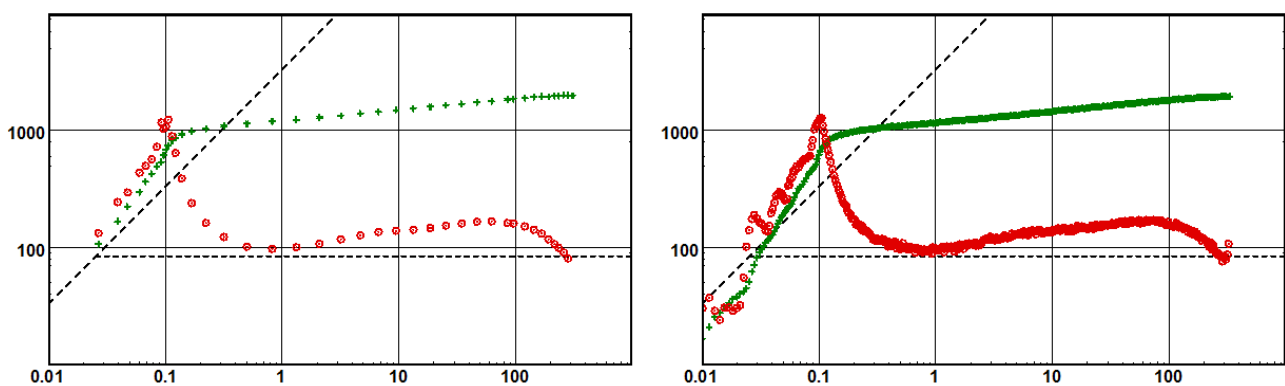


Fig. 13.F.5 – Partial reload to repopulate a build-up with original data

13.G Production Analysis of PDG data

The data presented in the section on 'Pressure Transient Analysis of PDG data' can also be transferred to the Ecrin PA module (Topaze) in order to perform Production Analysis. The result of this drag-and-drop is shown below. When the producing rates are transferred, the cumulative production is also calculated.

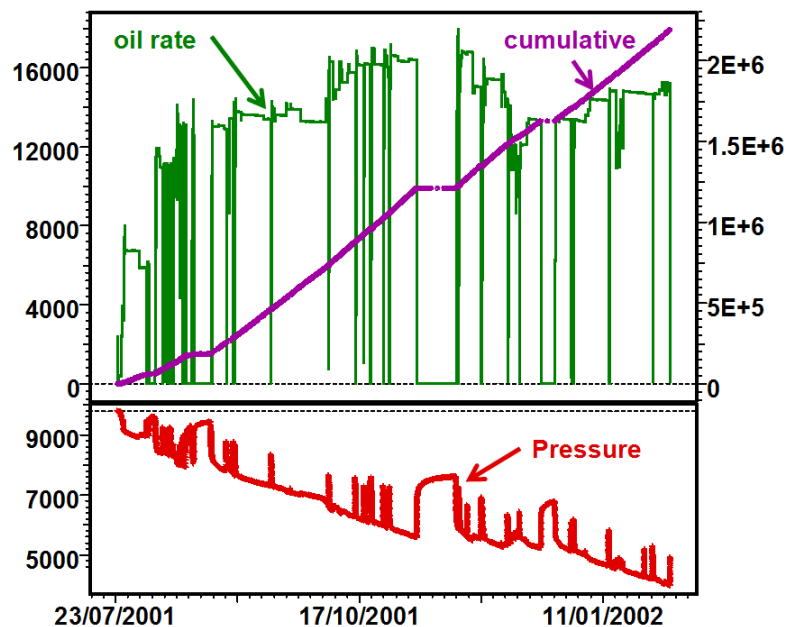


Fig. 13.G.1 – Production Analysis history plot

Traditional analysis techniques, using type-curves (e.g. Fetkovich) or straight lines (e.g. Arps) are based on the assumption of a constant pressure production. This is the 'old stuff' described in the chapter Production Analysis. Just looking at the above figure it is clear that the constant pressure assumption is rarely valid; for any practical purpose the traditional (old) methods are not very useful. There is no way to select a reliable curve match in the Fetkovich type curve plot or draw a reliable decline in the Arps plot (there is no decline).

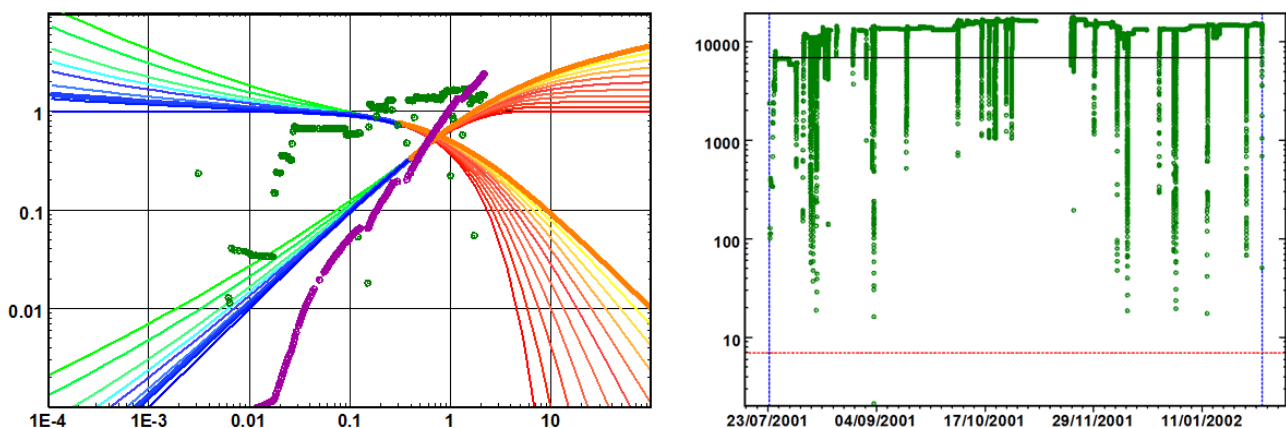


Fig. 13.G.2 – Fetkovich type-curve and Arps plot

The next step in Production Analysis is the use the modern tools that also takes into account the pressure history. The loglog plot, showing rate normalized pressure, and the Blasingame plot, which plots the productivity index, can be highly scattered as they plot against material balance time, see illustrations below. The models, which are plotted as continuous lines, will jump back and forth when the rate changes. The diagnostic capability is limited as we are essentially matching a cloud of measured points against a cloud of simulated points.

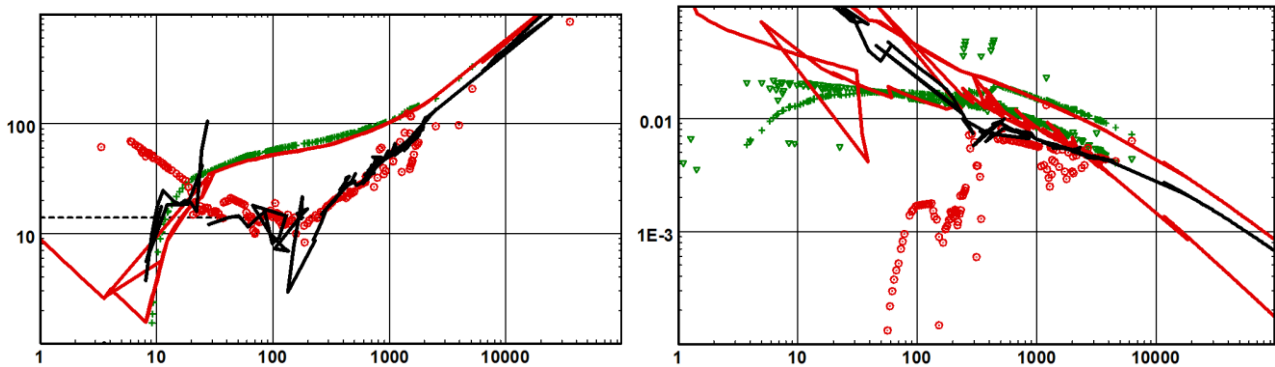


Fig. 13.G.3 – Loglog and Blasingame plots with model 'matching'

Therefore, in the majority of cases the only diagnostic tool will be the history plot, and the goal will be to globally history match the data (see below). Forecasting of the well performance from an anticipated producing pressure is also illustrated below. To improve confidence in the process it is always recommended to use the models found in the PTA of the buildups and constrain the PA model with that model, eventually integrating the evolution of skin with time.

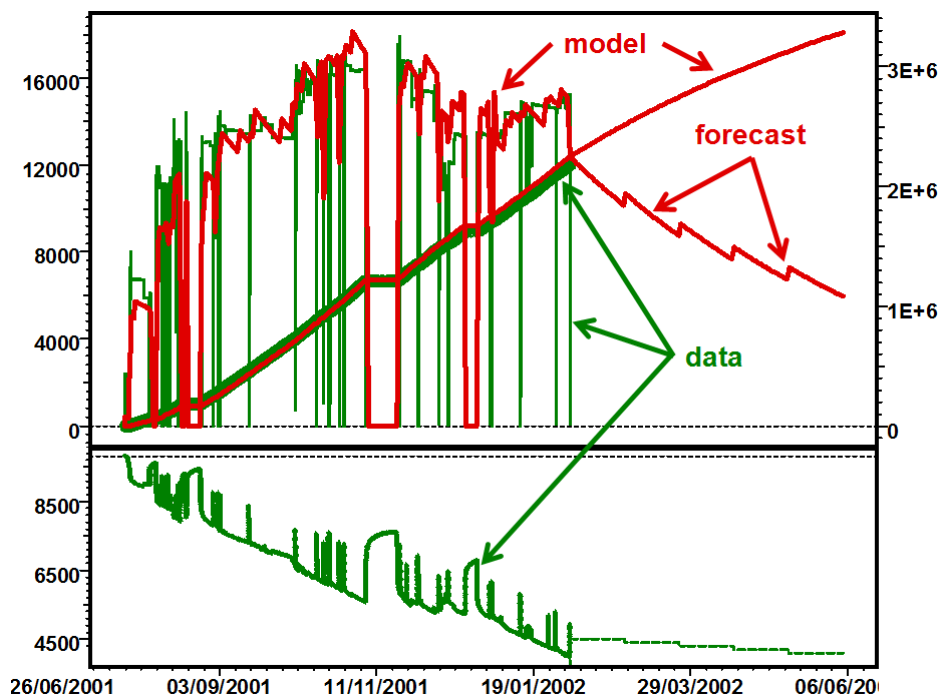


Fig. 13.G.4 – History match and forecast

13.H Applications and data flow

This section is very software related. However, even if you are not an ECRIN user it has generic interest as it describes the problem our technical group encountered in implementing PDG data processing. This integration took place in a single environment (Ecrin). This grouped, in its original version, three components; a PDG module (Diamant), a PTA module (Saphir) and a PA module (Topaze). The goal of the initial version of this integrated environment was to get together the three aspects of the PDG data processing described in this chapter. In the integrated environment, filtered data are transferred between the PDG and the PTA/PA modules by single drag-and-drop or using various other internal options. In the next session we will refer to PDG, PTA and PA processes / modules in order to avoid repetition of commercial software product names. We will also refer to workstation solution when the PDG process is performed by Diamant in Ecrin, and to a client / server solution when the process is performed on a dedicated machine in a shared environment (Diamant Master).

When this integrated environment was released and tested on a few pilot sites, there was one bit of good news and two bad. The good news was that this process was exactly what operators needed to face the challenge brought by PDG data. However we quickly faced two major issues: the poor access to the data historian and the lack of sharing of this process within a workgroup.

13.H.1 Accessing the historian: Workstation solution

The historian databases in which PDG data are stored were not designed to provide fast access to, typically, 30 million data points. Even sequential access is poor. It is even worse when a process needs to navigate 'randomly' within the data.

The wavelet processing and filtering can handle 100,000 data points per second. The ability of a data historian to deliver the points will be typically 100 to 1,000 times less.

One of the first adaptations of our workflow was a mirroring of the raw data. This is sequential and is done, once for all, with only incremental loads on a daily or weekly basis. The data is mirrored using a storage option in order to have fast and random access to the raw data, using a direct binary access format sped up by an indexing that have immediate access to the first data of every calendar day.

The workflow is described in the following figure. There are distinct processes:

- Data mirroring: The engineer connects to the right tag and the mirroring starts as a background process. Because there may be several gauges involved, the mirroring will cycle in an infinite loop on the different gauges until the end of the tags is reached. When the end is reached for a given tag, the mirroring process will re-connect and update the mirror on a timing controlled by the engineer.
- Data filtering: When there is enough data in the mirror to start working on it, typically 100,000 points, the engineer may define the wavelet algorithm and post-filtering according to the process described in section Wavelet filtration - practice. The filtering is executed until the end of the mirror is reached. Once this is done the process will return to the mirror on a timing controlled by the engineer (typically it will require 100,000 more points) and filter the next pack of data.

- PTA and PA: By drag and drop the filtered data is sent from Diamant to the Saphir and Topaze modules for analysis.
- Partial reload: When a build-up is selected, the engineer can, from Diamant, return to the mirrored data and replace a range of filtered points by the original points, or filtered data with a more refined setting.
- Storage: While mirrored data are stored in the dedicated BLI files, all the rest, including the serialization, is stored in a dedicated Diamant file.

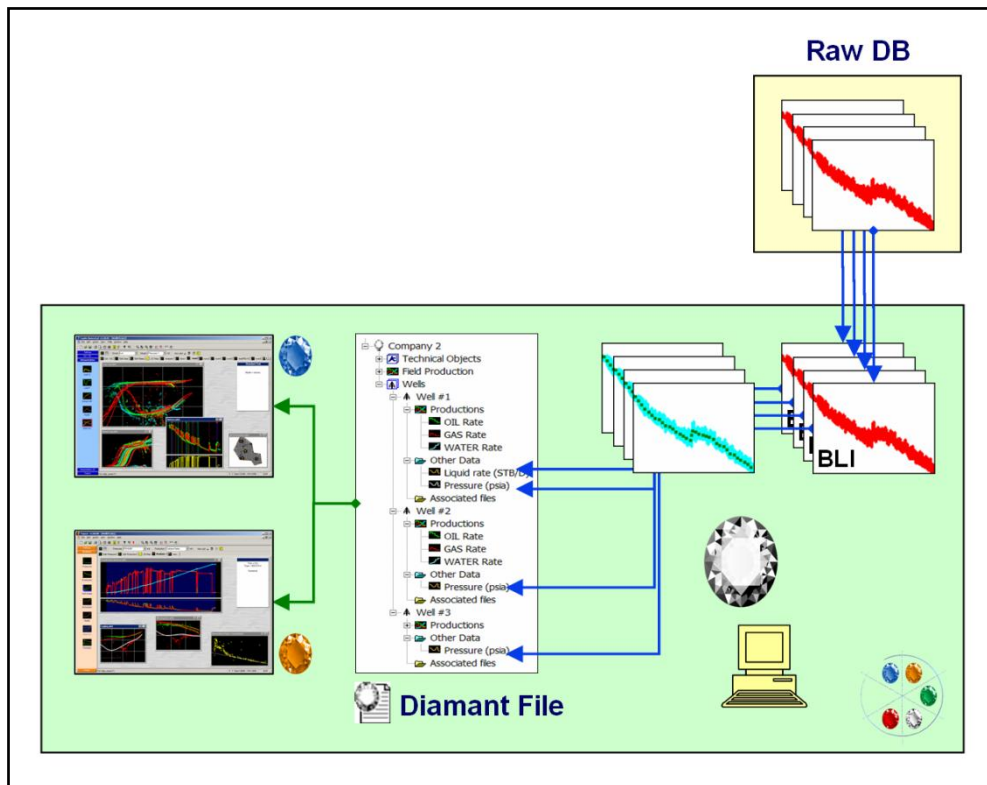


Fig. 13.H.1 – Workstation version of the PDG work flow

The workflow of the workstation solution turned out to be satisfactory in the case of relatively small structures where only a few engineers are involved in this process. However, in the pilot tests performed by large operators very serious issues pointed to the limitations of a workstation solution:

- The result of the filtration was not shared within a workgroup.
- The resulting filtered data were stored in KAPPA proprietary format the required KAPPA application to read. There was no export to third party databases.
- Each engineer would have access to the data historian, considerably increasing its work load.

13.H.2 Sharing data within a workgroup: Client/Server solution

In order to address the limitations of the workstation solution, a Client / Server solution was implemented under the name Diamant Master. The workflow is described in the following figure.

The solution runs on a dedicated server that is continuously mirroring and filtering the data. Export to a third party database allows filtered data to be permanently shared and accessible to third party applications. Filtered data and other objects are stored in a local database and are accessible and may be shared by all engineers. Mirroring is done only once for each gauge. A given gauge may be subject to several filtering options, but the result is also shared.

Some engineers, given the privilege, may be entitled to mirror tags and create new filters. Others will just take the result of the filtration and drag-and-drop into their analysis applications.

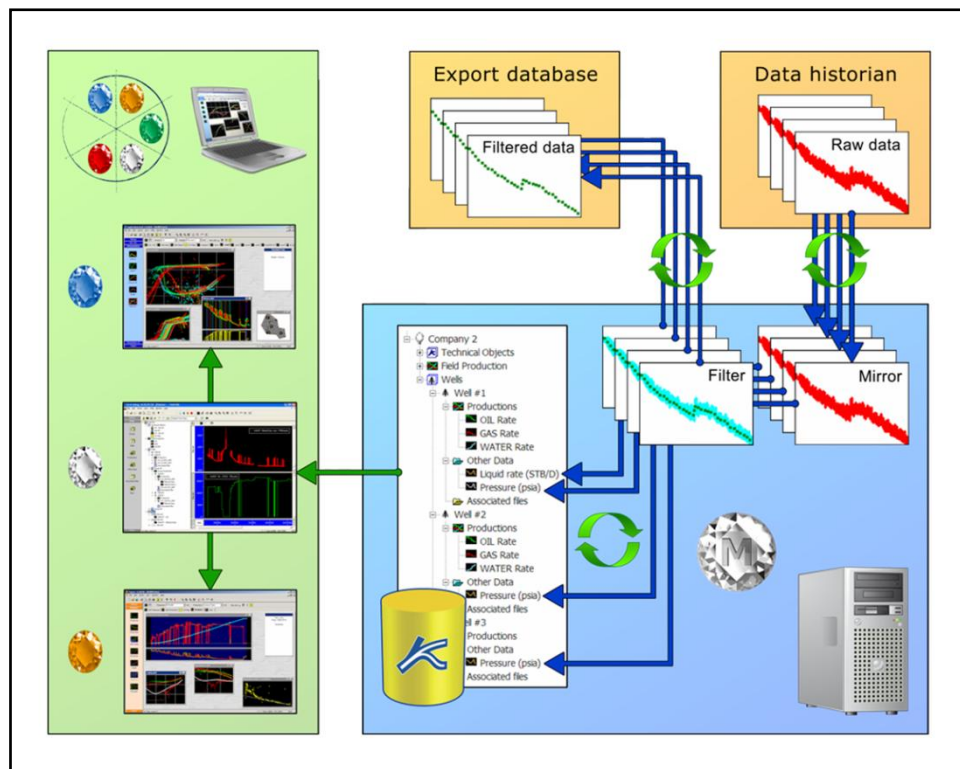
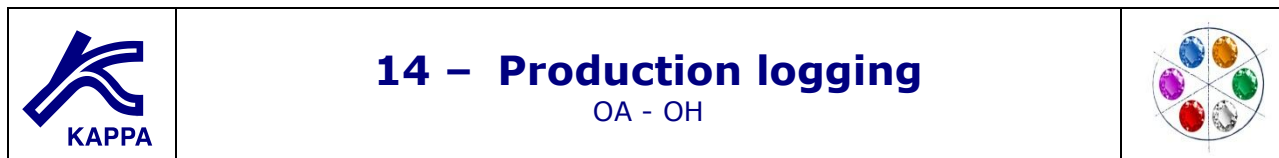


Fig. 13.H.2 – Client / Server version of the PDG work flow



14.A Introduction

This chapter is not an exhaustive manual on the interpretation of Production Logs (PL). It does not go into as much details as what is done for PTA and PA. However it summarizes pretty well the history and current status of the methodology, and how PL Interpretation integrates in the analysis of Dynamic Data.

The first production logs were temperature surveys run in the 1930's. The first spinner based flowmeters appeared in the 1940's. They were complemented by fluid density and capacitance tools in the 1950's. Together with some PVT correlations and Flow Models, these were the elements required to perform what we will call today a 'classical' multiphase interpretation.

The first probe tools were introduced in the 1980's. Although they acquired local measurements at discrete points across the borehole cross section the initial objective was to reduce the local measurements to a normal pipe averaged value. In the late 1990's, these probes were packaged into complex tools that began to measure the velocity and holdup distributions across the pipe in order to address the challenges of understanding the flow in complex, horizontal, near horizontal wells.

PL interpretation was too long overlooked by the Industry. It is not part of a standard formation in Petroleum Engineering departments. To our knowledge only Imperial College in the UK has an education module dedicated to PL. With a few noticeable exceptions most oil companies used to consider that PL was a simple process of measuring downhole rates. Specialized interpretation software was developed and used by Service Companies to process the data, either on-site or in a computing center. This situation changed in the mid-90's, when commercial PL software became more accessible within the industry, and oil companies began to realize that PL Interpretation was, indeed, an interpretation process and not just data processing.

PL is an in-well logging operation designed to describe the nature and the behavior of fluids in or around the borehole, during either production or injection. We want to know, at a given time, phase by phase and zone by zone, how much fluid is coming out of or going into the formation. To do this the service company engineer runs a string of dedicated tools:



Fig. 14.A.1 – An example of tool string

PL may be run for different purposes: monitoring and controlling the reservoir, analyzing dynamic well performance, assessing the productivity or injectivity of individual zones, diagnosing well problems and monitoring the results of a well operation (stimulation, completion, etc). In some companies the definition of PL extends up to what we call Cased Hole Logging, including other logs such as Cement Bond Logs (CBL), Pulse Neutron Capture Logs (PNL), Carbon/Oxygen Logs (C/O), Corrosion Logs, Radioactive Tracer Logs and Noise Logs. In this chapter we will focus on Production Logging per se, and explain the main methods to interpret classical and multiple probe Production Logs.

14.B What Production Logging is used for

PL can be used at all stages of the well life, during the natural production of the well, at the time of secondary or tertiary recovery, or when using injection wells.

It is the authors' recommendation that PL be run at early stage of the life of the well, in order to establish a baseline that will be used later when things go wrong. This is generally done when PL is identified as a necessary reservoir engineering tool (for example in extremely layered formations), otherwise it will be a hard sell to Management.

Too often Production Logs are run when 'something' has gone wrong...

At the end of a successful interpretation, the PL engineer will have a good understanding of the phase-by-phase zonal contributions. When multiple probe tools (MPT) are used this will be complemented by very good looking tracks describing the areal flow.

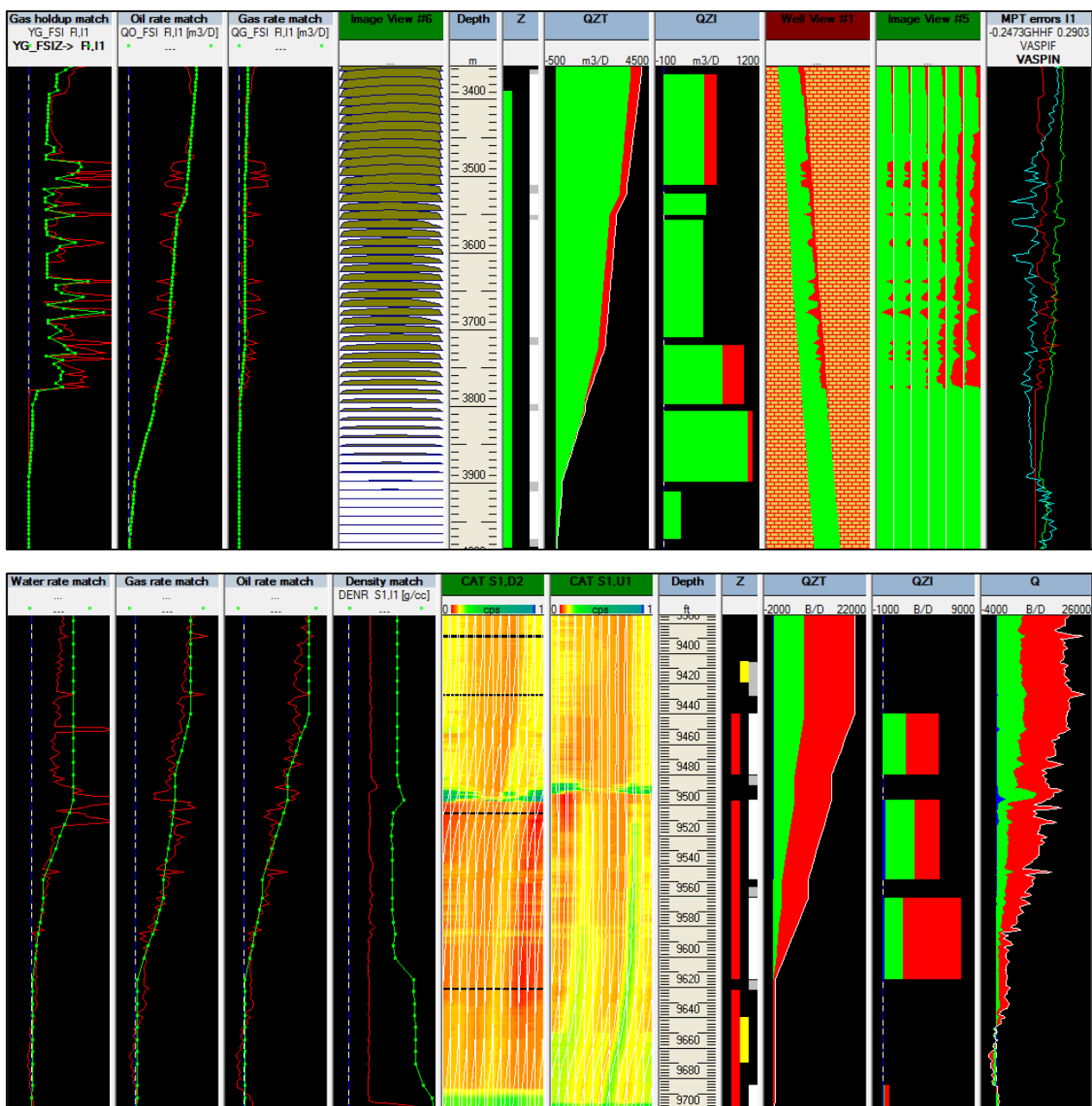


Fig. 14.B.1 – MPT interpretations in Emerald (FSI top and MAPS bottom)

PL allows the qualification and /or the quantification of a certain number of operational issues: Formation cross-flow, channeling of undesired phases via a poor cement, gas and water coning, casing leaks, corrosion, non-flowing perforations, etc.

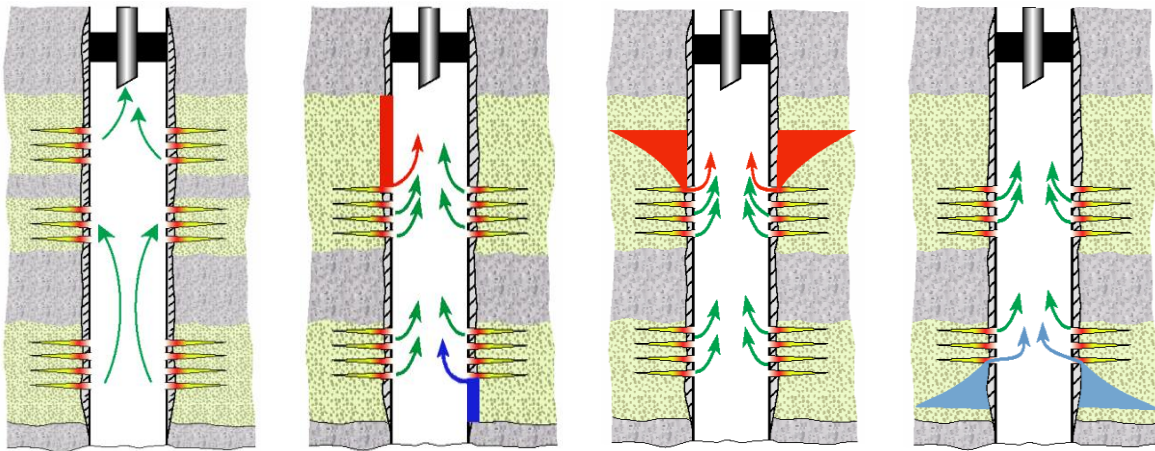


Fig. 14.B.2 – Examples of usage: Crossflow, Channeling, Gas Coning and Water Coning

Production Logging can also be used to identify fracture production and early gas or water breakthrough via high permeability layers. During shut-ins the movement of a water or oil column can also be identified.

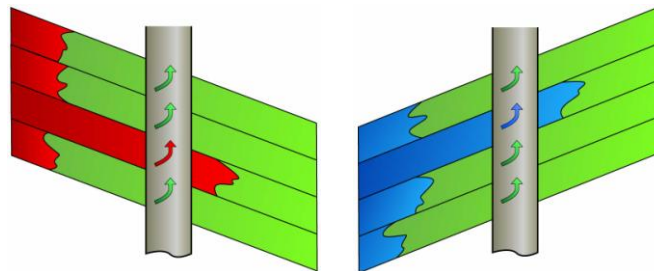


Fig. 14.B.3 – Early gas or water breakthrough

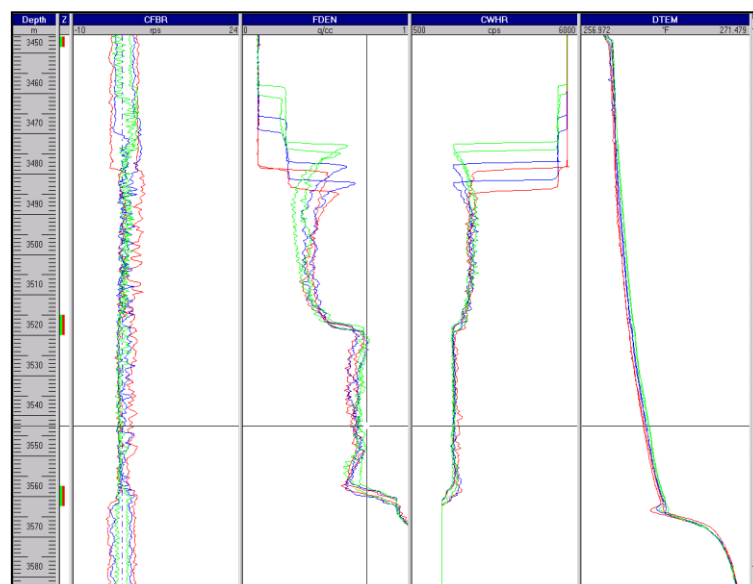


Fig. 14.B.4 – Rise of a water column during a shut-in

14.C Classical Production Logging Tools

The schematic of a typical PL job is shown in the figure below, left. During a stabilized flow period (production, injection or shut-in) the production logging tool string, hanging on a cable controlled by a logging unit, is run up and down in front of the contributing zones at different speeds. There are also static transient surveys, referred to as 'stations', where the tool is immobilized at different depths. From these runs the PL interpretation engineer will calibrate the tools, then calculate a flow profile.

PL tool strings may be run with surface read-out, using a mono-conductor cable, or on slickline. Surface read-out allows a real time quality control of the data at surface. The logging program can then be adjusted depending on the results. The slickline option is less expensive and easier to run. However it is a blind process, as data are stored in the tool memory. There is no way to check the data before the string is pulled out. Power requirement also limits the range of tools that can be run on slickline.

A typical, classical tool string is shown in the figure below, right. Sensors are not located at the same measure point of the string. As measurements are presented vs. depth, they are not synchronized for a given depth, and this may become a serious issue when flow conditions are not stabilized. In some cases one may have to stop the tool and check for the transients, in order to discriminate noisy tools and real effects. Conversely, when running stationary surveys tools are not recorded at the same depth. This issue of time vs. depth is the reason why compact tools are recommended to minimize errors due to this limitation.

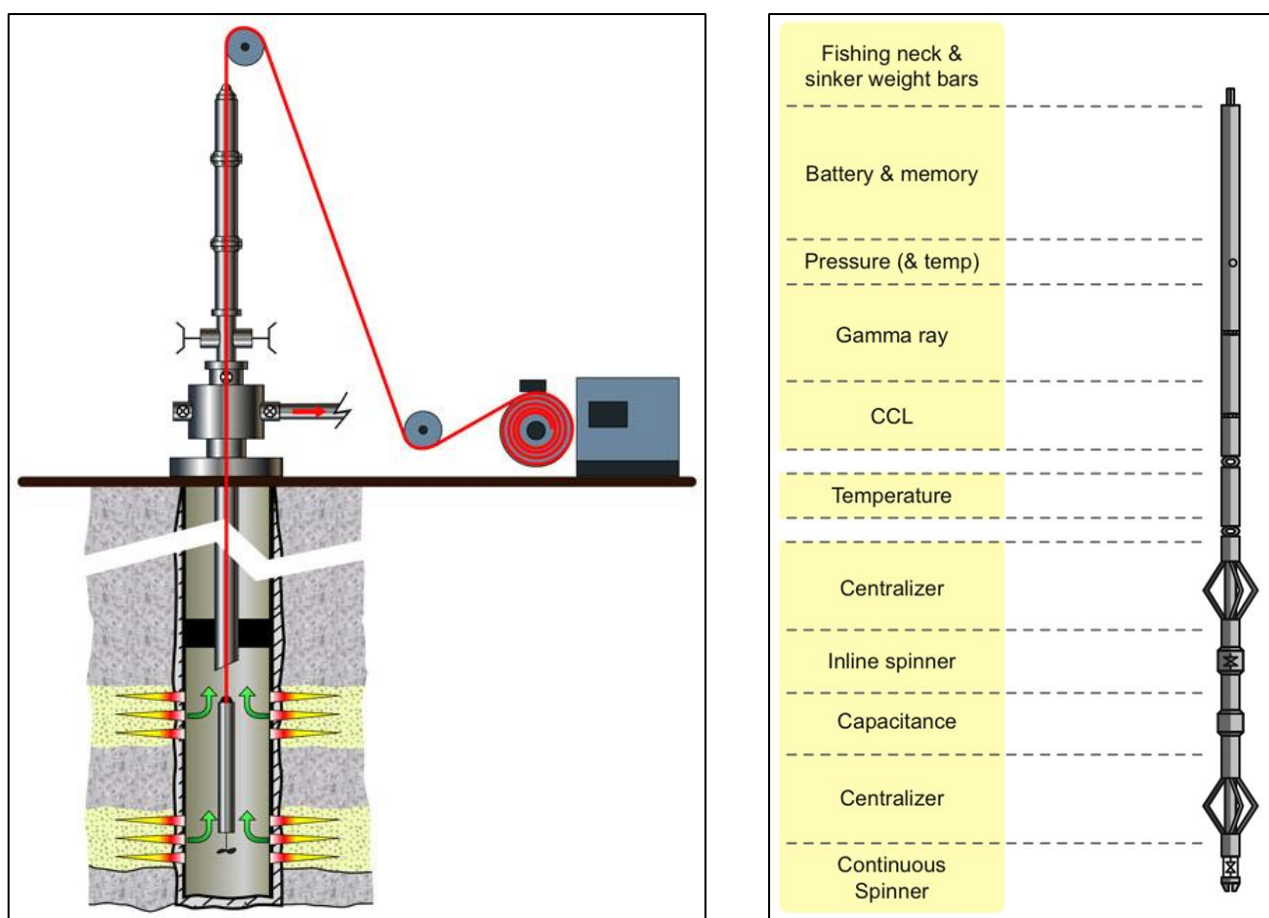


Fig. 14.C.1 – Schematics of PL operations and PL tool string

14.C.1 Flowmeters (spinners)

These are THE tools naturally associated to Production Logging. Despite numerous attempts to use other technologies, the spinner based tools remain the primary way to assess fluid velocities. Even the latest multiple probe tools use micro-spinners placed at strategic points in the wellbore cross-section.

Spinners are of various types, material and shapes, depending on usage. They turn with as little friction as possible, and include internally located magnets which will activate powered Hall effect switches, generating a pulse several times per revolution. If the magnets are somewhat asymmetric they will give a way for the tool to detect the direction of the rotation.



Fig. 14.C.2 – Various types of spinners – Schematic of the Hall effect – Courtesy Sondex

The spinners are packaged in several types of tools. There are three main types of flowmeters: Inline, Fullbore and Petal Basket. Other types are not described here.



Fig. 14.C.3 – Inline, Fullbore and Petal Basket flowmeters – Courtesy Sondex

Inline flowmeters have small diameters and can be used to log in completions with restricted diameters (tubing, scaled up wells, etc). Conversely they have a low sensitivity and must be selected to log high rates / high velocity wells. Because of the small spinner size, a good centralization of the tool is required.

Fullbore flowmeters have larger blades that are exposed to a larger part of the flow cross-section. The blades collapse in order to pass the tubing and other restrictions. They expand and start turning when the cross-section becomes large enough. Fullbore flowmeters have a good sensitivity and can be run for a wide range of flow rates and velocities. There may be sometimes issues with injectors, where the blades may collapse when the flow coming from above becomes too large. A lot of tools (see below) combine the fullbore spinner with a X-Y caliper that will protect the blade, and expand / collapse the tool. Such set-up combining two tools in one, creates a more compact tool string.



Fig. 14.C.4 – PFCS Fullbore flowmeter with built-in X-Y caliper – Courtesy Schlumberger

Petal Basket flowmeters concentrate the flow towards a relatively small spinner. They are very efficient at low flowrates. However they are not rugged enough to withstand logging passes, and are really designed for stationary measurements and the tool shape often affects the flow regime.

It is important to realize that spinner based flowmeters do not measure rates. They do not even calculate the fluid velocity. The output of a spinner based flowmeter is a spinner rotation in RPS (or CPS for some tools). The process of converting RPS to apparent velocity, then average velocity, and then ultimately rates, is the essence of Production Logging Interpretation and requires additional measurements and assumptions. This is described later in the Chapter.

14.C.2 Density tools

In single-phase environments spinner measurements may get us flow rates. However, when several phases flow at the same time the problem becomes under-defined, and one needs to get additional measurements in order to discriminate possible solutions.

To schematize we will need at least one more tool to get two-phase interpretations, and at least a third one to get three-phase interpretations. Without the minimum number of tools, additional assumptions will be needed.

If there are more tools than necessary, one will not be able to match all measurements exactly at the same time, because of the nature of the calculations done (more on this later).

The first natural complement of the spinner type flowmeters are density tools. In a two-phase environment, measuring the fluid density will allow discriminating the light phase and the heavy phase, provided that we have a good knowledge of the PVT. There are four main tools that may give a fluid density: gradiomanometers, nuclear density tools, tuning fork density tools (TFD) and... pressure gauges after differentiation.



Fig. 14.C.5 – Schematic of a gradiomanometer; nuclear density tool; TFD tool; pressure differentiation

14.C.2.a Gradiomanometers

The tools measure the difference of pressure between either sides of a sensing chip. The direct calculation ($P_2 - P_1$) must be corrected for the hydrostatic pressure of the internal column of silicon oil in order to get the effective pressure ($P_B - P_A$). This pressure then has to be corrected for deviation and friction effects in order to get a corrected density.

$$\rho_{fluid} = \frac{[P_2 - P_1] - \Delta p_{fric} - \Delta p_{acc}}{gh \cos(\theta)} + \rho_{so}$$

The acceleration term is generally ignored. For a given surface the friction gradient is a function of the friction factor (f , calculated from the Reynolds number and the surface roughness) the density, the relative velocity, the friction surface and the flow area:

$$\left[\frac{dP}{dZ} \right]_{friction} = \frac{f \rho V^2}{8} \times \frac{S}{A}$$

We generally split the friction into tool friction and pipe friction:

$$\left[\frac{dP}{dZ} \right]_{friction} = \left[\frac{dP}{dZ} \right]_{pipe} + \left[\frac{dP}{dZ} \right]_{tool} = \frac{f_p \rho V^2}{2} \times \frac{D}{(D^2 - d^2)} + \frac{f_t \rho V_t^2}{2} \times \frac{d}{(D^2 - d^2)}$$

14.C.2.b Nuclear density tool

This tool sends gamma rays from one side of a chamber and detects them on the other side. The gamma ray attenuation will only be a function of the fluid density inside the chamber. There is no correction for friction or deviation required.

The issue is whether the fluid present in the chamber is representative of the flow through the pipe. The tool shows very quickly its limitations in deviated wells with segregated flow. The existence of a radioactive source is also an issue.

14.C.2.c Tuning Fork Density (TFD)

The TFD operates by measuring the effect of the fluid on a resonant fork. As for nuclear density tools there is no need to correct for frictions and deviation.

This is a pretty recent type of tool and we will have to wait a little more to assess its efficiency.

14.C.2.d Pseudo-density from pressure

We calculate the derivative of the pressure with respect to measured depth, and then have to correct for friction and deviation. Generally this will be used on pressure acquired during slow passes.

14.C.3 Capacitance and holdup tools

The holdup of a phase at any given depth, is the volume fraction occupied by that phase. The Figure opposite shows a heavy (blue) and light (red) phases and indicates the corresponding holdups.

The holdups are usually noted 'Y'; they add up to 1 by definition.

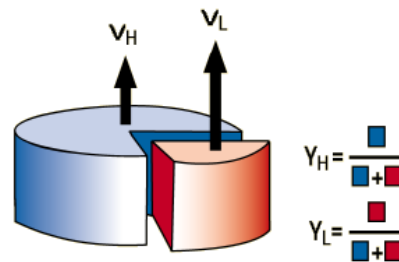


Fig. 14.C.6 – Definition of holdup

Capacitance and holdup tools are designed to provide the holdup of a particular phase. This series of tools are a complement to the spinners in order to differentiate multiphase flow.

14.C.3.a Capacitance tools for water holdup

This is a tool based on the difference of dielectric constants between water and hydrocarbons.

This tool will provide correct measurements when the water holdup is less than 40%. The tool response, given as a calibration curve, is unique and highly non-linear.

This tool is also subject to delays in the response by filming (down passes) and wetting effects (up passes), hence the risk of the wrong positioning of the fluid contact.



Fig. 14.C.7 – Capacitance tool
Courtesy Weatherford

14.C.3.b Gas holdup tools (GHT)

This tool is designed to calculate the gas volume fraction in the fluid. A transmitter emits gamma rays; the measurement discriminates the gas based on the amount of back scatter, knowing that the gas has a low electron density and a low back scatter.

The tool gives a measurement across the wellbore with no influence of the formation behind the casing. It is not sensitive to deviation and requires no friction correction.

The negative is that it uses a radioactive source and must be run centralized. Raw counts have to be corrected by the pipe ID, prior knowledge of certain PVT properties, and results may be affected by scale.



Fig. 14.C.8 – Gas holdup tool
Courtesy Sondex

14.C.4 Pressure and Temperature sensors

Pressure and Temperature measurements are used directly or indirectly and they constitute two very important components of any PL string.

Pressure is required for PVT calculations; it can be used as an indication of the production stability; it can supplement a missing / faulty density measurement when differentiated; it provides one of the key information with SIP.

Pressure gauges can be split into Strain gauges or Quartz gauges. With strain gauges, the mechanical distortion caused by the applied pressure is the primary measuring principle. There are several sensor types based on Bourdon tubes, thin-film resistors, sapphire crystals, etc.

In Quartz gauges, a quartz sensor oscillates at its resonate frequency. This frequency is directly affected by the applied pressure.

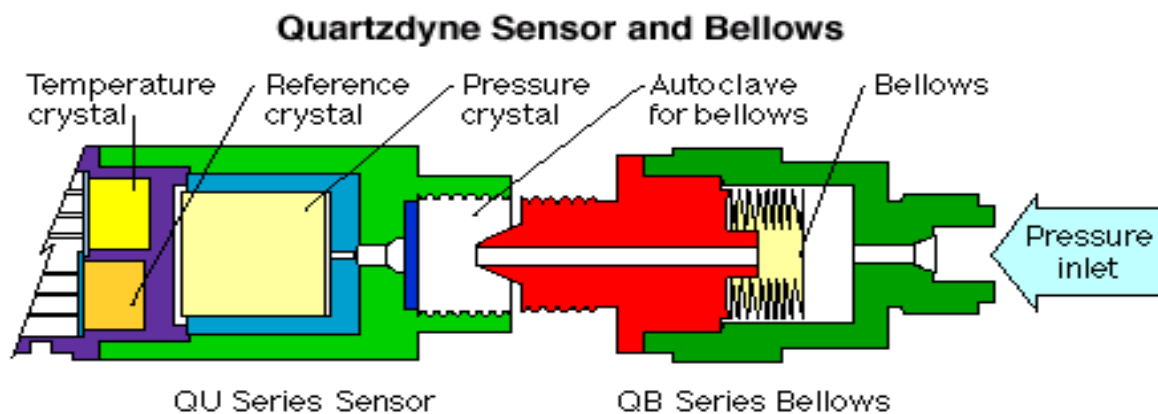


Fig. 14.C.9 – Quartz sensor example

Courtesy Quartzdyne

Like the Pressure, the Temperature is used in PVT calculations. It can also reveal flow outside the wellbore because of cement channeling leak for instance. The Temperature can be used quantitatively, provided an adequate forward model for calculations is available.



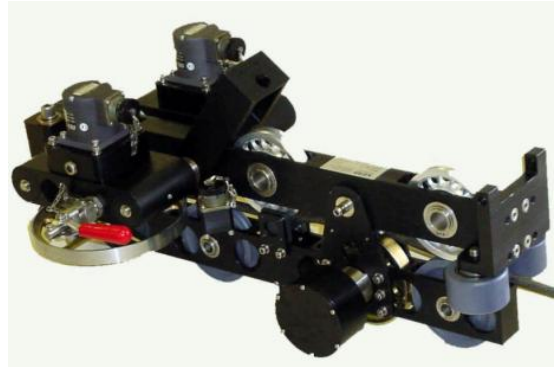
Fig. 14.C.10 – Temperature sensor

Courtesy Spartek

14.C.5 Depth and ID devices

14.C.5.a Depth measurement

The depth is measured at surface by measuring the length of the cable run in hole. The depth measurement does not consider possible stretch of the cable or conversely slack due for instance to deviation or restrictions. A Tension measurement can be used to spot such cases. As mentioned earlier the log data needs to be offset in time to be displayed at the same depth. This is because the various sensor measurement points are at different depths.



*Fig. 14.C.11 – Depth measuring device
Courtesy NOV ELMAR*

14.C.5.b Depth correction: Open Hole Gamma Ray

The tool '0' is set at surface when the log is run. The first task in the data QAQC is to set the log data consistently with the other available information: completion, perforations, etc. This can be achieved by loading a reference Open-Hole Gamma Ray and shifting the acquired data so that the PL and Open-Hole curves overlay. The signal may not be strictly the same, due to completion, scale, etc.

14.C.5.c Depth correction: Cased Hole CCL

An alternative to the Gamma Ray for depth correlation is a CCL measurement that will react in front of the Casing Collars, at known depths.

14.C.5.d ID calculation: Calipers

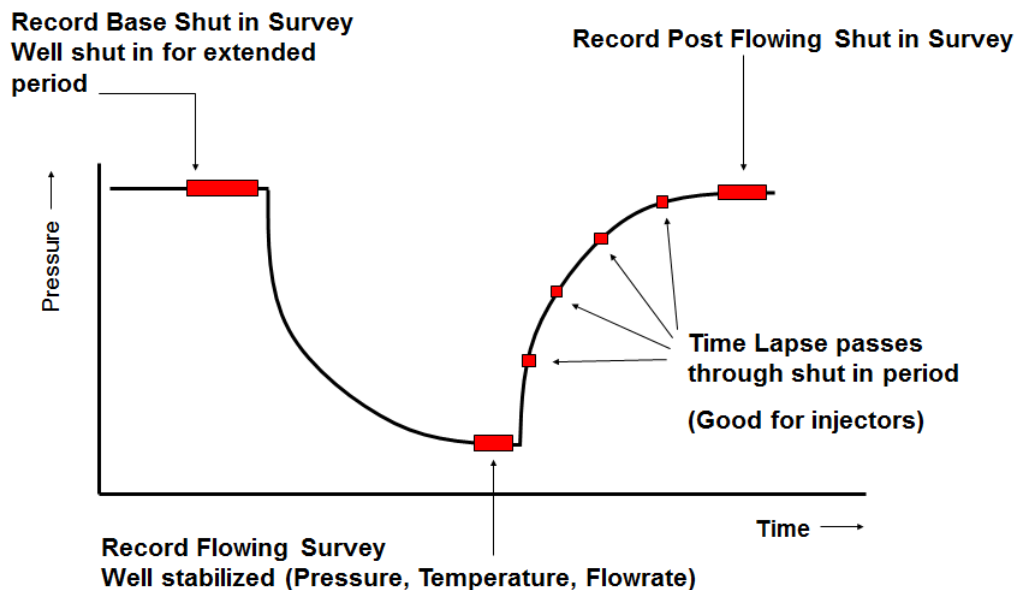
Calipers are mechanical devices used to calculate the cross-section of the wellbore. They are critical since the cross-section must be known to convert velocities to flowrates. Even in cased holes, a completion diagram may not reflect the reality. Calipers can be integrated in the spinner tool or as a separate device. They usually measure the diameter in two orthogonal directions; in this case they are referred to as X-Y calipers. For such calipers, the ID at every depth is calculated as: $\sqrt{(X^2 + Y^2)}$



*Fig. 14.C.12 – Independent X-Y caliper; X-Y caliper combined with fullbore spinner
Courtesy Sondex and Schlumberger*

14.D A typical PL job sequence

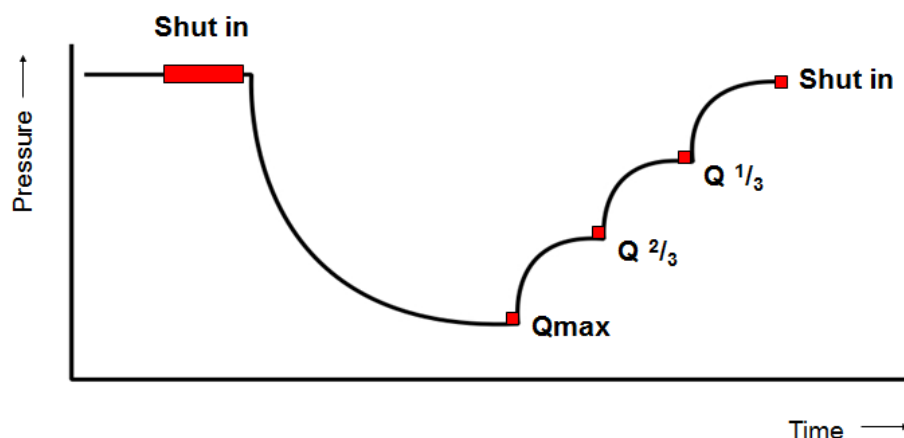
The basic assumption in Production Logging is that the well is in steady state. It is therefore important that the well be stabilized before running the tools. A typical job will consist in several surveys corresponding to different surface conditions. Shut-in surveys are also recorded with the goal being to calibrate the tools in an environment where the phases are segregated. Shut-ins can also reveal crossflow due to differential depletions; they provide a reference gradient in shut-ins; they provide a baseline for a number of measurements in flowing conditions, e.g. Temperature.



Part of the job planning is to account for the time it will take for the well to be stable. The notion of stability is defined as a pressure variation over time since we know from Welltest that the flowing pressure will usually not be strictly constant. Time lapsed passes will be interesting to record evolution with time, for instance, the warmback following an injection period.

Multirate PL and SIP

In order to get Selective Inflow Performance (or SIP) it is necessary to achieve more than one rate. Typically, 3 rates and a shut-in are recorded, as illustrated below.



14.E Typical job

In a single phase situation, a typical tool string will comprise Temperature and Pressure, Spinner, and Caliper. No further information is required, assuming of course that the flow conditions are indeed single-phase. It is not uncommon to encounter fluids downhole that are not produced at surface. If in doubt, it is always better to add a fluid identification tool in the string (density or holdup) before.

In a multiphase situation, there are $n-1$ additional unknowns, n being the number of phases. So in two-phase flow a density or holdup is required, and in 3 phase two such independent measurements are required.

For all tools but the spinner, one pass would be sufficient for calculation. However, comparing several passes for other tools is a way of judging the well stability. Having multiple passes also provides more chances to have a representative measurement if the data is bad on some section of some passes.

The spinner calibration, which is explained next, requires several passes at various logging speed. A typical job will comprise 3-4 down and 3-4 up passes, as illustrated below. Passes are normally numbered by increasing speed, and the slow passes are recorded first. This means that Down 1 is normally the first and slowest pass in the well.

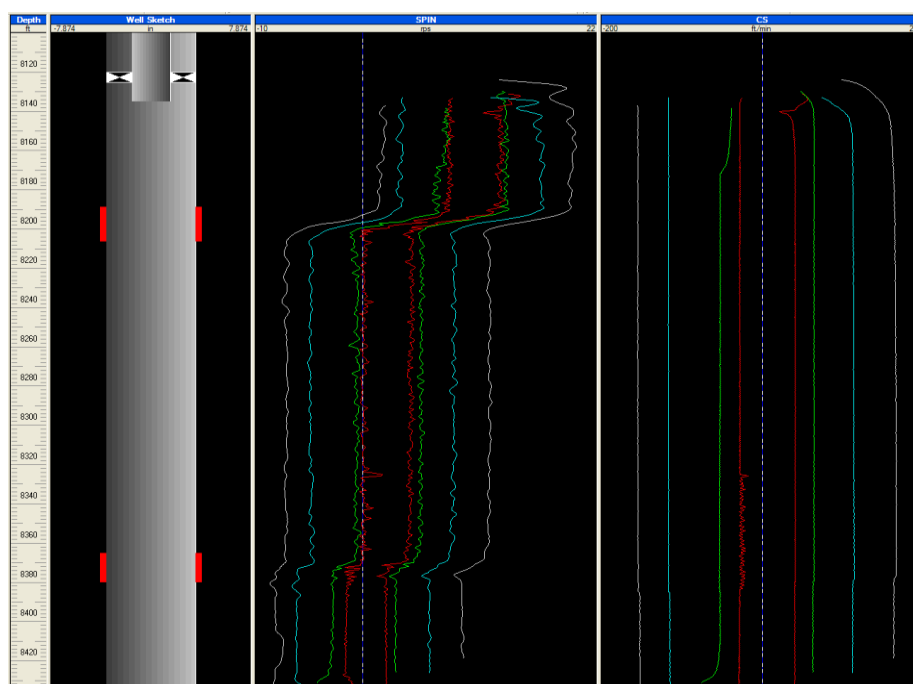


Fig. 14.E.1 – Spinner and cable speed for an 8-pass job

Stations may be recorded for certain tools that require it. In addition the ability to display the measurement of a station versus time is a further indication of well stability or instability.

14.F Data loading, QA/QC, and reference channels

The first task after the job is run is to load and review the log data for QA/QC. The following is a list of checks and possible actions.

Data editing - general: telemetry errors can introduce spikes on data which in turn will upset the scaling and make the QA/QC difficult. De-spiking should be achieved beforehand to avoid this problem using for instance a median filter. Some tool responses may also be noisy, for instance nuclear tool responses, and will usually deserve a processing with a low-pass filter.

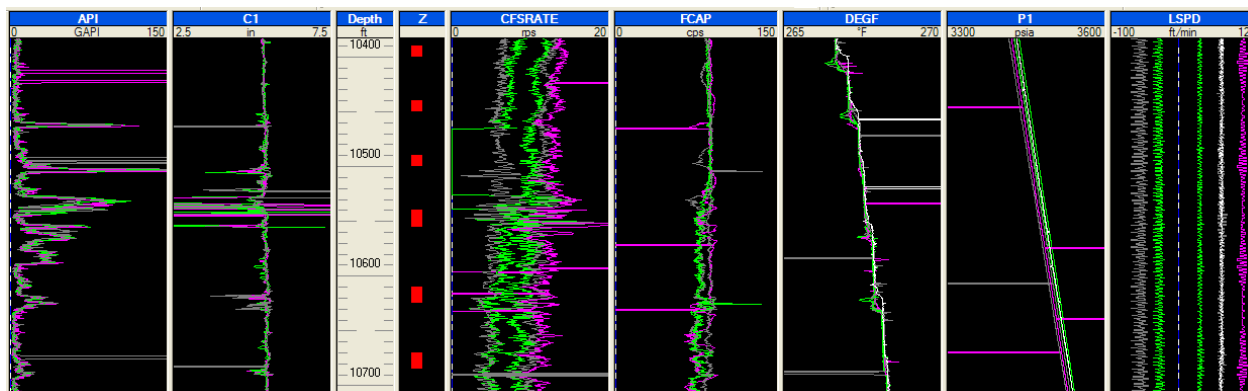


Fig. 14.F.1 – Example of telemetry spikes

Data editing – spinner / cable speed: when starting fast passes ‘yoyo’ effects may be seen. Similarly oscillations may appear on the flowmeter as a result of the cable sticking/slipping along the length of the completion. Those can be edited out with a sliding window averaging.

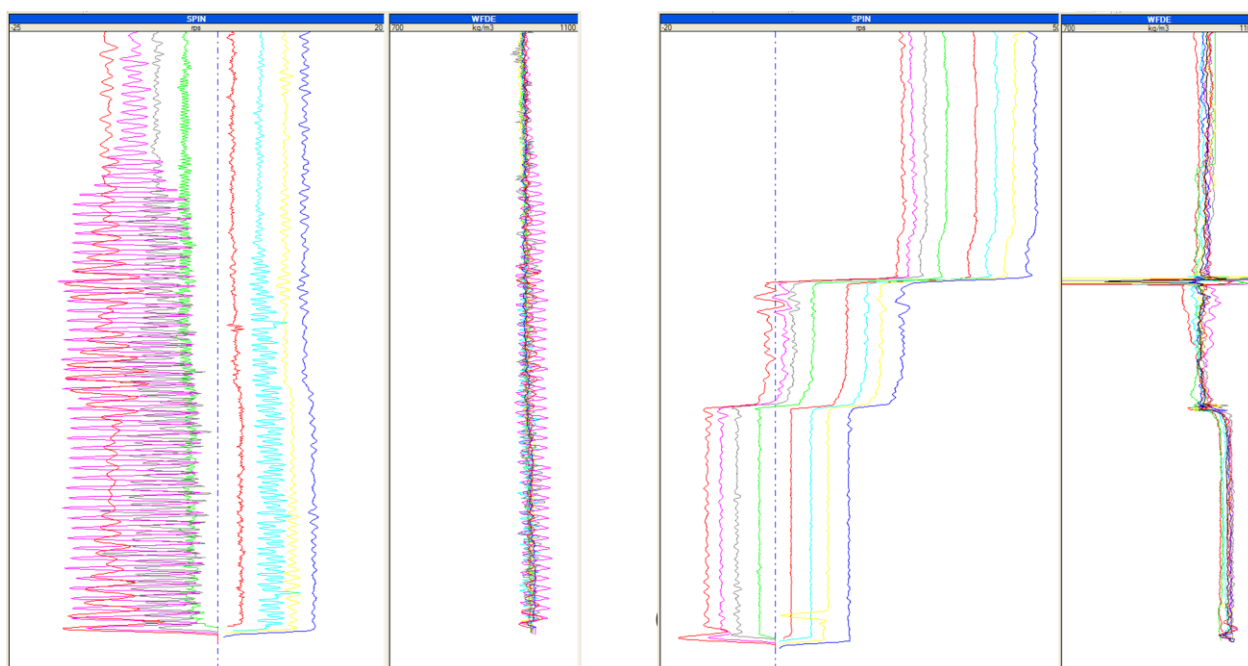


Fig. 14.F.2 – Stick & slip (left) and yo-yo at start of passes (right)

Unsigned spinners will need to be corrected before processing, on Up passes in producers and Down passes on injectors.

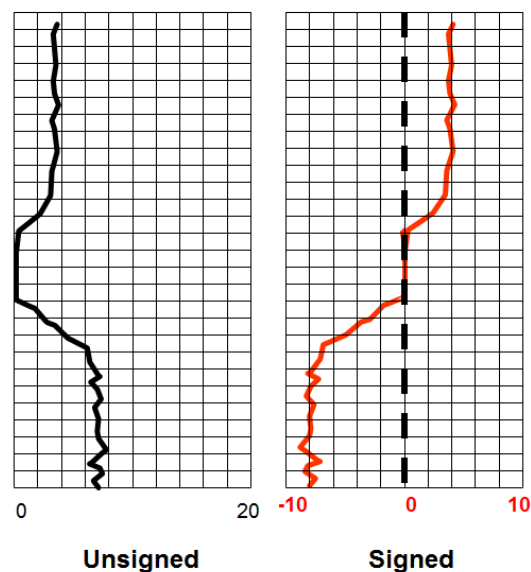


Fig. 14.F.3 – Comparison of unsigned/signed responses

Depth matching: using the Gamma Ray or CLL all the available data should be set with coherent depth. Sometimes the depth correction might require more than a shift.

Repeatability: the repeatability of readings from one pass to another will be an indication of the well stability. Some tool readings are affected by the cable speed when the fluid mixture changes drastically (density, temperature for instance) and this should be noted as it will orient the choice of reference channels for the calculations.

Consistency: a first consistency check between sensors can be done at this stage. Beware that some tools will need corrections before they can provide a quantitative answer (e.g. a pseudo density – dP/dZ - in a deviated well). Some tools react to what happens behind the tubing or casing (e.g. the Temperature) and will behave differently from the spinner.

Qualitative analysis: once all data have been cleaned, most of the questions can be answered qualitatively but there are some pitfalls, like mistaking a change in spinner response to an inflow/outflow when it is due to a change of ID.

Reference channels: for any measurement that will be used quantitatively in the interpretation, a single curve must be selected or built. Most of the time this curve will be the slowest down pass but some editing or averaging may be necessary. This procedure will not apply to the spinner that needs to be calibrated first, in order to calculate velocities, before we can define or build the reference velocity channel.

14.G Spinner calibration and apparent velocity calculation

To conduct a quantitative interpretation, the spinner output in RPS needs to be converted into velocity. The relation between RPS and velocity depends on, amongst other things, the fluid property and for this reason, an in-situ calibration is required.

14.G.1 Spinner response

The spinner rotation depends on the fluid velocity relative to the spinner; this is a function of the fluid velocity and the tool velocity. The usual sign conventions consider that the tool velocity is positive going down and negative coming up. Similarly, the spinner rotation is counted positive when the fluid is seen by the spinner as coming from below, and negative when it is seen as coming from above. With these conventions, the spinner rotation is relative to the sum: Cable Speed + Fluid Velocity.

The response of an ideal spinner run in a static fluid would be as plotted below, with 2 distinct response lines for Up passes (negative CS) and Down passes (positive CS).

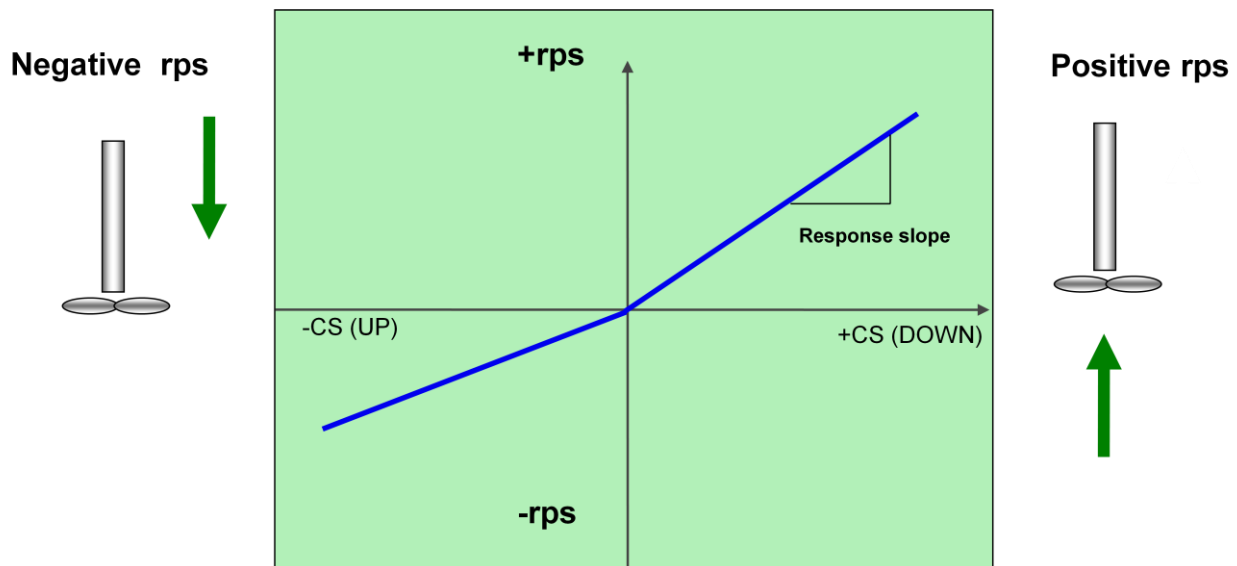


Fig. 14.G.1 – Ideal spinner response (in a no-flow zone)

- (1) The rps value is a linear function of the velocity; the response slope depends on the spinner pitch; i.e. its geometry only.
- (2) The spinner rotates with the slightest movement of the tool, i.e. the slightest movement of fluid relative to the tool.
- (3) The negative slope is lower, typically as the tool body acts as a shield; this is not the case with a symmetrical tool like an in-line spinner.

In reality, the response is affected by the fluid properties as well as the bearing friction. The equation below is a possible representation (SPE Monograph Vol. 14; Hill A.D.):

$$rps = aV_{fs} - \frac{b}{\rho V_{fs}} - c \sqrt{\frac{\mu}{\rho V_{fs}}}$$

For PL interpretation we will consider that the calibration is still a straight line. Since this line is approximating a non-linear function, it may vary with the encountered fluid. In addition, the tool response is shifted by a threshold velocity, the minimum velocity required for the spinner to rotate. This threshold velocity will depend on the fluid; typical numbers for a fullbore spinner are 3 to 6 ft/mn in oil, 10 to 20 ft/mn for gas.

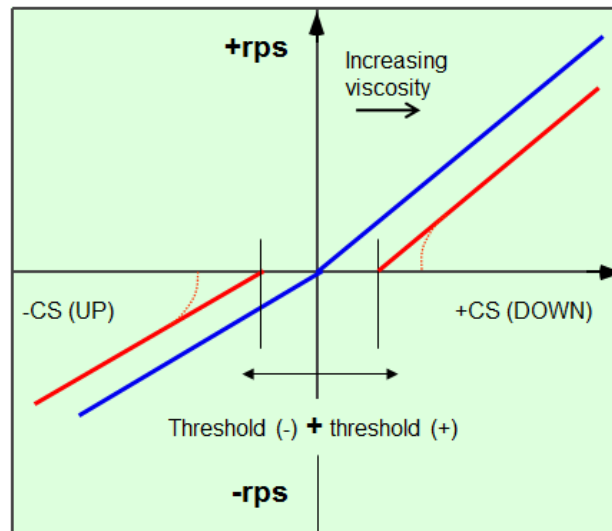


Fig. 14.G.2 – Real spinner response (in a no-flow zone)

The plot above represents the spinner response in a no-flow zone as a function of the cable speed. If the fluid is moving at some velocity V_{fluid} , the tool response will be the same, but shifted to the left by V_{fluid} as shown below. The reason behind the shift is that since the spinner reacts to the sum of ($V_{\text{fluid}} + \text{Cable Speed}$), the rps value for a CS value 'X' in V_{fluid} , is the response to a CS value of $(X + V_{\text{fluid}})$ in the no-flow zone.

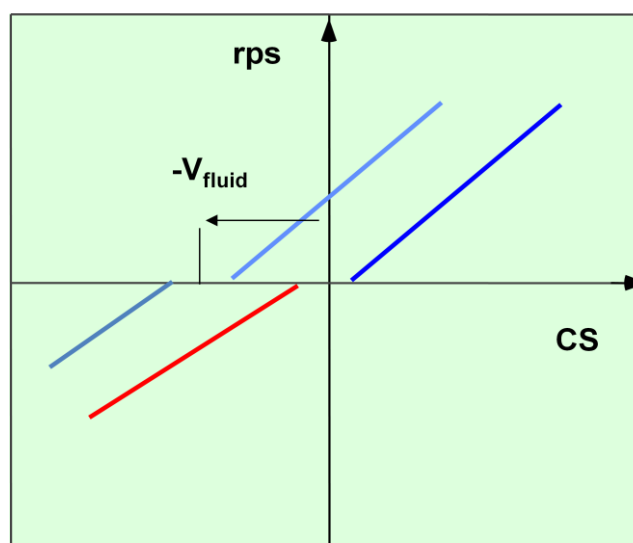


Fig. 14.G.3 – Real spinner response in a no-flow zone, and a zone with production

14.G.2 Spinner in-situ calibration

In practice the objective is to build the calibration response in-situ to take into account the changing fluid properties, and their effect on the spinner calibration. On the schematic below, the fluid velocity is represented on the left. 6 passes have been run and the spinner response is shown on the right.

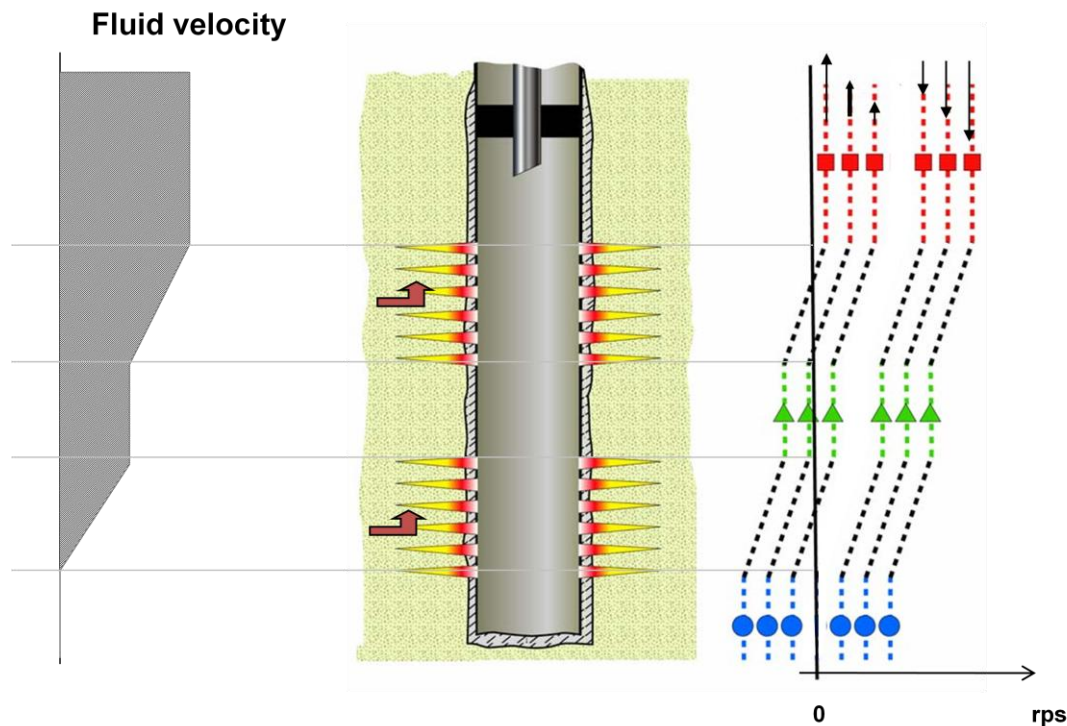


Fig. 14.G.4 – Fluid velocity (left) and spinner response for the 6 passes (right)

Three stable intervals are considered represented by the sections in blue, green, and red. The corresponding points are plotted on a rps vs. cable speed plot and the lines are drawn by linear regression:

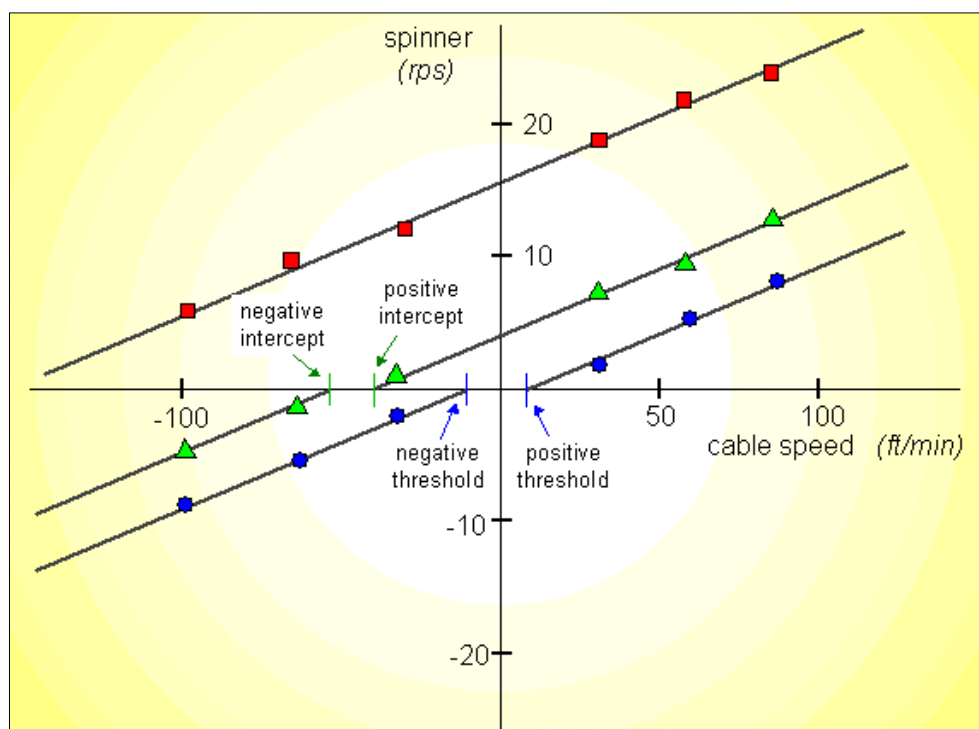


Fig. 14.G.5 – In-situ calibration for the case above

Historically when doing hand calculations, the usual method was to consider a spinner calibration zone in stable regions in-between every perforations, as above. The velocity was then calculated directly from the cross-plot for every zone. Today's idea is that you only put in spinner calibration zones because you think there has been a change of slope or threshold, (usually due to a change of fluid type). In theory a single phase well only needs one spinner calibration zone. In reality, having multiple zones – as long as they are stable - ensures that any change is properly captured.

14.G.3 Velocity from calibration: threshold handling and V_{apparent}

The calibration does not give the fluid velocity directly and some calculation or assumptions remain to be done. If the response of the various sections were strictly parallel we know from the previous discussion that the fluid velocity could be obtained by estimating the horizontal translation between say the positive line of a given zone, and the positive line of the no-flow zone. This method is fine for manual analysis but it is quite limitative. A general approach needs a systematic way of handling slope and threshold variations.

14.G.3.a Threshold options

Below are the options given in Emeraude.

Unique value of (+) and (-) thresholds for all zones

The apparent velocity for a point on a positive line is calculated based on the slope of that line and the common positive threshold. The apparent velocity for a point on a negative line is calculated based on the slope of that line and the common negative threshold. This mode is suitable in case of single-phase fluid.

Distinct thresholds, unique ratio threshold(-)/[Intercept(-) – Intercept(+)]

This ratio is equal by default to $7/12 = 0.583$ but can be set from the value of a no-flow zone. Obviously this can be used only on zones with both a positive and negative intercepts.

Independent Thresholds

This mode allows different thresholds for each calibration zone and is the most general one. Note that the only problem with this mode is that on a zone where there is fluid movement, at best, we can get the sum of the thresholds. Deciding the positive and the negative can be done bluntly (i.e. halving the sum) or based on the split on the no-flow zone.

14.G.3.b Apparent Velocity

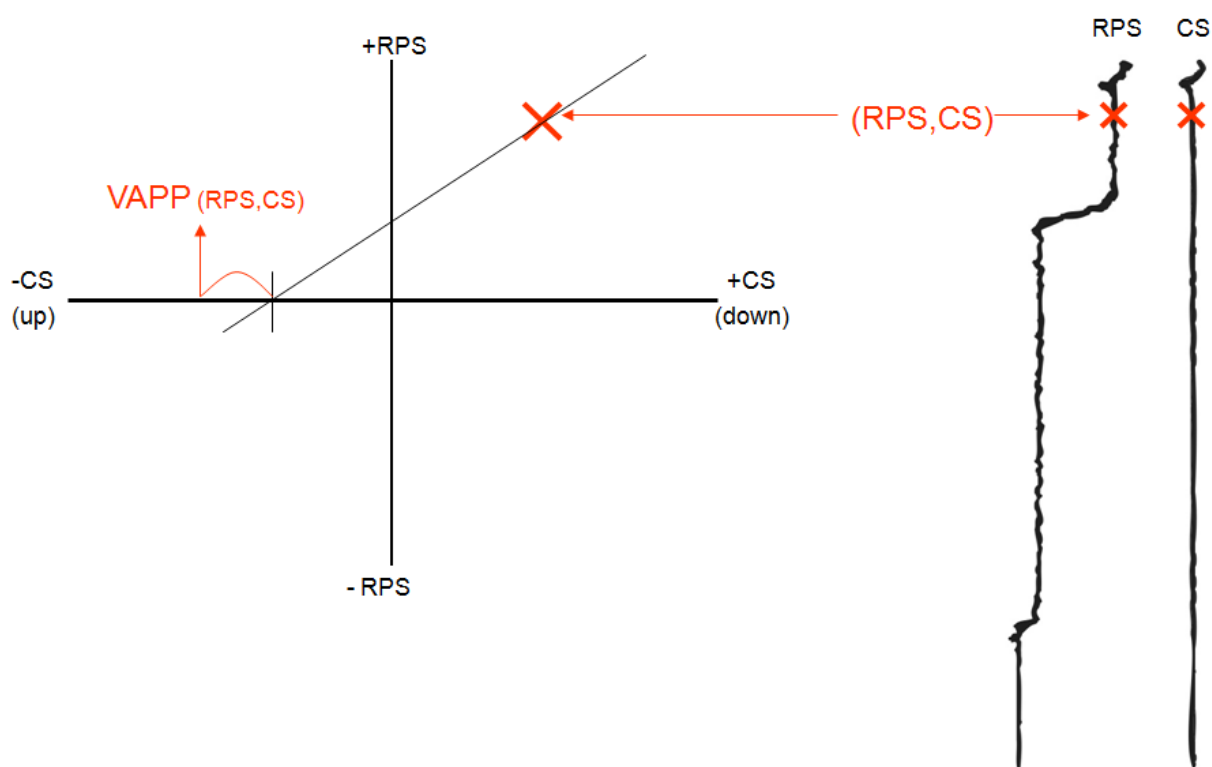
No matter what method is used we will end up with a measurement of velocity that represents the fluid velocity seen by the spinner. This value is the average velocity in the cross-section covered by the spinner and it is different from the actual fluid average velocity. For this reason it is referred to as apparent velocity, noted V_{apparent} or V_{APP} .

14.G.4 Apparent velocity log

After the calibration is complete and the threshold mode has been selected, the goal is to obtain a continuous apparent velocity curve representing the velocity at every depth.

The slope and threshold values for a calibration zone will apply to all calculations performed within that zone. Data above the top calibration zone will use the top calibration, and data below the bottom calibration zone will use the bottom calibration. In between consecutive calibration zones the possible options are to move linearly from the values of a zone to the value of the other, or to make this change occur sharply. From the previous discussion on spinner response we know that the difference in spinner response is caused by the change in fluid. Because the change in fluid property is local (to a particular inflow zone) rather than spread over a large interval, a sharp transition is probably more liable. Emeraude offers all the possibilities: progressive change, sharp change, or a mix of both.

Having decided how to obtain a slope and threshold for any depth, the procedure to get the apparent velocity curve for a given pass is as follows: for a given measuring point, we have the cable speed and the spinner rotation. From graphing the point on the calibration plot, we follow the slope, get the intercept and correct by the threshold.



Producing one apparent velocity channel per pass allows an overlay and is a further check of the well stability and the calibration adequacy. When this check has been made, the multiple apparent velocity curves are typically replaced with a single average value (median stack or lateral average). This single apparent velocity curve is the sole information required for quantitative analysis.

14.H Single phase interpretation

Rate calculations may be performed on each depth frame or averaged on calculation zones of interest. Such calculation zones could be the calibration zones, the top of each perforation zones, but in most cases the engineer will define where the rate calculations are relevant.

The spinner calibration allows us to get the apparent velocity, V_{APP} , everywhere there is a measurement.

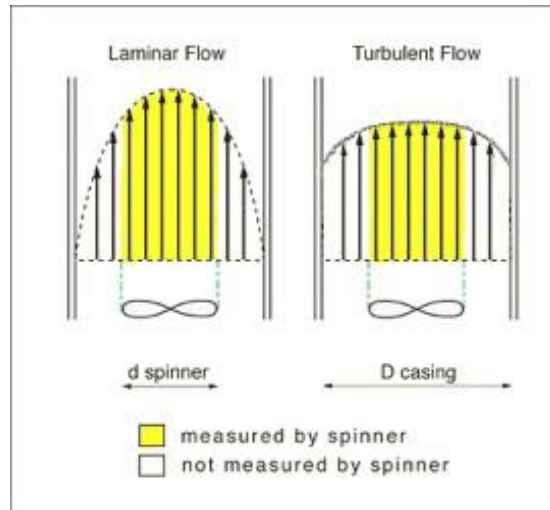


Fig. 14.H.1 – Velocity profiles and spinner sampling section

To get a single phase rate we need the total average flow velocity, which can be expressed from V_{APP} with some correction factor usually noted VPCF: $V_M = VPCF \times V_{APP}$.

14.H.1 Velocity profile correction factor

Historically, and at least for any manual interpretation, VPCF is taken as 0.83. More generally this factor can be calculated from the Reynolds number and the ratio of blade diameter to pipe diameter using the correlation illustrated in the figure below.

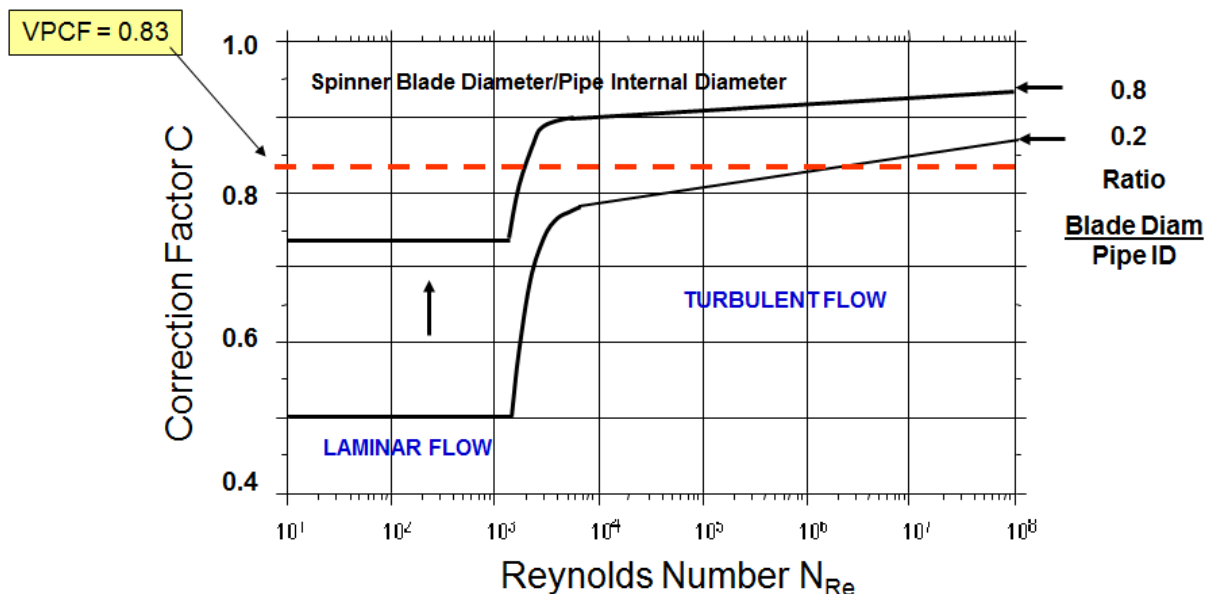


Fig. 14.H.2 – VPCF vs. Reynolds number for different ID ratios

Under a value of 2000 for the Reynolds number the flow is laminar with a parabolic velocity profile. In this situation, the maximum velocity is twice the average leading to VPCF of 0.5 for a small blade diameter. When the Reynolds number increases, the correction factor increases from 0.5 and its value tends asymptotically to 1. Also, as the blade diameter tends to the pipe ID, the correction factors moves towards 1.

The Reynolds number is expressed below for fluid density ρ in g/cc, diameter D in inches, velocity in ft/sec and viscosity in cp:

$$N_{Re} = 7.742 \times 10^3 \frac{\rho D v}{\mu}$$

Obviously, the value we are seeking - the fluid velocity - is part of the equation meaning that an iterative solution is required.

The classical solution is to assume a value of velocity, typically based on a VPCF of 0.83, then calculate the Reynolds number, from which a new value of VPCF would be calculated, hence a corrected estimation of the flow velocity.

The process would go on until the solution eventually converges.

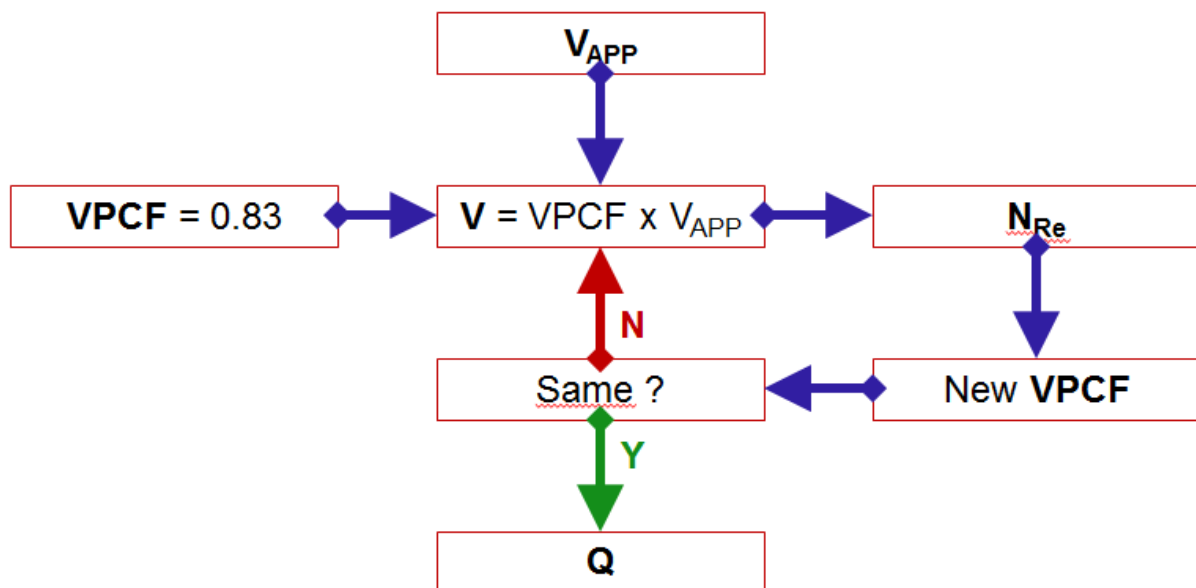


Fig. 14.H.3 – Single phase interpretation workflow

In modern software, this has been replaced by a regression algorithm, and the single phase calculation is only a specific case of what is done for much more complicated processes like multiphase rate calculations or the processing of multiple probe tools.

The principle of the nonlinear regression process is that we take as unknowns the results we wish to get, here the single-phase downhole rate Q .

The target will generally be the observed tool measurement.

In the case of a single phase calculation the target is the apparent velocity calculated after the spinner calibration.

From any value of Q in the regression process, we calculate the velocity, hence the Reynolds number, hence the VPCF, hence a simulated apparent velocity.

This allows to create a function $V_{APP} = f(Q)$. We then solve for Q by minimizing the standard deviation between the simulated apparent velocity and the measured apparent velocity.

$$Q \rightarrow v \rightarrow N_{Re} \rightarrow VPCF \rightarrow V_{APP}$$

$$\text{Simulated Apparent Velocity : } V_{APP} = f(Q)$$

$$\text{Measured Apparent Velocity : } V_{APP}^*$$

$$\text{Minimize Error Function : } Err = (V_{APP} - V_{APP}^*)^2$$

14.H.2 Single phase interpretation results

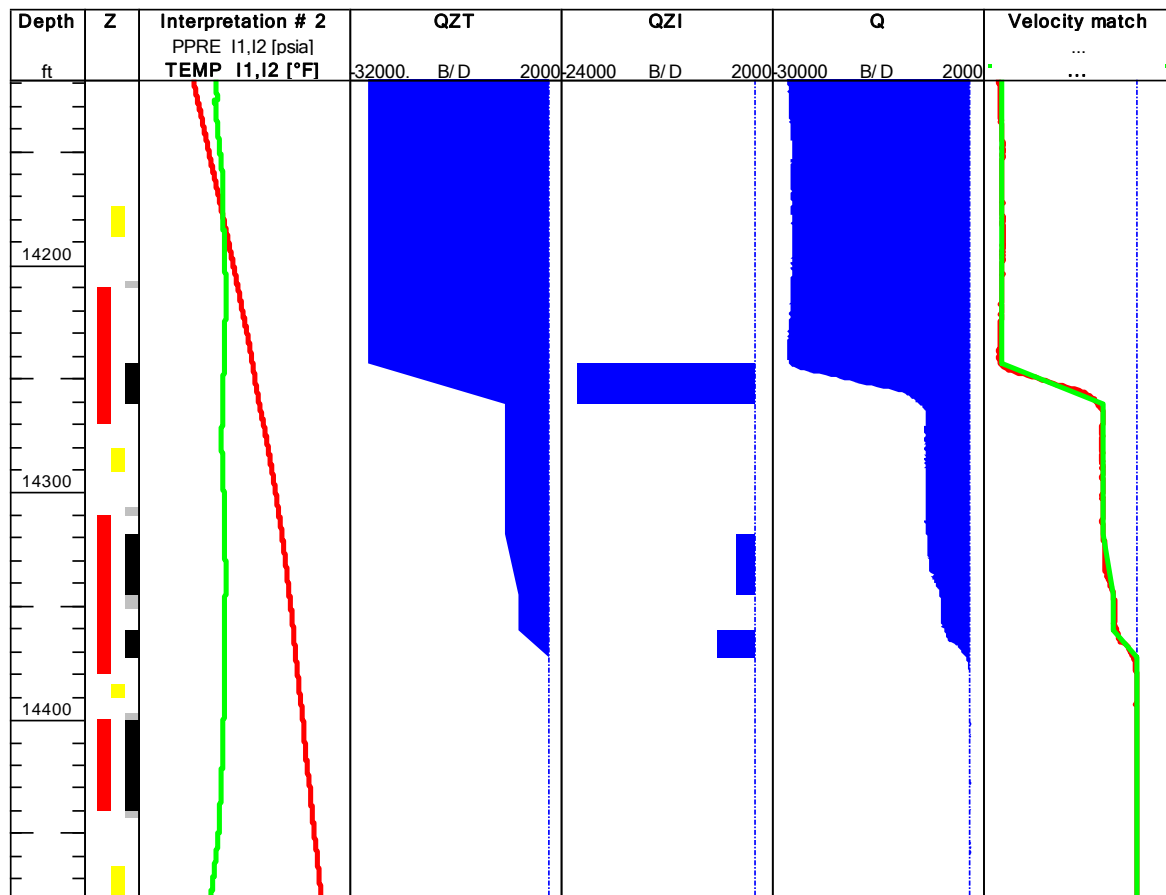


Fig. 14.H.4 – Typical log presentation for a single-phase interpretation

The previous figure is a typical presentation of results.

In this water injector, five different calculation zones (grey) were selected to isolate the contributions.

The non-linear regression described previously was executed on all of them to get Q.

The results are summarized by the QZT track where the value of a given calculation zone is extended up to the inflow zone above, and down to the inflow below.

Inflow zones (black) can be distinct from the perforations (red) simply to capture the fact that not all the perforation interval may produce or in this case, take fluid.

The QZI track represents contributions or injections and they are obtained by the difference of the rate above and below an inflow.

The last rate track, noted Q, represents the application of the non-linear regression at every depth, the point being to obtain a continuous log everywhere faithful to the log data.

Having this log provides in particular a guide to refine the position of calculation zones.

In the complete log (Q) or for the zone rates (QZT) the calculation of the rate at Depth 1 is independent of the calculation at Depth 2. As a result those rates may entail contributions of a sign or amplitude that is not physically justified.

We can address this potential inconsistency in a global regression process described later in this document.

The final track above shows the target V_{APP} and the simulated equivalent in green. Note that we arbitrarily decided to take the apparent velocity as the target function, rather than the real tool response in RPS.

We could have integrated the spinner calibration in the regression process and matched the RPS measurements for the different selected passes.

The simulated (green) curves and the QZT logs are referred to as schematics in Emeraude.

14.H.3 Matching surface conditions

It is possible to apply a global gain on the rate calculations.

This may be relevant if one wants to match the production above the top producing zone with the measured surface rates (if one relies on this). Numerically it amounts to allow a multiplier to VPCF.

14.I Multiphase interpretation

In single phase interpretation the spinner alone is providing the answer, even if the determination of the correction factor needs a good grasp of the downhole conditions to have a representative density and viscosity. In multiphase flow there are at least as many unknowns as we have phases, i.e. one rate per phase. Actually due to the fact that different phases do not flow at the same velocities the number of unknowns is larger, including not only rates but also holdups.

14.I.1 Definitions

14.I.1.a Holdups

This definition was given before but it is repeated for clarity. The holdup of a phase is the volume fraction occupied by that phase. The Fig. opposite shows a heavy (blue) and light (red) phases and indicates the corresponding holdups.

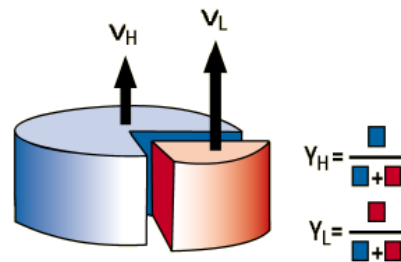


Fig. 14.I.1 – Definition of holdup

The holdups are usually noted 'Y'; they add up to 1 by definition.

In two phases with a heavy ('H') and a light phase ('L'): $Y_H + Y_L = 1$

In three phases with water ('w') oil ('o') and gas ('g'): $Y_w + Y_o + Y_g = 1$

14.I.1.b Phase velocities

The average velocity of a particular phase is obtained from the rate of that phase, its holdup,

and the cross sectional area by:

$$V_p = \frac{Q_p}{A \times Y_p}$$

14.I.1.c Slippage velocity

The slippage velocity is the difference between the velocities of two distinct phases. When light and heavy phases are considered, the slippage velocity is usually defined as the difference between the light phase velocity and the heavy phase velocity, namely:

$$V_s = V_L - V_H$$

When going uphill, the light phase will move faster and V_s will be positive. The opposite situation will be encountered when going downhill where the heavy phase will go faster. The slippage velocity is not something the PL tool measures, nor are the phase rates (at least with conventional tools). Getting the rate values will only be possible if we can estimate the slippage value using a correlation. There are many correlations available in the literature, empirical or more rigorously based. For the time being let us simply assume that such correlation will be available to us if we need it.

14.I.2 Starting with 2-phase...

For 2-phase flow, the alternatives will be water-oil, water-gas, and oil-gas. Even though the general approach that we advocate is using non-linear regression, we describe here a deterministic approach which value is to explain the concepts in a simple situation, and to introduce the basic notions / presentations that will be used in the general case. Recalling the definitions above and using the subscript 'H' for heavy and 'L' for light we can write:

$$Y_H + Y_L = 1 \quad Q_H + Q_L = Q_T$$

$$V_S = V_L - V_H = \frac{Q_L}{A \times Y_L} - \frac{Q_H}{A \times Y_H} = \frac{Q_T - Q_H}{A \times (1 - Y_H)} - \frac{Q_H}{A \times Y_H}$$

Solving for Q_H gives: $Q_H = Y_H \times [Q_T - (1 - Y_H) \times V_S \times A]$

And to finish: $Q_L = Q_T - Q_H$

Holdup is a quantity we can measure directly, or infer from density. If we measure mixture density and know the individual phase densities downhole, holdup can be obtained as shown below:

$$\rho = \rho_H Y_H + \rho_L Y_L \Rightarrow Y_H = \frac{\rho - \rho_L}{\rho_H - \rho_L}$$

Note that when density is measured with a gradiometer the reading needs to be corrected for frictions. This correction requires the knowledge of velocity and the fluid properties so like in single phase, such a calculation will necessitate an iterative solution scheme.

Since we know how to calculate the total rate from the single phase equivalent, all we need is a way of determining the slippage velocity. In the simplest situations, this could be done manually. The chart below shows the Choquette correlation, representative of bubble flow in vertical well for an oil-water mixture.

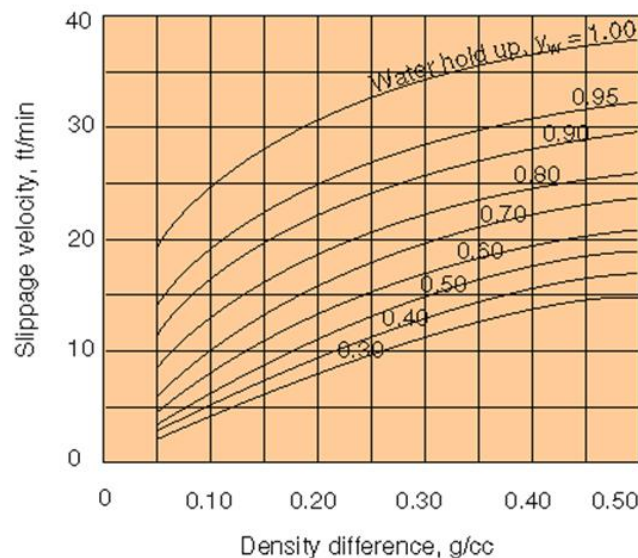


Fig. 14.I.2 – Choquette bubble flow chart

With such a chart, the slippage is obtained from the holdup and density difference. With a spinner and a density measurement, the steps of a manual deterministic approach would be straightforward:

- (1) Estimate Q_T from V_{APP} and $VPCF = 0.83$
- (2) Estimate Y_H from ρ and ρ_H and ρ_L . Iterate for frictions and VPCF as desired
- (3) Get V_s from the Choquette chart
- (4) Estimate Q_H and thus Q_L

In a general situation, the slippage velocity is given as a function of the rates, the fluid properties (densities, viscosity, surface tensions, etc). The manual approach must be modified.

14.I.3 General solution using non-linear regression

The suggested workflow as in single phase, relies on using non-linear regression to find the rates that minimize an objective function defined by the error between the target measurements, and the simulated equivalent. In the case above for instance all we need is a forward model that from an assumption of the rates Q_H and Q_L calculates the simulated V_{APP} and Density. In a general situation, the steps are as follows:

- (1) From the rates, the fluid and the local geometry, get the slip velocities
- (2) From the slip velocities and the rates get the holdups
- (3) From the holdups calculate the fluid mixture properties
- (4) Calculate the simulated tool response using the relevant model (eg VPCF, friction equations, etc).

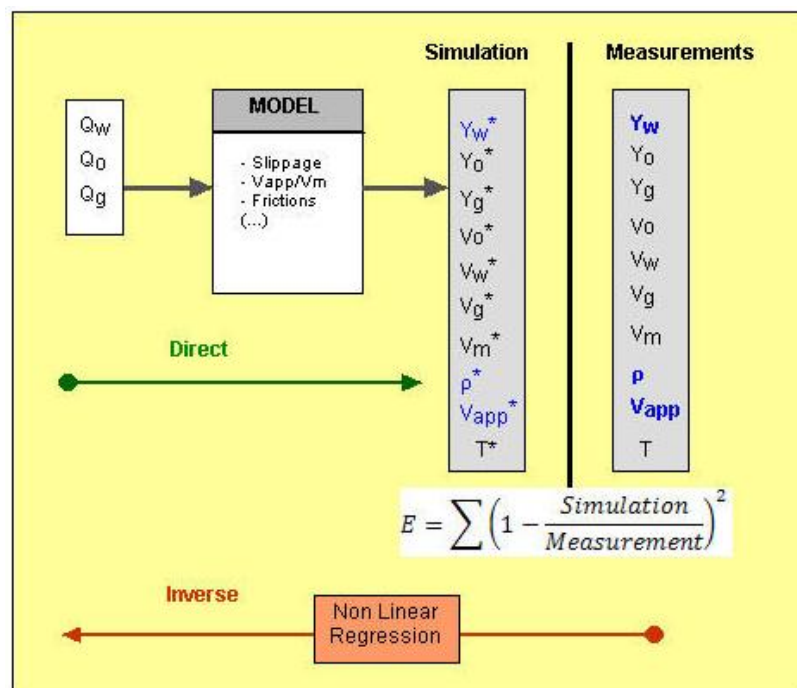


Fig. 14.I.3 – Methodology using non-linear regression

The interest of such an approach is that any number and type of measurements can be chosen as targets provided that they are sufficient and the problem is not undetermined (insufficient measurements for the number of unknowns). Having redundant measurement is also possible where the regression will try and find a compromise based on the confidence assigned by the user to the different measurements.

It is important to realize in the above procedure that slippage correlations are a necessary evil to relate the rates to holdups because holdups are the quantities we are best at measuring. When PL can measure phase rates or phase velocities directly, which is the Holy Grail of Production Logging, the procedure can do away with slippage correlations.

14.I.4 Flow models and correlations

Slippage correlations have been derived for a number of situations either empirically, or by solving the general momentum balance equation in which case the correlation is said to be 'mechanistic'. In general the behavior of the slippage velocity will strongly depend on the nature of the flow regime encountered. Whereas a water-oil mixture moving upward can often be considered in bubble flow, liquid-gas mixtures will give rise to much more complex regimes, as illustrated below with one of the classical empirical correlations by Duns and Ross.

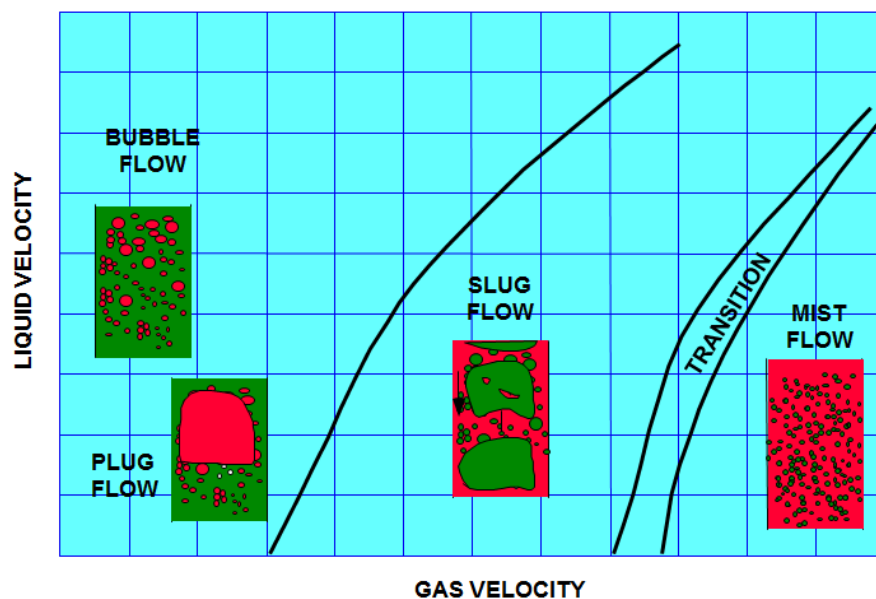


Fig. 14.I.4 – Duns and Ross flow map

In each regime, a specific slippage correlation will be applicable with extreme cases like Mist flow, where no slip exists between the two phases. Many correlations will start with a determination of the flow regime using a flow map, and continue with the application of the corresponding slippage equation. Slippage correlations can be organized in the following categories:

Liquid-Liquid: This category gathers bubble flow correlations (e.g. Choquette), correlations developed for stratified flow (e.g. Brauner) and combinations of those.

Liquid-Gas: This is by far the largest population with many empirical correlations (Duns and Ross, Hagedorn & Brown, Orkiszewski, etc) and mechanistic models (Dukler, Kaya, Hassan & Kabir, Petalas & Aziz, etc). Most of those correlations have been primarily designed for representing wellbore pressure drops in the context of well performance analysis.

Three phase: There are very few such correlations and when they exist they are for a very specific situation, e.g. stratified 3-phase flow (Zhang). In practice, three-phase slippage / holdup prediction from rates are done using two 2-phase models, typically for the gas-liquid mixture on one hand and the water-oil mixture on the other hand.

14.1.5 Graphical presentation

A graphical presentation albeit based on a 2-phase analogy, can help understand some previous concepts and provides a means of comparing different correlations.

For a given mixture rate Q , we consider the possible mixture and plot the corresponding mixture density. The X axis value range from 0 (100% Light phase) to Q (100 % Heavy phase). The density at those end points is the relevant single phase density. The equation derived previously for Q_H is now used to express Y_H :

$$Y_H = \frac{Q_H}{[Q_T - (1 - Y_H) \times V_s \times A]}$$

This equation shows that without slippage, the heavy phase holdup would be equal to the heavy phase cut. This situation is represented by the red line on the plot below. With slippage velocity on the other hand, V_s is positive uphill hence the equation above tells us that Y_H should be higher than the cut. The curve representing the case with slippage is thus above the no-slip line. An opposite situation would be expected downhill.

Another way of considering the plot below, is to realize that for a given cut, the higher the slippage, the heavier the mixture will be. This is because the light phase is going faster and therefore occupies less volume in the pipe. The light phase is 'holding up' the heavy phase, leading to more heavy phase present at any depth than there would be with no slippage. For a given solution with slippage, the density will read heavier than if there is no slip.

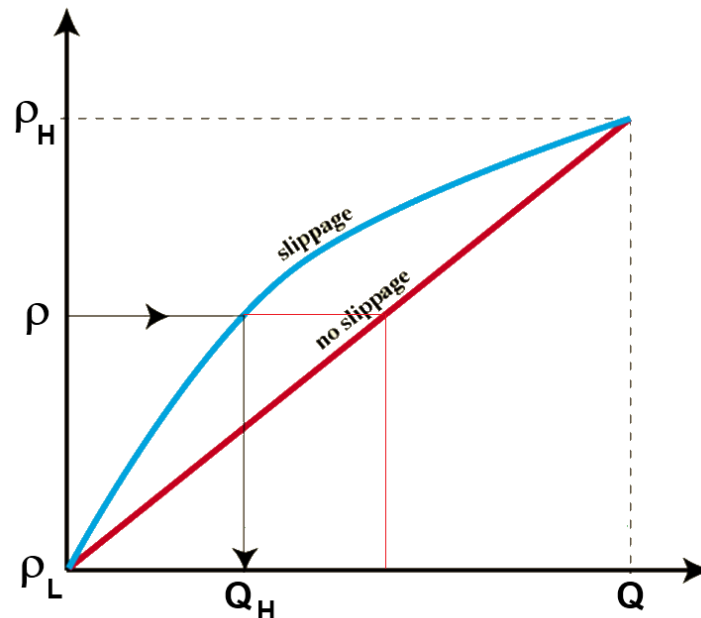


Fig. 14.1.5 – Density vs. heavy phase rate with and without slippage

We can look at this plot from a last perspective. If we have a measurement of density, the solution we should find (or that the non-linear regression will find) is seen graphically by interpolating the relevant curve for this density value.

14.I.6 Emeraude Zoned approach and the Zone Rates plot

The simplest interpretation method in Emeraude, called the Zoned approach, amounts to using the regression described previously on a set of user defined calculation zones. As in single phase, the zones are selected in the stable intervals above and below the inflow zones.

For each zone, a non-linear regression is performed, and the result of this regression presented graphically in the Zone Rates plot. The Y-scale can display density or holdups as relevant. Below is an illustration in a 2-phase oil-gas situation with spinner and density. The dashed line represents the measured density. The current solution is such that for the selected correlation (Dukler) the predicted density value (horizontal dotted line) is similar to the measured one (horizontal dashed line).

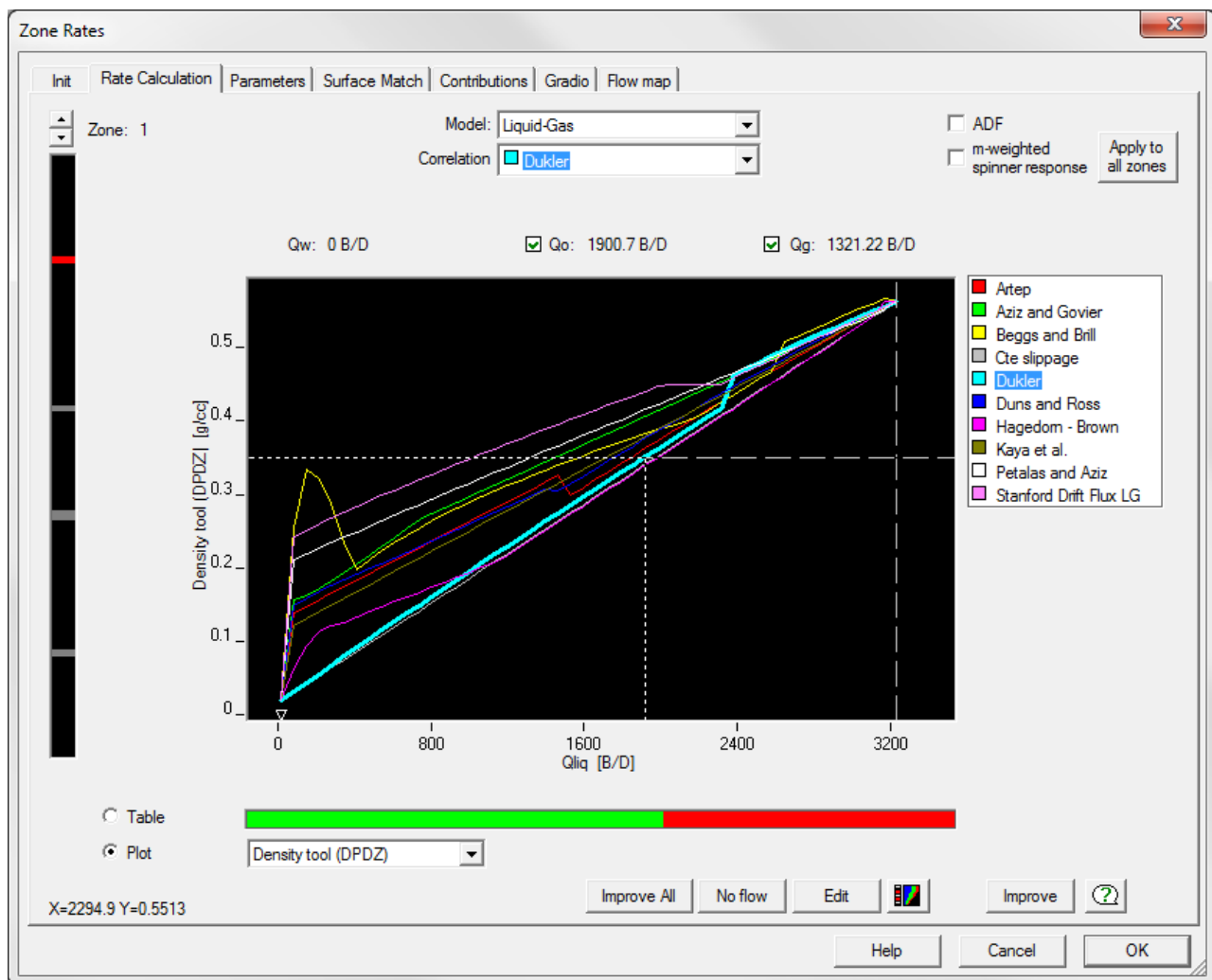


Fig. 14.I.6 – Emeraude Zone Rates dialog

Each colored line represents a different correlation. As we did previously, one way to look at this graph is to consider how different the rate solution will be depending on the selected correlation... The rationale behind a proper selection is to start by ruling out the correlations developed for situations not applicable to the particular test. Beyond this first elimination, it is possible to check which correlation is the most consistent with additional information, surface rates in particular. This selection is a very important step of the analysis, and at least should be noted and justified. Software defaults will not be a sufficient excuse.

14.I.7 Multiphase interpretation results

Below is a typical presentation. In this vertical oil-gas producer, 3 different (grey) calculation zones were selected to isolate the contributions of the two (red) perforations. The non-linear regression described previously was executed on all three calculation zones to get Q_o and Q_g . Actually on the bottom zone, the rate was set to 0 and water holdup to 1. On other zones we have only two measurements (spinner, and density) and we imposed $Q_w=0$, so the regression solved only for Q_o and Q_g . The results are summarized by the QZT track where the value of a given calculation zone are extended up to the inflow zone above, and down to the inflow below.

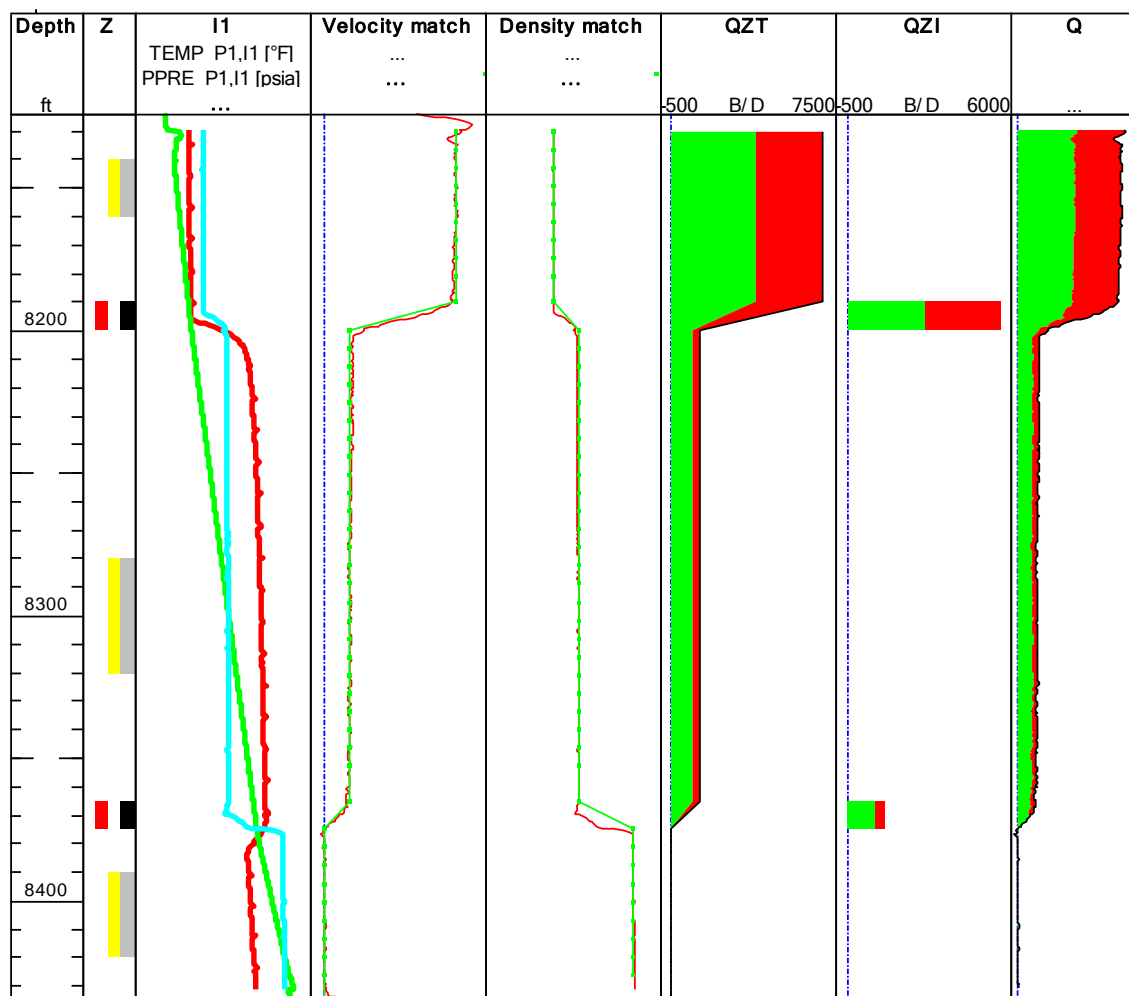


Fig. 14.I.7 – Typical multiphase result; Zoned approach

The QZI track represents contributions or injections and they are obtained basically by the difference of the rate above and below an inflow. The Q track represents the application of the non-linear regression at every depth frame.

The two match views show the comparison between target (red) and simulated (green) measurements. The simulated curves are obtained by feeding at every depth the known rates into the forward model, including in particular the slip correlation. The simulated curves and the QZT logs are referred to as schematics in Emeraude.

14.I.8 Local versus global regression

The Zoned approach described previously executes a series of unrelated non-linear regressions on the calculation zones; the contributions are then obtained by taking the difference of the rates above and below for each phase. By proceeding this way there is no guarantee that in the end the contributions of a given zone will be of the same sign.

To avoid this, it is possible to solve for the entire well at once with a single regression, the global regression, where the unknowns are the zone contributions, dQ 's. Since the contributions are the direct unknowns we can impose some sign constraints upfront. For each iteration the assumption of the dQ 's translates into a series of Q 's on the calculation zones, which can be injected into the forward model to calculate the objective function. Here again the objective function is evaluated on the calculation zones only; and to this error, other components might be added such as a constraint using the surface rates.






		Local	Global
	 Q_w^1, Q_o^1, Q_g^1	$E^1 = \Sigma (\text{meas}^1 - \text{sim}^1)^2$	$E = \Sigma (\text{meas}^1 - \text{sim}^1)^2$
dQ_w^1, dQ_o^1, dQ_g^1			+
	 Q_w^2, Q_o^2, Q_g^2	$E^2 = \Sigma (\text{meas}^2 - \text{sim}^2)^2$	$\Sigma (\text{meas}^2 - \text{sim}^2)^2$
dQ_w^2, dQ_o^2, dQ_g^2			+
	 Q_w^3, Q_o^3, Q_g^3	$E^3 = \Sigma (\text{meas}^3 - \text{sim}^3)^2$	$\Sigma (\text{meas}^3 - \text{sim}^3)^2$

Fig. 14.I.8 – Local vs. global regression

Note that whether the regression is local or global the end result is only influenced by the solution on the few user defined calculation zones. This is why we call this approach the 'Zoned' approach.

14.I.9 The Continuous approach

The clear advantage of the Zoned approach is speed, since only a few points are required to get an answer, even if the Global regression is finally run. Its main drawback is that the results are driven by the choice of calculation zones. A way to remove this dependency is to run a Global regression with the errors evaluated *everywhere* on the logs, and not only at a few points. We could for instance seek to minimize the difference between the data and the simulated measurement logs (the schematics) everywhere. When we look at match views however, we see that the schematics are very square in shape; this is because between inflow zones the mass rate does not change, and since we honor a slip model, there are little variations in holdups and deduced properties – see Fig. on previous page for instance.

The only way to account for the changes seen on the data is to let the holdups differ from the model prediction, locally, and at the same time to complement the objective function by a term measuring how far the solution deviates from the slip model prediction. More precisely, with the Continuous approach the Global regression can be modified as follows.

The **main regression loop** is still **on the contributions** but the objective function considers an error on the log points. In turn, at each depth, the simulated log values are evaluated by running a second **regression on the holdups** to minimize an error made of the difference between simulated and measured values, and at the same time, a **new constraint** using the slip model holdup predictions. In cases where one can do without the slip model, this new constraint is obviously not included.



Fig. 14.I.9 – Global regression in Continuous mode

14.I.9.a Illustration with a 3-Phase example

The Fig. below shows the result of the Zoned approach on a 3-phase example. The calculation zones (grey) were defined – see how the second perfo has been split. Local regressions have been run, followed by a Global regression with the constraint that all contributions are ≥ 0 .

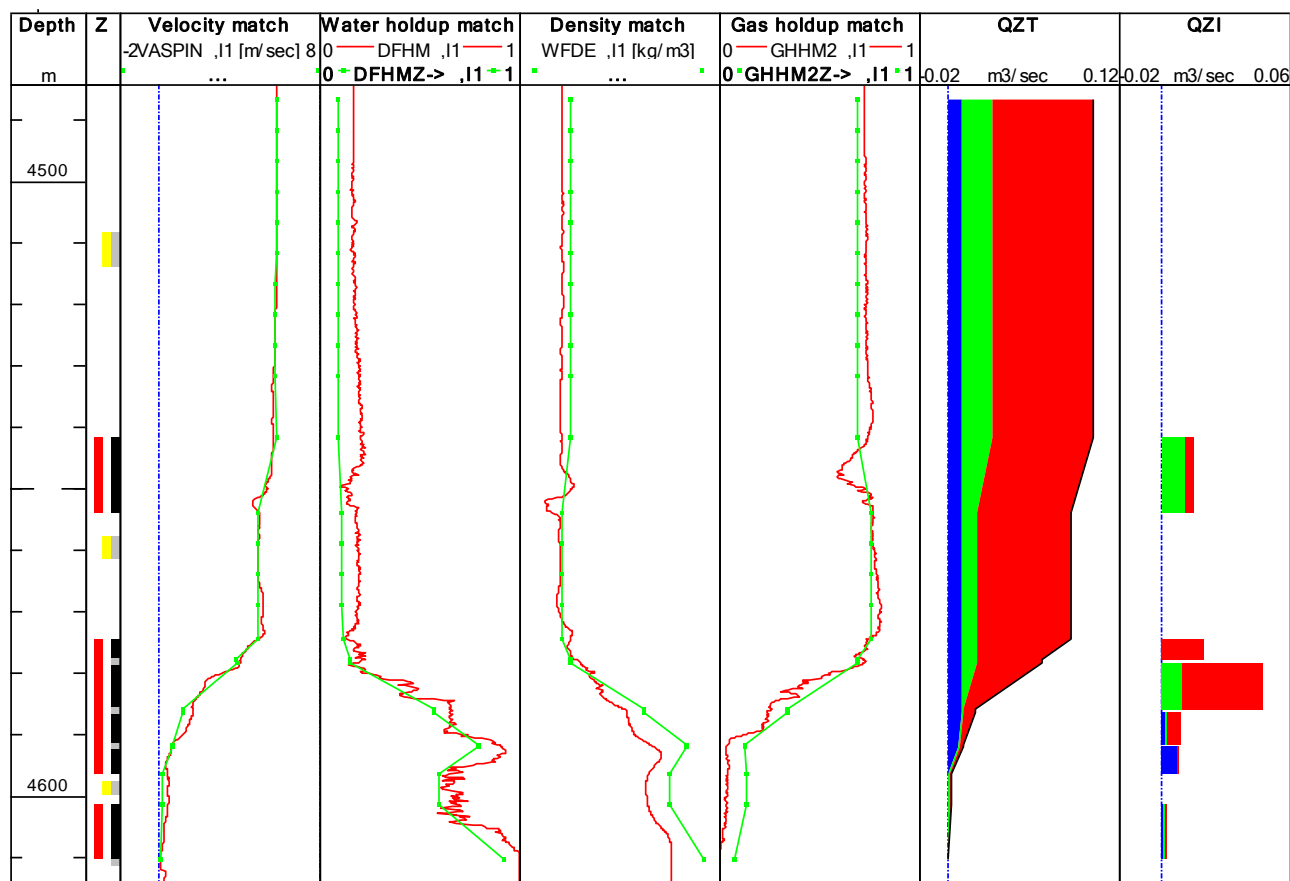


Fig. 14.I.10 – Example of zoned approach result in Emeraude

This example is now interpreted with the Continuous approach and the Global regression rerun. In the end, there are certain differences. The match looks better overall, but at the expense of not honoring the slip models. The deviation from the slip models is indicated in the rightmost track (line=model, markers=solution). *Note that the number of depth samples on the logs is user defined.*

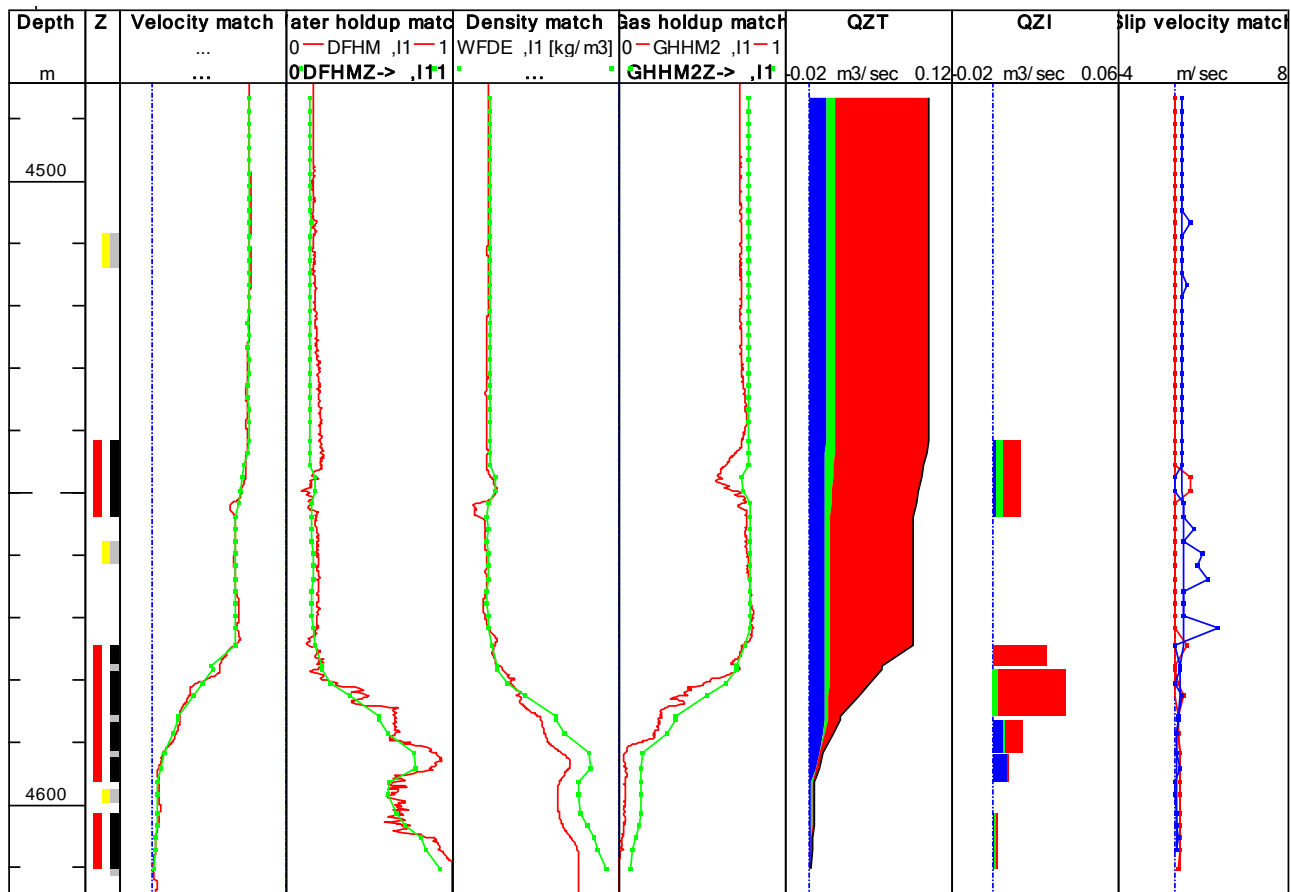


Fig. 14.I.11 – Example of continuous approach result in Emerald

14.I.9.b So?

In the above example there is no drastic benefit to use the Continuous method. But there are cases where reverse will apply, for instance when the data is unstable between contribution intervals. In this case, the location of the calculation zones may dangerously impact the Zoned method results. Note however, that the continuous method is also influenced by the location of the calculation zones *inside the inflows*, since the way the inflows are split has a direct influence on the shape of the simulated logs over the inflows. Another situation where the Continuous method might provide a better answer is with temperature, since the temperature is essentially an integral response. In Emerald the two methods, Zoned and Continuous, are offered in parallel and you can switch from one to the other at any stage.

It is important to stress that a nice looking match does not necessarily mean a right answer. It all comes down at some stage to the interpreter's judgment. Also, any regression is biased by the weights assigned to the various components of the objective function. Different weights will lead to different answers; starting point will also be critical as a complex objective function will admit local minima. So the Continuous approach is not a magical answer, and more complex does not necessarily mean better. The Continuous approach is more computing intensive and a bit of a black box.

14.J Slanted and Horizontal wells

Even though the solutions presented up to now are in principle applicable to any well geometry, things get terribly complex in deviated or horizontal wells. The response of a conventional tool in these environments can be unrepresentative of the flow behavior; in addition, even if the tool responses can be trusted, the slippage models can turn out to be inadequate.

14.J.1 Apparent down flow

In a slanted well with significant water holdup, the water phase tends to be circulated around while the light phase is going up. As the light phase occupies a small section of the pipe, the spinner will mostly see the water going down and a straight analysis will come up with a negative water rate.

The heavy phase is not limited to water and could also be oil.

One way to deal with this situation is to use a dedicated model considering that the heavy phase is essentially static while the light phase moves up at a speed proportional to the slippage velocity. The only requirement is to have some holdup measurement, and to deduce the slippage velocity by matching this holdup.

Another possible way of dealing with this situation is to use the temperature quantitatively as one of the target measurements. This obviously requires a forward temperature model representing the necessary thermal exchanges between the fluid, the reservoir, and the well.

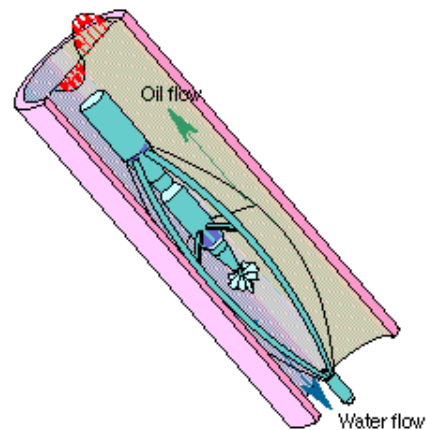


Fig. 14.J.1 – Flow recirculation

14.J.2 Horizontal wells

The first problem in horizontal well logging is that the tools do not go down by gravity. Dedicated conveyance systems are required, the two families being coiled tubing, or tractors. The conveyance may affect the measurements as for instance, with tractors, sometimes all the power goes into the tractor running in and one is only able to log coming up.

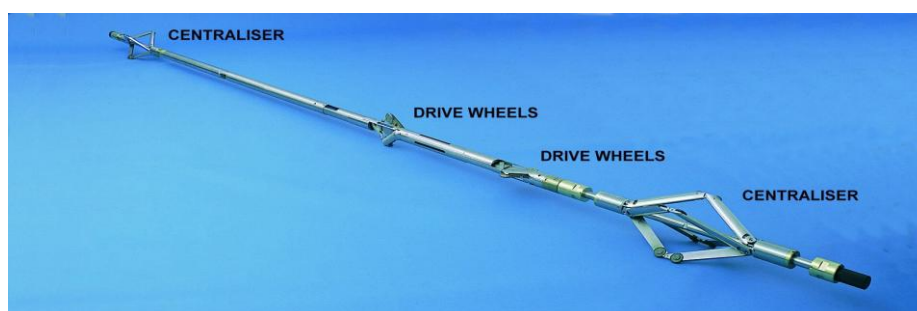


Fig. 14.J.2 – Tractor example; Courtesy Sondex

Horizontal wells are rarely strictly horizontal and unfortunately, slippage velocities hence holdups are very sensitive to slight changes of deviation around the horizontal.

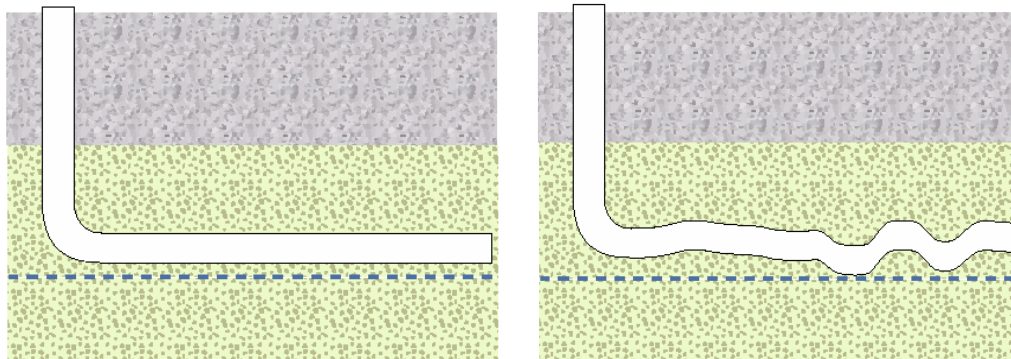


Fig. 14.J.3 – Horizontal well trajectory; ideal and real

The pictures below taken in the Schlumberger Cambridge Research flow loop show this dependence. A 50-50 rate mixture is flown with water and oil. A blue dye is injected in the water and at the same time a red dye in the oil. At 90° both phases move at the same speed and the holdups are 50% each. At 88° , i.e. going uphill by only 2 degrees, the oil flows much faster and its holdup decreases significantly. Conversely, going downhill by 2° at 92° , the situation is reversed with the water going faster.

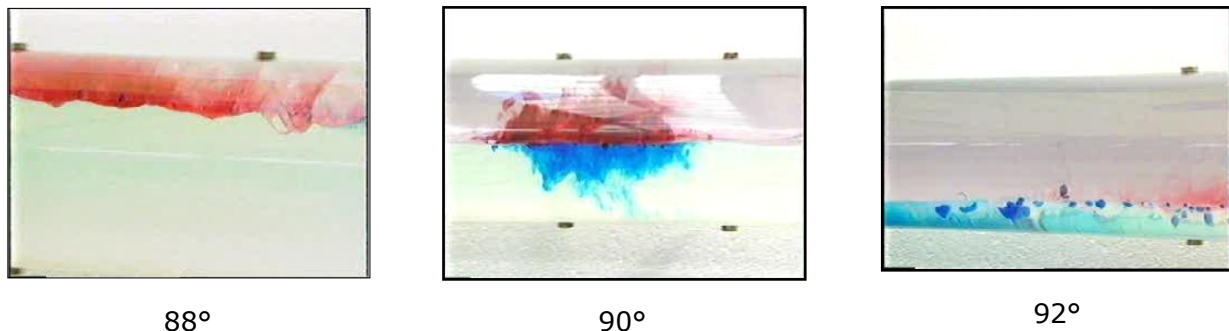


Fig. 14.J.4 – Slippage dependence around horizontal; Courtesy Schlumberger

It is not difficult to imagine that with undulations, the change from one behavior to the other will not be immediate, leading to intermittent regimes such as waves. In this situation, the response of conventional tools will most of the time be useless. Even if they were reliable, slippage models that capture the physical behaviors in this situation are few.

The undulation of the wellbore will also create natural traps for heavy fluids in the lows and light fluid in the highs. Those trapped fluids will act as blocks and obviously impact the tool responses when they occur. A last condition worth mentioning is that the completion may offer flow paths not accessible to the conventional tool, e.g. with a slotted liner and multiple external packers for instance.

For all the above reasons, specific tools were developed, called Multiple Probe Tools, or MPT. The goal with those tools is to replace a single value response with a series of discrete points in order to better characterize the flow behavior, and ultimately to remove the need for slippage models.

14.K Multiple Probe Tools (MPT), or Array Tools

14.K.1 Schlumberger FloView – *Courtesy Schlumberger*

The FloView is a generic name that includes the PFCS and the DEFT. The tools include 4 or 6 water holdup probes that use the electrical conductivity of water to distinguish between the presence of water and hydrocarbons.

In a water continuous phase, current is emitted from the probe tip and returns to the tool body. A droplet of oil or gas has only to land on the probe tip to break the circuit and be registered.

In an oil continuous phase a droplet of water touching the probe tip will not provide an electrical circuit. Instead, the water droplet must connect the electrical probe to the earth wire. This requires a larger droplet than is needed for gas or oil detection in a water-continuous phase.

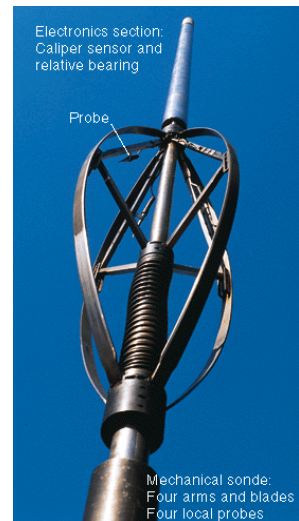


Fig. 14.K.1 – DEFT

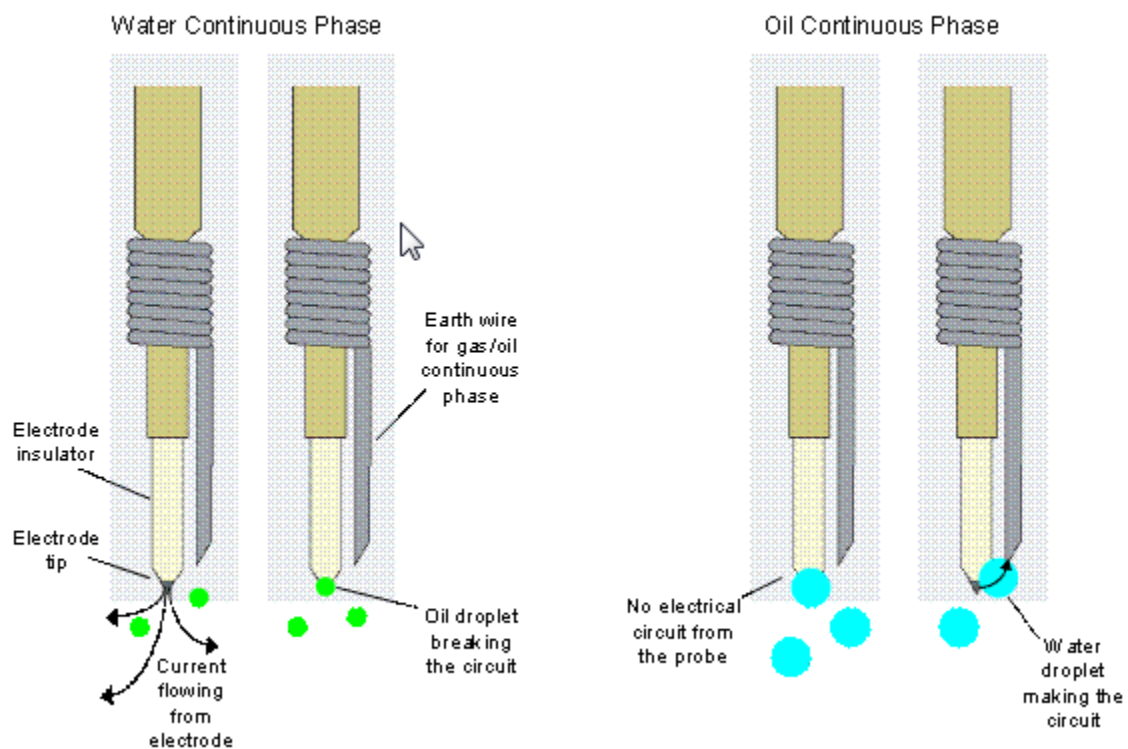


Fig. 14.K.2 – Theory of FloView Probe Operation, *Courtesy Schlumberger*

The signal from the FloView probe lies between two baselines, the continuous water-phase response and the continuous hydrocarbon-phase response. To capture small transient bubble readings a dynamic threshold is adjusted close to the continuous phase and then compared with the probe waveform. A binary water holdup signal results, which when averaged over time becomes the probe holdup. The number of times the waveform crosses the threshold is counted and divided by 2 to deliver a probe bubble count.

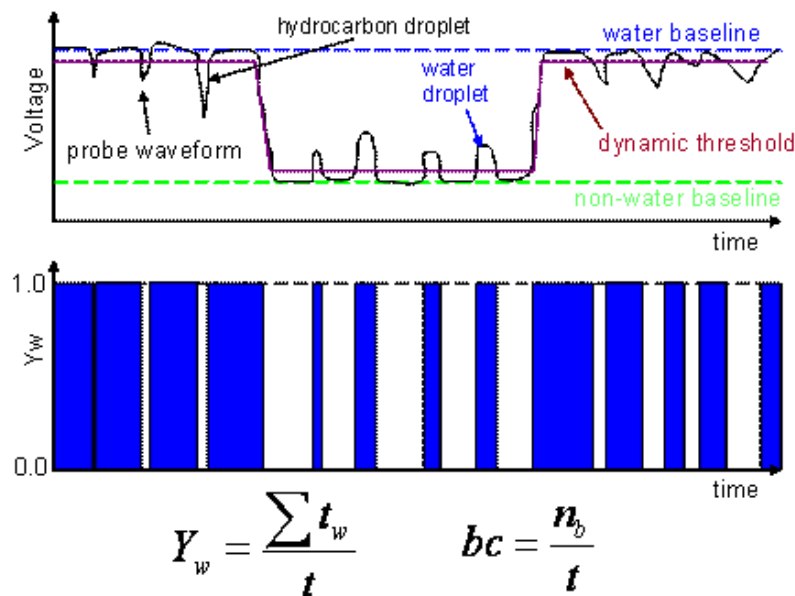


Fig. 14.K.3 – FloView Probe Waveform Processing, Courtesy Schlumberger

14.K.2 Schlumberger GHOST – Courtesy Schlumberger

The GHOST comprises 4 gas holdup probes. The probes use the refractive indices of gas, oil, and water to distinguish between the presence of gas and liquid.

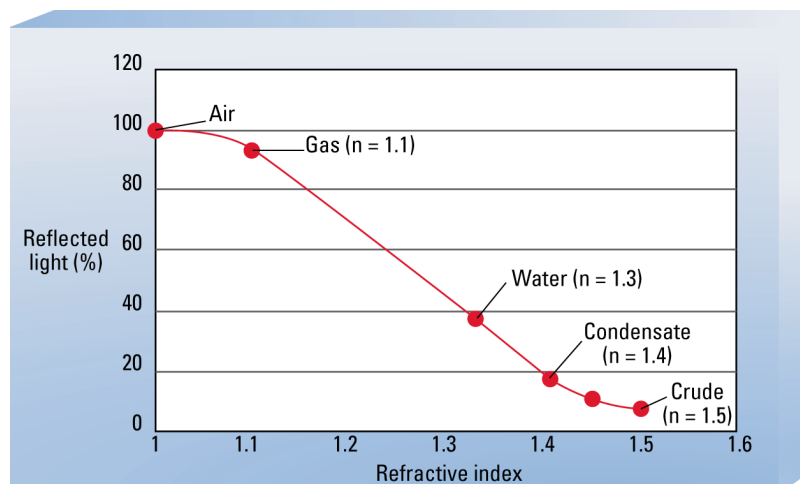


Fig. 14.K.4 – Reflected Light versus Refractive Index, Courtesy Schlumberger

Light emitted at a suitable frequency is fed down an optical fiber through a Y-coupler and finally to an optical probe made from synthetic sapphire crystal. Light that does not escape is returned via the Y-coupler to a photodiode and is converted to a voltage.

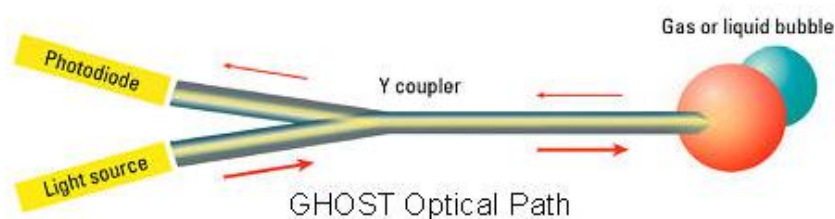


Fig. 14.K.5 – Sensor Optical Path, Courtesy Schlumberger

The signal from the optical probe is at or below the gas baseline and at or above the oil baseline. To capture small transient bubble readings a dynamic threshold is adjusted close to the continuous gas phase and close to the continuous liquid phase. The threshold is then compared with the probe waveform to deliver a binary gas holdup signal, which is averaged over time. The number of times the waveform crosses the threshold is counted and divided by 2 to deliver a probe bubble count.

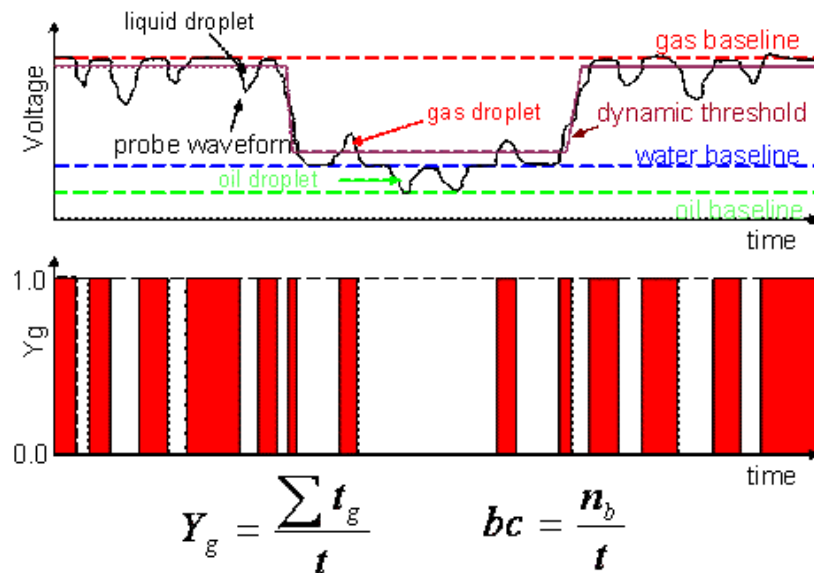


Fig. 14.K.6 – Optical Probe Waveform Processing, Courtesy Schlumberger

14.K.3 Schlumberger FloScanner (FSI) – Courtesy Schlumberger

The FSI combines 5 micro-spinners (MS) with 6 FloView probes (Electrical - Ep) and 6 GHOST probes (Optical - Op). The tool is designed to sit on the low side of the pipe by gravity, hence providing water holdup, gas holdup, and velocity profiles on a vertical axis.

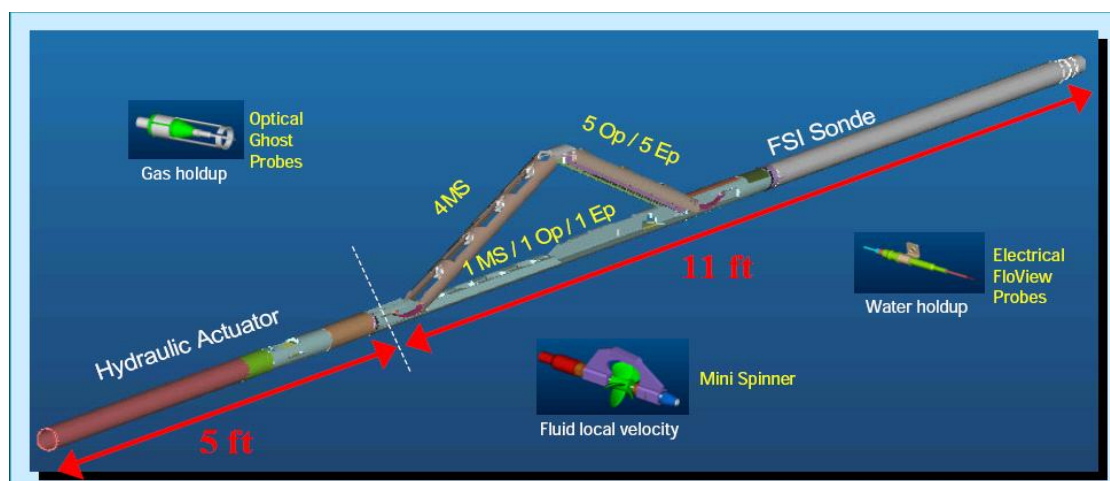


Fig. 14.K.7 – FSI tool geometry; Courtesy Schlumberger

The operation principle of the holdup sensors is the one explained in the previous sections. The calibration of the individual FSI spinners is pretty straightforward, as the spinners are supposed to be in the same vertical location from one pass to the other.

14.K.4 Sondex MAPS: CAT / RAT / SAT

14.K.4.a CAT: Capacitance Array Tool



Fig. 14.K.8 – CAT; Courtesy Sondex

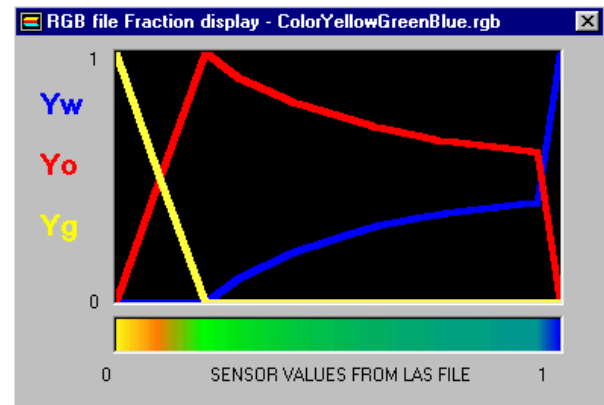


Fig. 14.K.9 – Normalized values in [Gas-Oil] then [Oil-Water] mixtures

The CAT uses 12 capacitance probes distributed on a circumference. As with any capacitance sensor, the CAT probes discriminate mostly between water and hydrocarbons. The contrast in dielectric values for oil and gas may however be used to differentiate the two fluids.

In a stratified environment the probe response can be used to get holdup values using 2 two-phase calibrations as represented on the graph above. When the probe normalized response is between 0 and 0.2 a gas-oil system is considered, and from 0.2 to 1, an oil-water system. To solve in three phase without any assumption about the local holdups, a 3-phase response can be used as shown below. This response is an extension of the previous graph that constitutes the intersection of the surface with the side walls.

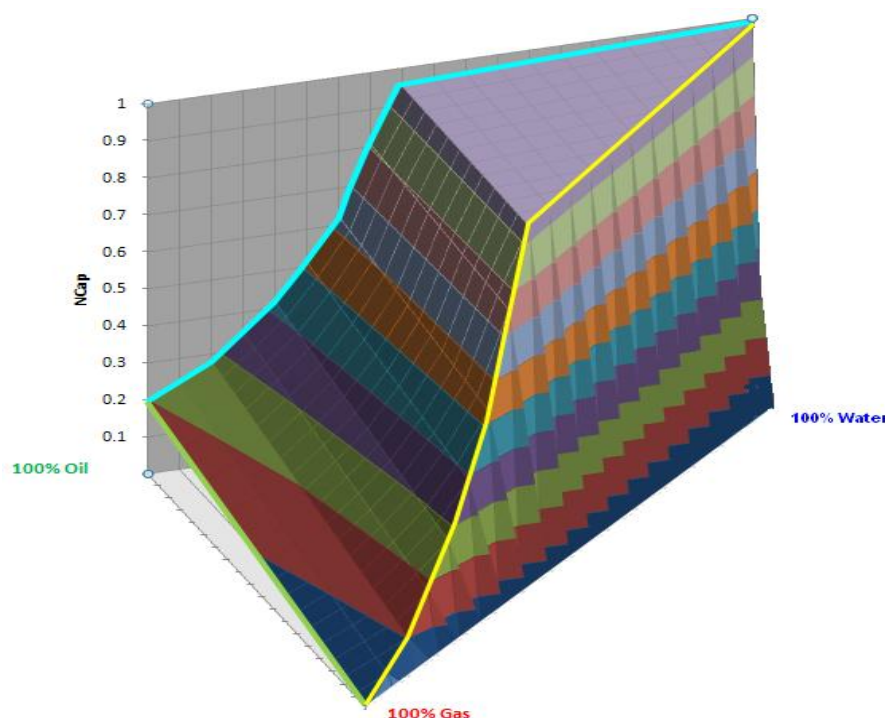


Fig. 14.K.10 – 3-Phase CAT response - Note the 2-phase segments:
Oil-Gas Oil-Water Gas-Water

14.K.4.b RAT: Resistance Array Tool

The tool incorporates 12 sensors arranged on a circumference. The sensors mechanics comprise (1) a probe tip that ultimately connects to the sensor electronics input and (2) a reference contact, typically at earth potential.

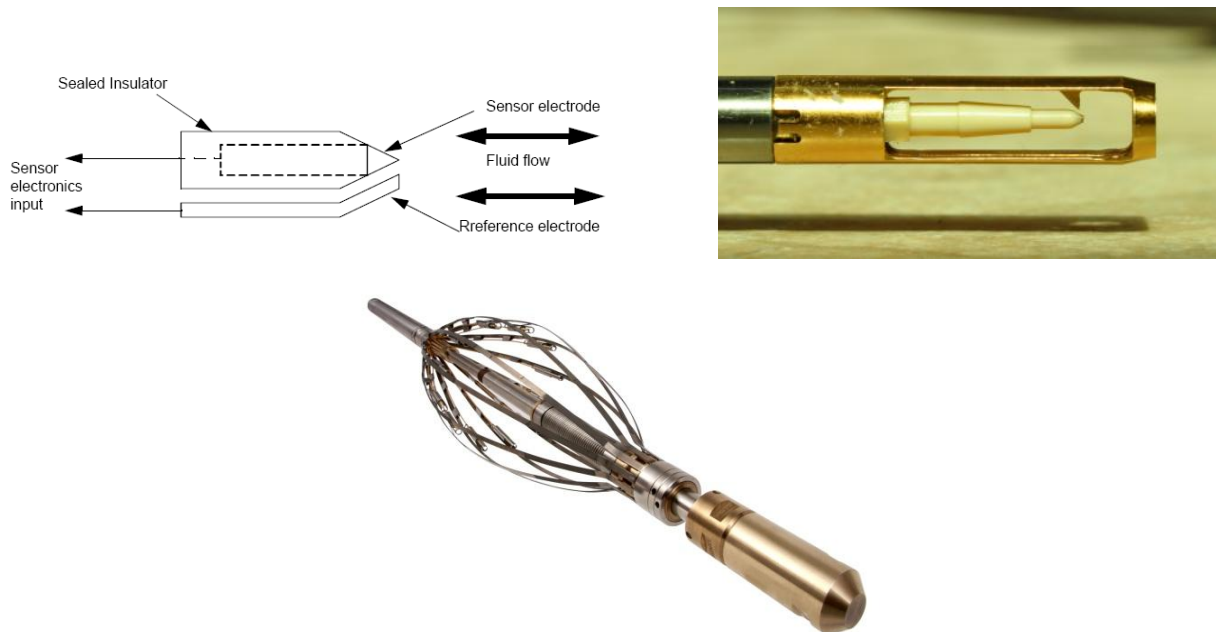


Fig. 14.K.11 – RAT, and RAT probes

Courtesy Sondex

Resistance measurements are made between the probe tips, and result in a number that is proportional to the logarithm of the resistance detected between the electrodes, and therefore the fluid resistivity. The field outputs include a mean resistivity and a standard deviation over a small time window, as well as histograms. The usual processing is based on the mean resistivity, R , considered to be a linear function of the conductive water resistivity R_c and the insulating hydrocarbon resistivity R_i .

The water holdup is thus obtained directly as:
$$Y_w = \frac{R - R_i}{R_c - R_i}$$

14.K.4.c SAT: Spinner Array Tool



Fig. 14.K.12 – SAT, and SAT probes

Courtesy Sondex

The SAT uses 6 micro spinners distributed again on a circumference. One of the complexities of the SAT is that the MAPS tool string can usually freely rotate, hence a SAT spinner will typically be at a different position in the pipe at a given depth for distinct passes. This makes the spinner calibration in flowing conditions problematic.

14.L MPT interpretation

For any MPT tool, the exact position of the probes at a given depth is determined from the tool geometry, the local diameter, and the tool bearing which is part of the acquired measurements. The first required step of a quantitative analysis is to move from the discrete values, to a 2D representation. Having this 2D representation will then serve two purposes:

- (1) Integration of the individual properties to have representative average
- (2) Combination of the local properties to get phase rates, and integration

Imagine for instance that we know holdups and velocity everywhere. Locally we can assume that there is no slippage and at every location in the cross-section, calculate the phase rates as the local velocity multiplied by the local holdup. By integrating the phase rates, we can get average phase rates directly, and therefore produce a final result without the need for slippage models.

14.L.1 Mapping models

Mapping models assume horizontal stratification. If the flow regime is segregated then a conventional analysis from the average holdups and velocity will be adequate.

14.L.1.a Linear model

The linear model defines the measurement of interest by a number of variables representing the values of that measurement along the local vertical axis. There are as many variables as there are distinct valid projections of probe readings on this axis. The values are then extended laterally. Without further constraints, the linear model will go exactly through the projected values. This is illustrated below with a RAT pass. The 12 projections define the values of water holdup on the vertical axis, and those values are extended laterally. The colored 2D map of the water holdup (water = blue and oil = green) shows segregation but the holdup does not strictly decrease from bottom to top.

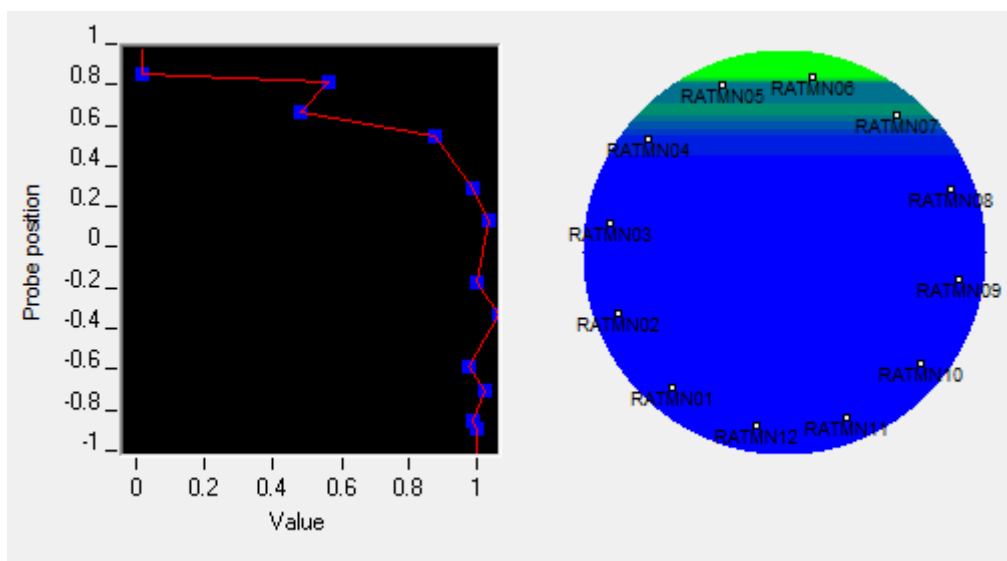


Fig. 14.L.1 – RAT mapping with the linear model; no constraint

To correct the previous situation it is possible to alter the linear model using gravity segregation constraints, i.e. imposing that water hold-up decreases from bottom to top, or gas holdup increases from bottom to top.

A non-linear regression can be used to try and match the values and satisfy the constraints at the same time. The result is shown below.

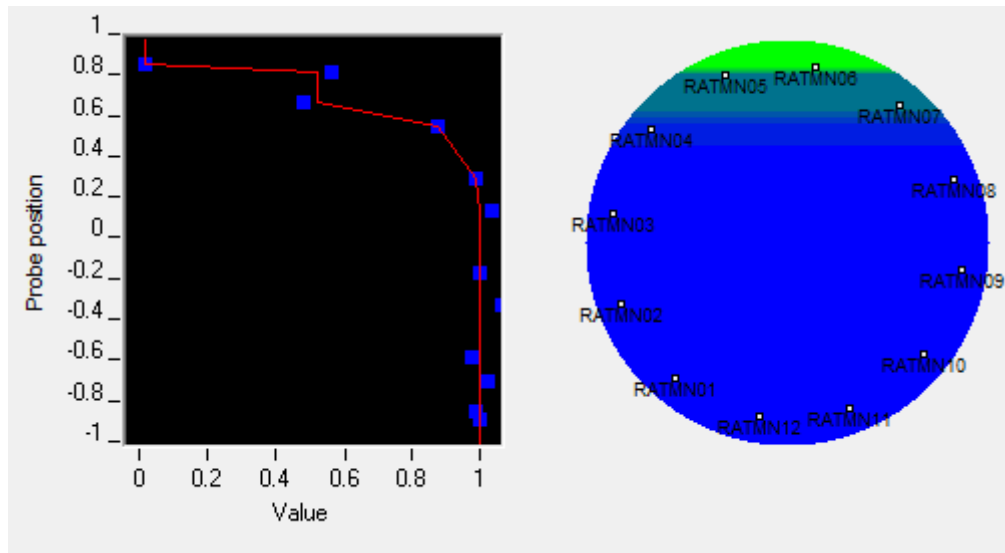


Fig. 14.L.2 – RAT mapping with the linear model; segregation constraint applied

14.L.1.b MapFlo holdup model

This model is restricted to Schlumberger holdup measurements. It can be used with PFCS, DEFT, GHOST, FSI or even combinations. All the model tries to match, like the linear model, is the projection of the measurements on the vertical axis. The MapFlo model is based on 2 parameters and produces the typical shapes/responses shown below.

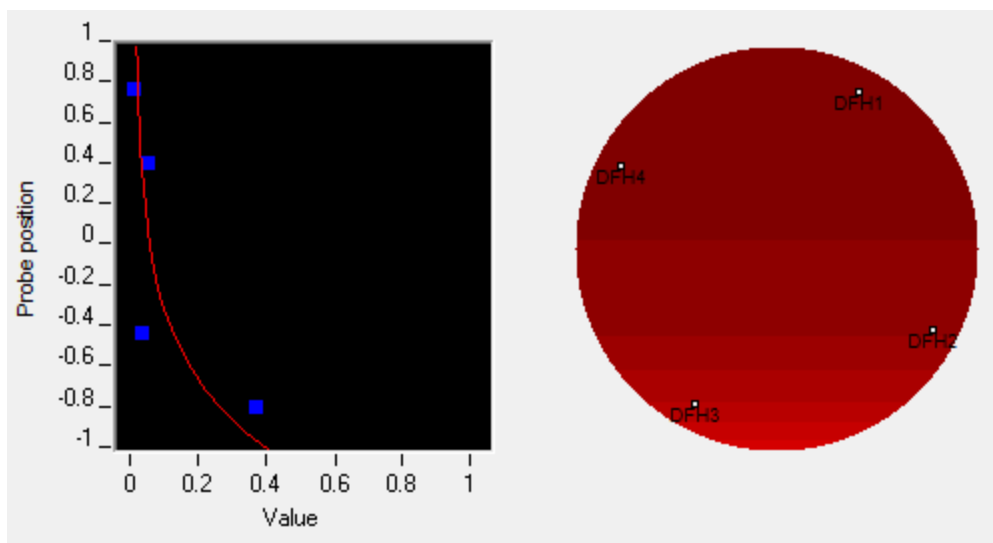


Fig. 14.L.3 – PFCS mapping with the MapFlo model

14.L.1.c Prandtl velocity model

This model can be used for the FSI velocity mapping.

Like MapFlo it is driven by 2 parameters. The main idea behind this model is to obtain the velocity profile by applying a linear transformation of the holdup profile and then rounding the profile near the pipe walls. More precisely, the velocity profile is obtained with the equation below, regressing on α and β to match the velocity projections.

$$[(Y_w - Y_g) \times \alpha + \beta] \times \left(1 - \left|\frac{z}{r}\right|\right)^{1/7}$$

The next Figure shows how the vertical holdup and velocity profiles were obtained on an FSI example with MapFlo and Prandtl combined.

The water holdup is 0 everywhere; the gas holdup profile is shown in red (see the Y_g scale at the bottom). The velocity profile is displayed with the yellow curve; one spinner was ignored in this case. The squares represent the discrete measurements (blue= Y_w , red= Y_g , yellow= V).

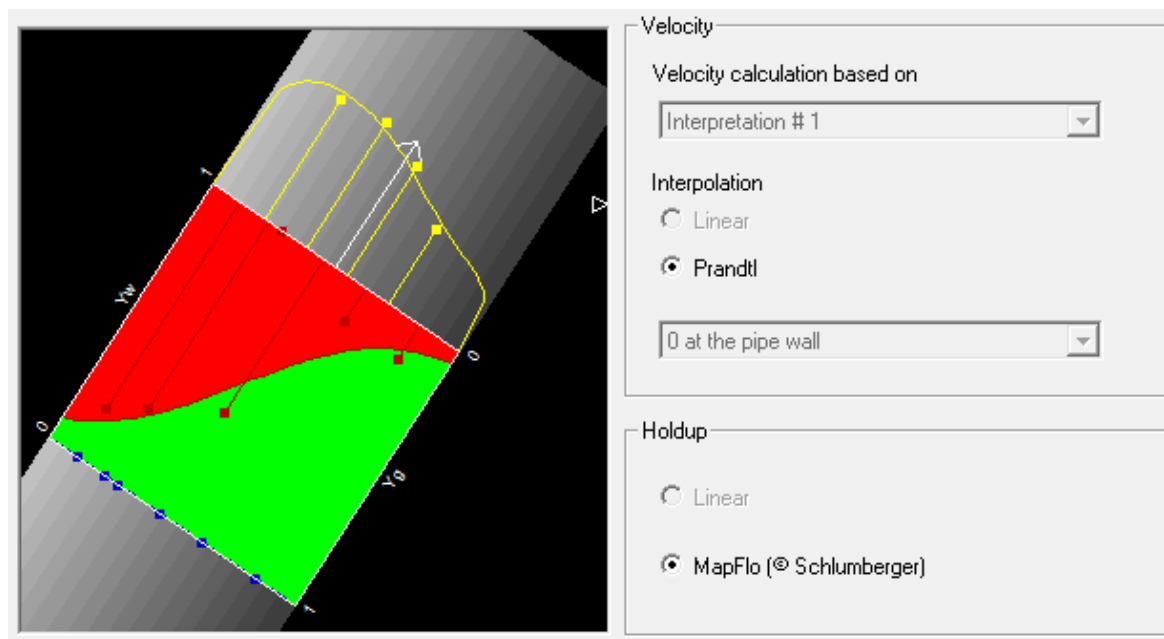


Fig. 14.L.4 – FSI mapping in a deviated well with Mapflo and Prandtl

It should be noted that the Prandtl model rounds the edge of the velocity on the entire circumference and not just at the top and bottom.

A typical 3d velocity profile is shown in the following figure.

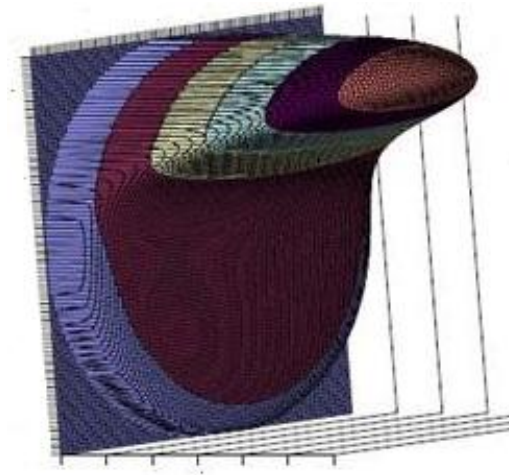


Fig. 14.L.5 – A typical Prandtl Velocity Profile; Courtesy Schlumberger

14.L.2 Mapping options

We saw how the basic framework used to map the 2D models is based on non-linear regression. This framework offers a lot of flexibility in the number of inputs as well as the inclusion of external constraints. We mentioned the ability to associate gravity segregation constraints with the linear model. It is also possible to constrain the process by the value of conventional tool, e.g. a density tool for instance.

Finally, the optimization can be based on several passes at the same time if the conditions are stable from one pass to the other. When the tool rotates (MAPS, PFCS, GHOST) this provides the ability to multiply the points of measurements in the cross-section at every depth and can compensate for faulty probes.

14.L.3 Integration

The mapping allows integrating over the cross-section at every depth in order to get average values.

$$Y_w = \frac{\int_S Y_w \times dS}{S}; Y_g = \frac{\int_S Y_g \times dS}{S}; Y_o = \frac{\int_S Y_o \times dS}{S}; V = \frac{\int_S V \times dS}{S}$$

As explained earlier, with the assumption of no local slippage, we can use the local velocity and holdups to obtain phase rates.

$$Q_w = \frac{\int_S Y_w \times V \times dS}{S}; Q_o = \frac{\int_S Y_o \times V \times dS}{S}; Q_g = \frac{\int_S Y_g \times V \times dS}{S}$$

14.L.4 Interpretation

The interpretation is conducted using the process outputs: holdups, phase rates, total velocity together with any additional tool available. Even though the answers we are seeking are in essence already provided (we have the phase rates everywhere) the interpretation is still a required step to come up with actual zone contributions, possibly honoring additional constraints (sign, surface rates).

Using the Continuous method is the best choice as it contains a built-in mechanism to by-pass any slippage model on the recognition that enough information is supplied. Below is a typical output example for an FSI job.

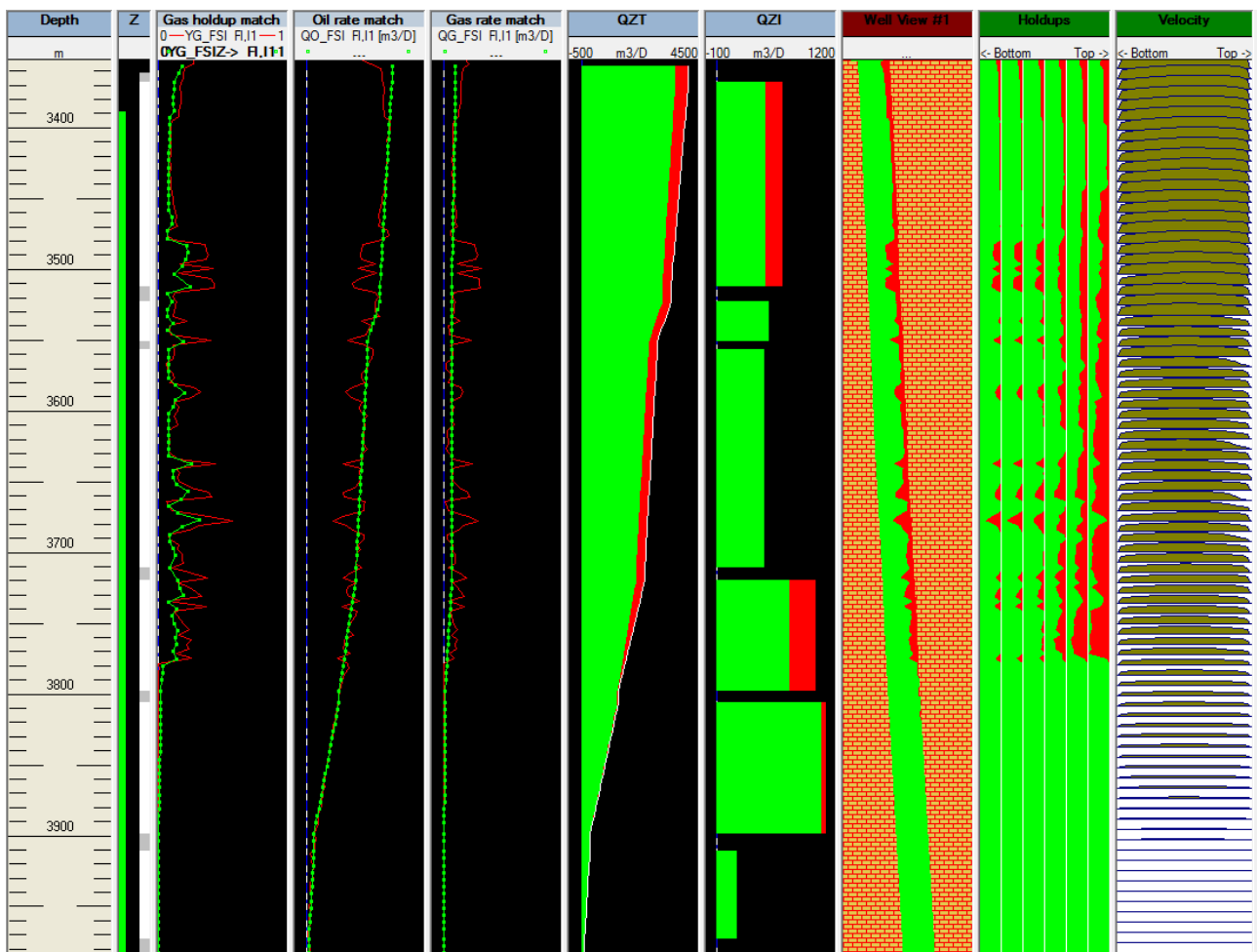


Fig. 14.L.6 – FSI Interpretation

14.M SIP

Selective Inflow Performance (SIP) provides a mean of establishing the steady state inflow relationship for each producing layer.

The well is flowed at several different stabilized surface rates and for each rate, a production log is run across the entire producing interval to record simultaneous profiles of downhole flow rates and flowing pressure. Measured in-situ rates can be converted to surface conditions using PVT data.

The SIP theory is strictly valid for single-phase.

To each reservoir zone corresponds, for each survey/interpretation, a couple [rate, pressure] used in the SIP calculation.

For the pressure, the interpretation reference channel is interpolated at the top of the zone.

For the rate, the value used in the SIP is the contribution. It is calculated for a given reservoir zone as the difference between the values interpolated on the schematic at the top and the bottom of that zone.

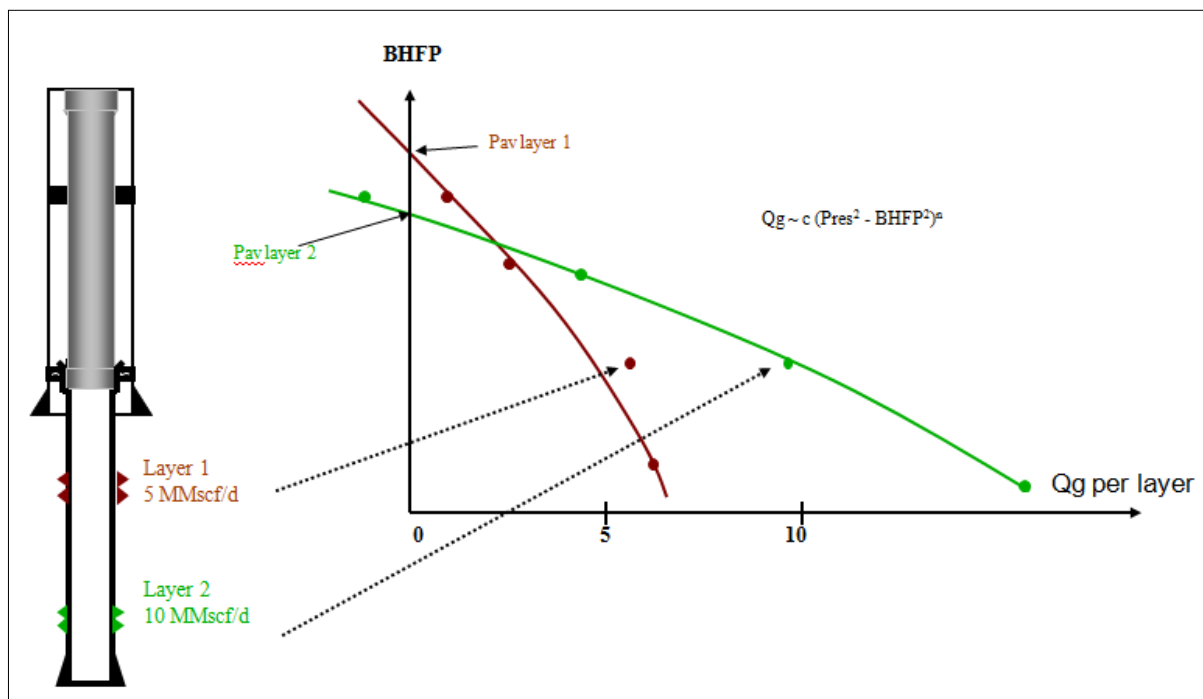


Fig. 14.M.1 – SIP example with 2 layers, 3 rates and a shut-in survey

14.M.1 IPR Type

Different IPR equations can be used: Straight line, C&n, and LIT relations. In the case of a gas well, the pseudo pressure $m(p)$ can be used instead of the pressure p to estimate the gas potential.

Straight line: $Q = PI \times (\bar{p} - p)$

LIT (a & b): $\bar{p}^2 - p^2 = a \times Q + b \times Q^2$

or $m(\bar{p}) - m(p) = a \times Q + b \times Q^2$

Fetkovitch or C&n: $Q = C \times (\bar{p}^2 - p^2)^n$

or $Q = C \times (m(\bar{p}) - m(p))^n$

It is possible to generate the SIP after correcting the pressures to a common datum. This is typically done using the shut-in pressure profile for the estimation of the hydrostatic head between layers. A pressure corrected SIP highlights the eventual crossflow between layers.

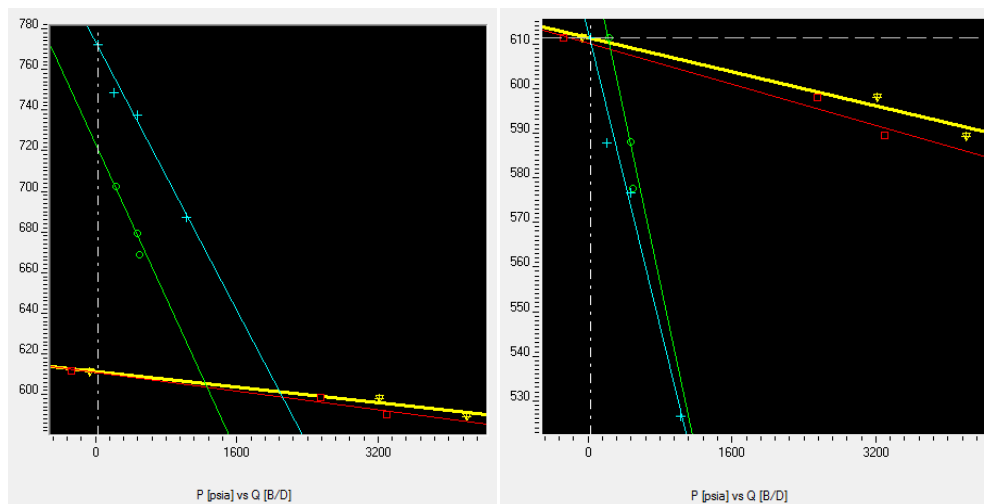


Fig. 14.M.2 – SIP example without and with datum correction

14.N Temperature

Temperature can be used quantitatively to replace a missing or faulty spinner provided an adequate temperature model is available. This model should provide the temperature everywhere in the wellbore, from an assumed distribution of contributions. Such a model needs to capture the following:

- Temperature changes occurring inside the reservoir (compressible effects, friction). Those are often reduced to simply a Joule-Thomson cooling/heating but the reality is more complex
- Temperature changes in the wellbore: due to convection (transport), conduction to the surrounding, changes of enthalpy in front of inflows, and changes due compressible effects in the wellbore

It is beyond the scope of this chapter to describe the Emeraude temperature models in details. There are currently two such models, the most advanced one capturing all the above effects by solving numerically a general energy equation coupled to a mass balance equation. Below is an example match in an apparent downflow situation.

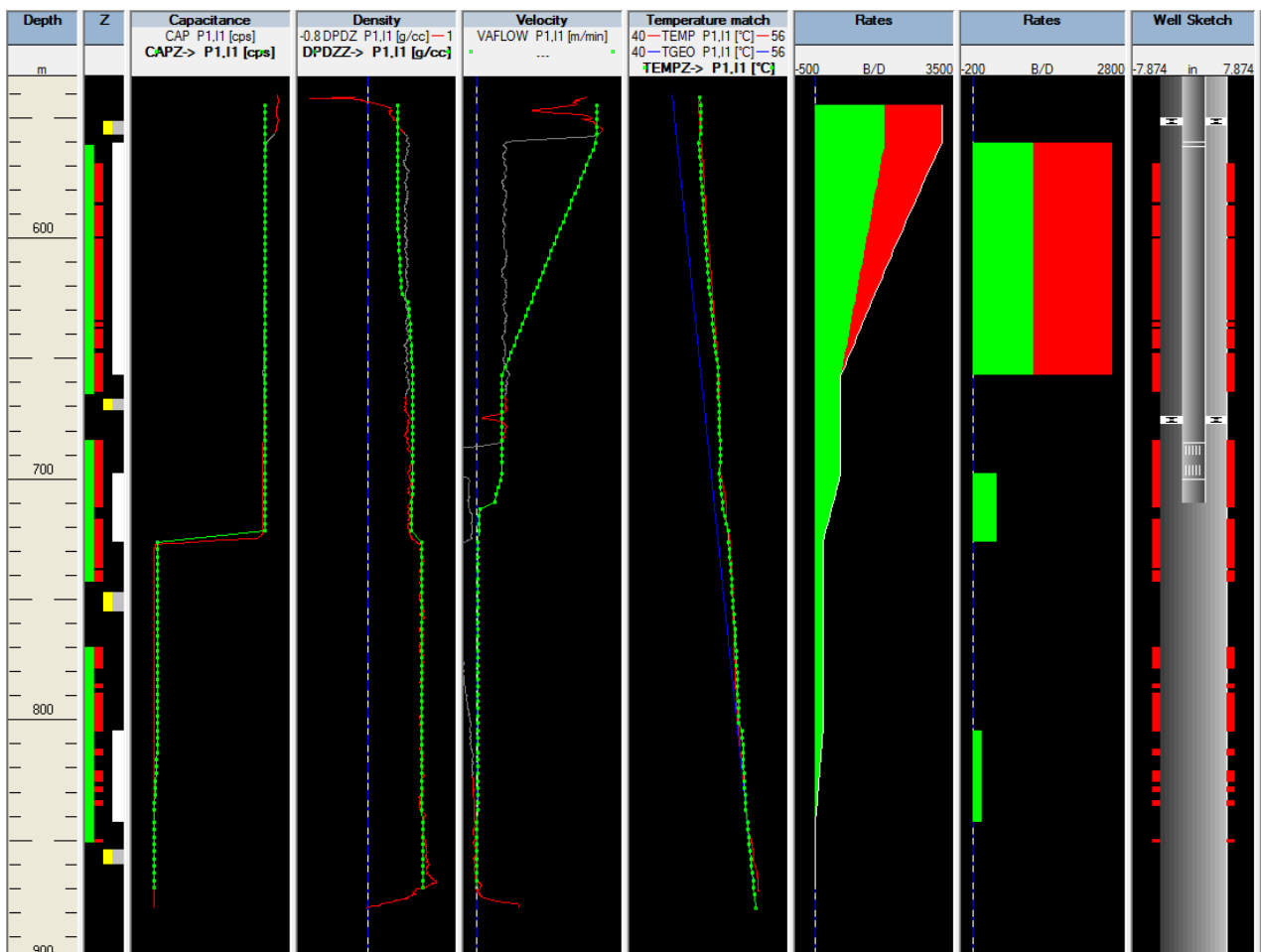


Fig. 14.N.1 – Temperature match in Emeraude

Working with temperature requires a large number of inputs, typically: geothermal profile, rock thermal properties, fluid heat capacities, thermal properties of the completion elements, reservoir petrophysical properties, etc. If those parameters are not available, they become additional degrees of the freedom of the problem leading to multiple answers. In any case, the discrimination of the phases still needs fluid identification measurements like density or holdups.



TABLE OF CONTENTS



1 – INTRODUCTION	3
1.A WHAT IS THE PURPOSE OF THIS BOOK?	3
1.B WHAT IS DYNAMIC DATA ANALYSIS?	5
1.C PRESSURE TRANSIENT ANALYSIS (PTA).....	8
1.D PRODUCTION ANALYSIS (PA).....	12
1.E PERMANENT DOWNHOLE GAUGES	14
1.F OTHER CANDIDATES FOR DYNAMIC DATA ANALYSIS (DDA)	15
1.F.1 Formation testers	15
1.F.2 Temperature diffusion	15
1.G BOOK CONTENT.....	16
1.H HOW MANY EQUATIONS DO YOU WANT?.....	17
1.I OTHER BOOKS FOR REFERENCE	18
2 – THEORY	19
2.A DIFFUSION EQUATION	19
2.A.1 Darcy's law	19
2.A.2 The diffusivity equation	20
2.A.3 Diffusion in a homogeneous isotropic reservoir	22
2.B INITIAL, WELL AND OUTER BOUNDARY CONDITIONS	24
2.B.1 Initial conditions	24
2.B.2 Well conditions	24
2.B.3 Outer boundary conditions	25
2.C LINE SOURCE SOLUTION IN A HOMOGENEOUS INFINITE RESERVOIR	26
2.C.1 Derivation.....	26
2.C.2 The Line Source Solution	28
2.D WELLBORE STORAGE AND SKIN	30
2.D.1 Wellbore storage	30
2.D.2 Skin	31
2.D.3 Derivation.....	33
2.D.4 Behavior.....	35

2.E	OUTER BOUNDARY CONDITIONS	36
2.E.1	<i>Major types of boundaries.....</i>	36
2.E.2	<i>Derivation for a circular reservoir.....</i>	37
2.E.3	<i>Pseudo-Steady State flow</i>	38
2.F	COMPLEX PRODUCTION HISTORIES – SUPERPOSITION IN TIME	40
2.F.1	<i>The principle of superposition</i>	40
2.F.2	<i>Build-up superposition.....</i>	41
2.F.3	<i>Multirate superposition</i>	42
2.G	OTHER MEANS TO SOLVE AND MODEL A DIFFUSION PROBLEM	43
2.G.1	<i>Superposition in space of analytical models (image wells).....</i>	43
2.G.2	<i>Semi-analytical solutions</i>	44
2.G.3	<i>Boundary elements</i>	45
2.G.4	<i>Numerical models</i>	45
2.H	PHYSICAL MEANING OF DIFFUSION	46
2.H.1	<i>Reference case</i>	46
2.H.2	<i>Effect of 'unknown' parameters</i>	48
2.H.2.a	Wellbore storage.....	48
2.H.2.b	Skin	49
2.H.2.c	Permeability	50
2.H.2.d	Reservoir size	51
2.H.3	<i>Effect of 'known' parameters</i>	52
2.H.3.a	Wellbore radius.....	52
2.H.3.b	Porosity	53
2.H.3.c	Total compressibility	54
2.H.3.d	Viscosity	55
2.H.3.e	Thickness	56
2.H.3.f	How about rates?	57
2.H.4	<i>Conclusions.....</i>	58
2.H.4.a	on this series of designs.....	58
2.H.4.b	on the equations	58
2.H.5	<i>Effect of errors on the different input parameters</i>	59
2.I	THE CASE OF DRY GAS	61
2.I.1	<i>The PVT of real dry gas</i>	61
2.I.2	<i>Derivation of the real dry gas diffusion</i>	62
2.I.3	<i>Diffusion of real dry gas</i>	63
2.I.3.a	Standard pseudopressures	63

2.I.3.b	Normalized pseudopressures	64
2.I.4	Non-Darcy flow	65
3	– PRESSURE TRANSIENT ANALYSIS	67
3.A	INTRODUCTION	67
3.B	THE OLD STUFF	68
3.B.1	<i>IARF and Semilog plots</i>	68
3.B.2	<i>Drawdown response and MDH plot</i>	68
3.B.3	<i>Build-up response and Horner plot</i>	70
3.B.4	<i>Shut-in after a complex production and superposition plot</i>	72
3.B.5	<i>Complex productions and rate normalized superposition plot</i>	73
3.B.6	<i>Other specialized plots</i>	75
3.B.7	<i>IPR & AOF</i>	76
3.C	THE 'RIGHT' STUFF	77
3.C.1	<i>Before the Bourdet Derivative</i>	77
3.C.2	<i>Definition of the Bourdet Derivative</i>	78
3.C.3	<i>Bourdet Derivative & Infinite Acting Radial Flow (IARF)</i>	79
3.C.4	<i>Bourdet Derivative & Wellbore Storage</i>	80
3.C.5	<i>The original idea behind the Bourdet Derivative</i>	80
3.C.6	<i>Bourdet Derivative & other flow regimes</i>	81
3.C.7	<i>Bourdet Derivative & Other models</i>	82
3.C.8	<i>Modeling</i>	82
3.D	THE USE OF MODERN DECONVOLUTION	83
3.D.1	<i>What is deconvolution? Why do we need it?</i>	83
3.D.1.a	<i>The need</i>	83
3.D.1.b	<i>Mathematical formulation</i>	84
3.D.2	<i>Deconvolution Method 1 (von Schroeter et al., 2004)</i>	85
3.D.2.a	<i>Problem unknowns</i>	85
3.D.2.b	<i>Problem objective function</i>	86
3.D.2.c	<i>Deconvolution in plain English</i>	87
3.D.2.d	<i>Field data application</i>	87
3.D.2.e	<i>Main limitation of von Schroeter et al. method</i>	88
3.D.3	<i>Deconvolution Method 2 (Levitan, 2005)</i>	89
3.D.4	<i>Deconvolution Method 3 (Houzé et al., 2006-2010)</i>	91
3.D.4.a	<i>Variant 1: Using Levitan method after Method 3</i>	92
3.D.4.b	<i>Variant 2: Using Method 3 on all build-ups</i>	93

3.D.4.c	Remaining limitations	93
3.D.5	<i>Pi</i> influence on the deconvolution	94
3.D.5.a	Implementation in Saphir	95
3.D.6	Using sensitivity to assess the validity of a deconvolution	96
3.D.7	Conclusion (in 2010)	98
3.E	MODERN PTA METHODOLOGY	99
3.E.1	Initialization	99
3.E.2	Loading Data	100
3.E.3	Quality Control	101
3.E.4	Editing data	102
3.E.5	Extraction and diagnostic	103
3.E.6	Deconvolution	104
3.E.7	Diagnostic	105
3.E.8	Model generation	105
3.E.9	Model refinement	107
3.E.10	Sensitivity study	107
3.E.11	Reporting Guidelines	108
3.F	TEST DESIGN	109
3.F.1	Safety	109
3.F.2	Objectives	109
3.F.3	What data, what quality at what cost?	110
3.F.4	Type of test	112
3.F.5	Scenario	112
3.F.6	The final program	115
3.G	OPERATIONAL CONSIDERATIONS: GATHERING DATA	116
3.H	QUALITY ASSURANCE AND QUALITY CONTROL	117
3.H.1	Introduction	117
3.H.2	Background	117
3.H.3	The concept of Differential Pressure Analysis	118
3.H.4	Basics	119
3.H.5	Pressure correction	120
3.I	MORE ON QA/QC	121
3.I.1	Diagnosing phase segregation from differential pressure	121
3.I.2	Impact on the diagnostic	123
3.I.3	Gauge drift	123

3.I.4 Phase redistribution	124
3.J THE CASE OF DRY GAS	126
3.J.1 Diffusion of real dry gas	126
3.J.2 Correcting the pressure to sandface.....	126
3.J.3 Gas material balance	127
3.J.3.a Using pseudotime functions.....	128
3.J.3.b Integrating the material balance correction in the analytical model.....	129
3.J.3.c Using a numerical model.....	130
3.J.4 Non-Darcy flow	130
3.J.4.a Simulating non-Darcy flow with a rate dependent skin model	130
3.J.4.b Simulating non-Darcy flow with a numerical model.....	132
4 – PRODUCTION ANALYSIS (PA).....	133
4.A INTRODUCTION AND A BRIEF HISTORY	133
4.B THE OLD STUFF	135
4.B.1 Arps.....	135
4.B.2 Fetkovich	138
4.B.3 Gas material balance \bar{P}/Z vs Q plot.....	140
4.C THE RIGHT STUFF	141
4.C.1 Blasingame plot.....	141
4.C.2 Loglog plot.....	144
4.C.3 Material balance (Normalized rate-cumulative) plot.....	146
4.C.4 Flowing gas material balance plot	147
4.C.5 P-Q diagnostic plot.....	149
4.C.6 History plot.....	150
4.D THE CASE OF DRY GAS	151
4.D.1 Diffusion of real dry gas.....	151
4.D.2 The old Stuff	151
4.D.2.a Fetkovich	151
4.D.2.b Gas material balance \bar{P}/Z vs Q plot	152
4.D.3 The right stuff	152
4.D.3.a Blasingame plot	152
4.D.3.b Loglog plot	153
4.D.3.c Material balance (Normalized rate-cumulative) plot	154
4.D.3.d Flowing gas material balance plot and P-Q diagnostic plot	155

4.D.4	<i>General major gas issues</i>	155
4.D.4.a	Correcting the pressure to sandface	155
4.D.4.b	Gas material balance correction	155
4.D.4.c	Non-Darcy flow	157
4.E	MODERN PA METHODOLOGY	158
4.E.1	<i>Preparing a project and loading data</i>	159
4.E.2	<i>Editing data</i>	160
4.E.3	<i>Extraction and diagnostics</i>	160
4.E.4	<i>Model generation</i>	161
4.E.5	<i>Model refinement</i>	162
4.E.6	<i>Forecast</i>	162
4.E.7	<i>Sensitivity study</i>	163
4.E.8	<i>Reporting Guidelines</i>	163
4.F	PA VERSUS PTA.....	164
4.F.1	<i>Introduction</i>	164
4.F.2	<i>Common tools</i>	165
4.F.3	<i>PSS vs. IARF</i>	165
4.F.4	<i>Diagnostic capabilities</i>	165
4.F.5	<i>Validity of the PTA hypothesis in Production Analysis</i>	166
5	– WELLBORE MODELS	167
5.A	INTRODUCTION	167
5.B	CONSTANT WELLBORE STORAGE.....	168
5.B.1	<i>Loglog analysis</i>	168
5.B.2	<i>Specialized analysis (Cartesian plot)</i>	169
5.B.3	<i>Sensitivity analysis on the wellbore storage coefficient</i>	170
5.C	CHANGING WELLBORE STORAGE	171
5.C.1	<i>Analytical models</i>	171
5.C.2	<i>Combining pseudo-time and a constant storage model</i>	172
5.C.3	<i>Numerical pressure dependent wellbore storage</i>	173
6	– WELL MODELS	175
6.A	INTRODUCTION	175
6.B	VERTICAL WELL WITH CONSTANT SKIN	176
6.C	VERTICAL WELL WITH CHANGING SKIN.....	178
6.C.1	<i>Rate dependent skin</i>	178

6.C.2	<i>Time dependent well model</i>	179
6.C.3	<i>Time dependent skin</i>	180
6.D	HIGH CONDUCTIVITY FRACTURE.....	181
6.D.1	<i>Hypotheses</i>	181
6.D.2	<i>Behavior</i>	182
6.D.3	<i>Loglog Analysis</i>	184
6.D.4	<i>Sensitivity to different parameters</i>	185
6.D.4.a	Choice of fracture model	185
6.D.4.b	Sensitivity to the half fracture length.....	185
6.D.4.c	Sensitivity to the reservoir permeability	186
6.D.5	<i>Specialized Analysis</i>	187
6.D.6	<i>Adding wellbore storage</i>	188
6.D.7	<i>Skin effect</i>	188
6.D.7.a	Fracture Geometrical Skin	188
6.D.7.b	Model Skin and Total Equivalent Skin.....	189
6.D.7.c	Influence of skin	190
6.E	LOW CONDUCTIVITY FRACTURE	191
6.E.1	<i>Hypothesis</i>	191
6.E.2	<i>Behavior</i>	191
6.E.3	<i>Loglog Analysis</i>	192
6.E.4	<i>Sensitivity to different parameters</i>	193
6.E.4.a	Sensitivity to $k_f w_f$	193
6.E.4.b	Sensitivity to the half fracture length.....	194
6.E.5	<i>Specialized analysis</i>	194
6.E.6	<i>Adding wellbore storage</i>	195
6.E.7	<i>Skin effect</i>	196
6.E.7.a	Fracture Geometrical Skin	196
6.E.7.b	Model Skin and Total Equivalent Skin.....	196
6.F	LIMITED ENTRY WELL.....	198
6.F.1	<i>Hypothesis</i>	198
6.F.2	<i>Behavior</i>	198
6.F.3	<i>Loglog Analysis</i>	199
6.F.4	<i>Sensitivity to different parameters</i>	200
6.F.4.a	Sensitivity to the anisotropy	200
6.F.4.b	Sensitivity to the vertical distance to a constant pressure boundary	201
6.F.5	<i>Specialized analysis</i>	202

6.F.6	<i>Adding wellbore storage</i>	202
6.F.7	<i>Skin effect</i>	203
6.F.7.a	<i>Skin components</i>	203
6.F.7.b	<i>Influence of skin</i>	204
6.G	<i>HORIZONTAL WELLS</i>	205
6.G.1	<i>Hypothesis</i>	205
6.G.2	<i>Behavior</i>	206
6.G.3	<i>Loglog analysis</i>	207
6.G.4	<i>Sensitivity to different parameters</i>	207
6.G.4.a	<i>Contributing horizontal section, h_w and position</i>	207
6.G.4.b	<i>Sensitivity to the anisotropy</i>	209
6.G.5	<i>Adding wellbore storage</i>	209
6.G.6	<i>Skin effect</i>	210
6.H	<i>MORE ON HORIZONTAL WELLS</i>	211
6.H.1	<i>The flow regimes and incomplete data</i>	211
6.H.1.a	<i>Early time radial flow</i>	211
6.H.1.b	<i>Linear flow</i>	212
6.H.2	<i>Horizontal anisotropy</i>	214
6.H.3	<i>Fractured horizontal well</i>	215
6.H.3.a	<i>Sensitivity</i>	215
6.H.3.b	<i>Adding wellbore storage</i>	217
6.H.3.c	<i>Skin</i>	218
6.H.4	<i>Field examples</i>	218
6.I	<i>SLANTED WELLS</i>	219
6.I.1	<i>Behavior</i>	220
6.I.2	<i>Sensitivity to different parameters</i>	220
6.I.3	<i>Adding wellbore storage</i>	223
6.I.4	<i>Skin</i>	224
6.I.5	<i>Slanted well multilayer</i>	224
6.I.5.a	<i>Hypothesis</i>	224
6.I.5.b	<i>Behavior</i>	225
6.J	<i>MULTILATERAL WELLS</i>	228
6.J.1	<i>Hypothesis</i>	228
6.J.2	<i>Behavior</i>	229

7 – RESERVOIR MODELS..... 231

7.A	INTRODUCTION	231
7.B	HOMOGENEOUS RESERVOIR	232
7.B.1	<i>Homogeneous Sensitivity to parameters</i>	234
7.B.1.a	Skin	234
7.B.1.b	Permeability	235
7.B.1.c	Wellbore radius.....	236
7.B.1.d	Porosity	237
7.B.1.e	Total compressibility.....	238
7.B.1.f	Viscosity	239
7.B.1.g	Thickness.....	240
7.B.1.h	... and how about rates?.....	241
7.C	DOUBLE-POROSITY RESERVOIR	242
7.C.1	<i>Hypothesis</i>	242
7.C.2	<i>Loglog behavior</i>	243
7.C.3	<i>Specialized analysis</i>	247
7.C.4	<i>Effect of wellbore storage</i>	248
7.C.5	<i>Skin</i>	249
7.D	EXTENSIONS OF THE DOUBLE-POROSITY RESERVOIR	250
7.D.1	<i>Multiple porosities</i>	250
7.D.2	<i>Hypothesis</i>	250
7.D.3	<i>Loglog behavior</i>	252
7.D.4	<i>Effect of wellbore storage</i>	253
7.D.5	<i>Effect of skin</i>	254
7.E	DOUBLE-PERMEABILITY RESERVOIRS	255
7.E.1	<i>Hypothesis</i>	255
7.E.2	<i>Loglog behavior</i>	256
7.E.3	<i>Effect of wellbore storage</i>	258
7.E.4	<i>Skin</i>	258
7.E.5	<i>Field examples</i>	259
7.F	EXTENSION OF DOUBLE-PERMEABILITY RESERVOIRS	260
7.F.1	<i>Multiple layers</i>	260
7.F.2	<i>Numerical double permeability</i>	261
7.G	MULTILAYERED RESERVOIRS	263
7.G.1	<i>Hypothesis</i>	264
7.G.2	<i>How to build a multilayer model</i>	265

7.H	COMPOSITE RESERVOIRS	268
7.H.1	<i>Hypothesis</i>	268
7.H.2	<i>Loglog behavior</i>	270
7.H.3	<i>Specialized analysis</i>	272
7.H.4	<i>Effect of wellbore storage</i>	272
7.H.5	<i>Skin</i>	274
7.H.6	<i>Extensions of the composite reservoir</i>	275
7.H.7	<i>Numerical models</i>	277
7.H.8	<i>When should we use a composite model?</i>	278
7.H.8.a	Changes of reservoir properties	278
7.H.8.b	Fluid front	278
7.H.8.c	Gravel packs and the invaded zone	278
7.H.8.d	Match any old weird response.....	278
7.I	RESERVOIR ANISOTROPIES	279
7.I.1	<i>Vertical anisotropy</i>	279
7.I.2	<i>Horizontal anisotropy</i>	280
7.J	ANALYTICAL COMBINATIONS OF RESERVOIR MODELS	281
7.J.1	<i>Double permeability radial composite</i>	281
7.J.2	<i>Double permeability double porosity layers</i>	282
7.J.3	<i>Double porosity radial composite</i>	282
7.J.4	<i>Just a comment on the above described models</i>	283
8	– BOUNDARIES.....	285
8.A	INTRODUCTION	285
8.B	DIFFERENT TYPES OF BOUNDARIES	286
8.B.1	<i>Description of a boundary behavior</i>	286
8.B.2	<i>No flow boundaries</i>	287
8.B.3	<i>Constant pressure boundaries</i>	288
8.B.4	<i>Aquifers</i>	288
8.B.5	<i>Leaky boundaries</i>	289
8.B.6	<i>Conductive boundaries</i>	289
8.C	SINGLE SEALING FAULT	290
8.C.1	<i>Behavior</i>	290
8.C.2	<i>Semilog analysis</i>	290
8.C.2.a	Drawdown response	291

8.C.2.b Build-up response	291
8.C.3 Loglog analysis.....	292
8.C.4 Influence of the boundary distance	293
8.C.5 The case of shut-ins after a short production time	293
8.C.6 Remarks on the sealing fault model	294
8.D INTERSECTING FAULTS.....	295
8.D.1 Description	295
8.D.2 Behavior.....	295
8.D.3 Semilog analysis.....	296
8.D.3.a Drawdown response	296
8.D.3.b Build-up response	297
8.D.4 Loglog analysis.....	297
8.D.5 Remarks on the intersecting faults model	298
8.D.6 Example of intersecting faults match with field data	298
8.E TWO PARALLEL FAULTS.....	299
8.E.1 Description	299
8.E.2 Behavior.....	299
8.E.3 Semilog analysis.....	300
8.E.4 Loglog analysis.....	300
8.E.5 Specialized analysis	301
8.E.6 U-Shape reservoir.....	303
8.E.7 Remarks on the parallel faults model.....	304
8.E.8 Field example.....	304
8.F CLOSED SYSTEMS	305
8.F.1 Description	305
8.F.2 Behavior.....	306
8.F.3 Semilog analysis.....	307
8.F.4 Loglog analysis.....	307
8.F.5 Specialized analysis	308
8.F.6 Closed system versus drainage area	309
8.F.7 Other remarks on the closed systems.....	309
8.F.8 Example of matches with field data	310
8.G CONSTANT PRESSURE BOUNDARIES	311
8.G.1 Description	311
8.G.2 Behavior.....	311

8.G.3	<i>Semilog analysis</i>	312
8.G.4	<i>Loglog analysis</i>	312
8.G.4.a	Drawdown response	312
8.G.4.b	Build up response	313
8.G.5	<i>Constant pressure vs. closed system</i>	315
8.H	LEAKY AND INCOMPLETE BOUNDARIES.....	317
8.H.1	<i>Leaky fault</i>	317
8.H.1.a	Behavior	317
8.H.1.b	Semilog analysis	318
8.H.1.c	Loglog analysis	319
8.H.2	<i>Incomplete boundary</i>	320
8.H.2.a	Behavior	320
8.H.2.b	Semilog analysis	321
8.H.2.c	loglog analysis	322
8.I	CONDUCTIVE FAULTS	323
8.I.1	<i>Behavior</i>	324
8.I.2	<i>Semilog analysis</i>	325
8.I.3	<i>Loglog analysis</i>	325
8.J	COMBINATION WITH OTHER RESERVOIR AND WELL MODELS.....	328
8.K	ASSESSING BOUNDARY EFFECTS	329
8.L	RADIUS OF INVESTIGATION VS MINIMUM RESERVES	331
8.M	SUPERPOSITION EFFECTS.....	332
8.M.1	<i>Can we see a fault in a build-up and not in the drawdown?</i>	332
8.M.2	<i>Superposition effect consequence on the boundaries diagnosis</i>	333
8.M.3	<i>Conclusion</i>	334
8.N	TYPICAL ERRORS DIAGNOSING A BOUNDARY EFFECT	335
8.N.1	<i>Incorrect production history</i>	335
8.N.2	<i>End effect in the derivative calculation</i>	336
8.N.3	<i>Gauge drift</i>	337
8.N.4	<i>Reservoir trends</i>	337
8.N.5	<i>Interference from other wells</i>	337
8.O	DECONVOLUTION	339
8.P	CONCLUSION	341
9	PVT	343
9.A	INTRODUCTION	343

9.B	PHASE EQUILIBRIUM	344
9.B.1	<i>Single-component fluids</i>	344
9.B.2	<i>Multi-component fluids</i>	345
9.C	CLASSIFICATION OF RESERVOIR FLUIDS	347
9.D	PHASE DESCRIPTION	349
9.D.1	<i>Oil - Classical Black-Oil (BO) formulation</i>	349
9.D.2	<i>Wet gas</i>	351
9.D.3	<i>Modified Black Oil (MBO) PVT Formulation</i>	351
9.D.4	<i>Water production</i>	353
9.E	FLUID PROPERTIES	354
9.E.1	<i>Gas properties</i>	354
9.E.2	<i>Oil properties</i>	356
9.E.3	<i>Water properties</i>	357
9.F	USE OF PVT DATA IN DDA (OIL)	359
9.F.1	<i>Single-phase oil</i>	359
9.F.2	<i>Perrine</i>	359
9.G	USE OF PVT DATA IN DDA - CONTINUED (OIL)	361
9.G.1	<i>Single phase oil pseudopressure</i>	361
9.G.2	<i>Multiphase pseudopressure</i>	361
9.H	USE OF PVT DATA IN DDA (GAS).....	362
9.H.1	<i>Dry gas</i>	362
9.H.2	<i>Wet gas and condensate single phase analog</i>	362
9.I	USE OF PVT DATA IN DDA - CONTINUED (GAS).....	363
9.I.1	<i>Multiphase pseudopressures for condensate</i>	363
9.J	GETTING PROPERTIES FROM PVT STUDIES	364
9.J.1	<i>Constant Composition Expansion (CCE)</i>	364
9.J.2	<i>Differential Liberation Expansion (DLE)</i>	365
9.J.3	<i>Separator Tests</i>	366
9.J.4	<i>Converting Fluid Study Results</i>	367
9.K	OBTAINING PROPERTIES FROM PVT CORRELATIONS	368
9.K.1	<i>Gas correlations</i>	368
9.K.1.a	<i>Z factor</i>	368
9.K.1.b	<i>Gas viscosity</i>	369
9.K.2	<i>Oil correlations</i>	369
9.K.2.a	<i>Pb and Rs</i>	369

9.K.2.b Oil FVF.....	370
9.K.2.c Oil viscosity	370
9.K.2.d Oil isothermal compressibility	370
9.K.3 Water correlations	370
9.K.3.a Water FVF	371
9.K.3.b Water Compressibility	371
9.K.3.c Gas solubility	371
9.K.3.d Water Viscosity	371
9.K.4 Correlation: feeding and matching	371
9.L 'COMPOSITIONAL' PVT FROM BO (AND MBO) MODEL	373
9.L.1 2-Phase envelope	373
9.M EQUATIONS OF STATE	376

10 – NUMERICAL MODELS 377

10.A INTRODUCTION	377
10.B BUILDING COMPLEX GEOMETRIES	379
10.B.1 Building a 2D model	379
10.C PRINCIPLES OF VORONOI / PEBI GRIDDING	382
10.C.1 What is a Voronoi grid	382
10.C.2 Building the Voronoi grid	383
10.C.3 Local 3D refinement for specific well geometries	387
10.C.3.a Vertical wells	387
10.C.3.b Fractured (fully penetrating) wells.....	388
10.C.3.c Limited entry wells	388
10.C.3.d Limited entry fractured wells	389
10.C.3.e Horizontal wells	389
10.D HANDLING LINEAR PROBLEMS	391
10.D.1 A 'super-analytical model'	391
10.D.2 Formulation	392
10.E HANDLING LINEAR PROBLEMS (ADVANCED)	394
10.E.1 Modeling composite zones	394
10.E.2 Using field data	395
10.E.3 Double-porosity reservoirs	398
10.E.4 Modeling permeability anisotropy.....	399
10.E.5 Modeling multi-layer reservoirs (with or without cross-flow).....	401
10.F HANDLING NONLINEAR PROBLEMS	403

10.F.1	<i>Non-Darcy flow</i>	404
10.F.2	<i>Flow with Water and Hydrocarbons (Oil OR Gas)</i>	406
10.F.3	<i>Unconsolidated formations</i>	407
10.F.4	<i>How about three-phase flow?</i>	409
10.F.5	<i>Changing well controls</i>	410
11	– PTA: SPECIAL TEST OPERATIONS	413
11.A	INTRODUCTION	413
11.B	FORMATION TESTS	414
11.B.1	<i>Tool description</i>	414
11.B.2	<i>Test sequence</i>	415
11.B.3	<i>Standard Pressure Transient Analysis</i>	416
11.B.4	<i>Specific Formation Test Analysis</i>	417
11.C	SLUG TESTS	420
11.C.1	<i>Test sequence</i>	420
11.C.2	<i>Buildup analysis using slug rates</i>	421
11.C.3	<i>Slug test analysis</i>	422
11.D	MULTILAYER TESTS	426
11.D.1	<i>Introduction</i>	426
11.D.2	<i>Available models</i>	426
11.D.3	<i>Standard tests</i>	428
11.D.4	<i>Using Production Logs</i>	429
11.D.4.a	<i>Stabilized rate acquisition</i>	429
11.D.4.b	<i>Transient rate acquisition</i>	429
11.D.5	<i>Designing a multilayer test</i>	430
11.D.6	<i>Multilayer analysis workflow</i>	431
11.D.6.a	<i>Preparation of the data</i>	431
11.D.6.b	<i>Getting the global results</i>	432
11.D.6.c	<i>Multilayer model building and first run</i>	433
11.D.6.d	<i>First improve of the model</i>	434
11.D.6.e	<i>Final model adjustment</i>	436
11.D.6.f	<i>The solution uniqueness</i>	438
11.E	INTERFERENCE TESTS	439
11.E.1	<i>Homogeneous, sensitivity to parameters</i>	441
11.E.2	<i>Influence of wellbore storage and skin</i>	443
11.E.3	<i>Multilayer numerical: An overview</i>	443

<i>11.E.4 Other application of the numerical model</i>	445
<i>11.E.5 Interference testing and real life</i>	447
11.E.5.a The signal	447
11.E.5.b The tests	449
<i>11.E.6 Pulse tests</i>	451
11.E.6.a The old stuff	452
11.E.6.b The right stuff	452
<i>11.E.7 Vertical interference tests</i>	453

12 – WELL MODELING & PERFORMANCE ANALYSIS..... 455

12.A INTRODUCTION	455
12.B INFLOW PERFORMANCE RELATIONSHIP AND A.O.F.	455
<i>12.B.1 The IPR types</i>	456
12.B.1.a Straight line Constant IPR:	456
12.B.1.b Darcy Equation	456
12.B.1.c C&n IPR.....	457
12.B.1.d Gas LIT IPR.....	458
12.B.1.e Vogel Oil IPR for Solution gas drive reservoir	458
<i>12.B.2 Different types of multirate tests</i>	459
<i>12.B.3 Different IPR/AOF calculation methods</i>	460
12.B.3.a The Rawlins and Shellhardt method (C&n)	460
12.B.3.b The LIT Method	461
12.B.3.c Jones method	462
12.C INTAKE MODELS IN PTA AND PA	464
<i>12.C.1 Classic pressure correction</i>	464
<i>12.C.2 Correction methods</i>	464
12.C.2.a Flow correlations for oil.....	465
12.C.2.b Flow correlations for gas	465
12.C.2.c Lift curves.....	466
<i>12.C.3 General calculation method</i>	466
<i>12.C.4 Correcting gauge data vs. correcting model</i>	466

13 – PERMANENT GAUGES & INTELLIGENT FIELDS 467

13.A WHAT PDG DATA CAN BRING	467
13.B CHALLENGES OF PDG DATA.....	469
<i>13.B.1 Storage and access</i>	469
<i>13.B.2 Smart reduction</i>	469

13.C	WAVELET FILTRATION – AN OVERVIEW	471
13.D	WAVELET FILTRATION - THEORY	473
13.D.1	<i>Wavelet and scaling functions</i>	<i>473</i>
13.D.2	<i>Wavelet filtration with a single frequency.....</i>	<i>474</i>
13.D.3	<i>Wavelet filtration with multiple frequencies</i>	<i>475</i>
13.D.4	<i>Parameters controlling wavelet processing</i>	<i>476</i>
13.D.5	<i>Selection of the initial time step / frequency.....</i>	<i>477</i>
13.E	WAVELET FILTRATION - PRACTICE.....	478
13.F	PRESSURE TRANSIENT ANALYSIS OF PDG DATA	481
13.G	PRODUCTION ANALYSIS OF PDG DATA	484
13.H	APPLICATIONS AND DATA FLOW	486
13.H.1	<i>Accessing the historian: Workstation solution</i>	<i>486</i>
13.H.2	<i>Sharing data within a workgroup: Client/Server solution.....</i>	<i>488</i>
14	– PRODUCTION LOGGING	489
14.A	INTRODUCTION	489
14.B	WHAT PRODUCTION LOGGING IS USED FOR	490
14.C	CLASSICAL PRODUCTION LOGGING TOOLS	492
14.C.1	<i>Flowmeters (spinners).....</i>	<i>493</i>
14.C.2	<i>Density tools.....</i>	<i>495</i>
14.C.2.a	Gradiomanometers.....	496
14.C.2.b	Nuclear density tool	496
14.C.2.c	Tuning Fork Density (TFD)	496
14.C.2.d	Pseudo-density from pressure	496
14.C.3	<i>Capacitance and holdup tools</i>	<i>497</i>
14.C.3.a	Capacitance tools for water holdup.....	497
14.C.3.b	Gas holdup tools (GHT)	497
14.C.4	<i>Pressure and Temperature sensors</i>	<i>498</i>
14.C.5	<i>Depth and ID devices</i>	<i>499</i>
14.C.5.a	Depth measurement.....	499
14.C.5.b	Depth correction: Open Hole Gamma Ray	499
14.C.5.c	Depth correction: Cased Hole CCL.....	499
14.C.5.d	ID calculation: Calipers.....	499
14.D	A TYPICAL PL JOB SEQUENCE	500
14.E	TYPICAL JOB	501
14.F	DATA LOADING, QA/QC, AND REFERENCE CHANNELS.....	502

14.G	SPINNER CALIBRATION AND APPARENT VELOCITY CALCULATION	504
14.G.1	<i>Spinner response</i>	504
14.G.2	<i>Spinner in-situ calibration</i>	506
14.G.3	<i>Velocity from calibration: threshold handling and V_{apparent}</i>	507
14.G.3.a	Threshold options	507
14.G.3.b	Apparent Velocity.....	507
14.G.4	<i>Apparent velocity log</i>	508
14.H	SINGLE PHASE INTERPRETATION	509
14.H.1	<i>Velocity profile correction factor</i>	509
14.H.2	<i>Single phase interpretation results</i>	511
14.H.3	<i>Matching surface conditions</i>	512
14.I	MULTIPHASE INTERPRETATION	513
14.I.1	<i>Definitions</i>	513
14.I.1.a	Holdups	513
14.I.1.b	Phase velocities	513
14.I.1.c	Slippage velocity	513
14.I.2	<i>Starting with 2-phase</i>	514
14.I.3	<i>General solution using non-linear regression</i>	515
14.I.4	<i>Flow models and correlations</i>	516
14.I.5	<i>Graphical presentation</i>	517
14.I.6	<i>Emeraude Zoned approach and the Zone Rates plot</i>	518
14.I.7	<i>Multiphase interpretation results</i>	519
14.I.8	<i>Local versus global regression</i>	520
14.I.9	<i>The Continuous approach</i>	520
14.I.9.a	Illustration with a 3-Phase example.....	521
14.I.9.b	So?	522
14.J	SLANTED AND HORIZONTAL WELLS	523
14.J.1	<i>Apparent down flow</i>	523
14.J.2	<i>Horizontal wells</i>	523
14.K	MULTIPLE PROBE TOOLS (MPT), OR ARRAY TOOLS	525
14.K.1	<i>Schlumberger FloView – Courtesy Schlumberger</i>	525
14.K.2	<i>Schlumberger GHOST – Courtesy Schlumberger</i>	526
14.K.3	<i>Schlumberger FloScanner (FSI) – Courtesy Schlumberger</i>	527
14.K.4	<i>Sondex MAPS: CAT / RAT / SAT</i>	528
14.K.4.a	CAT: Capacitance Array Tool	528

14.K.4.b	RAT: Resistance Array Tool	529
14.K.4.c	SAT: Spinner Array Tool	529
14.L	MPT INTERPRETATION	530
14.L.1	<i>Mapping models</i>	530
14.L.1.a	Linear model	530
14.L.1.b	MapFlo holdup model.....	531
14.L.1.c	Prandtl velocity model	532
14.L.2	<i>Mapping options</i>	533
14.L.3	<i>Integration</i>	533
14.L.4	<i>Interpretation</i>	534
14.M	SIP	535
14.M.1	<i>IPR Type</i>	536
14.N	TEMPERATURE.....	537